3

SID 63-600-9

SATURN S-II MATERIALS AND PROCESSES DEVELOPMENT DURING LAST HALF OF 1967

31 June 1968

Prepared by

Materials and Processes Branch
of
Research, Engineering, and Test

Approved by

H. E. Dale
Assistant Program Manager
and Chief Program Engineer

SPACE DIVISION
NORTH AMERICAN ROCKWELL CORPORATION

N64-75949 (ACCESSION NUMBER)
429 (PAGES)
CR-113332 (NASA CR OR TMX OR AD NUMBER)
(THRU) none (CODE) (CATEGORY)
FACILITY FORM 602

FOREWORD

This report is submitted in compliance with SID 61-366A, revised 10 August 1966, DRL 004, Line Item 79, DRD SE 716, NASA-200. The work described was performed between 15 June 1967 and 15 December 1967 by the Research, Engineering and Test Department of the Space Division of North American Rockwell, Inc., in support of the Saturn S-II Program.

This report deals with Saturn S-II material engineering and studies associated with such processes as welding, corrosion prevention, and sealing and spray foaming of thermal insulation. This is the tenth semiannual report on this activity.

TECHNICAL REPORT INDEX/ABSTRACT

ACCESSION NUMBER							DOCUMENT SECURITY CLASSIFICATION	
							UNCLASSIFIED	

TITLE OF DOCUMENT

SATURN S-II MATERIALS AND PROCESSES DEVELOPMENT DURING SECOND HALF OF 1967

LIBRARY USE ONLY

AUTHOR(S)

CARR, W.A.

CODE	ORIGINATING AGENCY AND OTHER SOURCES	DOCUMENT NUMBER
QN085057	MATERIALS AND PROCESSES BRANCH, RESEARCH, ENGINEERING, AND TEST, SPACE DIVISION, NR	SID63-600-9

PUBLICATION DATE	CONTRACT NUMBER
31JUNE68	NAS7-200

DESCRIPTIVE TERMS

WELD SURFACE DISCONTINUITIES, INTERNAL WELD DISCONTINUITIES, STRESS RELIEF AREAS OF CIRCUMFERENTIAL WELDS, FRACTURE TOUGHNESS OF WELDMENTS, FAILURE ANALYSIS, CORROSION PREVENTION, SEALING, ABLATIVE INSULATION, FOAM INSULATION, ADHESIVES

ABSTRACT

THIS REPORT IS SUBMITTED IN COMPLIANCE WITH SID 61-366A, REVISED 10 AUGUST 1966, DRL 004, LINE ITEM 79, DRD SE716, CONTRACT NAS7-200. THE WORK DESCRIBED WAS PERFORMED BETWEEN 15 JUNE 1967 AND 15 DECEMBER 1967 BY THE RESEARCH, ENGINEERING, AND TEST DEPARTMENT OF THE SPACE DIVISION, NORTH AMERICAN ROCKWELL INC., IN SUPPORT OF THE SATURN S-II PROGRAM.

THIS REPORT DEALS WITH SATURN S-II MATERIAL ENGINEERING AND STUDIES ASSOCIATED WITH SUCH PROCESSES AS WELDING, CORROSION PREVENTION, SEALING, AND SPRAY FOAMING OF THERMAL INSULATION. THIS IS THE TENTH SEMIANNUAL REPORT OF THIS ACTIVITY.

CONTENTS

	Page
WELD SURFACE DISCONTINUITIES	1
INSPECTION OF S-II-1 STAGE AT KSC	3
INSPECTION OF S-II-2 STAGE AT KSC	7
POST-PNEUMOSTATIC INSPECTION OF S-II-3 STAGE	9
INSPECTION OF LH_2 TANK ON S-II-3 STAGE AT MTF	11
INSPECTION AND ELIMINATION OF WELD SURFACE DISCONTINUITIES ON S-II-5	13
SURFACE DISCONTINUITIES IN 2014-T651 ALUMINUM WELDS ON SATURN S-II	15
INTERNAL WELD DISCONTINUITIES	19
INVESTIGATION OF CAUSES OF INTERNAL DISCONTINUITIES IN HORIZONTAL ALUMINUM WELDS	21
METALLURGICAL EXAMINATION OF AFT LOX BULKHEAD WELDS ON S-II-9	25
METALLURGICAL INVESTIGATION OF UNUSUAL WELD STRUCTURE ON THE I-MERIDAN WELD OF S-II-10 FORWARD FACING SHEET	27
MINISTAGE FORWARD LH_2 BULKHEAD WELD EVALUATION	33
STRESS RELIEF AREAS OF CIRCUMFERENTIAL WELDS	35
SIMULATED WELD RELIEF SPECIMEN TESTS, PHASE I	37
SIMULATED WELD RELIEF SPECIMEN TESTS, PHASE II	45
STRESS RELIEF AREA EVALUATION	59
FRACTURE TOUGHNESS OF WELDMENTS	63
FRACTURE TOUGHNESS OF 2014-T651 WELDMENTS, PHASES I AND II	65
FRACTURE TOUGHNESS OF 2014-T651 WELDMENTS, PHASE III	93
WELDING, MISCELLANEOUS	121
MECHANICAL TESTING AND METALLURGICAL EXAMINATION OF WELDED 2014-T651 ALUMINUM SHEET AFTER FLATTENING WITH MAGNETIC HAMMER	123

Page

EVALUATION OF INCONEL 82 WELD FILLER MATERIAL FOR S-II LH_2 FEEDLINES 129
METALLURGICAL EVALUATION OF QUALITY OF LONGITUDINAL WELD IN A SAMPLE OF 321 CRES TUBING 131
METALLURGICAL INVESTIGATION OF CRACKING OF REPAIR WELD ON J-SECTION 135

MECHANICAL JOINT EVALUATION 143
SHEAR DEFORMATION TESTS ON S-II THRUST BLOCK BOLTS 145
TORQUE DEGRADATION TESTS FOR BOLTING RING MECHANICAL JOINTS AT X_B 299.380 UTILIZING RTV SEALANT UNDER BEARING SURFACES 149

FAILURE ANALYSIS 155
FAILURE ANALYSIS OF 321 STAINLESS BELLOWS P/N 1001531-413 157
FAILURE ANALYSIS OF S-II LH_2 TANK UPPER AND CENTER FRAME ASSEMBLIES, P/N's V7-312409 AND V7-312212 165
METALLURGICAL INVESTIGATION OF FRAMES AND CAP ANGLES FROM S-II-7 185

CORROSION 187
METALLURGICAL EVALUATION OF CORRODED RETAINER, P/N V7-315563 189
PACE WIANCKO PRESSURE TRANSDUCER FAILURES CAUSED BY ELECTRICAL SHORTING 191
CAUSE OF SHORT TRANSVERSE SURFACE ATTACK OF S-II LH_2 QUARTER-PANELS 195
CORROSION TESTS ON BURST DIAPHRAGMS, P/N 38762-100 215
CORROSION PROTECTION OF BURST DIAPHRAGMS, P/N 38762-100 217
CORROSION PROTECTION OF THE LH_2 TANK J-AREA . . 219
CORROSION OF PMS SUPPORT HOUSING COVERS, P/N V7-480268 221

LOX COMPATIBILITY AND CLEANING 225
LOX COMPATIBILITY DETERMINATIONS OF CONTAMINATED RIVETS 227

Page

EVALUATION OF COATINGS ON HI-SHEAR RIVET COLLARS 229
EVALUATION OF COATINGS ON CHERRY RIVETS . . . 231
FLUORESCENT TESTS ON LOX TANK CONTAMINATION . 233

SEALING 235
LEAKAGE CORRELATIONS: WATER VERSUS LOX . . . 237
LEAK TEST RESULTS ON RD BOLTS 241
COLORING AGENT FOR FOIL ADHESIVE, NARMCO 7343 . 243
PROPELLANT TANK FOIL SEALING PROBLEMS . . . 245
FOIL SEAL PEEL TESTS ON PRIMER M 249
THOR TANK FOIL SEAL TEST 253

ABLATIVE INSULATION 257
PREPARATION OF INTERSTAGE STRUCTURE FOR MB0130-074 ABLATIVE MATERIAL 259
DEVELOPMENT OF THERMAL PROPERTY DATA ON MB0130-074 ABLATIVE MATERIAL (KOROTHERM 790-005) 261

FOAM-FILLED HONEYCOMB INSULATION 273
DEVELOPMENT OF PROCEDURES APPLICABLE TO EMERGENCY REPAIR OF SIDEWALL INSULATION PRIOR TO LAUNCH 275
MINIMUM SATURN S-II TANK WALL TEMPERATURE FOR ADHESIVE APPLICATION 291
TEST DATA FOR A POLYURETHANE-COATED NYLON FABRIC TO REPLACE MEMBRANE SEAL 295
EVALUATION OF SILICONE RUBBER FLEXIBLE CLOSEOUT SEAL INSTALLATION AT EXTREME COLD TEMPERATURES 297
EVALUATION OF NYLON CLOSEOUT DOUBLER FOR USE UNDER FAIRINGS ON SATURN S-II 313

FOAM INSULATION 317
PIGMENTED SPRAY FOAM - PRELIMINARY DATA ON SELECTROFOAM SYSTEMS 319
ENVIRONMENTAL VERIFICATION TESTING OF CPR 369-3 SPRAY FOAM INSULATION 325
DESIGN VERIFICATION, SPRAY-ON FOAM INSULATION, 3-POUND DENSITY 351
DETERMINATION OF MAXIMUM TEMPERATURE LIMITATIONS OF SPRAY FOAM INSULATION 373

Page

QUALIFICATION TESTS OF SPRAYABLE POLYURETHANE FOAM INSULATION (CPR 369-3) FOR S-II TANK SIDEWALL 391
OVERLAP PRIMER STUDY ON CPR 369-3 FOAM AND EVALUATION OF CRYOGENIC STRAIN COMPATIBILITY OF NOPCO BX-250 SPRAY FOAM INSULATION . . . 397
MATERIAL PROPERTIES OF NOPCO BX-250 SPRAY FOAM 409
COMPARATIVE BLOCK SHEAR PROPERTIES OF BX-250A FOAM SPECIMENS PERPENDICULAR TO RISE . . . 421
DEVELOPMENT OF NEW PROCEDURE FOR FLATWISE TENSILE TESTING OF SPRAY FOAM INSULATION MATERIAL 425
THERMOPHYSICAL PROPERTIES OF NOPCO SPRAY FOAM BX-250A 429
OVERLAP JOINT PROCESSING TECHNIQUES 437
FLAMMABILITY/EXPLOSIBILITY HAZARD ASSOCIATED WITH APPLICATION OF SPRAY FOAM (NOPCO BX-250) . 443
SIMULATED DEBOND AREAS IN SPRAY FOAM INSULATION 447
DEVELOPMENT AND VERIFICATION OF CPR 349-3 POUR FOAM MATERIAL FOR NONSPRAYABLE APPLICATION AND SMALL REPAIRS ON S-II INSULATION 451
CRYOGENIC STRAIN COMPATIBILITY OF CPR 349-3 POUR FOAM 465

ADHESIVES AND PRIMERS 473
EVALUATION OF MECHANICAL PROPERTIES OF CHEMICAL FILM, EPOXY PAINT SURFACE FOR ADHESIVE BONDING 475
EVALUATION OF M-602 PRIMER CURED AT 240 F . . 479
ADHESIVE AND PRIMER COMPATIBILITY WITH M-602 . . 483

PLASTICS 487
TEFLON CORRUGATED TUBING PRESSURE TEST . . . 487

NEW SPECIFICATIONS 491
MATERIAL SPECIFICATIONS 491
PROCESS SPECIFICATIONS 493
INDEX TO PREVIOUS REPORTS 495

ILLUSTRATIONS

Figure		Page
1	Sketch of Planes Examined Metalligraphically	28
2	Microstructure Across Top of Weld, Magnification 50X	31
3	Specimen Ready for Testing (Outboard Side View)	38
4	Specimen Ready for Testing (Inboard Side View)	39
5	Specimen Deformation Behind Weld Land Relief	40
6	Applied Load Versus Average Tensile Stress at Selected Strain Gauge Locations	42
7	Edge View of Failed Specimen	43
8	Specimen Ready for Testing - Weld Land Side	46
9	Specimen Ready for Testing - Back Side	47
10	Specimen 4 Showing Flaw Locations	48
11	Load Versus Average Tension and Shear - Specimen 3 Strain Gauge Data	50
12	Load Versus Average Tension Stress - Specimen 6 Strain Gauge Data	51
13	Specimen 2 After Loading to 200, 000 Pounds	52
14	Specimen 4 After Failure at 145, 250 Pounds	54
15	Closeup of Specimen 4 Failure Edge	55
16	Specimen 5 After Failure at 152, 000 Pounds	56
17	Test Specimen Configuration	60
18	Determination of Weld Nugget Yield Strength	67
19	Test Specimen With Starter Notch 4 Inches Wide x 5/16 Inch Thick x 20 Inches Long	69
20	Fatigue Test Fixturing Fatigue Crack Growth (First Setup)	70
21	Modified Load Fixture Fatigue Crack Growth (Second Setup)	71
22	Final Fixturing Fatigue Crack Growth (Third and Final Setup)	72
23	Failed 6-Inch-Wide Specimen	73
24	Failed 4-Inch-Wide Specimen	74
25	Failed 4-Inch-Wide Specimen With Weld Notch	75
26	Load-Strain Curves of Specimen TI-10 at Room Temperature	78
27	Load-Strain Curves of Specimen C at -320 F	79
28	Load-Strain Curve of Specimen T-1-B at -423 F	80

Figure		Page
29	Gross Failure Stress Versus Normalized Flaw Depth, Room Temperature Test	82
30	Gross Failure Stress Versus Normalized Flaw Depth at -423 F	83
31	Typical Fatigue Flaw Photomacrographs	84
32	Photomacrograph of Weld Cross Section - Arrow Indicates Direction of Fatigue Flaw in Weld Nugget	85
33	Weld Land Tests, 22.8 ksi, Room Temperature Proof Load, -423 F Test	87
34	Defectometer Reading Versus Actual Crack Depth— Tight Fatigue Cracks	88
35	Weld Tests, 5/8 Inch Thick, -423 F (Specimen T11-3)	89
36	Weld Tests, 5/8 Inch Thick, -423 F (Specimen T11-2)	90
37	Weld Tests, 5/8 Inch Thick	91
38	Test Specimen - Transverse Weld	95
39	Test Specimen - Longitudinal Weld	96
40	Load-Strain Curve, Specimen S3-IT-2319 Filler Wire Weld Nugget at Room Temperature	98
41	Specimen 34-4, Room Temperature, Static, 4043 Filler Wire, 0.035-Inch Depth Second Pass Flaw	102
42	Specimen 34-11, Room Temperature, Static, 4043 Filler Wire, 0.055-Inch Depth Second Pass Flaw	102
43	Specimen 35-3, -300 F, Static, 4043 Filler Wire, 0.085-Inch Depth Second Pass Flaw	103
44	Specimen 32-2, -300 F, Static, 4043 Filler Wire, 0.180-Inch Depth Second Pass Flaw	103
45	Specimen 33-12, -423 F, Static, 4043 Filler Wire, 0.053-Inch Depth Second Pass Flaw	104
46	Specimen 34-3, -423 F, Static, 4043 Filler Wire, 0.062-Inch Depth Second Pass Flaw	104
47	Specimen 32-10, Room Temperature, -Cyclic, 4043 Filler Wire, 0.160-Inch Depth Second Pass Flaw	105
48	Specimen 35-7, -423 F, Cyclic, 4043 Filler Wire, 0.104-Inch Depth Second Pass Flaw	105
49	Specimen 35-12, -423 F, Static, 4043 Filler Wire, 0.108-Inch Depth First Pass Flaw	106
50	Specimen 33-1, -423 F, Cyclic, 4043 Filler Wire, 0.150-Inch Depth First Pass Flaw	106
51	Failure Stress Versus Normalized Flaw Depth, 4043 Filler Wire, Transverse Welds, Room Temperature Tests	107
52	Failure Stress Versus Normalized Flaw Depth, 4043 Filler Wire, Transverse Welds, -240 F and -300 F Tests	108

Figure		Page
53	Failure Stress Versus Normalized Flaw Depth, 4043 Filler Wire, Transverse Welds, -423 F Tests	109
54	Specimen S3-3, -423 F, Static, 2319 Filler Wire, 0.188-Inch Depth	112
55	Specimen S1-10, Room Temperature, Cyclic, 2317 Filler Wire, 0.098-Inch Depth	112
56	Specimen S4-14, Cyclic, 2319 Filler Wire, 0.160-Inch Depth	113
57	Specimen S1-15, -423 F, Cyclic, 2319 Filler Wire, 0.165-Inch Depth	113
58	Failure Stress Versus Normalized Flaw Depth, 2319 Filler Wire, Transverse Welds, Room Temperature Test	114
59	Failure Stress Versus Normalized Flaw Depth, 2319 Filler Wire, Transverse Welds, -240 F and -300 F Tests	115
60	Failure Stress Versus Normalized Flaw Depth, 2319 Filler Wire, Transverse Welds, -423 F	116
61	Failure Stress Versus Flaw Depth, Longitudinal Weld Specimens, 4043 Filler Wire	119
62	Photomicrograph of As-Welded, Transverse Section of Weld Showing Typical Metal Thinning	133
63	Photomicrograph of Planished Transverse Section of Weld, Showing Typical Metal Thinning	133
64	Photomicrograph of Specimen 4C Depicting Macrostructure of Weld Area of Figure 65	137
65	Photomicrograph of Specimen 4C Depicting Microstructure of Area in Figure 64	137
66	Photomacrograph of Specimen 5B Depicting Macrostructure of Weld and Indicating Area Shown in Figure 67	138
67	Photomicrograph of Specimen 5B Depicting Microstructure of Area Indicated in Figure 66	138
68	Photomacrograph of Specimen 6A Depicting Macrostructure of Weld and Indicating Area Shown in Figure 69	139
69	Photomicrograph of Specimen 6A Depicting Microstructure of Area Indicated in Figure 68	139
70	Photomacrograph of Specimen 8B, Depicting Macrostructure of Weld and Indicating Area Shown in Figure 71	140

Figure		Page
71	Photomicrograph of Specimen 9B Depicting Microstructure of Area Indicated in Figure 70	140
72	Photomacrograph of Specimen 8B, Depicting Macrostructure of Weld and Indicating Area Shown in Figure 73	141
73	Photomicrograph of Specimen 8B Depicting Microstructure of Area Indicated in Figure 72	141
74	Photomacrograph of Specimen XB Depicting Macrostructure of Weld and Indicating Area Shown in Figure 75	142
75	Photomicrograph of Specimen XB Depicting Microstructure of Area Indicated in Figure 74	142
76	Test Setup Showing Clevis Loading Arrangement and Special Deflectometer	146
77	Autographic Load Deflection Curve	147
78	Sketch of Test Specimen, 3/8-Inch-Diameter Bolts	150
79	Fracture in Second Convolution of Region A on Outer Surface (Outside Diameter) of Bellows	159
80	Fracture in Second Convolution of Region A on Inner Surface (Inside Diameter) of Bellows	160
81	Fracture in Second Convolution of Region B on the Outer Surface	161
82	Fracture in Second Convolution of Region B on Inner Surface (Inside Diameter) of Bellows	162
83	Photomacrograph of Fracture A at Magnification of 10X	163
84	Cracked Upper Frame Prior to Disassembly From the LH_2 Tank Panel	166
85	Upper and Lower Segments Showing Similarity of Fractures	168
86	Deformation of Upper Left-Hand Rivet Holes of Figures 119a and 119b, Respectively	169
87	Edge View of Remated Frame Segments, Looking Inboard Showing Buckling in Region of Sheared Rivets Adjacent to Tank Wall	170
88	Views of Upper Frame Fraction Through Cap Angle Demonstrating Impingement Damage and Offset	171
89	Fracture Faces of Frame Web and Cap Angle Members Showing Staining	172
90	Schematic of Nonuniform Staining of Fracture Surfaces	173
91	Schematic of Location of Replicas Taken From Fracture Surface	174

Figure		Page
92	Mode Replicas Taken From Upper Left-Hand Frame Member Fracture Surfaces	176
93	Edge Replicas Taken From Upper Left-Hand Frame Member Fracture Surface	177
94	Edge Replicas Taken From Lower Right-Hand Frame Member Fracture Surface	178
95	Edge Replicas Taken From Lower Right-Hand Frame Member Fracture Surfaces	179
96	Upper Cap Angle Extension Showing Surface Defects in Radius	180
97	Replicas Taken From Suspected Origin of Upper Frame Cap Angle Extrusions	182
98	Extrusion Defects Discovered in the Upper Frame Cap Angle	183
99	Photomicrographs of Panel Sections As-Received and After LAD Environmental Exposure	200
100	Panel Section Processed One Time Through LAD Solutions	201
101	Test Coupon Processed 10 Times Through LAD Solutions	202
102	Test Coupon Processed 10 Times Through LAD Solutions	203
103	Test Coupon Processed One Time Through LAD Solution	204
104	Photomicrograph of Panel Sections After Environmental Exposure	206
105	Test Coupons After Processing 10 Times Through LAD Solutions and Environmental Exposure	207
106	Panel Section Processed One Time Through LAD Solutions and Salt Spray	208
107	Test Coupons Processed One Time Through LAD Solutions and Salt Spray	209
108	Photomicrograph of Panel Sections After Processing One Time and Salt Spray	210
109	Photomicrograph of Test Coupon After Processing One Time and Salt Spray	211
110	Photomicrographs of Bare Aluminum Panel Section After Salt Spray	213
111	Photomicrographs of Bare Aluminum Test Coupons After Salt Spray	214
112	Support Housing Cover	222
113	Photomicrograph of 0.003-Inch Depth of Corrosion on Part 1	223

Figure		Page
114	Photomicrograph of 0.0025-Inch Depth of Corrosion on Part 2	223
115	Correlation of LOX Leakage at -320 F With Water Leakage at Room Temperature	239
116	Round Test Panel With Patches Applied	255
117	Dog-Bone Panel With Patches Applied	256
118	Ablative Material Specimen Holder Configuration—Hyperthermal Tunnel Plasma Jet Test Facility	263
119	Cross-Section Specimen Holder Positioned in Hyperthermal Tunnel Plasma Jet Facility	266
120	Time/Temperature History—0.015-Inch-Thick Korotherm 790-005 Ablative Specimens	267
121	Time/Temperature History—0.030-Inch-Thick Korotherm 790-005 Ablative Specimens	268
122	Time/Temperature History—0.045-Inch-Thick Korotherm 790-005 Ablative Specimens	269
123	Plasma Jet Test Sequence, 25-Second Period	270
124	Ablative Material Specimen After Test in Plasma Jet	271
125	Insulation Repair Area Prepared for Application of Spray Foam (CPR 369) at Ambient Temperature	277
126	Air-Motor-Driven Cutting Tool Removing Section of Defective Skin	278
127	Application of CPR 369-3 Foam Using Glascraft Gun Forming U-Shape Pattern Around Periphery of Repair	279
128	Trimming the Spray Foam Insulation Repair, Using a Carpenter's Hand Saw	280
129	CPR 369-3 Spray Foam Repair Finished to Surface of Core and Flush With Adjacent Tedlar Skin Insulation Leak-Checked at Ambient Using Helium at 5 psi	281
130	Application of CPR 369-3 Foam to Prechilled (<-280 F) Insulation Repair Area Using Glascraft Gun	282
131	Application of CPR 369-3 Foam Across Peripheral Area of Repair Insulation (Aluminum Plate is at <-280F)	283
132	Sealing Left-Hand Peripheral Area of Chilled (-280 F) Repair Using CPR 369-3 Foam and Glascraft Gun	284
133	Cross-Section of CPR 369-3 Spray Foam Applied into 3/4-Inch Cell Honeycomb With Aluminum Backing Plate (Aluminum Plate Immersed in LN_2)	285
134	Tedlar Laminate Cut as Shown With Knife 1/16 x 16 Inch (Note Chilled Helium Purge Escaping Through Crack)	286

Figure		Page
135	Application of Johns Manville B-FF Tape to Prechilled (-80 F) Tedlar Surfaces Over Cracked Area; Iron is Approximately 475 F	287
136	Typical Repair Area—Core Removed to HT-424 Surface of Tank Wall—Primed With Primer M	288
137	Application of CPR 369 Foam in Center Section of Insulation Repair Area	289
138	Modified Joint Configuration for Flexible Closeout Seal	298
139	Closeup of Cracked Rubber Doubler and Tedlar Skin, Panel 252A	300
140	Flexible Closeout Seal Pulled Back Exposing Cracked Nylon/Tedlar Skin, Panel 252A	301
141	Panel 252A After Second Test Cycle	303
142	Closeup of Cracked Flexible Closeout Seal, Panel 252A	304
143	Flexible Closeout Seal Pulled Back Exposing Cracked Tedlar/Nylon Skin	305
144	Panel 272 Prior to Bonding in Cork and Foam Filler Strips	307
145	Panel 272 After First Test, 17 Purge Cycles	308
146	Panel 272 Closeup of Cracked Lower Flexible Closeout Seal	309
147	Nylon Closeout Doubler Panel Configuration	314
148	Cryogenic Test Tank After Pressurization Failure	316
149	Hard Spot Details Bonded to Bolting Ring Test Tank 538	327
150	Schematic - Application Technique of Spray Foaming Section 3 of Bolting Ring Test Tank 538	328
151	Machined Foam and Hard Spot Details in Cavity 3 of Bolting Ring Test Tank 538	329
152	Bolting Ring Test Tank 538 Showing Machined Foam and Hard Spot Details	330
153	Test Assembly for Bolting Ring Test Tanks	331
154	Processing Sequence for Locating and Bonding of Hard Spot Details in Predetermined Locations in Spray Foam Insulated S-II Bolting Ring Section	333
155	Bonded Hard Spot Details in Test Tank 547	334
156	Test Tank 538 Prior to Environmental Testing	335
157	Test System Schematic for Combined Environmental Testing of S-II Insulation	336
158	Typical Test Setup for Combined Environment Tank Test of S-II Insulation	337
159	Test Tank Aerodynamic Heating Profile	339
160	Bolting Ring Test Tank 538 After Environmental Tests	340

Figure		Page
161	Bolting Ring Test Tank 538 After Environmental Testing With Hypalon Coating Removed	339
162	Bolting Ring Test Tank 538 After Dissection of Form in Failure Areas	342
163	30- x 30-Inch Test Tank 539 After Test	345
164	30- x 30-Inch Test Tank 539 After Test—With Hypalon Coating Partially Removed	346
165	30- x 30-Inch Test Tank No. 539 After Test—Showing Depth of Cracks in Foam Structural	347
166	Bolting Ring Test Tank 547 Before Test	348
167	Bolting Ring Test 547 After Test—Showing Ballooning of Hypalon Coating Removed	349
168	Bolting Ring Test Tank 547 After Test—Showing Foam Surface With Hypalon Coating	350
169	Specimen Plate Setup Before Foaming	352
170	Specimen After Application of Spray Foam	354
171	Sketch of Foam Composite Tension Specimen	355
172	Sketch of Foam Composite Tension Specimen Configuration	356
173	Six-Inch Debond 30 x 30-Inch Tank Specimen	359
174	Twelve-Inch Debond 30- x 30-Inch Tank Specimen	360
175	Bulkhead Configuration Composite Test Specimen	36[illegible]
176	Twelve-Inch Debond 30- x 30-Inch Tank After Test	370
177	Twelve-Inch Debond 30- x 30-Inch Tank After Dissection	371
178	Six-Inch Debond 30- x 30-Inch Tank After Dissection	372
179	Typical Specimen Configuration for Determining Effect of Elevated Temperatures on Spray Foam Insulation	375
180	Radiant Heat/Altitude Chamber Test Apparatus	376
181	Cork-Insulated Spray Foam Specimen After Exposure to Peak Temperature of 890 F	377
182	CPR 369-3 Spray Foam Specimens After Environmental Testing at 925 F and 0.2-Torr Pressure	379
183	CPR 369-3 Spray Foam Specimens After Environmental Testing at 875 F and 920 F at 0.2-Torr Pressure	380
184	CPR 369-3 Spray Foam Specimens After Environmental Testing at 800 F and 810 F at 0.2-Torr Pressure	381
185	CPR 369-3 Spray Foam Specimens After Environmental Testing at 720 F and 770 F at 0.2-Torr Pressure	382
186	CPR 369-3 Spray Foam Specimens After Environmental Testing at 690 F at 0.2-Torr Pressure	383
187	Effect of Aerodynamic Heat Profile on Hypalon-Coated Foam Specimens After Exposure to 590 F and 650 F at 0.2-Torr Pressure	384

Figure		Page
188	Hypalon-Coated Foam Specimens After Exposure to 590 F and 650 F at 0.2-Torr Pressure	385
189	Hypalon-Coated Foam Specimens After Exposure to 710 F and 750 F at 0.2-Torr Pressure	386
190	Hypalon-Coated Foam Specimens After Exposure to 810 F and 820 F at 0.2-Torr Pressure	387
191	Hypalon-Coated Foam Specimens After Exposure to 930 F and 1035 F at 0.2-Torr Pressure	388
192	Effect of Aerodynamic Heat Profile on Ablative-Coated CPR 369-3 Spray Foam in 0.2-Torr Pressure	389
193	Ablative-Coated CPR 369-3 Spray Foam Specimens After Environmental Testing at 625 F and 0.2-Torr Pressure	390
194	S-II Sidewall Foam Insulation Test Panel 542 Before Test	392
195	S-II Sidewall Foam Insulation Test Panel 544 Before Test	393
196	S-II Sidewall Foam Insulation Test Panel 542 After Test	394
197	S-II Sidewall Foam Insulation Test Panel 544 After Test	395
198	Test Panel Configuration for Overspray and Interface Strength Evaluation	399
199	Test Panel 555, Showing Vacuum Bell Bonded Over Debond Area in Foam-Tank Interface	401
200	Cross-Section of Overlap Interfaces on Control Foam Specimens and Foam Specimens With Primer M-Coated Overlaps	404
201	Cross-Section of Overlap Interfaces on Foam Specimens Coated With PRC 1535 Primer and Furane 8018 Resin System	405
202	Cross-Section of Overlap Interfaces on Foam Specimens Coated With PRC 410 and PRC 1531 Primer Systems	406
203	Cross-Section of Overlap Interfaces on Foam Specimens Coated With De Sota 390-003 Resin, Furan's Epo Coat 25-3-946 Resin and Proseal 775 Primer Systems	407
204	Debond Test Panel 555 After Test and Dissected	408
205	Block Shear Specimens, Type I and Type II Configuration	422
206	Configuration of Flatwise Tensile Test Specimens	426
207	Sketch of Load-and-Strain Measuring Fixture for Foam Flatwise Tensile Testing	427

Figure		Page
208	Flatwise Tensile Specimen Installed in Loading Fixture	428
209	Helium Absorption Versus Time	436
210	Cross-Section of Overlap Joint Using Processing Method 1	439
211	Cross-Section of Overlap Joint Using Processing Method 2	440
212	Cross-Section of Overlap Joint Using Processing Method 3	441
213	Cross-Section of Overlap Joint Using Processing Method 4	442
214	Spray Foam and 20- x 20-Inch Foam-In-Place Repair on 30- x 30-Inch Test Tank	461
215	Final Configuration of 30- x 30-Inch Cryogenic Tank Test With Foam-In-Place Repair	462
216	Final Setup of Shaker, Cryogenic Test Tank, and Hydraulic Actuator	463
217	PQV Test Values Obtained After Cryogenic Testing	464
218	Fixturing for Pouring of Cryogenic Strain Compatibility Specimen	467
219	Fixture Clamped in Position and Foam Poured	468
220	Configuration of Cryogenic Strain Compatibility Specimens	469
221	Specimens 445, 446, and 447 Prior to Test	470
222	Specimens 445 and 447 After Test	471
223	Panel B-1—M-602 Cured 6 Hours at 290 F and Adhesive Applied, Cured, and Tested	486
224	Test Setup With 14-Inch Tube	488
225	Straight Line Position of 26-Inch Tube at 50 psig	489
226	Straight Line Position of 26-Inch Tube After Relief of Pressure	490

TABLES

Table		Page
1	Summary of MRD Actions and Rework Results on S-II-1	4
2	S-II-3 LH_2 Tank - Inspection Data on Stress - Corrosion-Susceptible Parts	12
3	Summary of Penetrant-Identified Defects on S-II-5	14
4	Welding Conditions	16
5	Mechanical Properties of 2014-T651 Welds	18
6	Schedule Life Cycle Loading for Ministage Weld Tensile Specimens	33
7	Results of Weld Tensile Strength Tests of 2014 Aluminum Weld Tensile Specimens From Ministage Bulkhead	34
8	Tension Test Results Summary	57
9	Test Results Summary	61
10	Average Yield Strength of 2014-T651 Weldments Using 4043 Filler Wire	77
11	Typical Test Data - Surface Flawed Specimens	81
12	Representative Test Data - Weld Land Specimens	86
13	Uniaxial Tests - 2319 Filler Wire Weld Nugget - Specimen Average	97
14	Typical Transverse Weld Tests - 4043 Filler Wire	99
15	Typical Transverse Weld Tests - 2319 Filler Wire	110
16	Typical Longitudinal Weld Tests - 4043 Filler Wire Welds	117
17	Porosity Measurements of Tensile Coupons	124
18	Summary Data After Magnetic-Hammer Flattening, of Inspection, Alignment, and Tensile Properties of the 5/16-Inch Thick Weld Specimen	126
19	Minus 423 F (LH_2 Immersion) Weld Tensile Test Data	130
20	Description of Welding Procedures and Material Combination Used on Original Weld Joints	135
21	Description of Welding Procedures and Material Combinations Used to Weld Repair the Panels in Table 11	136
22	Torque Degradation Room Temperature Test Results Summary, 3/8-Inch-Diameter Bolts	151

Table		Page
23	Torque Degradation Room Temperature Results Summary, 7/16-Inch-Diameter Bolts	152
24	Torque Versus Thermal Cycle Results, 3/8-Inch-Diameter Bolts, 0.040-Inch-Thick Skin Bonded Per LA0106-033, Foil Seal Bonded With 0.010-Inch Thick Narmco, and RTV Accelerated Cure	152
25	LH_2 Panel Processing Operations at Los Angeles Division	197
26	Test Schedule	199
27	Impact Test Data of Rivets	228
28	Impact Test Data of Coatings on Hi-Shear Rivet Collars	230
29	Impact Test Data of Cherry Rivet Coatings	231
30	Leakage Test Results on Unsealed Bolts	242
31	Average Peel Test Data on Bonded Foil Specimens Using Narmco 7343	244
32	Comparison, of Foil Peel Strength Properties of Various Polyurethane Adhesives	248
33	Back Pressure Required to Delaminate Foil Seal Bondlines	251
34	Room Temperature Flatwise Tensile Tests	260
35	Average Lefkoweld 109 Room Temperature Tensile Shear Results	293
36	Average Narmco 7343 Room Temperature Tensile Shear Results	294
37	Physical and Chemical Data of Selectrofoam Systems	321
38	Average Flatwise Tensile Strength, Parallel to Rise	322
39	Average Flatwise Compressive Strength, Parallel to Rise	322
40	Thermal Expansion Data	323
41	Legend of Specimen Code	357
42	Vibration Levels	363
43	Results of CPR 369 Spray Foam Composite Tensile Tests	364
44	Foam Physical Properties Data	369
45	Specimen Data for Overlap Joint Processing Evaluation	398
46	Average Flatwise Tensile Test Data at Room Temperature, +200 F, -100 F, -300 F, and -423 F Parallel to Rise	410
47	Average Flatwise Tensile Test Data at Room Temperature, +200 F, -200 F, -300 F, and -423 F Perpendicular to Rise	410

Table		Page
48	Average Flatwise Compressive Test Data at Room Temperature, +200 F, -100 F, -320 F, and -423 F Parallel to Rise	411
49	Average Flatwise Compressive Test Data at Room Temperature, +200 F, -100 F, -320 F, and -423 F Perpendicular to Rise	411
50	Average Block Shear Test Data at Room Temperature, +200 F, -100 F, -300 F, and -423 F Parallel to Rise	412
51	Average Block Shear Test Data at Room Temperature, +200 F, -100 F, -300 F, and -423 F Perpendicular to Rise	412
52	Poisson's Ratio of BX-250A at Room Temperature, +200 F, -100 F, -300 F, and -423 F, Average Valves	414
53	Properties of BX-250A Foam Components and Mix	415
54	Thermal Conductivity Test Data of Nopco BX-250A Foam	416
55	Average Water Absorption Test Data	417
56	Average Thermal Expansion Test Data	417
57	Average Closed Cell-Porosity Test Data	418
58	Round Guarded Calorimeter Test Data	419
59	Average Block Shear Test Data — Type-I Configuration Specimens	423
60	Average Block Shear Test Data — Type-II Configuration Specimen	423
61	Apparent Density Test Results (Average)	430
62	Water Absorption Test Results (Average)	430
63	Thermal Conductivity Test Results	431
64	Thermal Expansion Test Result Average	433
65	Closed-Cell Test Results	434
66	Specific Heat Test Results	434
67	Flammability Test Results	435
68	Results of Flammability Tests On Airborne Droplets During Spray Operation	444
69	Results of Dust Explosion Tests	445
70	Average Flatwise Tensile Data Perpendicular to Rise, CPR 349-3 Pour Foam	453
71	Average Flatwise Tensile Data Parallel to Rise, CPR 349-3 Pour Foam	453
72	Average Flatwise Compressive Data Perpendicular to Rise, CPR 349-3 Pour Foam	454
73	Average Flatwise Compressive Data Parallel to Rise, CPR 349-3 Pour Foam	454

Table		Page
74	Average Block Shear Data Perpendicular to Rise, CPR 349-3 Pour Foam	455
75	Average Block Shear Data Parallel to Rise, CPR 349-3 Pour Foam	455
76	Average Water Absorption of CPR 349-3 Pour Foam (ASTM D-2127-62T)	455
77	Thermal Conductivity of CPR 349-3 in Direction Parallel to Foam Rise (ASTM C-177-63)	456
78	Average Thermal Expansion of CPR 349-3 (ASTM D-696-44)	457
79	Effect of Temperature and Relative Humidity on Density of CPR 349-3	458
80	Heat Sink Effect	459
81	Average Primer Lap Shear Test Data	477
82	Average Cure Lap Shear Test Data	481
83	Average Lap Shear Test Controls	481
84	Adhesion of Cured Adhesive Films to M-602	485

WELD SURFACE DISCONTINUITIES

PROGRESS SUMMARY

After pneumostatic test of the S-II-6, an unusually high incidence of small linear surface penetrant indications were found during inspection of the LH_2 tank welds. Because these weld beads are shaved flush, the penetrant indications would actually be subsurface discontinuities in the original weld bead. The small size of the discontinuities precluded their being revealed during the radiographic inspections. Because of the penetrant indications found on the S-II-6 tank welds, all previous tanks were reinspected and a comprehensive study program of the welds was initiated. Where a penetrant indication was found, it was removed by grooving, and the size of the groove-out was documented. All penetrant indications were found to be caused by subsurface microporosity or oxide films. The details of all penetrant indications and their dispositions on LOX and LH_2 tanks on stages S-II-1, S-II-2, S-II-3, and S-II-5 are presented in this report.

A program was initiated to determine the cause and structural effect of such surface defects. The overall test plan and basic results are presented.

INSPECTION OF S-II-1 STAGE AT KSC

INTRODUCTION

This section presents a report on the inspection of the welds of the LOX and LH_2 tanks of the subject stage. All accessible welds were subjected to radiographic and/or penetrant inspection.

Radiographs taken at KSC were compared with those taken during fabrication to determine if stage operations to date had caused propagation of the previously identified internal defects. Penetrant inspection was used to locate defects similar to those found on later fabricated stages.

All surface defects found during this inspection were removed by localized grooving with a carbide tip ball mill. Caustic etch and penetrant inspection were used to verify the removal of each defect.

RESULTS

In the LOX tank, five defects were identified by penetrant inspection in three separate locations. In the LH_2 tank, 13 defects were found by penetrant inspection in five separate locations.

CONCLUSIONS

All defects found through penetrant inspection were associated with subsurface microporosity (0.005-inch diameter or less). The grooving of each defect showed a typical pattern of the indication being removed on the initial use of the ball mill. Application of the etchant and penetrant solution would then reveal scattered porosity in the grooved-out area. Most groove depths shown in Table 1 were necessary to remove porosity of a sharp nature or linear orientation.

In addition to those defects found through penetrant inspection, nine questionable areas were identified through the review of radiographs. These questionable areas were as follows:

1. A crack was suspected in the aft LOX bulkhead dollar weld

   Disposition—One section of the doubler was removed to afford penetrant inspection and improved radiographic definition.

Table 1. Summary of MRD Actions and Rework Results on S-II-1

LOX TANK	
MRD 47705:	Two 0.030-inch, L-shaped penetrant indications were found at the intersection of the aft LOX bulkhead I meridian and the LOX tank girth weld.
Rework:	Two grooveouts were made to a final depth of 0.019 inch and 0.024 inch. Penetrant inspection at final depth showed microporosity in the bottom of the groove and in the surrounding area.
MRD 47706:	One 0.060-inch chevron-shaped indication was found in the girth weld between the J- and K-weld intersections.
Rework:	A grooveout was made to a final depth of 0.057 inch. This indication was typical of the oxide film type with considerable porosity being encountered as grooving progressed.
MRD 47707:	Two 0.125-inch L-shaped indications were found on LOX girth weld between meridians G and H of the aft LOX bulkhead.
Rework:	This indication appeared to be linear microporosity. A final groove depth of 0.061 inch was required to remove all linear indications. The weld in this area had 0.020 inch of reinforcement.
LH_2 TANK	
MRD 47733:	One 0.125-inch transverse indication was found on the weld joining Cylinders 5 and 6 adjacent to Splice 2.
Rework:	The indication was typical of the oxide film type. Final groove depth was 0.009 inch. The groove was free of porosity at final depth.
MRD 47734:	A group of six indications were found in a 0.250-inch area on the weld joining Cylinders 2 and 3 at Stringer 95 + 7-1/2 inches.
Rework:	This area appeared to be discolored and rough as would be the case if a repenetration weld had been made from the outboard side. Microporosity was encountered just below the surface. Final groove depth was 0.046 inch.

Table 1. Summary of MRD Actions and Rework Results on S-II-1 (Cont)

MRD 47735:	Two 0.020-inch transverse indications were found approximately 0.030 inch apart located on the weld joining Cylinders 5 and 6 at Stringer 123 + 6 inches.
Rework:	Microporosity was encountered just below the surface. Final groove depth was 0.010 inch.
MRD 47736:	One 0.125-inch longitudinal indication was found on the weld joining Cylinders 5 and 6 at Stringer 131 + 2 inches.
Rework:	Microporosity was found just below the surface. Final groove depth was 0.013 inch.
MRD 47737:	Three 0.025-inch transverse indications were found on the B-meridian weld of the forward LH_2 bulkhead, and one area was found to contain surface porosity. These indications were spaced approximately 5 inches apart.
Rework:	Grooves of 0.071, 0.072, 0.064 and 0.030 inch were required to remove these indications. Microporosity was encountered in each of the grooveouts.

Results—The radiographic image was attributed to a concentration of silicon in a repair area.

2. Seven crater cracks were suspected in previously grooved areas or weld stop points of the LH_2 tank.

   Disposition—The insulation was removed from the outboard surface, and both of the inboard and outboard surfaces were caustic-etched and penetrant-inspected.

   Results—All surfaces were found free of defects, with the exception of the inboard surface of one area. Crack-like defects were found adjacent to the area in question; however, these defects were attributed to selective chemical attack as a result of the etchant solution used and the dwell time.

3. Incomplete penetration was suspected of the F meridian weld of the forward LH_2 bulkhead.

   Disposition—A 4-inch long groove approximately 0.010 inch deep was made in the suspect area. Caustic etching and penetrant inspection were performed.

   Results—The area was found to contain linear surface porosity along the weld root edge.

INSPECTION OF S-II-2 STAGE AT KSC

INTRODUCTION

This section presents results of the inspection of the S-II-2 stage at KSC. The inspection techniques and the procedures used were identical with those used for the S-II-1 stage.

RESULTS

LOX Tank

Three defects were removed in two locations. Only one of these defects was crack-like in nature.

LH_2 Tank

The LH_2 tank was found to be defect-free.

CONCLUSIONS

The singular crack-like defect in the LOX tank was found to be associated with subsurface porosity.

The defect-free condition of the LH_2 tank is evidence of the thoroughness of the inspection performed at MTF and verifies that no additional defects were opened during static firing operations.

POST-PNEUMOSTATIC INSPECTION OF S-II-3 STAGE

The results of penetrant inspection of the S-II-3 stage after the pneumostatic test are presented in this section. The inspection techniques and procedures used in this inspection were identical with those employed on S-II-1 and S-II-2 stages.

All surface defects found during this inspection were removed by grooving the weld with a carbide tip ball mill. Caustic etching and penetrant inspection were used to verify the removal of the defects. Rework procedures were as follows:

Groove in 0.005-inch increments to a maximum depth of 0.030 inch

Etch and penetrant-inspect at each increment

M&P and NASA examination at each increment

Acceptance upon mutual agreement of M&P and NASA that the defect had been removed or reduced to an acceptable condition.

RESULTS

A total of 37 indicated defects were removed from the inboard surface of welds in the LH_2 tank. Four indications were reevaluated, and no rework was required.

CONCLUSIONS

The groove depths employed were necessary to remove the linear oxide films with and without porosity (as established by the NASA guidelines) that were revealed by the penetrant inspection.

It appeared that some of the defects resulted from a preferential chemical attack of segregated eutectics during prepenetrant inspection etching and were not oxide films produced by the welding operation.

INSPECTION OF LH_2 TANK ON S-II-3 STAGE AT MTF

INTRODUCTION

The S-II-3 stage LH_2 tank was fluorescent penetrant-inspected on the inboard circumferential and vertical weld areas. The designated brackets of the LH_2 probe assembly were visually inspected for stress corrosion. (See Table 2.)

RESULTS

Two linear defects were found in two circumferential welds. These defects were not located in the stress relieved areas.

Visual inspection of the probe assembly brackets revealed no evidence of stress corrosion; however, scratches and gouges were found on the surface of six brackets.

CONCLUSIONS

The linear defects were found to be associated with subsurface oxides and porosity. The scratches and gouges occurred during intank installation of systems at the Seal Beach facility.

COMMENTS

Cylinders 2 and 3 Circumferential Weld

A defect was reported as a 0.020-inch transverse linear indication that was located 773.9 inches from Position I.

Rework—The weld in the defective area was removed to the parent metal surface, and a pore with a stringer oxide 0.010 inch in length remained. This was accepted by Material Review.

Cylinders 3 and 4 Circumferential Weld

A defect was reported as a 0.125 transverse linear indication that was located at 1205 inches from Position I.

Rework—The defect was removed at a depth of 0.021 inch.

Stress Corrosion Inspection

Eleven 2024-T4 aluminum brackets were visually inspected for evidence of stress corrosion in the fillets and around the holes.

Rework—All areas damaged by scratches and gouges were polished and chem-filmed.

Table 2. S-II-3 LH_2 Tank Inspection Data on Stress-Corrosion-Susceptible Parts

Part Number	Part Name or Function	Location	Present Finish and Condition
V7-480158 1	Clevis probe support, bulkhead, LH_2	Forward bulkhead near access door	Acceptable
V7-480158 2	Clevis probe support, bulkhead, LH_2	Forward bulkhead near access door	Acceptable
V7-480242 1	Fitting bracket	XB362 Stringer 211	Scratched or chipped on radius of bracket
V7-480242 2	Fitting bracket	XB362 Stringer 210	Scratched or chipped on radius of bracket
V7-480272-3	Bracket support probe, LH_2 tank	XB814 Stringer 209	Scratched or chipped on edge of bracket
V7-480272-5 1	Bracket support probe, LH_2 tank	XB434 Stringer 209	Acceptable
V7-480272 3	Bracket support probe, LH_2 tank	XB580 Stringer 209	Scratched or chipped around hole
V7-480272 4	Bracket support probe, LH_2 tank	XB655 Stringer 209	Scratched or chipped around hole
V7-480272 5	Bracket support probe, LH_2 tank	XB734 Stringer 209	Scratched or chipped around hole
V7-480276	Bracket support probe, upper LH_2 tank	XB860 Stringer 209	Acceptable

INSPECTION AND ELIMINATION OF WELD SURFACE DISCONTINUITIES ON S-II-5

Linear surface indications were found in welds of the LH_2 tank of the S-II-5 stage by post-pneumostatic fluorescent penetrant inspection. General rework of defects was performed in accordance with standard grooveout procedures. The detailed steps taken were as follows:

1. The defect was grooved out with a tungsten-carbide tipped ball mill in depth increments of 0.010 inch.

2. Each increment was etched and penetrant-inspected.

3. M&P and NASA concurrence that defect has been removed or reduced to an acceptable condition.

4. The grooveout was polished to a 63 RMS finish and chem-filmed per Process Specification MA0109-003.

RESULTS

Table 3 shows that all defects were shallow, with the exception of the pore at the bottom of one defect. Radiographic inspection of grooveout repairs indicated that these areas contained porosity and/or oxide within the allowable limits of Process Specification MA0107-016, Machine Fusion Welding of Aluminum Alloys for Saturn S-II Vehicle.

The linear discontinuities found on the S-II-5 were caused by tight oxide films and/or subsurface porosity and were not cracks as described on the MRD's. These defects were considered to have no adverse effect on the weld integrity of the LH_2 tank.

Table 3. Summary of Penetrant-Identified Defects on S-II-5

Defect	Location	Groove Depth (inches)	Comments
2 transverse cracks 0.030 inch + 0.050 inch	Inboard Cylinders 2 and 3 circumferential weld	0.017	Defect removed completely
1 oxide fold and tail - 0.060 inch	Inboard Cylinders 4 and 5 circumferential weld	0.018	Defect removed completely
1 linear crack 0.085 inch	Outboard Cylinders 2 and 3 circumferential weld	0.002	Defect removed completely
1 linear crack 0.070 inch	Outboard Cylinders 2 and 3 circumferential weld	0.003	Parent metal defect near weld edge removed completely
1 linear crack 0.045 inch	Outboard Cylinders 2 and 3 circumferential weld	0.010	Defect removed to within acceptable limits
1 transverse crack 0.070 inch	Inboard Cylinders 5 and 6 circumferential weld	0.032	Defect removed to within acceptable limits
1 oxide pore 0.050-inch deep (total)	Inboard Cylinders 5 and 6 circumferential weld	0.020	Pore is at bottom of grooveout. Total depth is 0.050 inch. Acceptable as is.

SURFACE DISCONTINUITIES IN 2014-T651 ALUMINUM WELDS ON SATURN S-II

INTRODUCTION

During dye-penetrant inspection after pneumostatic testing of stages S-II-2, S-II-3, and S-II-4, numerous small transverse and longitudinal linear indications were observed on the root side of the horizontal welds.

The possibility that these indications may have been the result of welding procedures, prompted a study of certain welding variables that could be the cause of the surface discontinuities. The study involved two test phases as follows:

Phase I - To determine if life cycle testing of 2014-T651 welds would produce linear defects on the root side of weld

Phase II - To determine if various welding conditions contribute to the production of linear defects after the welds on 2014-T651 aluminum were subjected to pneumostatic test conditions.

CONCLUSIONS

The specimens in Phases I and II did not indicate any evidence of root side defects through the use of fluorescent penetrant inspection under 10X optical aid after the specimens were subjected to life cycle and simulated pneumostatic test conditions.

PROCEDURE AND RESULTS

Phase I

Test plates of 0.250-inch-thick 2014-T651 aluminum were welded in the horizontal position with a 3/32-inch diameter, 45-degree bevel tungsten. A standard square butt design and the DC TIG straight polarity process were used. The welding conditions are given in Table 4.

Test plates were radiographically inspected to the Saturn S-II fusion welding specification MA0107-016. All welds met the specification requirements.

Table 4. Welding Conditions

Phase	Filler Wire Type	Pass	Remarks
I	4043 1/16-inch diameter	Penetration cover	Free fall welds
II	4043 1/16-inch diameter	Continuous tack penetration cover	Procedure - A (1) Free-fall weld
II	4043 1/16-inch diameter	Continuous tack penetration cover	10-CFH Argon gas with hand held cup on penetration side of weld. Procedure A (1) free-fall weld
II	4043 1/16-inch diameter	Penetration cover	Procedure B (2) Free-fall weld
II	4043 1/16-inch diameter	Continuous tack penetration cover	Pre-Gap 0.030 inch. Procedure A free-fall weld.
II	4043 1/16-inch diameter	Continuous tack penetration cover	SS backup bar with 0.032-inch-deep 3/8-inch-wide groove. Procedure A (1)
II	4043 1/16-inch diameter	Penetrant cover	SS backup bar with 0.032-inch-deep 3/8-inch-wide groove. Procedure B (2)
II	2319 1/16-inch diameter	Continuous tack penetration cover	Procedure A (1). Free-fall weld.

Note:

(1) Procedure A

Pass 1 - 75-percent penetration continuous tack
Pass 2 - Full penetration
Pass 3 - Cover pass

(2) Procedure B

Pass 1 - Full penetration pass
Pass 2 - Cover pass

After machining, radiographic examination of the specimens was again performed; all welds met the requirements of the fusion welding specification MA0107-016.

The specimens were uniaxially tensile-tested and inspected to the following schedule:

1. Six cycles 1 to 25,000 psi at room temperature
2. Two hundred cycles 1 to 7000 psi at room temperature
3. Fluorescent penetrant inspection
4. Fifty cycles 1 to 16,000 psi at -320 F
5. Fluorescent penetrant inspection
6. Radiographic inspection
7. Four cycles 1 to 29,000 psi at room temperature
8. One hundred twenty-five cycles 1 to 8,500 psi at room temperature
9. Fluorescent penetrant inspection
10. Thirty-five cycles 1 to 18,500 psi at -320 F
11. Fluorescent penetrant inspection
12. Pull to failure at -320 F

The mechanical properties of these specimens are given in Table 5. No defects were detected in any of the penetrant inspection steps. Specimens were fluorescent penetrant-inspected on both sides.

Phase 2

Test plates were welded through the use of the conditions and procedures given in Table 4. A radiographic inspection was made (same as in Phase I); all welds met specification requirements. The specimens were then tested and inspected to the following schedule:

1. Fluorescent penetrant-inspected per MQ0501-004.
2. Room temperature cycled five times from 4.6 ksi to 46 ksi.
3. Fluorescent penetrant-inspected per MQ0501-004.

No defects were detected by fluorescent penetrant inspection before or after cycling.

Table 5. Mechanical Properties of 2014-T651 Welds

Specimen No. (1)	Ultimate Stress F_{tu} (ksi)	Percent Elongation 2-Inch Gauge Length	Test Temperature (F)
1-1	60.4	5.5	-320
3-1	55.5	4.5	-320
3-2	63.5	5.0	-320
7-1	62.0	5.5	-320
7-2	62.1	5.5	-320
9-1	61.4	4.7	-320

(1) Longitudinal weld specimens

INTERNAL WELD DISCONTINUITIES

PROGRESS SUMMARY

X-ray inspection of welds is used to inspect nondestructively for internal discontinuities. Most, but not all, of the X-ray indications are readily traced to the type of internal discontinuity that is responsible for the indication. In the remaining cases, the type of discontinuity that causes a particular X-ray indication is unique to the type of weld being examined. Four of these situations were studied. They were horizontal welds in LH_2 tanks, gore to waffle aft LOX bulkhead welds, I-meridian welds, and forward LH_2 bulkhead welds. In each case the cause of the X-ray indication was determined.

INVESTIGATION OF CAUSES OF INTERNAL DISCONTINUITIES IN HORIZONTAL ALUMINUM WELDS

INTRODUCTION

The LH_2 tank of the Saturn S-II is composed of 2014-T651 aluminum cylinders that are stacked one on top of the other. Cylinder 1 is joined to a 2219-T62 J-ring. The circumferential joints are welded in the horizontal position. The occurrence of internal discontinuities in these welds is not uncommon.

An investigation was conducted to determine if strain gauge sealer adjacent to the weld joint, or the scraping and galling of the mating surfaces of the cylinders (a condition that occurs during preweld fitup operations), causes internal discontinuities.

Also investigated was the effect of using Teflon spacers or tape between test plates. The spacers would be removed before welding, while the Teflon tape would be left in the joint during welding. The Teflon spacers and tape were proposed as a means of eliminating the scraping and galling conditions.

CONCLUSIONS

Test plates of 2014-T651 welded to 2014-T651 or 2219-T62 in which the mating surfaces were scraped and galled were radiographically acceptable.

Strain gauge sealer applied to the back side of the weld joint causes internal discontinuities in the resultant weld.

Teflon spacers will prevent scraping and galling during fitup of the cylinders. However, internal discontinuities will be produced in the area of the Teflon spacers.

Teflon tape cannot be left in a joint during welding.

PROCEDURE

Test Plate 1

This was a control plate 0.250-inch-thick 2014-T651 welded to 2014-T651 in the horizontal position (free fall) using the dc straight polarity GTA process. The test panels were cleaned before welding using a scrape and draw file method. Subsequent to removing the weld bead reinforcement, top and bottom, the plate was radiographically inspected. All test plates in this investigation were prepared under these same conditions.

Test Plate 2A

This plate also consisted of 0.250-inch-thick 2014-T651 panels. One panel was filed to produce a sine wave pattern in the joint. After the panels were set up in the horizontal position with an applied load of 30 pounds per foot, the upper panel was moved parallel to the joint ten times for a distance of one inch to produce galling and scraping. The panels were welded without removing the applied load.

Test Plate 2B

Test plate 2B was produced in the exact same manner as test plate 2A, with the exception that the lower panel was 2219-T62 instead of 2014-T651.

Test Plate 3

To determine the effect of the strain gauge sealer, a 0.250-inch-thick panel of 2014-T651 aluminum was coated along a 12-inch length of the back side of the joint in a 1-1/2-inch-wide band from the panel edge. During preweld cleaning, 6 inches of the sealer was removed to determine the adequacy of the cleaning process. The panel was then welded to a cleaned panel of the same material in such a manner that the sealer was on the top side of the joint.

Test Plate 4

Two panels of 2014-T651 aluminum, with a square butt joint, were preweld cleaned and set up in the horizontal position with three pieces of 1/16-inch-thick Teflon spacer inserted at equal intervals between the panels. An applied load and a forced relative motion (same as test panels 2A and 2B) were induced on the upper plate. The spacers were then removed without relaxing the applied load and the panels were welded.

Test Plate 5

This test was the same as test 4, except that the Teflon spacers were replaced by a thin 1/4-inch-wide Teflon tape, and the tape was left in the joint during welding.

RESULTS

The radiographic quality of test panels 1 through 4 was acceptable to the criteria of MA0107-016F, with the exception of test plate 3 (in the region of the unremoved sealer) and test plate 4 (in the areas of the Teflon spacers). In this latter test plate, there were three distinctive areas of internal discontinuities ranging in length from 5/8-inch to 1-5/16-inch clusters centered on the Teflon spacer locations. These results indicate that the galling and scraping of cleaned mating surfaces are not detrimental to weld quality, and any attempt to prevent surface abrasion by the use of Teflon spacers will only tend to degrade weld quality rather than improve it.

METALLURGICAL EXAMINATION OF AFT LOX BULKHEAD WELD ON S-II-9

INTRODUCTION

Radiographic inspection of the gore-to-waffle weld of the aft LOX bulkhead of the S-II-9 revealed a faint dark indication running parallel to the weld. A weld sample showing a similar indication was evaluated. The subject material was 2014-T6 welded with 4043 filler wire.

The evaluation was conducted to determine the nature of the X-ray-located imperfection.

CONCLUSION

The microstructure had no defects that could be construed as the cause of the X-ray-located imperfection.

PROCEDURE

The imperfection was sectioned transverse to its longitudinal direction. The section was mounted and polished for microexamination. The mating surface of the first section was also mounted and polished to ensure a complete examination of the imperfection.

Both mounts were submitted to X-ray for views perpendicular to the polished surface.

RESULTS AND DISCUSSION

The microstructure of the mounted sections showed no defects that could be related to the X-ray indication. These mounted sections were X-rayed 90 degrees to the polished surface, and in each instance no defect or imperfection was indicated.

METALLURGICAL INVESTIGATION OF UNUSUAL WELD STRUCTURE ON I-MERIDIAN WELD OF S-II-10 FORWARD FACING SHEET

INTRODUCTION

An unusual pattern of curved low-density areas was observed in the radiographs of the I-meridian weld of the S-II-10 forward facing sheet. The I-meridian had been processed as follows:

1. Penetration pass
2. Cover pass
3. Local repair by manual welding
4. Re-fusion pass over entire weld with the same parameters used previously for the cover pass.

A welded panel, made with the same welding procedures shown for the I-meridian, was investigated. The radiographs of this panel contained curved low density areas similar to those in the radiographs of the I-meridian weld.

The purpose of this investigation was to identify the cause of the low density lines in the radiographs of the submitted sample and the I-meridian weld.

CONCLUSION

The low density lines of the radiograph are associated with differences in orientation of large dendrites in the re-fused zone of the weld.

PROCEDURE

Metallographic Examination

Metallographic specimens were prepared so that planes through the low-density lines (as shown at A in Figure 1) and across the lines (as shown at B in Figure 1) could be examined.

NOTE: THE CROSS-HATCHED PLANE AT "A" REPRESENTS A SECTION THROUGH THE LOW-DENSITY LINES. PLANES AT "B" REPRESENT TOP AND BOTTOM SURFACE PLANES FROM WHICH A MINIMUM OF MATERIAL WAS REMOVED IN POLISHING.

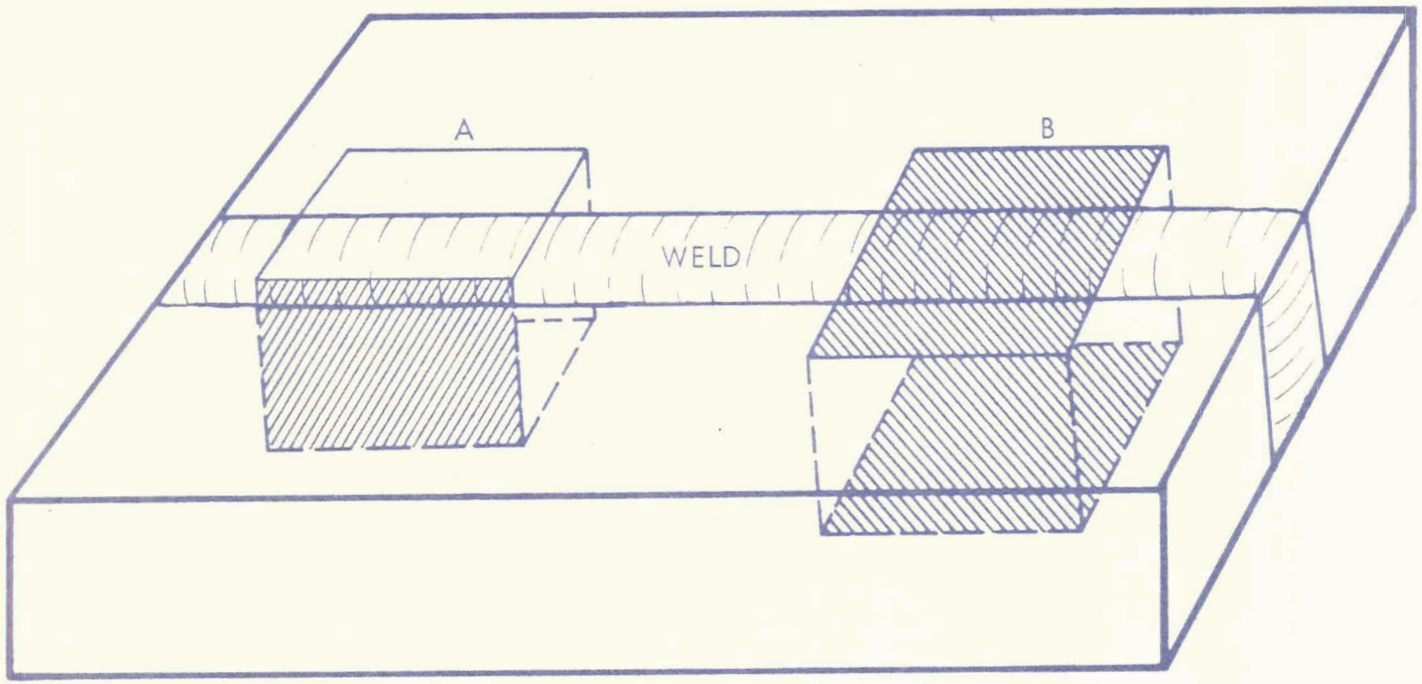

Figure 1. Sketch of Planes Examined Metalligraphically

SPACE DIVISION OF NORTH AMERICAN ROCKWELL CORPORATION

Microprobe Analysis

Microprobe analysis was made along the outer edges of the weld, on a plane across the top side of the weld (shown at B in Figure 1).

RESULTS AND DISCUSSION

Metallographic Examination

Metallographic examination of sections through the lines (shown at A in Figure 1) did not reveal any microstructural differences from the top side to bottom side of the weld that bore any relationship to the pattern of lines in the radiograph.

Upon examination of planes across the lines (shown at B in Figure 1), it was observed that the microstructure described a pattern similar to that of the low-density lines on the top side of the weld but not on the bottom side. A series of photomicrographs to illustrate the microstructural pattern on the top side of the weld is shown in Figure 2. It should be noted that the curved pattern of solidification is more prominent on the right side than on the left. This difference is due to the fact that more material was removed in preparation from the left side than from the right. Thus, the depth of this condition below the top side after removal of the reinforcement and removal of a slight additional amount of material during polishing was not great.

The microprobe traces along the weld revealed higher silicon content at the dendrite cell boundaries and some differences in silicon content from point to point were shown, but the pattern of silicon segregation did not show a pattern similar to that of the low-density lines on the radiograph. Traces for copper also failed to show a pattern of segregation that conformed to the pattern of low-density lines on the radiograph.

Based on the metallographic observations and the microprobe analysis, it was concluded that the low-density lines in the radiographs of the submitted sample were caused by differences in the orientation of large dendrites in the re-fused zone of the weld, and it is reasonable to assume that the low density lines in the radiographs of the I-meridian weld of the S-II-10 were also caused by differences in orientation of large dendrites.

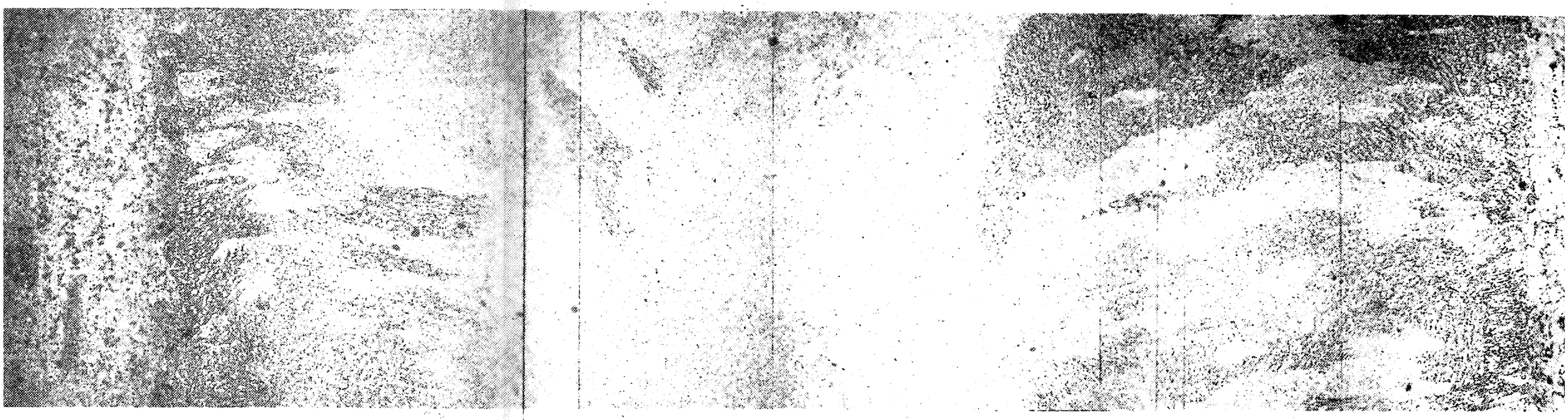

Figure 2. Microstructure Across Top of Weld, Magnifica

FOLD-OUT #1

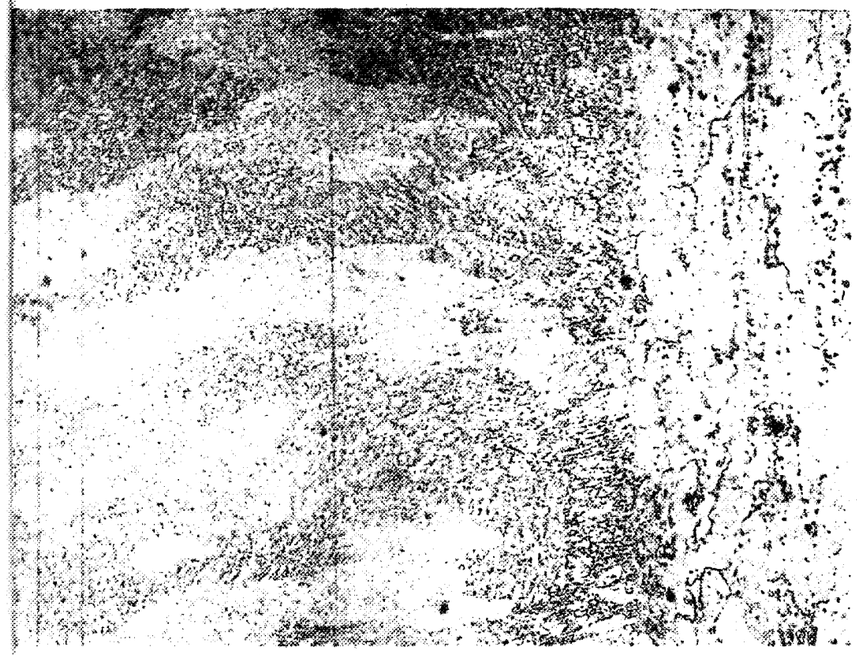

e 2. Microstructure Across Top of Weld, Magnification 50X

FOLD-OUT #2

MINISTAGE FORWARD LH_2 BULKHEAD WELD EVALUATION

INTRODUCTION

Examination of the welds on the ministage forward LH_2 bulkhead showed excessive copper concentrations as evidenced by heavy white lines in X-rays. Ten sections were removed from this bulkhead and investigated.

This investigation was conducted to evaluate the strength properties of weld tensile specimens having excessive copper concentration in the weld.

PROCEDURE

The sections of the ministage bulkhead were machined into weld tensile specimens and tested with a Model PS-60 Riehle Universal test machine. Specimens 2, 4, and 7 were tested to failure at room temperature. Specimens 3, 5, 6, 8, 9, and 10 were tested to failure at -300 F.

Prior to destructive testing of specimens 8, 9, and 10, they were life-cycle loaded in accordance with the schedule listed in Table 6.

Table 6. Schedule Life Cycle Loading for Ministage Weld Tensile Specimens

Number of Cycles	Temperature (F)	Load Level (psi)
6	75	25,000
200	75	7,000
50	-320	16,000
4	75	29,000
125	75	8,500
35	-320	8,500

RESULTS

The results of the metal weld tensile tests at room temperature and at -300 F are listed in Table 7.

DISCUSSION

A review of the weld tensile data reveals that the 10 weld passes used to make these welds caused a degradation of the material, because 2014-T651 is time-temperature sensitive. This sensitivity is reflected in the relatively low and scattered tensile properties. The radiographs of some of the test specimens indicated a high eutectic concentration. Because the weld history of all the specimens is essentially the same, it can be assumed that the same eutectic condition exists in all the specimens and is only visible in some specimens because of favorable orientation. The existence of the eutectic (whose formation is time-temperature dependent) supports the assumption that the material was subjected to excessive heat input.

Table 7. Results of Weld Tensile Strength Tests of 2014 Aluminum Weld Tensile Specimens From Ministage Bulkhead

Specimen Number	Test Temperature (F)	Ultimate Stress (psi)	Elongation (3/4-inch) (percent)
1	Not tested		
2	75	32,200	5.3
3	-300	44,700	4.0
4	75	36,300	5.3
5	-300	31,400	4.0
6	-300	36,300	4.0
7	75	30,800	4.0
*8	-300	34,900	2.7
*9	-300	45,300	4.0
*10	-300	35,900	2.7

*Specimens life cycled per Table 6 before destructive testing.

STRESS RELIEF AREAS OF CIRCUMFERENTIAL WELDS

PROGRESS SUMMARY

The circumferential tank welds on the S-II-1 through S-II-7 stages are stress-relieved by using a machined radius relief in the weld land. This machined relief was to assist in unloading highly stressed areas near the crossover welds by yielding. If yielding does occur during tank pressurization, it sometimes causes undesirable dimpling.

To determine the effectiveness of the stress relief, a program was conducted to test simulated tank weld specimens to failure. The test specimens were instrumented with strain gauges to determine the exact stress distribution in the weld land relief and adjacent material. An additional study was conducted by using a machined straight ramp in the weld land.

SIMULATED WELD RELIEF SPECIMEN TESTS, PHASE I

INTRODUCTION

The ultimate tensile strength and the stress distribution under load of a specimen that simulates the S-II-7 stage weld land relief and adjacent material were investigated. Stress distribution was determined with strain gauge instrumentation. Of interest in this program also was the determination if the localized dimpling, which occurred behind the S-II-7 stage weld land relief during pneumostatic testing, could be duplicated on a test specimen.

PROCEDURE

Two test specimens were fabricated, and strain gauges were positioned on the specimens as shown in Figures 3 and 4.

Each specimen was tension-loaded in a 200,000-pound-capacity Riehle testing machine. All strain gauges were electrically connected to a consolidated systems multichannel recorder, which made a permanent record both on tape and on chart paper of strain measurements at each load increment. Figures 3 and 4 are closeup photographs of each side of the specimen. Load was applied to the specimen in 14,000-pound increments, and strain measurements were taken at each increment. Also, after strain measurements were recorded at each load increment, the load was reduced to 14,000 pounds, and strain measurements again were recorded. For the first test, the specimen was incrementally loaded to 126,000 pounds, and then the test was terminated. The second test specimen was incrementally loaded to failure. During testing, local deformation on the backside of the weld relief radius was checked with a dial indicator.

RESULTS

Specimen Deformation

Figure 5, taken at 112,000 pounds load, visually displays the deformed area behind the weld relief radius by the appearance of light under the straight edge. This was the load at which the dimpling first became visually apparent.

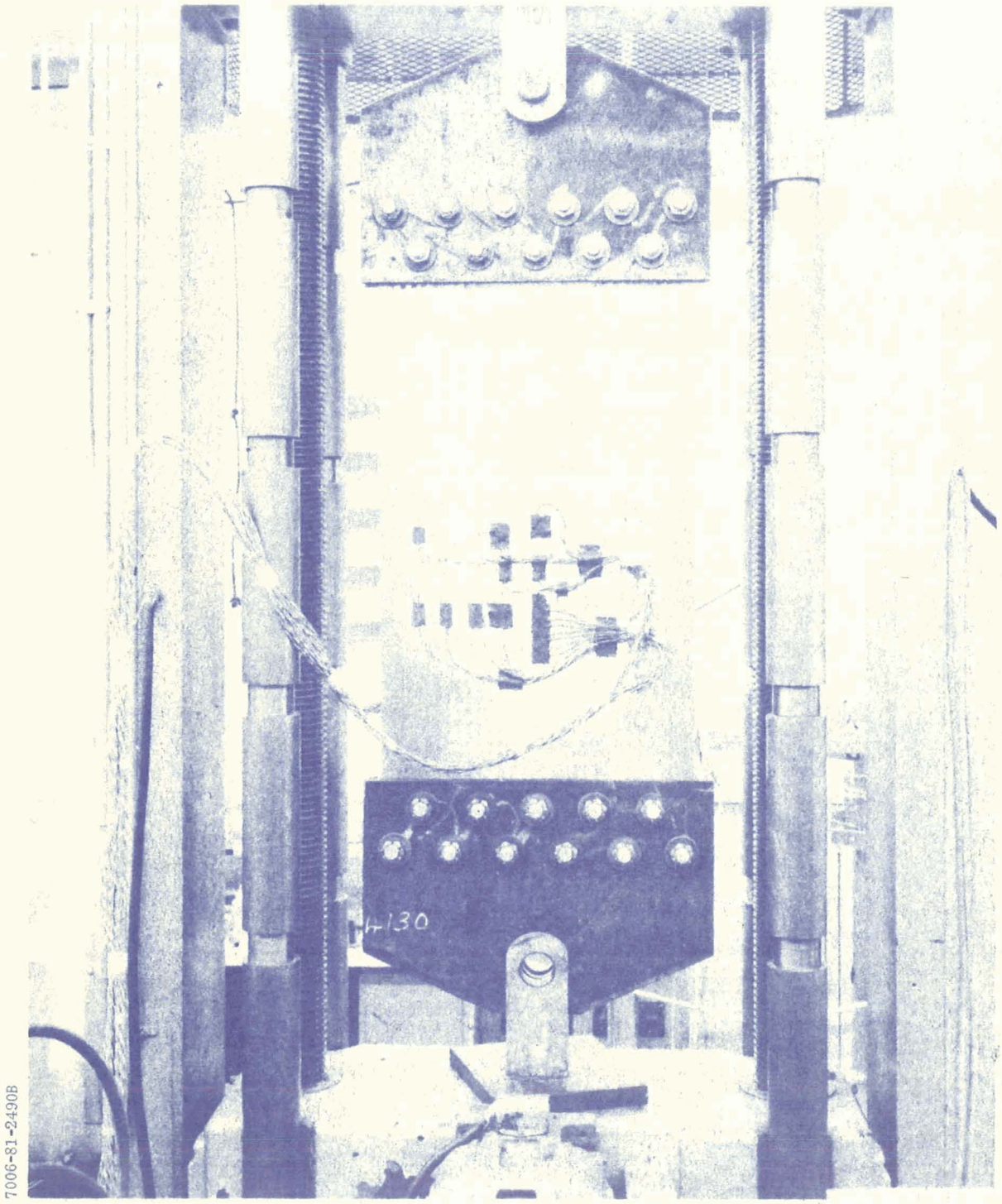

Figure 3. Specimen Ready for Testing (Outboard Side View)

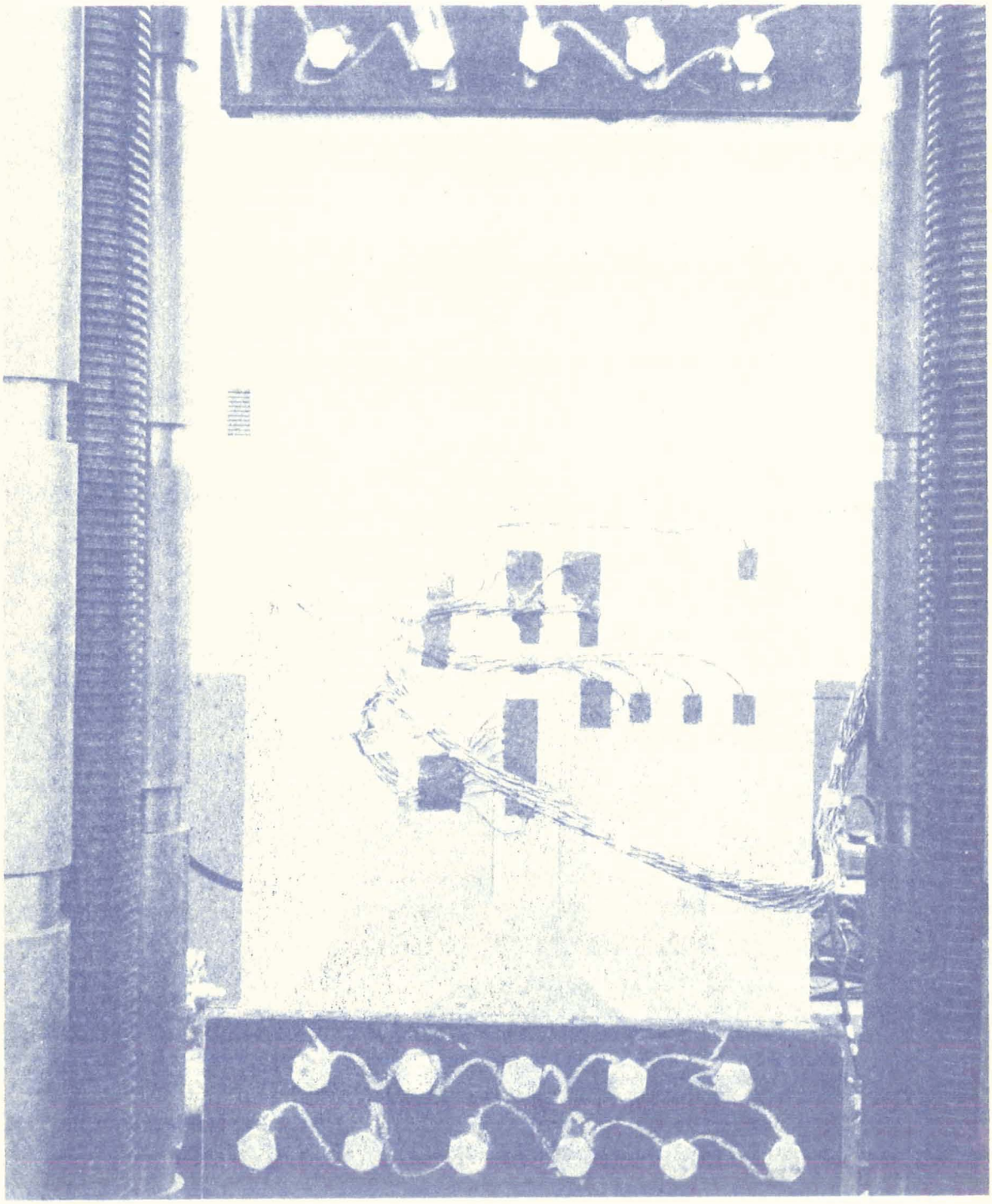

7006-81-2400C

Figure 4. Specimen Ready for Testing (Inboard Side View)

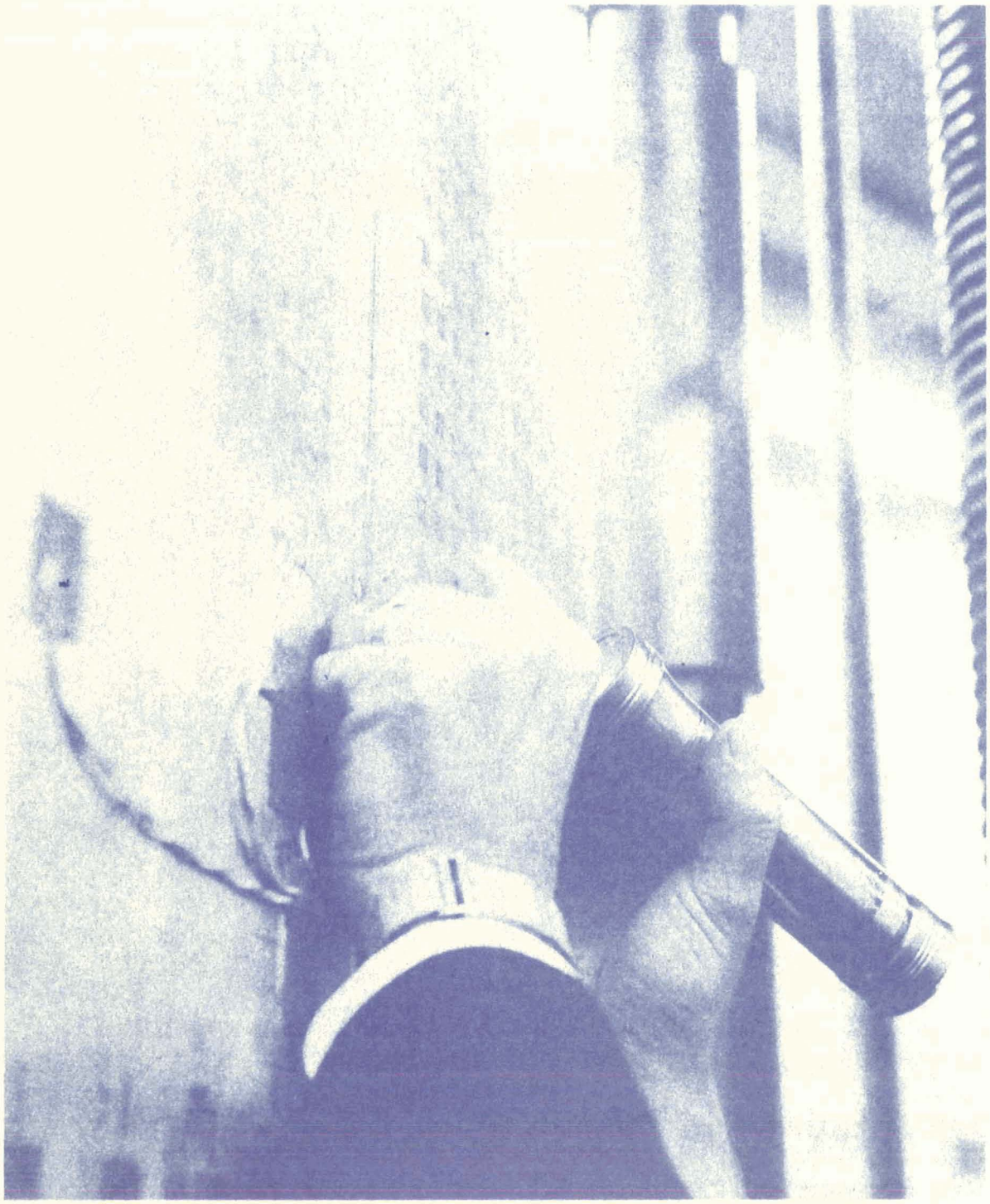

7006-81-2490D

NOTE: PHOTO TAKEN AT 112,000 POUNDS LOAD

Figure 5. Specimen Deformation Behind Weld Land Relief

Strain Gauge Data

A summary graph of a portion of the strain gauge data is shown in Figure 6. These curves, which represent stress parallel to the longitudinal axis, were plotted by averaging the readings from the two gauges that were back-to-back at specified locations.

Specimen Failure

The specimen failed during the second test at 196,500 pounds. Failure occurred at the bottom of the radius in the weld land relief. Figure 7 shows the failed edge of the specimen.

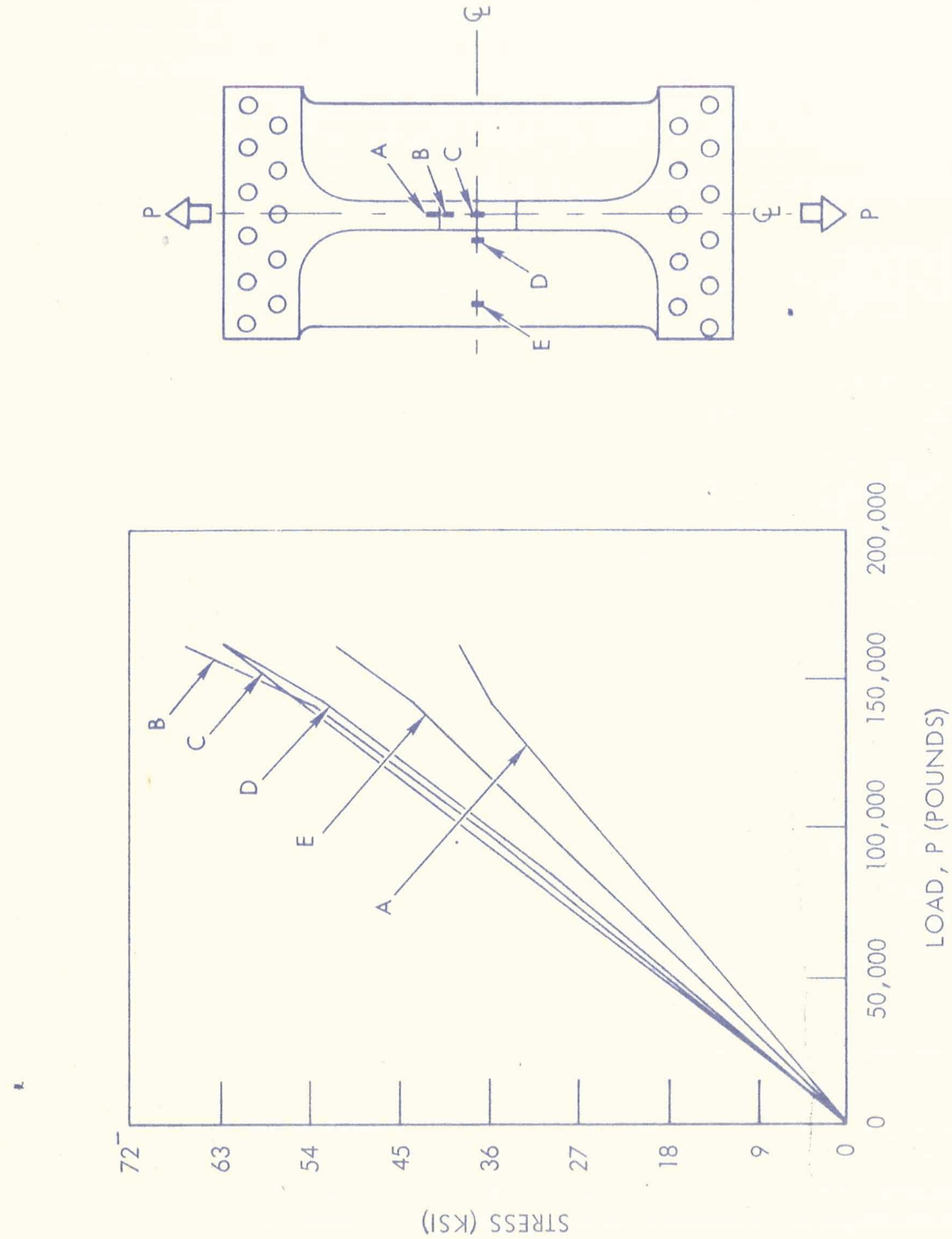

Figure 6. Applied Load Versus Average Tensile Stress at Selected Strain Gauge Locations

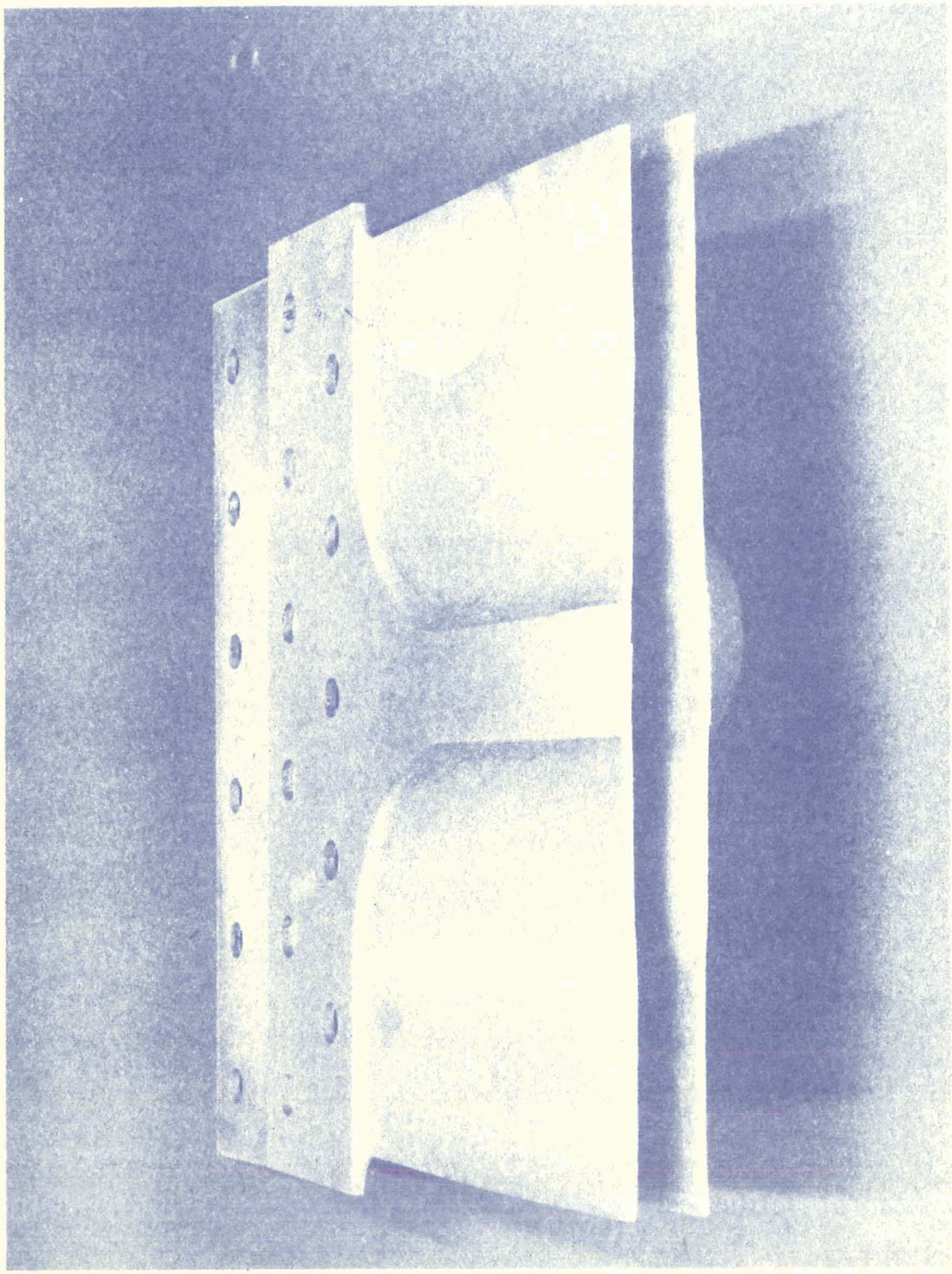

7006-81-2497A

Figure 7. Edge View of Failed Specimen

SIMULATED WELD RELIEF SPECIMENS TESTS, PHASE II

INTRODUCTION

Based on the results of Phase I, the test program for evaluating specimens simulating the S-II-7 stage weld land relief and adjacent material was continued. Six welded test specimens, 2 feet by 4 feet, were tension-loaded to failure. Stress distribution under load was measured with strain gauges on two specimens, and the effects of purposefully introduced weld material cavity flaws were determined with two other specimens.

PROCEDURE

Specimen Fabrication

Specimen halves were machined from 2016-T6 aluminum sheet and then welded together by the Seal Beach Facility Production Welding Group. The panels were next drilled at both ends for installation of testing load plates and the weld land were machined for stress relief.

Strain Gauge Installation

Two of the six test panels were strain gauge-instrumented to determine stress distribution under load. Test panel 3 was instrumented with biaxial gauges for tensile and shear data; test panel 6 was instrumented with axial gauges for longitudinal tensile data only.

Testing

Each specimen was tension-loaded in a 200,000-pound-capacity Riehle Universal testing machine (Figures 8 and 9). All strain gauges were electrically connected to a consolidated Systems multichannel recorder, which made a permanent record of all strain versus load measurements.

Specimen Flawing

Small flaws were drilled into two of the specimens with a dentist's drill. The flaws were located in the weld metal at each end of the weld land relief. Figure 10 is a photograph of a flawed specimen showing the exact location of each flaw.

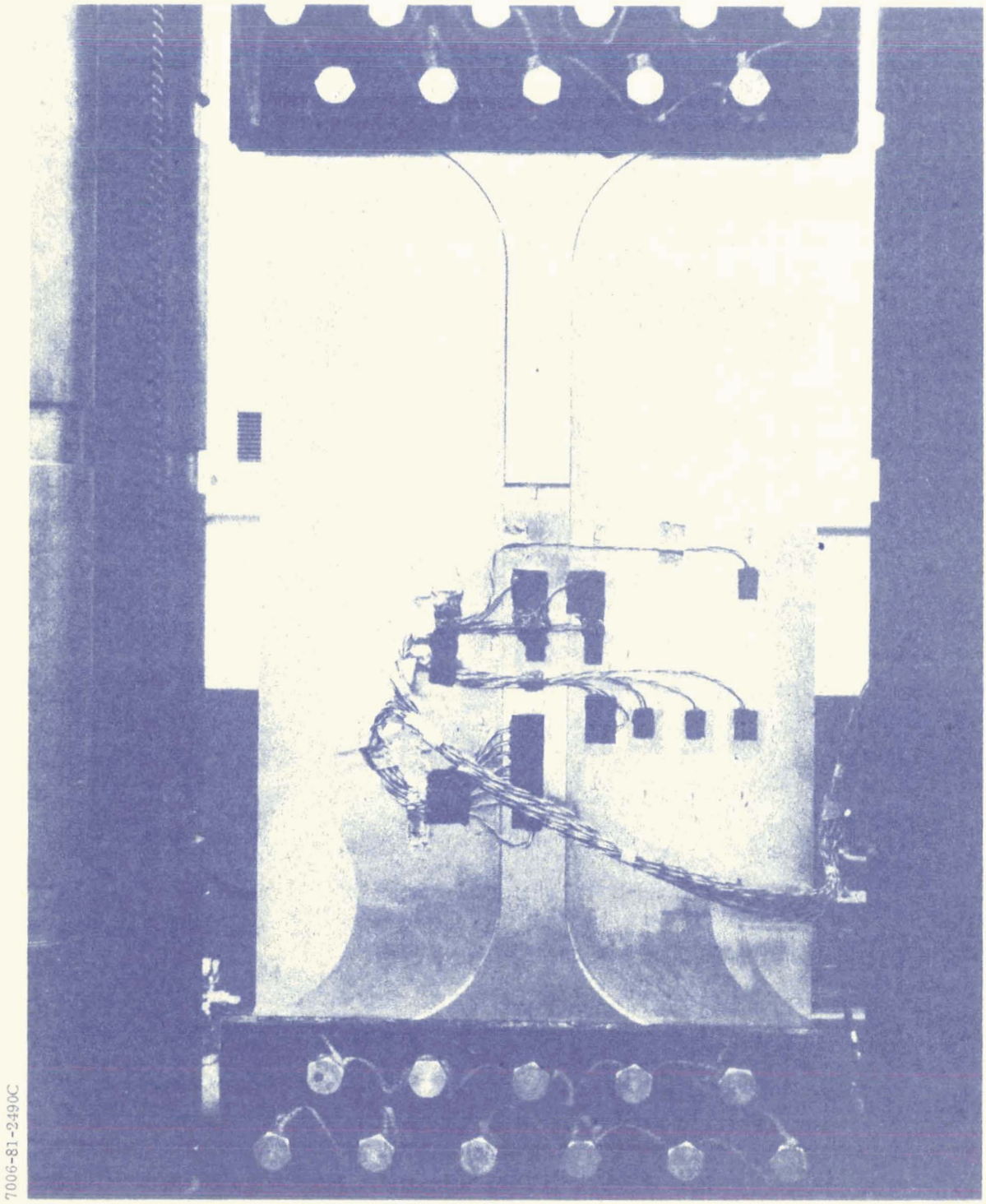

7006-81-2490C

Figure 8. Specimen Ready for Testing - Weld Land Side

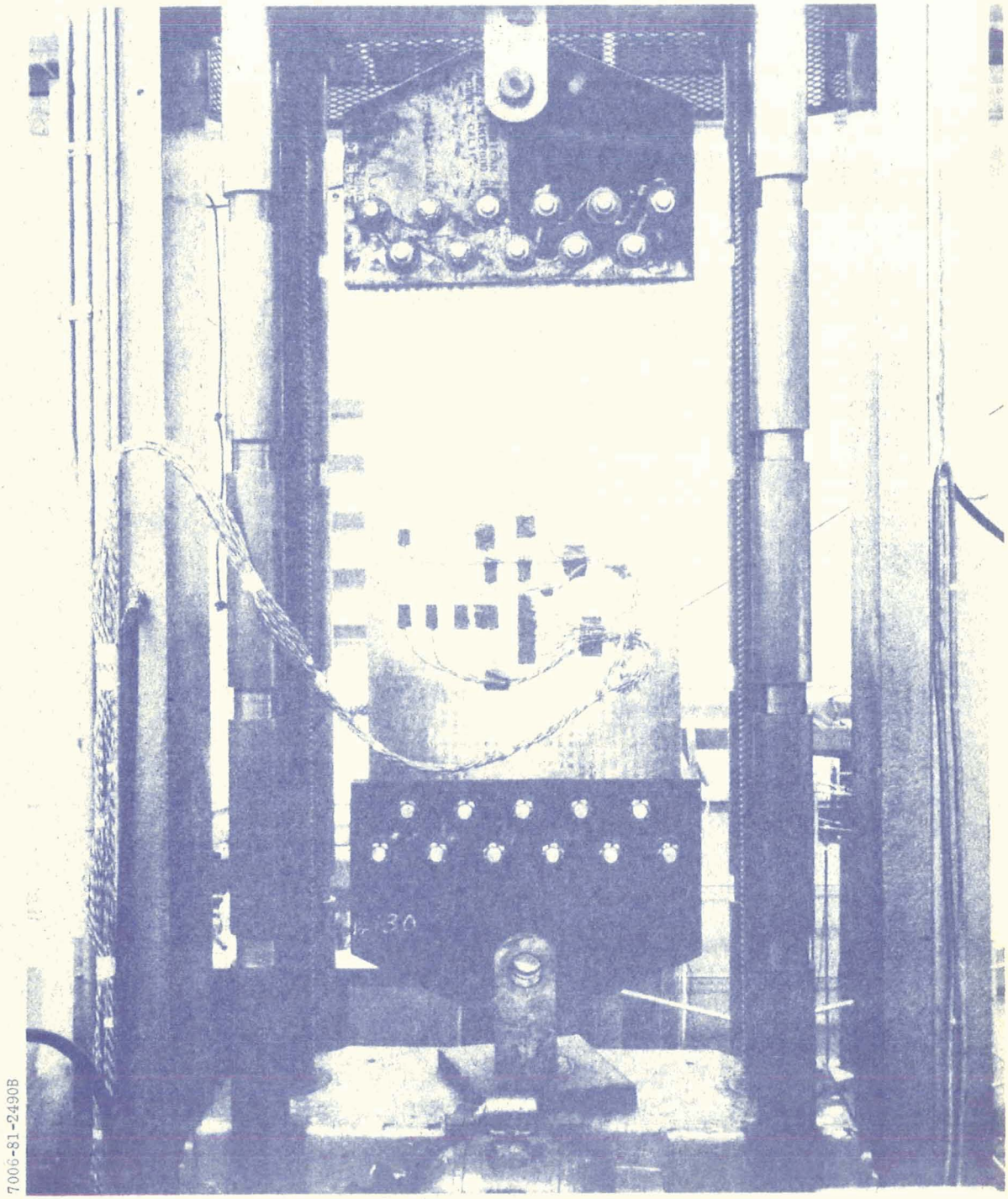

Figure 9. Specimen Ready for Testing - Back Side

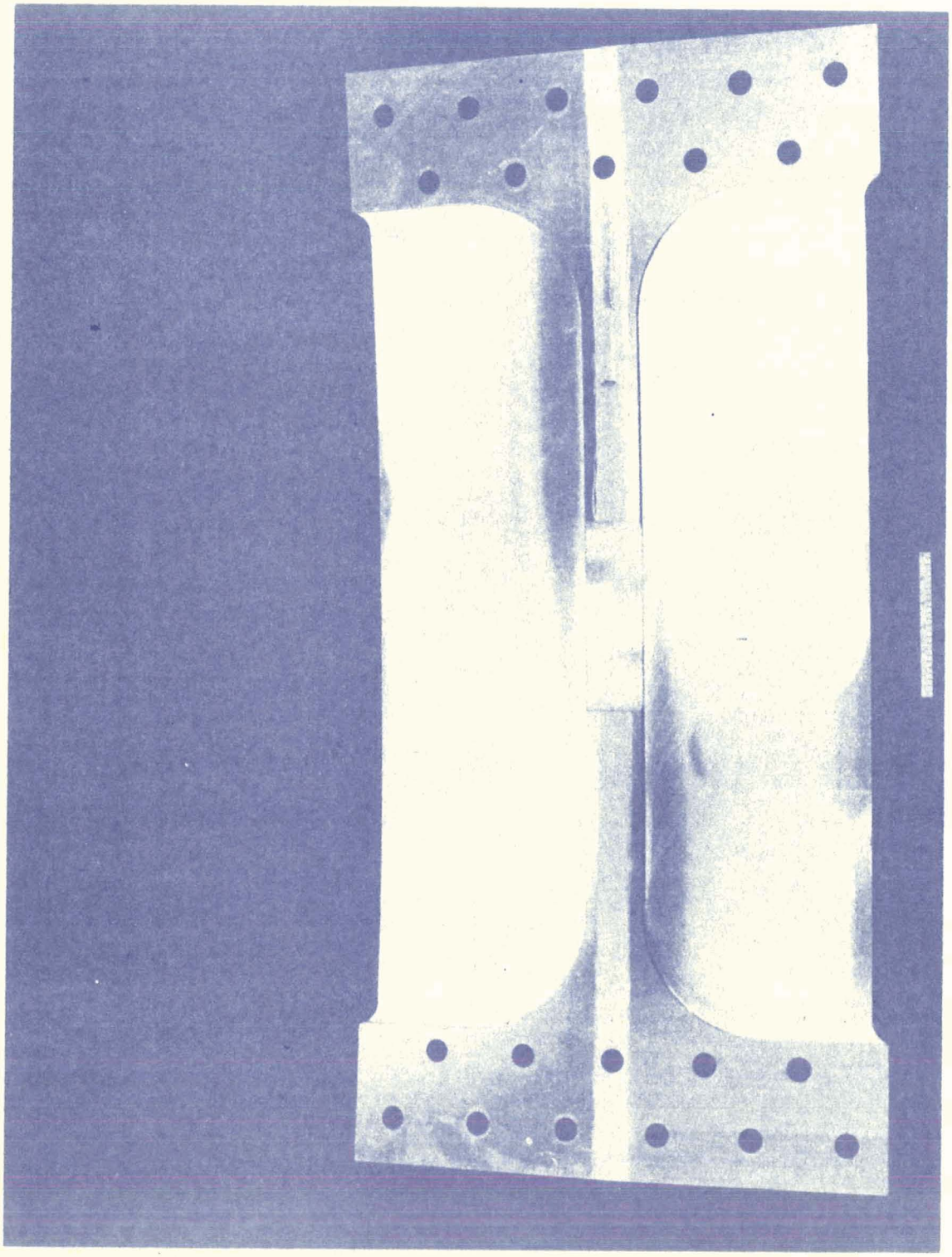

Figure 10. Specimen 4 Showing Flaw Locations

RESULTS

Strain Gauge Data

Figures 11 and 12 show the strain gauge data in graphic form. These curves were plotted by averaging data from gauges located back-to-back.

Test Results

Test results are summarized in Table 8; a test history of each specimen is detailed in the following paragraphs.

Specimen 1 was tested without having a relief machine into the weld land. The specimen was loaded to 200,000 pounds (which is the capacity of the Riehle University testing machine) then unloaded and removed from the machine. The specimen did not have any creases across the weld area, which occur when the specimen has a weld land relief. The specimen was then shipped to the Los Angeles Division, placed in a 440,000-pound-capacity Tineus Olsen test machine, and was loaded to failure, which occurred at 240,500 pounds. Failure occurred approximately 16 inches from the end.

Specimen 2 was relieved in the weld land. The specimen was loaded to 200,000 pounds, unloaded, shipped to the Los Angeles Facility, and loaded to failure, which occurred at 207,750 pounds. The specimen failed through the end radius in the relief. During the initial loading, creases behind the weld land relief became visible under a straight edge at 90,000 pounds and were first noticeable without a straight edge at 130,000 pounds. Figure 13 is a photograph of a specimen that had been loaded to 200,000 pounds; two creases behind each weld land relief radius are readily noted in the photo.

Specimen 3 was relieved in the weld land and the specimen was strain-gauged. The specimen was loaded to 200,000 pounds in 10,000-pound increments starting at 80,000 pounds, unloaded, shipped to the Los Angeles Facility, and loaded to failure, which occurred at 205,750 pounds. The specimen failed through the end radius in the relief. Again, the two creases behind each weld land relief radius could be readily seen.

Specimen 4 was relieved in the weld land, and flaws were drilled into the weld metal adjacent to each radius in the relief. Flaw size was 1/8 inch long by 1/32 inch wide by 3/64 inch deep. Flaw locations are shown in Figure 10. At 80,000 pounds load, a crack was visible in the bottom of one flaw, and a crease was visible behind the flaw. The crease was 0.010 inch deep and elongation over the flaw was 0.005-inch with a one inch gauge length.

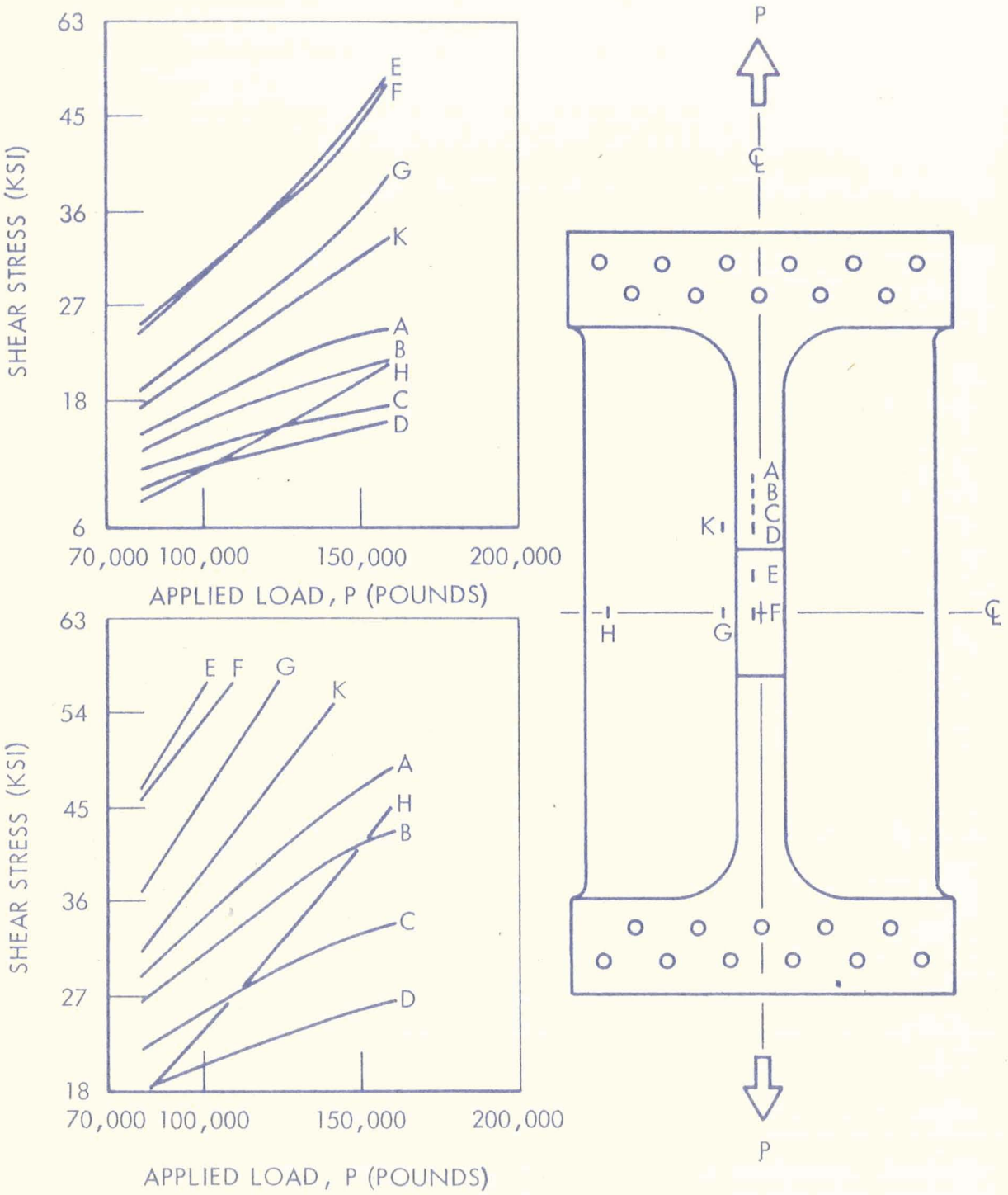

Figure 11. Load Versus Average Tension and Shear Specimen 3 Strain Gauge Data

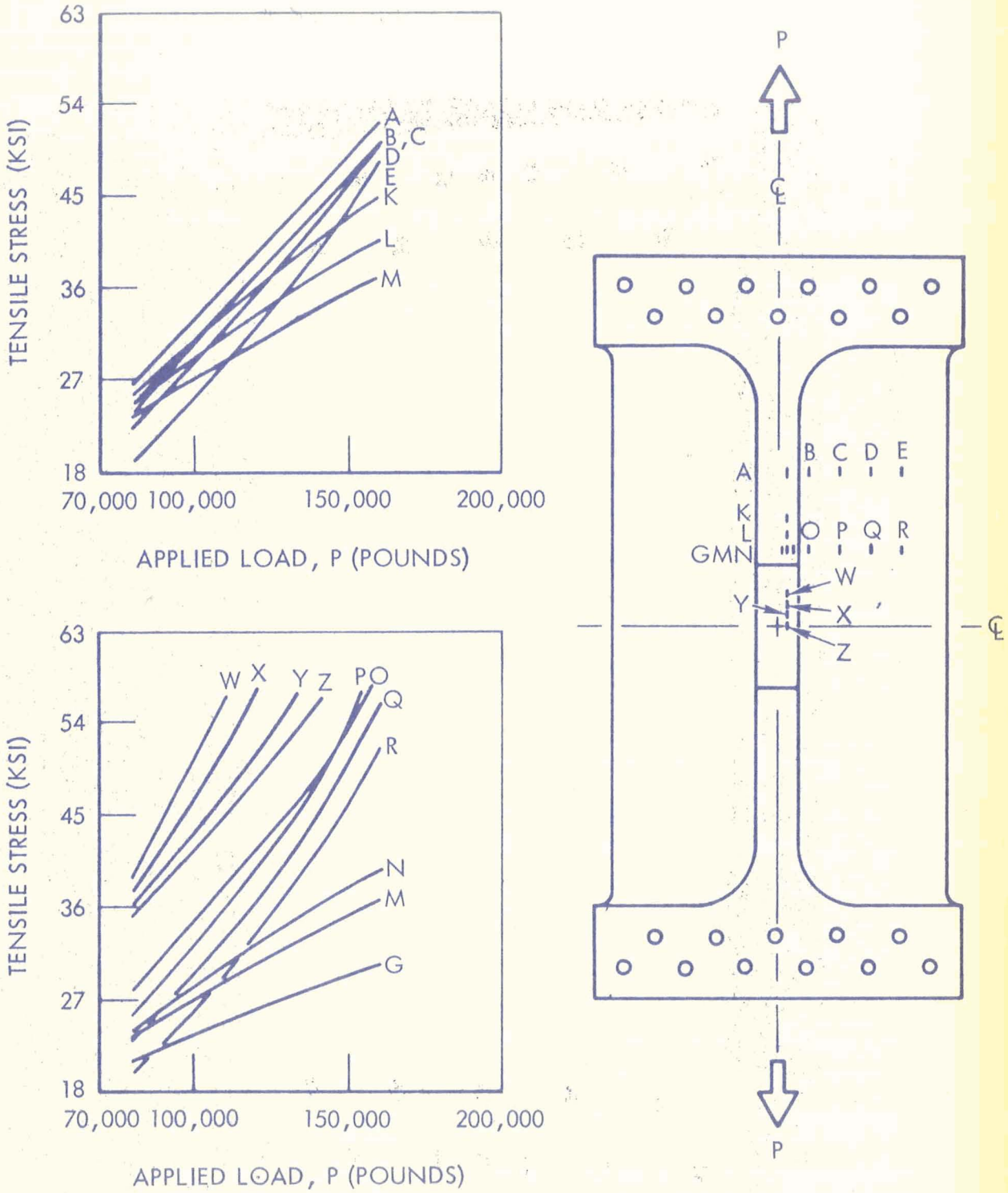

Figure 12. Load Versus Average Tension Stress
Specimen 6 Strain Gauge Data

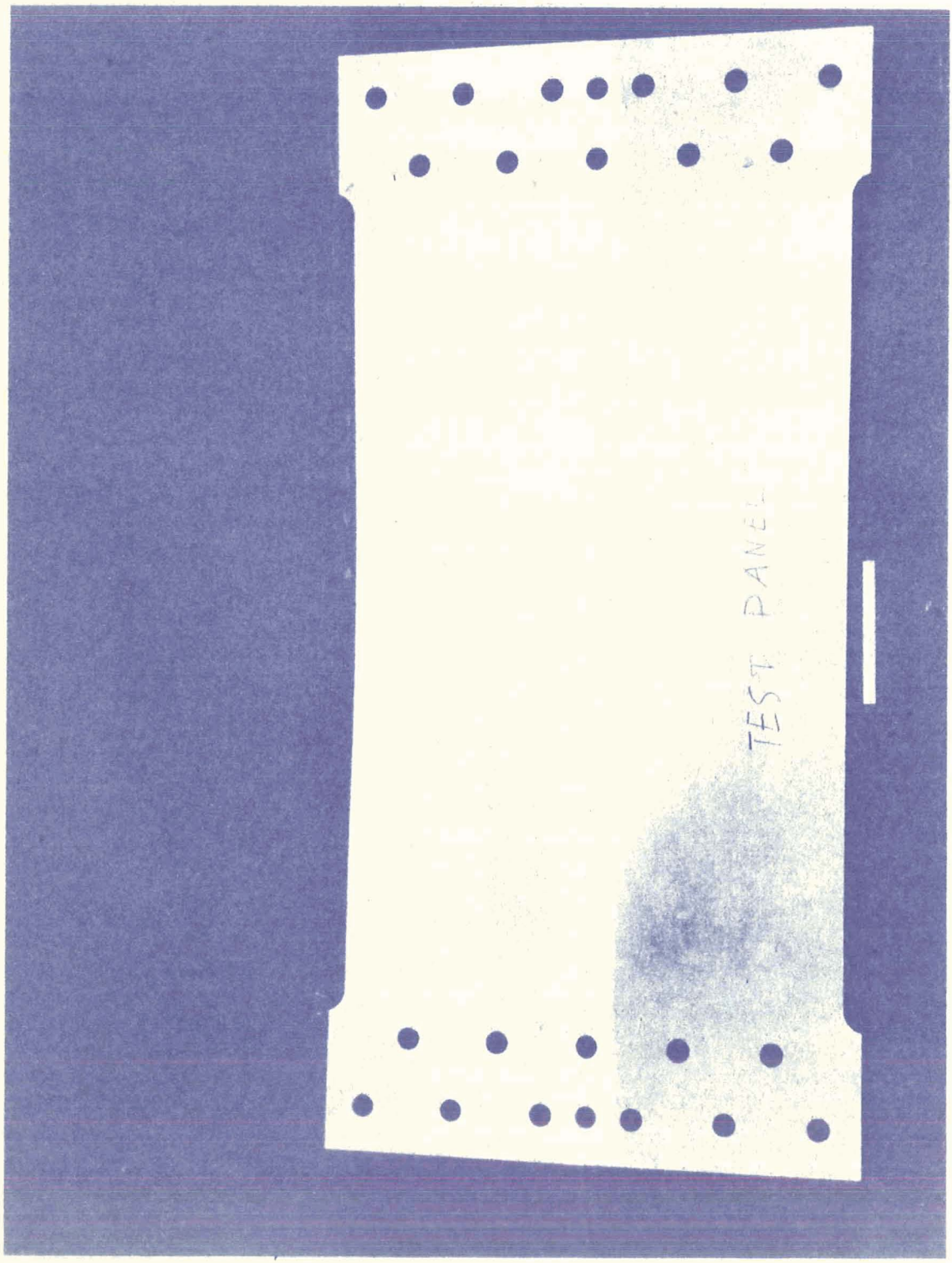

(NOTE CREASES BEHIND WELD LAND RELIEF.)

Figure 13. Specimen 2 After Loading to 200,000 Pounds

The specimen was next loaded to 106,000 pounds and unloaded. A crack was now visible in the bottom of the second cavity. The crease depth was 0.013 inch, and the elongation measurement remained unchanged. The specimen was next loaded to 121,000 pounds and unloaded. The crease depth increased to 0.015-inch, and the elongation increased to 0.008 inch. The specimen was then loaded to 136,000 pounds and unloaded. A crack was now visible on the back side of the specimen behind the flaw. The specimen was then loaded to failure, which occurred at 145,250 pounds. Figure 14 is a photograph of the failed specimen showing that failure occurred through a flaw. Figure 15 is a closeup of the failure edge, giving an indication of the flaw configuration.

Specimen 5 was relieved in the weld land, except that the relief end was cut into a straight ramp configuration instead of the usual radius configuration. The ramp was 1.50-inches long, and the overall relief length was 10.50 inches. Flaws were drilled into the weld metal adjacent to each ramp. Flaw size was 1/8 inch long by 1/32-inch wide by 1/6 inch deep. The specimen was loaded to 83,000 pounds and unloaded. A crack was visible in the bottom of both flaws and creases were visible on the back side that were 0.010 inch deep. A load of 108,500 pounds was next applied and removed, and the crease depth increased to 0.025-inch. A load of 124,000 pounds was next applied then removed; and the crack in one flaw now extended out of the flaw into the parent material for 7/16 inch, and a crack was visible in the back side. The specimen was then loaded to failure, which occurred at 152,000 pounds. Figure 16 is a photograph of the failed specimen, showing that failure occurred through one of the flaws.

Specimen 6 was radius relieved and strain-gauged. Load was applied in 10,000 pound increments, starting at 80,000 pounds and up to failure, which occurred at 192,000 pounds. Failure occurred through one radius in the weld land relief. Strain gauge data are summarized in Figure 12. Table 8 summarizes the tension test results.

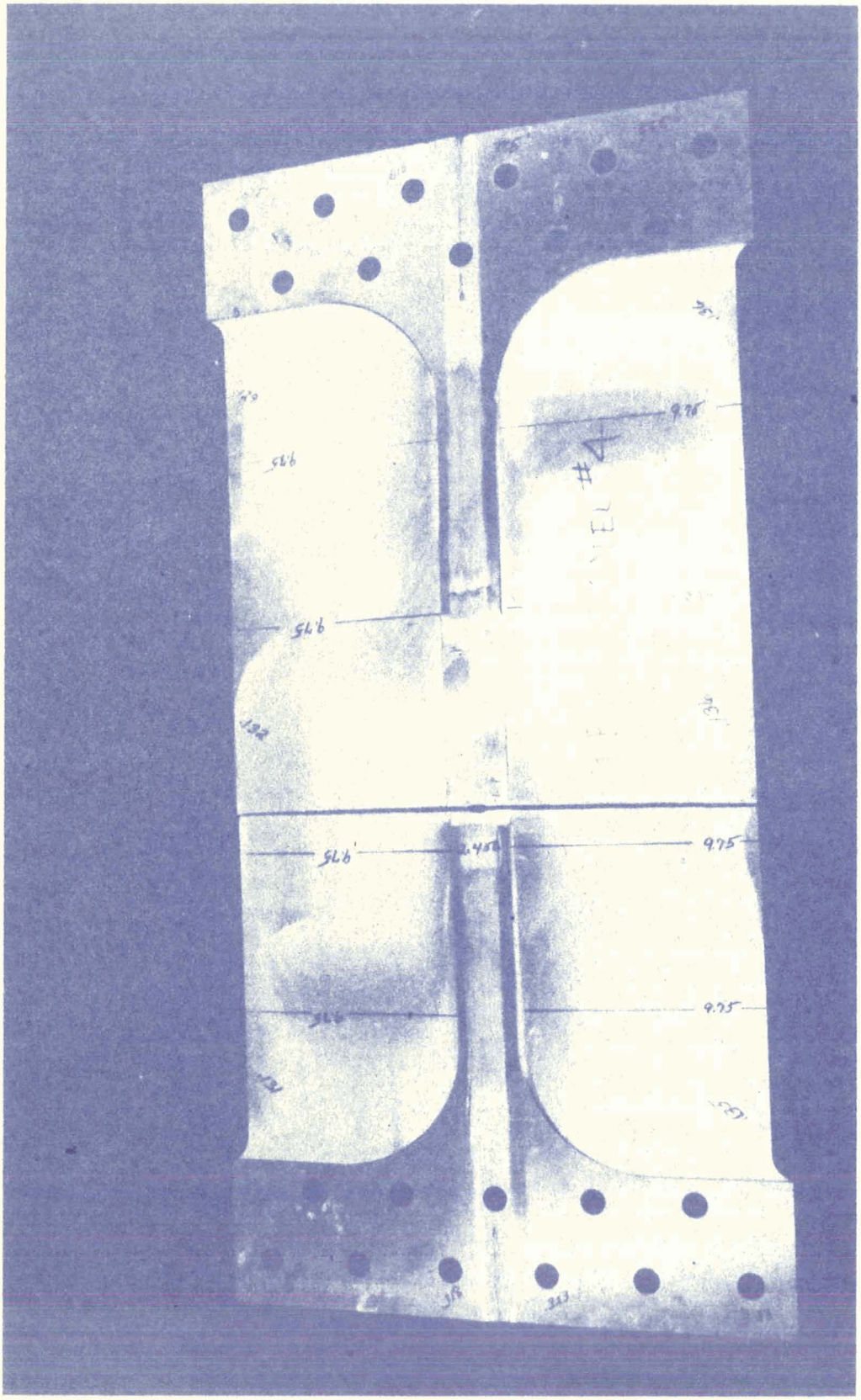

7006-81-2405F

NOTE: FAILURE OCCURRED THROUGH ONE OF THE FLAWS

Figure 14. Specimen 4 After Failure at 145,250 Pounds

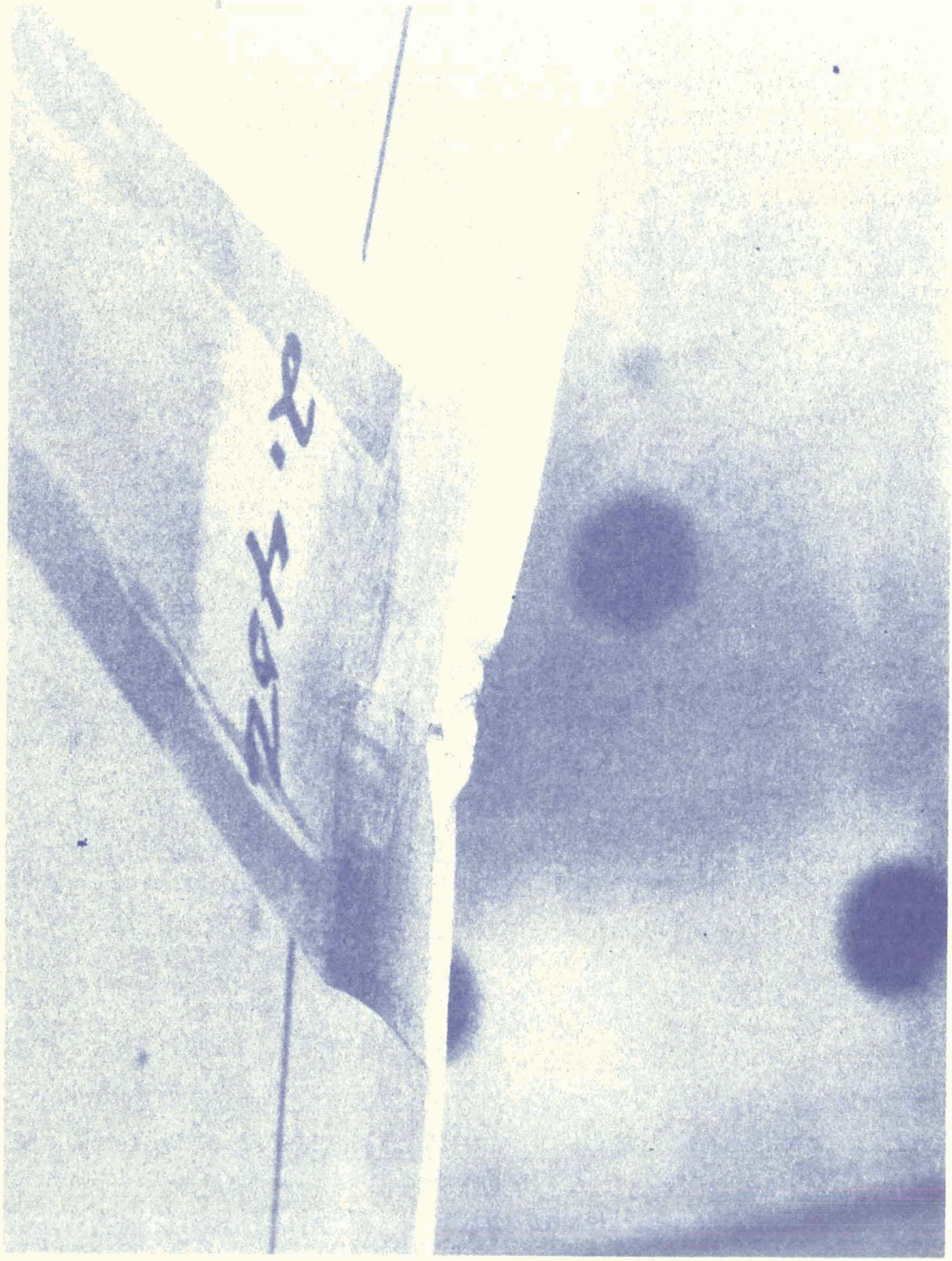

7006-81-2504

NOTE: FLAW CONFIGURATION. FLAW DIMENSIONS WERE
1/8 X 1/32 X 3/64 INCH

Figure 15. Closeup of Specimen 4 Failure Edge

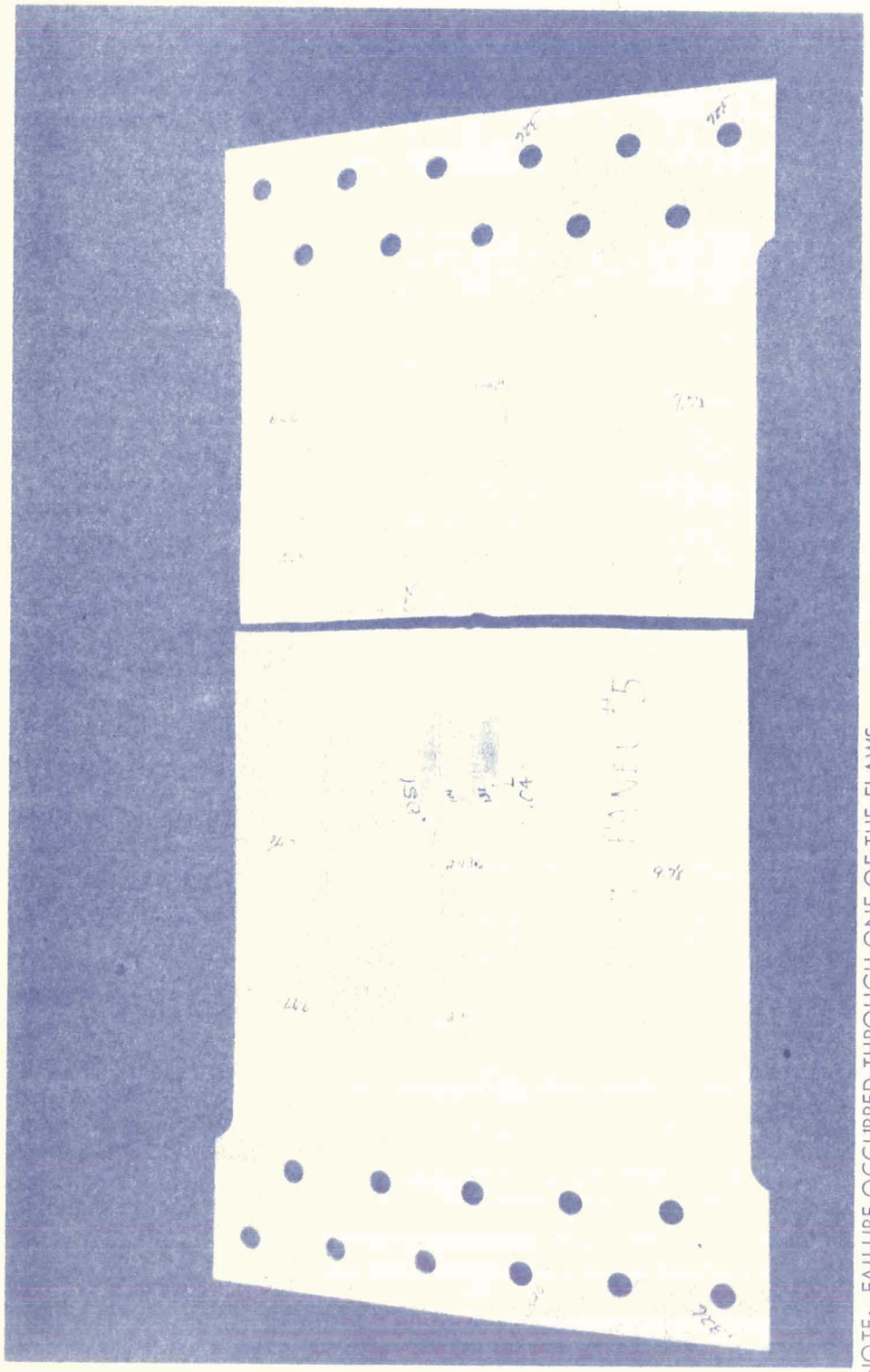

NOTE: FAILURE OCCURRED THROUGH ONE OF THE FLAWS

7006-81-25041

Figure 16. Specimen 5 After Failure at 152,000 Pounds

Table 8. Tension Test Results Summary

Specimen Dimensions (Weld Land With Adjacent Skin Material Tension-Tested at Room Temperature)

Specimen Number	Type of Relief	Skin Width (T_1+T_2) (inches)	Skin Thickness (inches)	Land Width (T_3) (inches)	Land Thickness (inches)	X-Sectional Area* (inches^2)	Failing Load (pounds)	Average Failing Stress (ksi)	Comments
1	None	19.45	0.137	2.52	0.321	3.474	230,500	66.4	
2	Radius	19.43	0.139	2.47	0.180	3.147	207,750	66.0	
3	Radius	19.07	0.137	2.51	0.166	3.030	205,750	67.9	Specimen strain-gauged.
4	Radius	19.50	0.134	2.45	0.173	3.037	145,250	47.8	Two flaws drilled into specimen 1/8 x 1/32 x 3/64 inch deep. (See Figure 43 for location.) Failure occurred through flaw.
5	Ramp	19.55	0.136	2.44	0.181	3.101	152,000	49.0	Two flaws drilled into specimen 1/8 x 1/32 x 1/16 inch deep. Failure occurred through flaw.
6	Radius	19.47	0.138	2.48	0.177	3.126	192,000	61.4	Specimen strain-gauged.

*Through weld land relief

STRESS RELIEF AREA EVALUATION

INTRODUCTION

Tension tests were conducted on specimens that simulate the S-II-7 vehicle LH_2 tank horizontal weld land with a machined relief. Specimens were tested with both a radius relief in the weld land, which is common to S-II-7, and with a modified straight ramp relief in the weld land, which is a proposed correction for the dimples and cracks found on S-II-7 opposite the weld land reliefs after stage pneumostatic pressurization.

The purpose of this program was to determine the ultimate failing load (at room temperature and at -423 F) of specimens that simulate the S-II-7 vehicle LH_2 horizontal weld land configuration, with both radius and modified straight ramp relief of the weld land, after the specimens had been proof-loaded to 49 ksi and cyclic-loaded for 70 cycles to 30 ksi.

PROCEDURES

Twenty test specimens were fabricated from 2016-T6 aluminum, welded, and radiographically inspected in accordance with MA0107-016, and machined to the standard radius relief configuration as shown in Figure 17. All specimens were then proof-loaded in tension to 49 ksi, radiographically inspected, and 10 of the specimens reworked to the modified straight ramp relief as shown in Figure 17. Five radius-relieved and five ramp-relieved specimens were then loaded in tension at room temperature from zero to 30 ksi and back to zero for 70 cycles and then loaded to failure. The remaining five ramp-relieved and five radius-relieved specimens were loaded in tension from zero to 30 ksi and back to zero for 35 cycles at room temperature, for 35 cycles at -423 F, and then fail tested at -423 F.

RESULTS

Table 9 summarizes the test results for all specimens.

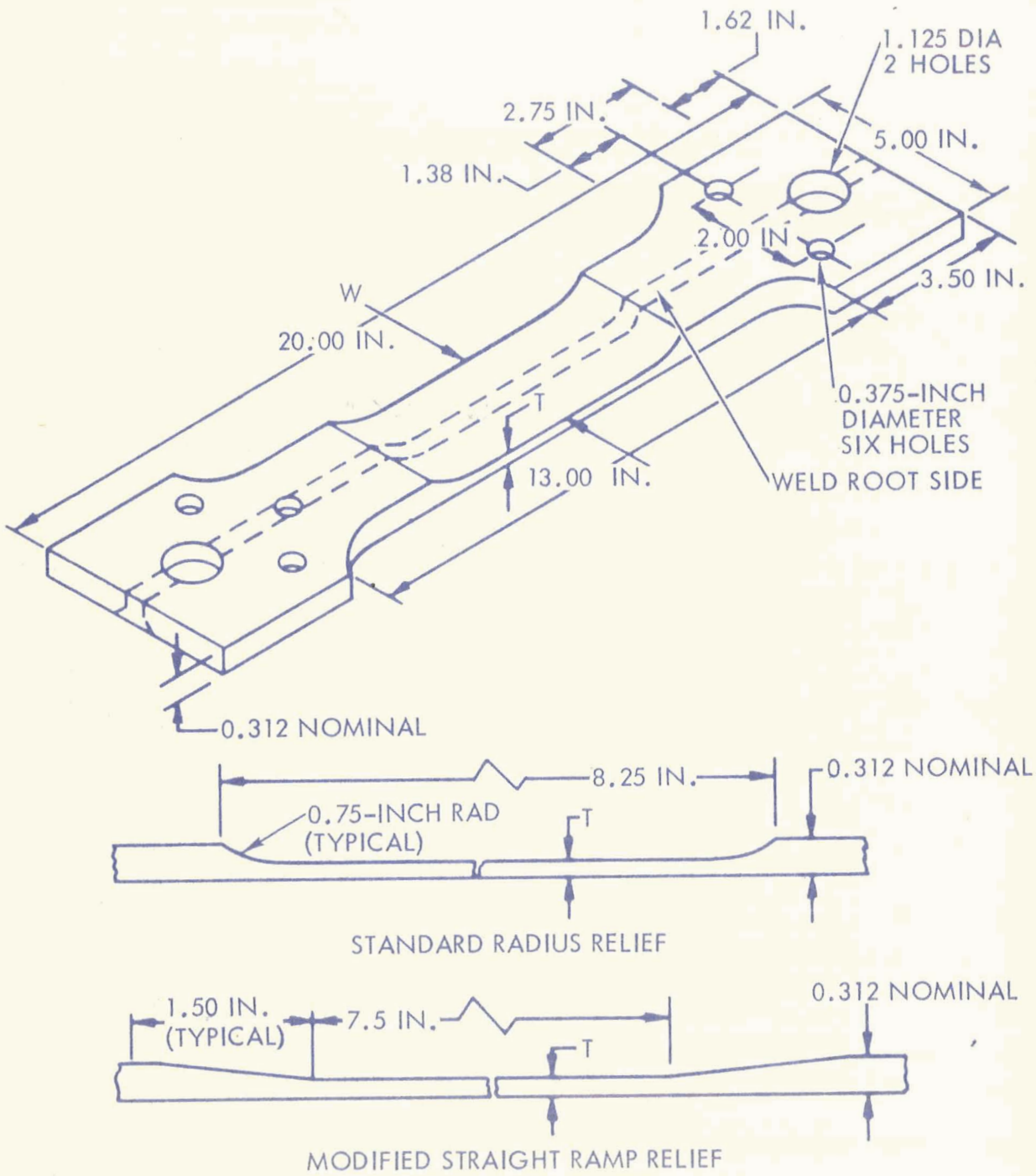

Figure 17. Test Specimen Configuration

Table 9. Test Results Summary

(Weld Land Relief Specimens Proof-Loaded to 49 ksi, Cyclic Loaded to 30 ksi, and Then Fail Tested)

Type of Relief	Number of Cycles at Room Temperature (for 30 ksi)	Failing Stress (ksi) Room Temperature	Number of Cycles at -423 F	Failing Stress (ksi) -423 F	Weld X-Ray Results (Read per MA0107-016G)
Radius	70	61.3			Acceptable
Radius	70	60.4			Acceptable
Radius	70	60.6			Acceptable
Radius	70	61.7			Acceptable
Radius	70	60.8			Rejected*
Radius	35		35	78.3	Acceptable
Radius	35		35	77.7	Acceptable
Radius	35		35	76.4	Acceptable
Radius	35		35	76.2	Acceptable
Radius	36		35	77.7	Acceptable
Ramp	70	61.0			Acceptable
Ramp	70	60.5			Acceptable
Ramp	70	60.5			Acceptable
Ramp	70	61.6			Acceptable
Ramp	70	62.6			Acceptable
Ramp	35		35	80.9	Acceptable
Ramp	35		35	77.8	Acceptable
Ramp	35		35	78.0	Acceptable
Ramp	35		35	75.2	Acceptable
Ramp	35		35	72.7	Rejected*

*Oxide inclusion (0.060 inch), Failed through inclusion.

FRACTURE TOUGHNESS OF WELDMENTS

PROGRESS SUMMARY

The fracture mechanics method of analysis is the best engineering method used to determine the effects of sharp discontinuities on a structure. A fracture mechanics was conducted to determine the fracture toughness of typical S-II weldments. Both Laboratory and Test and Manufacturing departments prepared weldments. Numerous tests were conducted at room temperature and at -423 F.

FRACTURE TOUGHNESS OF 2014-T651 WELDMENTS, PHASES I AND II

INTRODUCTION

Fracture mechanics is a stress analysis approach to the problem of rapid fracture caused by sharp defects. Basically, it states that a defect will propagate rapidly if the stored elastic energy in the system exceeds the energy required to form additional crack surface. Fracture mechanics of analysis and testing are among the best available methods for engineering analysis of the effects of sharp discontinuities in a structure.

This program was established as a preliminary effort to obtain data for better evaluation of S-II weldments in the presence of sharp cracks or defects.

PROGRAM SUMMARY

Weldments

Two thicknesses, 5/8-and 5/16-inch, of 2014-T651 aluminum alloy plate were welded, using 4043 filler wire with two passes from one side.

Standard Specimen Tests of Welds

Uniaxial tensile tests were conducted on specimens from the 5/8-inch-thick weldments.

Tests were conducted at room temperature, -320 F, and -423 F, using 1/8-inch grid length strain gauges on the weld nugget to determine the discrete yield strength of the weld metal. Room temperature tests were also conducted on specimens using a 3/8-inch gauge length extensometer across the weld nugget to determine the variation in weld material properties.

Fracture Toughness Tests - Transverse Welds in Uniform Thickness Specimens

Tests were conducted at room temperature, -300 F, and -423 F on specimens 1/4 inch, 3/8 inch, 1/2 inch, and 5/8 inch thick by 6 inches in width, fabricated from the 5/8-inch-thick weldments. Tests were also conducted at -423 F on specimens 1/4 inch thick and 5/8 inch thick by 4 inches in width fabricated from the 5/8-inch weldments.

Fracture Toughness Tests - Weld Land Specimens

Tests were conducted at room temperature and at -423 F on weld land specimens with a 5/16-inch-thick land fabricated from the 5/16-inch-thick weldments. Some of these specimens were given a 22.8-ksi proof load at room temperature and then tested to failure. Crack size before and after the proof test is given in the data.

Tests at room temperature and at -423 F were conducted on weld land specimens with a 0.280-inch (nominal) thick land fabricated from the 5/16-inch-thick weldments. The starter notch was removed on these specimens after fatigue cracking to allow X-ray examination of the specimens before and after a 22.8-ksi proof test at room temperature.

Metallographic Examination

Specimens were examined for evidence of fatigue damage after fatigue cracking. A specimen with a low apparent K value was examined, and extension of fatigue cracks by a room temperature proof load were examined.

TEST PROCEDURES

Two thicknesses of 2014-T651 plate were welded by using 4043 filler wire for specimen blanks. Material was welded by using two passes from one side in accordance with MA0107-016F. Strips of 5/8-inch-thick plate, 12 inches wide by 36 inches long, were welded to produce specimen blanks 24 by 36 inches. Strips of 5/16-inch-thick plate, 10-1/4 inches wide and 72 inches long, were welded to produce specimen blanks 21 inches wide by 72 inches in length. All welds tested passed dye-penetrant and X-ray inspection.

Yield strength of the weld nugget was determined on 1/2-inch-thick by 3/4-inch-wide uniaxial specimens (Figure 18) machined from the 5/8-inch-thick welded blanks. The weld was instrumented with strain gauges with a 1/4-inch grid length, as shown in Figure 18. Tests were conducted at room temperature, -320 F, and -423 F. For the cryogenic tests, compensating gauges cemented to unstressed pieces of the same alloy were used to compensate for thermal contraction of the material during cooling.

Standard 3/4-inch-wide uniaxial specimens were machined from the welded test blanks. The specimens were surface-machined to 1/2 inch and tested at room temperature, using a 3/8-inch gauge length across the weld nugget for the strain measurement.

Specimen blanks 6 inches wide by 20 inches long and 4 inches wide by 20 inches long, with the weld centered on the 20-inch dimension, were

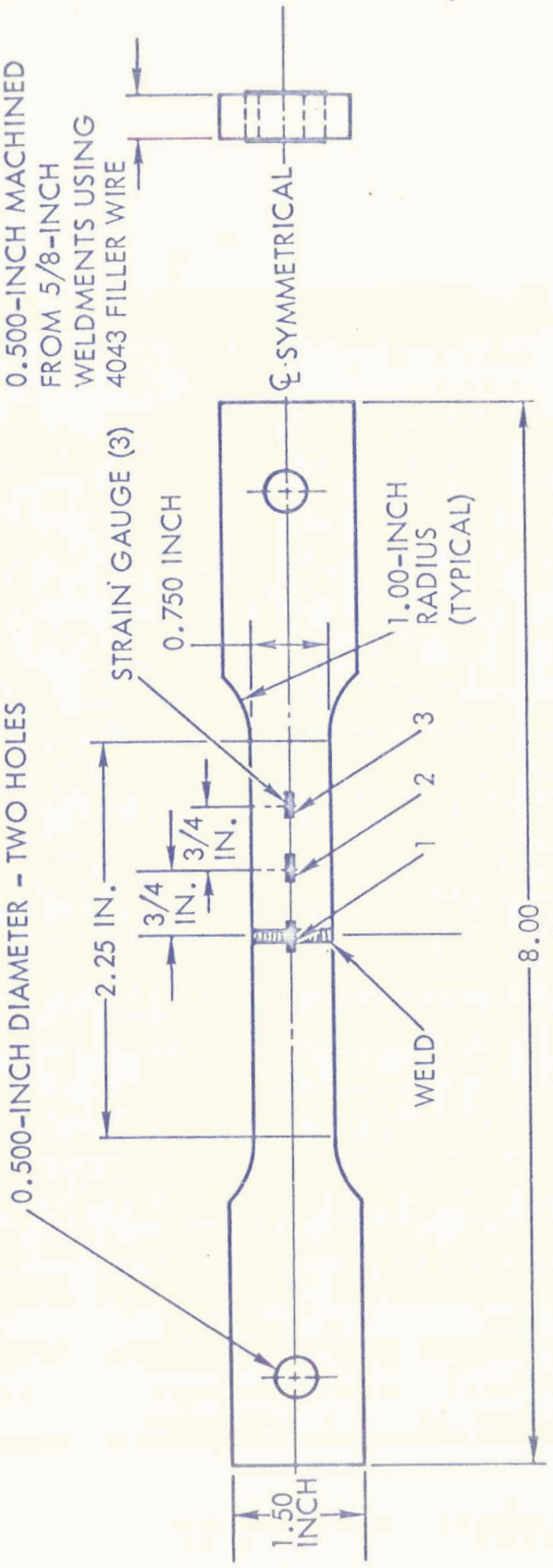

Figure 18. Determination of Weld Nugget Yield Strength

machined from the 5/8-inch-thick weldments. Specimen blanks 4 inches wide by 20 inches long were machined from the 5/16-inch weldments.

Starter notches were produced by two methods, and both were successful. The notches were centered on the weld nugget and parallel to the weld nugget (transverse to the specimen length). A typical 4-inch-wide specimen with a starter notch is shown in Figure 19. Starter notches were machined using a tungsten Elox electrode in an electric discharge machine. Starter notches also were machined by using a 1-inch-radius swing on a fly cutter with a standard mill.

Flaw growth from the starter notch was (in most cases) done on the full thickness welded blank. The fatigue flaw growth was done in bending fatigue through the use of a Sonntag SF-1U fatigue machine. The first fatigue flaws on 5/8-inch-thick material were grown using a tension-tension (+100 percent, +10 percent) stress cycle using the fixturing shown in Figure 20. The starter notch is on the upper surface of the specimen, even with the edge of the lower clamping fixture. Later in the program, a redesigned loading fixture was adopted as shown in Figure 21. This fixture allowed better control of stress and use of a tension-compression stress cycle. The final fixture used is shown in Figure 22. Crack growth observations and size estimates were made using a binocular microscope.

Specimens 6 inches wide from 5/8-inch-thick weldments were notched and fatigue-cracked in the 5/8-inch thickness. Part of the specimens were tested as 5/8-inch-thick specimens. The rest were machined to thicknesses of 1/4 inch, 3/8 inch, and 1/2 inch on the face opposite the flaw, they were then tested.

Specimens 4 inches and 6 inches wide from 5/8-inch-thick weldments were notched and fatigue cracked and tested with 5/8-inch thickness.

Specimens 4 inches wide from 5/8-inch-thick weldments were machined on the second pass side to 1/4 inch, and then notched and fatigue cracked to obtain crack depths near the first and second pass weld interface.

Specimens 4 inches wide from 5/16-inch weldments were notched and fatigue-cracked and then machined to simulate an S-II weld land.

Specimens were measured and then tested in calibrated universal test machines at room temperature, -300 F, and -423 F. Failed-test specimens are shown in Figures 23, 24, and 25. Tests at -300 F were cooled with gaseous nitrogen in a controlled cold chamber. Tests at -423 F were tested using liquid hydrogen as a coolant.

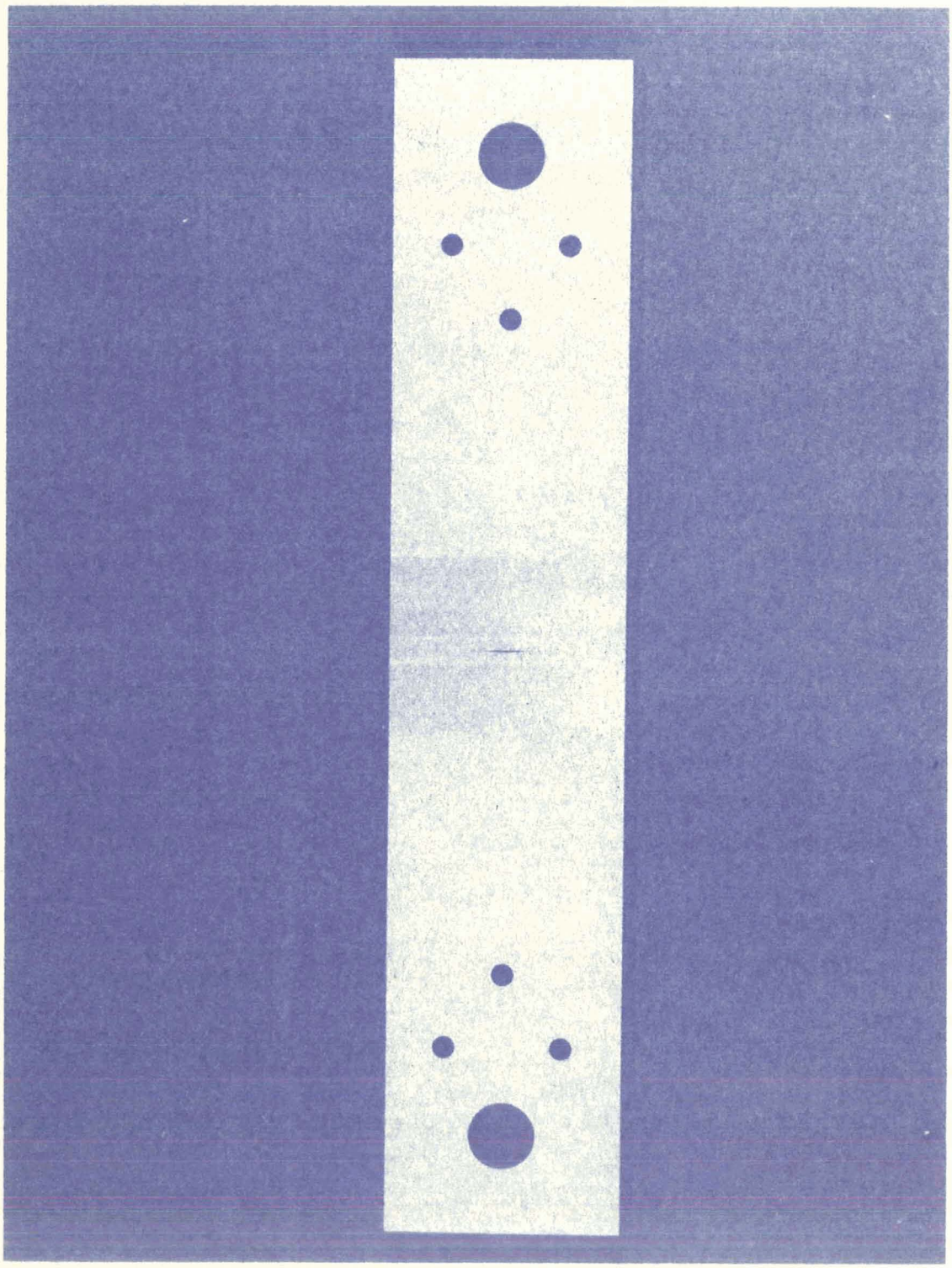

7006-81-2420E

Figure 19. Test Specimen With Starter Notch 4 Inches Wide x 5/16 Inch Thick x 20 Inches Long

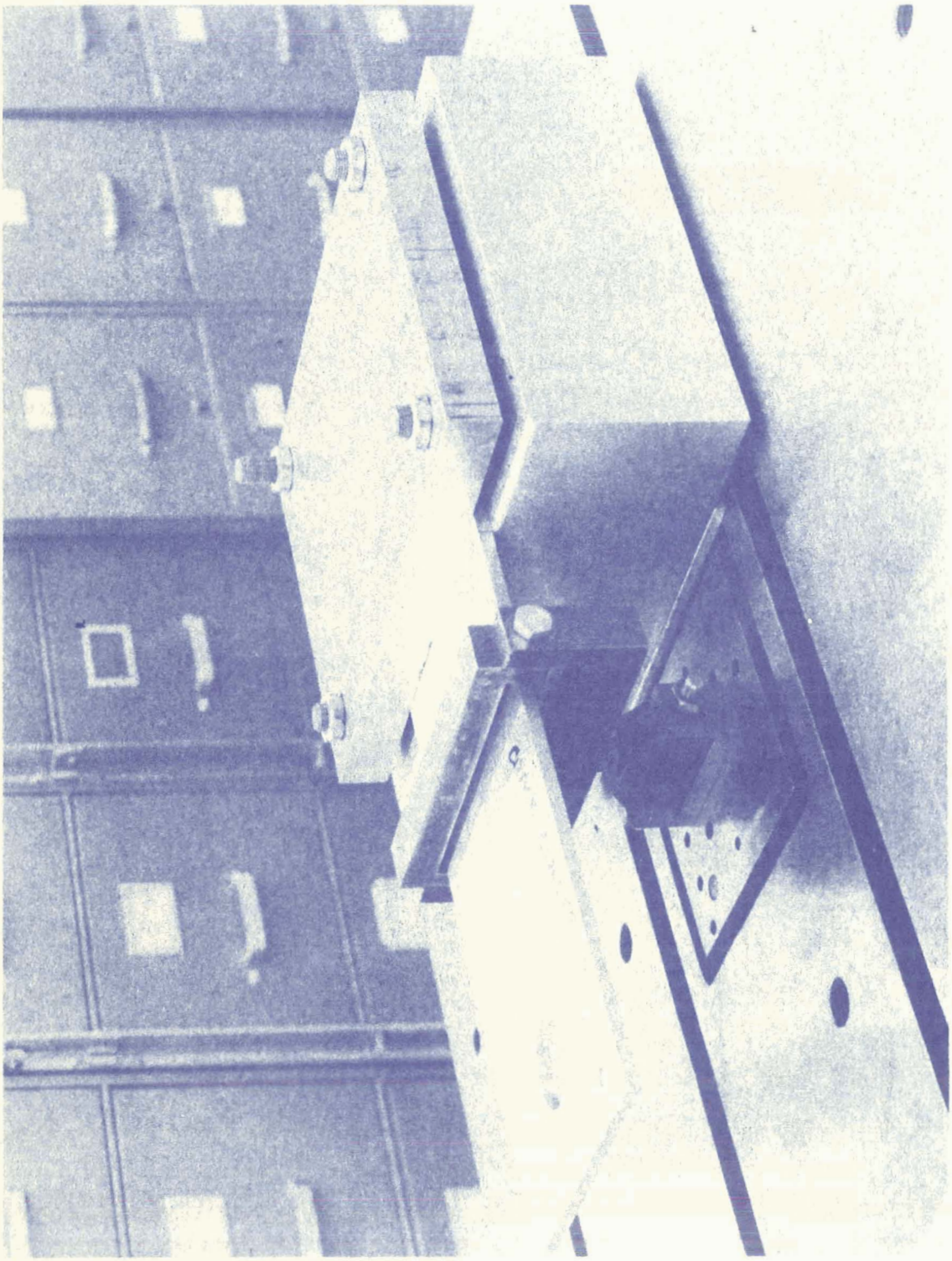

7006-81-2420B

Figure 20. Fatigue Test Fixturing Fatigue Crack Growth (First Setup)

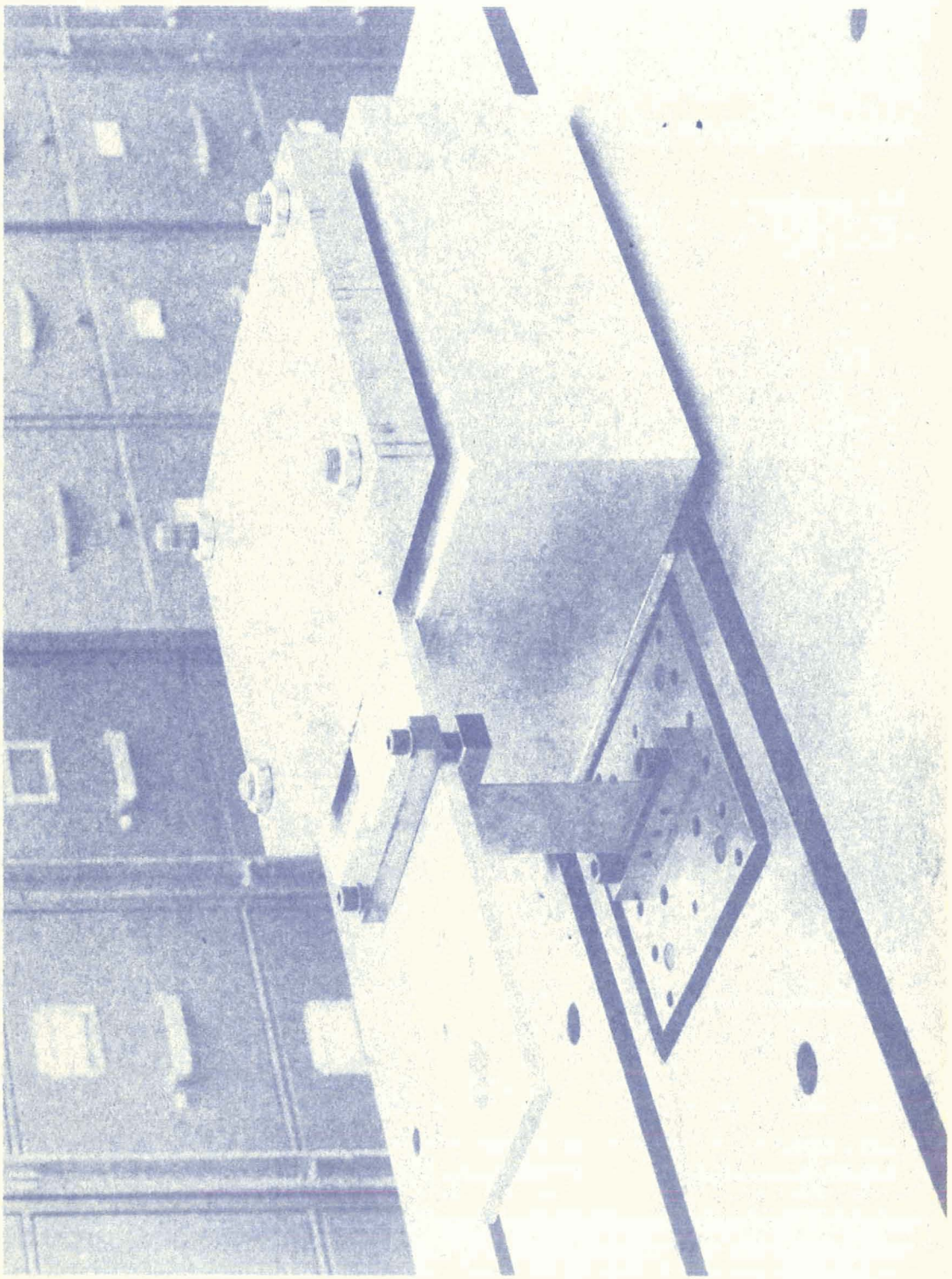

7006-81-2420A

Figure 21. Modified Load Fixture Fatigue Crack Growth (Second Setup)

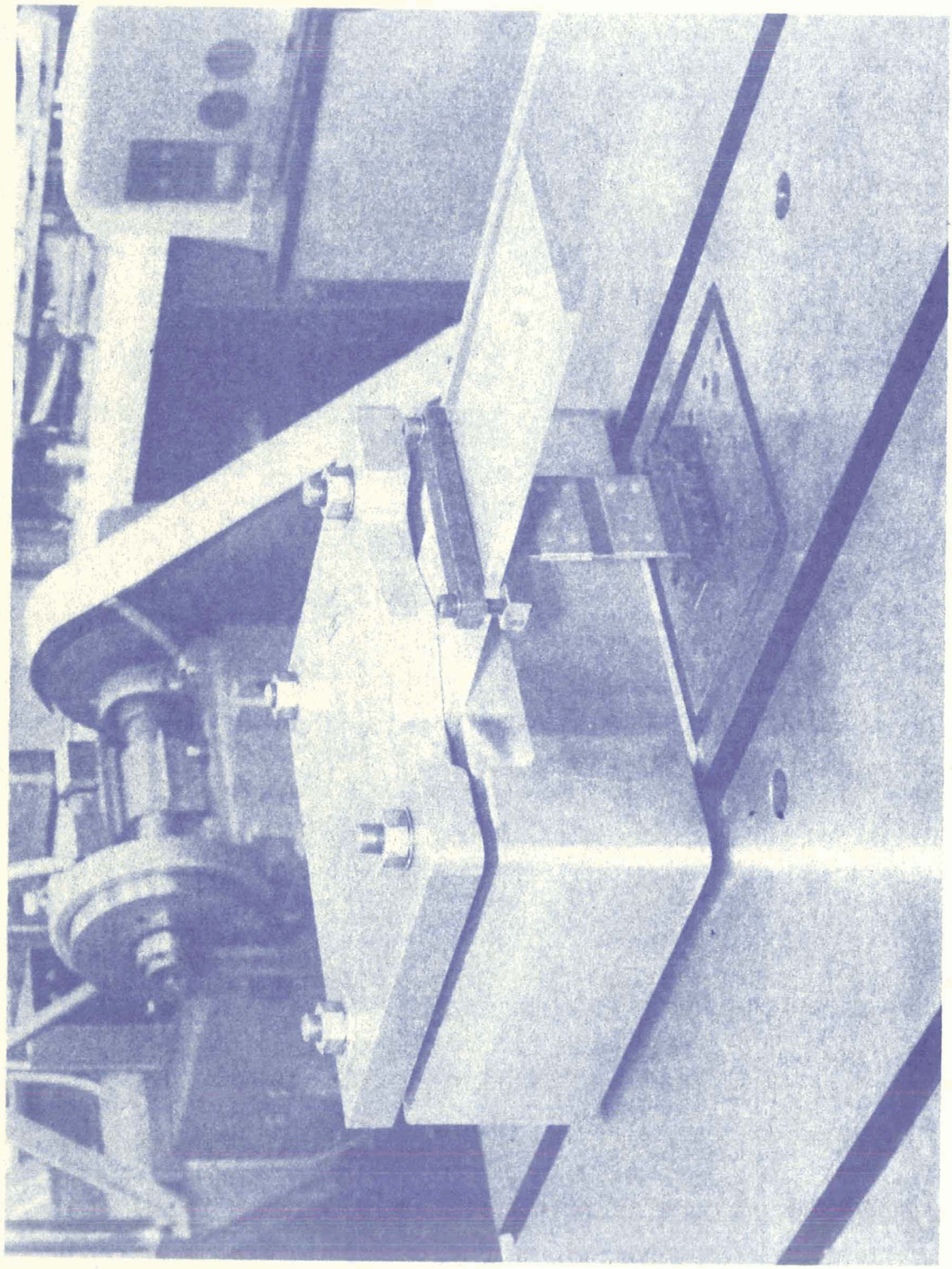

7006-81-2456A

Figure 22. Final Fixturing Fatigue Crack Growth (Third and Final Setup)

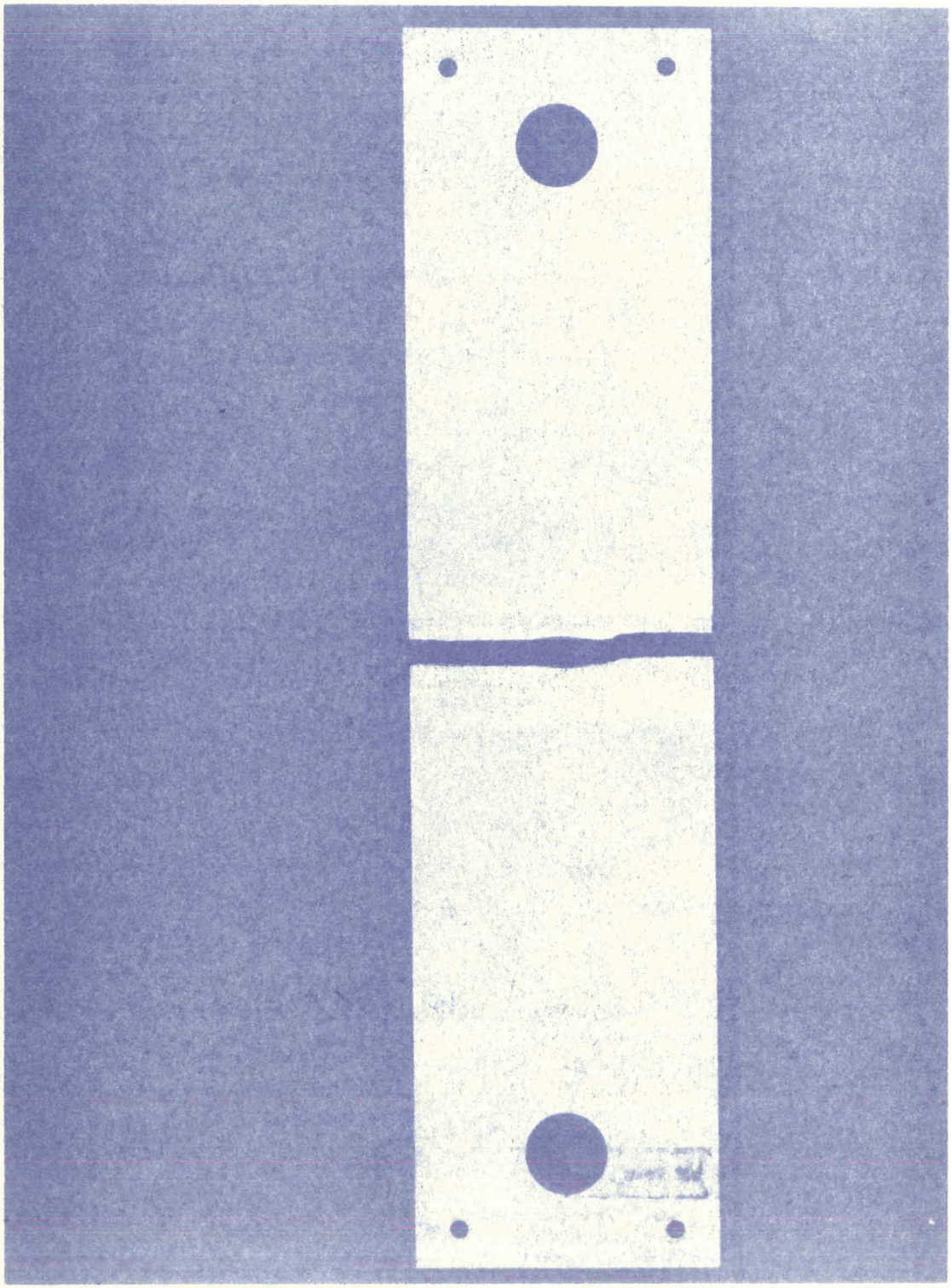

7006-81-242OF

Figure 23. Failed 6 Inch Wide Specimen

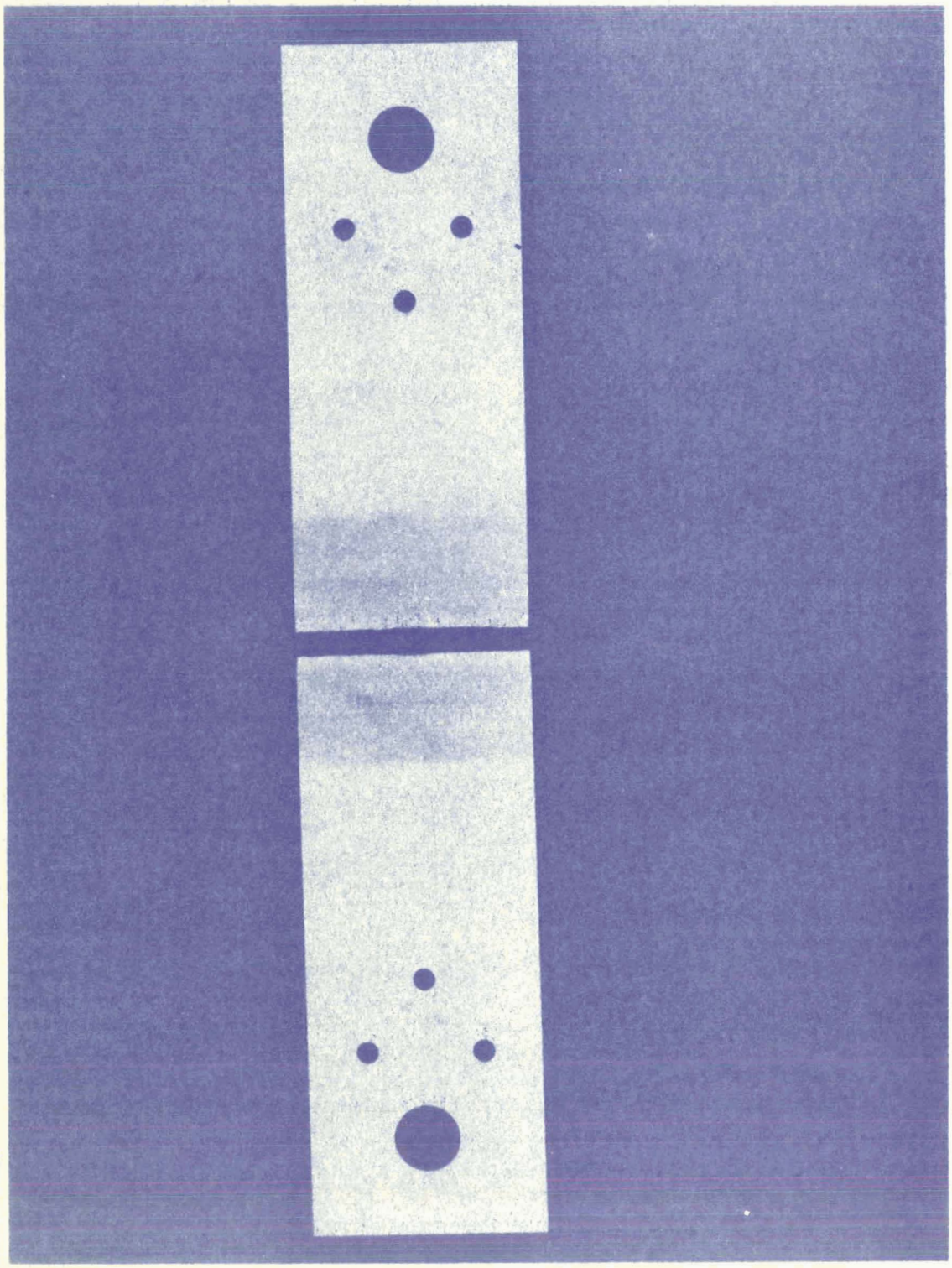

7006-81-2420D

Figure 24. Failed 4-Inch-Wide Specimen

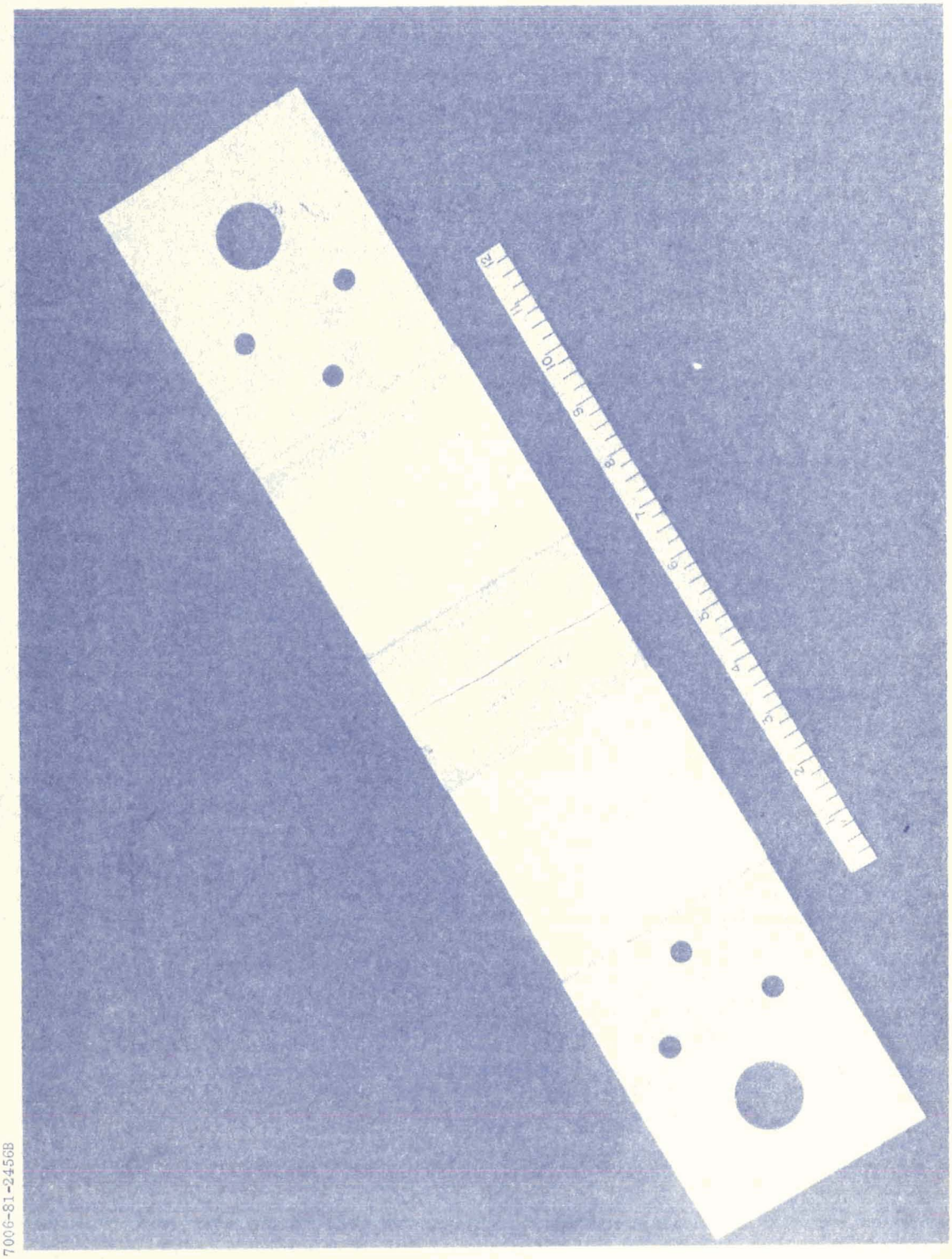

Figure 25. Failed 4-Inch-Wide Specimen With Weld Notch

Selected specimens were taken for metallographic examination. Photomacrographs were taken of specimen fatigue cracks after test. X-rays were taken after fatigue-cracking and after applying the proof test stress to a series of weld land specimens.

Several specimens were checked with a defectometer after fatigue cracking for comparison of the instrument reading with the measured depth after testing. The defectometer is an eddy current instrument manufactured by Sperry Products.

CALCULATIONS

The flaw shape factor (Q) was obtained from a plot of a/2C versus Q, based on the relationship:

$$Q = \Phi^2 - .212\,(\sigma/\sigma\,ys)^2 \text{ where}$$

Φ = complete elliptical integral of the second kind

a = flaw depth

2c = flaw width

σ = gross failure stress, ksi

σys = yield strength of the test material (weld nugget) at the temperature of test, ksi

Ratios of $\sigma/\sigma ys$ from 0 to 1.00 were used to obtain Q. For actual ratios above 1.00, the 1.00 line was used.

For the weld land tests where bending stress was involved with a consequent indeterminate stress adjacent to the crack tip, the 1.00 line was used.

Stress intensity factors (K) were taken from a plot of gross failure stress (σ) versus normalized flaw depth (a/Q). This plot was based on the relationship:

$$K^2 = 1.21\,\pi\,\sigma^2\,(a/Q)$$

For the weld land tests, apparent K's were not calculated because of the indeterminate stress in the region of the crack tip.

TEST RESULTS

Mechanical properties obtained on 4043 filler wire weldments are presented in Table 10. Typical load strain curves for the weld nugget, the heat affected zone, and the parent metal are shown in Figures 26, 27 and 28.

Table 10. Average Yield Strength of 2014-T651 Weldments Using 4043 Filler Wire (1/4-Inch Grid Length Strain Gauge on Weld-Nugget)

Test Temperature (F)	F_{tu} (ksi)	F_{ty} (ksi)
RT	26.15	47.55
-320	33.6	54.45
-423	41.2	56.0

Note: Two-pass weld, from one side, welded as 5/8-inch-thick plate. Specimen machined to 1/2 inch thick x 3/4 inch width x 2.25 inches gauge length. Weld transverse to load direction.

RT = room temperature

Typical test results on 5/8-inch-thick weldments fatigue-cracked as 5/8-inch-thick material and machined to 1/4 inch, 3/8 inch, 1/2 inch, and 5/8 inch (not machined) for test are given in Table 11. Plotted test results at room temperature are presented in Figure 29, and -423 F test results are shown in Figure 30. Photomacrographs of representative fatigue cracks are shown in Figure 31. For the -300 F and -423 F tests, sections adjacent to the crack were etched and photographed to determine the location of the first and second weld pass interface with respect to the crack tip. Representative photographs are shown in Figure 32.

Representative test results on weld land specimens are shown in Table 12. Typical fatigue flaws and flaw growth during proof stress are shown in Figure 33. A plot of gross failure stress versus normalized flaw depth is shown in Figure 34.

Test results on 5/8-inch-thick weldments tested at -423 F are plotted in Figure 30. Photographs of the fatigue flaws after test are shown in Figures 35, 36, and 37.

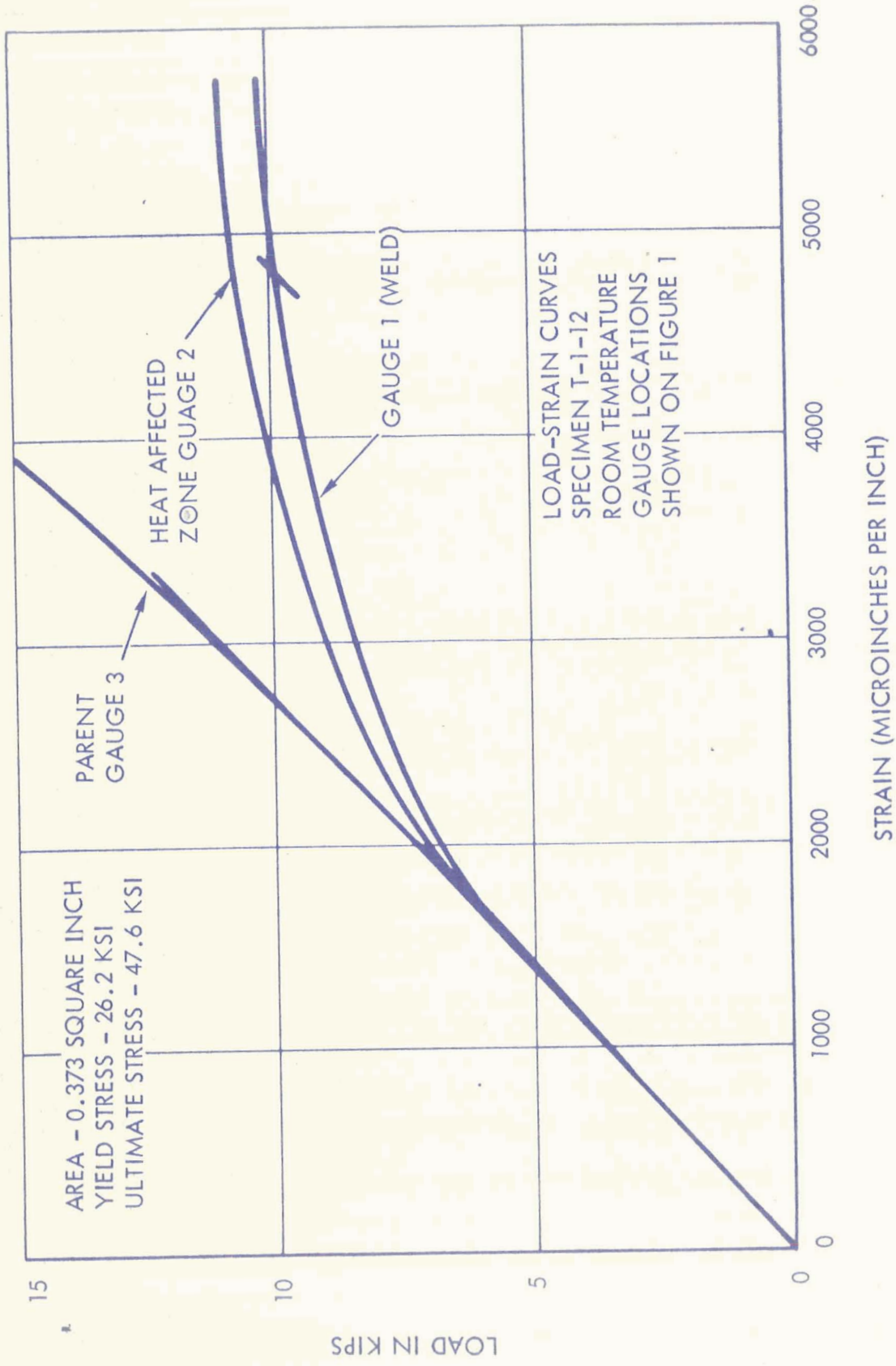

Figure 26. Load-Strain Curves of Specimen TI-10 at Room Temperature

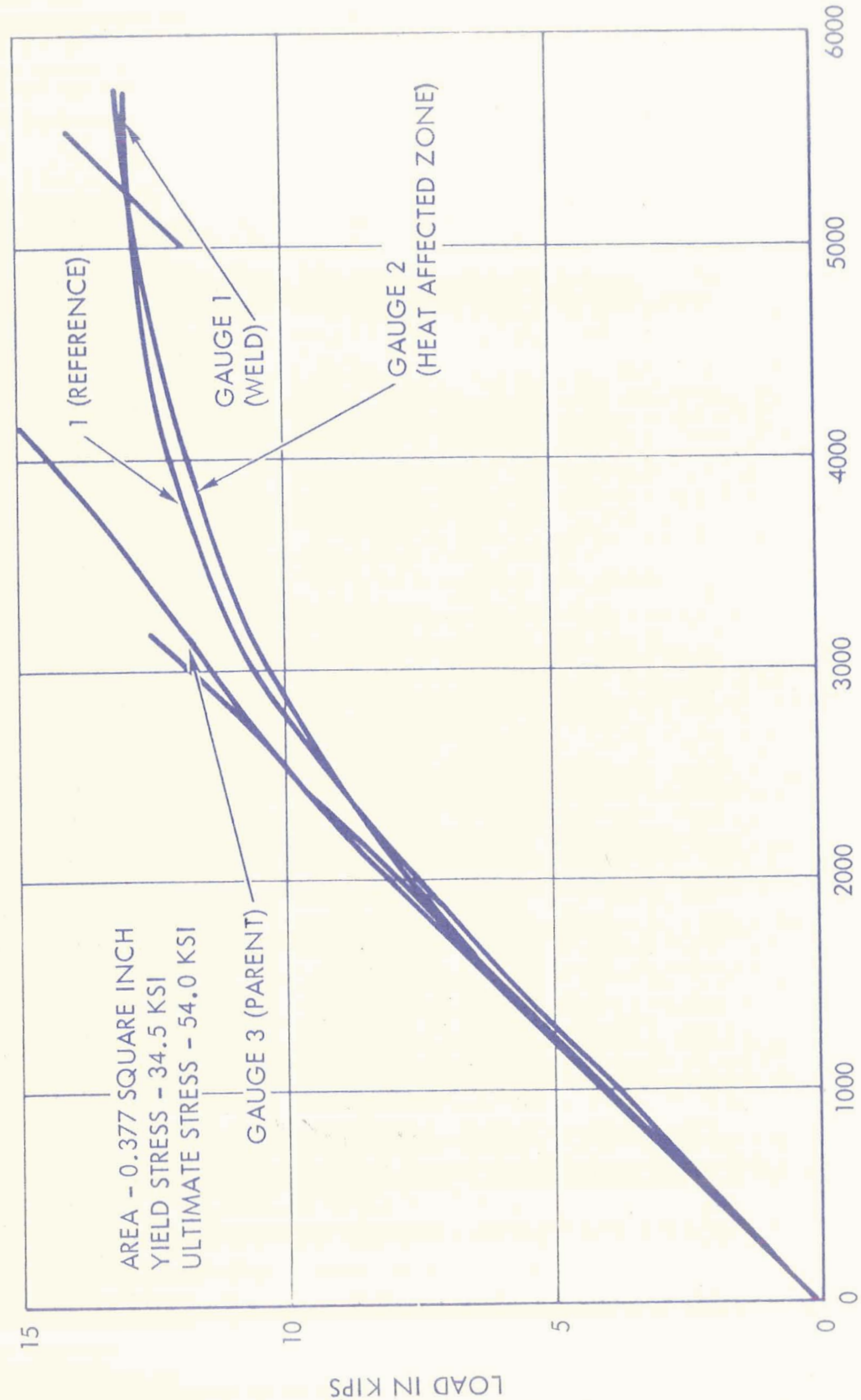

Figure 27. Load-Strain Curves of Specimen C at -320 F

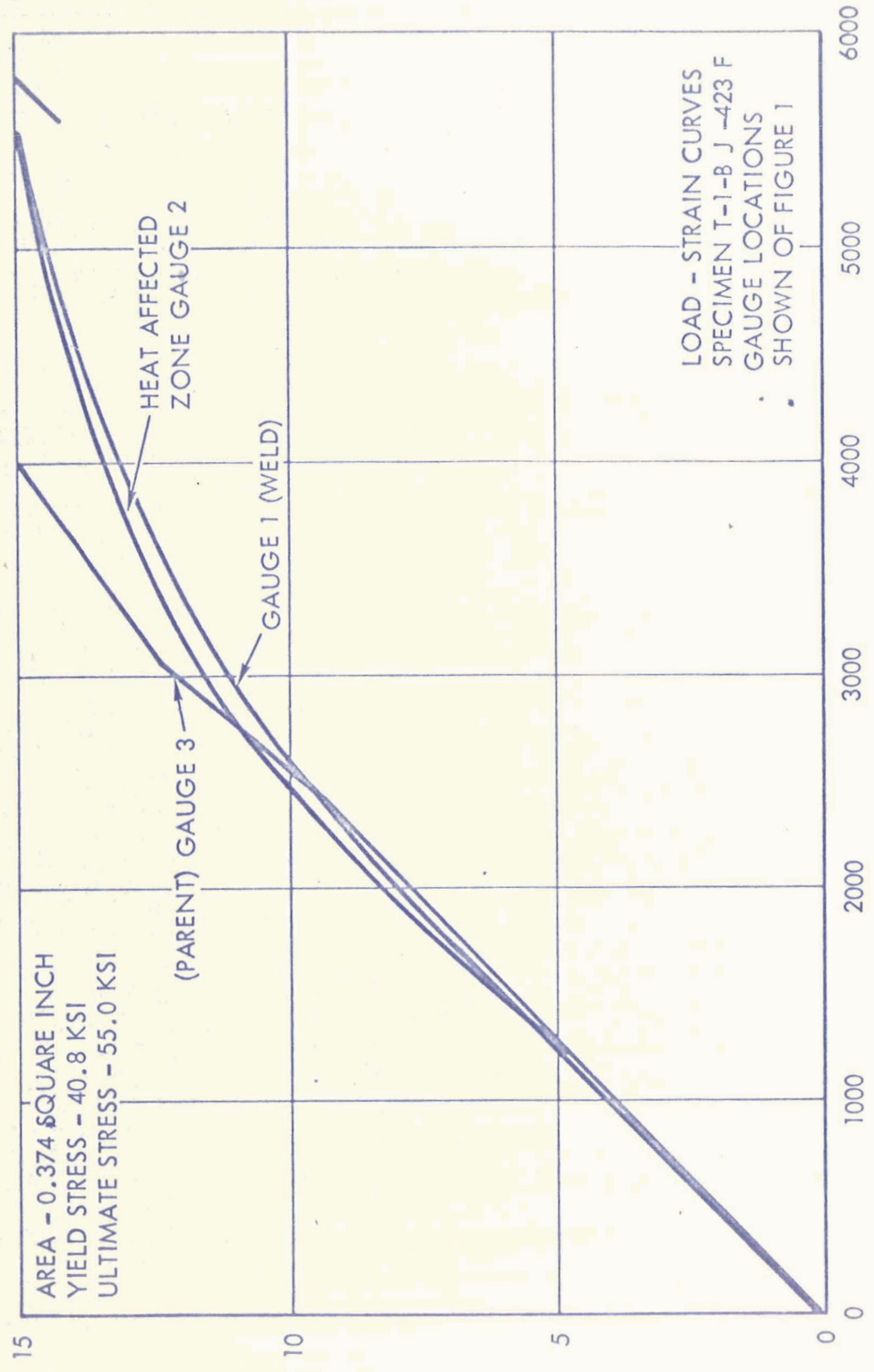

Figure 28. Load-Strain Curve of Specimen T-1-B at -423 F

Table 11. Typical Test Data Surface Flawed Specimens

Specimen Number	Specimen Thickness (inches)	Gross Failure Stress (ksi)	Test Temperature (F)	Fatigue Crack Data				a/Q (inches)	Apparent K ksi $\sqrt{in.}$	Side of Weld Flawed	Depth (inches) From Flawed Side to First and Second Pass Interface
				Stress (ksi)	Cycles 1000	Crack Depth (a) (inches)	Crack Width (2c) (inches)				
P1-1	0.252	31.99	RT	20	280						
				30	70						
				40	100	0.130	0.720	0.125	21.7	First pass	0.080
P1-2	0.254	28.00	RT	30	31						
				35	20						
				32.5	40	0.160	0.650	0.132	19.8	First pass	0.160
T4-3	0.244	29.03	RT	20	60	0.130	0.850	0.138	21.0	First pass	0.170
T7-3	0.377	21.88	RT	20	43	0.280	1.04	0.207	19.5	First pass	0.150
T5-1	0.505	22.40	RT	20	55	0.235	1.31	0.214	20.2	Second pass	0.050
T4-2	0.635	30.79	RT	20	100	0.175	0.630	0.133	21.5	First pass	0.170
T3-4	0.630	17.98	RT	20	75	0.380	1.63	0.299	19.0	First pass	0.250
T3-2	0.630	19.11	-300	20	100	0.350	1.455	0.259	19.2	First pass	0.190
T3-3	0.630	13.36	-300	20	110	0.425	1.970	0.337	16.0	First pass	0.240
P2-2	0.250	23.58	-423	25	40	0.170	1.04	0.150	18.0	First pass	0.150
P2-3	0.249	20.07	-423	25	40	0.177	1.00	0.151	15.3	First pass	0.140
P2-1	0.246	17.60	-423	30	30	0.200	1.60	0.189	14.8	First pass	0.190

Note: 5/8-inch-thick 2014-T656 weldments using 4043 weld rod;
Fatigue flawed in bending using an Elox starter and a +100 percent, +10 percent stress cycle using fixture shown in Figure 57;
Specimen dimensions: 5/8 inch thick x 20 inches long x 6 inches wide; RT-room temperature;
aQ-normalized flaw depth.

SPACE DIVISION OF NORTH AMERICAN ROCKWELL CORPORATION

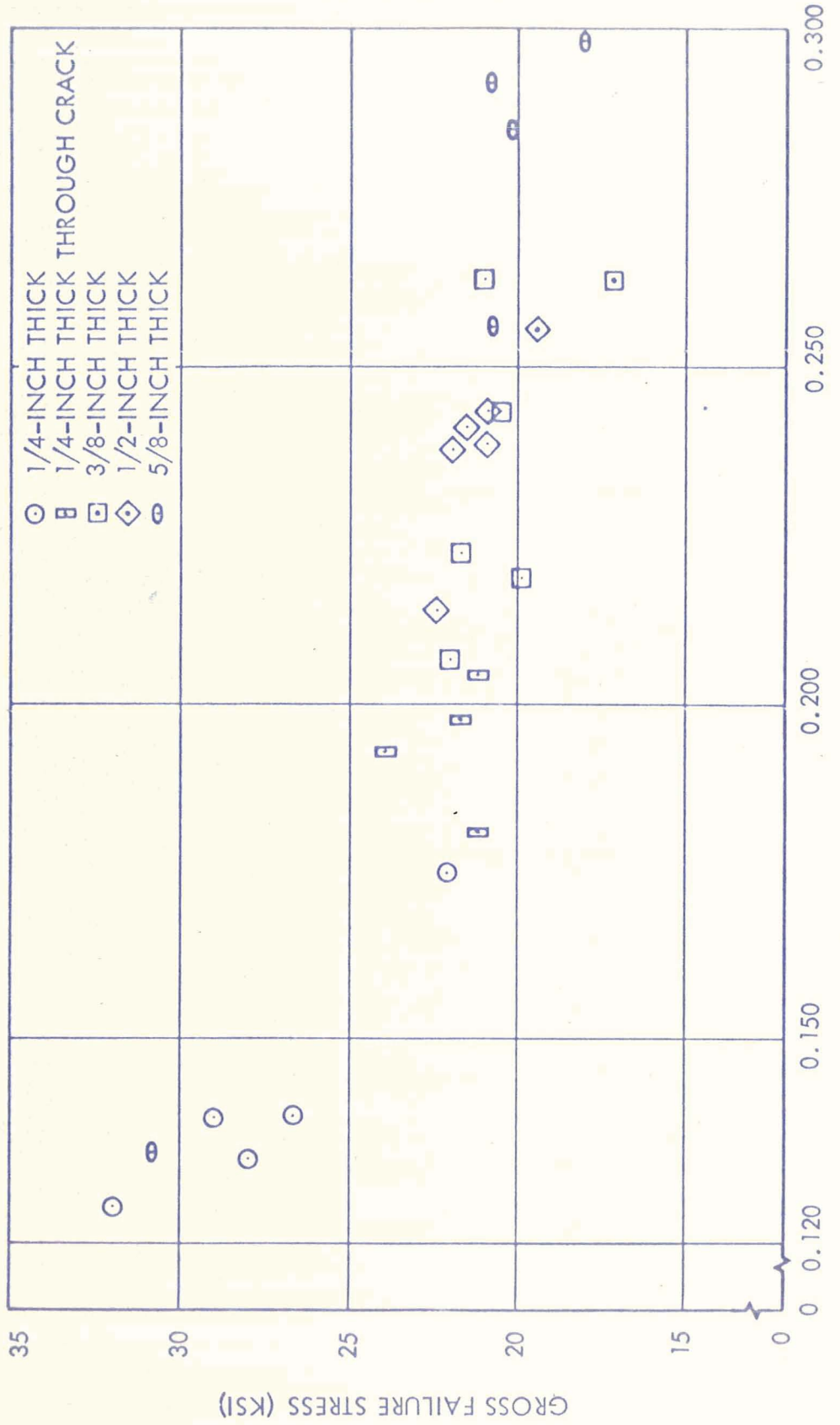

Figure 29. Gross Failure Stress Versus Normalized Flaw Depth, Room Temperature Test

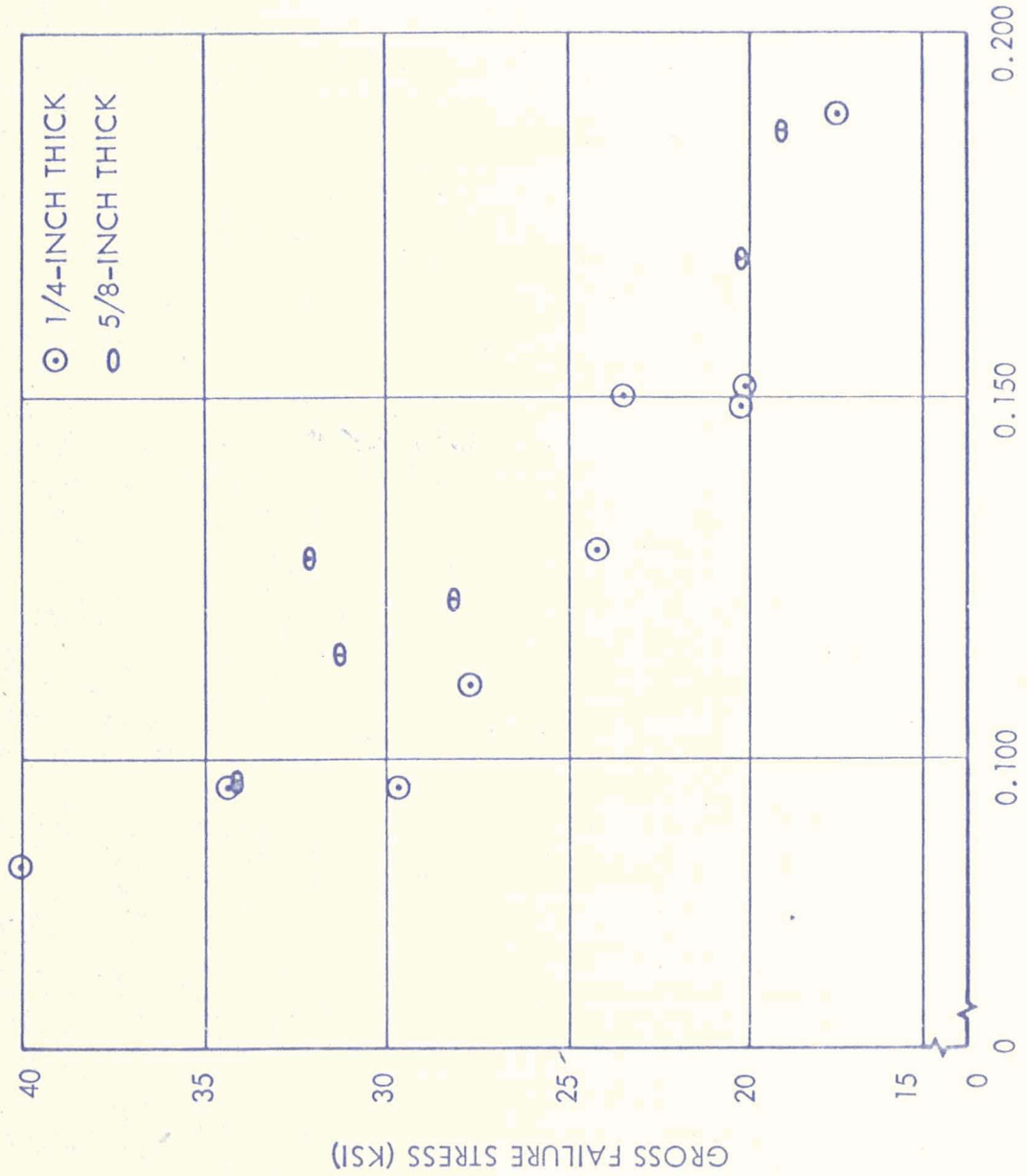

Figure 30. Gross Failure Stress Versus Normalized Flaw Depth at -423 F

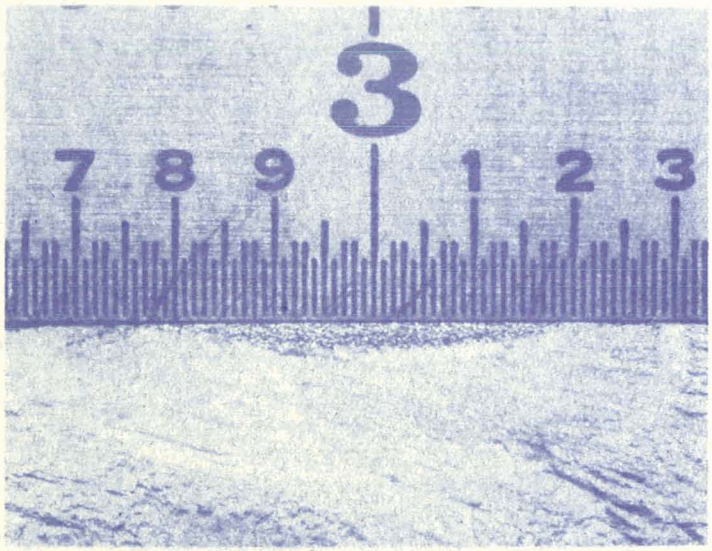

(A) FATIGUE FLAW
SPECIMEN PL-2
FLAW 0.160-INCH DEPTH
X 0.650-INCH WIDTH

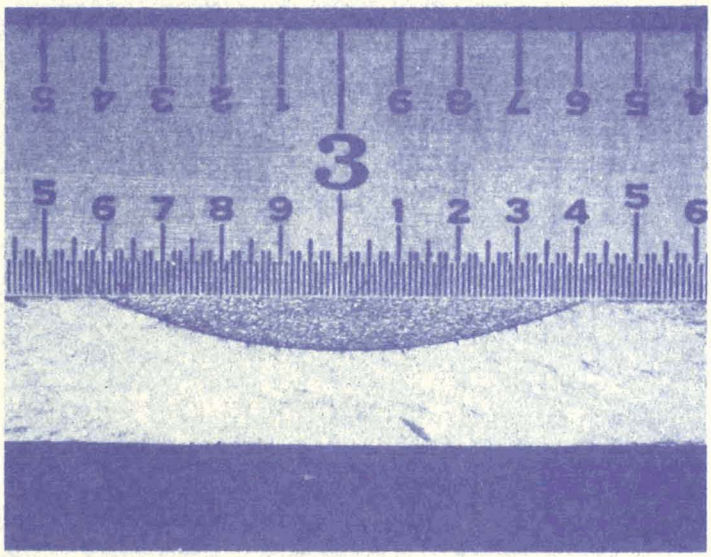

(B) FATIGUE FLAW SPECIMEN T6-4
FLAW - THROUGH X 1.12-INCH
WIDTH

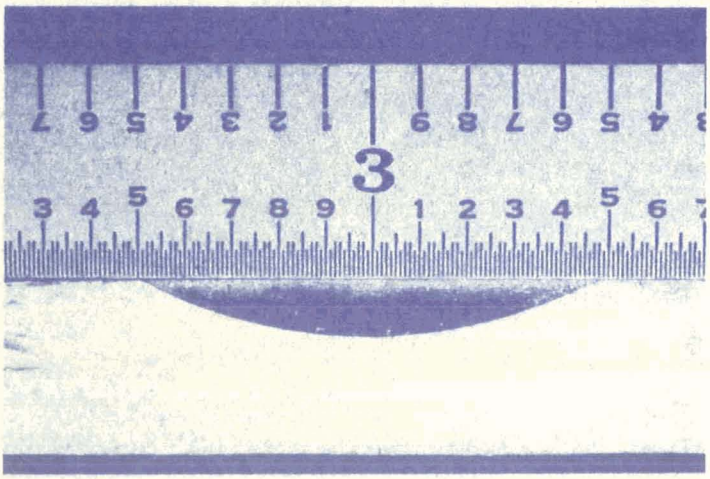

(C) FATIGUE FLAW
SPECIMEN T8-4
FLAW 0.355-INCH DEPTH
X 1.44-INCH WIDTH

Figure 31. Typical Fatigue Flaw Photomacrographs

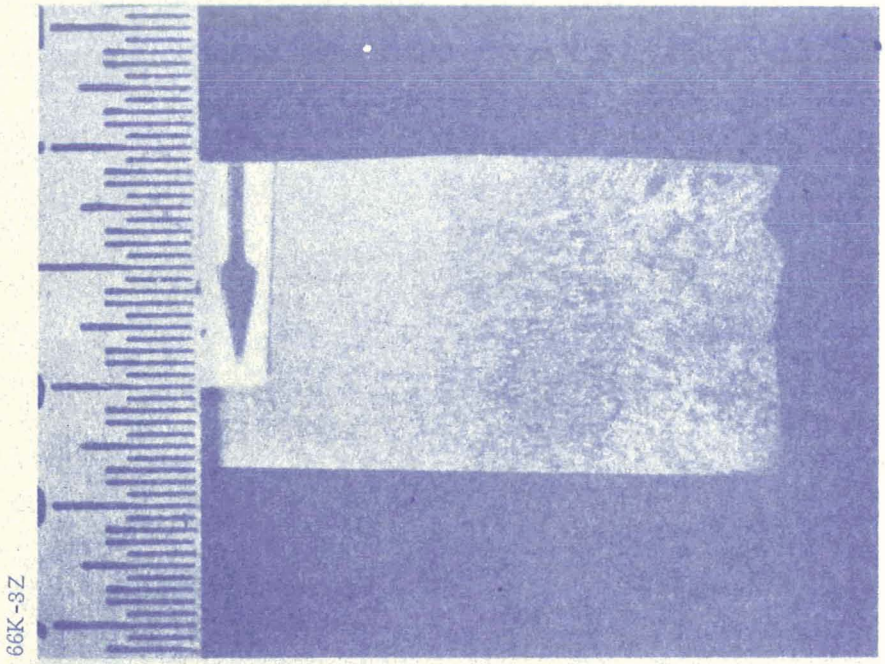

66K-3Z

(A) SPECIMEN P2-4
-423 F TEST
FATIGUE FLAW
0.146-INCH DEPTH
APPARENT K 15.2
1/4-INCH THICK
SPECIMEN
WELD INTERFACE
0.140-INCH DEEP

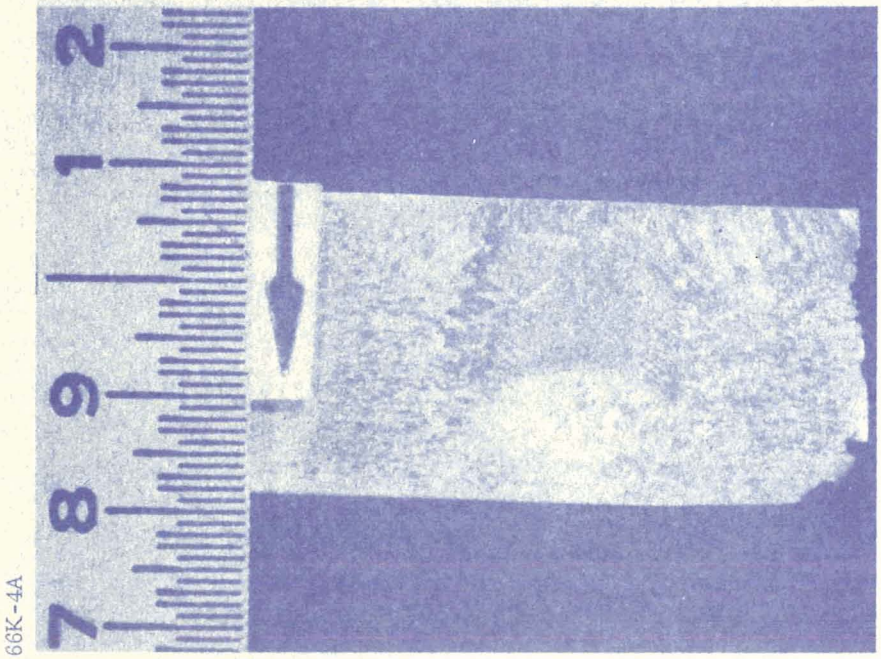

66K-4A

(B) SPECIMEN P2-2
-423 F TEST
FATIGUE FLAW
0.170-INCH DEPTH
APPARENT K 18.0
1/4-INCH THICK
SPECIMEN
WELD INTERFACE
0.145-INCH DEEP

Figure 32. Photomacrograph of Weld Cross Section - Arrow Indicates Direction of Fatigue Flaw in Weld Nugget

Table 12. Representative Test Data - Weld Land Specimens

Specimen Number	Weld Thickness (inches)	Gross Failure Stress (ksi)	RT Proof Stress (ksi)	Test Temperature (F)	Fatigue Crack Data					Flaw Identity	a/Q (inches)
					Maximum Stress (ksi)	Stress Cycle (percent)	Cycles (1000)	Crack Depth (a) (inches)	Crack Length (2c) (inches)		
D30-10	0.331	25.38	0	RT	14	±100	25	0.050	0.497	No proof test	0.051
D30-4	0.335	23.32	0	RT	14	±100	60	0.112	0.495		0.095
D31-12	0.330	25.32	0	-423	14	±100	35	0.055	0.508		0.061
D32-12	0.330	23.71	0	-423	14	±100	21	0.062	0.515		0.067
D36-8	0.323	25.15	22.8	-423	14	±100	88	0.114	0.461	Fatigue	0.091
								0.158	0.485	Proof	0.105
D32-6	0.331	25.09	22.8	-423	18	±100, -80	55	0.102	0.519	Fatigue	0.093
								0.151	0.520	Proof	0.109
D35-5	0.317	25.45	22.8	-423	18	±100	150	0.136	0.518	Fatigue	0.105
					19		45	0.152	0.650	Proof	0.126
D30-1	0.288	29.05	22.8	-423	14	±100	7	0.107	0.440	Fatigue	0.086
					13		70	0.122	0.510	Proof	0.100
D30-2	0.288	29.49	22.8	-423	14	±100	25	0.102	0.395	Fatigue	0.079
					13		70	0.118	0.400	Proof	0.084

RT - room temperature
aQ - normalized flaw depth

SPACE DIVISION OF NORTH AMERICAN ROCKWELL CORPORATION

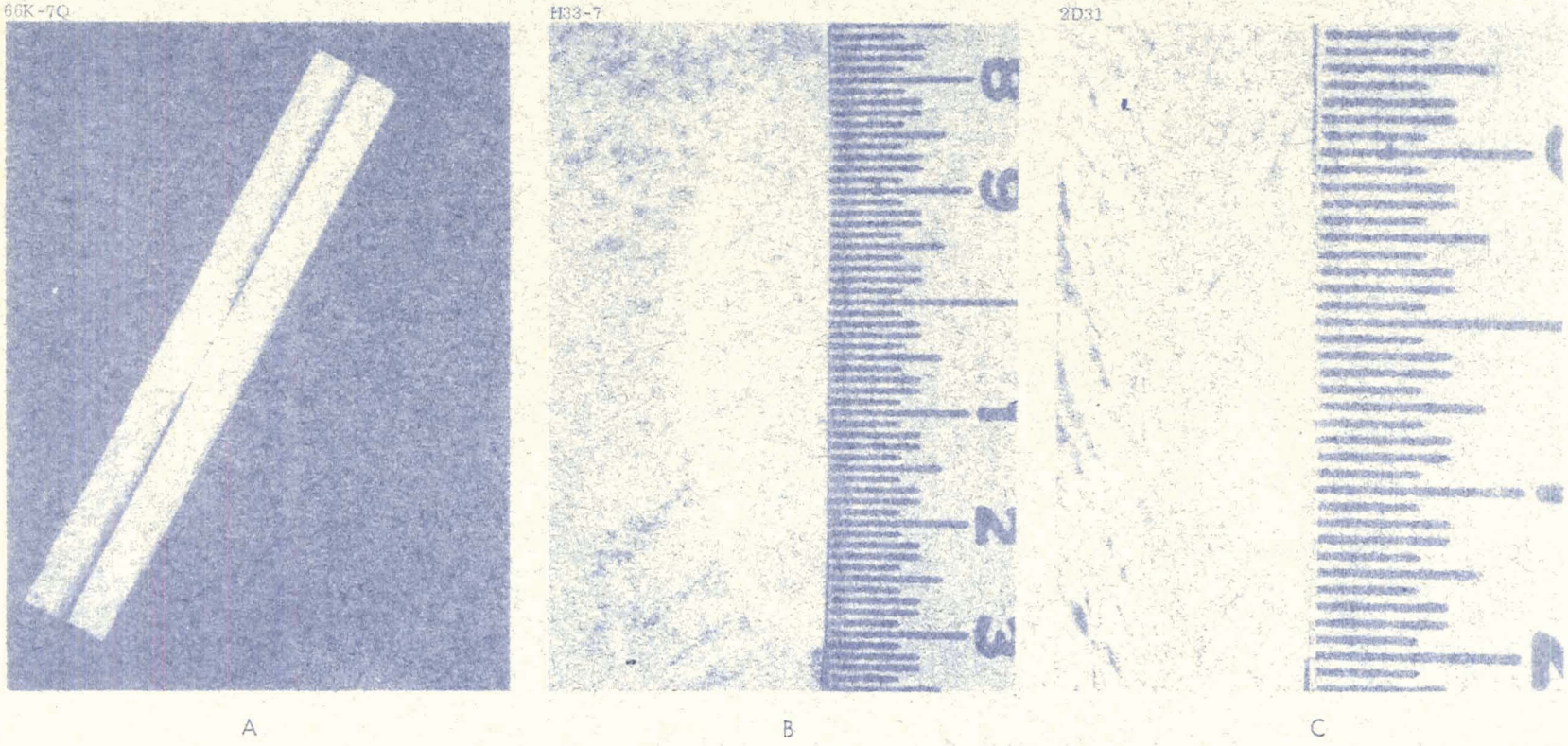

A - FAILURE SURFACE SPECIMEN 33-7
B - SPECIMEN 33-7, FATIGUE FLAW 0.126-INCH DEPTH X 0.524-INCH WIDTH
C - SPECIMEN 31-2, FATIGUE FLAW 0.047-INCH DEPTH X 0.274-INCH WIDTH

Figure 33. Weld Land Tests, 22.8 ksi, Room Temperature Proof Load, -423 F Test

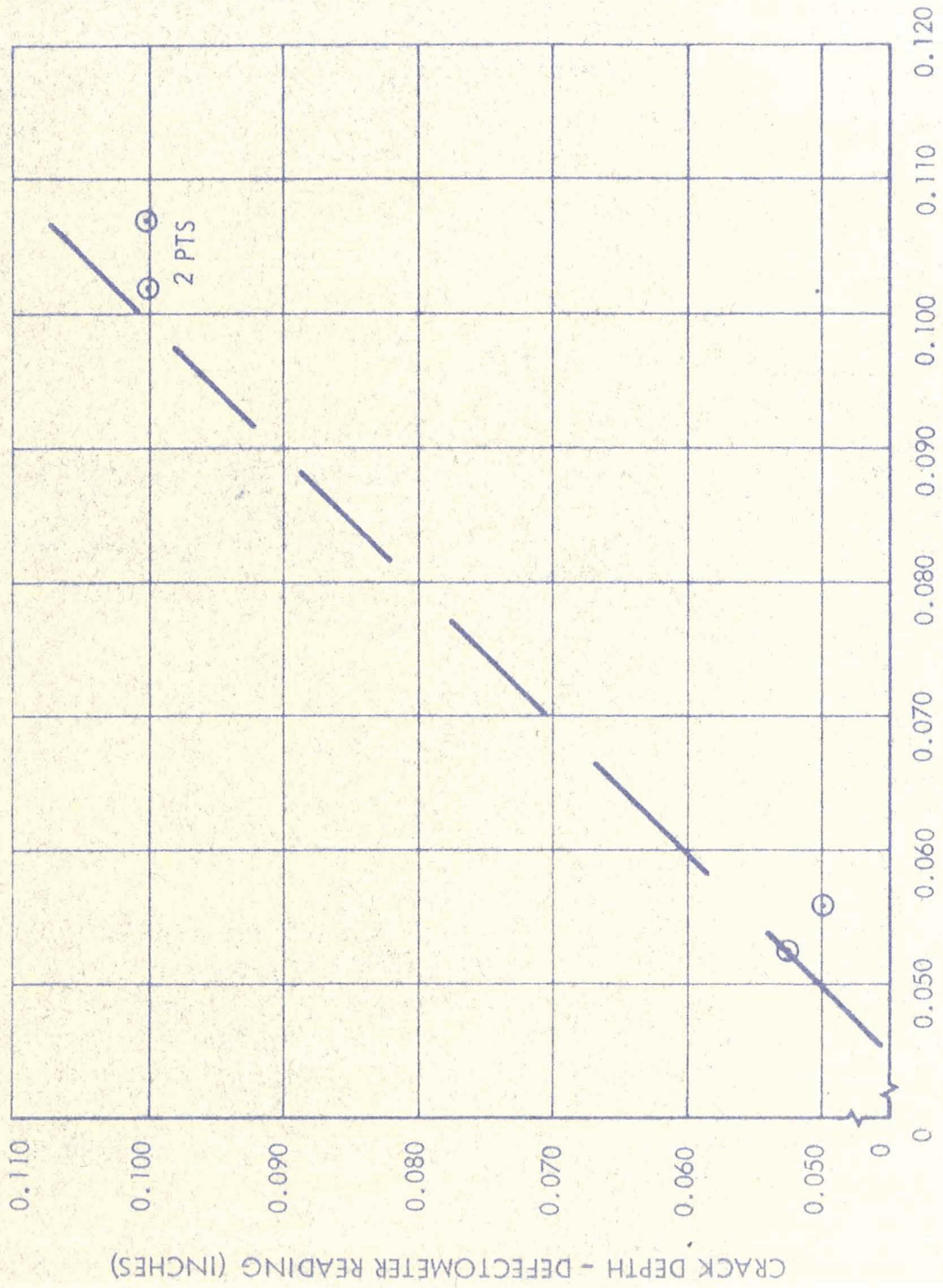

Figure 34. Defectometer Reading Versus Actual Crack Depth—Tight Fatigue Cracks

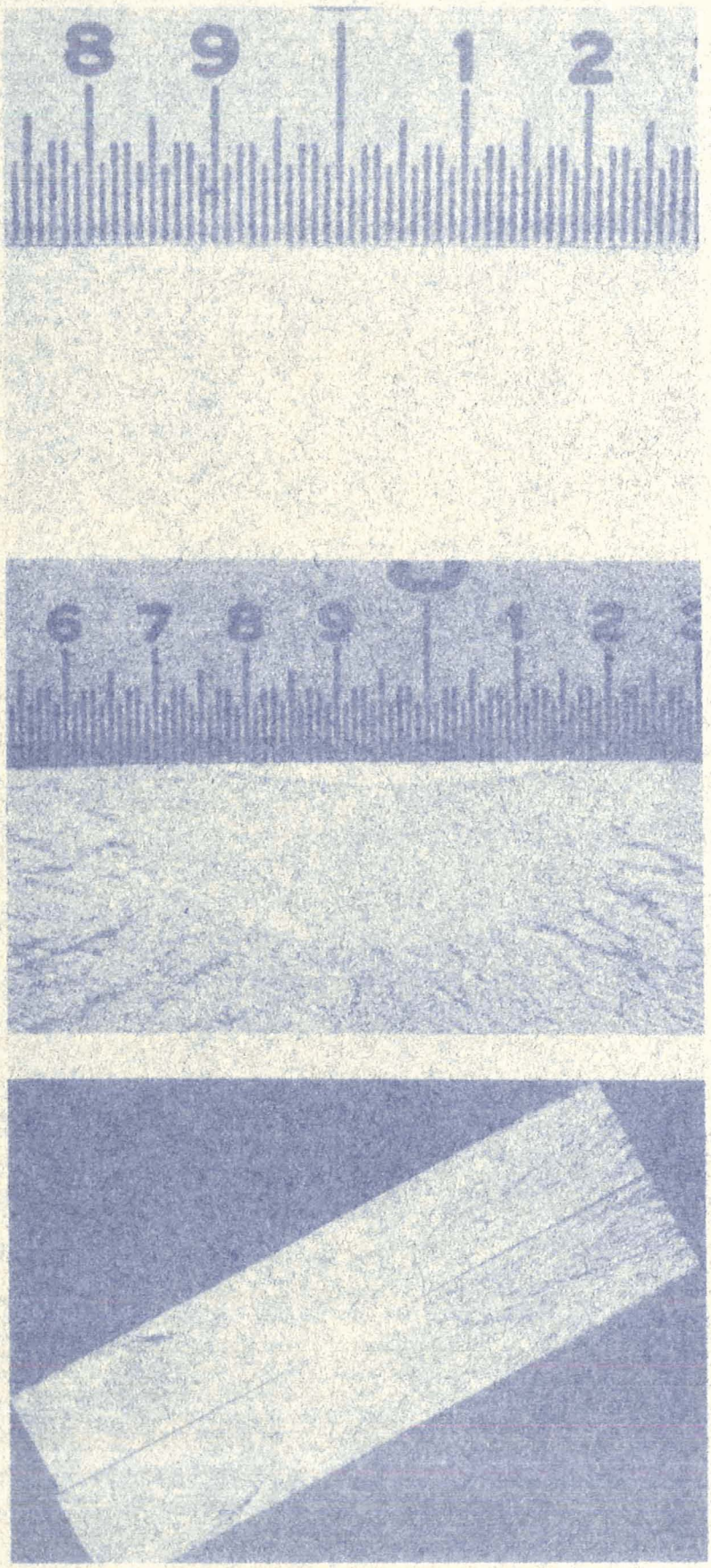

A - FAILURE SURFACE, SPECIMEN T11-3

B - SPECIMEN T11-3, FATIGUE FLAW 0.182" DEPTH x 0.558" WIDTH

C - SPECIMEN T11-4, FATIGUE FLAW 0.202" DEPTH x 0.605" WIDTH

Figure 35. Weld Tests, 5/8-Inch Thick, -423 F (Specimen T11-3)

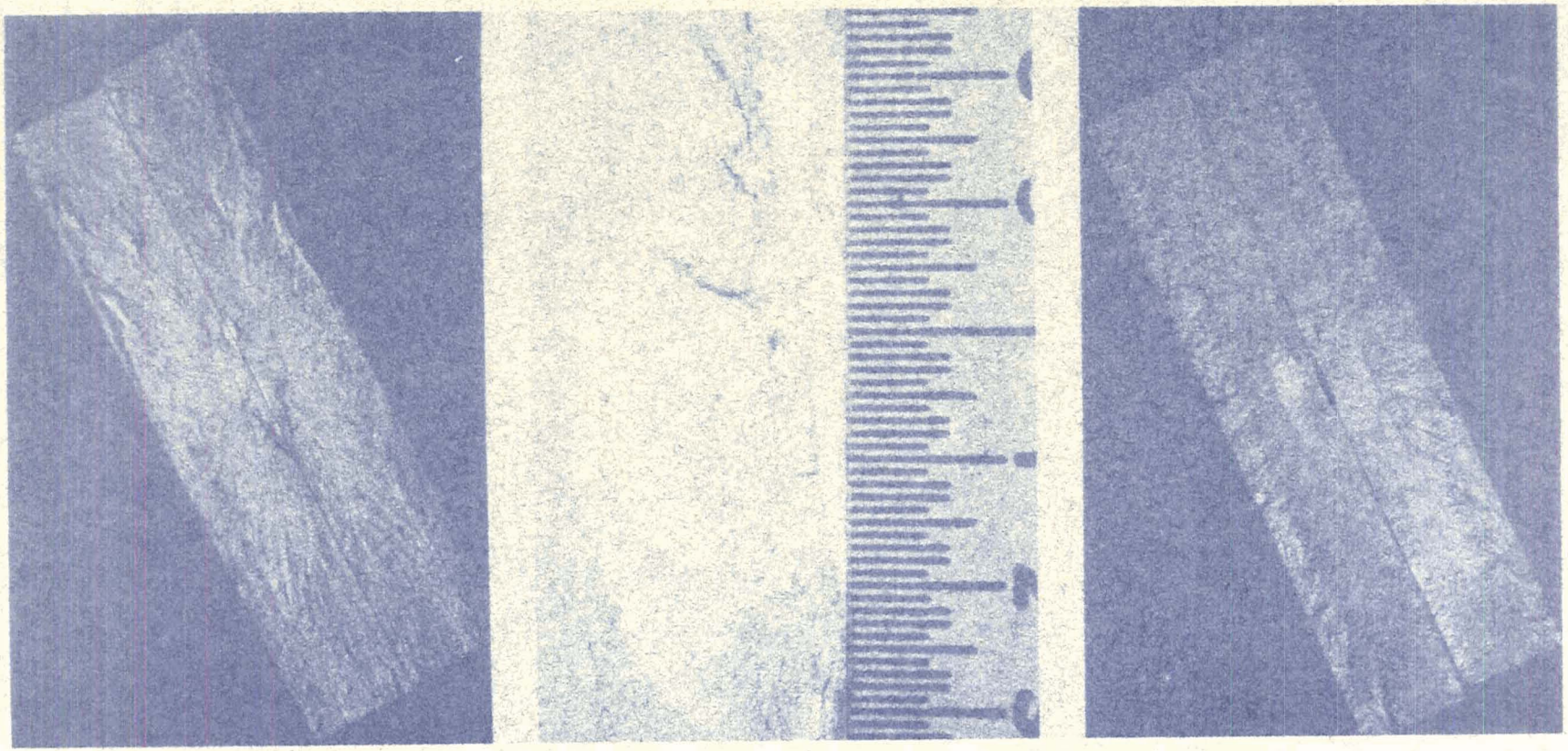

A B C

A - FAILURE SURFACE, SPECIMEN T11-2

B - SPECIMEN T11-2, FATIGUE FLAW 0.215" DEPTH x 0.639" WIDTH

C - FAILURE SURFACE, SPECIMEN T11-6

Figure 36. Weld Tests, 5/8-Inch Thick, -423 F (Specimen T11-2)

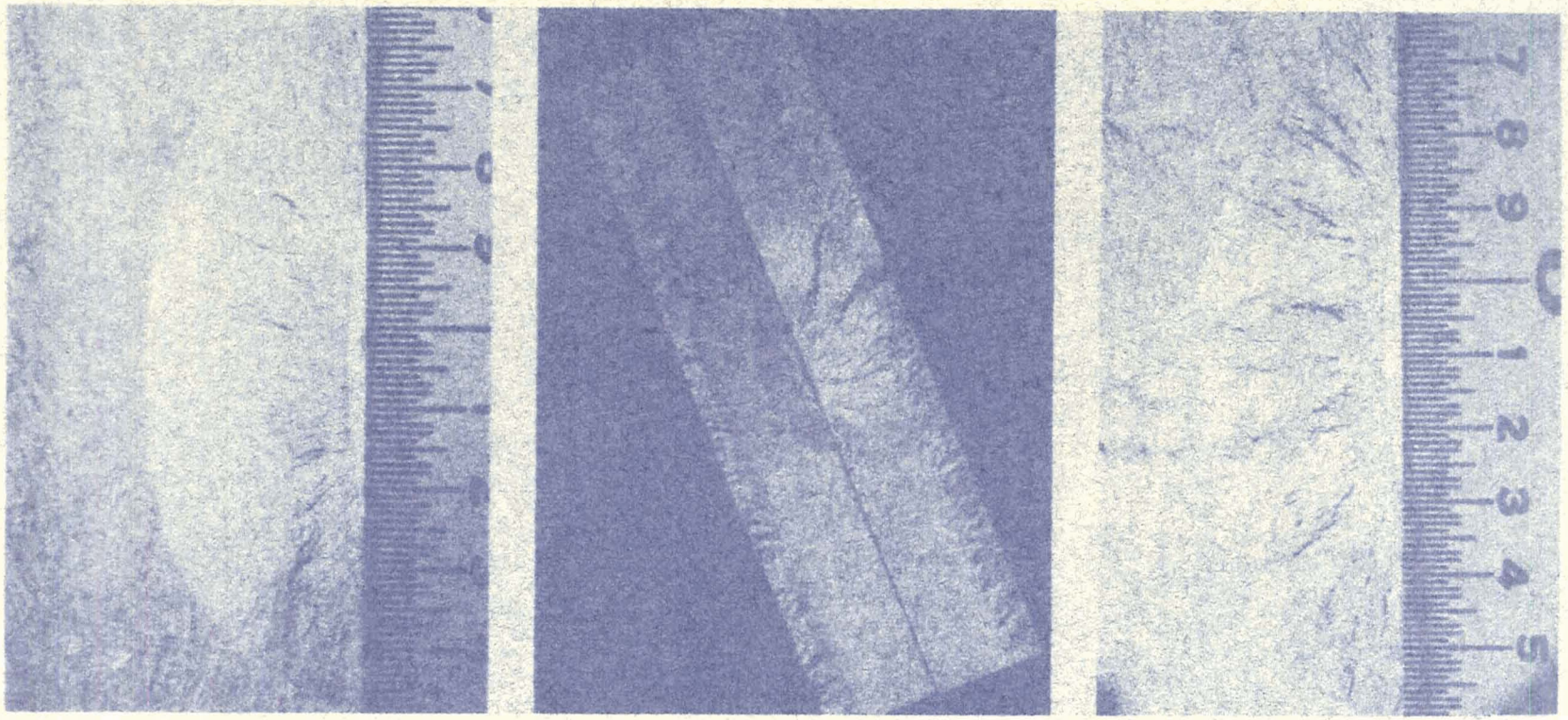

A B C

A - SPECIMEN T11-6, FATIGUE FLAW 0.276" DEPTH x 0.854" WIDTH

B - FAILURE SURFACE, SPECIMEN T11-1

C - SPECIMEN T11-1, FATIGUE FLAW 0.283" DEPTH x 1.003" WIDTH

Figure 37. Weld Tests, 5/8-Inch Thick

METALLOGRAPHIC EXAMINATION

Examination for Fatigue Damage in Broken Specimens

Specimen T4-1 and T4-2, tested at room temperature, were examined for evidence of plastic deformation at the crack tip and for other damage during fatigue cracking. The fracture face was bisected through the center of the crack. On one side of the center cut, parallel cuts were made so that the end of the fatigue crack and the beginning of the tension fracture could be examined.

No evidence of damage was observed in the microradiographs. In the fatigue portion of the crack profile, the fracture was mostly transgranular; while in the tension portion, the fracture was intergranular. No evidence of fatigue damage was observed adjacent to the fatigue crack or at the point of transition from fatigue to tension.

DISCUSSION

Metallographic examination of failed specimens and specimens sectioned after fatigue cracking revealed no evidence of plastic deformation or damage at the crack front that could be attributed to the cyclic stress history of the specimen.

No significant difference was observed in the load-strain curves on tests of the weld nugget before and after fatigue cracking.

A plot of K values versus the crack depth (a) $\div$ weld thickness indicates a K range of 18 to 22 $\sqrt{\text{inch}}$ for the room temperature tests. The data indicate a probable minimum value of K of 18 ksi $\sqrt{\text{inch}}$ for the 4043 filler wire 2014-T656 welds at room temperature.

A plot of crack dept $\div$ weld thickness versus apparent K showed a broad scatter band for the -423 F tests. However, theory indicates that the values with about a 50-percent crack depth for the thicker (5/8-inch) specimens would be the most valid for K. More tests would be required to establish a range or minimum values.

Surface cracks were fairly easy to identify with X-ray techniques after the room temperature proof test at 22.8 ksi on weld land specimens. This is believed to be caused by the bending mode of stress distribution.

The stress distribution on a land-type configuration would make surface cracks on the surface opposite the land (outer surface of the vehicle) critical at loads, while the inner (land side) surface of the weld would be noncritical.

FRACTURE TOUGHNESS OF 2014-T651 WELDMENTS, PHASE III

INTRODUCTION

Briefly, fracture mechanics states that a sharp defect will propagate rapidly if the stored elastic energy in the system exceeds the energy required to form new surface.

The purpose of this program was to acquire additional fracture toughness data on typical Saturn S-II 5/16-inch-thick weldments produced with Manufacturing tooling by Manufacturing personnel.

PROGRAM SUMMARY

Weldments

All weldments were prepared from 5/16-inch-thick 2014-T651 plate. Weldments using 4043 filler were made in the horizontal position, weldments using 2319 filler wire were welded in the vertical position by Manufacturing.

Specimens

All tests were on uniform (5/16-inch-thick) specimens. Transverse weld fracture toughness specimens, 4 inches wide by 20 inches long, were prepared from the 4043 and 2319 filler wire weldments. Three-inch gauge width longitudinal weld fracture toughness specimens were prepared from the 4043 filler wire weldments. Standard material property specimens with transverse welds were prepared from both the 4043 and the 2319 filler wire weldments.

Testing

The yield strength of the 2319 weld nugget was determined at room temperature, -300 F, and -423 F through the use of back-to-back strain gauges on the weld nugget. Standard uniaxial tests were conducted on the 4043 and 2319 filler wire weldments at room temperature, with a 3/8-inch gauge length extensometer across the weld nugget. Transverse fracture toughness tests were conducted at room temperature, -240 F, -300 F, and -423 F on weldments with both types of filler wire. Cyclic tests were conducted as indicated in the table footnotes prior to static loading to failure.

Fracture toughness tests on longitudinal specimens were conducted at room temperature, -300 F, and -423 F with weldments using 4043 filler wire only. Data for specimens cyclic-loaded prior to testing to failure are given in the table footnotes.

TEST PROCEDURES

All welded specimen blanks were fabricated from 5/16-inch-thick 2014-T651 plate in accordance with MB0170-021. The parent metal grain direction was in all cases parallel to the direction of the weld bead. All edges to be welded were machine-finished prior to welding. Pieces 6 x 72 inches were joined to form a 12- x 72-inch-long welded blank for longitudinal specimens. Pieces 10-1/4 x 72 inches were joined to form a 20-1/2 x 72-inch long welded blanks for transverse specimens. Blanks for longitudinal and transverse specimens were welded in the horizontal position by using 4043 filler wire and two passes from the one side in accordance with MA0107-016F.

Blanks for transverse specimens were welded in the vertical position on the Seal Beach Manufacturing vertical splice tool by Manufacturing personnel. All welded blanks passed dye-penetrant and X-ray inspection.

Yield strength of the 2319 weld nugget was determined on 3/8-inch gauge width by 0.250-inch-thick uniaxial test specimens with back-to-back 1/8-inch grid length strain gauges on the weld nugget. Tests were conducted on calibrated Universal test machines. Standard uniaxial specimens were taken from transverse weld specimen blanks and tested at room temperature by using a 3/8-inch gauge length extensometer across the weld.

Transverse weld specimens (Figure 38) were machined from the welded specimen blanks with 4043 filler wire and from the welded specimen blanks with 2319 filler wire. Longitudinal weld specimens (Figure 39) were machined from weld blanks with 4043 filler wire. A starter notch was either Elox machined or fly-cut in the specimens.

Fatigue cracking of the specimens was accomplished in bending on an SF-10 Sonntag fatigue tester shown in Figure 22. Crack growth observations were made with the use of a binocular microscope. All cracks were transverse to the direction of specimen loading.

Specimens were tested in calibrated Universal test machines with a load rate of 0.05 inch per minute of head travel. Cyclic tests were cycled as shown at the end of the data tables and then tested as previously outlined. The -240 F and -300 F tests were conducted in a controlled test chamber through the use of vaporizing liquid nitrogen as a coolant. Liquid hydrogen was used as a coolant for the -423 F tests.

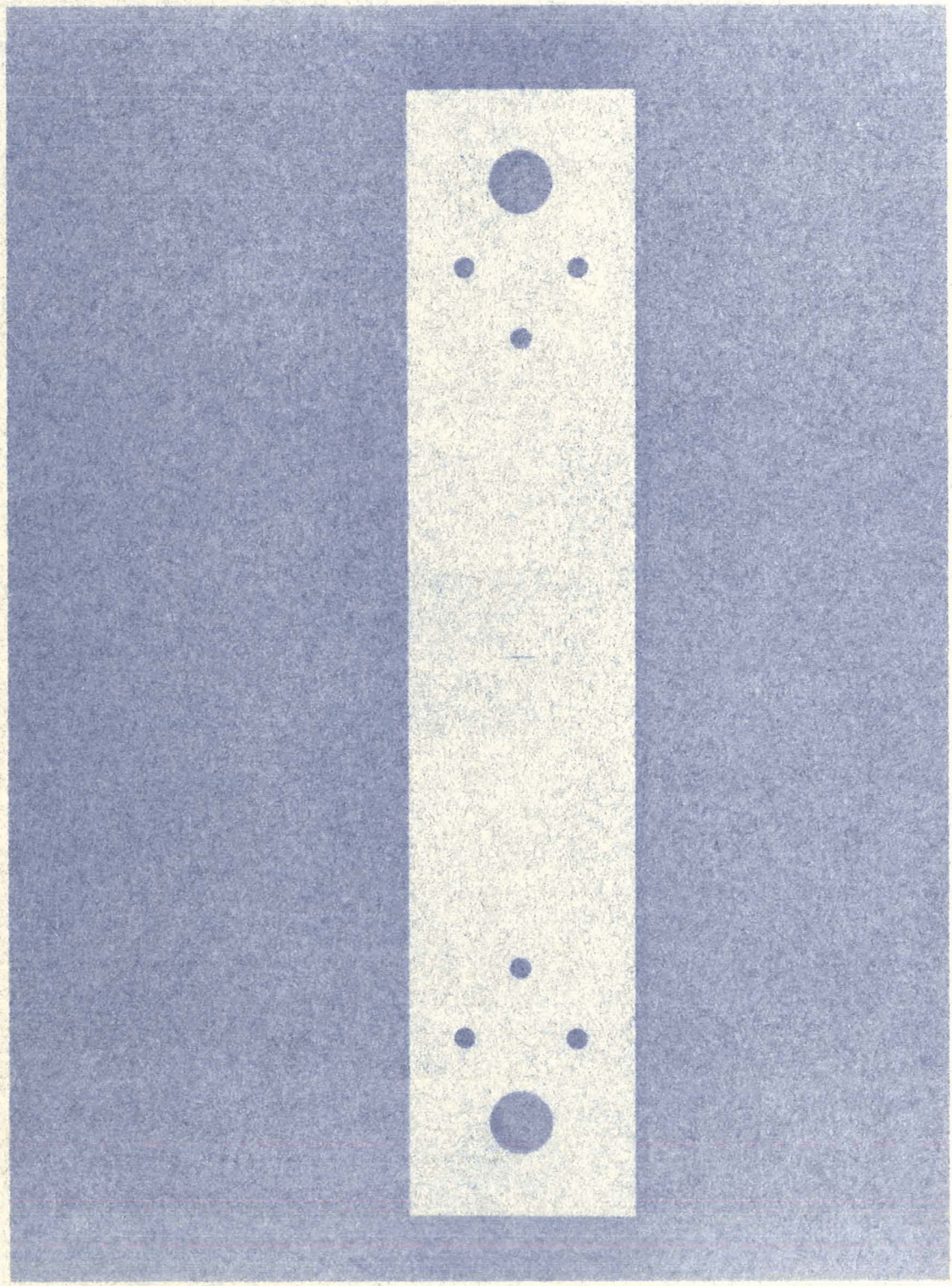

7006-81-2420E

Figure 38. Test Specimen - Transverse Weld

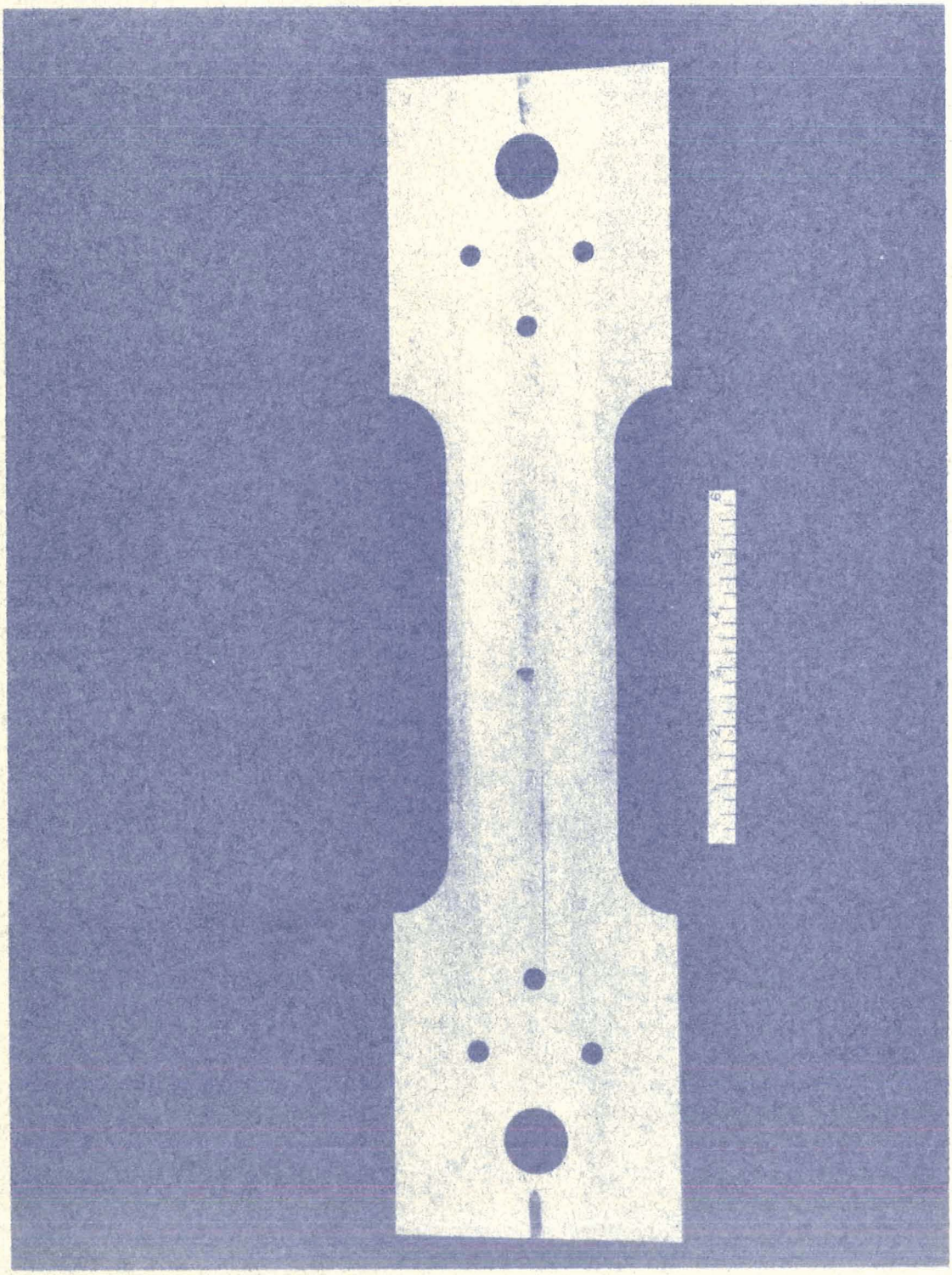

7006-81-2528A

Figure 39. Test Specimen - Longitudinal Weld

TEST RESULTS

Results on strain-gauged specimens tested at room temperature, -300 F, and -423 F to determine the yield strength of the 2319 filler wire weld nugget are presented in Table 13. A typical load-strain curve is shown in Figure 40.

Typical data for the transverse weld tests with 4043 filler wire are presented in Table 14. Typical flaws are shown in Figures 41 through 50. Plots of failure stress versus normalized flaw depth are shown in Figure 51, 52, and 53.

Typical data for the transverse weld tests with 2319 filler wire are presented in Table 15; typical flaws are shown in Figures 54 through 57. Graphs of failure stress versus normalized flaw depth are shown in Figures 58, 59, and 60.

Typical data for the longitudinal weld tests with 4043 filler wire are presented in Table 16. A plot of failure stress versus normalized flaw depth is shown in Figure 61.

No significant difference was observed between specimens using tension-tension and tension-compression stress cycles for fatigue flaw growth.

In fatigue cracking of longitudinal and transverse specimens with starter notches on the first pass side, trouble was encountered in using reversed bending stress. There was a tendency to fatigue-crack the specimen on the second pass side at the edges, in the weld or in the heat affected zone, before obtaining the desired crack growth in the starter notch on the first-pass side. Trouble of this type was not encountered for specimens with starter notches on the second-pass side. The trouble was attributed to residual tensile stress on the second-pass side. The cure used was of an unbalanced stress cycle (a low stress on the second-pass side where crack growth on the first-pass side was required).

Table 13. Uniaxial Tests - 2319 Filler Wire Weld Nugget - Specimen Average

Test Temperature	F_{tu} (ksi)	F_{ty} (ksi)
RT	48.9	25.35
-300	58.2	33.15
-423	63.85	41.35

RT - room temperature

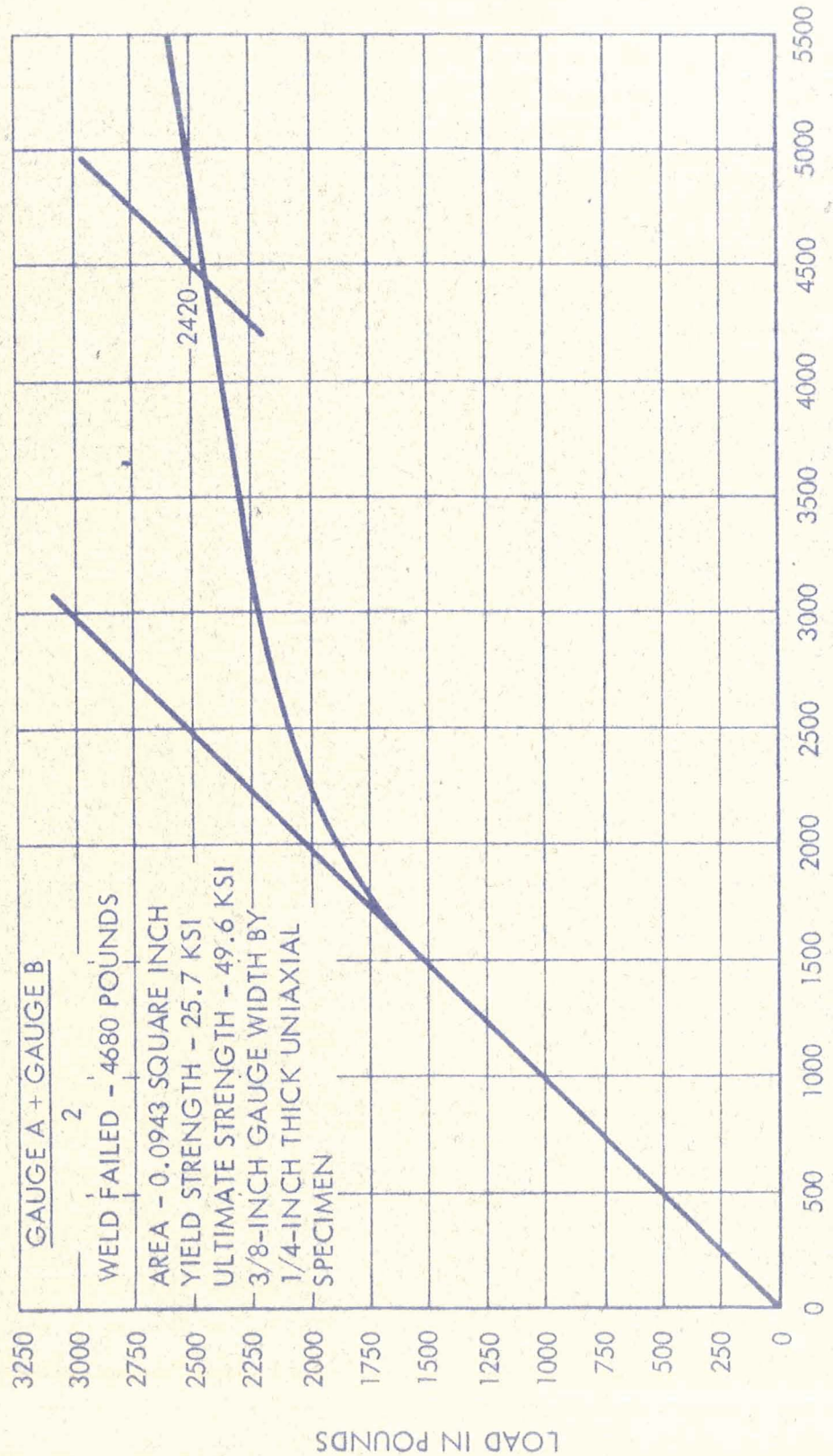

Figure 40. Load-Strain Curve, Specimen S3-1T-2319
Filler Wire Weld Nugget at Room Temperature

Table 14. Typical Transverse Weld Tests - 4043 Filler Wire

Weld Thickness (inches)	Gross Failure Stress (ksi)	Fatigue Crack				a/Q (inches)	Apparent K ksi $\sqrt{in.}$
		Stress (ksi)	Cycles (1000)	Crack Depth (a) (inches)	Crack Width (2c) (inches)		
TEMPERATURE: ROOM TEMPERATURE; TEST TYPE: STATIC; NOTCHED ON SECOND-PASS SURFACE							
0.330	30.51	14 15	60 60	0.119	0.519	0.100	19.0
0.332	28.05	16	25	0.142	0.615	0.118	19.1
TEMPERATURE: -240 F; TEST TYPE: STATIC, NOTCHED ON SECOND-PASS SURFACE							
0.320	33.28	14 13	30 90	0.105	0.476	0.090	19.5
0.322	29.09	14 13	40 40	0.163	0.579	0.116	19.7
TEMPERATURE: -300 F; TEST TYPE: STATIC; NOTCHED ON SECOND-PASS SURFACE							
0.315	36.03	14 13	40 220	0.060	0.369	0.059	17.3
0.317	38.06	14 13	50 150	0.060	0.425	0.062	18.6
TEMPERATURE: -423 F; TEST TYPE: STATIC, NOTCHED ON SECOND-PASS SURFACE							
0.316	31.62	13	40	0.092	0.442	0.081	16.8
0.332	29.00	16	83	0.142	0.533	0.104	18.5

Table 14. Typical Transverse Weld Tests - 4043 Filler Wire (Cont)

Weld Thickness (inches)	Gross Failure Stress (ksi)	Fatigue Crack				a/Q (inches)	Apparent K ksi $\sqrt{\text{in.}}$
		Stress (ksi)	Cycles (1000)	Crack Depth (a) (inches)	Crack Width (2c) (inches)		
TEMPERATURE: ROOM TEMPERATURE; TEST TYPE: CYCLIC; NOTCHED ON SECOND-PASS SURFACE							
0.331	33.86	14	21	0.049	0.502	0.061	16.2
0.332	30.50	14	70	0.090	0.485	0.086	17.0
TEMPERATURE: -423 F; TEST TYPE: CYCLIC; NOTCHED ON SECOND-PASS SURFACE							
0.315	31.90	15 14	15 10	0.148	0.506	0.102	19.8
0.308	32.71	15	42	0.135	0.558	0.103	20.5
TEMPERATURE: ROOM TEMPERATURE; TEST TYPE: STATIC; NOTCHED ON FIRST-PASS SURFACE							
0.318	39.28	14 13	22 120	0.033	0.325	0.038	15.0
0.317	37.04	14	102	0.074	0.388	0.068	19.0
TEMPERATURE: -300 F; TEST TYPE: STATIC; NOTCHED ON FIRST-PASS SURFACE							
0.317	42.32	14 13	22 10	0.054	0.393	0.056	19.5
0.324	39.74	14 13	40 125	0.070	0.376	0.065	19.7
TEMPERATURE: -423 F; TEST TYPE: STATIC; NOTCHED ON FIRST-PASS SURFACE							
0.319	43.06	14 13	20 135	0.054	0.389	0.057	20.0
0.316	43.51	14 13	40 130	0.073	0.408	0.066	21.5

Table 14. Typical Transverse Weld Tests - 4043 Filler Wire (Cont)

Weld Thickness (inches)	Gross Failure Stress (ksi)	Fatigue Crack				a/Q (inches)	Apparent K ksi $\sqrt{\text{in.}}$
		Stress (ksi)	Cycles (1000)	Crack Depth (a) (inches)	Crack Width (2c) (inches)		
TEMPERATURE: ROOM TEMPERATURE; TEST TYPE: CYCLIC; NOTCHED ON FIRST-PASS SURFACE							
0.316	31.11	14	50	0.099	0.459	0.086	18.0
TEMPERATURE: -423 F; TEST TYPE: CYCLIC; NOTCHED ON FIRST-PASS SURFACE							
0.322	38.79	15 14	20 60	0.096	0.425	0.077	20.6
0.317	32.20	15 14	20 160	0.152	0.552	0.107	20.5

Note: Nominal 4-inch specimens. Failure stress based on weld thickness. Cyclic tests: One cycle room temperature 11,000 psi 34 cycles at test temperature 6,6000 psi, then static tested to failure.
a/Q - normalized flaw depth

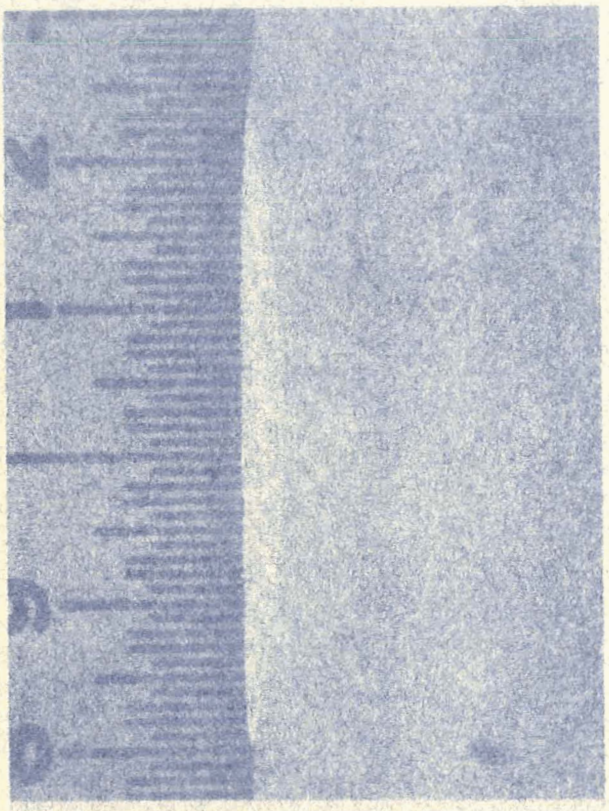

Figure 41. Specimen 34-4, Room Temperature, Static, 4043 Filler Wire, 0.035-Inch Depth Second Pass Flaw

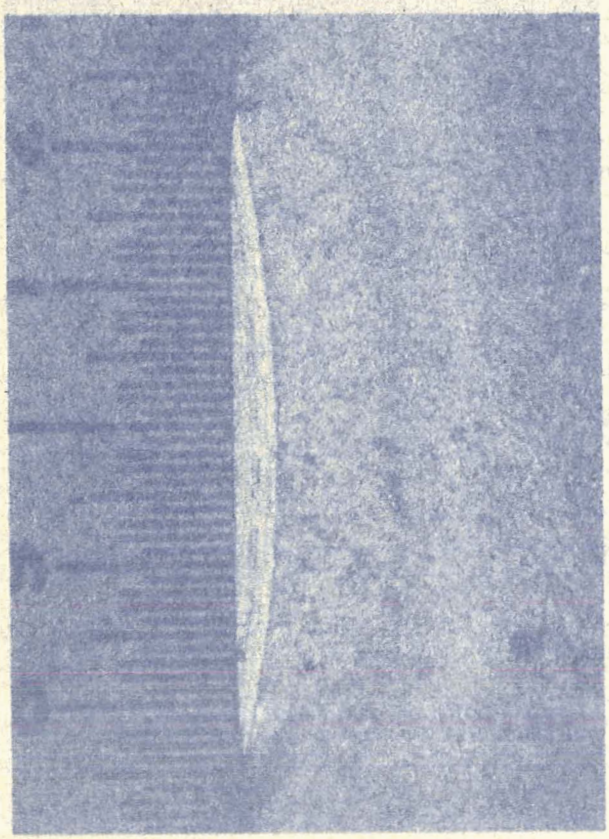

Figure 42. Specimen 34-11, Room Temperature, Static, 4043 Filler Wire, 0.055-Inch Depth Second Pass Flaw

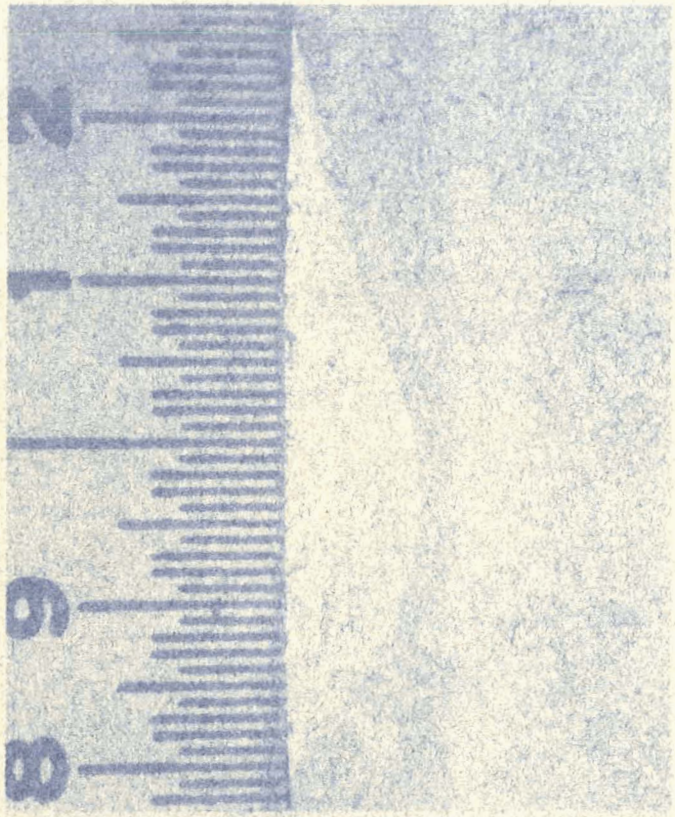

Figure 43. Specimen 35-3, -300 F, Static, 4043 Filler Wire, 0.085-Inch Depth Second Pass Flaw

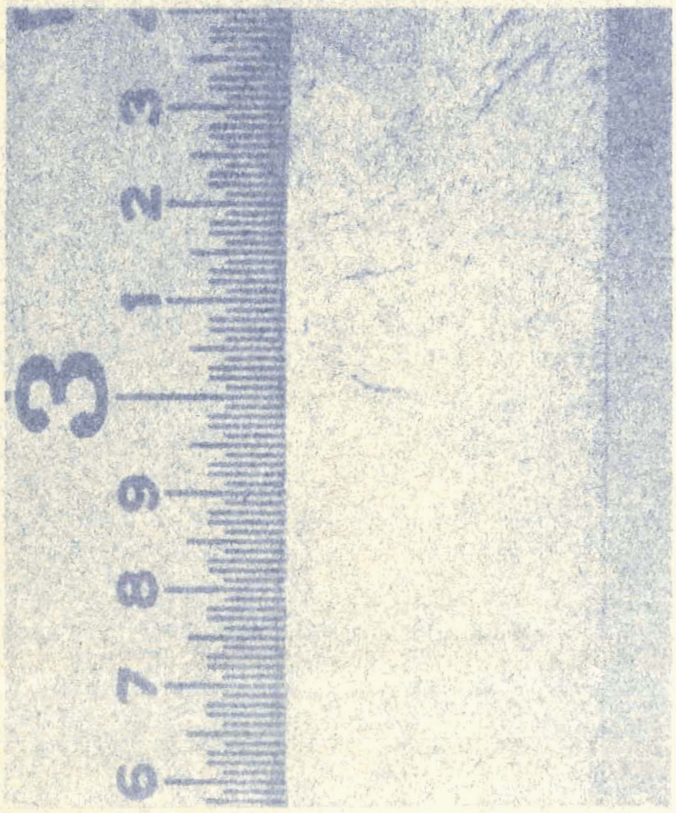

Figure 44. Specimen 32-2, -300 F, Static, 4043 Filler Wire, 0.180 Inch Depth Second Pass Flaw

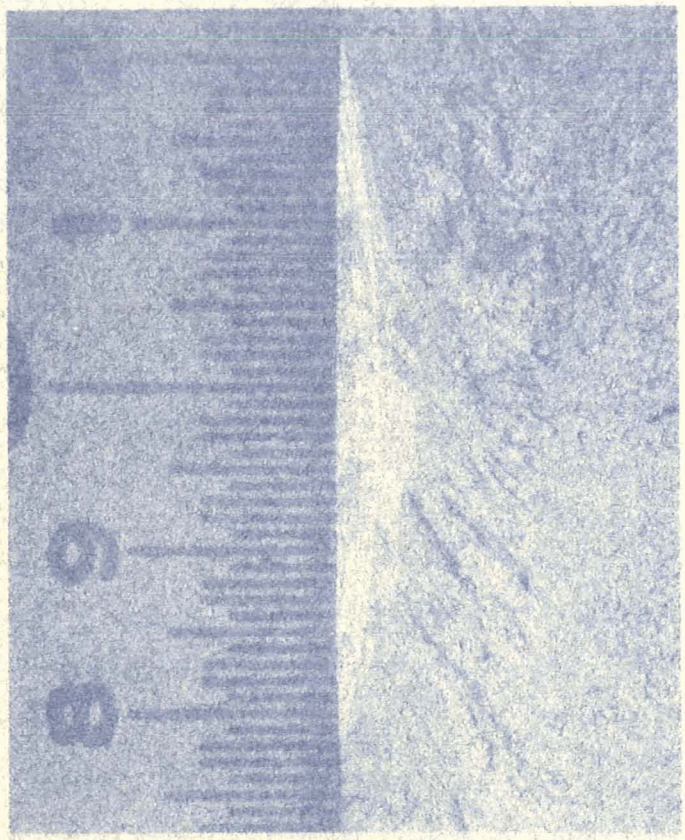

Figure 45. Specimen 33-12, -423 F, Static, 4043 Filler Wire, 0.053-Inch Depth Second Pass Flaw

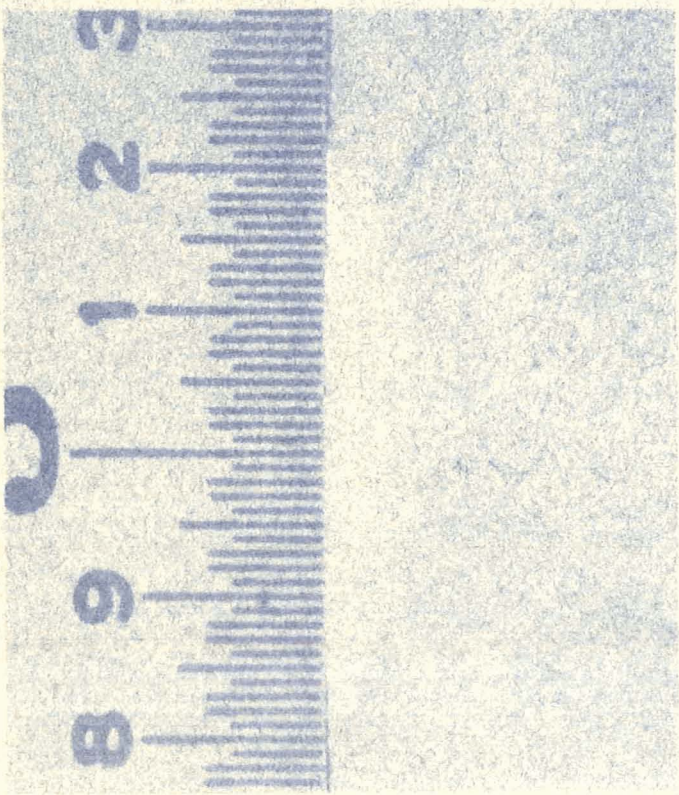

Figure 46. Specimen 34-3, -423 F, Static, 4043 Filler Wire, 0.062-Inch Depth Second Pass Flaw

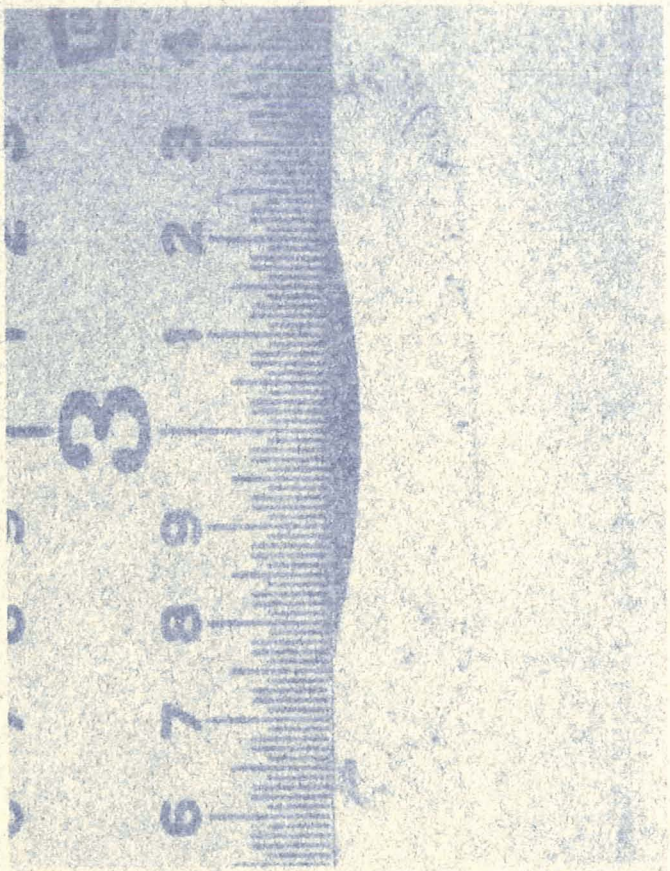

Figure 47. Specimen 32-10, Room Temperature, -Cyclic, 4043 Filler Wire, 0.160-Inch Depth Second Pass Flaw

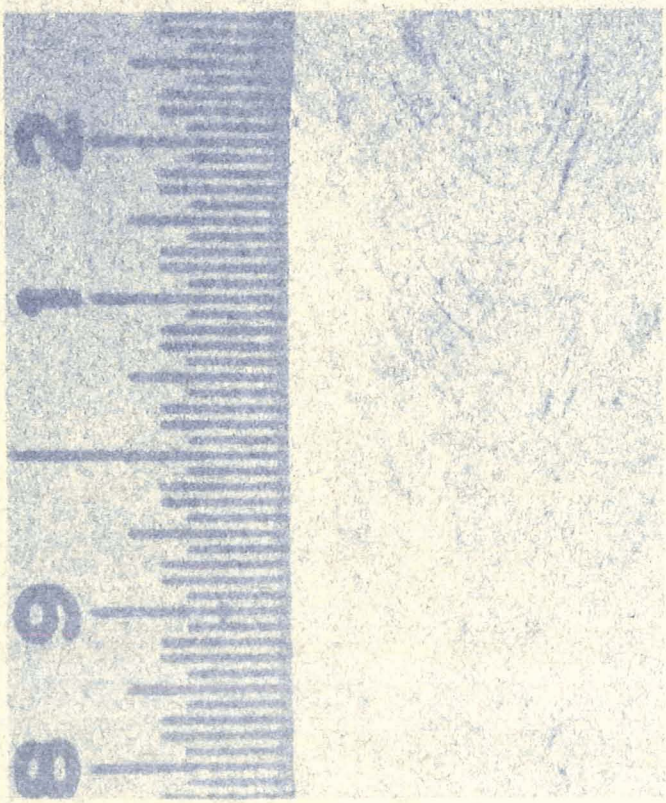

Figure 48. Specimen 35-7, -423 F, Cyclic, 4043 Filler Wire, 0.104-Inch Depth Second Pass Flaw

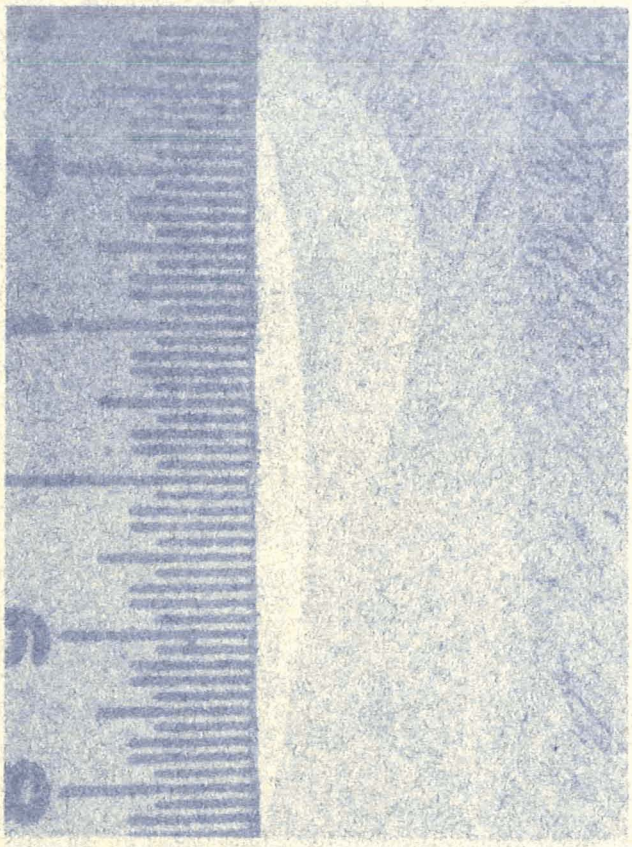

Figure 49. Specimen 35-12, -423 F, Static, 4043 Filler Wire, 0.108-Inch First Pass Flaw

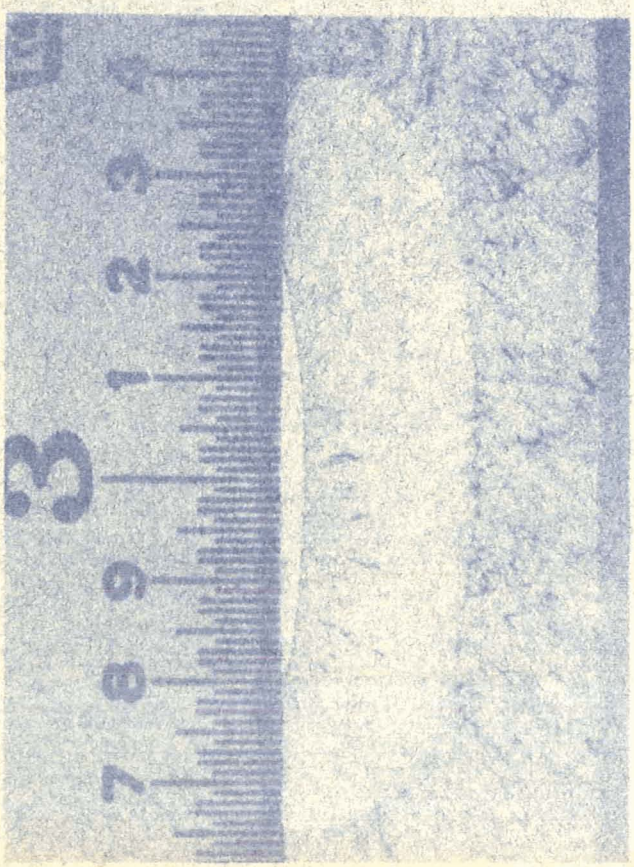

Figure 50. Specimen 33-1, -423 F, Cyclic, 4043 Filler Wire, 0.150-Inch First Pass Flaw

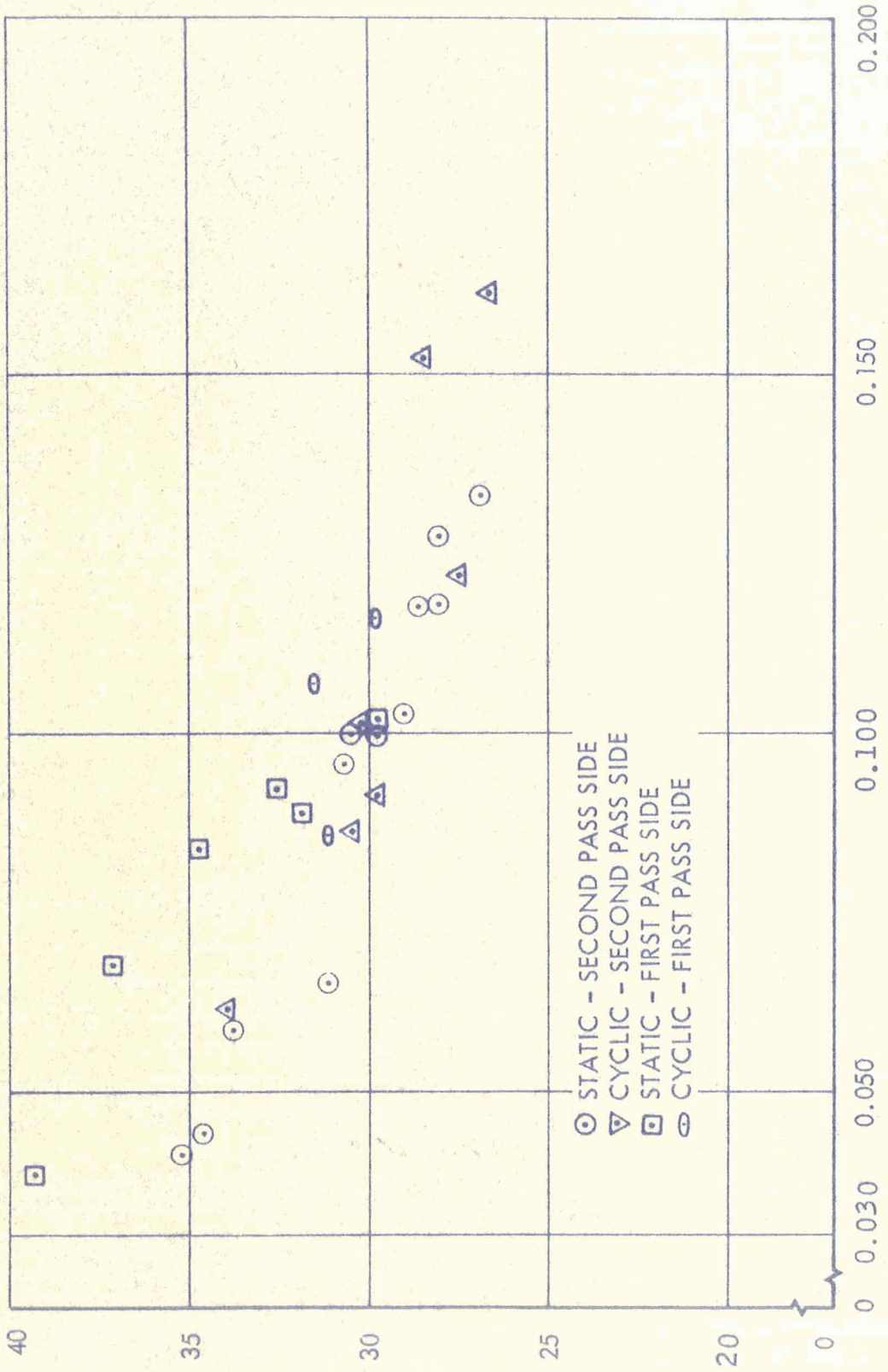

Figure 51. Failure Stress Versus Normalized Flaw Depth, 4043 Filler Wire, Transverse Welds, Room Temperature Tests

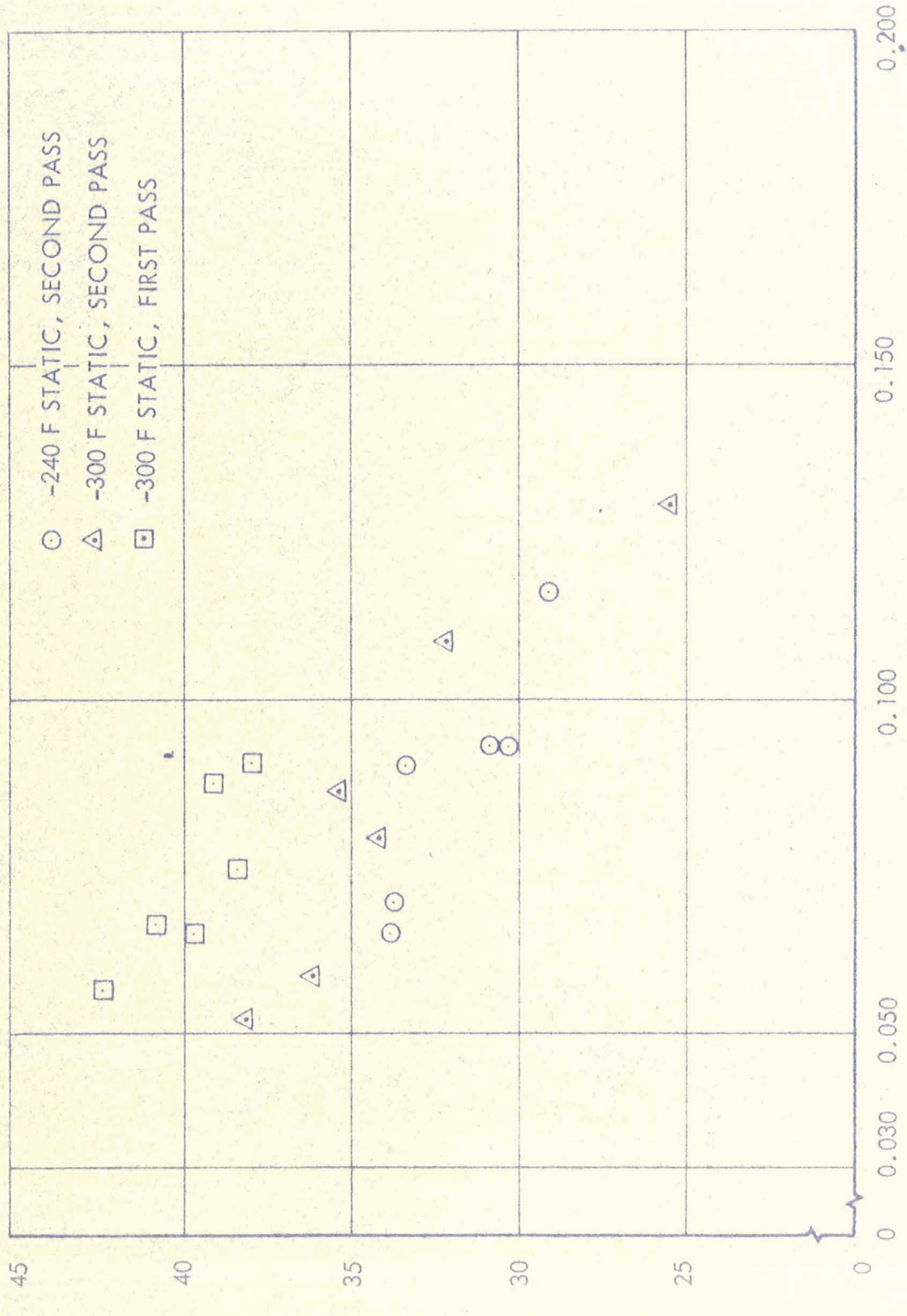

Figure 52. Failure Stress Versus Normalized Flaw Depth, 4043 Filler Wire, Transverse Welds, -240 F and -300 F Tests

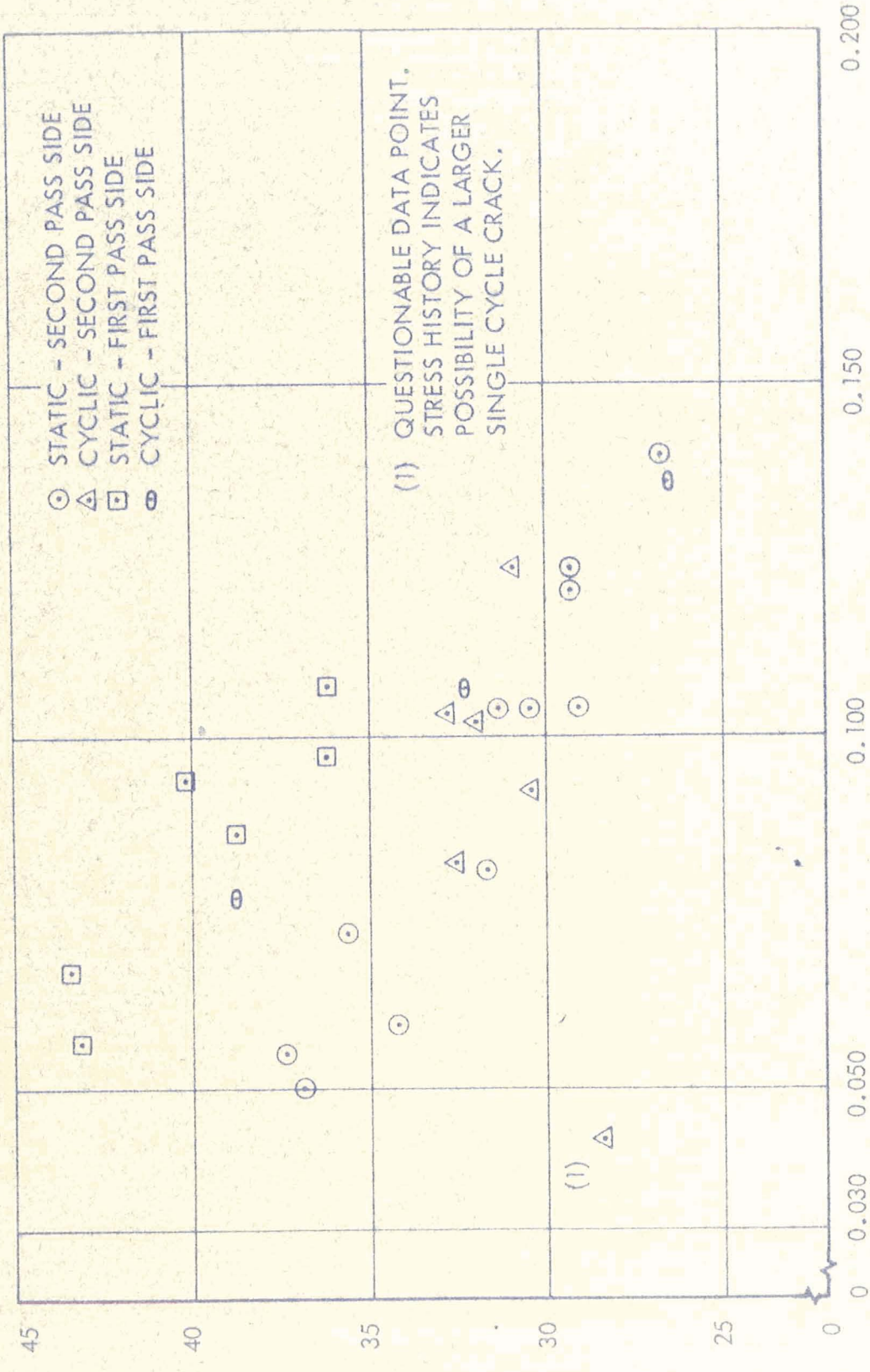

Figure 53. Failure Stress Versus Normalized Flaw Depth, 4043 Filler Wire, Transverse Welds, -423 F Tests

Table 15. Typical Transverse Weld Tests - 2319 Filler Wire

Weld Thickness (inches)	Gross Failure Stress (ksi)	Fatigue Crack				a/Q (inches)	Apparent K ksi $\sqrt{\text{in.}}$	Side of Weld Notched
		Stress (ksi)	Cycles (1000)	Crack Depth (a) (inches)	Crack Width (2c) (inches)			
ROOM TEMPERATURE TESTS - STATIC								
0.329	26.91	20	120	0.170	0.693	0.142	19.8	Second pass
0.321	27.68	20	107	0.195	0.793	0.163	21.5	Second pass
-240 F - STATIC								
0.332	36.22	18	60	0.100	0.503	0.093	21.2	Second pass
0.330	29.12	18	115	0.146	0.524	0.108	19.0	Second pass
-300 F - STATIC								
0.329	40.29	18 17	60 40	0.089	0.480	0.083	22.2	Second pass
0.332	40.03	16	180	0.089	0.603	0.090	23.1	Second pass
-423 F - STATIC								
0.330	27.35	18	50	0.160	0.566	0.110	17.8	Second pass
0.324	23.57	18	70	0.184	0.727	0.134	17.0	Second pass

Table 15. Typical Transverse Weld Tests - 2319 Filler Wire (Cont)

Weld Thickness (inches)	Gross Failure Stress (ksi)	Fatigue Crack				a/Q (inches)	Apparent K ksi $\sqrt{\text{in.}}$	Side of Weld Notched
		Stress (ksi)	Cycles (1000)	Crack Depth (a) (inches)	Crack Width (2c) (inches)			
ROOM TEMPERATURE - CYCLIC								
0.322	36.44	14	160	0.067	0.515	0.072	19.3	Second pass
0.323	34.39	14	170	0.077	0.457	0.075	18.9	Second pass
-240 F - CYCLIC								
0.330	37.67	18	80	0.088	0.487	0.085	21.2	Second pass
0.328	34.95	17	100	0.103	0.570	0.099	21.2	Second pass
-330 F - CYCLIC								
0.331	38.72	17	70	0.086	0.511	0.085	21.5	Second pass
0.330	38.61	17	100	0.090	0.578	0.092	22.3	Second pass
-423 F - CYCLIC								
0.326	36.64	18 17	90 20	0.116	0.507	0.097	22.5	Second pass
0.329	34.32	17	100	0.106	0.580	0.097	20.7	Second pass

a/Q - normalized flow depth

Figure 54. Specimen S3-3, -423 F, Static 2319 Filler Wire, 0.188-Inch Depth

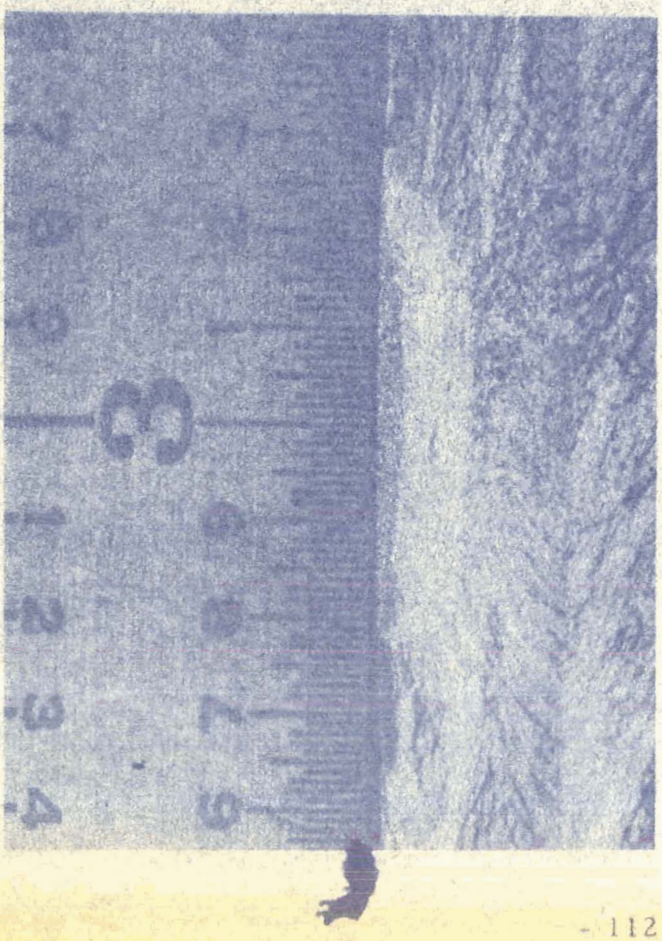

Figure 55. Specimen S1-10, Room Temperature, Cyclic, 2317 Filler Wire, 0.098-Inch Depth

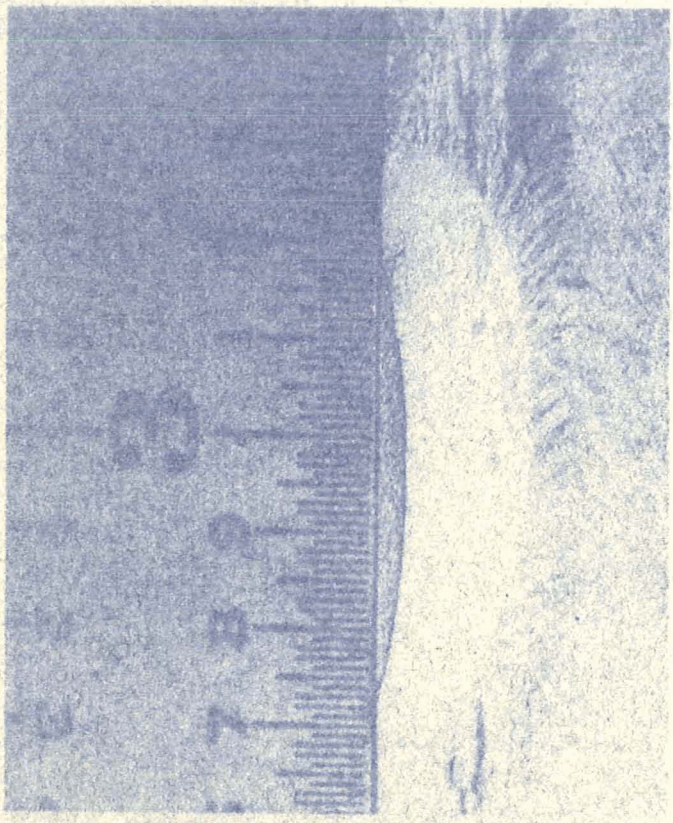

Figure 56. Specimen S4-14, -423 F, Cyclic, 2319 Filler Wire, 0.160-Inch Depth

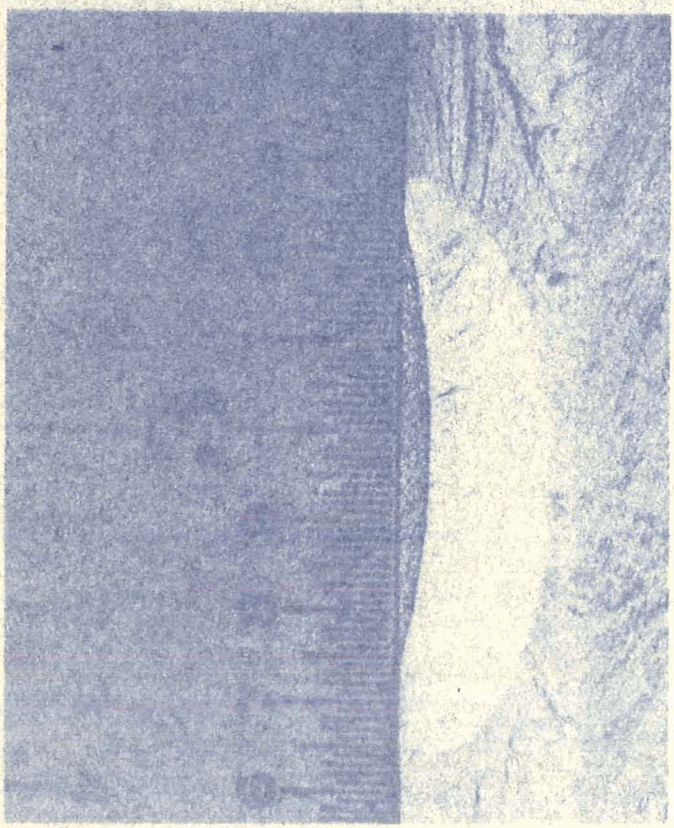

Figure 57. Specimen S1-15, -423 F, Cyclic, 2319 Filler Wire, 0.165-Inch Depth

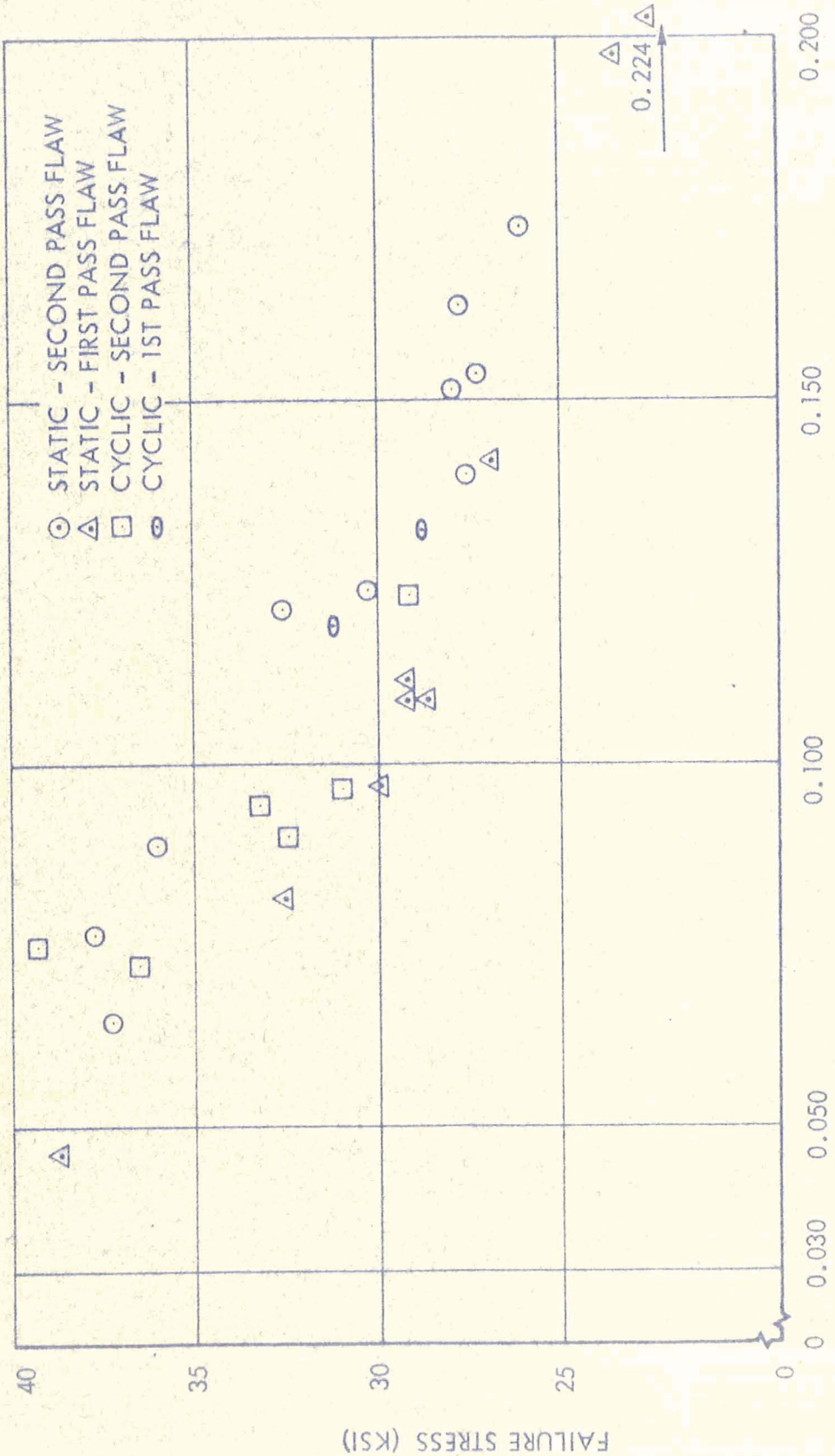

Figure 58. Failure Stress Versus Normalized Flaw Depth, 2319 Filler Wire, Transverse Welds, Room Temperature

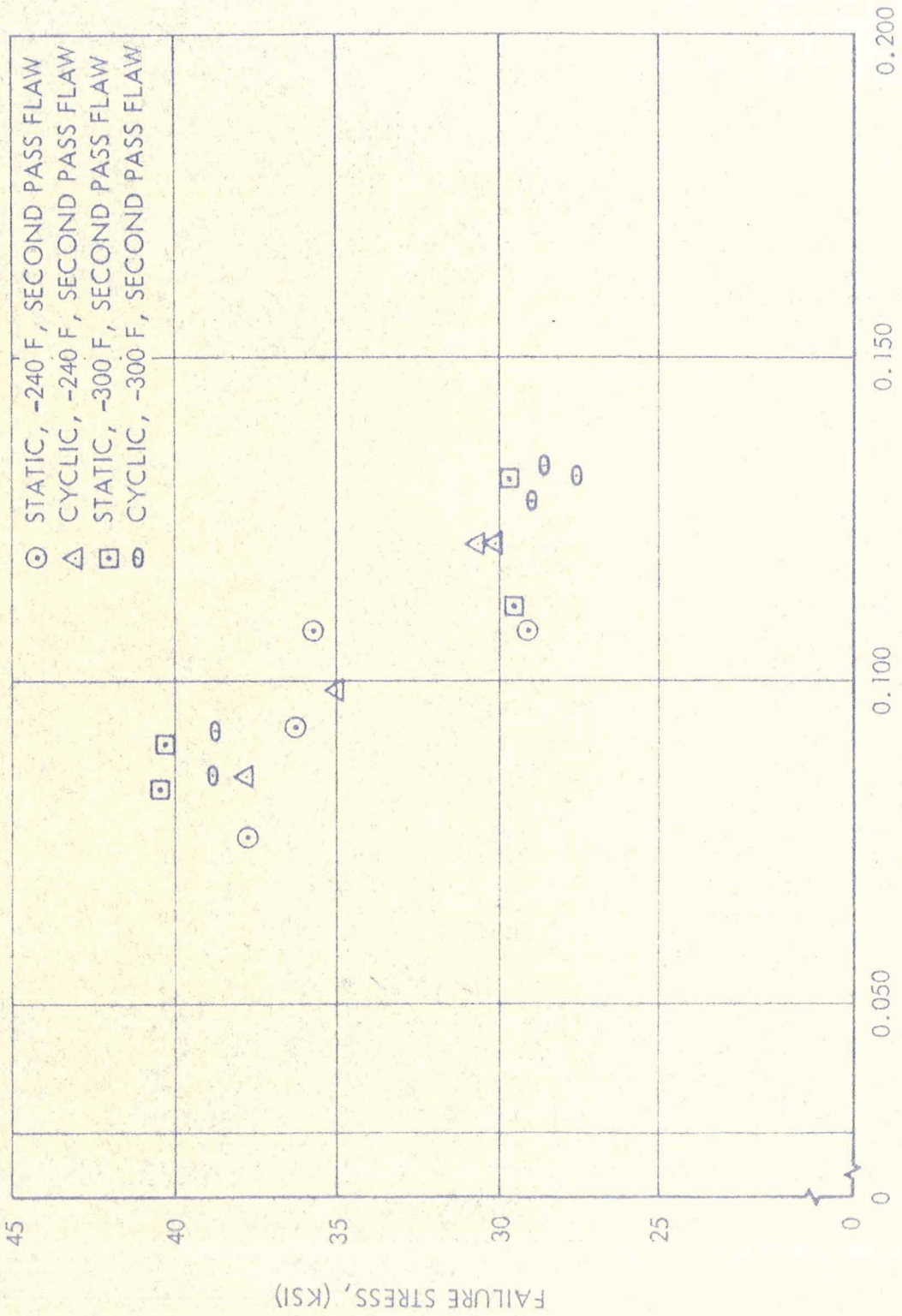

Figure 59. Failure Stress Versus Normalized Flaw Depth, 2319 Filler Wire, Transverse Welds, -240 F and -300 F Tests

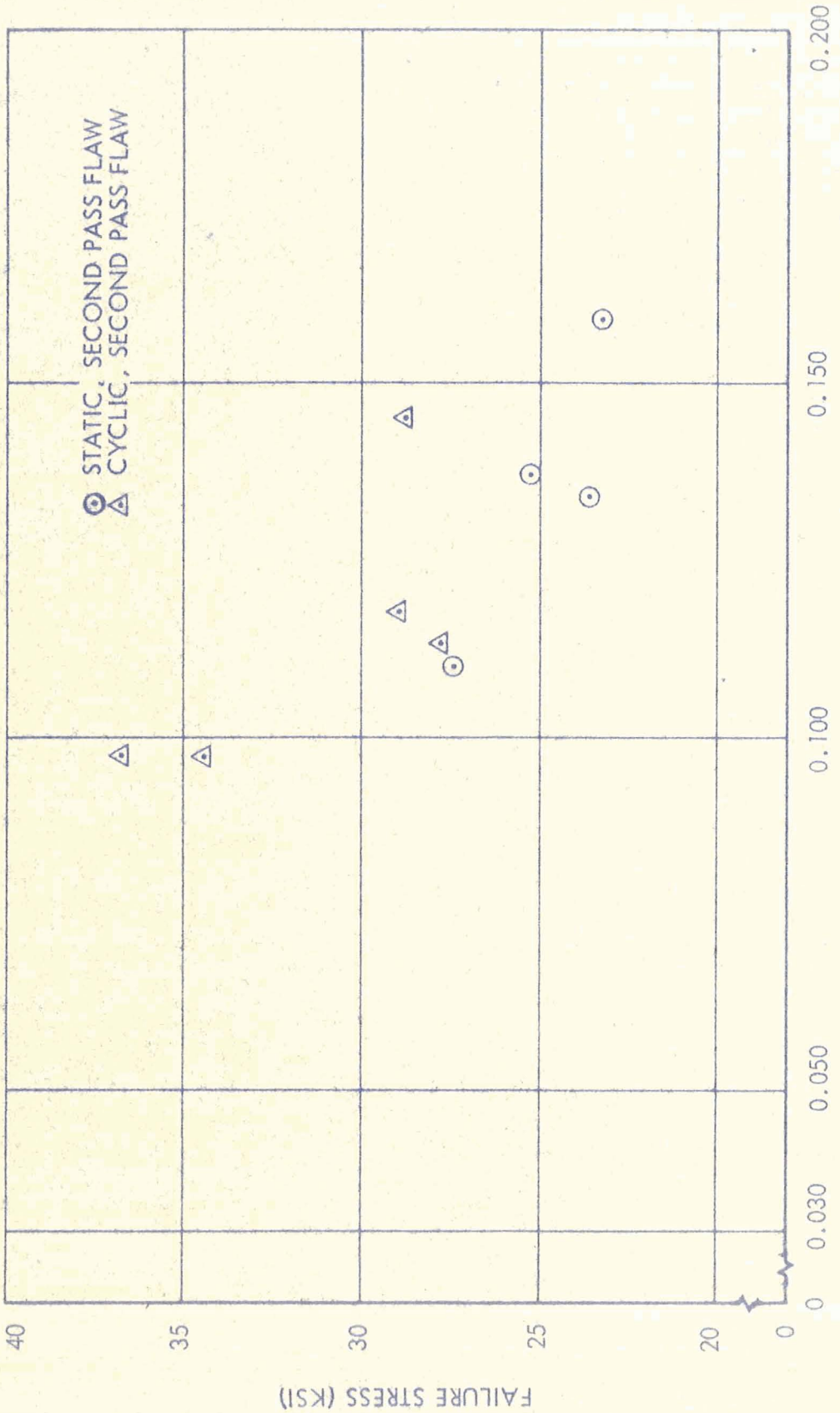

Figure 60. Failure Stress Versus Normalized Flaw Depth, 2319 Filler Wire, Transverse Welds, -423 F

Table 16. Typical Longitudinal Weld Tests - 4043 Filler Wire Welds

Weld Parent Thickness (inches)	Gross Failure Stress (ksi)	Fatigue Crack				a/Q (inches)	Side of Weld Notched
		Stress (ksi)	Cycles (1000)	Crack Depth (a) (inches)	Crack Width (2c) (inches)		
ROOM TEMPERATURE - STATIC							
0.336	58.40	15	20	0.116	0.369	0.080	Second pass
0.336	49.28	13	40	0.142	0.464	0.099	Second pass
-300 - STATIC							
0.334	59.14	15	30	0.073	0.384	0.067	Second pass
0.336	56.2	15	20	0.112	0.382	0.081	Second pass
-423 - STATIC							
0.338	57.12	12	82	0.073	0.366	0.066	Second pass
0.337	57.20	13	60	0.154	0.502	0.107	Second pass
ROOM TEMPERATURE - CYCLIC							
0.336	47.64	12	26	0.178	0.583	0.124	Second pass
0.337	47.02	13	10	0.195	0.695	0.142	Second pass

Table 16. Typical Longitudinal Weld Tests - 4043 Filler Wire Welds (Cont)

Weld Parent Thickness (inches)	Gross Failure Stress (ksi)	Fatigue Crack				a/Q (inches)	Side of Weld Notched
		Stress (ksi)	Cycles (1000)	Crack Depth (a) (inches)	Crack Width (2c) (inches)		
-300 - CYCLIC							
0.338	58.41	15	50	0.118	0.410	0.086	Second pass
0.338	56.06	12	30	0.166	0.513	0.111	Second pass
-423 - CYCLIC							
0.334	58.30	13	60	0.155	0.466	0.101	Second pass
0.331	59.30	13	65	0.160	0.482	0.105	Second pass

Note: Nominal 3-inch gauge width specimen. (Failure stress based on parent metal thickness.) Cyclic Tests: One cycle at room temperature to 33.7 ksi; 34 cycles at test temperature to 20.2 ksi, then tested to failure.
a/Q - normalized flaw depth

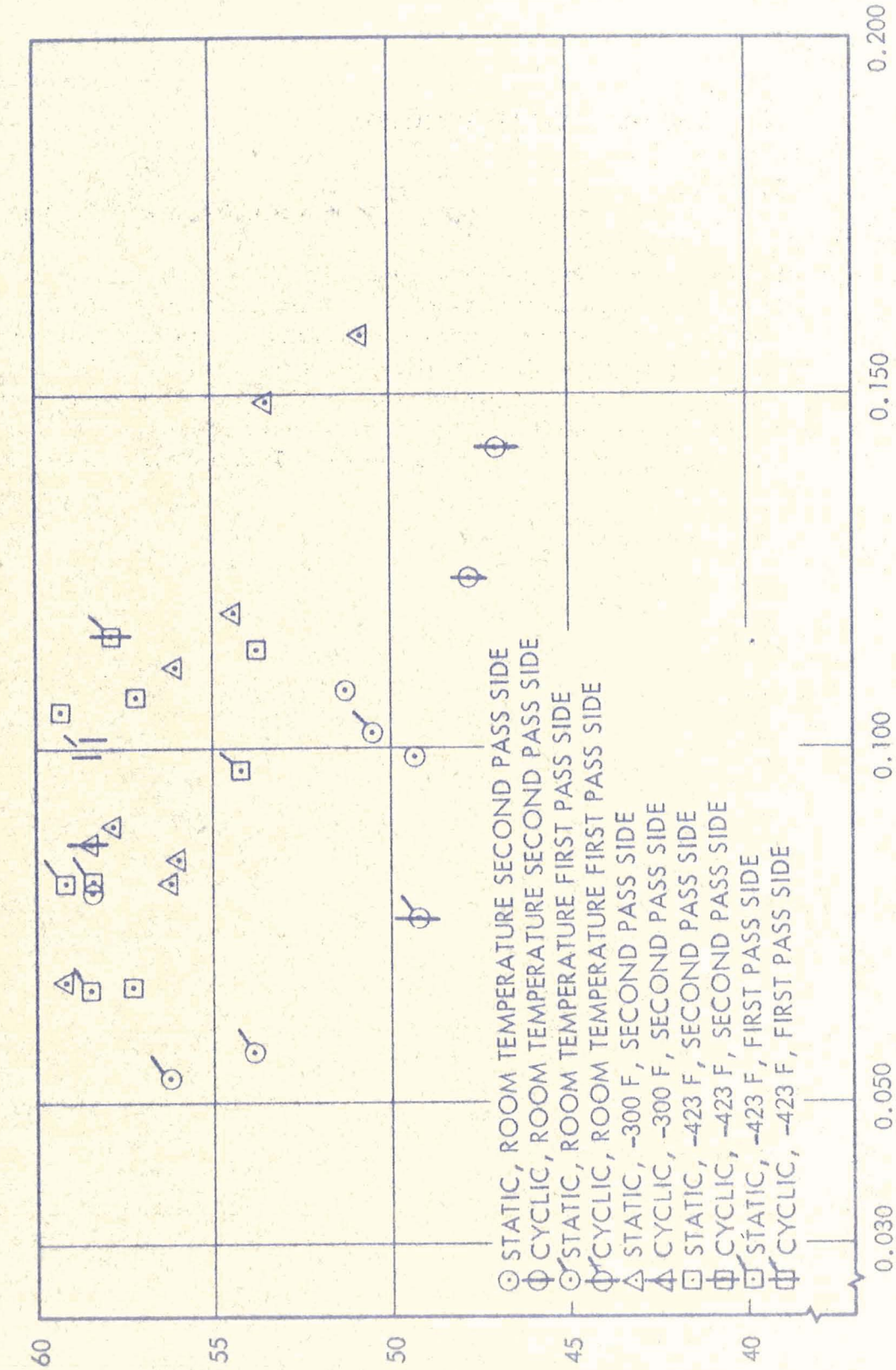

Figure 61. Failure Stress Versus Flaw Depth, Longitudinal Weld Specimens, 4043 Filler Wire

WELDING, MISCELLANEOUS

PROGRESS SUMMARY

Numerous miscellaneous welding studies were performed in support of the Saturn Program. One study includes repair welding; another covers the possible effect of magnetic-hammer flattening on the microstructure of the weld. A study was performed on the properties of dissimilar metal weldments (Haynes 718 to 321 CRES) to support feedline fabrication. The effect of weld thinning on feedline components also was studied, as was the effect of two-sided TIG welding on the mechanical properties of offset weld joints.

MECHANICAL TESTING AND METALLURGICAL EXAMINATION OF WELDED 2014-T651 ALUMINUM SHEET AFTER FLATTENING WITH MAGNETIC HAMMER

INTRODUCTION

This report covers the results of tests applied to the welds of 5/16-inch sheet after magnetic-hammer flattening.

The tests were conducted to determine the effect of porosity on the properties of welds subjected to correction of significant contour discrepancies, such as weld peaking, by magnetic-hammer flattening. Also determined was the effect of magnetic-hammer flattening on the microstructure and possible propagation of fractures initiating at pore sites.

CONCLUSIONS

No detrimental effect on porosity was observed in welded 5/16-inch panels after they were flattened by the magnetic hammer and no crack initiation occurred in the welds. However, two of the 5/16-inch panels cracked at the weld edge in the heat-affected zone.

PROCEDURE

Seven 5/16-inch-thick panels were fabricated, penetrant-inspected, radiographically inspected, and measured. The panels were subjected to flattening by a series of hits with the magnetic hammer in one or more passes along the length of the weld of each panel. After flattening, each panel was reinspected by penetrant and radiographic methods and compared with similar inspections applied before flattening.

Based on the radiographic inspection, two appropriate tensile coupons and one adjacent metallographic specimen were taken from each panel. (An appropriate coupon was one having a porosity level near the maximum allowed by Specification MA0107-016. As listed in the results in Table 17, the maximum was exceeded in 10 of the 14 coupons tested.)

Each coupon was radiographically and penetrant-inspected and measured for peaking and offset before tensile testing for ultimate strength and percent of elongation. The metallographic specimens were prepared and examined for evidence of microstructural change and for evidence of fracture at initiation sites at the pores.

Table 17. Porosity Measurement of Tensile Coupons

Panel No.	Identity of Tensile Coupons	Discontinuity Area* in Tensile Coupon (sq in. x 10^{-4})
B3-4-1	7	58.4
	9	21.8
B-3-4-2	19	22.8
	21	47.8
B3-4-3	4	14.1
	5	26.3
B3-4-4	16	29.4
	17	28.5
B3-4-5	13	31.6
	14	37.6
B3-4-6	1	18.9
	2	35.5
B3-4-7	11	43.8
	12	52.8

*Discontinuity limits per Welding Specification MA0107-016 are 24.63 x 10^{-4} per inch of weld or 0.004926 per 6 inches of weld.

RESULTS

The results of radiographic inspection before flattening were compared with radiographic inspection after flattening by X-ray films. No change was observed in the number, size, or contour of the porosity in the welds. Radiography results of the tensile coupons are also shown in Table 17.

After magnetic flattening, summary data of the alignment, inspection, and tensile properties of the 5/16-inch welds are shown in Table 18. In each instance, the tensile coupons broke at the weld edge.

Metallographic examination of specimens from each panel revealed no initiation of fracture in the porosity and no significant changes in microstructure of either weld or parent metal.

DISCUSSION AND SUMMARY

The ultimate strength of the 5/16-inch porosity panels was somewhat lower than that encountered in the control, repair, and cracked panels.

Averages are as follows for ultimate strength after flattening:

Control	Repair*	Cracked	Porosity
50.7 ksi	48.7 ksi	50.1 ksi	45.0 ksi
Range 49.4-51.3	37.4-52.9	46.3-52.2	42.7-49.2

*Average includes tensile tests outside repaired areas only.

The power employed for flattening was greater for the porosity panels than for the others. The average power per pass for each category is as follows:

Control	Repair	Cracked	Porosity
Average 3170 volts	3880 volts	4430*	4280 volts
Range 3000-3500	2400-5000	4000-5500	3000-6000

*One panel cracked at 5500 volts and suffered severely reversed peaking. The other panel in this category received 2-1/2 passes at 4000 volts.

Table 18. Summary Data After Magnetic-Hammer Flattening of Inspection, Alignment and Tensile Properties of the 5/16-Inch-Thick Weld Specimen

Coupon Number	Coupon Inspection Fluorescent Penetrant Indications	Magnetic-Hammer Flattening		Alignment/ Specimen		Mechanical-Property Results		
		No. of Passes	No. of Hits	Weld Angle	Weld Offset	UTS (ksi)	Percent Elongation	
							1/2-inch	2 inches
	Notch at weld-parent metal interface	1	33					
		1	32					
		1	31					
		1	16					
7				23'	0.0177	44.7	6.0	2.5
9				1°	0.0083	44.9	4.0	1.5
	Notch at weld-parent metal interface	1*	32					
19				2°22'	0.0164	42.7	5.0	2.0
21				2°40'	0.0027	42.7	4.0	1.5
		1	9*					
		1	9*					
		1	28					
		1	26					
		1	28					
4				1°	0.0133	49.2	8.0	2.5
5				46'	0.0064	48.3	6.0	2.5
	Notch at weld-parent metal interface	1**	34					
16				6°20'	0.0023	43.7	6.0	2.5
17				6°33'	0.0057	43.9	6.0	2.5

*Panel broke along weld near center of length during first pass.
**Specimen cracked along weld bead during first pass.
UTS—ultimate tensile strength

Table 18. Summary Data After Magnetic-Hammer Flattening of Inspection, Alignment and Tensile Properties of the 5/16-Inch-Thick Weld Specimen (Cont)

Coupon Number	Coupon Inspection Fluorescent Penetrant Indications	Magnetic-Hammer Flattening		Alignment/ Specimen		Mechanical Property Results		
		No. of Passes	No. of Hits	Weld Angle	Weld Offset	UTS (ksi)	Percent Elongation 1/2-inch	Percent Elongation 2 inches
	Notch at weld-parent metal interface	1 1 1	26 34 26					
13				1°36'	0.0000	42.9	4.0	1.7
14				1°46'	0.0017	45.9	4.0	1.7
	Notch at weld-parent metal interface	1 1 1 1	21 23 25 27					
1				46'	0.0114	46.3	6.0	2.5
2				18'	0.0084	45.4	6.0	2.5
	Notch at weld-parent metal interface	1 top 1 bottom 1 top 1 top 1 top 1 top	 37 28 24 39					
11				2°49'	0.0044	43.9	4.0	2.5
12				46'	0.0024	45.9	6.0	2.5

UTS—ultimate tensile strength

SPACE DIVISION OF NORTH AMERICAN ROCKWELL CORPORATION

EVALUATION OF INCONEL 82 WELD FILLER MATERIAL FOR S-II LH_2 FEEDLINES

INTRODUCTION

TIG butt welds of Haynes 718 alloy to 321 stainless steel with Inconel 82 filler material were used to fabricate Saturn LH_2 feedlines. Data required to determine if these welds would meet S-II design requirements included the strength and apparent ductility of TIG-welded Haynes 718 alloys to 321 stainless steel, using Inconel 82 filler material.

PROCEDURE

A welded panel of 0.050-inch gauge 321 stainless steel and 0.050-inch gauge Haynes 718 alloy was TIG welded with the Inconel 82 filler material. The panel was welded by the LH_2 feedline supplier, Solar Aircraft, San Diego.

The panel was machined into weld tensile test specimens and weld-bend test specimens. All specimens were fluorescent dye penetrant-inspected for cracks. The tensile specimens were then tested in liquid hydrogen (-423 F) to determine the ultimate strength, F_{tu}, and the percent elongation in 2-inch and 1/2-inch gauge lengths. A crosshead loading rate of 0.10-inch per minute was used.

The bend test specimens were bend-tested to the proper deflection, achieving the 45-degree included angle while the specimen was under load. The support span for the bend fixture was 2 inches and the loading ram had a 1/2-inch radius. After the bend tests, the specimens were again fluorescent dye penetrant-inspected for cracks.

RESULTS

The results of the tensile tests are listed in Table 19. The bend specimens yielded in the heat-affected zone of the Haynes 718 alloy. The fluorescent-penetrant inspection did not reveal cracks in any of the specimens inspected, before or after testing.

Table 19. Minus 423 F (LH_2 Immersion) Weld Tensile Test Data

Specimen Number	Ultimate Strength (ksi)	Percent Elongation		Remarks
		1/2 inch	2 inches	
1	181.1	20.0	22.5	Heat-affected zone in Haynes 718
2	176.2	26.0	24.5	Heat-affected zone in Haynes 718
3	168.0	24.0	22.0	Heat-affected zone in Haynes 718
4	168.0	26.0	25.0	Heat-affected zone in Haynes 718
5	173.2	24.0	31.5	Parent metal in Haynes 718
6	171.2	26.0	26.0	Heat-affected zone in Haynes 718

METALLURGICAL EVALUATION OF QUALITY OF LONGITUDINAL WELD IN SAMPLE OF 321 CRES TUBING

INTRODUCTION

Samples representative of the Saturn S-II LH_2 lines bellows assembly welds were evaluated for quality. Samples were supplied by Fairchild Precision Metals Products, San Diego, California.

Quality evaluation of the welds ascertained data to aid in the disposition of the bellows assemblies that did not meet procurement specification requirements. This evaluation determined the extent of thinning in the weld zone and the effect on the mechanical properties of the weld in question. Submitted radiographs were studied to determine the acceptability of the welded tubes in terms of specification ABMA 1050930b (Radiographic Inspection Procedures and Acceptance Standards for Fusion Welded Joints in Stainless and Heat-Resistant Steel).

CONCLUSIONS

Two of the samples did not meet the thinning tolerance of 0.0005-inch called out in the ABMA specification. Failure of the tensile coupons in the parent metal and not in the weld area was caused by work hardening in the planished weld area. Radiographs showed definite metal thinning and its acceptance, in accordance with the specification, could not be determined by examination of radiographs.

PROCEDURE

Four welded tubes were submitted, two of which were planished and two of which were as-welded. The as-welded tubes were to be used as control specimens. Radiographs accompanied all tubes. The tubes were made of 321 CRES steel and had a wall thickness of 0.005 inch.

Radiographs were examined to determine radiographic soundness and to establish the quality of metallographic and tensile specimens. Photomicrographs were taken of transverse and longitudinal weld sections in the planished and as-welded conditions. Microhardness tests were made in the weld, and the parent metal tensile coupons were machined to a subminiature, flat type configuration. Tensile coupons were tested at room temperature for F_{tu}, F_{ty}, and percent elongation.

RESULTS

Measurements made in metallographic examination clearly showed that two of the representative tubes did not meet the thinning requirements of ABMA 10509306, Radiographic Inspection Procedures and Acceptance Standards for Fusion Welded Joints in Stainless and Heat-Resistant Steel.

Samples for metallographic examination were sectioned transverse to the weld and showed metal thinning in the weld. Typical metal thinning observed in representative tubes is shown in the transverse sections in Figures 62 and 63. Longitudinal sections to the weld also exhibited metal thinning.

Tensile tests were not informative regarding mechanical properties of the planished welds. The work-hardening of the weld bead raised the strength of the weld to a level above that of the parent metal.

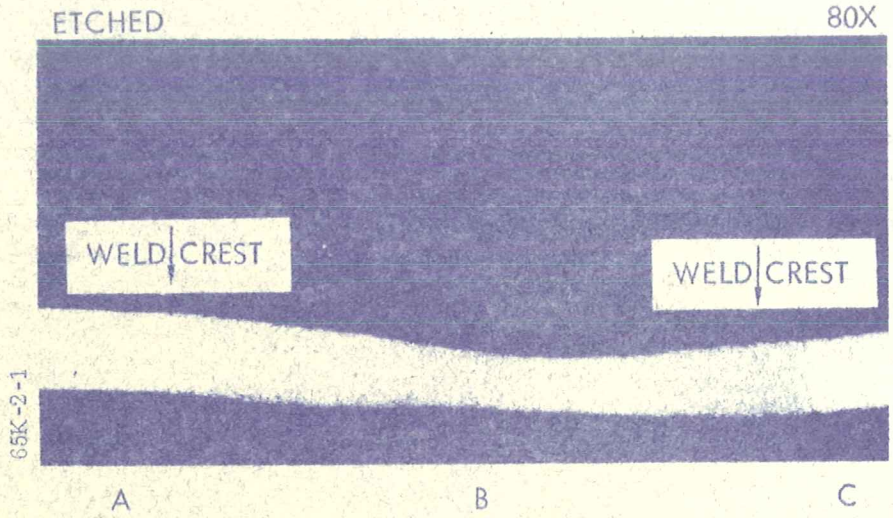

Figure 62. Photomicrograph of As-Welded, Transverse Section of Weld Showing Typical Metal Thinning

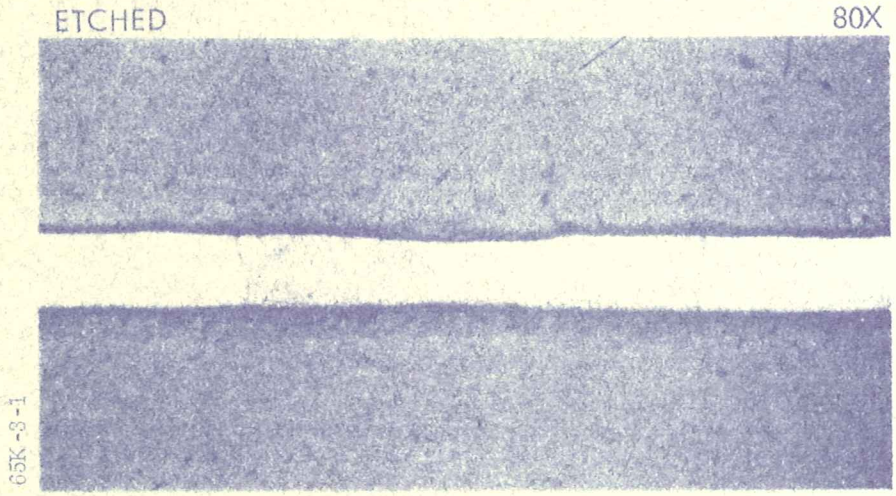

Figure 63. Photomicrograph of Planished Transverse Section of Weld, Showing Typical Metal Thinning

METALLURGICAL INVESTIGATION OF CRACKING OF REPAIR WELD ON J-SECTION

INTRODUCTION

Certification panel repair welds of 2014 welded to 2219 contained cracks on the dropthrough side of the weld. These panels were fabricated in preparation for repair welding of the J-section of Saturn vehicles. The parent metals used in the J-section after S-II-3, were 2219 welded to 2014.

Six fabricated panels employed various weld procedures and combinations of materials to establish a suitable repair method. A description of the various welding methods and material combinations is given in Tables 20 and 21.

Table 20. Description of Welding Procedures and Material Combination Used on Original Weld Joints

Panel Number	Parent Weld		Joint Preparation	Filler Wire	Weld Passes	Remarks
	2219-T6	2014-T651				
4	*	*	J-groove 3/16-inch wide 50 percent deep	4043	2	Dropthrough removed
5	*	*	Same	4043	2	Dropthrough not removed
6	*	*	Square butt	2319	4	Dropthrough not removed
7	*		Same	4043	4	Dropthrough not removed
8		*	Same	4043	3	Dropthrough not removed
X	*	*	J-groove	4043	3	Copper chill bar dropthrough removed

*Indicates the parent metal at the head of the column was used in making the panel.

Table 21. Description of Welding Procedures and Material Combinations Used to Weld-Repair the Panels in Table 20

Panel Number	Groove Out (percent)	Filler Wire	Weld Passes	Remarks
4	60	4043	3	Dropthrough removed
5	60	4043	3	Dropthrough not removed
6	60	2319	3-4	Dropthrough not removed
7	60	4043	3-4	Dropthrough not removed
8	60	4043	3-4	Dropthrough not removed
X	60	4043	3-4	Copper chilled

The investigation examined the six repair weld panels for cracks and other defects, such as porosity, excessive eutectic formation, and alignment and location.

CONCLUSIONS

Each weld repair procedure used on the six panels proved suitable for repairing J-welds. The use of a backup bar provided the most uniform microstructure with minimum eutectic concentrations. Various combinations of materials used in the six panels had no apparent detrimental effect on the microstructure of the repair welds.

RESULTS AND DISCUSSION

A dye-penetrant examination of the six submitted panels revealed no cracks or voids. Microexamination of the panels revealed no deleterious microstructural features, although some eutectic formations were noticed in the reheated zone of each panel. The magnitude of these concentrations, their locations, and alignment in regard to the surface was not considered detrimental to the quality of the weld.

The microstructures of specimens 4C, 5B, 6A, and 8B, are illustrated in Figures 64 through 71. The most severe eutectic formation was observed in specimen 8B (Figures 72 and 73). Specimen XB revealed the most uniform microstructure (Figures 74 and 75).

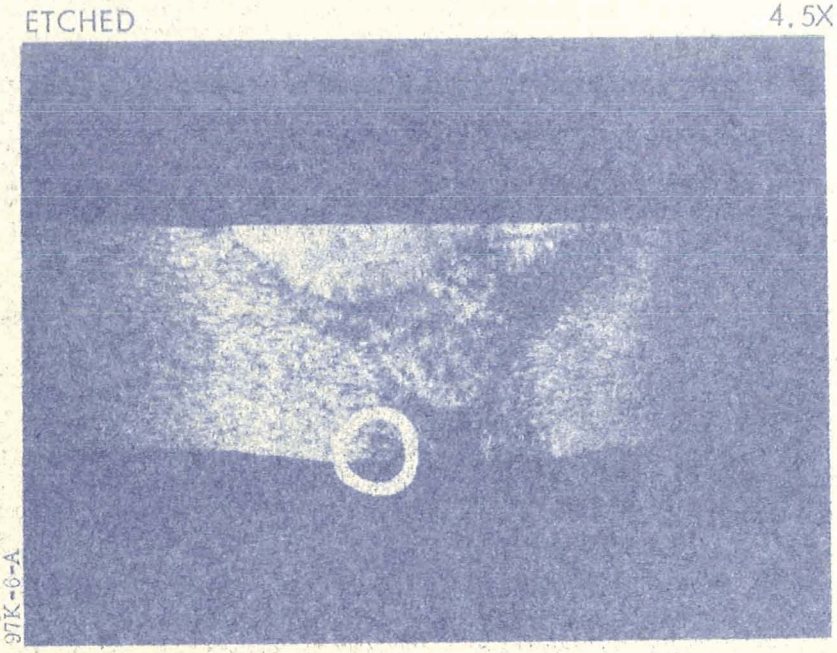

Figure 64. Photomicrograph of Specimen 4C Depicting Macrostructure of Weld Area of Figure 65

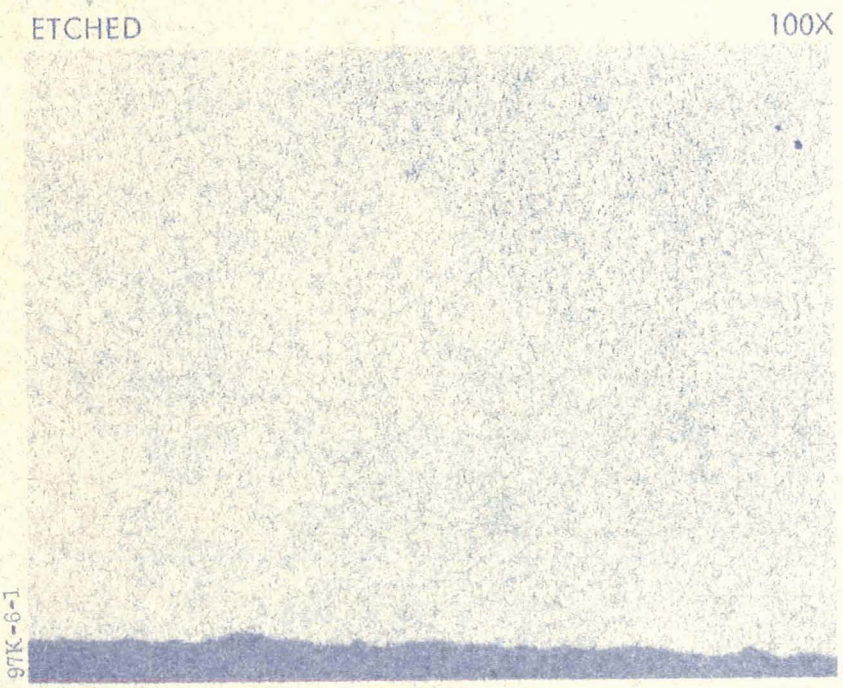

Figure 65. Photomicrograph of Specimen 4C Depicting Microstructure of Area in Figure 64

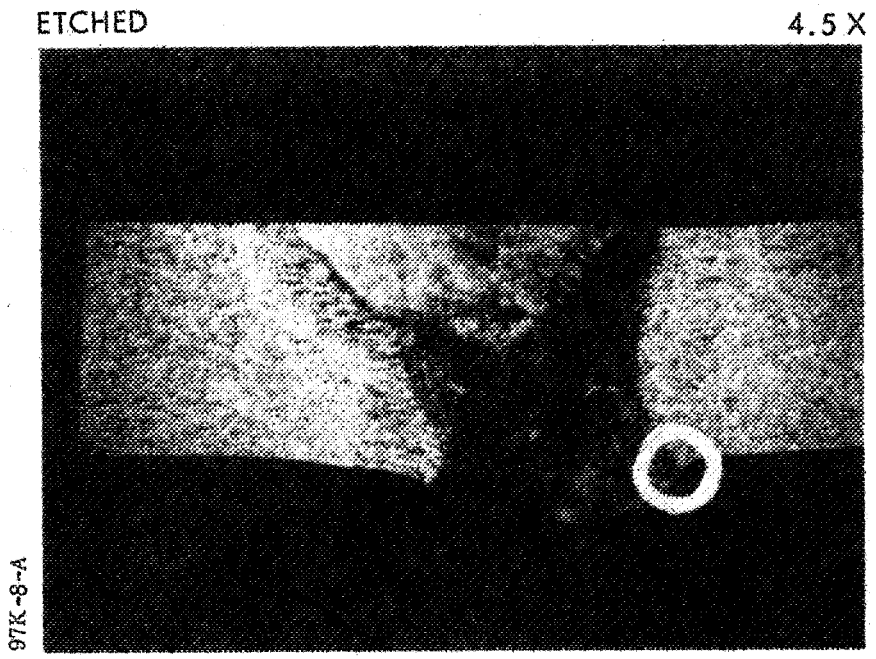

Figure 66. Photomacrograph of Specimen 5B Depicting Macrostructure of Weld and Indicating Area Shown in Figure 67

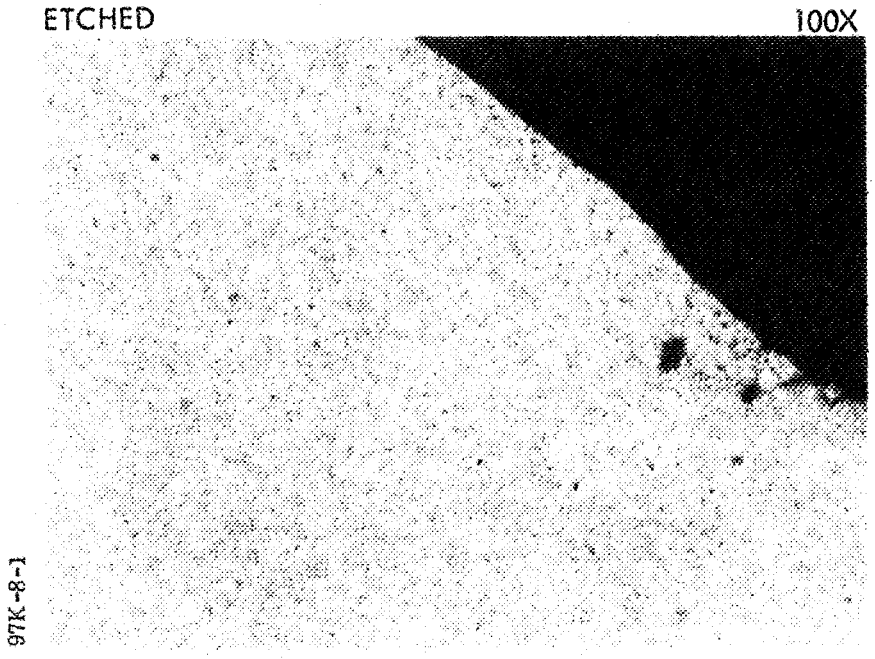

Figure 67. Photomicrograph of Specimen 5B Depicting Microstructure of Area Indicated in Figure 66

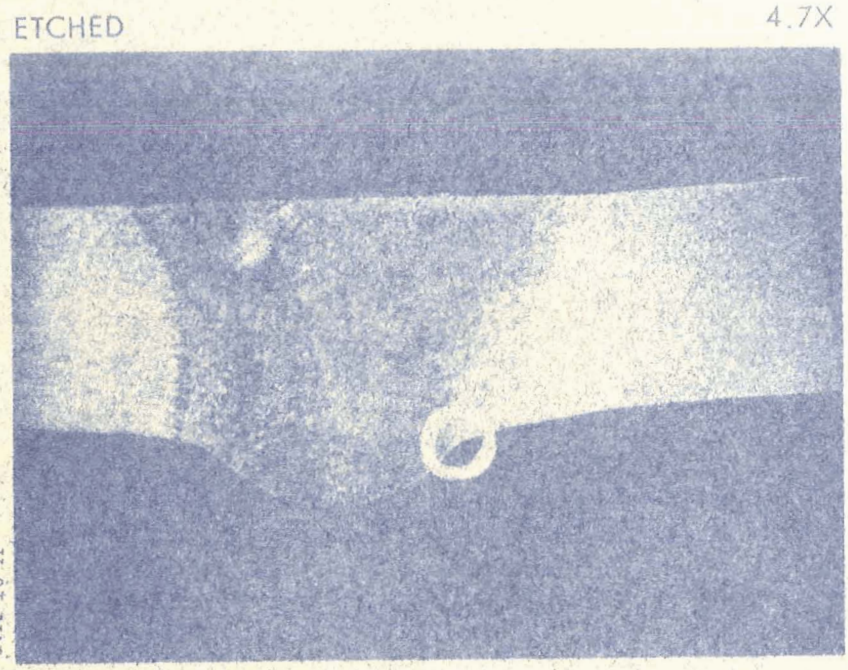

Figure 68. Photomacrograph of Specimen 6A Depicting Macrostructure of Weld and Indicating Area Shown in Figure 69

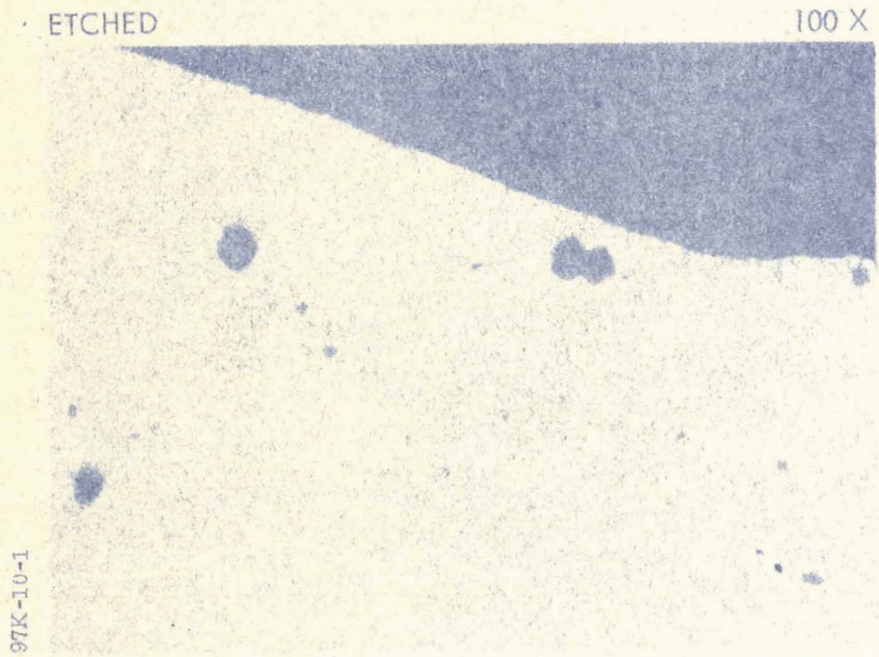

Figure 69. Photomicrograph of Specimen 6A Depicting Microstructure of Area Indicated in Figure 68

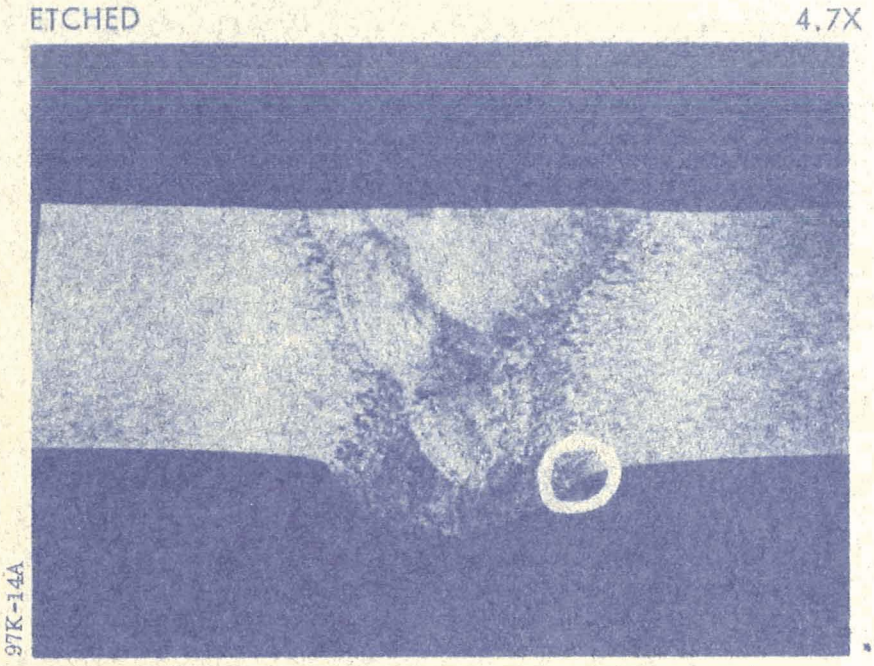

Figure 70. Photomacrograph of Specimen 8B, Depicting Macrostructure of Weld and Indicating Area Shown in Figure 71

Figure 71. Photomicrograph of Specimen 9B Depicting Microstructure of Area Indicated in Figure 70

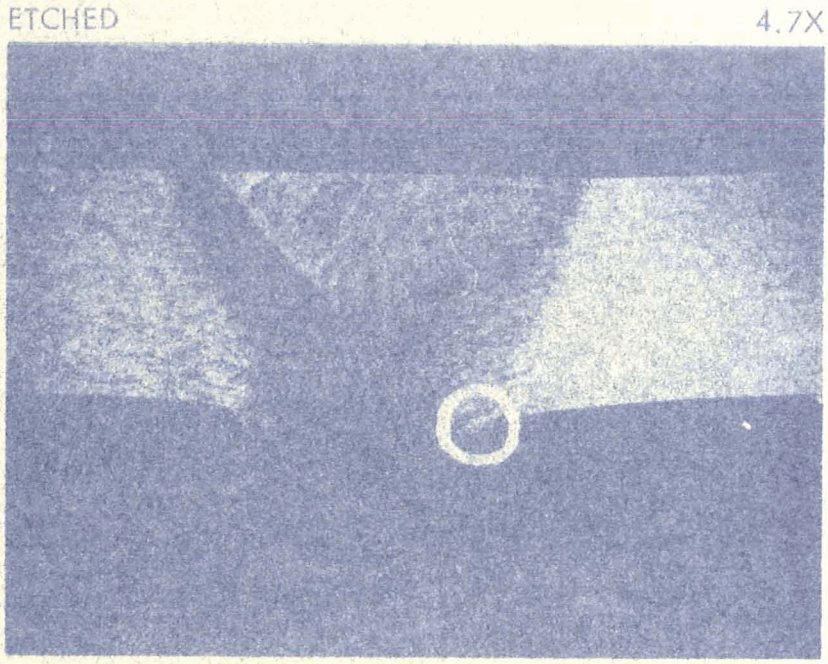

Figure 72. Photomacrograph of Specimen 8B, Depicting Macrostructure of Weld and Indicating Area Shown in Figure 73

Figure 73. Photomicrograph of Specimen 8B Depicting Microstructure of Area Indicated in Figure 72

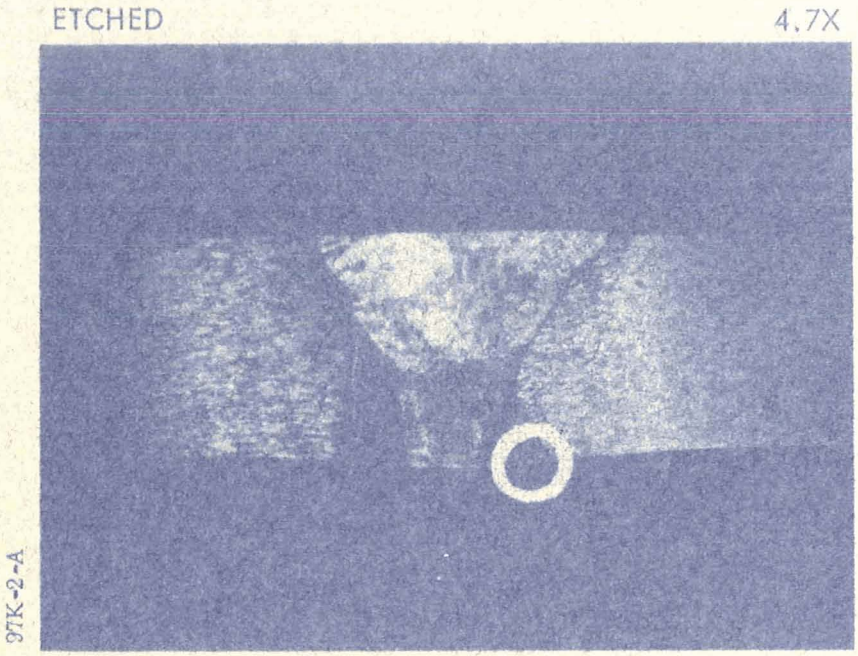

Figure 74. Photomacrograph of Specimen XB Depicting Macrostructure of Weld and Indicating Area Shown in Figure 75

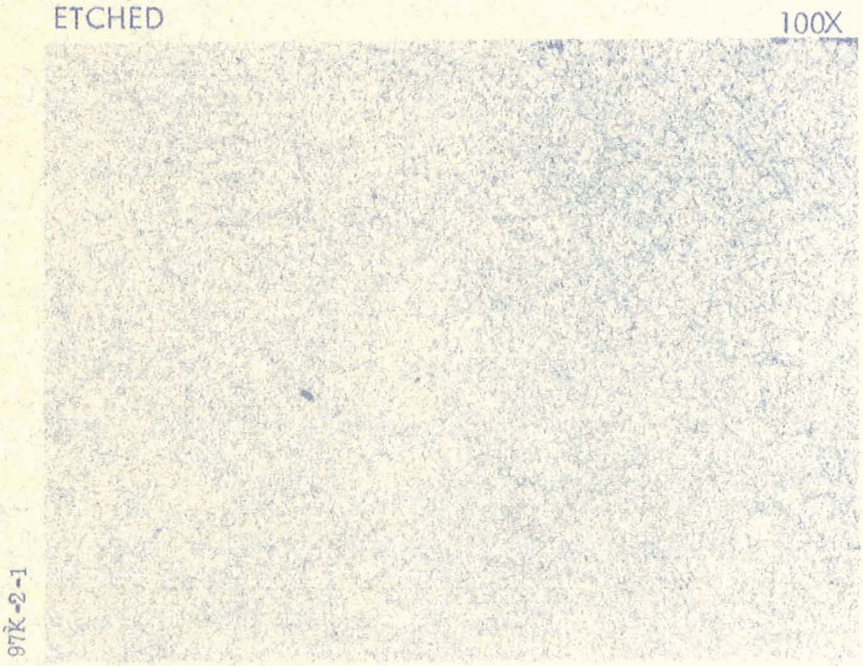

Figure 75. Photomicrograph of Specimen XB Depicting Microstructure of Area Indicated in Figure 74

MECHANICAL JOINT EVALUATION

PROGRESS SUMMARY

To aid in stress analysis, tests were performed on simulated S-II mechanical joints. One program investigated a lap shear joint used on the thrust structure; the other was concerned with torque relaxation in bolting ring joints using various sealants.

SHEAR DEFORMATION TESTS OF S-II THRUST BLOCK BOLTS

INTRODUCTION

Load-deflection data were required for stress analysis of the S-II stage thrust structure. Lap shear tests of 1/2-inch 2014-T651 aluminum plate bolted to 1 inch 2014-T651 aluminum plate with 5B502-10-22 bolts were conducted with representative bolts removed from the Saturn S-II-2 thrust structure after two field-duration static firings.

PROCEDURE AND RESULTS

The test setup and specimen are shown in Figure 76. The specimens were loaded and unloaded using a machine crosshead travel rate of 0.050 inch per minute. The average ultimate shear strength of the bolted joints was 17,640 pounds. A typical load-deflection curve is shown in Figure 77.

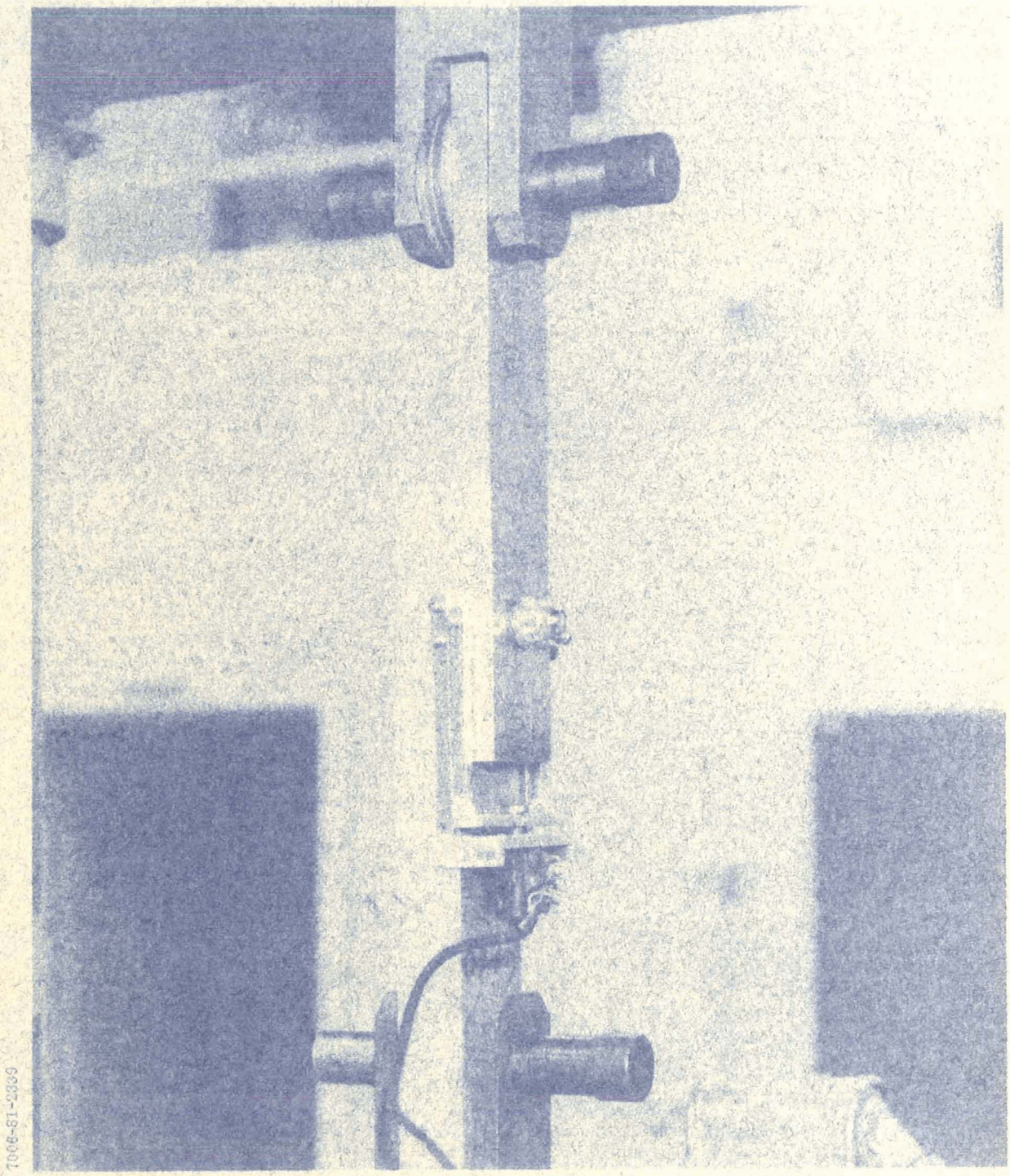

Figure 76. Test Setup Showing Clevis Loading Arrangement and Special Deflectometer

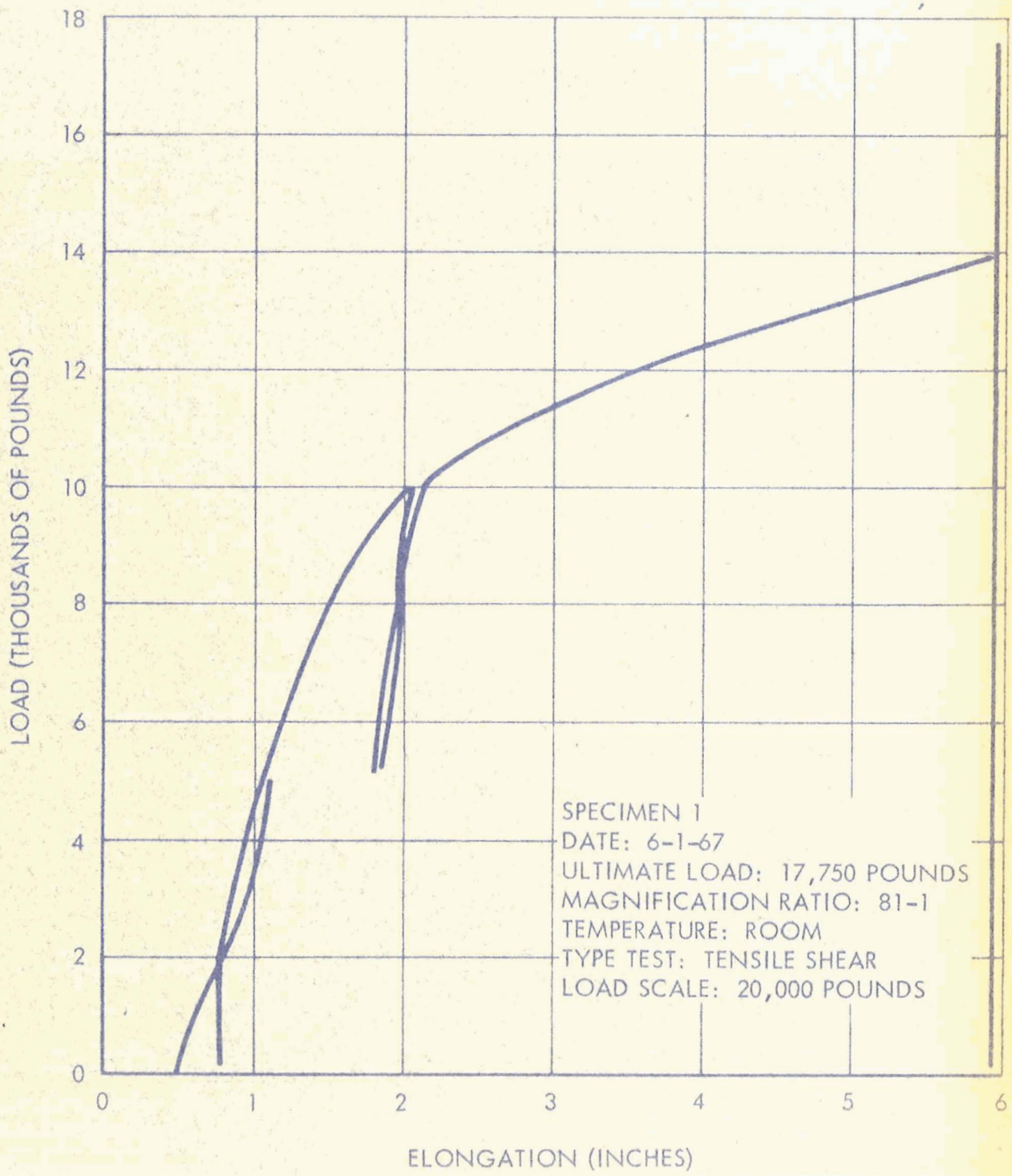

Figure 77. Autographic Load Deflection Curve

TORQUE DEGRADATION TESTS FOR BOLTING RING MECHANICAL JOINTS AT X_B 299.380 UTILIZING RTV SEALANT UNDER BEARING SURFACES

Torison tests were conducted on specimens simulating the bolting ring mechanical joints at X_B 299.380 on the S-II stage. The test specimens consisted of blocks of aluminum, cut and drilled to simulate the bolting ring fitup. These blocks were bolted together, torqued to specification requirements, and the torque degradation checked at various time intervals. Specimens with and without RTV sealant, Narmco sealant, and shim stock were tested, and tests were performed in conjunction with liquid nitrogen specimen thermal cycling. Nut torque versus bolt preload tests were also performed.

CONCLUSIONS

Nut torque degradation is caused by a loss in bolt tensile preload. The loss in bolt tensile preload in these tests proved to be caused by cold flow of the MIL-A-5092 Type II rubber base adhesive used to bond the shim stock in place.

RTV sealant applied to the bolt and nut threads and bearing surfaces has no appreciable effect on nut torque degradation or bolt preload. Narmco bonding material used for foil seal attachment had negligible effect on nut torque degradation.

PROCEDURE AND RESULTS

All tests used new bolts, nuts, and washers, and each item was used for one test only. The 3/8-inch-diameter bolts were RD111-4008-0620 parts, and the 7/16-inch-diameter bolts were RD111-4008-0720 parts. Appropriate RD114-8005 nuts were used with each bolt. All tests at -320 F were performed while the specimen was submerged in liquid nitrogen. Torque was applied to the specimens with a calibrated torque wrench.

Room Temperature Torque Degradation Tests

A typical test specimen prepared for these tests is shown in Figure 78. Each specimen was assembled and the nut tightened to the reported torque value. The nut-tightening torque was then checked at periodic time intervals. Representative results are shown in Tables 22 and 23.

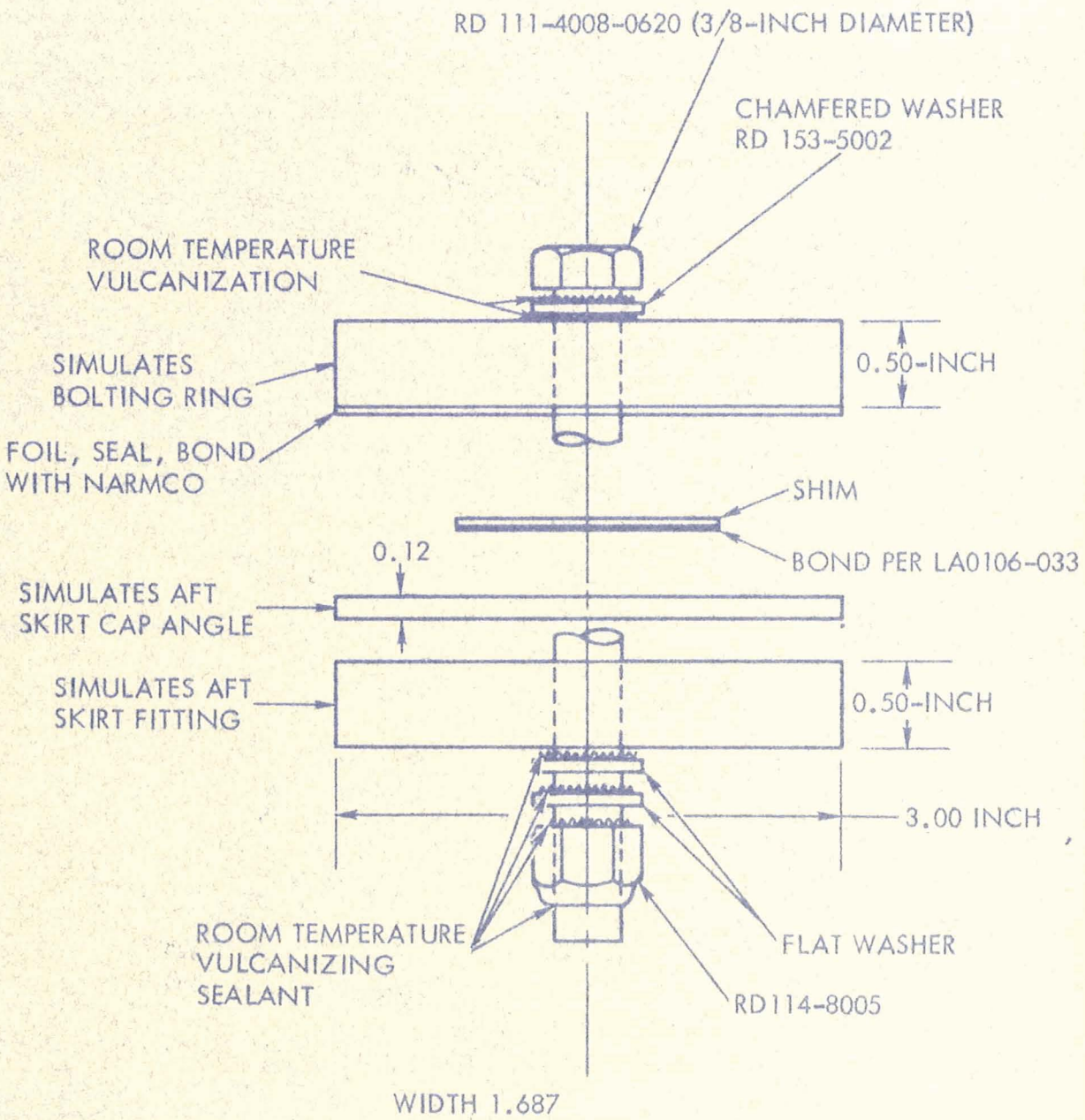

Figure 78. Sketch of Test Specimen, 3/8-Inch-Diameter Bolts

Table 22. Torque Degradation Room Temperature Test Results Summary, 3/8-Inch-Diameter Bolts

Shim Thickness (inches)	Narmco Thickness (inches)	RTV Sealed	Nut Torque (in. -lb) - Elapsed Time from Initial Nut Tightening
No shim	No Narmco	No	200 - nut tightened 200 - 2 hours 180 - 3.8 hours
0.015	0.005	Yes	200 - nut tightened 150 - 2 hours 170 - 2.5 hours 180 - 4.4 hours
0.015	0.005	Yes	200 - nut tightened 100 - 2 hours 170 - 2.5 hours 170 - 4.4 hours
0.040	0.010	Yes	200 - nut tightened 80 - 1.8 hours 170 - 2.2 hours 180 - 4.1 hours
0.040	0.010	Yes	200 - nut tightened 130 - 1.8 hours 180 - 2.2 hours 180 - 4.1 hours
No shim	0.015	Yes	200 - nut tightened 190 - 1.7 hours 190 - 2.2 hours 190 - 4 hours
No shim	0.020	Yes	200 - nut tightened 160 - 1.7 hours 180 - 2.1 hours 190 - 3.9 hours

Note: All specimens were tightened to 200 inch-pounds each time the torque was checked.

Table 23. Torque Degradation Room Temperature Test Results Summary, 7/16-Inch-Diameter Bolts

Shim Thickness (inches)	RTV Sealed	Nut Torque (in. -lb) - Elapsed Time from Original Nut Tightening
No shim	No	520 - nut tightened 500 - 1.3 hours 500 - 3.3 hours
No shim	Yes	520 - nut tightened 520 - 1.2 hours 520 - 1.7 hours 520 - 3.6 hours
0.040	Yes	520 - nut tightened 420 - 1.3 hours 460 - 1.7 hours 500 - 3.6 hours
Note: All specimens were tightened to 520 inch-pounds each time the torque was checked.		

Table 24. Torque Versus Thermal Cycle Results, 3/8-Inch-Diameter Bolts, 0.040-Inch-Thick Shim Bonded per LA0106-033, Foil Seal Bonded with 0.010-Inch-Thick Narmco, and RTV Accelerated Cure

Initial Torque RT (inch-pounds)	Nut Tightening Torque	
	43 hours (RT)	91 hours (RT)
200	40	200
200	90	200
200	70	200
200	55*	200
200	50*	220
200	70*	250
Note: Specimens retorqued to 200 inch-pounds at each check. *Specimens cooled to -320 F then brought back to room temperature for testing		

Torque Versus Thermal Cycle Tests

Table 24 details the results of these tests. The specimen configuration was as shown in Figure 78. In certain instances, the RTV and/or the shim stock and Narmco were omitted as noted in the table. In addition to the tests covered in the table, three specimens were torqued to 520 inch-pounds and tested at -320 F. With all three specimens, severe thread seizure was noted, and the breakaway torque exceeded 900 inch-pounds.

Torque Degradation Due to the Shim Stock

Three specimens were prepared as shown in Figure78, except that all adhesives and bonding material were omitted to determine if the shim stock was relaxing and relieving the bolt preload. The specimens were torqued to 200 inch-pounds and the tightening torque checked 2 days later. This tightening torque was 205, 205, and 210 inch-pounds.

Shim Stock Tests

Three shims were stack-loaded in compression to 5200 psi (the maximum anticipated on the S-II stage) and held for one-half hour. No measurable permanent set (which would have been evidenced by load dropoff) occurred during this test.

FAILURE ANALYSIS

PROGRESS SUMMARY

During the period covered by this report, three major component failures were thoroughly investigated. Two of these components failed during hydrostatic testing, and one during a flow test. In each case, the failure analysis covers two main areas. The first area is the determination of the origin of failure, the mode of fracture initiation and propagation, and the mechanism of fracture. The second area of investigation involves a metallurgical and chemical analysis of the material to verify that the materials and processes met all applicable specifications.

FAILURE ANALYSIS OF 321 STAINLESS BELLOWS, P/N 1001531-413

INTRODUCTION

A 321 stainless steel bellows, P/N 1001531-413, located in the Saturn LOX fill and drain line, ME271-0012-0005, failed during a flow test at Wyle Laboratories. The inside diameter of the bellows was 8 inches and the single ply wall was 0.020 inch thick. The bellows was manufactured by Stainless Steel Products.

Failure occurred in two places approximately 120 degrees apart in the outer diameter of the second convolution from one end. An analysis was made to determine the mode of fracture initiation and propagation and to determine if any metallurgical features of the part were significant in regard to initiation and propagation of fracture.

CONCLUSIONS

The fractures were initiated by fatigue at the inner surface of the second convolution. The sharp notches of the etched material surface intensified the sensitivity of the surface to the initiation of a fatigue failure.

PROCEDURE

The failed bellows was examined visually at magnifications up to 45X and photographed to illustrate significant features. The fracture faces were then subjected to fractographic examination.

RESULTS

Figure 79 and 80 illustrate the appearance of fracture A at the outer and inner wall surfaces respectively. Some fragmentation has occurred and small fragments are missing in Figure 80. Figures 81 and 82 illustrate the appearance of fracture B at the outer and inner wall surfaces, respectively. Fragmentation has occurred at both the inner and outer surfaces.

Figure 83 illustrates a composite of fracture magnification of 10X. The source of the replica for fractographic study is shown as are the fractographs. Location A1 on the figure shows the likely initiation site. Location A1-a shows the fracture near the inside diameter surface. A nonductile fracture is illustrated with microstriations indicative of fatigue

(magnification 2500X). Location A1-b shows the central zone of the fracture face. The fatigue striations are much more pronounced than in A1-a (magnification 5000X). Location A1-c shows the fracture near the outside diameter surface. The fatigue striations are quite evident (magnification 5000X). The fractographic results of fracture B were similar to those observed for fraction A. No discrete origin site could be defined.

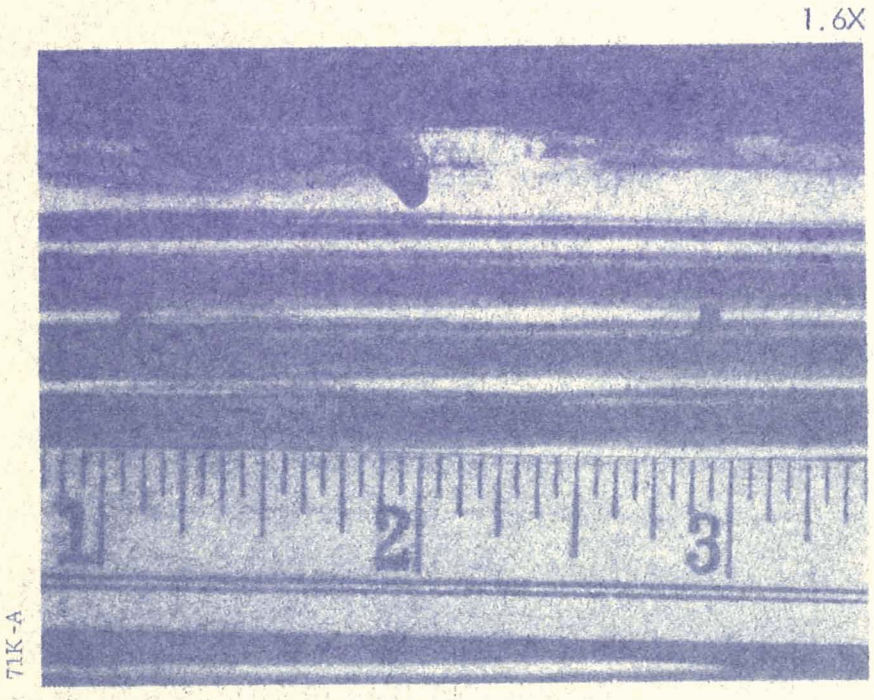

Figure 79. Fracture in Second Convolution of Region A on Outer Surface (Outside Diameter) of Bellows

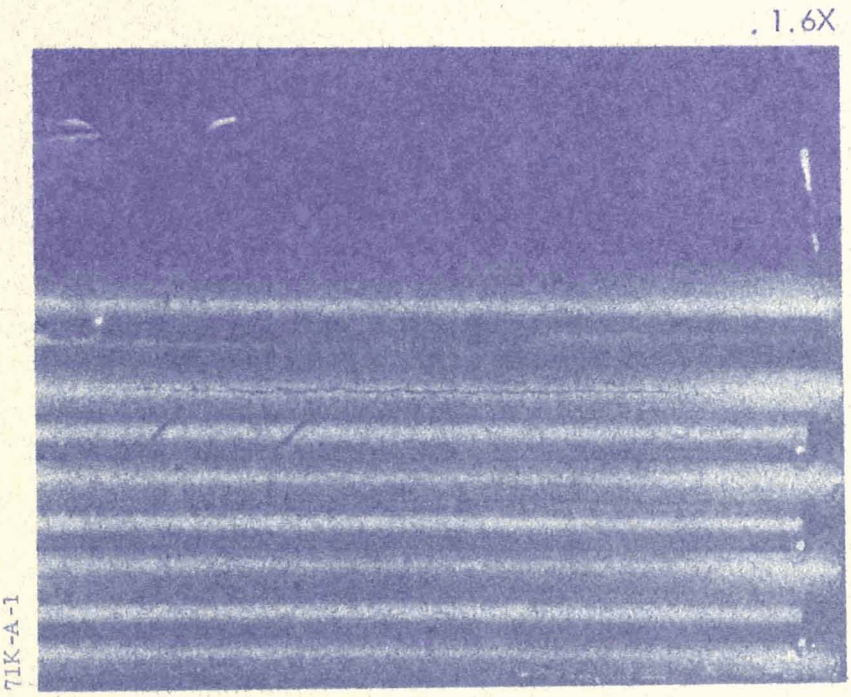

Figure 80. Fracture in Second Convolution of Region A on Inner Surface (Inside Diameter) of Bellows

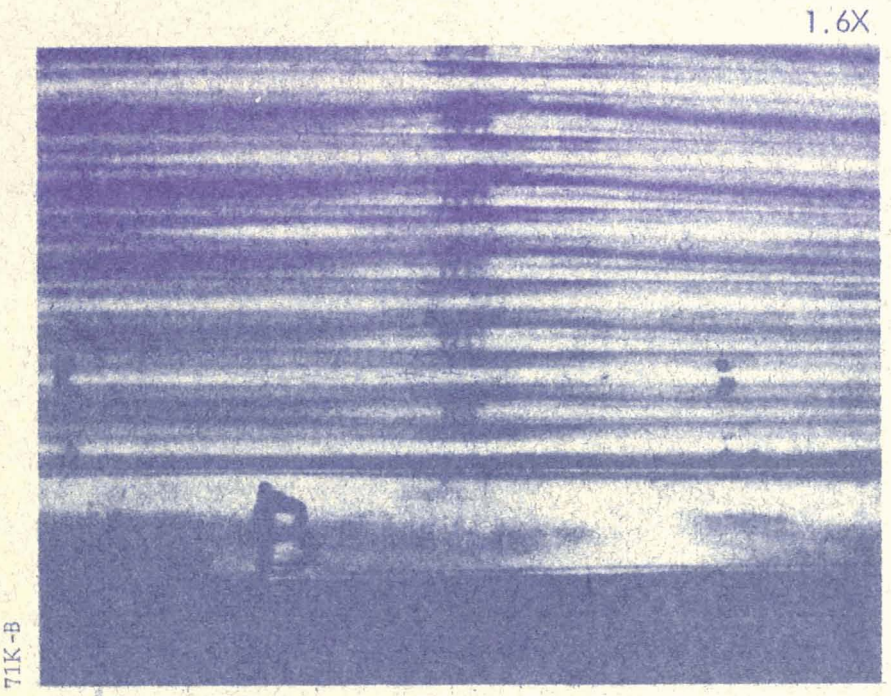

Figure 81. Fracture in Second Convolution of Region B on the Outer Surface

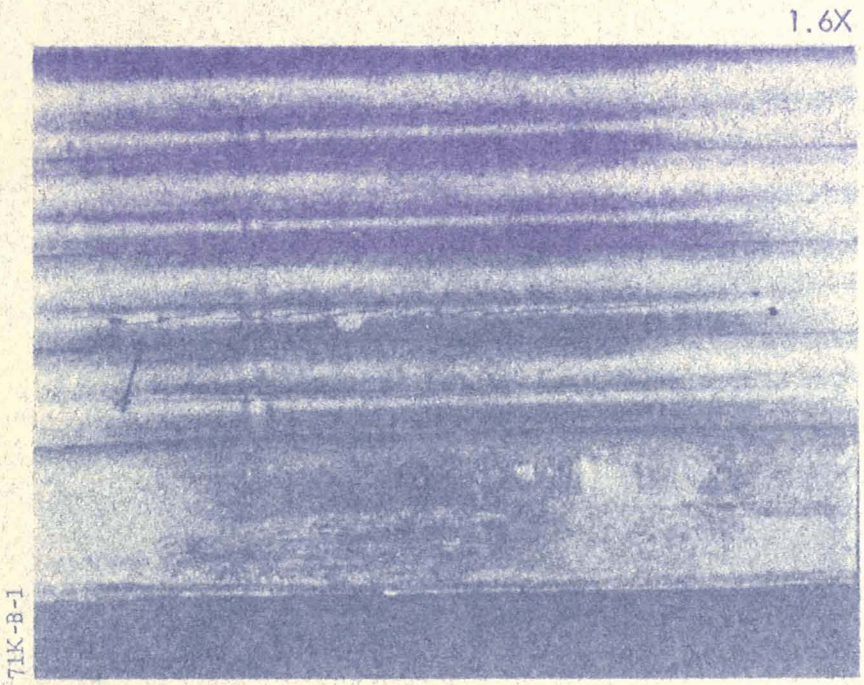

Figure 82. Fracture in Second Convolution of Region B on Inner Surface (Inside Diameter) of Bellows

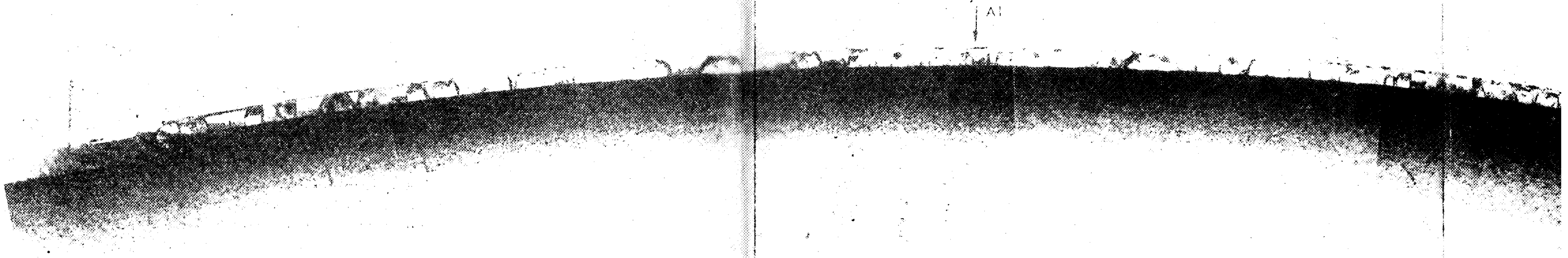

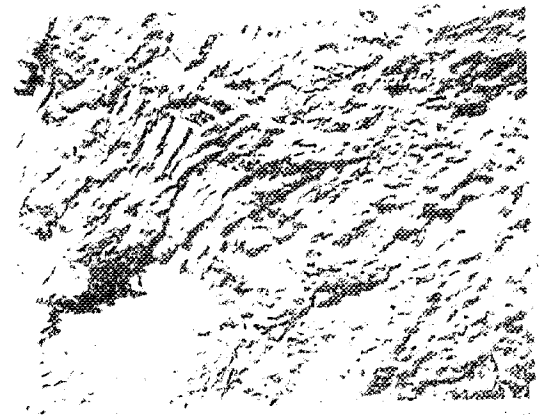

A1-a
2500X

A1-b
5000X

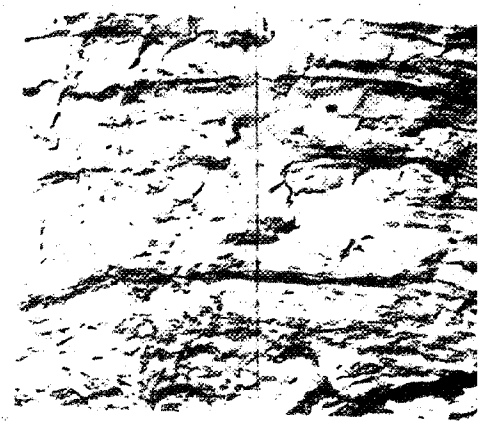

A1-c
5000X

FOLD-OUT #1

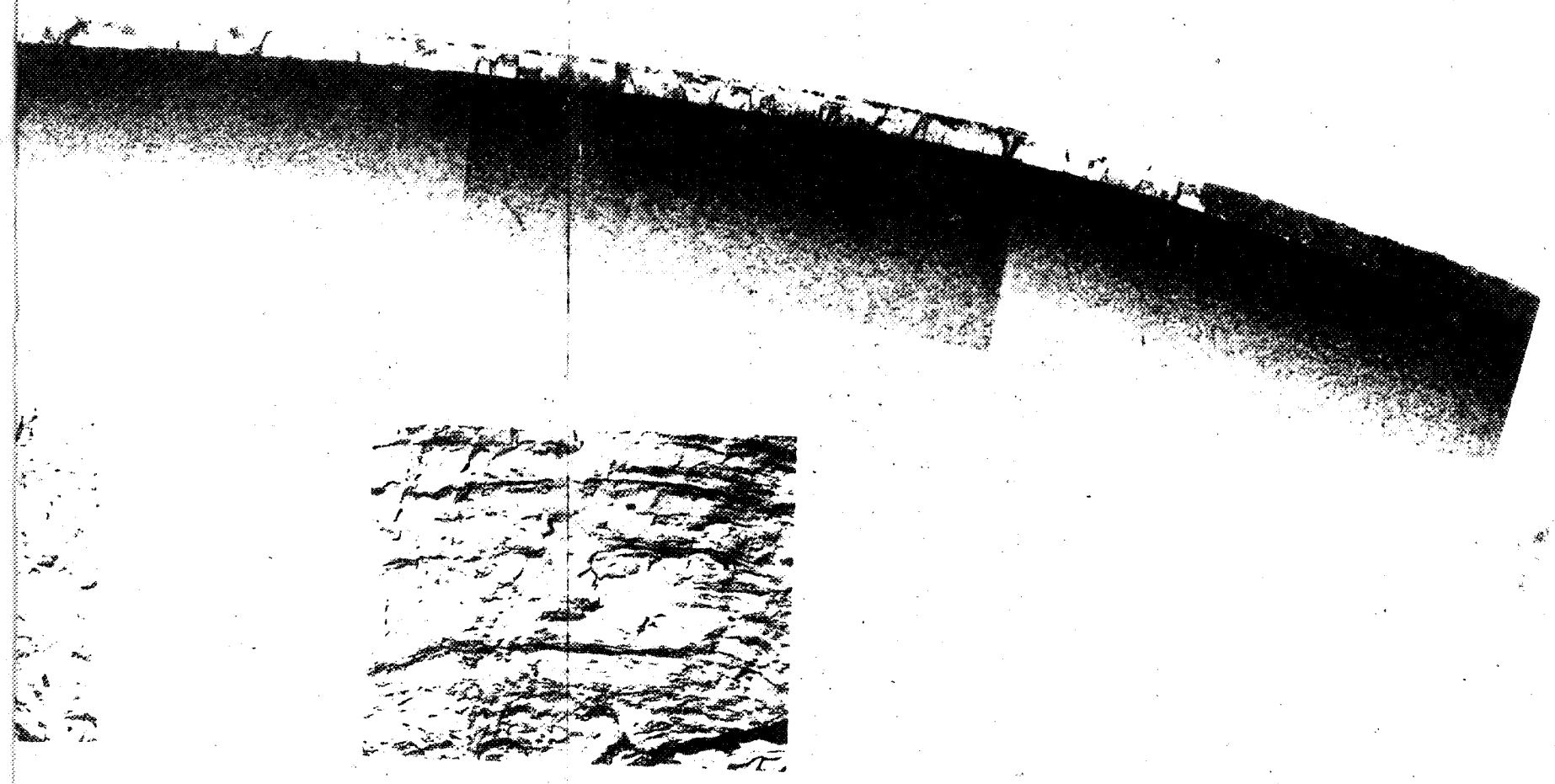

A1-c
5000X

Figure 83. Photomacrograph of Fracture A at Magnification of 10X

FOLD-OUT #2

FAILURE ANALYSIS OF S-II LH_2 TANK, UPPER AND CENTER FRAME ASSEMBLIES, P/N's V7-312409 AND V7-312212

INTRODUCTION

Inspection of the S-II-6 liquid hydrogen tank lower center cylinder assembly after hydrostatic testing at Seal Beach revealed two cracked aluminum frame assemblies in panel V7-312545 situated between tank splices 3 and 4. The frame assemblies referred to as upper and lower (rather than upper and center, as in the section title), constitute the upper two of three frame assemblies supporting this quarter panel. The quarter panel joins the common bulkhead structure at its lower extremity. Both frames were found similarly cracked through web lightening holes adjacent to tank splice 4. Segments of both cracked members were analyzed.

PROCEDURE

Visual, optical, and electron microscope techniques were used on the fracture surfaces and sectioned specimens to determine the origin of failure, direction of failure propogation and mechanism of fracture.

CONCLUSIONS

Fracture of both frame assemblies was initiated in the cap angle members and progressed outboard through the webs, ending with complete separation of the frame at the tank wall rib.

Fracture was initiated and propagated in a ductile manner under high tensile and bending stresses. No fatigue, corrosion, or other brittle fracture mechanism was involved. Fracture is believed to have resulted from an overloading condition.

Fracture of the upper frame cap angle was initiated at extrusion defects at the inner radius surface of the angle. Fracture of the lower angle, that was free from defects, occurred at the same respective location. The defects are not considered the primary cause for failure.

RESULTS

The appearance of cracks discovered in both upper and lower frame assemblies after hydrostatic testing, drying, and subsequent disassembly of the LH_2 tank section from the test fixture is shown in Figure 84. The

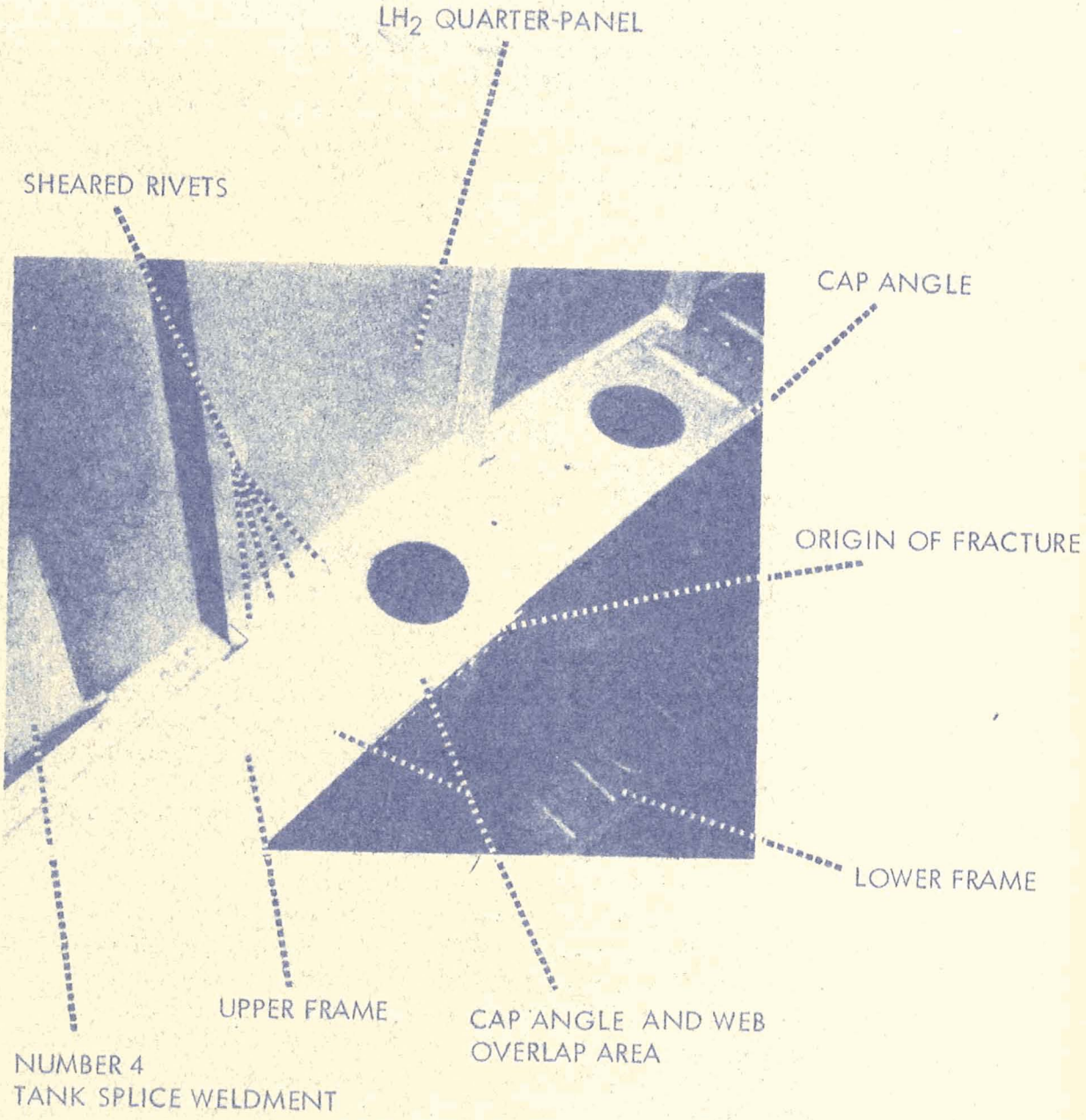

Figure 84. Cracked Upper Frame Prior to Disassembly From the LH_2 Tank Panel

upper frame crack is shown; the lower crack, directly beneath in the same panel bay, is not visible in the figure because of the camera angle. Unaffected portions of the lower frame are visible. The extreme similarity in gross damage suffered by both upper and lower frames is evident in Figure 85, where the cracked lightening hole segment of each frame is shown after removal from the tank and sectioning. As shown in Figure 85, four rivets attaching the frame webs to the panel rib were found sheared, again in both upper and lower frames, with the rivet head closest to the lightening hole of the upper frame missing entirely. Deformation of these rivet holes is illustrated in Figure 86.

Considerable buckling of the web adjacent to the tank wall, and offset of the web and frame cap angle on the inboard side of the lightening hole, were reported as evident before disassembly. The mating fracture surfaces of each were also found impinged on one another in this buckled and offset position. The impingement positions were readily reconstructed in Figure 85 from post-crack damage to fracture surfaces and cap angle rivets for both frames. Detailed views of buckling, offset, and impingement damage are shown in Figures 87 and 88.

Close visual and optical examination of the fracture surfaces revealed a nonuniform stain appearing intermittently throughout these surfaces. The stain was similar in color to that produced by chromate ion solutions on aluminum surfaces, with intensity varying from dark to light. Similar stains were noted on web and angle members, particularly on horizontal surfaces, both upper and lower, and in areas where liquid entrapment and capillary action would be expected to occur. Close examination of Figure 84, 85 and 88 will reveal stains around rivet heads, at frame-web lap joint crevices and on web surfaces. These stains are dark, in contrast to the alodine-treated aluminum surfaces on which they formed. Staining on fracture surfaces was intermittent; several regions completely free from stains were adjacent to surfaces quite heavily marked. A further peculiarity exists; in several instances, stains were found in fracture areas of a member, while no stains appeared in corresponding fracture areas of the mating member. These results are shown in Figure 89 for both cap angle and web members of both frames. Sketches of the entire fracture surfaces, showing the general stain pattern, are shown in Figure 90. No explanation can be offered for the erratic stain patterns detected.

Fractures contained in upper and lower frame segments (identified in Figure 85 as upper left-hand and lower right-hand) were examined under the electron microscope. These members were selected for examination since their fracture surfaces evidenced less obliteration from impingement with their mating members than did the latter. Figure 91 shows schematically the two members examined, indicating locations of edge (E) and mode (M) replicas made. Edge replicas, taken at an acute angle intersection of the

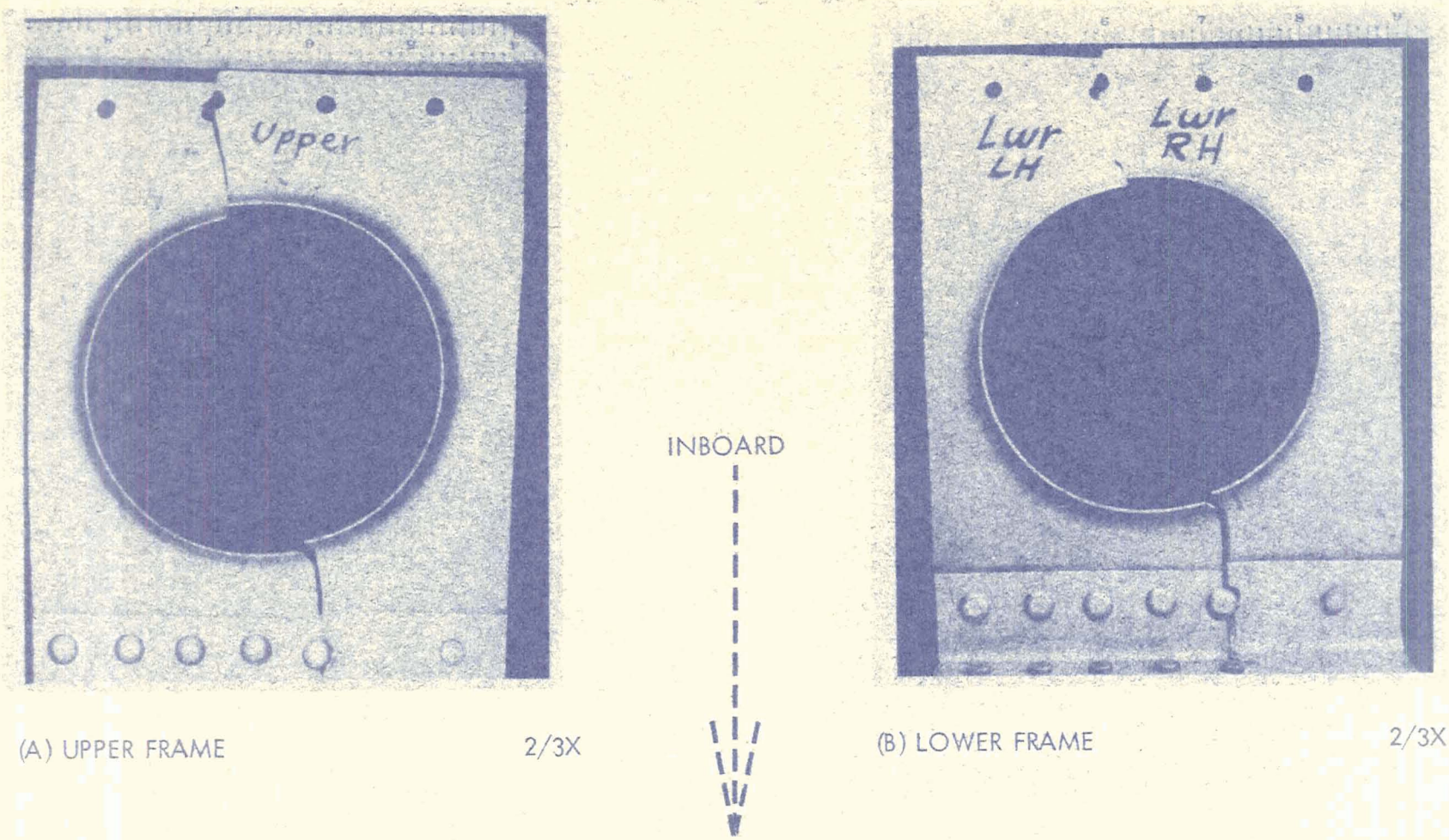

Figure 85. Upper and Lower Segments Showing Similarity of Fractures

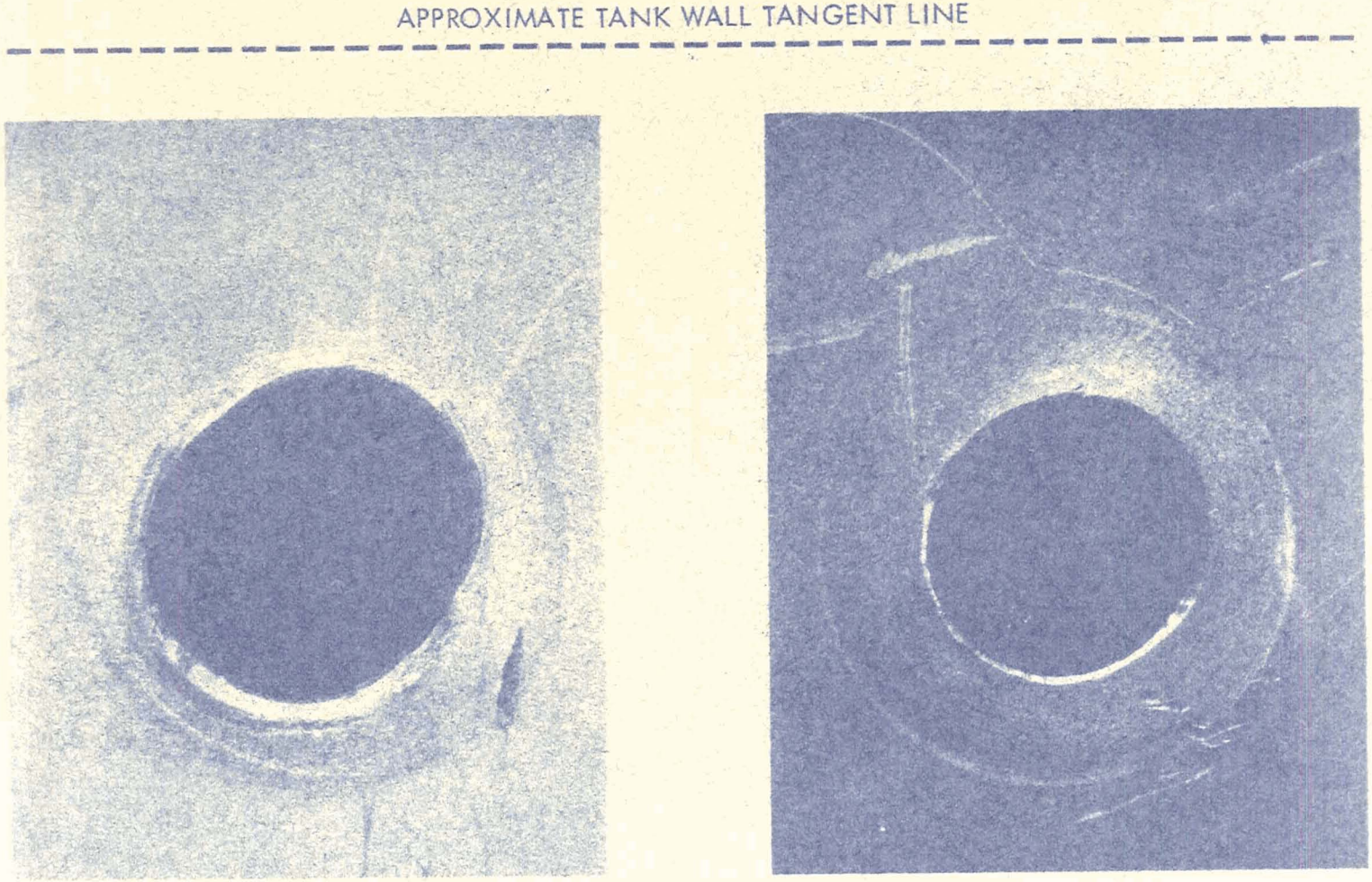

Figure 86. Deformation of Upper Left-Hand Rivet Holes of Figures 119a and 119b, Respectively

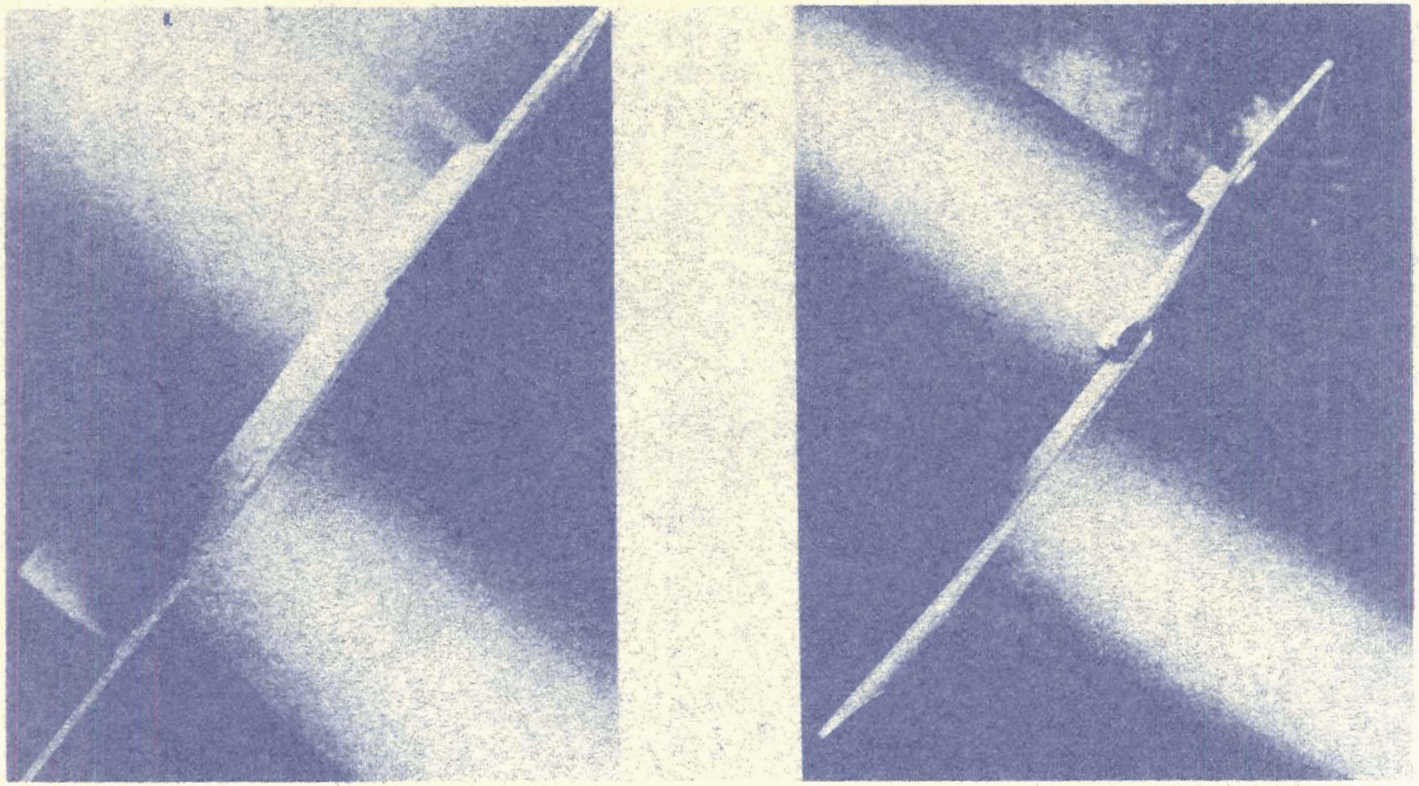

(A) UPPER FRAME NEAR IX (B) LOWER FRAME NEAR IX

Figure 87. Edge View of Remated Frame Segments, Looking, Inboard, Showing Buckling in Region of Sheared Rivets Adjacent to Tank Wall

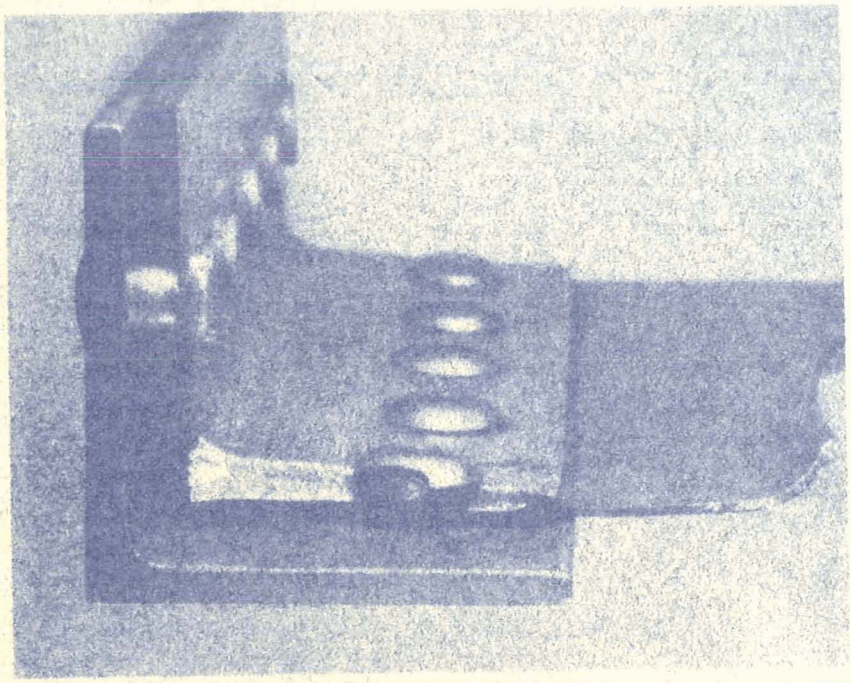

(A) NOTE DAMAGE TO RIVET HEADS 2X

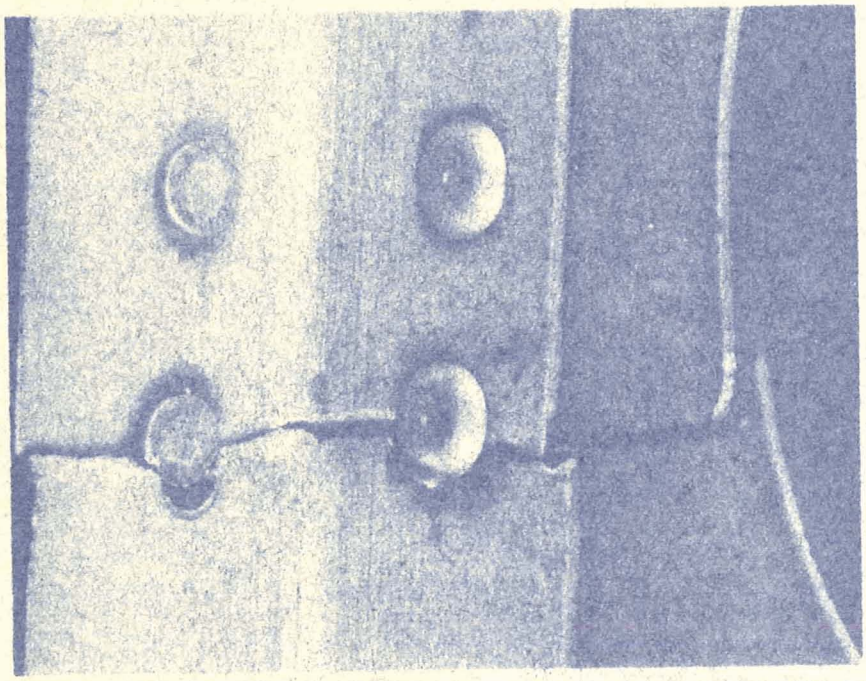

(B) OFFSET RECONSTRUCTION DEFINED BY RIVET DAMAGE AND ASSEMBLED WITH MATE 2X

TOP VIEW ROTATED ABOUT 90°

Figure 88. Views of Upper Frame Fraction Throught Cap Angle Demonstrating Impingement Damage and Offset

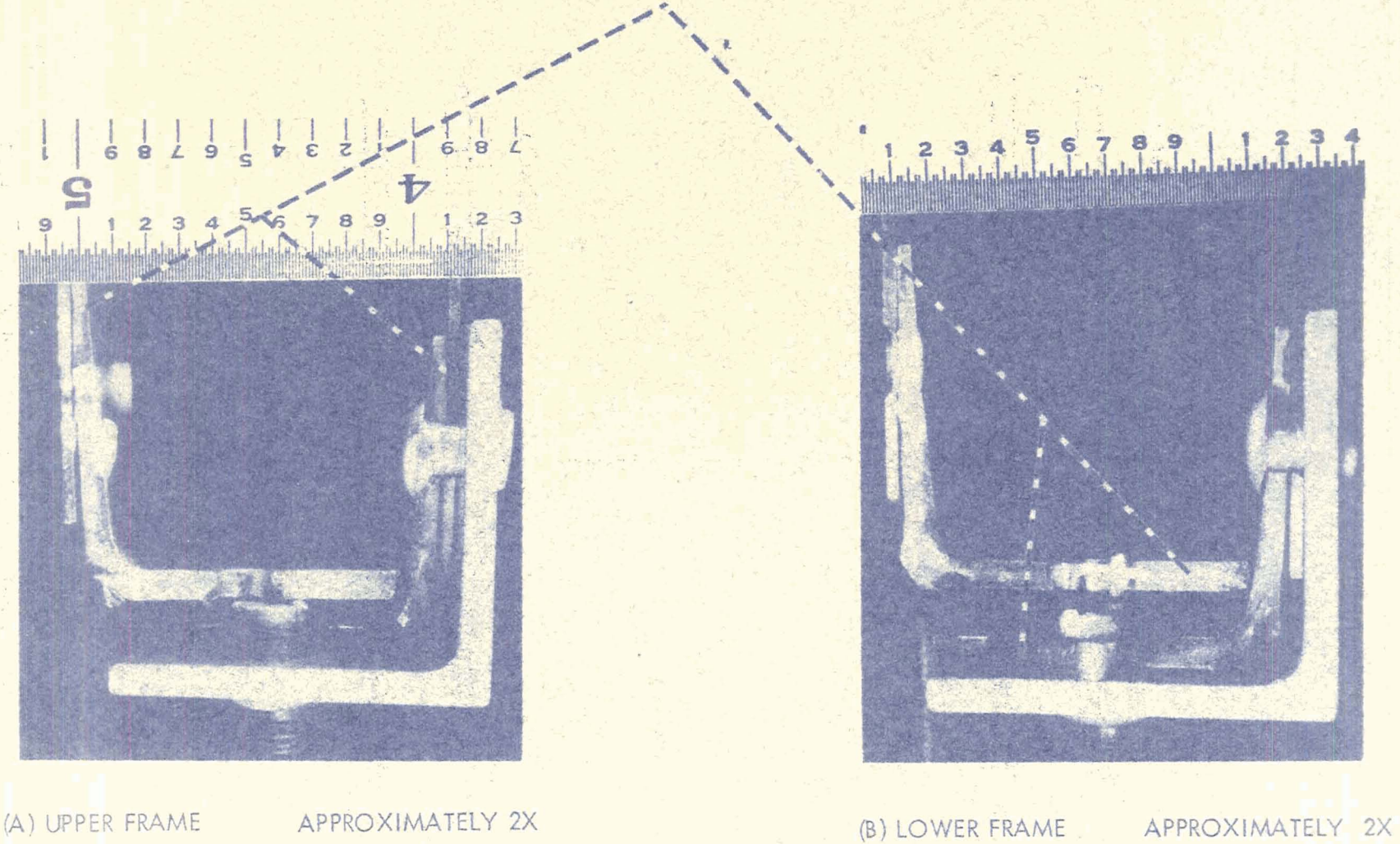

Figure 89. Fracture Faces of Frame Web and Cap Angle Members Showing Staining

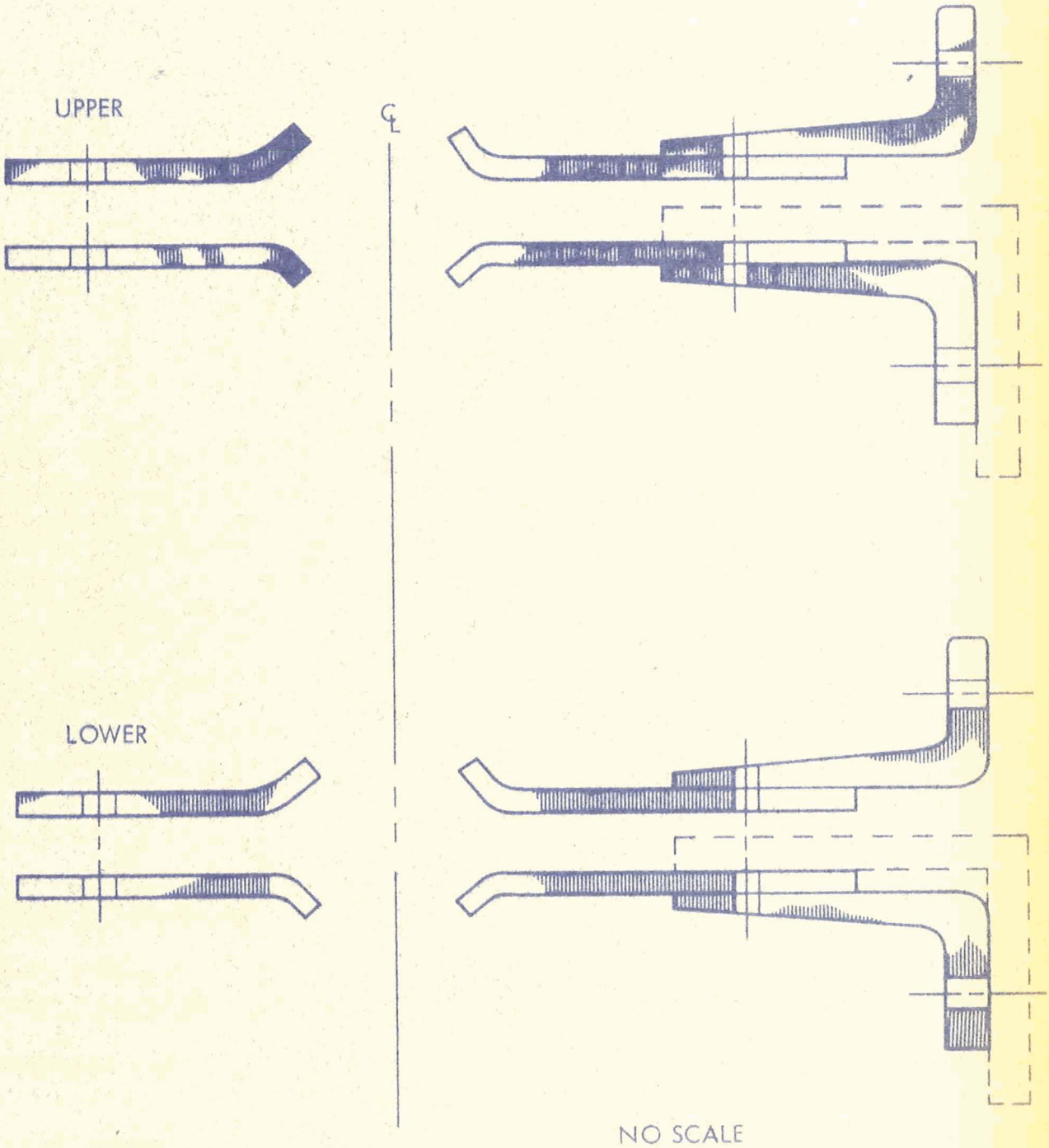

Figure 90. Schematic of Nonuniform Staining of Fracture Surfaces

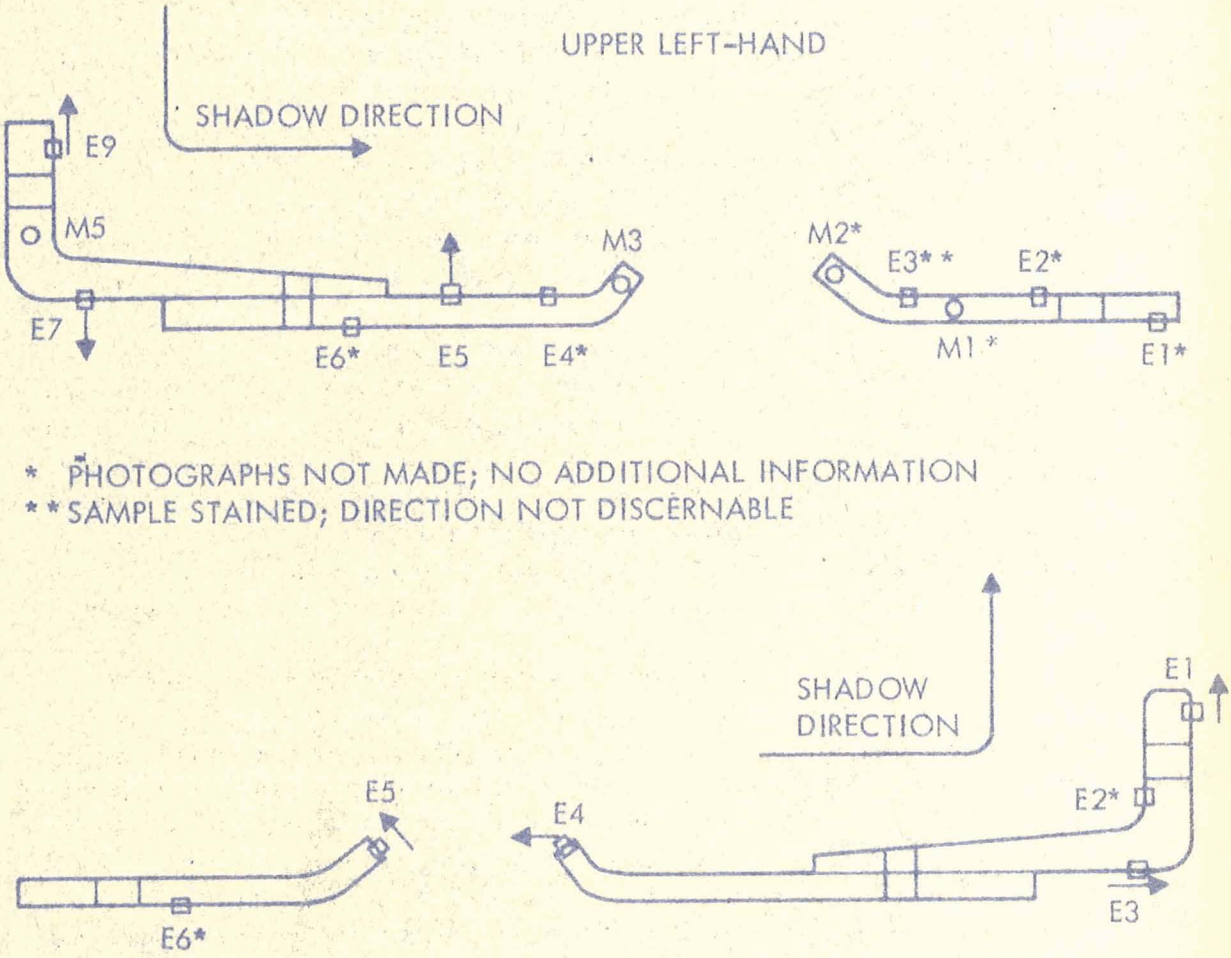

Figure 91. Schematic of Location of Replicas Taken From Fracture Surface

fracture with the specimen surface, reveal the direction of fracture propagation more adequately than do mode replicas, taken away from the edge and used to ascertain the mechanism of failure. Photographs taken of both edge and mode replicas, shown in Figures 92, 93, and 94, are coded numerically to Figure 91. Arrows placed adjacent to edge replica designations indicate the fracture direction determined at that location.

Review of mode replicas taken of the upper left-hand fracture surfaces revealed dimpled patterns typical of ductile, tensile fracture of aluminum alloys 2014-T6 (web) and 7075-T6 (cap angle extrusion). No evidence was noted of a corrosion or fatigue mechanism or other departure from a predominately static stress-induced mechanism. Photographs M3 and M5 of Figure 92 show representative views of replicas, the former in a rather coarse fracture area of the web and the latter of the frame cap angle. Some surface effects of staining noted in M5 are attributable to a post-cracking condition rather than an original fracture.

Edge replicas taken of the same member, representative of which are shown in Figure 92, produced less consistent results in regard to determination of gross fracture propagation direction. Several samples were stained, as shown by E3 of Figure 93, obliterating true dimple direction. A number, as shown by E5 and E7, indicated the crack propagation direction to be normal to the surface of the member. Without replication in corresponding areas of mating surfaces, conclusions drawn solely from the latter replicas are questionable.

Edge replicas taken from the lower left-hand member revealed considerably more decisive information. Fractographic evidence, together with some visual results, indicate that the crack emanates from an origin located in the cap angle extrusion at the intersection of the legs, and probably at the inner radius surface. Fracture directions noted in Figure 91 are taken from replicas represented in Figures 94 and 95. Again, post-crack staining obliterated some evidence: E2 and E6. The fracture appears to propagate from this location, up the vertical leg of the angle and simultaneously outboard, transmitting to the attached web, then through the lightening hole, and ending at the tank wall.

Close examinations were made of inner radius surfaces of upper and lower frame cap angle extrusions suspected as origins of failure. While the lower frame segments revealed no extraordinary cause for failure, except the possible stress-raising effect of the radius, examination of the upper cap angle extrusion produced a number of minute surface indications in the radius and adjacent to the fractures which were determined to be extrusion defects. These defects predominated in the upper left-hand members, while secondary cracks approximately parallel to the major crack were revealed in the upper right-hand member (Figure 96). A region identified as O on the right-hand

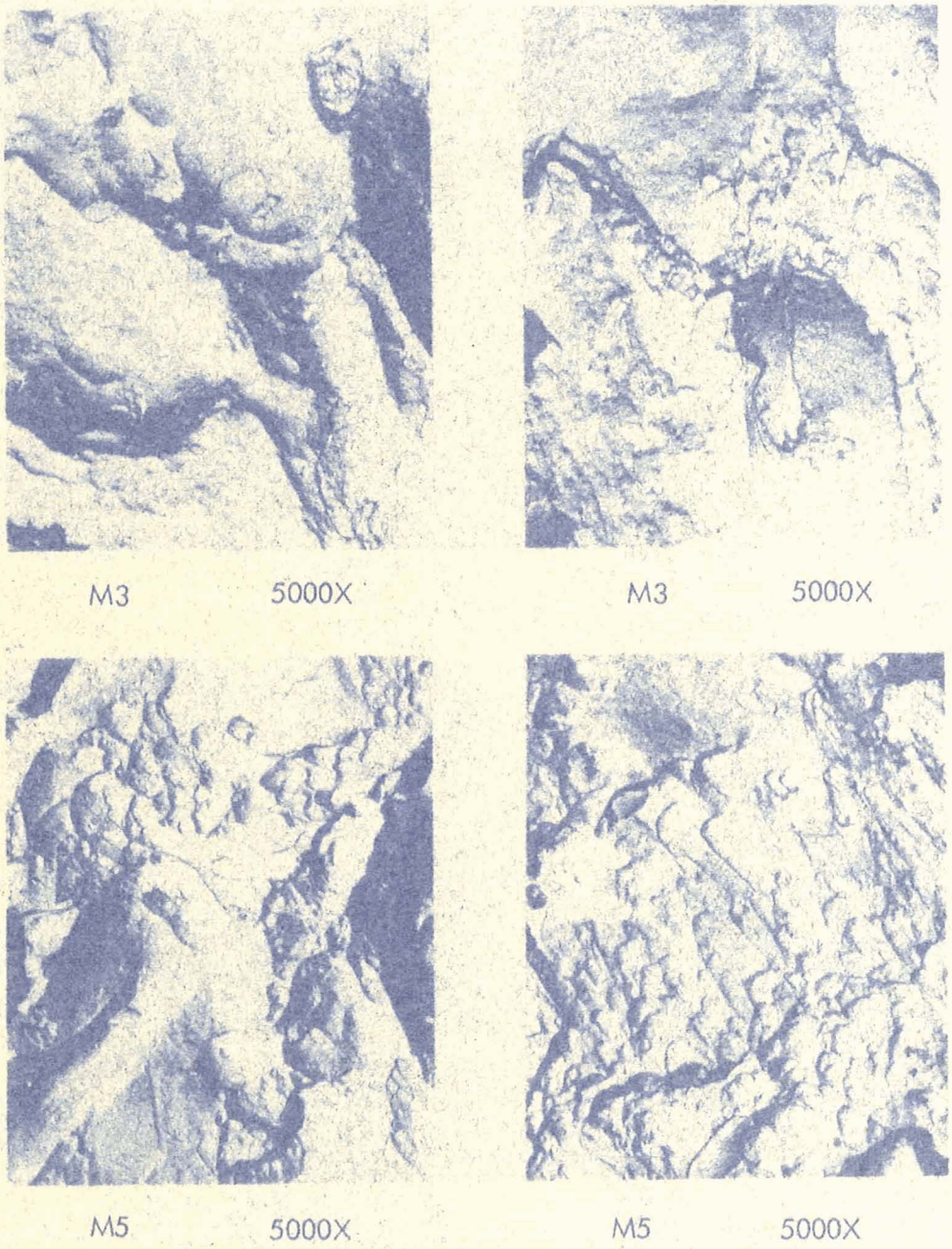

Figure 92. Mode Replicas Taken From Upper Left-Hand Frame Member Fracture Surfaces

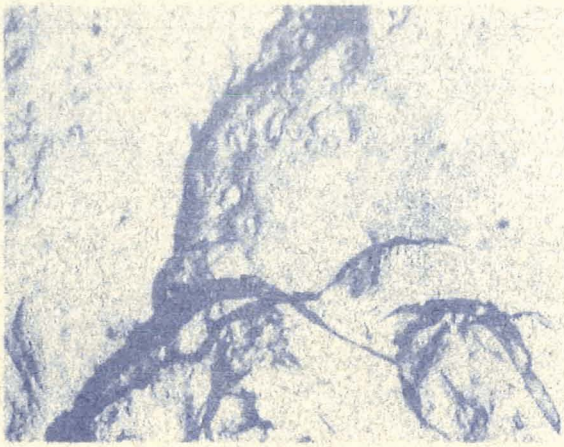

E3 5000X

E3 5000X

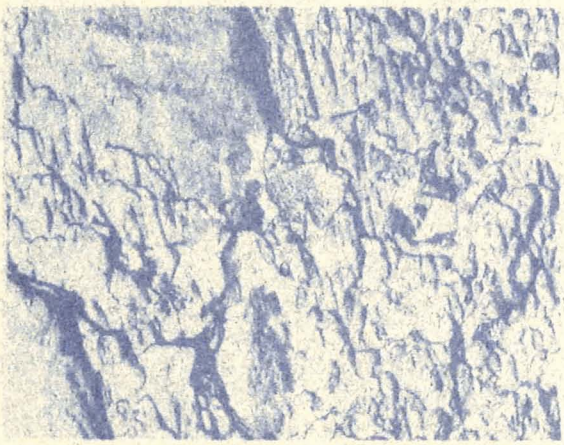

E5 5000X

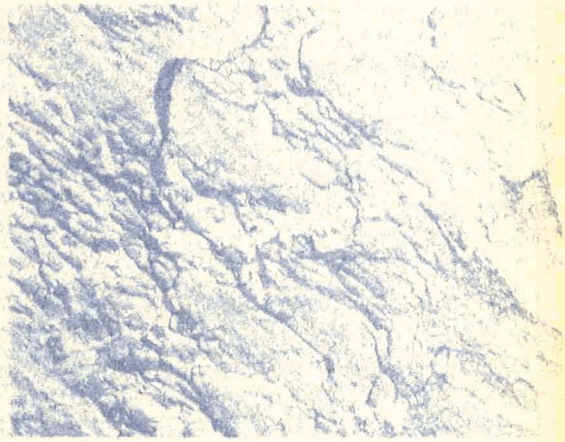

E7 5000X

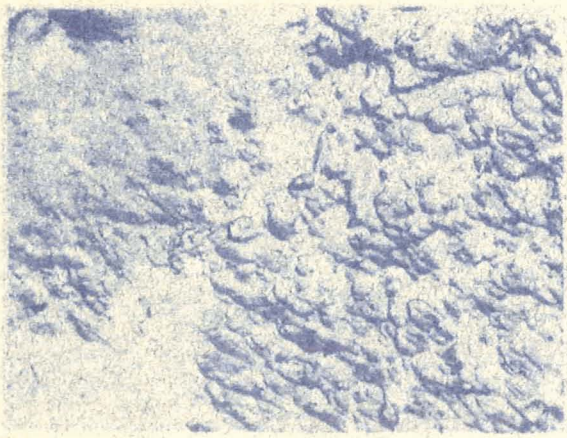

E9 5000X

E9 5000X

NOTE: DUPLICATE PHOTOS TAKEN PER LOCATION

Figure 93. Edge Replicas Taken From Upper Left-Hand Frame Member Fracture Surface

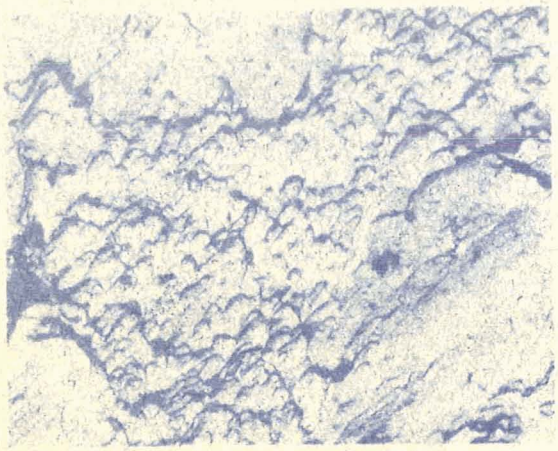

E1 5000X

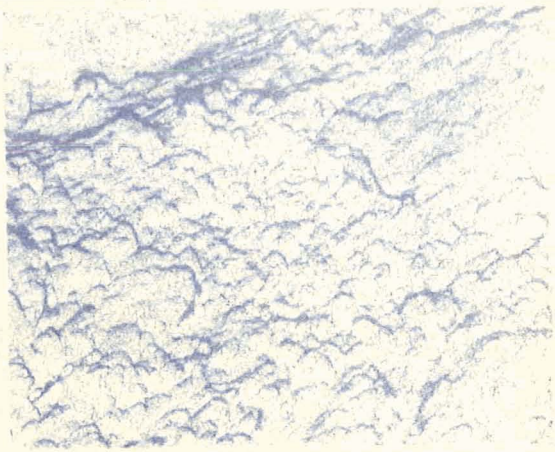

E1 5000X

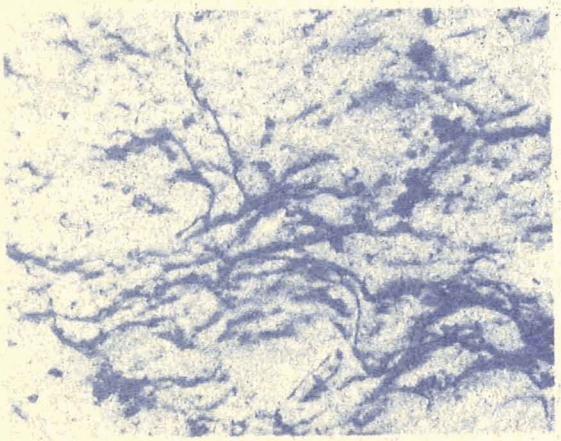

E2 5000X

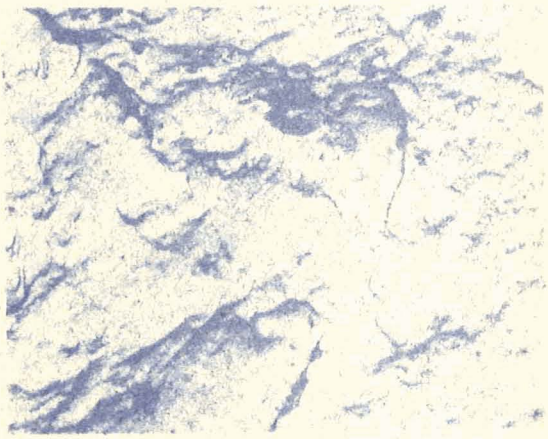

E2 5000X

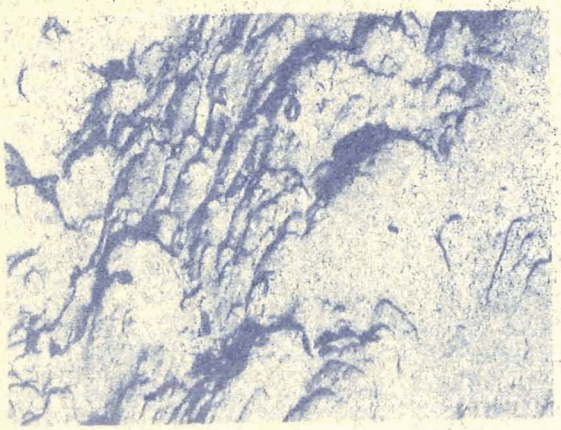

E3 5000X

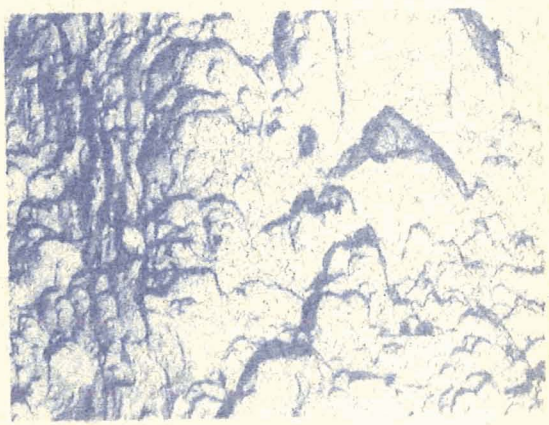

E3 5000X

NOTE: TWO PHOTOS TAKEN PER INDICATED LOCATION

Figure 94. Edge Replicas Taken From Lower Right-Hand Frame Member Fracture Surface

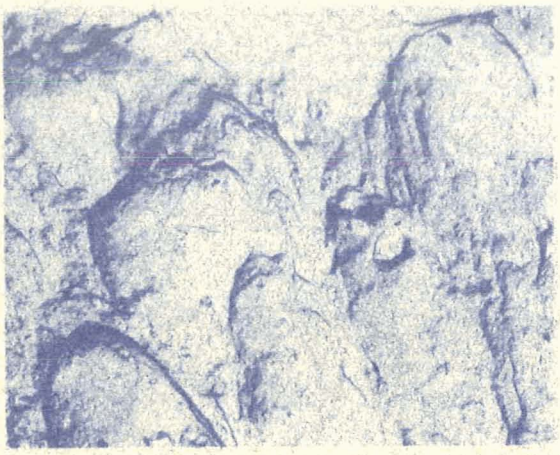

E4 5000X

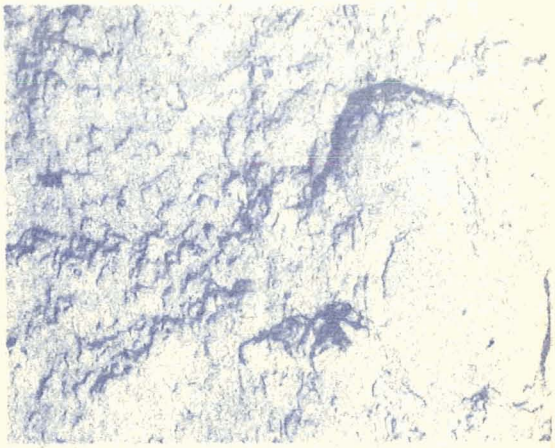

E4 5000X

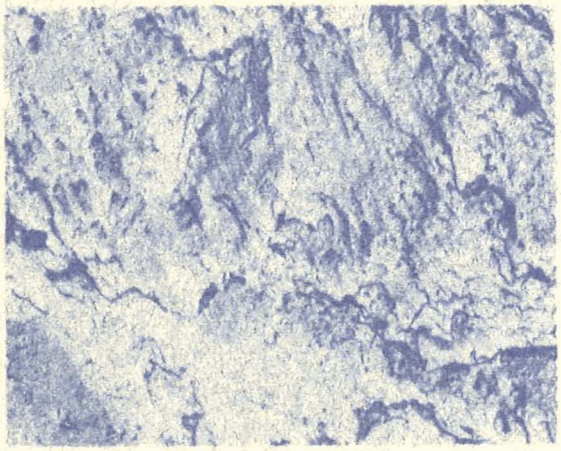

E5 5000X

E5 5000X

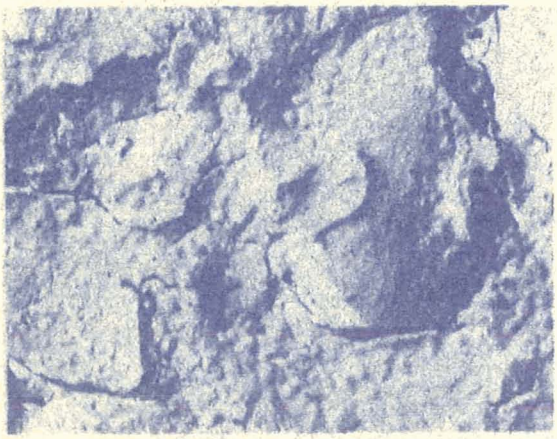

E6 5000X

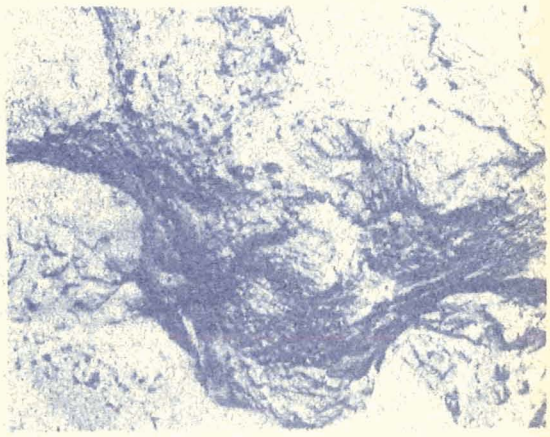

E6 5000X

NOTE: TWO PHOTOS TAKEN PER INDICATED LOCATION

Figure 95. Edge Replicas Taken From Lower Right-Hand Frame Member Fracture Surfaces

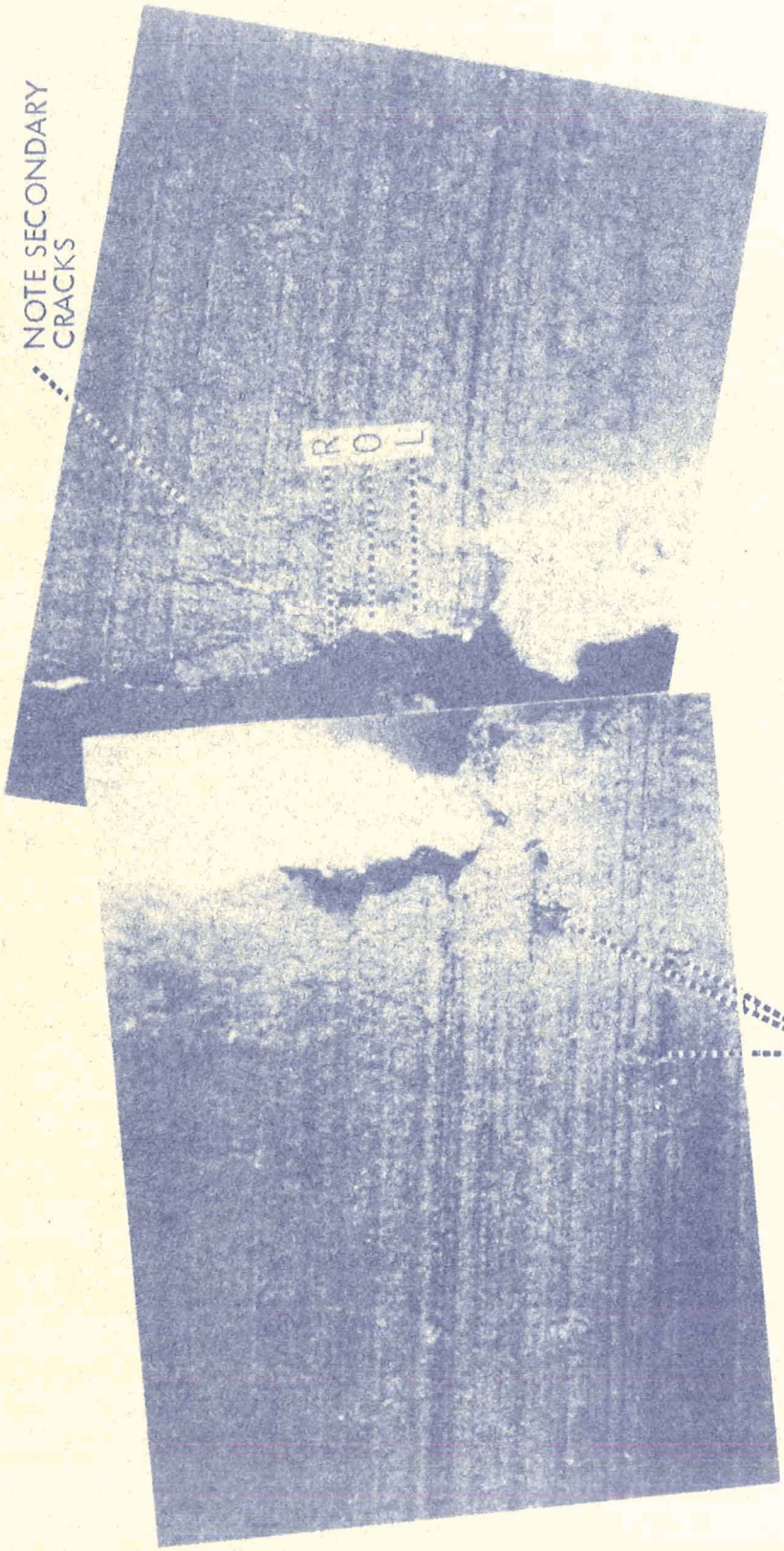

Figure 96. Upper Cap Angle Extension Showing Surface Defects in Radius

member of Figure 96 suspected as a point origin was replicated to determine fracture mechanism, and adjacent edge replicas, L and R, were examined to establish fracture direction (Figure 97). The mode replicas revealed equiaxed dimples, again indicating, ductile tensile-type failure with no other mechanism present. Adjacent-edge replicas also produced equiaxed dimples, providing no clue as to fracture propagation direction. The similarity in appearance of all six replicas suggests the possibility that all areas replicated fell within the origin, and that insufficient distance between L, O, and R locations was obtained to ensure location of remote surface material subjected only to progressive crack propagation during fracture.

Sections were taken through the surface blisters and secondary cracks, and these were examined metallographically. Two blisters, highly magnified in Figure 98, show the intergranular nature of the flaws considered defects incurred during hot extrusion of the angle in fabrication. The intergranular nature of the secondary cracks strongly suggested grain separation during extrusion. It is apparent that the overload conditions, which produced gross failure of the structure, resulted in fracture at or through these defects in this member. No evidence of corrosion was detected during this investigation. A photomicrograph composite showed a ductile, transgranular propagation of the fracture throughout the remainder of the section, indicating high static tensile loading as the driving force for fracture.

DISCUSSION

Failure of the frame assemblies is believed to have occurred during hydrostatic testing of the LH_2 tank section; staining of the freshly exposed fracture surfaces was produced by chromate additions used to inhibit the water used as the test medium. A combination of tensile stresses in the frame assemblies produced by imposed hydrostatic pressure, and bending stresses acting in the plane of the frame webs about an axis at or near the weld splice (produced by some configurational effect of the weld splice structure resisting uniform expansion of the tank circumference) acted to shear the four frame-attachment rivets initially, and subsequently initiate fracture in the frame cap angle members of both assemblies.

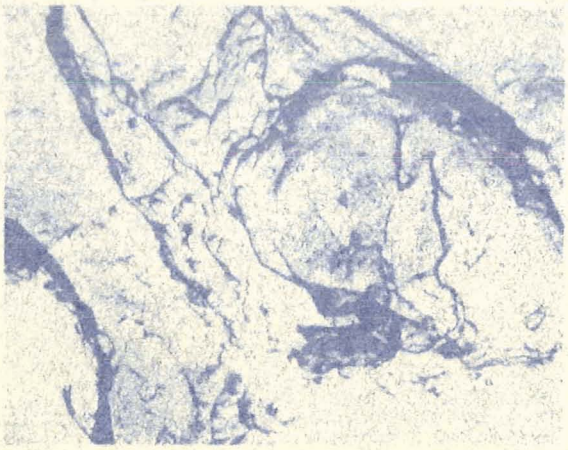

O MODE 5000X

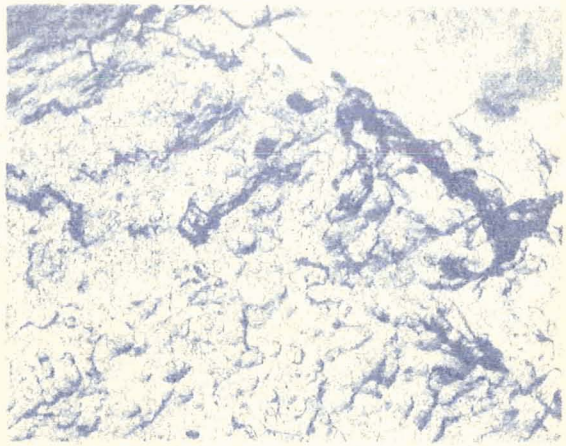

O MODE 5000X

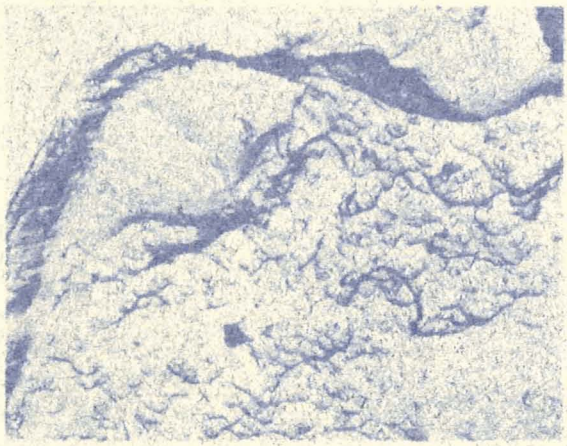

L EDGE 5000X

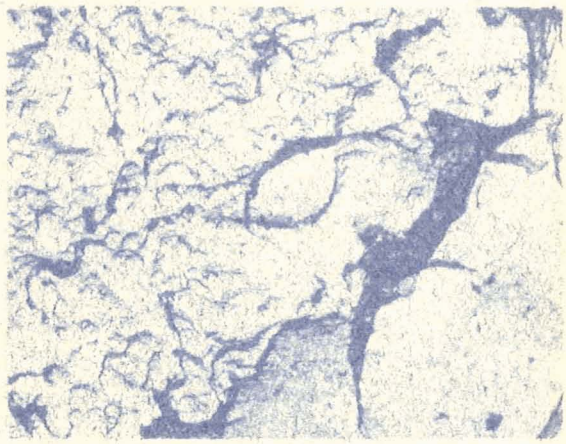

L EDGE 5000X

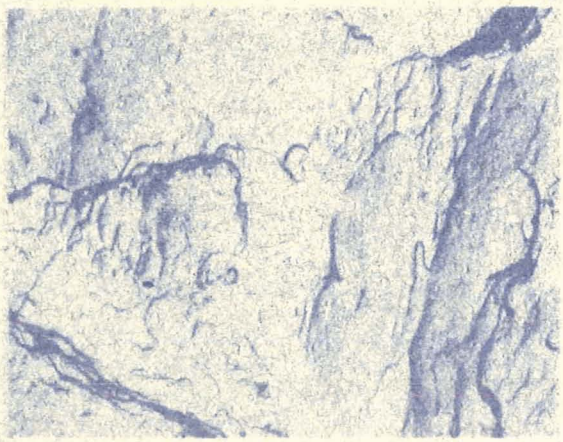

R EDGE 5000X

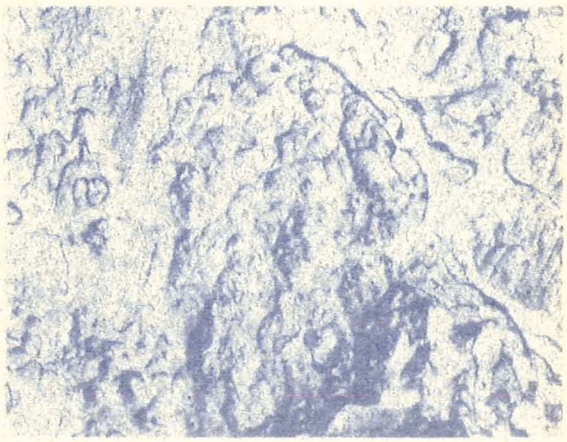

R EDGE 5000X

Figure 97. Replicas Taken From Suspected Origin of Upper Frame Cap Angle Extrusions

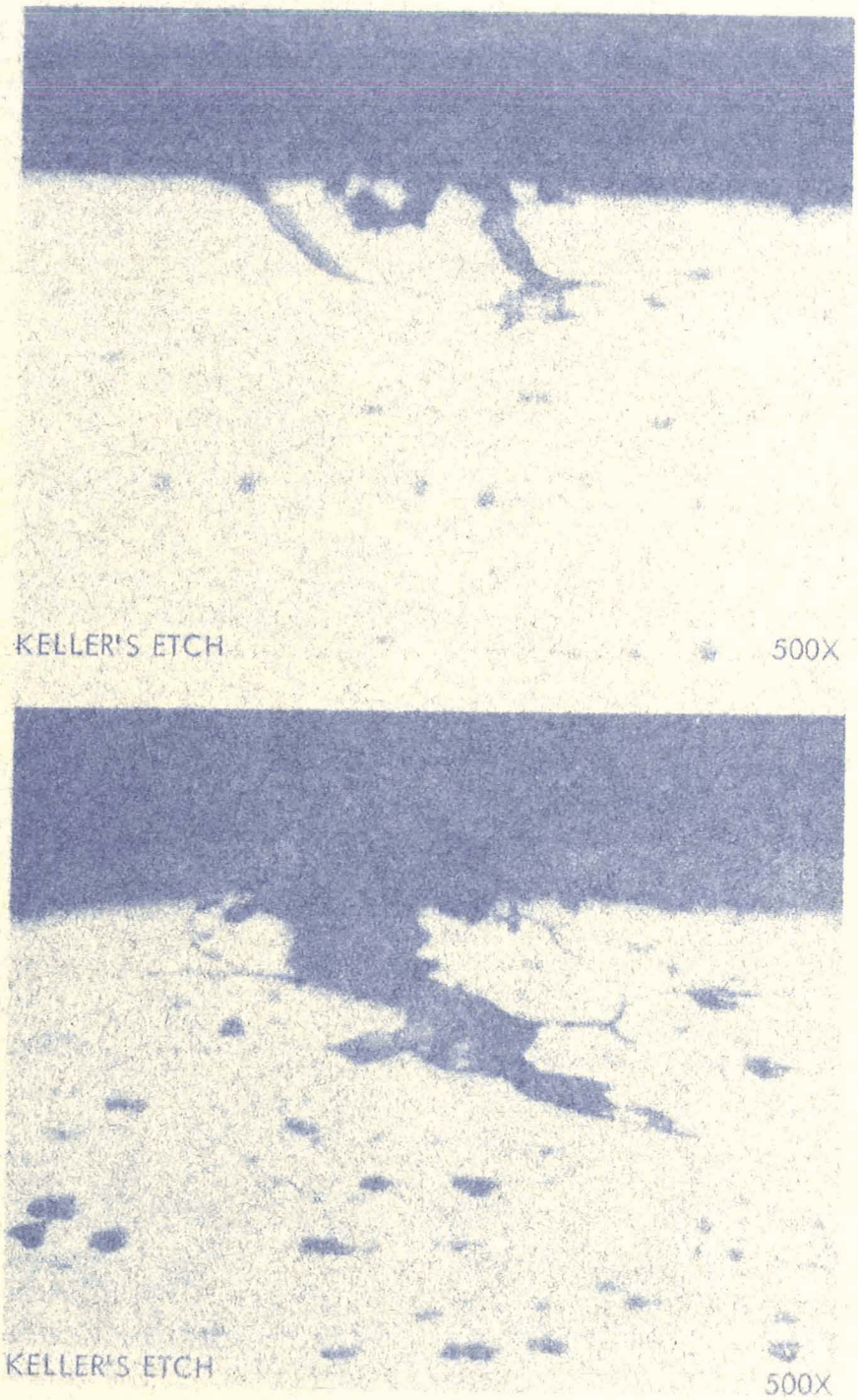

(SEE FIGURE 96)

Figure 98. Extrusion Defects Discovered in the Upper Frame Cap Angle

METALLURGICAL INVESTIGATION OF FRAMES AND CAP ANGLES FROM S-II-7

INTRODUCTION

During hydrostatic testing of the S-II-6, a structural failure occurred in the frame assemblies inside the LH_2 tank. The cracked frame assemblies were metallurgically analyzed, indicating that the failure occurred in a ductile manner resulting from an overloading condition. The material and processing procedures were found to be satisfactory.

Upon hydrostatic testing of the S-II-7, a similar cracking failure was encountered in the frame assemblies. Considering the results of the failure analysis on the S-II-6, the current investigation was limited to verification that the material and processing procedures were satisfactory in sections of the S-II-7 frame assemblies removed from areas adjacent to the cracks.

The frame assemblies consist of a 2014 aluminum alloy sheet stock frame (V7-312214) and a 2014 aluminum alloy extruded cap angle (V7-312220) joined by mechanical fasteners to form the frame assembly. The frame assemblies are then mechanically fastened to the inside of the liquid hydrogen tank.

CONCLUSION

The material properties and processing procedures were found normal and satisfactory.

PROCEDURE

Spectrographic analyses were performed on a sample from each of the three frames and each of the three cap angles. Tensile bars were fabricated from each of the three frames and cap angles. The bars were in the long transverse direction from the sheet stock frames and in the longitudinal direction from the extruded cap angles.

Samples for metallographic analyses were cut, mounted, polished, and observed at magnifications from 50 to 500 diameters. Both longitudinal and transverse samples were taken from each of the three frames and cap angles.

RESULTS

The results of the chemical analyses were normal and acceptable for 2014 aluminum alloy. The results of the tensile tests were normal and acceptable for 2014 sheet stock and 2014 extrusions, respectively. All samples examined exhibited a normal microstructure for 2014 aluminum alloy.

CORROSION

PROGRESS SUMMARY

Corrosion is an unrelenting hazard to any structure or system containing metallic materials. Corrosion may occur during raw material storage, manufacturing, installation, testing, or storage of the final assembly. Several problems were reviewed during the reporting period. In two cases involving small components, the corroded parts had not received the corrosion protective plating required by the drawings. In other cases, new protective coatings were applied to prevent corrosion. To reduce surface attack on the S-II LH_2 quarter-panels during manufacturing, an extensive investigation of processing parameters was conducted. Several changes were instituted to improve corrosion resistance of the film coating and to reduce detrimental environmental exposure.

METALLURGICAL EVALUATION OF CORRODED RETAINER, P/N V7-315563

INTRODUCTION

Two retainers, P/N V7-315563, from a ball lock assembly on the Saturn S-II umbilical connector were evaluated for existing corrosion. The retainer is maraging steel with an electroless nickel plate 0.001 inch to 0.0014 inch in thickness. The evaluation consisted of determining the electroless nickel plating thickness and depth of corrosion pits.

CONCLUSION

Tests showed no plating on the retainer and the depth of corrosion pits as 0.0014 inch to 0.0023 inch.

PROCEDURE AND RESULTS

Microsections were made of the retainers, and evaluation at 100X magnification showed no plating on the surface. To confirm this, a spectrographic analysis and a copper sulfate immersion test were performed. The spectrographic analysis showed no phosphorus, which would be a major constituent of the plating.

PACE WIANCKO PRESSURE TRANSDUCER FAILURES CAUSED BY ELECTRICAL SHORTING

INTRODUCTION

Pace Wiancko of Whittaker Corporation manufactures part ME449-0109-0003, a 0- to 15-psig pressure transducer used in five GSE S7-45, insulation purge control consoles. About 14 transducers are used in each unit. The transducers were failing at MTF and KSC. When disassembled at Pace Wiancko, a considerable wet, whitish aluminum oxide was found on the aluminum walls of the sensing chambers. Because the only entry into the chamber was an 0.020-inch hole, and the transducers were supposedly in a dry, nitrogen-purged enclosure, it was not evident as to how the corrosive agent was being introduced.

The purpose of this investigation was to determine the cause of corrosion in the transducer reference chamber and to determine a method of protecting the transducer from corrosion failures.

CONCLUSIONS

The GSE console is not purged with dry nitrogen during periods of inactivity. Over a period of time, the atmosphere inside the console becomes more extreme than normal outside MTF or KSC conditions. Thus, corrosion is caused by the ingress of moisture through the transducer's breath hole into the reference chamber. The insulation resistance, however, may drop below the five-megohm minimum requirement from the presence of moisture alone without corrosion.

Neither the internal painting of the chamber nor the addition of a desiccant assembly will guarantee a good insulation resistance or eliminate corrosion over an extended period of time under the extreme conditions experienced in the console at MTF.

Failed transducers that are found corroded can be cleaned. Testing indicates that some units are acceptable if they are cleaned and reassembled, saving a good portion of the reported $500 to $700 rework cost. Cleaning, however, is not the final solution because the parts corrode rapidly after being returned to service. This transducer is now under design change.

TEST AND RESULTS

Chemical Analysis on Failed Transducers

The six transducers examined at Pace Wiancko had five corrosion products differing in appearance: a clear jelly, a white jelly, a white paste, a brownish-white solid, and a clear yellow solid or gel. Chemical analysis showed all were different hydration states of aluminum oxide.

Humidity Testing of Transducers

Transducers, with attached desiccant bodies, were placed in a humidity chamber that cycled from 60 to 100 F and back to 60 F every 4 hours at 80- to 95-percent relative humidity for 14 days. The insulation resistance readings were taken 2 hours after removal from the humidity chamber. In this test, the desiccants 40-percent-expended color indicator did not change, indicating that very little moisture entered the chamber through the desiccant.

The desiccant bodies were removed from the two transducers and the chamber aluminum walls were painted with an epoxy-amine coating. Electrical contacts were protected with a silicone rubber. The transducers were placed in the humidity chamber using the same parameters just described. At the conclusion of the test, the insulation resistance was still good but not as good as obtained after the first test indicating the necessity of eliminating moisture from the reference chamber for best results.

Transducers with the internal coating were placed for 35 days in a humidity chamber cycling from 100 to 160 to 100 F every eight hours. This accelerated version of MIL-STD-810, Method 507, is an extreme corrosion test. After the test, the reference chamber was clean with no visual corrosion.

Salt Mist Chamber Exposure of Simulated Transducers

Cups of 2024 aluminum were machined and drilled to simulate the reference chamber of the transducers. A section of PH17-4 Mo honeycomb was placed in the cup and then pressed down and sealed, except for the 0.020-inch hole, with a plate of 301 CRES and silicone sealant. During 336 hours of 5-percent sodium chloride mist exposure at 95±5 F, the three units became completely corroded with deep pitting and white and green (copper) corrosion products. However, the interiors were bright, clean, and free of corrosion except around one silicone seal where seepage had occurred and on one spot on the cup bottom where a line of honeycomb rust was deposited.

This test proved that, with only small temperature variations (no breathing cycle), the internals of a transducer would not draw in a harmful amount of the corrosive external atmosphere.

OBSERVATIONS AND DISCUSSIONS

Six failed transducers from MTF were opened for observation. The following observations were significant:

Observation	Significance
Transducers S/N 50041, 50048, 50050, and 50066 were heavily corroded internally. Corrosion on the external surfaces was limited to areas where the steel mounting screws go through the aluminum body.	The corrosion is galvanically accelerated by the internal steel/aluminum couple.
Water was present in some of the transducers.	Entrapped, condensed moisture does not readily reevaporate, and remains as a corrosive agent.
All paper calibration stickers on the units appeared to have been water-soaked.	The GSE console is not sealed against water, and the transducers are exposed to water.

Effect of Drying on Transducer's Insulation Resistance

When units were dried by heat and vacuum after testing, the insulation resistance would improve. However, if the unit were disassembled, then immediately reassembled, the insulation resistance would improve an extra amount. Units that were not dried but were disassembled then reassembled also exhibited this marked improvement upward into an acceptable range.

CAUSE OF SHORT TRANSVERSE SURFACE ATTACK OF S-II LH_2 QUARTER-PANELS

INTRODUCTION

Corrosion and/or surface defects have been a problem on Saturn S-II hardware, particularly on ribs and stringers of LH_2 quarter-panels. Defects have been removed by grinding and/or etching, and in some instances it has been necessary to rework repeatedly to obtain satisfactory dye-penetrant readings. Rework of defects on one LH_2 quarter-panel resulted in removal of material below minimum strength requirements and the panel was scrapped. This panel is being used by the laboratory to determine the cause of defects.

Very little information was available regarding environmental exposure of the LH_2 quarter-panels between processing steps and the effect of exceeding specification limitations during chemical processing operations. An investigation was conducted to establish some of the factors which might cause the selective attack on the short transverse surfaces of Saturn S-II LH_2 quarter-panels.

The purpose of the investigation was as follows:

1. To determine the effect of excessive environmental exposure to 2014-T6 aluminum alloy between selected processing steps, and the effect of extended chemical processing times exceeding specification limitations in conjunction with excessive environmental exposure between selected process steps.

2. To determine any difference between processing 2014-T6 aluminum panels through used manufacturing chemical processing solutions and freshly prepared laboratory solutions, and the effect of accelerated environmental exposure on these panels.

3. To determine the effect of ac electrical leak on panels processed through laboratory chemical solutions simulating manufacturing processing solutions.

CONCLUSION

The current manufacturing sequence and a comparison to the former processing sequence are shown in Table 33. Four of the five immersion chemical film applications have been deleted and protection of the aluminum surface from corrosion is achieved by using an oil film or manual chemical film application. The results of this investigation show that the current processing sequence will improve the corrosion resistance of the chemical film coating because there is less etching of the LH_2 panel surfaces. This will provide smoother surfaces.

Tests, involving excessive environmental exposure, show that conditions at LAD can be more conducive to corrosion of 2014-T6 aluminum alloy than at the Seal Beach Facility during various periods of the year. Repeated chemical processing of 2014-T6 aluminum alloy produces rough and pitted surfaces, increasing susceptibility to corrosion. Specimens of 2014-T6 aluminum alloy, processed through LAD's chemical solutions, exhibited more severe corrosion than those processed through laboratory solutions after being exposed to five-percent salt spray for the same time period.

The ac electrical leak during chemical processing had no perceptible effect on 2014-T6 aluminum panels.

PROCEDURES AND RESULTS

The manufacturing sequence used at LAD for LH_2 quarter-panels was determined by review of planning tickets and visits to the facility. The planning sequence used in the past, the current planning sequence, and the resulting changes are shown in Table 25.

Sections approximately 12 inches square were cut from a scrap LH_2 quarter-panel, so that each section included a rib and a stringer. To obtain raw material not been previously exposed to corrosive environments, 0.010 inch was machined to approximately a 125-rms finish from each surface of the ribs and stringers. This investigation was limited to an examination of the selective attack on rib sections.

Trim stock from a LH_2 quarter-panel identified as 2014-T651 aluminum plate, Kaiser Mill Lot Number 247-412, was designated Material A. Another aluminum plate, designated Material B, was identified by spectrographic analysis and hardness test as 2014-T6 aluminum. Forty short transverse coupons of each material, 0.125 by 1 by 4 inches, were prepared from both longitudinal and transverse grain directions. The coupons were machined to approximately a 125-rms-surface finish.

Table 25. LH_2 Panel Processing Operations at Los Angeles Division

Former Sequence	Current Sequence	Current Protection
1. Plate received from supplier and stored	No change	Oil film
2. Plate requisitioned by using department	No change	Oil film
3. Machine 0.100 inch from one side only	No change	Oil film
4. Finish machine (horizontal mill)	No change	Oil film
5. Chemical film (immersion)	Operation deleted	Oil film
6. Finish machine (vertical mill)	No change	Oil film
7. Weigh and bench to remove excess material	No change	Oil film
8. Chemical film (immersion)	No change	Chemical film
9. Brake form contour	No change	Chemical film
10. Machine longitudinal stringer ends	No change	Manual chemical film
11. Clean	No change	Chemical film
12. Penetrant-inspect stringer ends	No change	Chemical film
13. Chemical film (immersion)	Operation deleted	Manual chemical film
14. Drill, tap, and deburr holes	No change	Manual chemical film
15. Chemical film (immersion)	Operation deleted	Manual chemical film

Table 25. LH_2 Panel Processing Operations at Los Angeles Division (Cont)

Former Sequence	Current Sequence	Current Protection
16. Penetrant-inspect entire panel	No change	Chemical film
17. Chemical film (immersion)	Operation deleted	Chemical film
18. Electrochemical etch Part Number, Serial Number, Etc.	No change	Chemical film
19. Install rubber stoppers	No change	Chemical film
20. Vinyl coat	No change	Chemical film and vinyl coat
21. Inspect - crate and transport to Seal Beach for etch and primer	No change	Chemical film and vinyl coat

One panel and one coupon of each grain direction from Materials A and B were subjected to the chemical film process solutions, as applicable, and within the environmental conditions shown in Table 26.

Panel sections 1 and 2 were sectioned at random. Photomicrographs of these sections are shown in Figure 99. Panel section 1 was a control sample, as sectioned from the scrap LH_2 panel; panel 2 was sectioned from the LH_2 panel and subjected to environmental exposure at LAD for 21 days, then processed through the Seal Beach LH_2 spray chamber. As shown in the photomicrograph, a pronounced corrosion pit developed after 21 days of environmental exposure.

Panels and coupons were processed through LAD by manufacturing personnel. One group of panel sections and coupons was processed once, and another group was processed ten times. The resulting surface finish is shown in Figure 100. Coupons A and B were pitted after chemical processing ten times. Figure 101 and 102 exhibit typical pits. Figure 103 shows typical surface obtained on the coupons after being processed through the tank solutions one time. After processing, the panels and coupons were subjected to prevailing outside environmental conditions at Seal Beach and LAD for 21 days.

Table 26. Test Schedule

Test Specimen	End Grain Direction	Processing Site and Cycles			Environmental Exposure (days)			Figure
		LAD	SB	Laboratory	LAD	SB	Salt Spray	
Panel section 2	Transverse		1		21			135
Coupons			1		21			
Panel section 3	Transverse	1						136
Coupons	Transverse	1						139
Panel section 4	Transverse	1	1		21			140
Coupons		1	1		21			
Panel section 5	Transverse	10	1			21		140
Coupons	Transverse	10	1			21		137, 138, 141
	Longitudinal	10	1			21		141
Panel section 6	Transverse	1					17	142, 144
Coupons	Transverse	1					17	145
	Longitudinal	1					17	143
Panel section 7	Transverse	1	1			21		140
Coupons		1	1			21		
		1	1			21		
Panel section 8	Transverse	10	1		1			140
Coupons	Transverse	10	1		21			141
	Longitudinal	10	1		21			141
Panel section 11	Transverse			1			17	144
Coupons	Transverse			1			17	145
	Longitudinal			1			17	
Panel section 12	Transverse						17	146
Coupons	Transverse						17	147
	Longitudinal						17	147

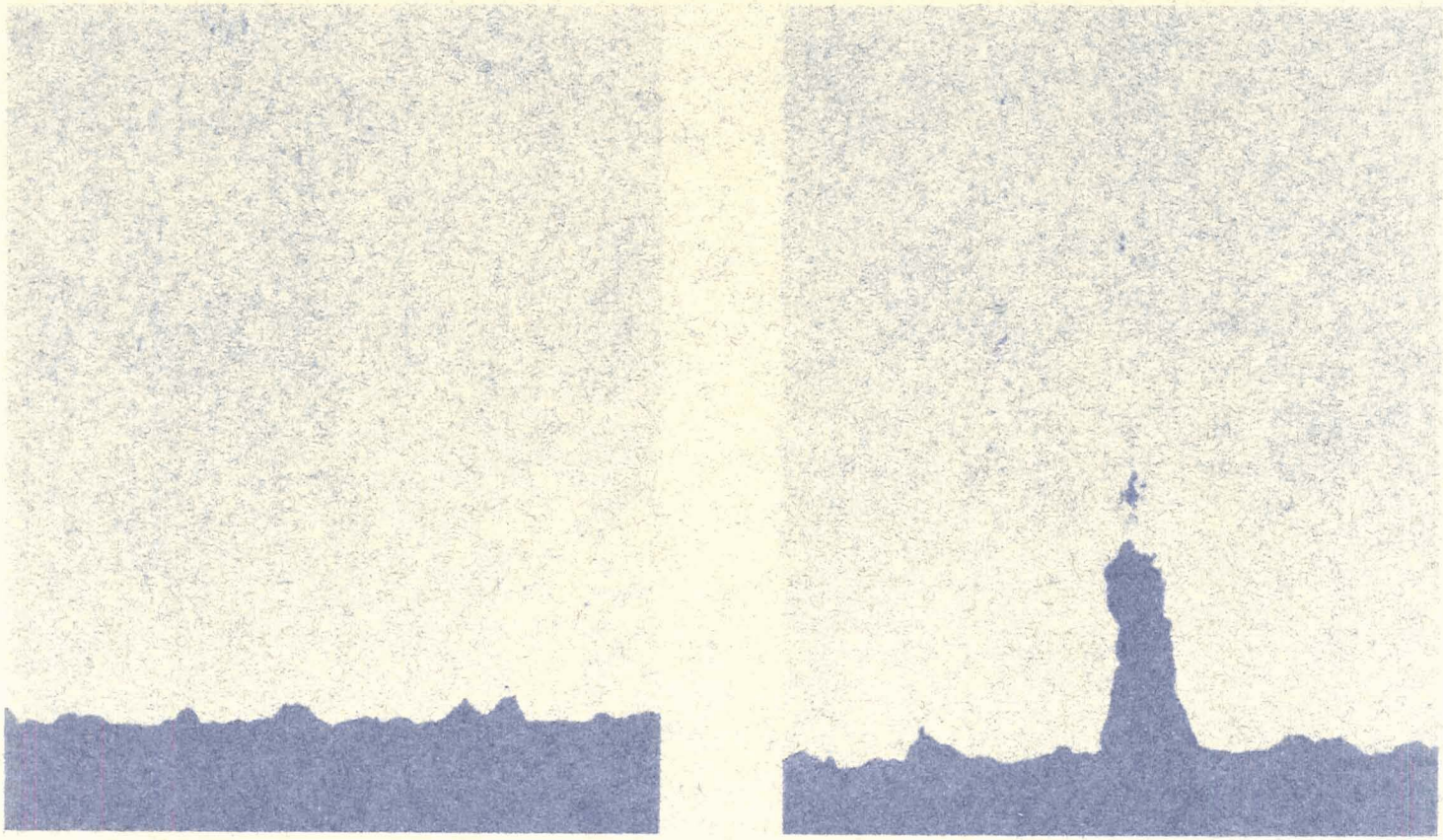

PANEL 1 (59K-16-1)
AS SECTIONED FROM LH_2 PANEL

PANEL 2 (59K-12-1) AFTER
21-DAY ENVIRONMENTAL EXPOSURE
AT LOS ANGELES DIVISION

NOTE: 100X MAGNIFICATION

Figure 99. Photomicrographs of Panel Sections As-Received and After LAD Environmental Exposure

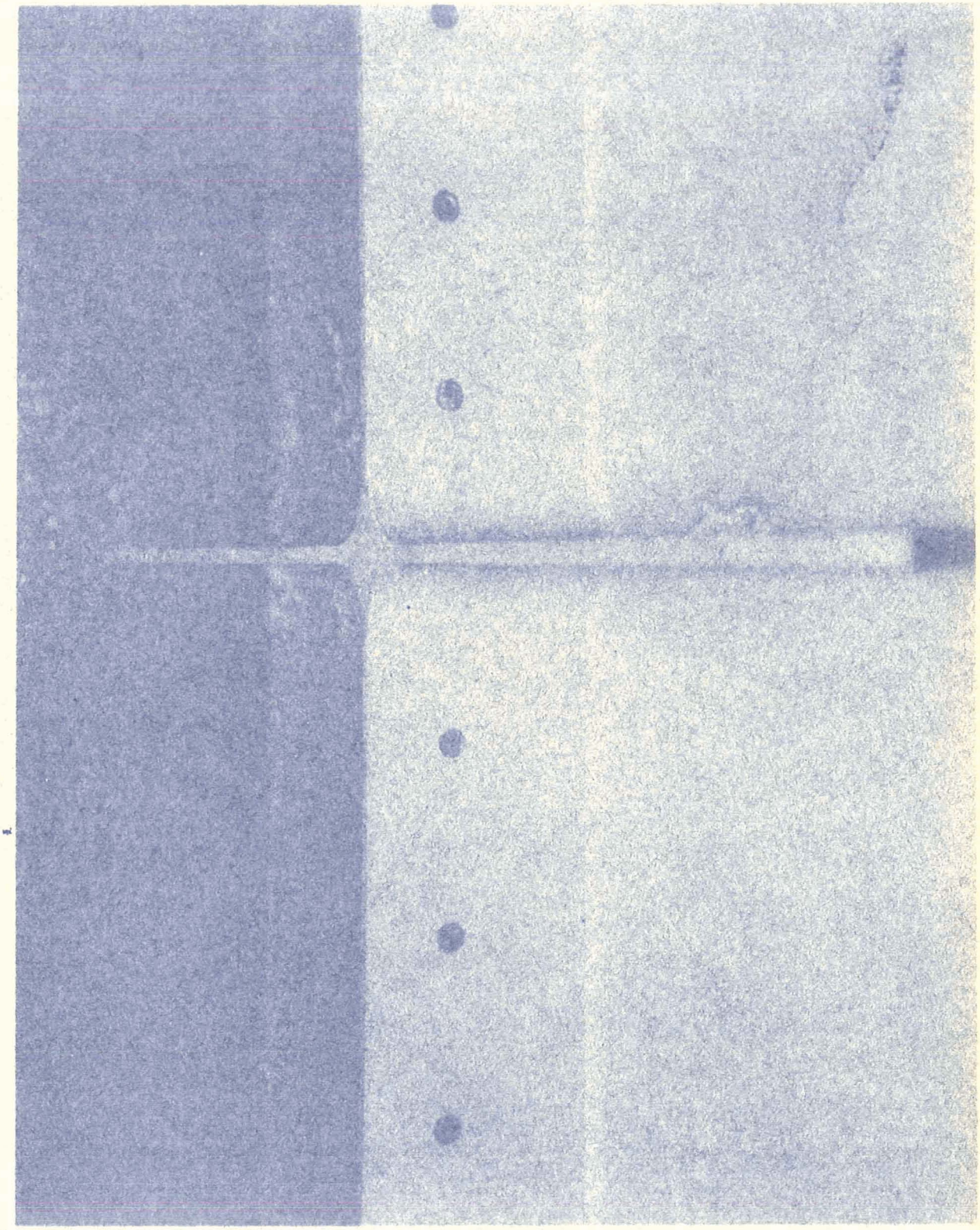

NOTE: 1X MAGNIFICATION PANEL 3

Figure 100. Panel Section Processed One Time Through LAD Solutions

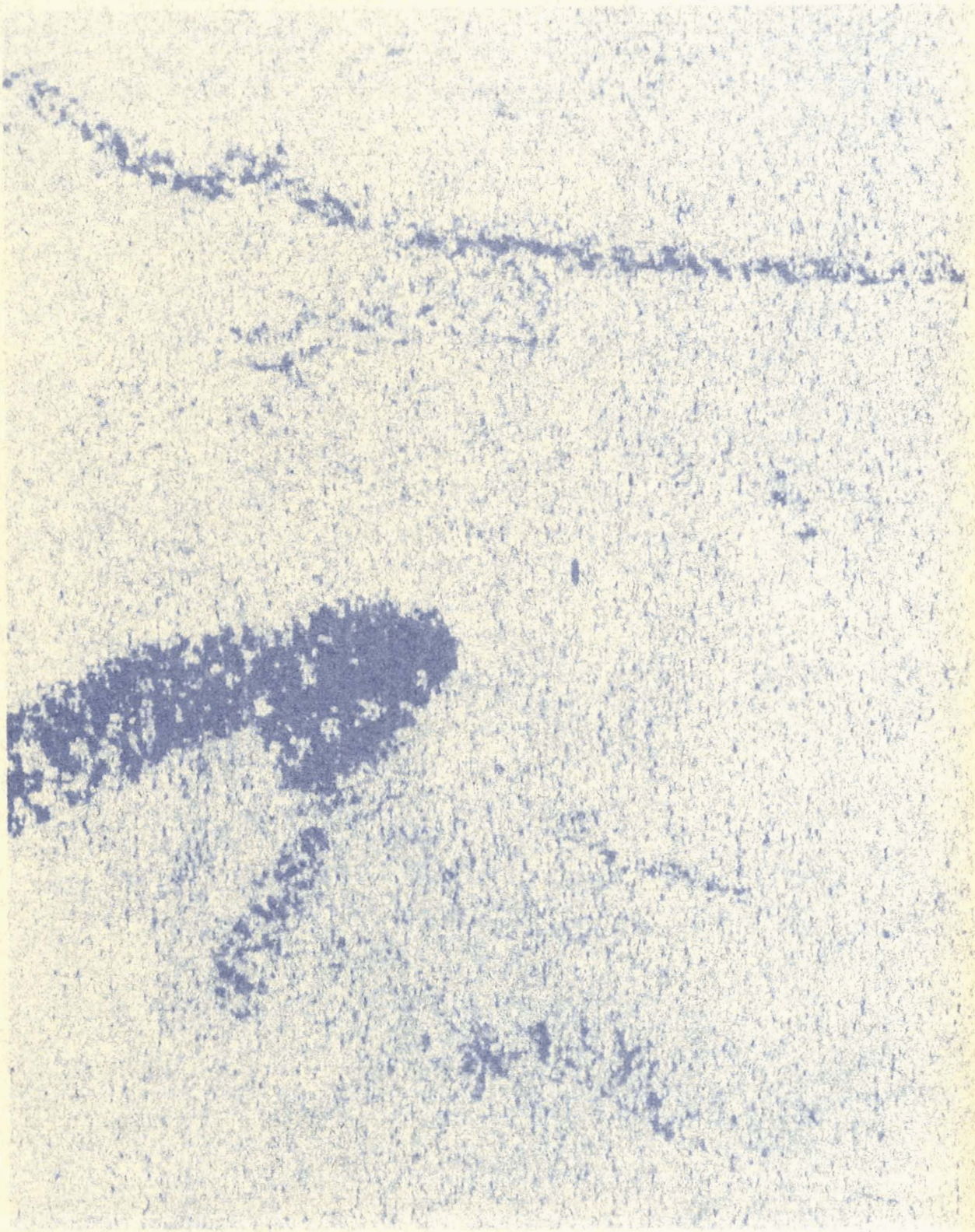

NOTE: 40X MAGNIFICATION TEST COUPON AT 5

Figure 101. Test Coupon Processed 10 Times Through LAD Solutions

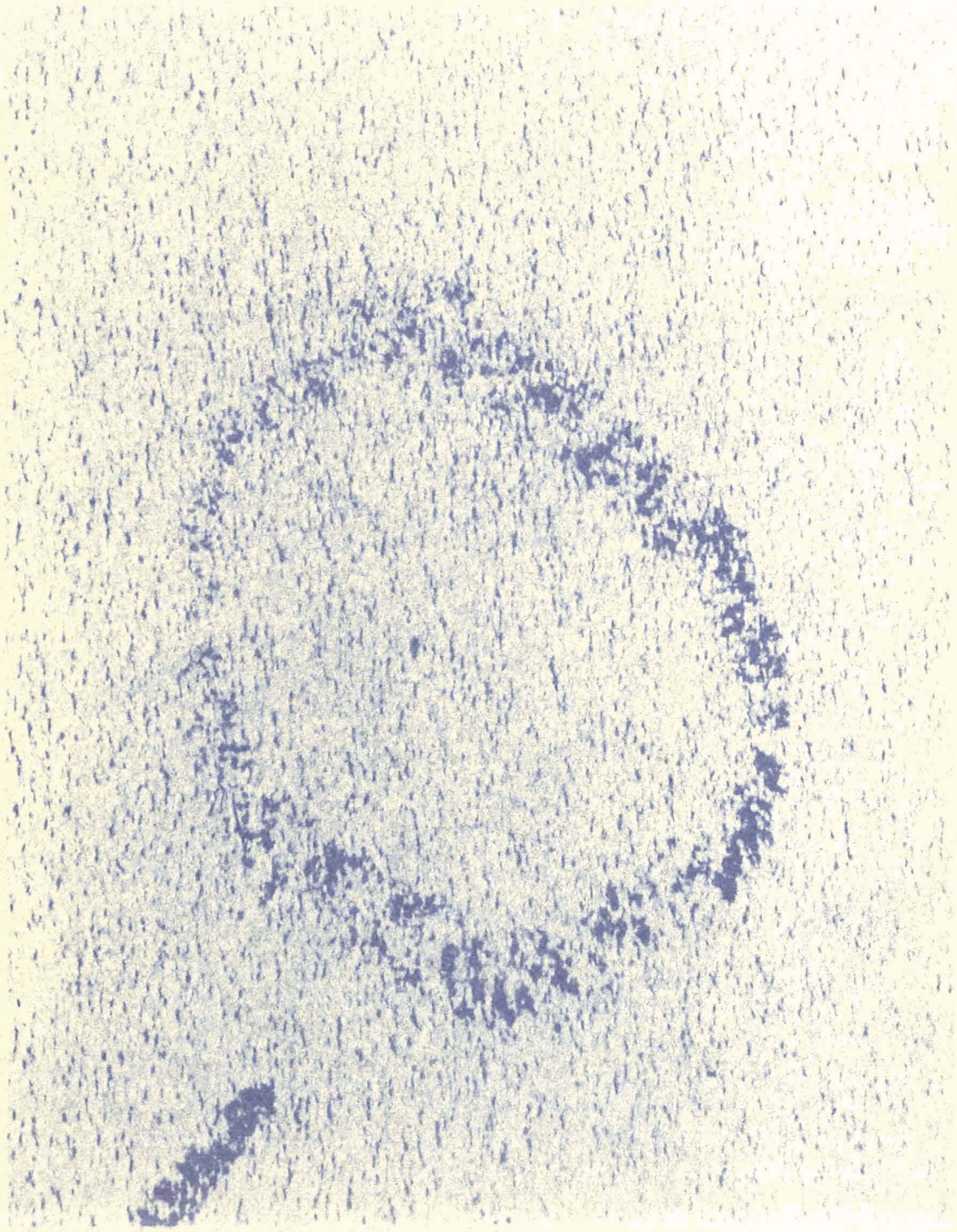

47K-BT-5

NOTE: 40X MAGNIFICATION

TEST COUPON BT-5

Figure 102. Test Coupon Processed 10 Times Through LAD Solutions

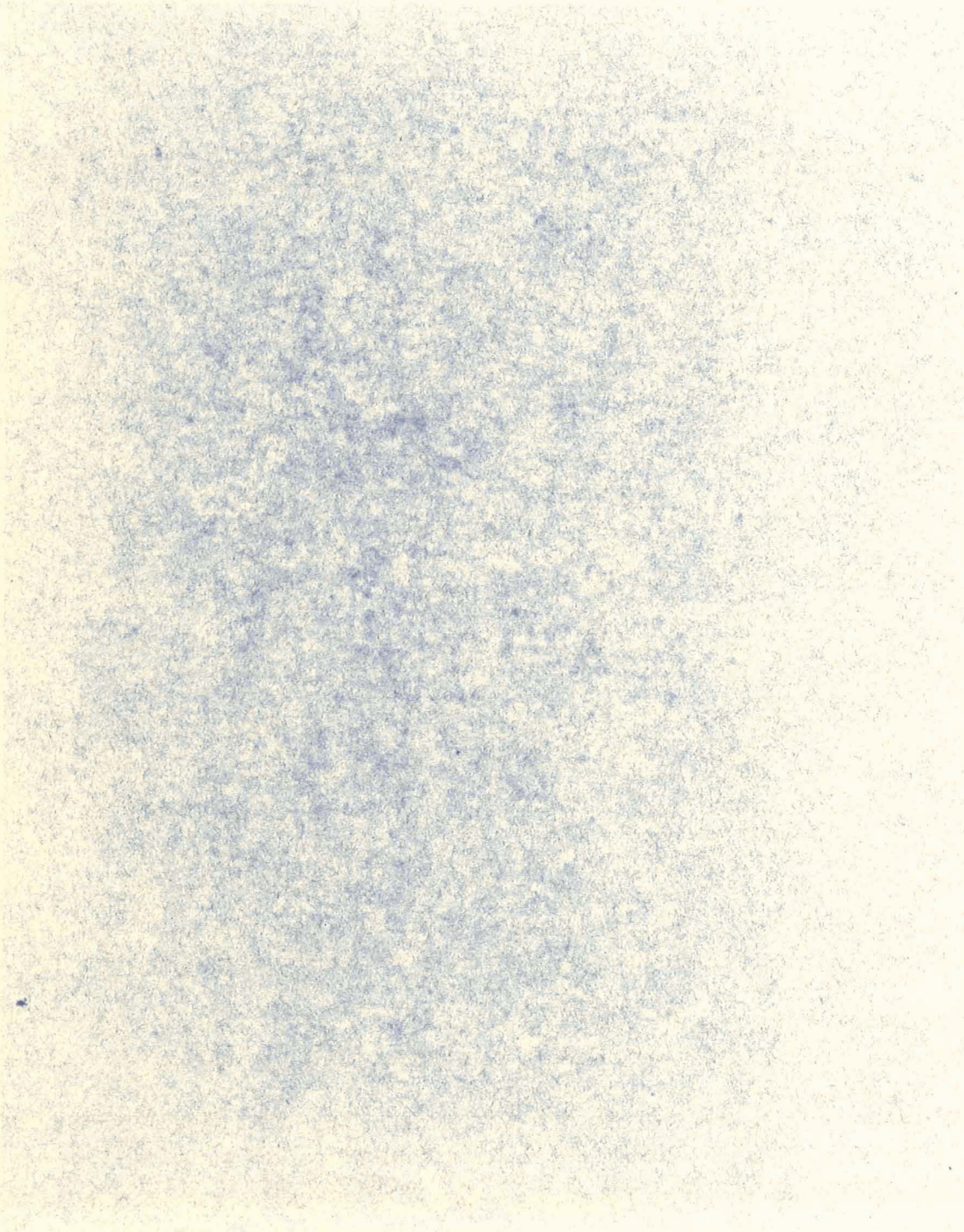

47K-AT-3

NOTE: 40X MAGNIFICATION

TEST COUPON AT-3

Figure 103. Test Coupon Processed One Time Through LAD Solution

After environmental exposure tests and LAD processing, the panel sections and test coupons were processed through the Seal Beach LH_2 panel spray chamber in the following sequence:

1. Spray alkaline clean
2. Chemical film strip
3. Deoxidize
4. Chemical film

A deionized water spray rinse followed each of the operations listed above. Figure 104 shows the effect to extended processing times and environmental exposure on panel sections. The panel sections processed through LAD solutions ten times have deeper pits than those processed once. The major difference, however, is between the pit depth and width caused by environmental exposure. This shows that environmental conditions at LAD are much more conducive to corrosion than at Seal Beach. Visual examination of coupons from the two different heats of 2014-T6 aluminum reveals more pitting on Material B than on Material A which is trim stock from the scrap LH_2 panel. This difference is shown in Figure 105, and the contrast is more pronounced on the coupons which were subjected to environmental exposure at LAD.

The chemical solutions in the laboratory tanks were prepared at maximum concentrations of the LAD specification requirements. The panel sections and associated test coupons were processed through the laboratory tanks using maximum specification immersion times. Three volts ac were applied to one panel section and one set of test coupons during immersion in the mild alkaline cleaner and the NA107A deoxidizer solutions. Evolution of gas from the specimens showed current flowing through the solutions. Examination of the panel sections and test coupons after processing revealed no significant change in surface condition, and there was no evidence of pitting or corrosion.

Panel section 6 and associated test coupons were processed through the LAD solutions. Panel section 11 and associated test coupons were processed through freshly prepared laboratory solutions. Both sets of specimens were then subjected to five-percent salt spray exposure test for 17 days. Figure 106 and 109 are photographs and photomicrographs of panel sections and test coupons after the exposure test. The test specimens processed through the LAD solutions exhibited many more corrosion products and much more pitting than the specimens processed through the laboratory solutions. Material B test coupons also exhibited much more pitting than the corresponding Material A coupons.

PANEL SECTION 5
AFTER 10 TIMES LAD PROCESS
AND 21-DAY SEAL BEACH
EXPOSURE

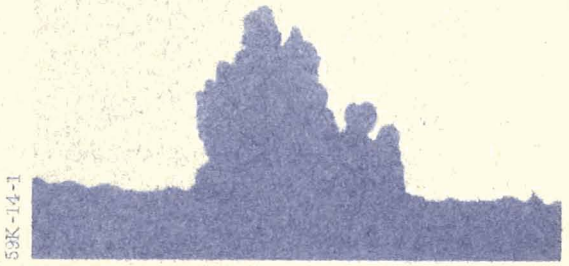

PANEL SECTION 8
AFTER 10 TIMES LAD PROCESS
AND 21-DAY LAD EXPOSURE

PANEL SECTION 7
AFTER ONE TIME LAD PROCESS
AND 21-DAY SEAL BEACH EXPOSURE

PANEL SECTION 4
AFTER ONE TIME LAD PROCESS
AND 21-DAY LAD EXPOSURE

NOTE: 100X MAGNIFICATION

Figure 104. Photomicrograph of Panel Sections After Environmental Exposure

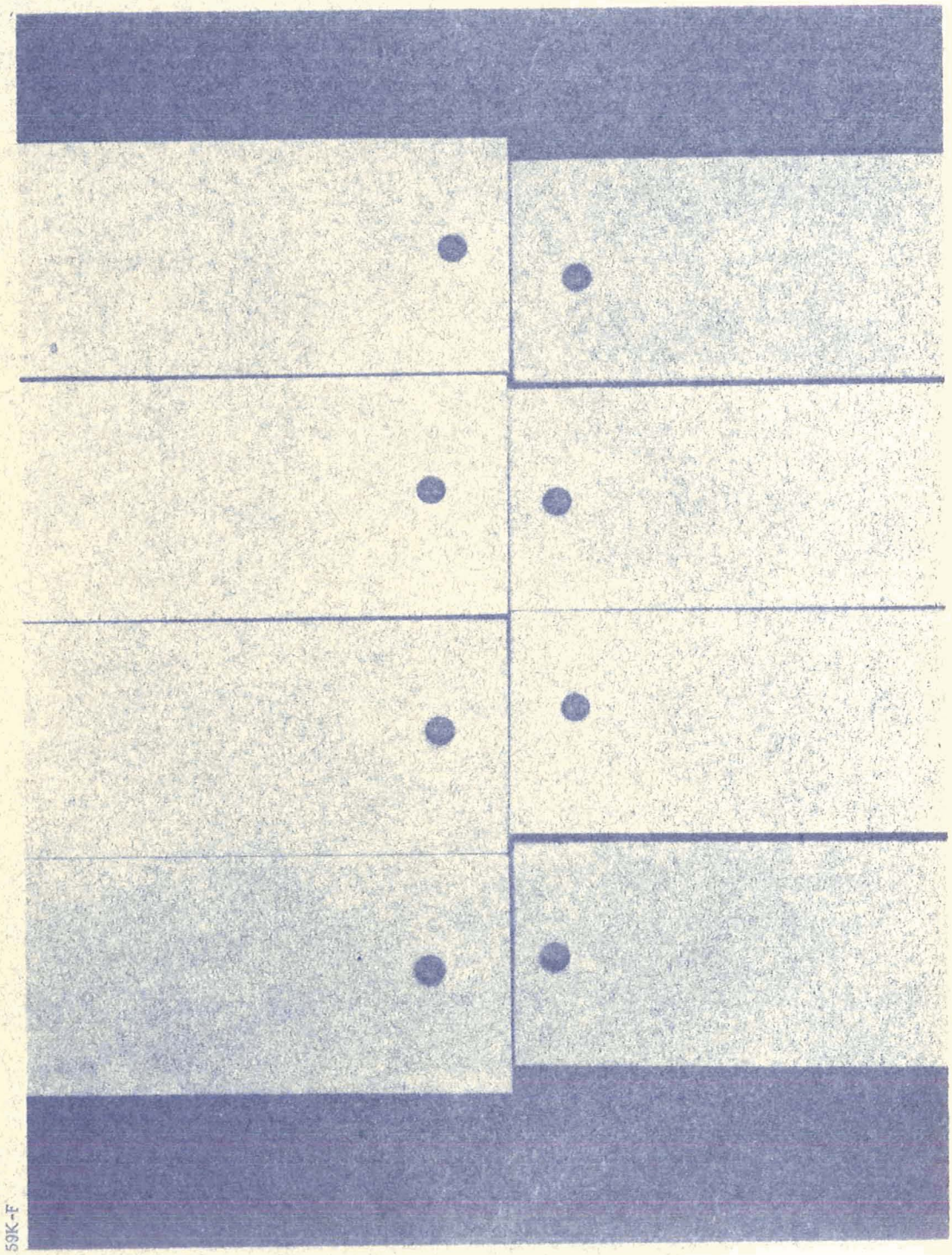

TEST COUPONS – SEE TEST SCHEDULE FOR PROCESSING

NOTE: 1X MAGNIFICATION

Figure 105. Test Coupons After Processing 10 Times Through LAD Solutions and Environmental Exposure

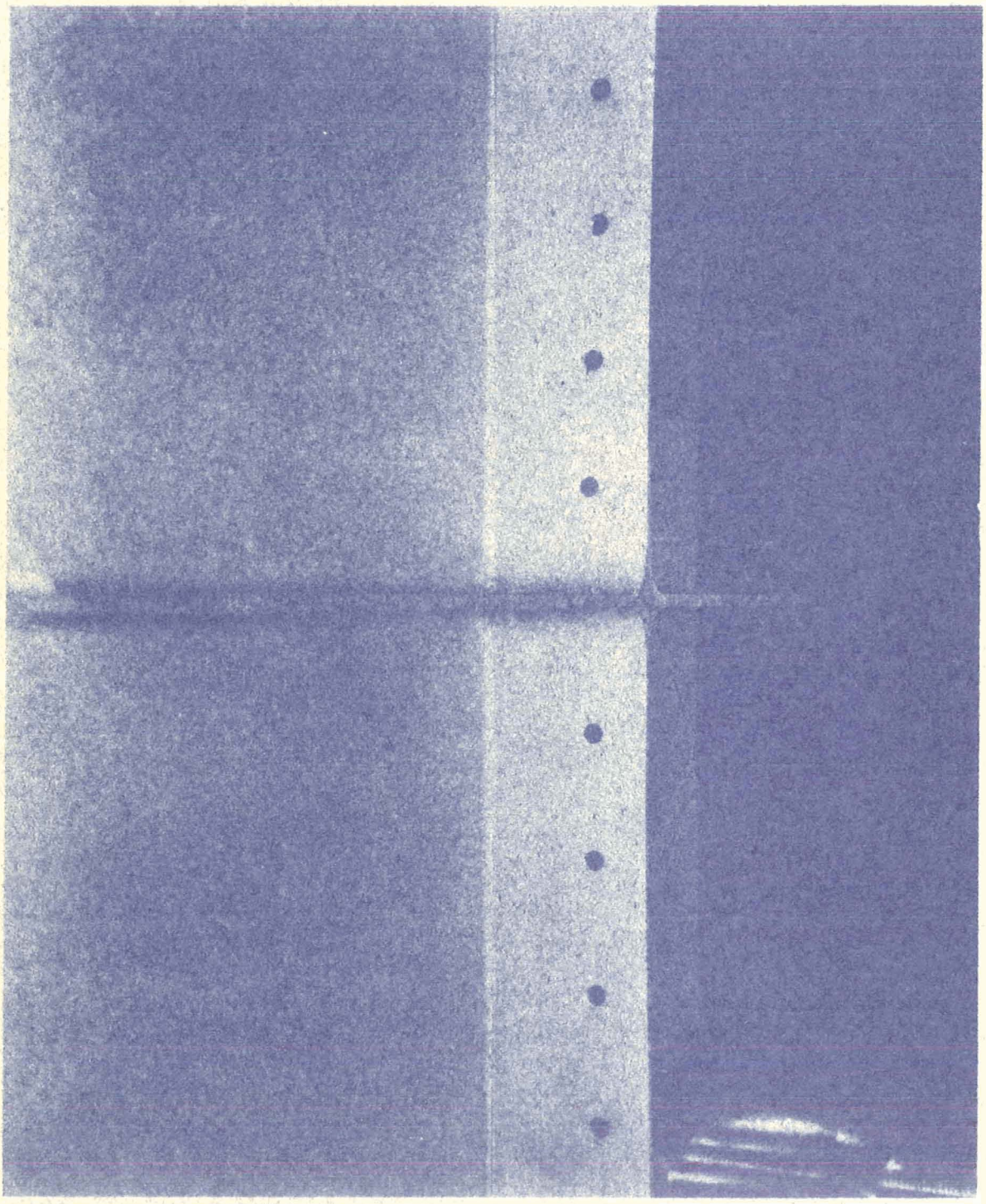

Figure 106. Panel Section Processed One Time Through LAD Solutions and Salt Spray

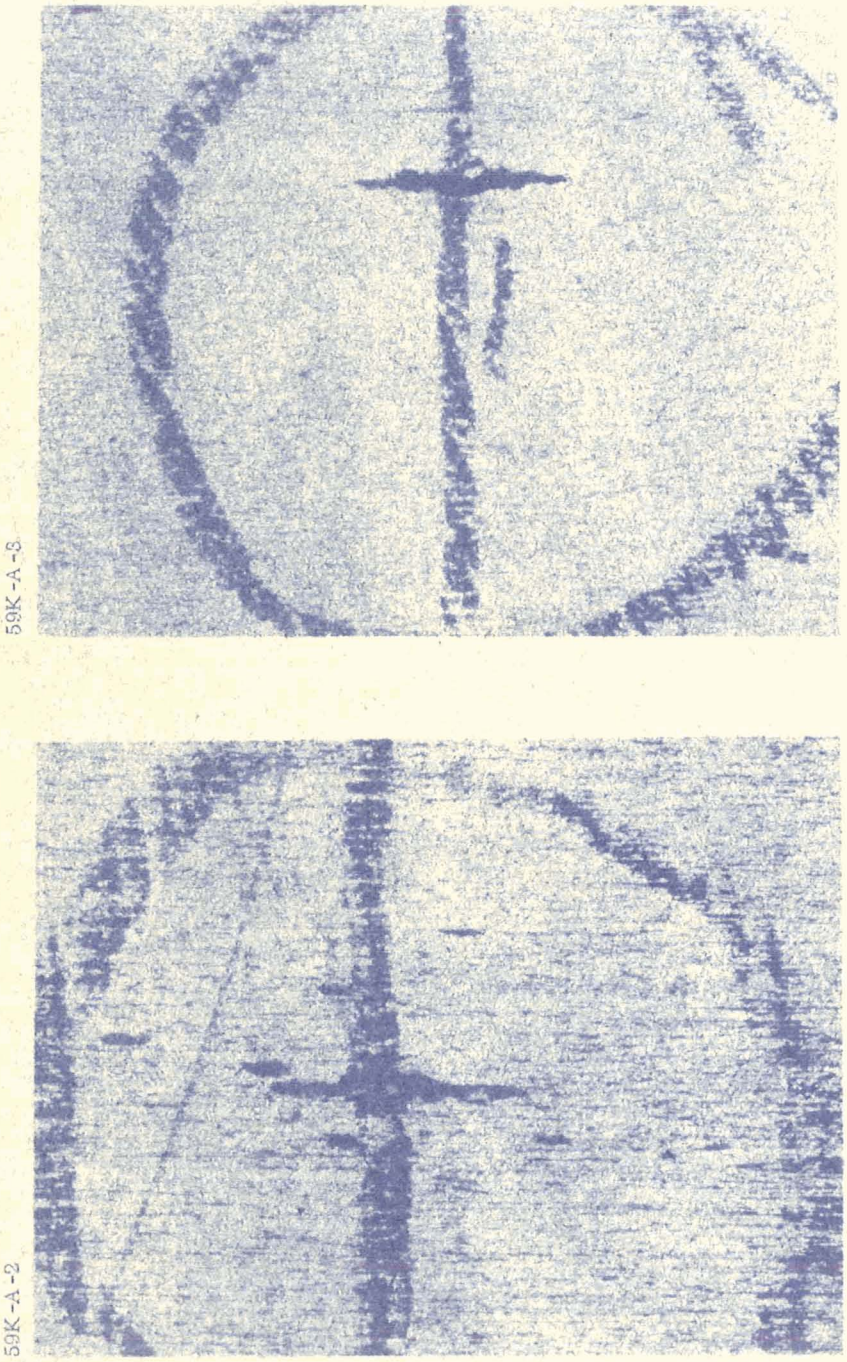

Figure 107. Test Coupons Processed One Time Through LAD Solutions and Salt Spray

59K-1-1

PANEL 6 100 X
AFTER ONE TIME LAD PROCESS
AND 17-DAY SALT SPRAY

59K-2-1

PANEL 11 100X
AFTER ONE TIME LABORATORY SOLUTIONS
AND 17-DAY SALT SPRAY

Figure 108. Photomicrograph of Panel Sections After Processing One Time and Salt Spray

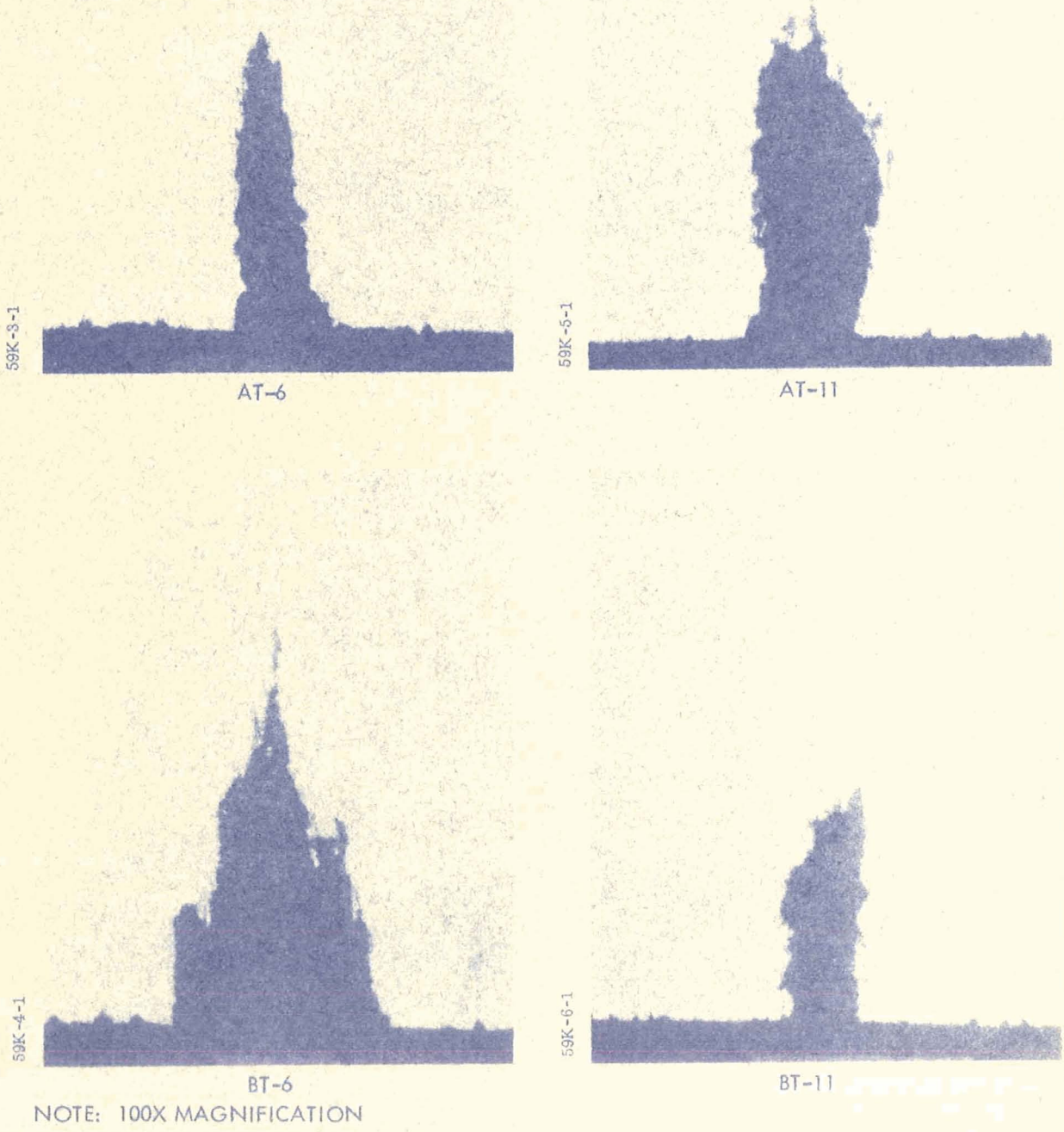

Figure 109. Photomicrograph of Test Coupon After Processing One Time and Salt Spray

A panel section and associated test coupons were subjected to 17 days exposure in a 5-percent salt spray chamber. These specimens were bare 2014-T6 aluminum with no previous coating or chemical treatment. Photomicrographs of typical pits which developed on these surfaces are shown in Figures 110 and 111. The pits developed on these test pieces were mode numerous and deeper than those formed on chemically processed test pieces exposed to an identical salt spray test.

DISCUSSION

Environmental exposure at LAD produced more surface attack and more contaminate deposit on test specimens than environmental exposure during the same time period on similar test specimens at Seal Beach. Since both sites are located approximately the same distance from the ocean, it is to be expected that salt air effect from the prevailing breezes would be similar. The Los Angeles Division site is located in a more industrialized area, however, and the atmosphere would be more polluted with contaminants than Seal Beach.

Material B exhibited more corrosion and pitting than material A when the test coupons were subjected to the same environmental conditions. Both of these materials were 2014-T6 aluminum alloys from different heats. This shows that inherent metallurgical characteristics of different heats of 2014 aluminum alloys affect the susceptibility to corrosion.

Examination of LH_2 quarter-panels now being received at Seal Beach reveals that corrosion has greatly diminished since the revised heading, storage, and overall processing have been used at the Los Angeles Division.

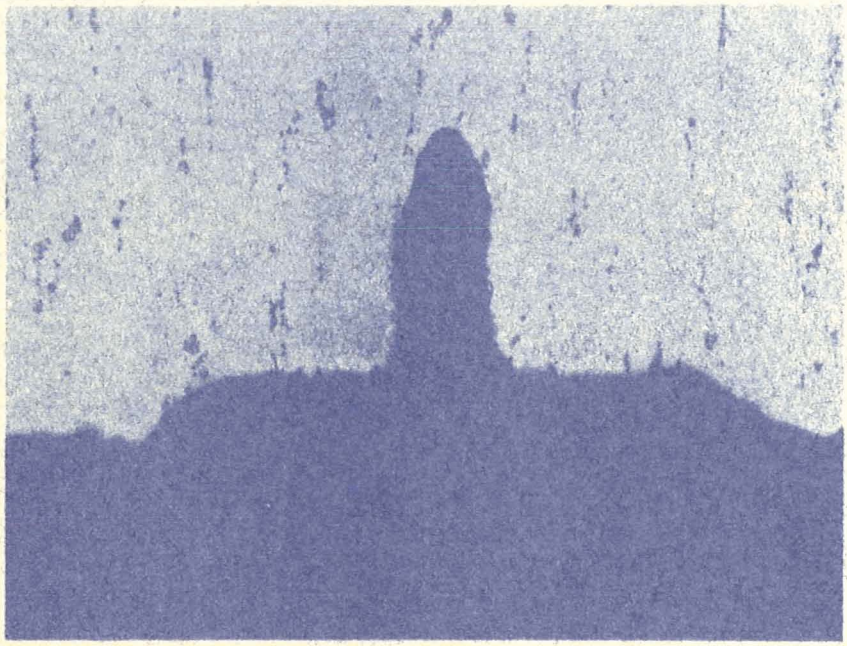

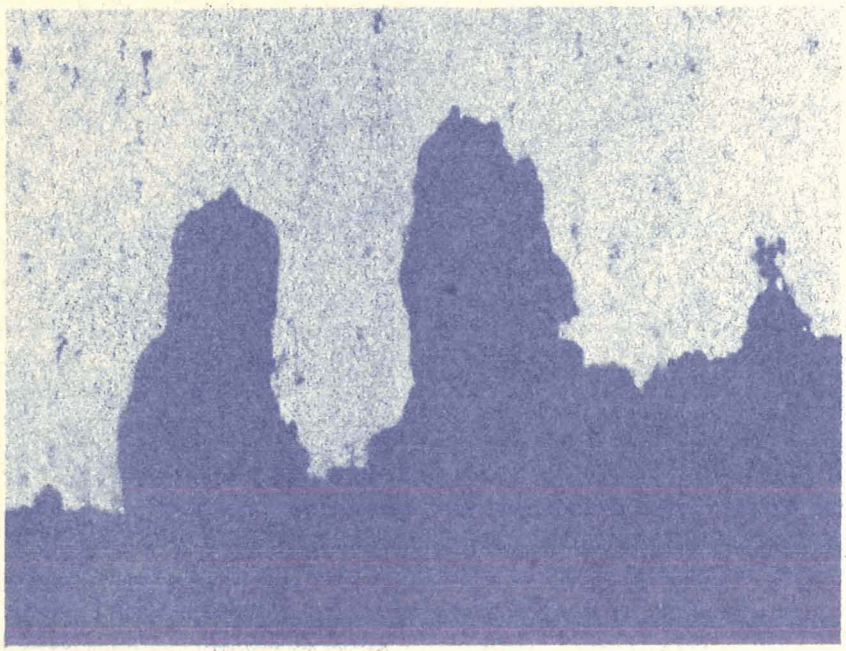

Figure 110. Photomicrographs of Bare Aluminum Panel Section After Salt Spray

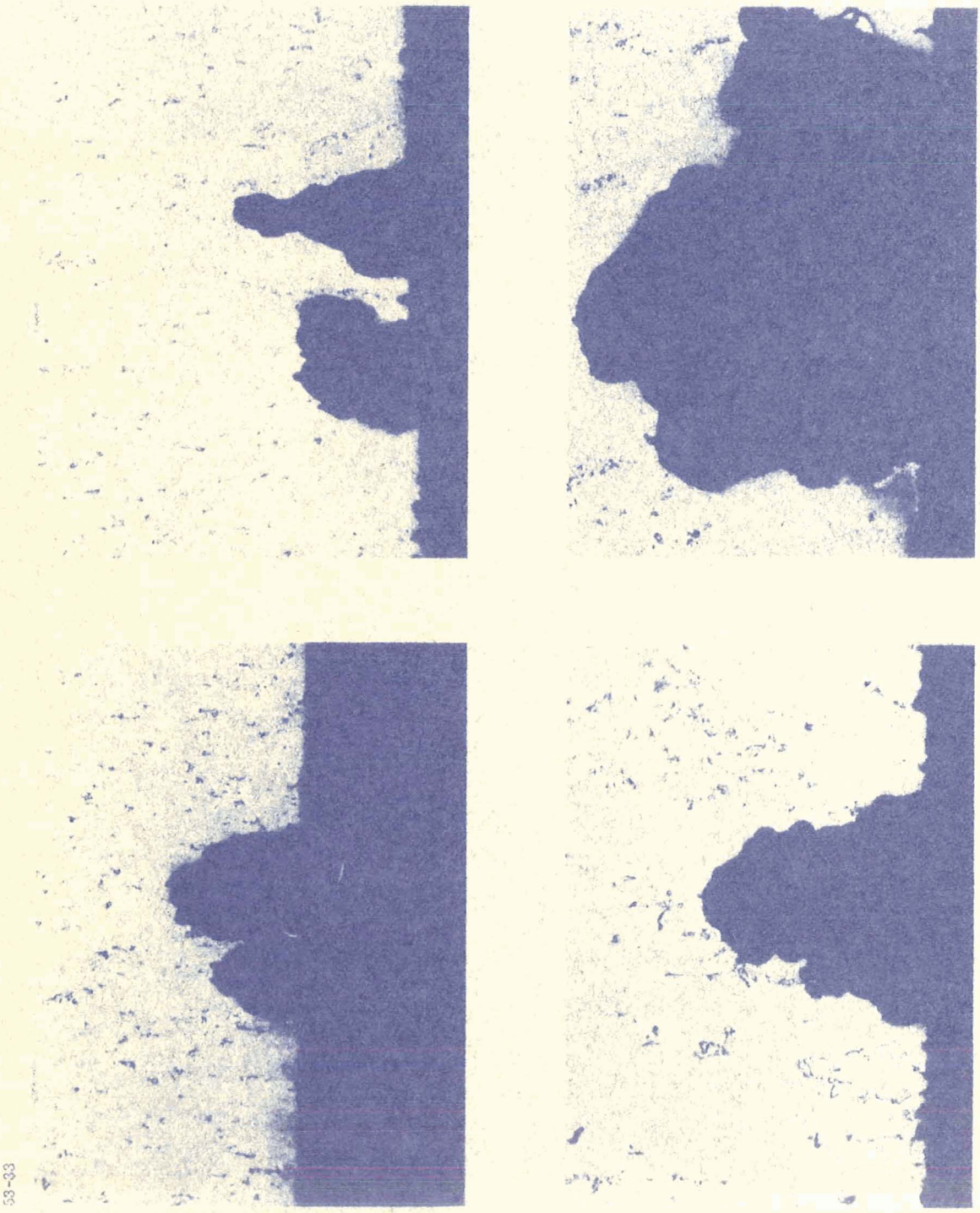

53-33

TEST COUPON BL-12
NOTE: 100X MAGNIFICATION

TEST COUPON BT-12

Figure 111. Photomicrographs of Bare Aluminum Test Coupons After Salt Spray

CORROSION TESTS ON BURST DIAPHRAGMS, P/N 38762-100

INTRODUCTION

One burst diaphragm is installed in each propellant feedline of the Saturn S-II stage. In the event of high pressure in one of the propellant lines because of a malfunction, the associated diaphragm will rupture, thus relieving the pressure overboard. It has been frequently necessary to replace the desiccant in the burst diaphragms after installation to guard against possible corrosion. Many man-hours are required to service the diaphragms and a more efficient means of protection is being sought.

To evaluate the use of a vapor phase inhibitor in lieu of a dessicant, the tests described below were conducted.

PROCEDURE AND RESULTS

The screens and rupture blades were removed from four burst diaphragm specimens and the diaphragms were viewed at 40X. There was no evidence of corrosion, pitting, or discontinuities on any of the test specimens that were protected as follows:

Serial Number	Protection
1099 and 1142	Rubber cap only
1151	Rubber cap containing VPI-250 crystals
1165	Rubber cap containing VPI paper

The specimens were placed in a chamber at room temperature. The temperature was raised gradually to 160 F during the first 2 hours and then maintained for six hours. The temperature was then returned linearly to room temperature during the next 16-hour period. This 24-hour period constituted one cycle. The relative humidity was maintained at 95 percent and the air velocity less than 150 feet per minute throughout the test. The cycles were repeated to extend the total time of the test to 168 hours. Examination of the specimens after exposure revealed no

perceptible difference in surface condition at 40X. The diaphragms of the test specimens were then coated with powdered iron, protected in the same manner (VPI-250 crystals and VPI paper) and exposed to the same conditions in the chamber for 168 hours. Examination revealed corrosion in varying degrees on all four specimens. There was no evidence that the VPI crystals or VPI paper inhibited corrosion during the humidity test. As a result of these tests, it does not appear feasible to use VPI materials for protection of burst diaphragms from corrosion.

CORROSION PROTECTION OF BURST DIAPHRAGMS, P/N 38762-100

INTRODUCTION

It was recommended that an epoxy primer be applied on burst diaphragms to protect them from corrosion. To evaluate the use of the epoxy primer, the test described below was conducted.

PROCEDURES AND RESULTS

Four burst diaphragms were viewed at 40X. There was no evidence of corrosion, pitting, or discontinuities on any of the test specimens. The specimens were protected as follows:

Serial No.	Protection
1165, 1151	Iron filings were covered by a 1.0- to 1.4-mil coat of Sherwin-Williams epoxy primer E42GP15, by spray application. The coating was air-dried for five days prior to humidity exposure
1099, 1142	Iron filings only

The specimens were then placed into a humidity chamber at a relative humidity of 95 percent and the temperature cycled from room temperature to 160 F for 160 hours. Examination at 40X magnification revealed that no corrosion was evident in the burst diaphragms containing iron filings, covered with Sherwin-Williams epoxy primer. Burst diaphragms containing only filings were badly corroded.

CORROSION PROTECTION OF LH_2 TANK J-AREA

INTRODUCTION

The epoxy primer coating used to protect the Saturn S-II LH_2 tank J-area groove from stress corrosion was suspected of causing contamination of the weld bead on the first cylinder weld. Coating the J-area by brushing or fill and drain is very difficult after the first cylinder is welded onto the J. Air-spray application of the coating after welding required development of a spray painting technique. A Binks spray gun having a 5-foot nozzle extension was investigated. This equipment originally designed for spray-coating pipe interiors appeared to be adaptable to J-groove spray painting.

The purpose of this investigation was to establish application techniques for air-spray coating the J-groove, using Binks Gun 62 with SA extension 52-227 and pressure cup 80-228, and to determine primer material requirements for application of a smooth, uniform film of primer MB0125-027, Finish System, Epoxy-Amine, Primer and Enamel.

CONCLUSIONS

Satisfactory 1- to 2-mil dry films were sprayed on the J-area groove using the Binks spray equipment with 25-psig air pressure on the gun, two-psig air pressure in the pressure cup, and the gun nozzle held 6 inches above the groove and with 1 foot per second gun travel speed. The MB0125-027 primer as now packaged was suitable for this application.

Specifications covering processing with this Binks spray equipment will require provision for careful controls to ensure a satisfactory primer film since there is no ready way to measure the actual film thickness on the J-area groove, nor to easily inspect the area visually.

PROCEDURES

MB0125-027 green epoxy primer was mixed in accordance with the specification. The Binks spray equipment was used to spray the primer onto flat test panels at nozzle distances of 1.5 to 8.0 inches above the panel and at gun travel speeds from 0.5 to 2.5 feet per second.

A section of J-area (V7-313117) was spray-coated with five passes at the optimum adjustment pressures. This J-section was not welded at the first cylinder. The LH_2 tank wall plate was taped to the J, allowing visual inspection of the groove after spraying. Specimens were cut from the coated J-section for photomicrograph film thickness measurement.

The sprayed films were visually examined for runs, sags, ripples, cratering, overspray, and dry overspray on the adjacent area. The sprayed films were recoated after one 5- and one 10-minute flash times.

RESULTS

The optimum spraying conditions for the Binks equipment were:

25-psig air pressure on the gun
Two-psig air pressure in the cup
Nozzle 6 inches above work
Travel speed 1 foot per second

A smooth, uniform primer film was sprayed averaging 0.4-mil dry film per pass. Three passes resulted in a continuous film of 1 to 2 mils.

DISCUSSION

The Binks spray gun and nozzle described is not adjustable, and has a fixed spray pattern. The only control is the air-pressure adjustment. Improved gun control and uniform film were obtained using a Teflon guide to hold the nozzle at the desired distance above the J-groove. The guide can be held against the first machined shoulder girdling the common bulkhead.

Some primer film of 0.1 to 0.2 mil dry thickness was deposited on the J-area walls near the gun nozzle, but no loose, flaking, or dry overspray particles were apparent.

CORROSION OF PMS SUPPORT HOUSING COVERS, P/N V7-480268

INTRODUCTION

During an inspection of stress-corrosion-susceptible parts on S-II-1 at KSC, corrosion was found on these three support housing covers in the LOX tanks. A metallographic analysis of the parts was conducted to determine the nature of the corrosion, and possible or probable causes.

CONCLUSIONS

The dark corroded areas (Figure 112) are the result of incorrect and careless application of electrochemical etchants.

PROCEDURE

The weight of coating was determined by weighing parts, determining the surface area, stripping the anodic coating from the parts, and then reweighing them. The difference in weight per surface area was calculated in milligrams per square foot.

The parts were sectioned and metallographic specimens were prepared. These specimens were examined for adhesion and coverage of dry lubricant, and for evidence of corrosion.

RESULTS

The weight of the coating was found to be 600 milligrams per square foot, which meets the minimum requirements of the anodizing specifications. The adhesion and coverage of the dry lubricant was as specified. The corrosion was of intergranular nature (Figures 113 and 114). Corrosion was found only in the darkened areas caused by the electrochemical etch. Spectrographic analysis conformed to the specified 2014 aluminum alloy. Traces of sodium were found in the dark residue.

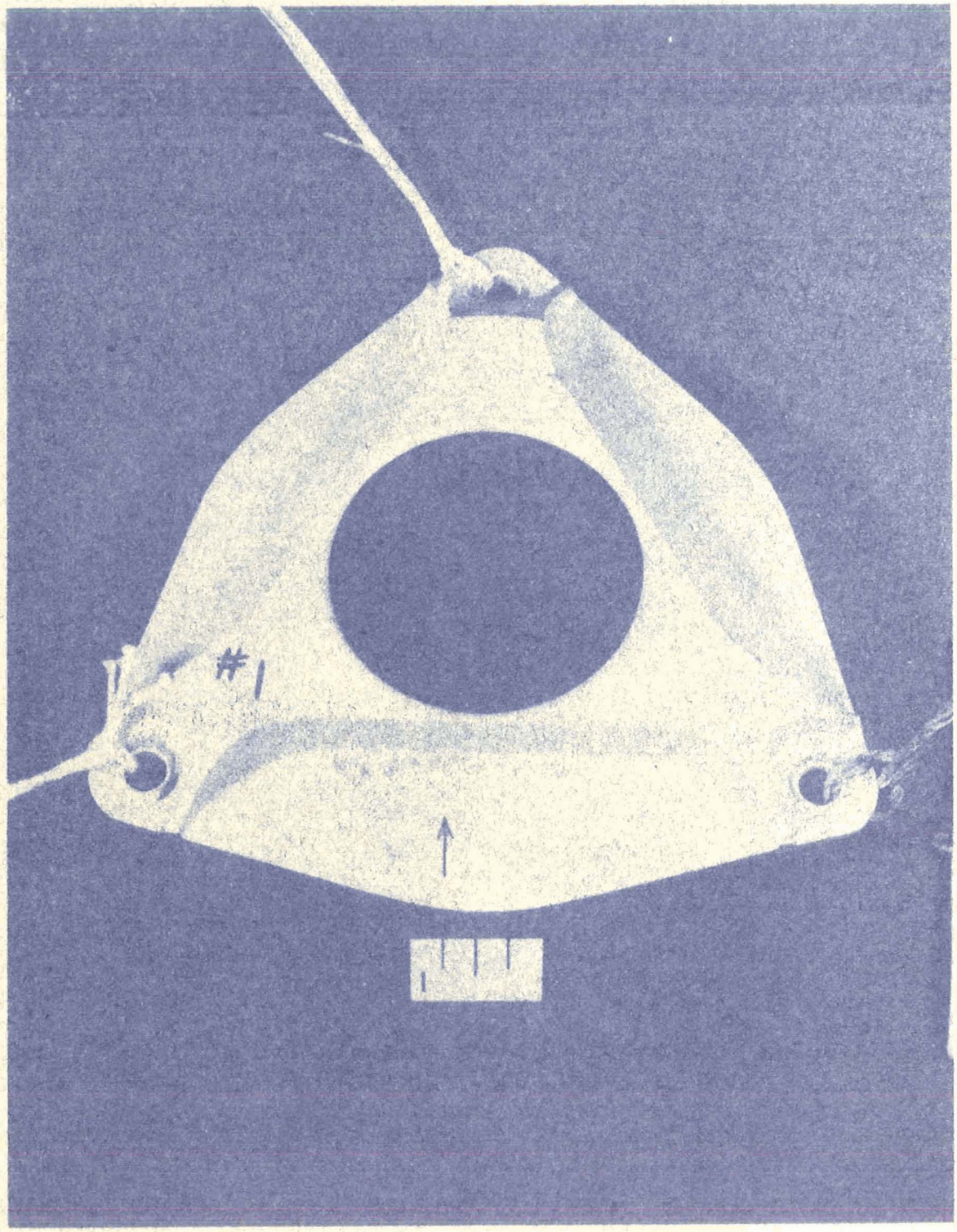

45K-A

NOTE: ARROW POINTS TO ELECTROCHEMICAL ETCHING AROUND THE PART NUMBER AND UNDER IT.
1X MAGNIFICATION

Figure 112. Support Housing Cover, Part 1

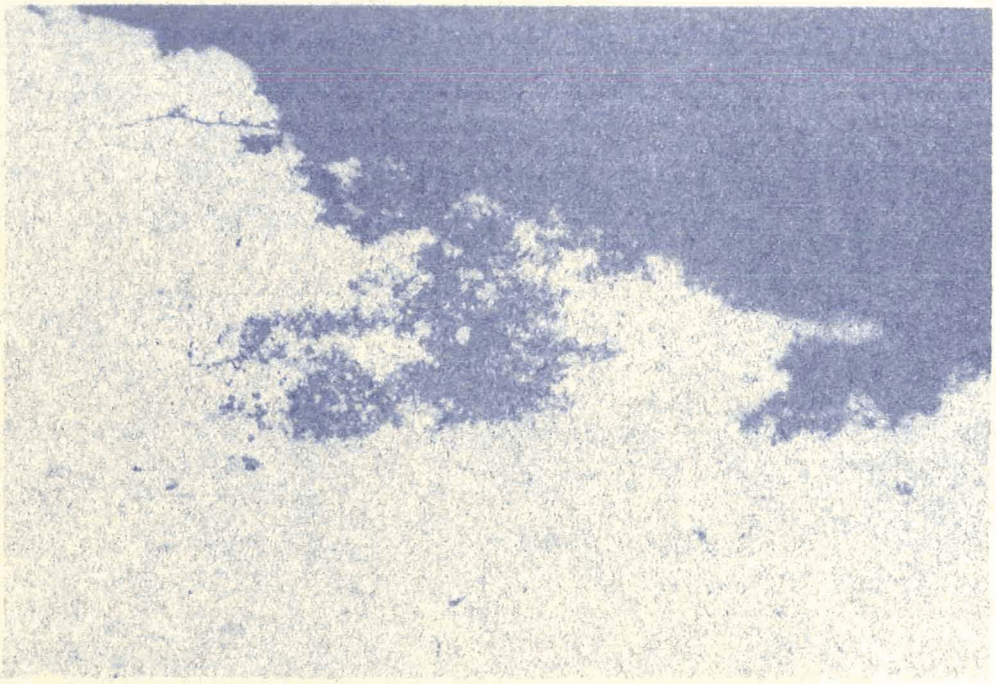

45K-1-1

NOTE: UNETCHED 400X MAGNIFICATION

Figure 113. Photomicrograph of 0.003-Inch Depth of Corrosion on Part 1

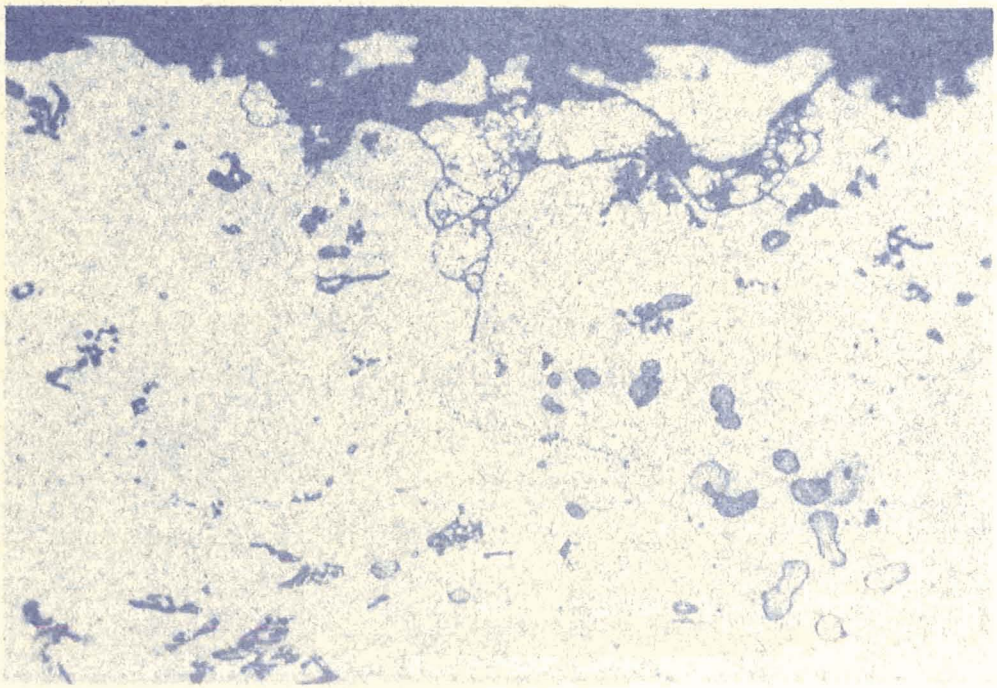

45K-2-1

NOTE: ETCHED 400X MAGNIFICATION

Figure 114. Photomicrograph of 0.0025-Inch Depth of Corrosion on Part 2

LOX COMPATIBILITY AND CLEANING

PROGRESS SUMMARY

All internal LOX tank surfaces and LOX wetted surfaces must be cleaned to remove all contamination that could be incompatible with LOX. After cleaning, inspection testing for evidence of fluorescence is accomplished by viewing under black light. Fluorescence is indicative of insufficient cleaning to remove LOX-incompatible materials. Three studies were conducted on rivets that fluoresced after cleaning. In another study, tests were conducted to determine if the fluorescence test indication is always associated with LOX-incompatible contamination.

LOX-COMPATIBILITY DETERMINATIONS OF CONTAMINATED RIVETS

INTRODUCTION

During final inspection of the S-II-3 LOX tank, a black light examination was made. Numerous DD-6 icebox rivets on the cruciform baffle located just to the right of the tank manhold revealed fluorescence from a hydrocarbon later identified as having carbon-double bonds and possible carbon-oxygen bonds. Further examination revealed fluorescence on cruciform baffle assemblies and the slosh baffle installed on S-II-4, and on the slosh baffles scheduled for installation on S-II-5 and S-II-6. All assemblies were fabricated by SD/NR-Tulsa.

The purpose of this investigation was to determine the LOX compatibility of the contaminated rivets removed from the S-II-6 slosh baffle assembly, using the standard LOX impact testing apparatus.

PROCEDURE

Specimen Source (Rivets)

Three sets of DD-6 rivets (20 per set) were removed from slosh baffle assemblies (S-II-6) by standard rivet removal procedures. The rivets selected for test were those exhibiting the highest degree of fluorescence under black light. New DD-6 rivets were obtained from manufacturing stock for test comparison purposes.

Impact Sensitivity Tests

The standard ABMA-type LOX impact sensitivity tester and procedures specified in MA0115-005, Testing Compatibility of Materials for Liquid Oxygen Systems, were followed except for specimen size.

RESULTS

Table 27 lists the specimen description, impact test energy, and results for each test series.

DISCUSSION

Although the contaminated rivet test specimens showed evidence of incompatibility when tested under standard LOX impact testing procedures,

the specimen size was considerably smaller than standard. This deviation makes the test results inapplicable to interpretation based on the acceptance requirements of MA0115-005 for LOX-compatible materials.

Table 27. Impact Test Data of Rivets

Specimen Description	Impact Energy (Foot-Pounds)	No. Tests/ No. Reactions
New DD-6 rivet (manufactured end)	72	0/20
Contaminated DD-6 rivets removed from slosh panel S-II-6, upset end	72	3/20
Contaminated DD-6 rivets removed from slosh panel, upset end	50	2/20
Contaminated DD-6 rivets removed from slosh panel, upset end	35	0/20
New DD-6 rivets (manufactured end) anodized, sealed in water, no heat treatment	72	0/6

EVALUATION OF COATINGS ON HI-SHEAR RIVET COLLARS

Hi-Shear rivets, alloy A-286, P/N HS92 and monel collars, HS60M, are used to attach bracketry to the torque tubes inside the Saturn S-II LOX tank. Twelve torque tubes are installed in the tank, and slosh baffles are attached to the brackets. Before receipt, the monel rivet collars are processed through black oxide, aluminum black dye, and lauric acid. The lauric acid serves as a lubricant for installation of Hi-Shear rivets. The Tulsa plant precleans the collars by vapor degreasing or Freon TF soaking before installation to remove the lauric acid. After installation of the rivets, the assembly is processed through a precision cleaning cycle at Seal Beach.

To determine the LOX compatibility of materials used on the monel collars and to evaluate the rivet preinstallation and post-assembly cleaning procedures, tests were performed.

PROCEDURE AND RESULTS

Seventy stainless steel and 30 aluminum wafers were cleaned and immersed in the following solution:

Material: Lauric acid-trichloroethylene solution
Concentration: 2.1 pounds lauric acid per gallon of trichloroethylene
Temperature: 145 F
Time: 2 minutes

After coating, the wafers were viewed under black light and showed no evidence of fluorescence. LOX impact tests at a 72 foot-pound energy level were performed on samples before and after use of various cleaning methods. Results are shown in Table 37.

Fifty-seven wafers punched out of 4130 sandblasted mild steel sheet stock were taken to Hi-Shear, Torrance, California, and processed as follows:

Black Oxide

Material: Hughto Black No. 15
Manufacturer: E. F. Houghton Co.
Composition: Sodium nitrite, sodium nitrate, sodium hydroxide

Black Dye

Material: Aluminum Black Bk
Manufacturer: Sandox Incorporated
Composition: Proprietary

Lauric Acid

Material: Lauric acid-trichloroethylene solution
Concentration: 2.1 pounds per gallon of trichloroethylene
Temperature and Time: 145 F, 2 minutes

After processing the test wafers at Hi-Shear, 20 wafers were cleaned in accordance with MA0110-018, and LOX-impact tested at 72-foot-pound energy level. The results are shown in Table 28. An infrared spectograph analysis performed on the aluminum black dye showed no evidence of organic matter. Further analysis by X-ray diffraction technique identified the dye as a black oxide of chromium.

DISCUSSION

Tests show that the current cleaning method before installation of Hi-Shear rivet and post-cleaning of the assembly satisfactorily remove the lauric acid coating.

Table 28. Impact Test Data of Coatings on Hi-Shear Rivet Collars

Material	Coating	Cleaning	LOX Impact
Aluminum	Lauric acid	None	3/20
Stainless steel	Lauric acid	None	3/20
Stainless steel	Lauric acid	Vapor degrease	0/20
Stainless steel	Lauric acid	Freon TF immersion	0/20
4130 Mild	Black Oxide + Black Dye + Lauric acid	Per MA0110-018	0/20
Aluminum	Black dye	None	0/20

EVALUATION OF COATINGS ON CHERRY RIVETS

INTRODUCTION

Cherry rivets, alloy 286, NR part number NAS-1398C6-4, manufactured by the Cherry Rivet Division of Townsend Company, are used to attach bracketry to torque tubes in the Saturn S-II LOX tank. Before receival, these rivets are lubricated with Drilube 700 (or Electrofilm 4396) and a tallow-paraffin film. Before installation, the rivets are solvent-cleaned at the Tulsa plant. After the brackets are attached to the torque tubes with Cherry rivets, the entire assembly is processed through a precision cleaning cycle at Seal Beach in accordance with MA0110-018.

To determine the LOX compatibility of the Cherry rivets after Tulsa and/or Seal Beach cleaning, LOX-impact tests were conducted.

PROCEDURE AND RESULTS

One set of 50 stainless steel wafers was coated with Drilube 700 by Drilube Company, Glendale, California. Another set of 50 stainless steel wafers was coated with Electrofilm 4396 by Electrofilm Incorporated, North Hollywood, California. Five wafers from each set were set aside for control samples and the remaining 45 wafers in each set were coated with paraffin and tallow by the Cherry Rivet Division. Impact tests with LOX were performed at 72-foot-pound energy level on the coated wafers after various cleaning procedures shown in Table 29.

Table 29. Impact Test Data of Cherry Rivet Coatings

Coating	Cleaning Procedure	Impact Test
Drilube 700, paraffin and tallow	Freon TF immersion	0/20
Electrofilm 4396, paraffin and tallow	Freon TF immersion	0/20
Drilube 700, paraffin and tallow	Per MA0110-018	0/20
Electrofilm 4396, paraffin and tallow	Per MA0110-018	0/20

A torque tube assembly containing Cherry rivets was rinsed with carbon tetrachloride, and the rinse solvent was analyzed on an infrared spectograph. The spectrographic analysis revealed no evidence of organic matter.

DISCUSSION

Tests show that current preinstallation and post-assembly cleaning procedures produce satisfactorily clean surfaces.

FLUORESCENT TESTS ON LOX TANK CONTAMINATION

INTRODUCTION

In accordance with the provisions of MA0610-001, Methods of Cleaning and Cleanliness Requirements for Saturn S-II Fuel and Oxidizer Tanks, fluorescent tests are performed on all internal LOX tank surfaces and all LOX wetted surfaces of components installed in the tank. Parts viewed with the black light must not exhibit fluorescence. Some parts that indicate fluorescence even after cleaning to specification fail the black light inspection. It has been necessary to accept and/or rework these parts through Material Review action.

As a result, an investigation was conducted to determine if the fluorescence commonly encountered in the stage LOX tank is caused by contamination.

RESULTS

Fluorescence appearing on as-received rivet heads is characteristic of some unsealed anodic coatings, and is not necessarily caused by contamination. Fluorescence on other surfaces usually results from tape residues deposited during masking operations. Chlorinated hydrocarbon, ketone or alcohol cleaning solvents will not effectively remove heat-affected tape residues.

Black light examination should not be the sole test method for detecting contamination. When unexplainable fluorescence occurs during black light inspection, further tests should be performed to determine the presence of organic contamination.

PROCEDURE AND RESULTS

The Seal Beach Facility was surveyed to determine which materials could show up as fluorescence in the LOX tank during black light inspection. It was learned that these materials consisted primarily of Krytox PR 240AC lubricant manufactured by DuPont, LOX Safe manufactured by Redel Co., a masking tape residue, and anodized rivet heads. Lubeco uses a masking tape when applying dry film lubricant to isolators subsequently cleaned and installed in the LOX tank. A sample of this tape, manufactured by Minnesota Mining and Manufacturing Company, was obtained and identified as Number 213.

The three nonmetallic materials were applied to aluminum panels with an unsealed sulfuric acid anodized coating, to aluminum panels with an Alodine 1200 coating, and to bare aluminum panels. The masking tape was removed after a simulated 3-hour cure at room temperature. There was no evidence of fluorescence on any of the samples when veiwed under black light.

Strips of the 213 tape were applied to another set of aluminum panels which had been processed as described above. The tape was cured on the panels at 300 F for 1 hour. After cooling, the tape was removed and the panels were examined under black light. There was no evidence of tape residue on the bare panels or the panels with a Chem-film coating. The anodized panels exhibited a very faint fluorescence where the tape was removed.

Methyl ethyl ketone, trichloroethylene, 1, 1, 1 trichloroethane and a mixture of 80-percent 1, 1, 1 trichloroethane and 20-percent isopropanol were wiped onto the tape residues. This cleaning operation did not change the fluorescence or perceptibly change the tape markings.

Unsealed anodized aluminum discs were placed between two strips of the 213 masking tape and cured in an oven at 300°F for 1 hour. After cooling to room temperature, the tape was removed and the discs were examined under black light. Nine of the discs exhibited fluorescence; these discs were impact-tested with LOX at a 72-foot-pound energy level and no reactions were observed.

One hundred rivets that exhibited fluorescence were obtained from North American Rockwell - Tulsa. Forty of the rivet heads were prepared for LOX-impact testing and twenty rivets were cleaned with a mixture of 80-percent 1, 1, 1 trichloroethane and 20-percent isopropyl alcohol. All forty rivet heads exhibited no reactions with LOX at a 72-foot-pound energy level; the cleaning operation did not perceptibly change the fluorescence.

Thirty rivets were then processed through the dichromate seal solution normally used to seal Type II anodized parts. After sealing, these rivets showed no fluorescence when viewed with a black light. It appears that the fluorescence caused by an inherent characteristic of the unsealed anodic coating rather than a contaminant.

SEALING

PROGRESS SUMMARY

Water and LOX leakage measurements were conducted to predict potential LOX leakage based on water leakage occurring during hydrostatic testing of the S-II aft LOX bulkhead.

Laboratory tests verified that retorquing the nuts and bolts of the S-II stage bolting ring would not damage the cured sealing compound used to seal the bolt head and nut surfaces.

The recurring problem of bubbles and voids under cryogenic aluminum foil seals was investigated. The addition of coloring to the adhesive and various methods of installing the aluminum foil seals were evaluated. The complete elimination of bubbles under the foil seals still remains a problem.

Laboratory tests simulating the foil sealing of the flush-head Huck bolts of the Thor tank on the off-pressure side indicated that the foil seals would generally withstand the back pressure of any leakage incurred during the static testing of the tank.

LEAKAGE CORRELATIONS: WATER VERSUS LOX

INTRODUCTION

Leakage correlation measurement tests were conducted to support prediction of potential LOX leakage based on water leakage rates large enough to be visible during hydrostatic testing of S-II aft LOX bulkheads.

CONCLUSIONS

LOX leakage, expressed as gas volume at room temperature at 1 atmosphere, numerically approximates 1000 times the water leakage through the same leak at the same pressure. The factor of 1000 can be used to simply calculate the LOX leakage equivalent to any slight water leakage during hydrostat. Pressure dependence data can be used for variance adjustment between hydrostatic test conditions and launch pad or flight conditions.

TESTING

Water leakage was collected and measured as liquid weight accumulated during measured periods of time. Liquid drop rates were measured as a check on flow uniformity during collection periods.

Oxygen leakage was collected and measured by water displacement as volume of gas accumulated during measured periods of time. A constant low flow of helium was passed through the exit plenum of the test fixture to prevent accumulation of LOX in the plenum. Oxygen leakage data were subsequently corrected.

Aluminum fixtures with CRES washers and bolts were used. Washers for initial attempts had relatively shallow, irregular grooves filed along a radius. Later, five were carefully machined to produce uniform V-shaped grooves 0.8 to 3.3 mils deep and approximately three times as wide as deep.

Attempts were made to measure comparative leakage by using 11 filed washers. However, all leaks became plugged by using water as a test medium, and correlative data were not produced. The leaks would typically pass water for a few minutes (long enough for a rough determination) but, during the time required for careful measurement, the leakage rate decreased (slowly at first—then quite rapidly) until complete plugging occurred. Flow

could sometimes be reestablished temporarily by a back-pressurization cycle up to 150 psig, but initial leakage values could not be attained.

Effort on subsequently filed washers (4220-3 through -11) involved a variety of steps to prevent plugging. Changes included: more elaborate fixture cleaning to the point where the last fixtures were ultrasonically cleaned, extremely careful assembly of fixtures, improved filtration of water to ensure removal of all particles larger than 0.45 microns; Chem-film treatment of aluminum parts to prevent aluminum oxide formation during test, and addition of 500 ppm sodium chromate to test water (hydrostatic test water formulation).

Data have been plotted on the overall correlation curve of Figure 115. The values represent smoothed values supported by the 30 data points developed.

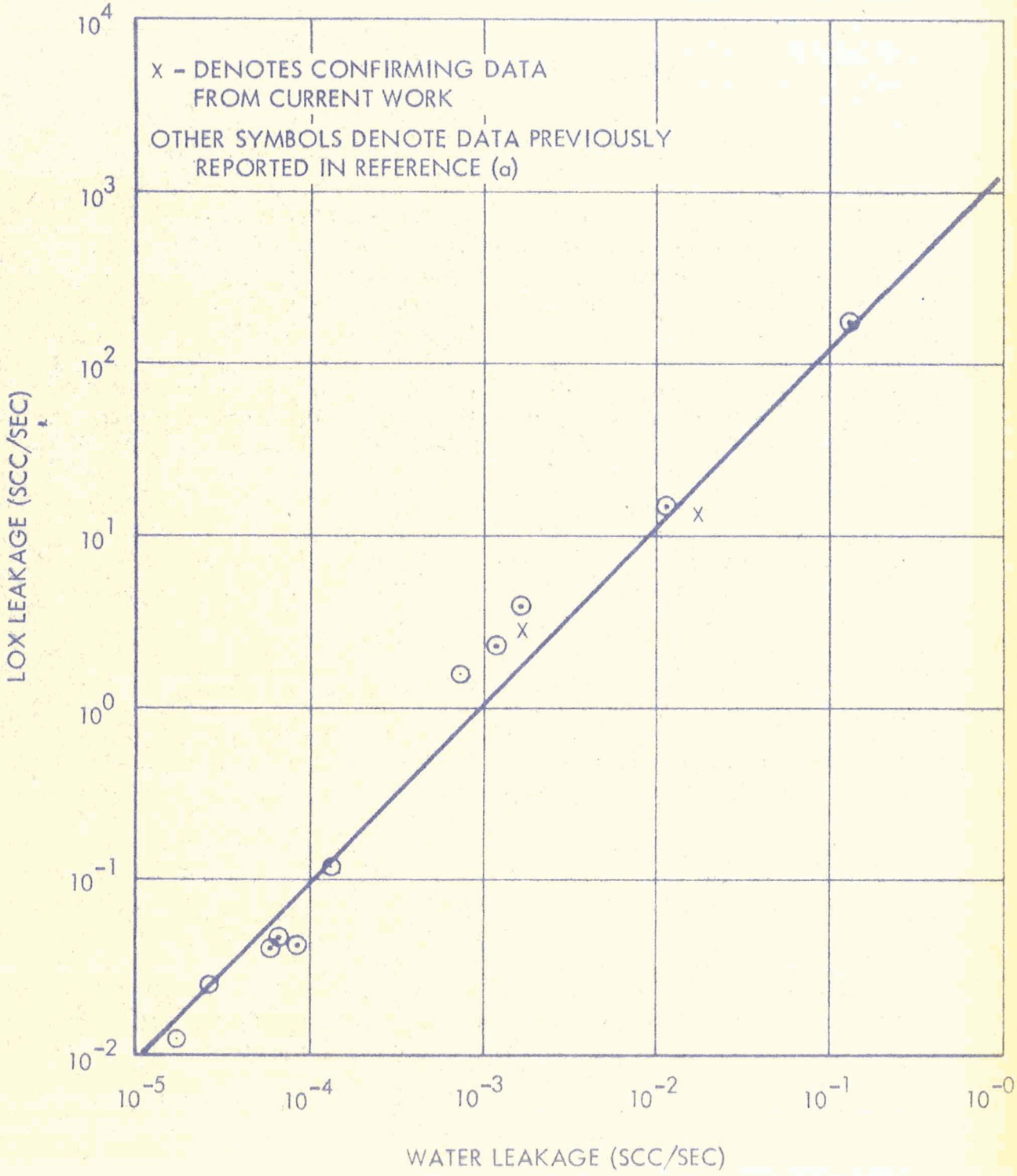

Figure 115. Correlation of LOX Leakage at -320 F With Water Leakage at Room Temperature

LEAK TEST RESULTS ON RD BOLTS

INTRODUCTION

Measurements of possible leakage around nuts or bolts in the S-II stage bolting ring were conducted. These bolt heads and nut surfaces are normally sealed with an RTV sealant compound; however, it is possible to destroy the original RTV bond by retorquing, and comparative leakage measurements under this condition were desired.

Special fixturing, fabricated to simulate the Saturn S-II bolting ring was installed with sealed and unsealed RD bolts, and the amount of leakage escaping past the bolts was determined.

CONCLUSIONS

The RTV compound provides effective sealing despite disruption of the bond by retorquing. Bolt head sealing was generally good without any RTV compound.

PROCEDURES

Bolts of 3/8-inch and 7/16-inch size were installed in the fixturing without sealant. The 3/8-inch bolts were torqued to 200 inch-pounds; the 7/16-inch bolts were torqued to 520 inch-pounds.

A second bolt series was assembled. Each bolt received a coating of GE 4004 silicone primer and a thin coat of RTV 560 on the washers and under the bolt head. A small bead of RTV sealant was applied to approximately 1/4-inch of the threads, but no sealant was applied directly to the nut. The 3/8- and 7/16-inch size bolts were torqued to 70- and 170 inch-pounds, respectively, and the RTV was fully cured. After the RTV was cured, the torque was increased to 200 inch-pounds and 520 inch-pounds for the 3/8-inch and 7/16-inch bolts, respectively.

A third series was torqued to 200- and 520 inch-pounds immediately after the RTV was applied. The RTV was fully cured before test.

The tests were conducted at room temperature and at -320 F with 2-psig helium pressure. Flowmeters were used to monitor the leakage.

RESULTS

Table 30 shows leakage rates on 3/8- and 7/16-inch RD bolts when assembled without sealant and pressurized to 2 psig with helium. No leakage occurred on any bolt sealed with RTV 560 at either room temperature or -320 F, with either single-torqued or retorqued assemblies. Detection limit is approximately 1×10^{-3} scc/sec.

Table 30. Leakage Test Results on Unsealed Bolts

Bolt Size (inch)	Leakage (scc per sec)			
	Past Head		Past Nut	
	RT	-320 F	RT	-320 F
3/8	0	0	0.8	1.8
3/8	0	0	1.0	4.2
3/8	0	0.6	0.9	2.8
7/16	0	0	0.6	3.1
7/16	0	0	0.7	3.6
7/16	0	0	0.7	3.1
RT - room temperature				

COLORING AGENT FOR FOIL SEAL ADHESIVE, NARMCO 7343

INTRODUCTION

Tests were conducted on various coloring agents added to make the clear Narmco resin visible when applied in thin, 5-mil bondlines in accordance with MAO606-038. This aids in estimating bondline thickness and uniformity of coating during resin application.

CONCLUSIONS

A red dye, rhodamine B, imparts a bright, translucent color and does not appear to degrade the physical properties of the resin. A concentration of 0.05 percent rohdamine B dye imparts sufficient color to the Narmco resin for most applications.

PROCEDURES

The dyes tested were thymol blue, anthroquinine violet R, isamine blue, copper phthalocyanine, anthracene, and rhodamine B base. These dyes were tested to determine their solubility in Narmco resin and methyl ethyl ketone.

Peel tests were conducted on 0.005-inch aluminum foil bonded to 0.20- x 1.0-inch 2024 aluminum strips using the Narmco resin, as provided, and on resin dyed with the final selected color.

RESULTS

All of the dye materials evaluated, except rhodamine B base were rejected because of poor solubility or incompatibility of these materials with methyl ethyl ketone or resin, or both. Visual tests of 1 to 5 mils of bondline indicated very satisfactory color by using 0.02 to 0.1 weight percent of rhodamine B. Table 31 compares the peel test results of the plain resin (control) and the dyed resin.

Table 31. Average Peel Test Data on Bonded Foil Specimens Using Narmco 7343

	Days Cured	Room Temperature Values (pounds)	-320 F Values (pounds)
Control (Plain) Specimens	1	17-1/4	-
	6	12-1/2	-
	9	12	-
	20	13-1/2	14
Modified (Colored) Specimens	1	19	-
	6	16	-
	9	16	-
	20	16	21

Note: 75 to 80 percent of the failures were adhesive from the foil.

PROPELLANT TANK FOIL SEALING PROBLEMS

INTRODUCTION

Excessive air pockets, bubbles, and/or voids in adhesive bondlines have been a recurring problem on various cyrogenic foil seal installations in the Saturn S-II propellant tanks. An investigation was conducted to determine the cause of air bubbles and voids in MB0120-024 polyurethane adhesive used in foil sealing according to Process Specification MAO606-038. Other polyurethane adhesive/sealants also were screened to determine if processing or physical properties were more adaptable to foil sealing applications.

CONCLUSIONS

Voids and air pockets can be eliminated on small foil seals of relatively simple configurations. However, on large foil seals of complex configurations (where the foil must be formed over contours and other structural irregularities) complete elimination of air pockets will be difficult to achieve. Once an air pocket is trapped under the foil during installation, the pocket is virtually impossible to eliminate.

Fine bubbles throughout the bondlines can be minimized to a large degree by deaerating the adhesive prior to application. Complete elimination of all fine bubbles can by achieved only by again deaerating the adhesive after application to the foil part. This approach is impractical from a production standpoint, and the few small bubbles entrapped during application of the adhesive are not detrimental to the sealing and adhesive functions.

Screening of polyurethane resins from suppliers other than the single source (Narmco 7343) presently qualified to MB0120-024 resulted in no improvement of processing characteristics and similar physical properties. Adding dye to the clear polyurethane helps appreciably in estimating adhesive thickness and uniformity of the film during application.

The following specific operations will aid in minimizing voids and bubbles in the foil seal adhesive bondlines:

1. Deaeration of the adhesive prior to application. This will eliminate trapped air bubbles mixed into the resin during catalyst addition. Deaeration also helps prevent entrapment of moisture within the resin that causes gas-bubble formation from water-resin chemical reaction.

2. Addition of a dye to the resin. This is a visual aid during application.

PROCEDURES

Test seals approximately 10 x 10 inches were fabricated from both 1100-0 aluminum foil and clear Mylar film, 5 mils thick. The seals were then bonded to a flat aluminum plate in an assorted combination of techniques to determine causes and effects of the following variables:

1. Deaerated and non-deaerated resin
2. Resin applied to one or both bonding surfaces
3. Resin thickness
4. Methods of mating bonding surfaces
5. Methods of working resin from under seals
6. Effects of vacuum bagging (one or both sides of edge-bonded seals)
7. Effects of edge-bonded or 100-percent bonding of seals
8. Careful and intentionally careless workmanship
9. Intentional air pocket entrapment
10. Dyeing the clear polyurethane resin

With the clear Mylar film it was possible to observe the effects of bubble and/or void entrapment and formation. When notable effects were observed with the Mylar, the same procedures were followed using aluminum foil. The foil bondlines were allowed to cure, and the foil was peeled from the mating panels to expose the bondlines. Comparisons were then made between the foil bondlines and Mylar bondlines.

Other sources of polyurethane resin similar to the Narmco 7343 were investigated. Narmco 7343 is basically Adiprene L-100, available from DuPont. The Adiprene L-100 was obtained and tested along with PR-5211 obtained from Products Research and Chemical Corporation.

Screening tests included aluminum foil 180-degree peel tests run at room temperature and -300 F. Processing characteristics were qualitatively compared to Narmco 7343. All test samples were cured a minimum of seven days at room temperature before testing.

RESULTS AND DISCUSSION

The most significant fact which evolved from the processing study was that once an air pocket (or void) was trapped within a bondline, it was virtually impossible to eliminate. Pressure and/or a vacuum bag diffused the air pocket over a wider area and resulted in an even larger unbonded area. Trying to force a visible air bubble (clear Mylar seals used) to the edge of a bondline using a Teflon paddle could be accomplished with narrow width bondlines, but with 100-percent bonded seals, most bubbles split into several smaller segments. The problem was further compounded by using actual foil, because the entrapped air pocket was not visible and was undetectable in a normal application. In general, all approaches evaluated to remove a trapped air pocket were unsuccessful. Prevention appears to be the cure.

Considerable effort was expended on prevention of voids (air pocket entrapment) within a bondline. Magnitude and frequency of voids were a direct function of foil application procedures. Incomplete resin coverage on bonding surfaces, uneven adhesive layers, careless mating of bonding surfaces, failure to flatten the foil seals with a Teflon paddle, and lack of positive pressure on the bondline during cure consistently led to bondline voids.

Air pockets and voids could be eliminated by first placing the foil down in one spot along one edge, while holding the opposite end of the foil a slight distance above the bond area, then gradually forcing the foil against the bond area, working across the seal. The adhesive was worked out ahead of the foil with a Teflon paddle as the foil was gradually applied.

The resin bondlines were a mass of fine bubbles (1/32-inch diameter or less) when the adhesive was not deaerated prior to application. Also, if deaerated adhesive were carelessly applied, fine bubbles would be worked back into the adhesive. The fine bubbles could only be completely eliminated by deaerating both bonding surfaces after application of the adhesive. This procedure can be accomplished readily in the laboratory on small test panels, but this would be impractical for a manufacturing operation where large seals are involved. Adding a dye to the clear resin aids considerably in visually determining bondline uniformity and estimating bondline thickness. Physical properties are not affected by addition of a dye. A screening of other commercial sources of polyurethane adhesive was conducted. Test data on Adiprene L-100 (from DuPont) and Pr-5511 (from Products Research and Chemical Corporation) are presented in Table 32.

Table 32. Comparison of Foil Peel Strength Properties of Various Polyurethane Adhesives

180-Degree Foil Peel Strength (pounds/inch)						
	Room Temperature			-300 F		
Adhesive Designation	Breakaway(1) Load (average)	Peel Range	Average Peel	Breakaway(1) Load (average)	Peel Range	Average Peel
Narmco 7343	17	11-17	14	45	17-23	19
PR-5211	24	15-20	17	> 50*	-	-
PR-5211 Plus 0.5 percent PR U8C color	27	16-21	19	> 50*	-	-
Adiprene L-100	17	9-16	12	53	19-23	22
Adiprene L-100 plus 0.5 percent PR U8C color	18	15-18	16	52	21-26	23

(1)Load Required to initiate peel

*Exceeded foil strength (foil broke prior to initiating peel, between 50 and 60 pounds).

FOIL SEAL PEEL TESTS ON PRIMER M

INTRODUCTION

A cursory evaluation of primer M (MB0120-042) was conducted to determine if its use would improve the polyurethane adhesive (Narmco 7343) bonding system. The evaluation involved determining the resistance of foil seal bondlines to delamination at room temperature and -320 F with and without the use of primer M.

CONCLUSIONS

Primer M slightly improved the room temperature peel characteristics of bonded foil seals, but definitely degraded the cryogenic peel characteristics of the polyurethane bondlines.

PROCEDURES

Six-inch diameter discs of 5 mil, 1100-0 aluminum foil were edge-bonded to 1/4-inch 2014-T6 panels so that a 4-inch diameter section in the center of the disc remained unbonded. A pressurization port was drilled through the backside of the 1/4-inch panel and located under the unbonded foil disc.

All test parts were processed according to the foil sealing specification MAO606-038 with the following exceptions:

1. Primer M (MB0120-042) was applied to both the foil discs and test panels on half on the test parts. Cure was 4 hours minimum at room temperature prior to resin application.

2. Teflon mold release was applied to all areas of the test parts where bonding was not desired and for accurate control of bondline width.

3. The Narmco 7343 bonding resin (MB0120-024) was deaerated before application. Actual resin cure time was 14 days at room temperature prior to test.

Test parts were gradually pressurized with nitrogen at room temperature and at -320 F until the first signs of delamination were evident (caused by peeling of the bondline). The pressure at this point was recorded. At

room temperature, the test parts were further pressured until complete bondline failure occurred. At cryogenics, initial peel and complete bondline failure occurred simultaneously, so no further pressurization was required.

RESULTS

The pressures required to initiate peel and to completely delaminate the foil seal bondlines are summarized in Table 33.

Table 33. Back Pressure Required to Delaminate Foil Seal Bondlines

Test Temperature (F)	Primer Type	Average Pressure at First Indication of Peel (psig)	Average Pressure Required for Complete Bondline Delamination (psig)	Type of Failure
RT	None (controls)	12	20	Adhesive from panel
RT	Primer M	14	22	Adhesive from foil
-320	None (controls)	50	50	Adhesive from panel
-320	Primer M	26	26	Adhesive from foil

RT - room temperature

THOR TANK FOIL SEAL TEST

INTRODUCTION

A Douglas Thor tank, received by North American Rockwell Saturn Engineering for evaluation of foam insulation was fastened together with several hundred flush-head Huck bolts. These constituted several hundred potential leak paths that could permit LH_2 to get under the foam insulation and blow it off. Saturn Engineering requested that foil patches be applied over the flush heads of the Huck bolts to avoid leakage. However, the flush-heads were on the exterior of the tank.

The process specification for foil sealing, MA0606-038, states that foil seal patches will be applied only on the pressure side or on the interior of the test article. Therefore, an evaluation program was necessary to determine if the foil patches could withstand the static back pressure. Initially, the tests were to be conducted at room temperature only, but the testing was extended to include cryogenic testing.

The evaluation consisted of the following two test objectives:

1. To determine if static back pressure would raise foil seal patches applied over flush-head Huck bolts on the low pressure side and

2. To determine if a back pressure would raise foil seal patches during a dynamic load cycling of a dog-bone tensile specimen containing leak paths and patches.

CONCLUSIONS

The foil patches generally will withstand the back pressure applied under the static and dynamic conditions which are imposed on the Douglas Thor tank during evaluation of the foam insulation.

PROCEDURES AND RESULTS

A round panel for static testing was abraded with Bear-Tex material and solvent wiped. The patch area of a dog-bone panel for dynamic testing was solvent wiped only. The 10-mil x 1-1/2-inch-diameter 1100 series aluminum foil patches were abraded with Bear-Tex material and solvent-wiped.

The Narmco 7343 adhesive was applied in accordance with MA0606-038, except that the resin was not applied on the pressure side of the test articles as specified in MA0606-038.

The round panel was bolted to a cryogenic flange (shown in Figure 116) and pressurized with nitrogen to 80 to 85 psig for 14 days. Periodic leak checks were conducted with helium pressure and monitored with a CEC helium tank leak detector. No leakage was observed. The round panel fixture was then filled with liquid nitrogen and held at 70 to 75 psig for 20 minutes to determine if the temperature and pressure would cause the patches to blister. Since it had been previously determined that the Huck bolts leaked slightly (4 cc per hour, maximum) before installation of the patches, it was considered possible that a small amount of LN_2 could get by the Huck bolt and blister the patch when the liquid nitrogen gasified. No blistering or leakage was detected.

The dog-bone panel, Figure 117, was load-cycled 50 times from 0 to 28,000 pounds with a pressure of 88-psig helium applied to the backside of the Huck bolts. After completion of the cyling test, a leak check was conducted while the panel was stressed and pressurized. There was no detectable leakage. After approximately 20 hours at a 28,000-pound load and 88-psig helium, another leak check was conducted with negative results. The dog bone was next immersed in LN_2 and load-cycled from 0 to 28,000 pounds for 25 cycles. No pressure was applied to the bolts during this cycling test. The test panel configuration was such that one Huck bolt was not connected to the pressurizing system. After the panel had returned to room temperature, a small blister was observed on the patch over the Huck bolt that had no pressurizing system. Neither this blister nor any of the other patches leaked when pressurized to 88 psig.

The pressurizing system was completely removed from the dog bone, and 15 load cycles from 0 to 28,000 pounds were conducted at -320 F. This test was conducted to determine if the liquid nitrogen would leak past the Huck bolts, under load, and become trapped under the foil and form other blisters. No additional blisters developed; another leak check also produced negative results.

A small hole was pierced in the blister and leak-checked again with negative results. The dog bone was then slowly stressed to determine at what load the Huck bolt leaked under the patch. This load was approximately 25,000 pounds, or 90 percent of the maximum load applied to the dog-bone panel during any of the testing.

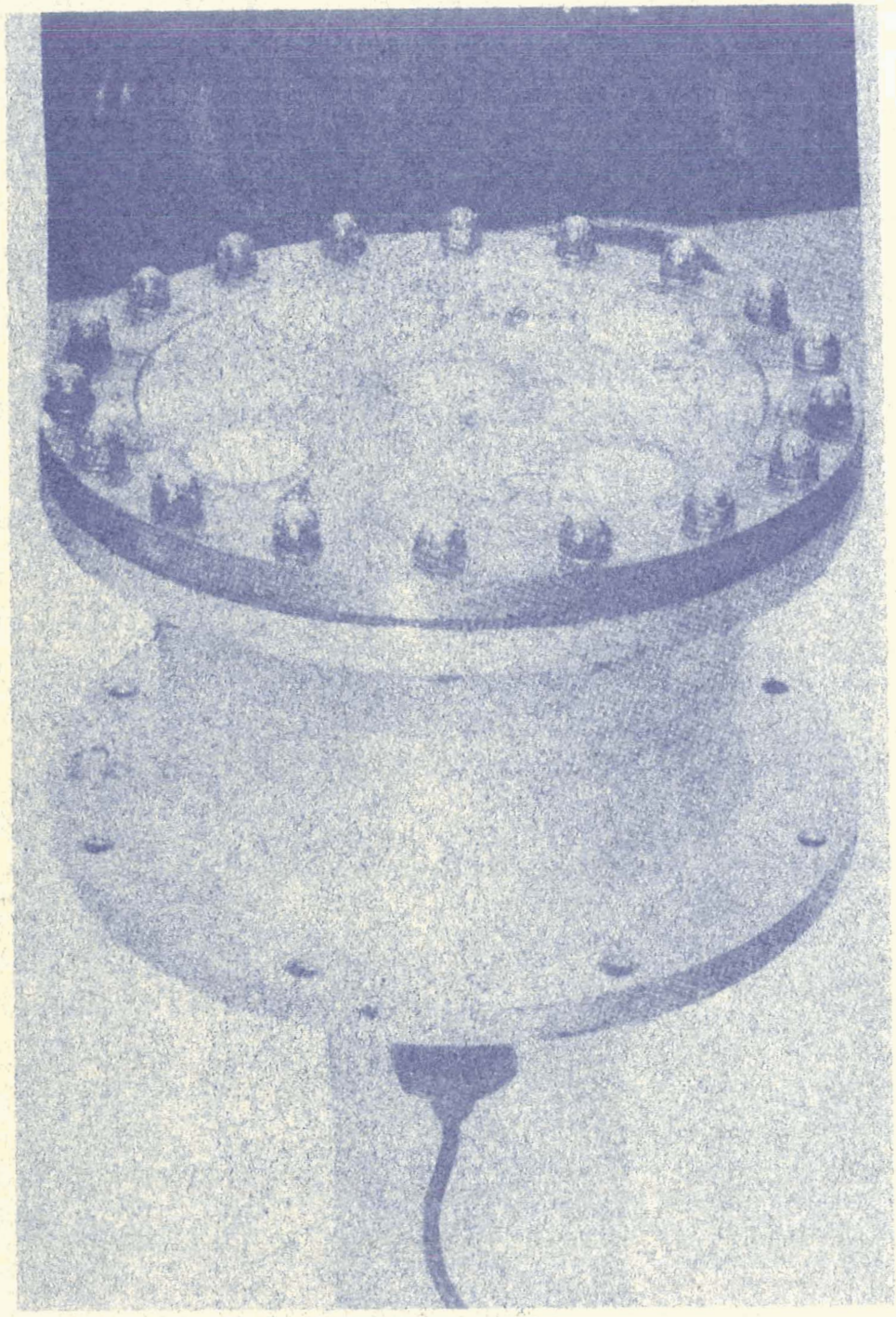

Figure 116. Round Test Panel With Patches Applied

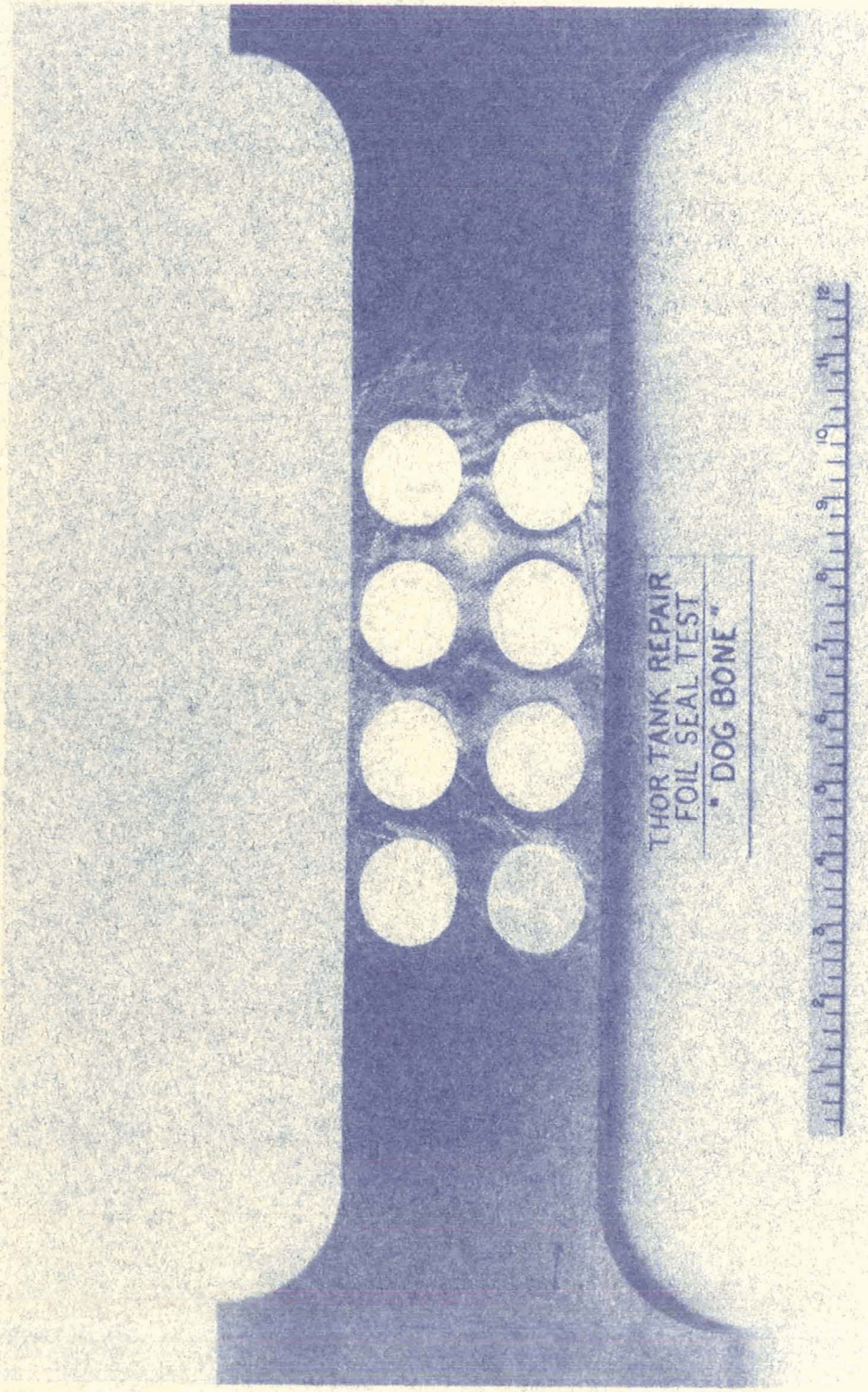

7006-81-2372C

Figure 117. Dog-Bone Panel With Patches Applied

ABLATIVE INSULATION

PROGRESS SUMMARY

Korotherm 790-005, a silica-filled isocyanate ablative material (MB0130-074), has been selected for insulating the internal surfaces of the S-II-4 and subsequent interstage structures. Test programs were conducted to determine structure surface preparation and to obtain thermal property data.

PREPARATION OF INTERSTAGE STRUCTURE FOR MB0130-074 ABLATIVE MATERIAL

INTRODUCTION

This investigation sought to determine whether solvent wiping of structure would provide adequate surface preparation for application of Korotherm 790-005 ablative material.

CONCLUSION

The surface preparation of the aluminum substrate by solvent wiping provides better adhesion than the cohesive strength of the applied ablative material.

PROCEDURE

Aluminum tensile blocks were solvent-wiped with methyl ethyl ketone, and Korotherm 790-005 material was applied by spraying in multiple applications with a DeVilbiss JG 5024 pressure pot spray gun with a No. 765 atomizing head. The thickness was built up to approximately 0.030 inch. Air supplied to the spraying equipment was checked for water content and dewpoint before spraying.

After a 48-hour cure, the other flatwise tensile block was secondarily bonded to the ablative material, using Narmco 7343/7139 adhesive and allowed to cure 24 hours at room temperature. The ablative flatwise tensile specimens were tested at room temperature in a Riehle Universal Test Machine. The tests were conducted after 72.0 to 72.5 hours of cure on the ablative material. Test data are listed in Table 34.

Table 34. Room Temperature Flatwise Tensile Tests

Specimen Number	Ultimate Flatwise Tension (psi)	Failure
1	136	Cohesive ablator
2	129	Cohesive ablator
3	161	Cohesive ablator
4	136	Cohesive ablator
5	146	Cohesive ablator
6	152	Cohesive ablator
	Average 143	

DEVELOPMENT OF THERMAL PROPERTY DATA ON MB0130-074 ABLATIVE MATERIAL (KOROTHERM 790-005)

INTRODUCTION

Korotherm 790-005 (MB0130-074) ablative coating is employed on the internal surfaces of the interstage structure on Saturn S-II-4 and subsequent stages to protect the interstages from the effects of base heating during the first 30 seconds of J-2 engine firing.

The purpose of this investigation was to develop thermophysical and ablative property data on the Korotherm 790-005 ablative coating.

CONCLUSIONS

The Korotherm 790-005 coating, in nominal 0.045-inch thicknesses, provided the required (< 300 F interface temperature) thermal protection to specimens simulating the interstage structure.

The thermocouple wires leading from the temperature sensor/ablative material interface clouded the results of the weight loss determinations. A accurate weight loss could not be determined on coating thicknesses less than 0.045 inch because of extremely low coating weights involved and the variables incurred from miscellaneous material constituents used in the test.

Thermal conductivity measurements could not be accomplished on the Korotherm 790-005 material at the 200 and 400 F temperature levels because the coating distorted when subjected to temperatures above 195 F.

PROCEDURE

Fabrication of Ablative Test Specimens

Specimens were fabricated in accordance with the design sketch shown in Figure 118, and in the following sequence.

The specimen holder assembly was fabricated by using MIL-C-7438, 5.7-3/16-20P (3003) aluminum honeycomb core. The core was bonded to

2014-T6 aluminum alloy facings in accordance with MA0106-033, using MB0120-048 Type-II adhesive. The aluminum surface of the specimen holder was prepared for application of the MB0130-074 ablative coating by applying MIL-C-5541 chemical film, according to MA0109-033; and MB0125-006 white epoxy primer, as required by MA0108-009. The specimen holder was trimmed to size and machined according to the design sketch.

The -3 insulator unit was machined from Johns Manville Marinite stock in conformance with the dimensions given. The -3 insulator was bonded into the specimen holder using MB0120-023 adhesive cured under contact pressure at room temperature for 24 hours.

The specimen holder, with -3 insulator installed, was sanded smooth and flush with wet sandpaper. Care was exercised to prevent damage or excessive removal of the MB0125-006 primer.

A dummy temperature sensor was installed in the 0.50-inch diameter counterbored receptable in the -3 insulator, flush with the surface of the MB0125-006 primer.

Korotherm 790-005 ablative compound was applied in three box coats to the specimen holder with a DeVilbiss JGA5024 pressure-pot spray gun, according to MA0606-042. The total coating thickness applied was approximately 0.060-inch. The coating was cured for 48 hours.

The dummy temperature sensor was removed by milling out the aluminum disc.

The -1 temperature sensor units were made from 0.125-inch-thick 2014-T6 aluminum alloy sheet. Iron-constantan 36-gauge wire thermocouples were spaced 0.75 inch apart and installed by peening the welded wire junctions into the surface of the aluminum sheet. Wire leads were individually passed through 0.015-inch-diameter holes predrilled in the aluminum sheet, as shown in Figure 118. The prepared aluminum sheet was spray-coated with MB0130-074 ablative compound, in accordance with MA0606-042.

Temperature-sensing units were extracted from the coated aluminum sheet by establishing the center point of the individual thermocouple installation, rough-cutting 0.75-inch squares out of the material around the thermocouples; and machining the 0.75-inch ablative-coated aluminum squares into 0.50-inch-diameter discs.

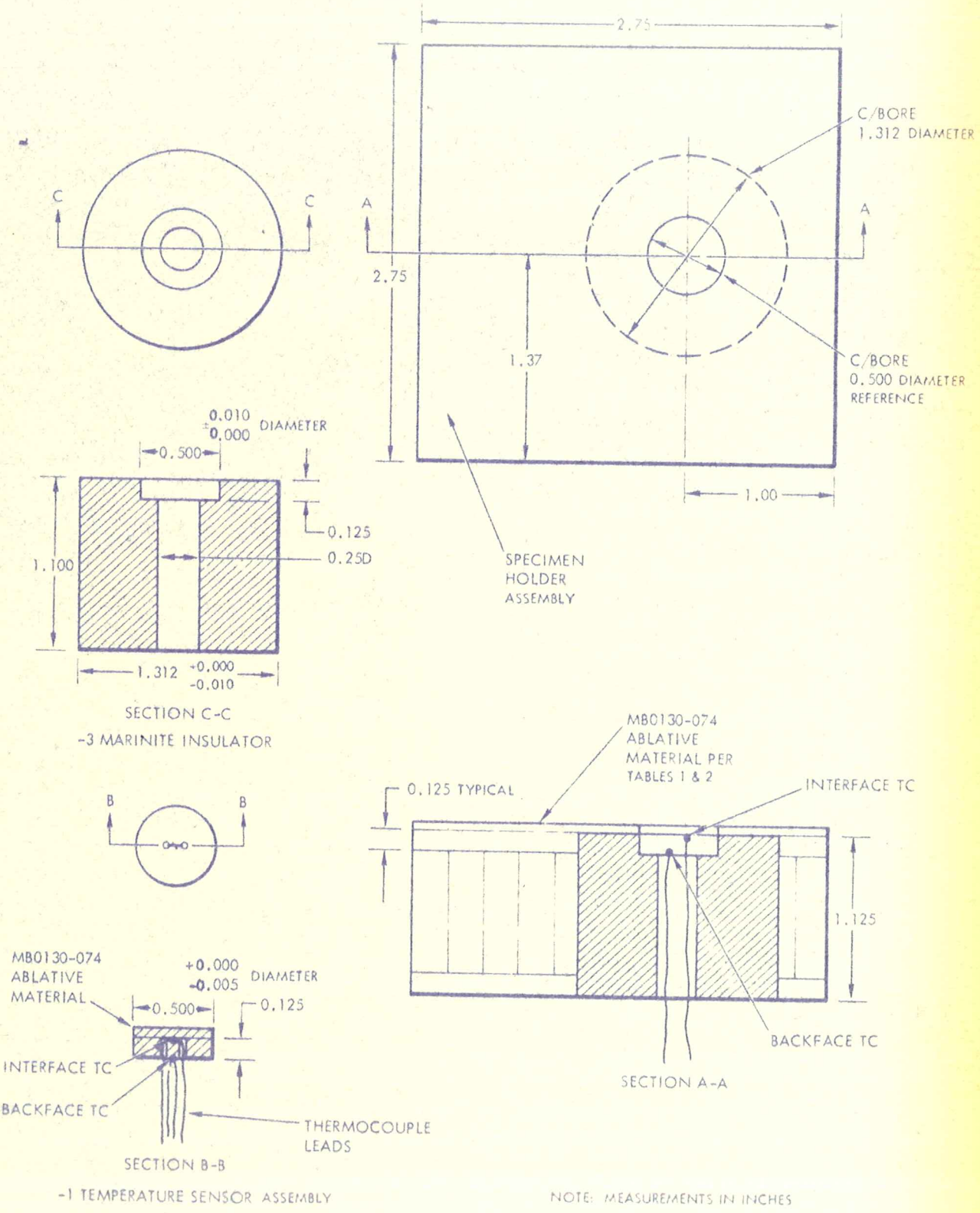

Figure 118. Ablative Material Specimen Holder Configuration—Hyperthermal Tunnel Plasma Jet Test Facility

The temperature sensor units were accurately weighed on an analytical balance, and then each was measured for thickness. A 30-gauge iron-constantan thermocouple was installed by peening the junction into the back surface of each temperature sensor unit.

The temperature sensor units were bonded into the -3 insulator receptacle, as shown in Figure 118, using the MB0130-074 ablative coating. The ablative material was trowelled smooth and flush around the edges of the temperature sensor and allowed to cure at room temperature for a minimum of 48 hours prior to test.

Testing

Testing of the ablative insulation specimens was accomplished in the Hyperthermal Tunnel Plasma Jet Facility. Testing parameters were adjusted in the plasma jet to provide the 8.0-Btu/ft^2/sec heat flux and convective flow environment that will be experienced by the ablative coating on the internal surfaces of the interstage during the first 30 seconds of J-2 engine firing.

The plasma jet settings to provide the 8.0-Btu/ft^2/sec heat flux were determined as follows: An iron-constantan asymptotic cold wall calorimeter was positioned in a specimen holder simulating the actual specimens to be tested, as shown in the test design sketch, Figure 119. The heat flux adjustments were made in the plasma jet initially by running the plasma for short three-second bursts, varying the electrical power and gas pressure to obtain the required 7.5 to 8.0-Btu/ft^2/sec heat flux.

After the final settings were determined, they were verified by testing the calibration specimen in the plasma for a 30-second duration. The final plasma jet settings and detailed operating procedures were as follows:

1. Evacuate the vacuum chamber of the plasma jet to a pressure of 0.50 cm mercury or less
2. Adjust nitrogen gas pressure to 100 psig
3. Start plasma jet
4. Set jet current to approximately 925 amperes and 56 volts dc
5. Allow plasma jet to stabilize as indicated by a straight trace on the current recorder

6. Position specimen by use of the swing arm into the center of the plasma stream; hold in position for 30 seconds, then remove specimen from plasma stream

Each ablative test specimen was tested for a nominal 30-second duration in accordance with the parameters listed above. Specimens were positioned in the plasma jet as shown in Figure 119.

RESULTS

Time-versus-insulation interface and backface temperatures are presented for the nominal 0.015-, 0.030- and 0.045-inch-thick ablative insulation specimens in Figures 120, 121, and 122 respectively.

All specimens tested demonstrated very even and smooth ablative characteristics. A typical ablation test is shown in Figure 123. A typical specimen after test is shown in Figure 124.

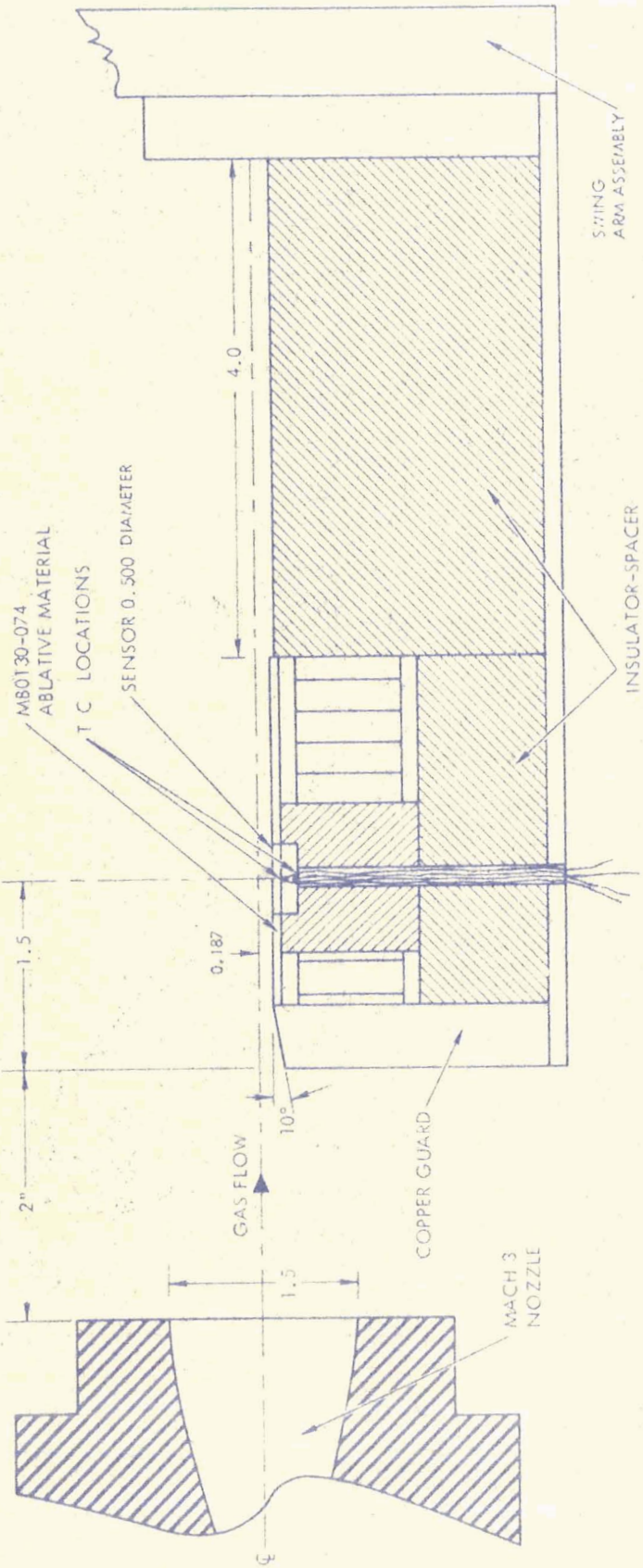

Figure 119. Cross-Section Specimen Holder Positioned in Hyperthermal Tunnel Plasma Jet Facility

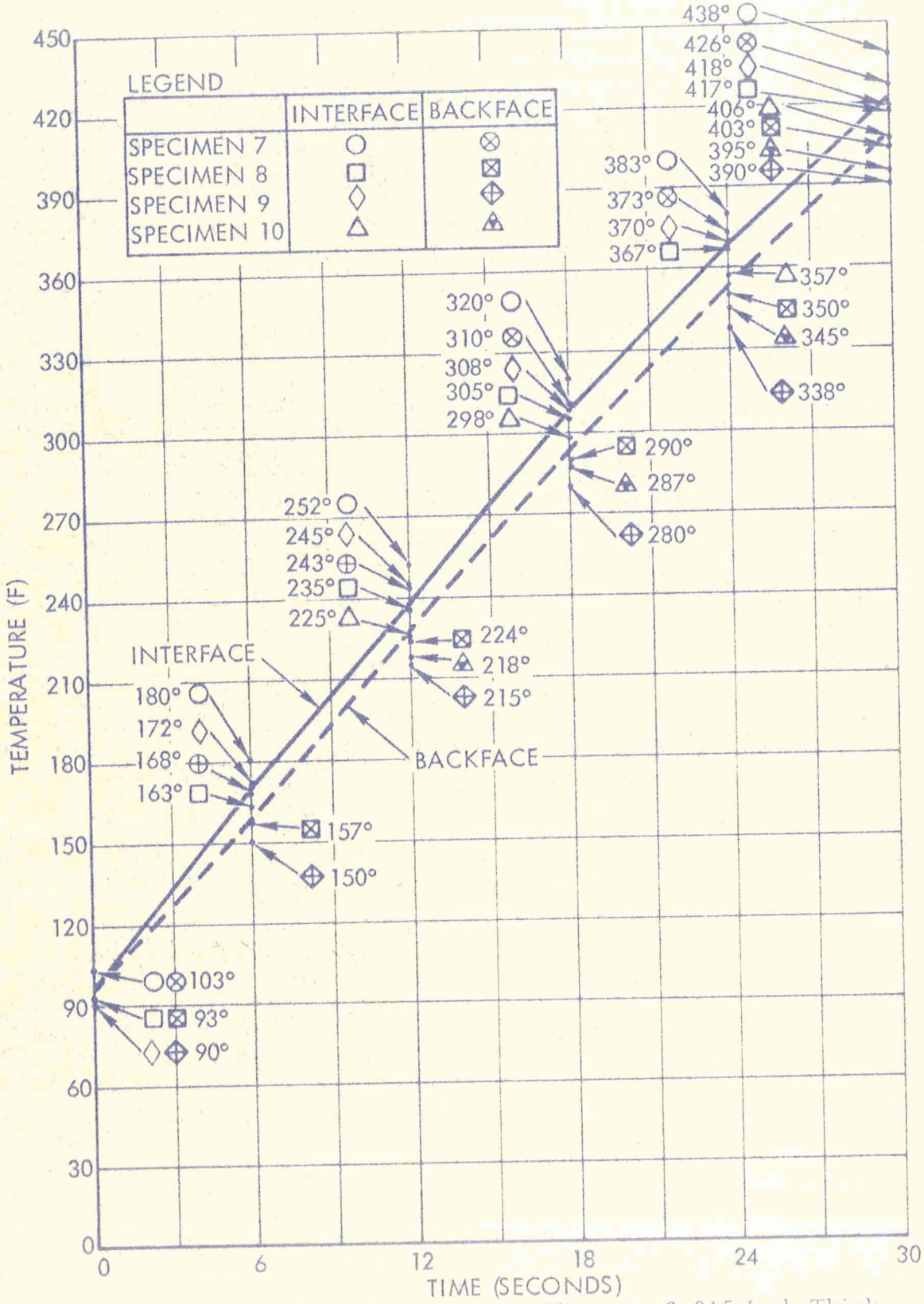

Figure 120. Time/Temperature History -0.015-Inch Thick MB0130-074 Ablative Specimens

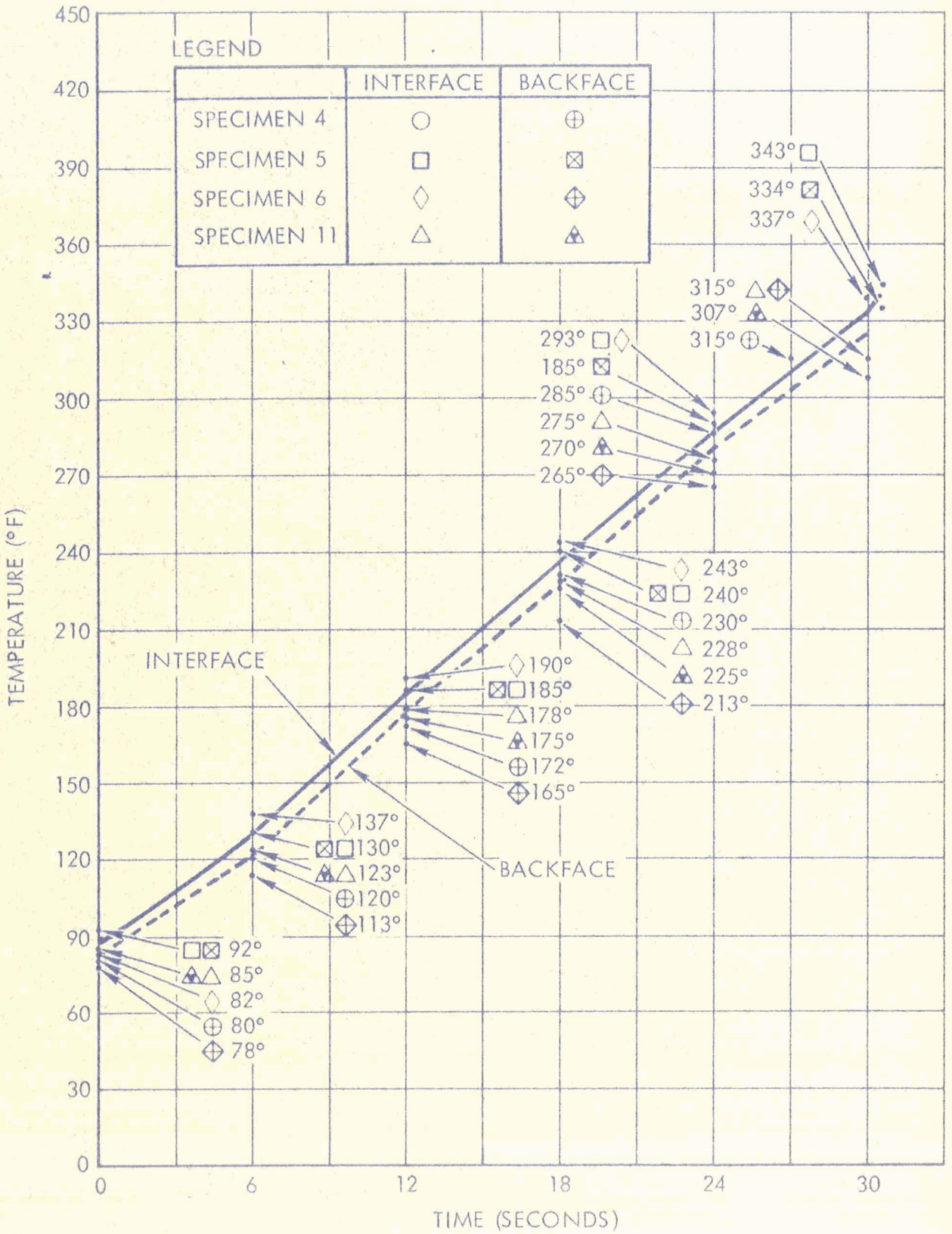

Figure 121. Time/Temperature History—0.030-Inch-Thick Korotherm 790-005 Ablative Specimens

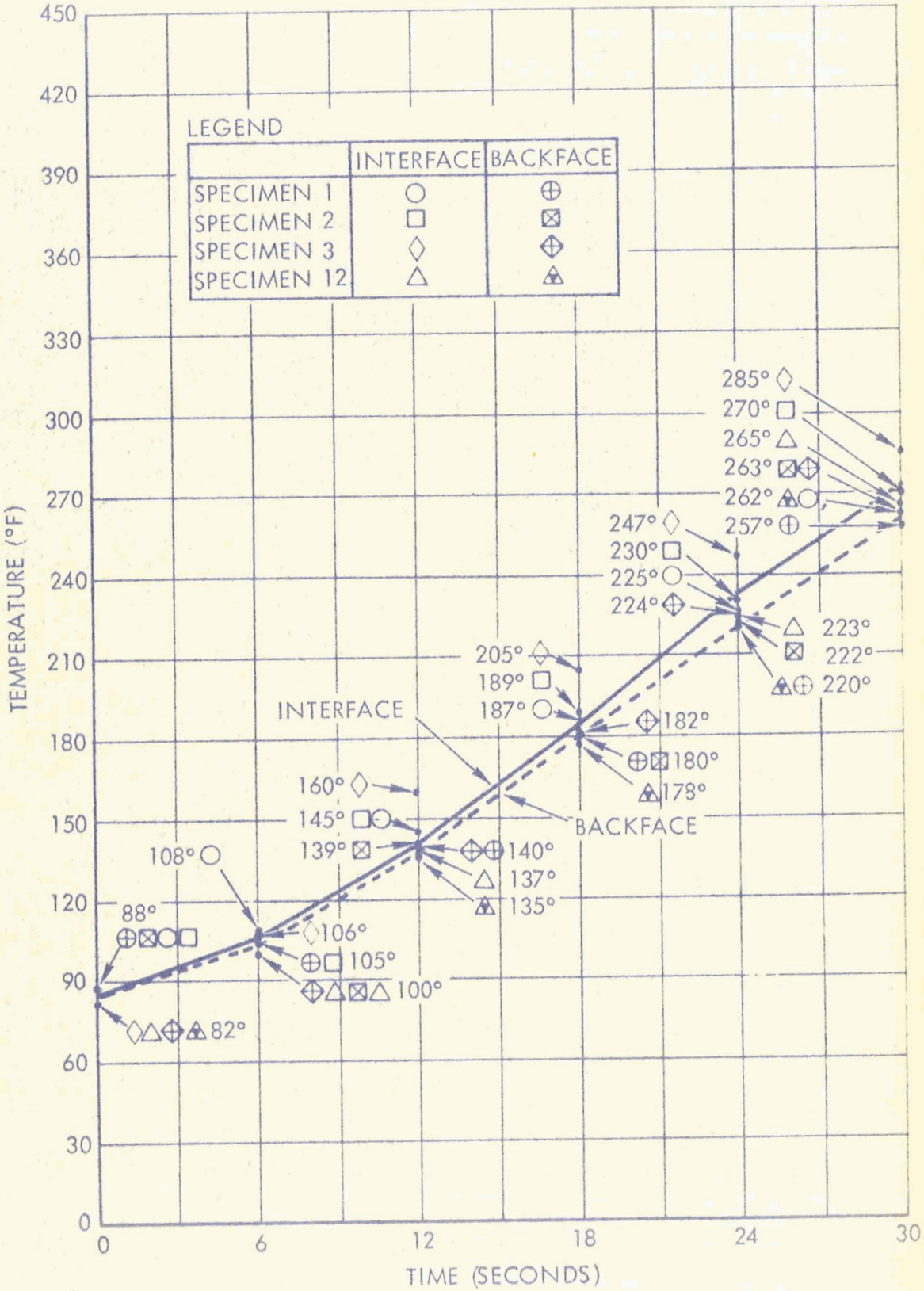

Figure 122. Time/Temperature History—0.045-Inch-Thick Korotherm 790-005 Ablative Specimens

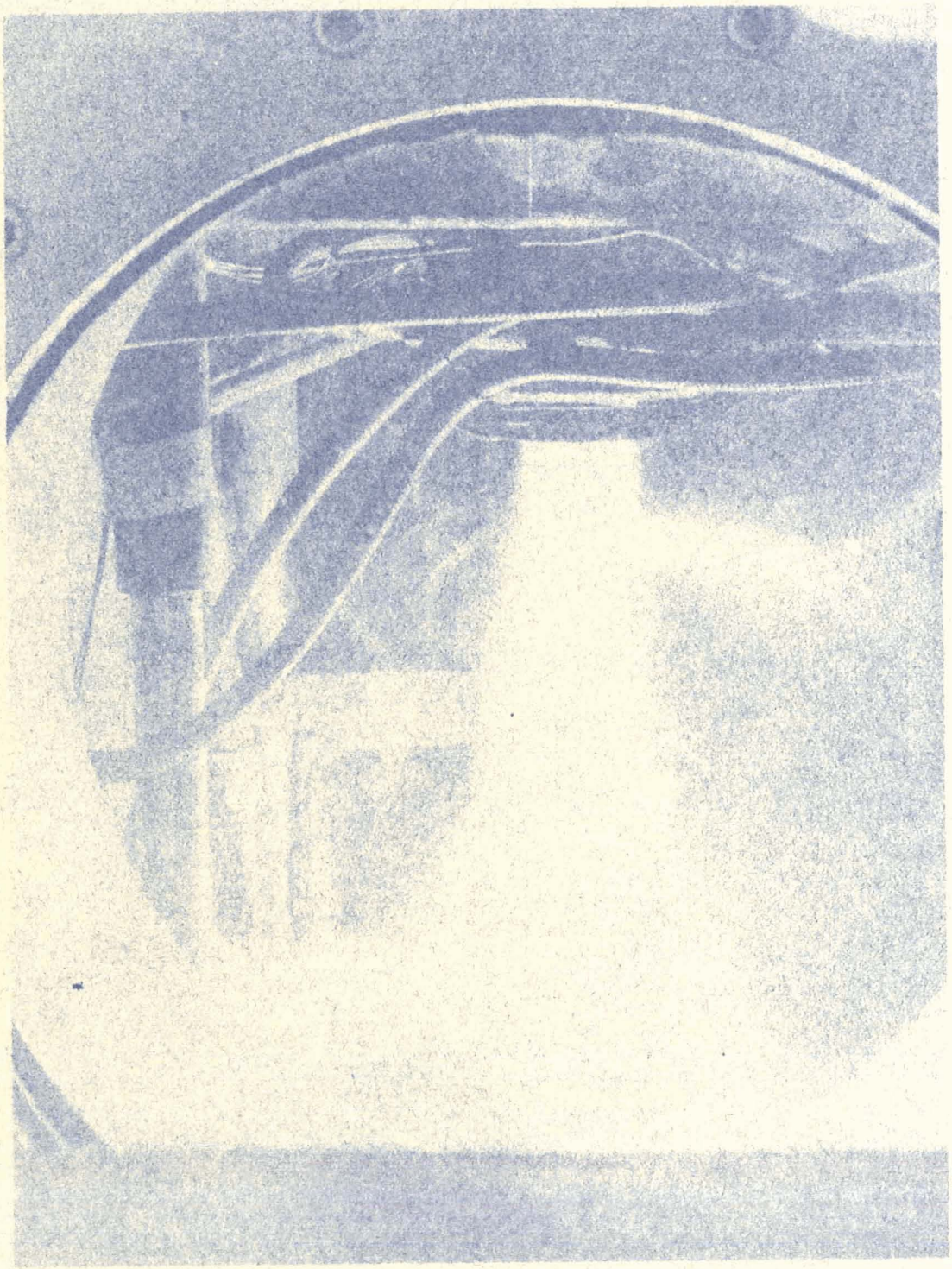

7006-81-2549C

Figure 123. Plasma Jet Test Sequence, 25-Second Period

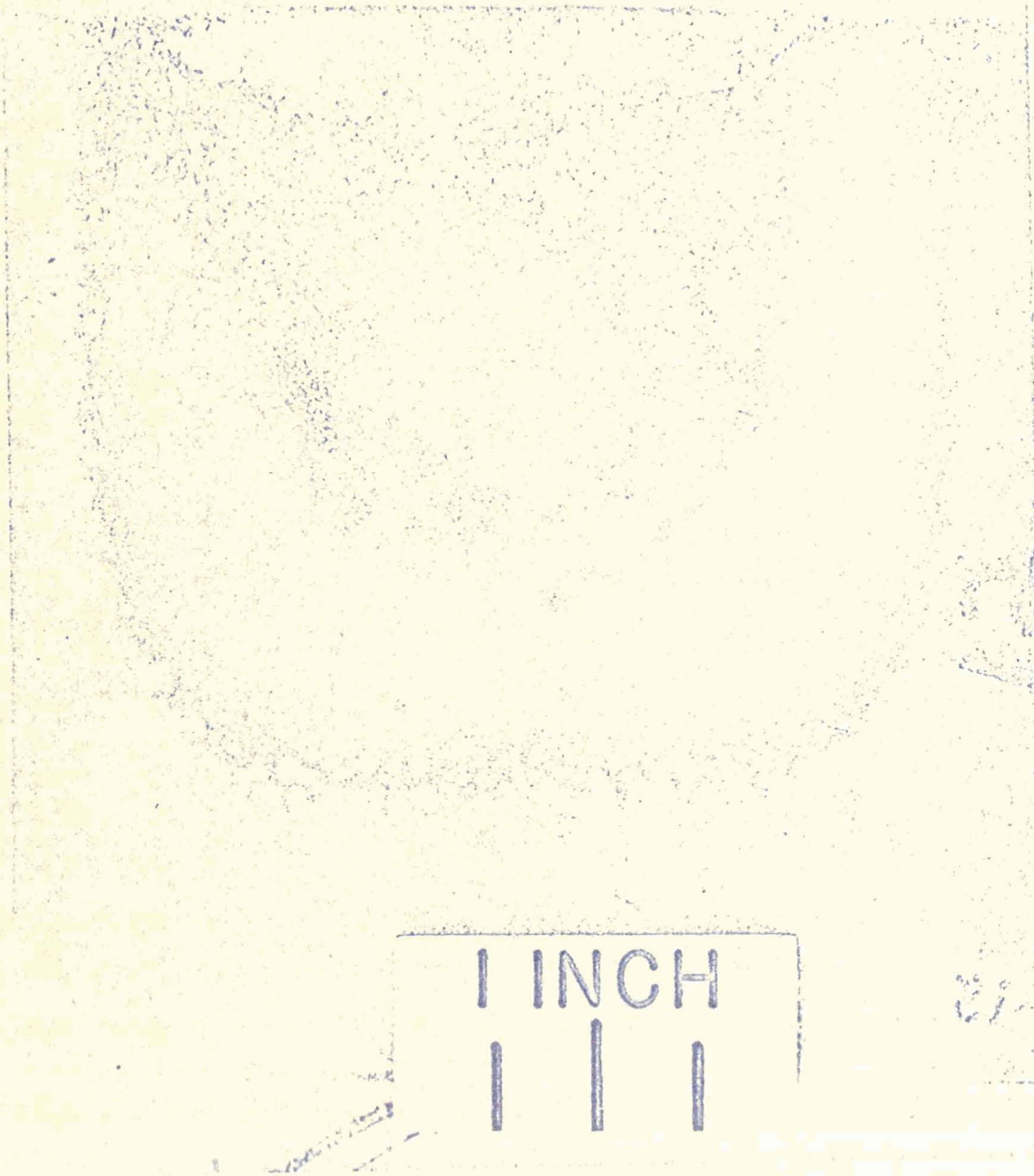

7006-81-2549D

Figure 124. Ablative Material Specimen after Test in Plasma Jet

FOAM-FILLED HONEYCOMB INSULATION

PROGRESS SUMMARY

Preliminary emergency repair procedures were developed and evaluated for possible use on the launch pad at KSC. The repair concepts were qualitatively demonstrated in laboratory tests. In addition, two room-temperature curing adhesives were tested to determine the minimum temperature that could be tolerated and still maintain mechanical properties.

A nylon fabric/polyurethane material was evaluated for use as a membrane seal on the LH_2 forward bulkhead. The function of the membrane seal is to prevent debris and water from entering the uninsulated area between the bulkhead and forward skirt while simultaneously permitting the slow escape of purging gases. The fabrics' two-dimensional flexibility during installation and temperature changes provides additional advantages.

Silicone rubber and nylon/polyurethane resin closeouts were evaluated for use under cryogenic conditions. It was determined that a change in the closeout joint configuration would allow the silicone rubber closeout to be used within its cryogenic capabilities. However, under fairings this capability is exceeded, and nylon/polyurethane resin closeouts must be employed.

DEVELOPMENT OF PROCEDURES APPLICABLE TO EMERGENCY REPAIR OF SIDEWALL INSULATION PRIOR TO LAUNCH

INTRODUCTION

Processes have been developed by the Laboratories and Test Department, in cooperation with S-II Engineering and Materials and Processes, to support repair of various defects that may occur in the sidewall insulation during the different phases of stage processing and just prior to launch (effective on the S-II-1 through the S-II-7 stages). The repair processes are tailored to meet the requirements of the S-II stage and available facilities when situated in the three following basic postures: on the pad and ready for tanking with the mobile service structure (MSS) in position, with the MSS removed and access to the stage provided by the STD-150 basket suspended from the launch umbilical tower (LUT) crane, or either prechilled or tanked with LH_2 with access to the stage provided by the STD-150 basket. The latter two requirements were subsequently deleted in accordance with a NASA directive. The basic concepts have been qualitatively demonstrated in preliminary laboratory tests.

PRELIMINARY DEVELOPMENT OF REPAIR CONCEPTS

During the preliminary development phase of the emergency repair program, several repair concepts were qualitatively evaluated and screened for possible application to the S-II stage during the final countdown period. Three basic emergency repair processes were evolved during the screening program:

1. For skin areas that become debonded from the foam-filled honeycomb core, the repair processes involve the use of a polyurethane spray foam applied to the open cells of the insulation.

   Figures 125 through 128 illustrate typical application sequence of spray foam at ambient conditions. Figures 129 through 132 show a typical application sequence of the foam at < -280 F temperatures. Figure 133 illustrates a cross-section of foam applied under < -280 F conditions.

   The repair concept is based on the spray foam partially sealing the repair area from adjacent helium-purged insulation. When time permits (2 hours prior to application of the helium purge), the spray foam repair is faced with a RTV silicone rubber fiberglass laminate.

2. Where cracked or torn skin or minor holes occur up to one-inch in width or diameter (with no skin-to-core debonds in the insulation), and while the stage is either at ambient temperature or in the chilled or tanked posture, an aluminum foil tape (Johns Manville B-FF) can be used as a repair procedure. Photographs showing the application of the Johns Manville B-FF tape at skin temperatures < -80 F while under 5 psig helium purge are presented in Figures 134 and 135.

3. Where the honeycomb core has become debonded from the tank wall, the Tedlar/nylon skin, core and foam within the cells are removed to the HT-424 adhesive surface, and the cavity is filled with the polyurethane spray foam. The spray foam is flush-finished with adjacent Tedlar film surfaces, then coated with the RTV silicone rubber/fiberglass laminate. This repair process is applicable to ambient temperature conditions only. Photographs of the spray application of a polyurethane foam to a simulated tank surface are presented in Figures 136 and 137.

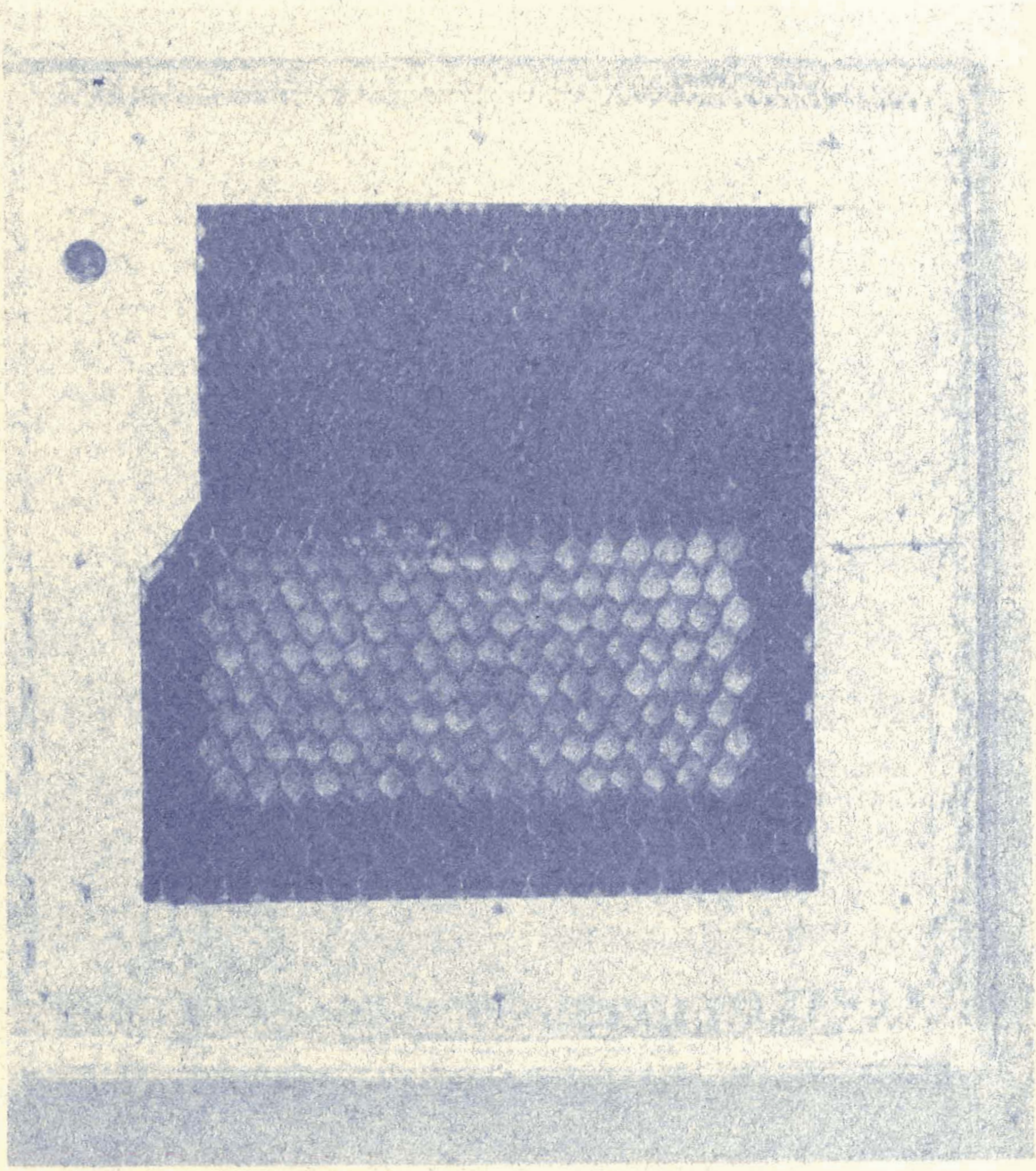

7006-81-2136C

Figure 125. Insulation Repair Area Prepared for Application of Spray Foam (CPR 369) at Ambient Temperature

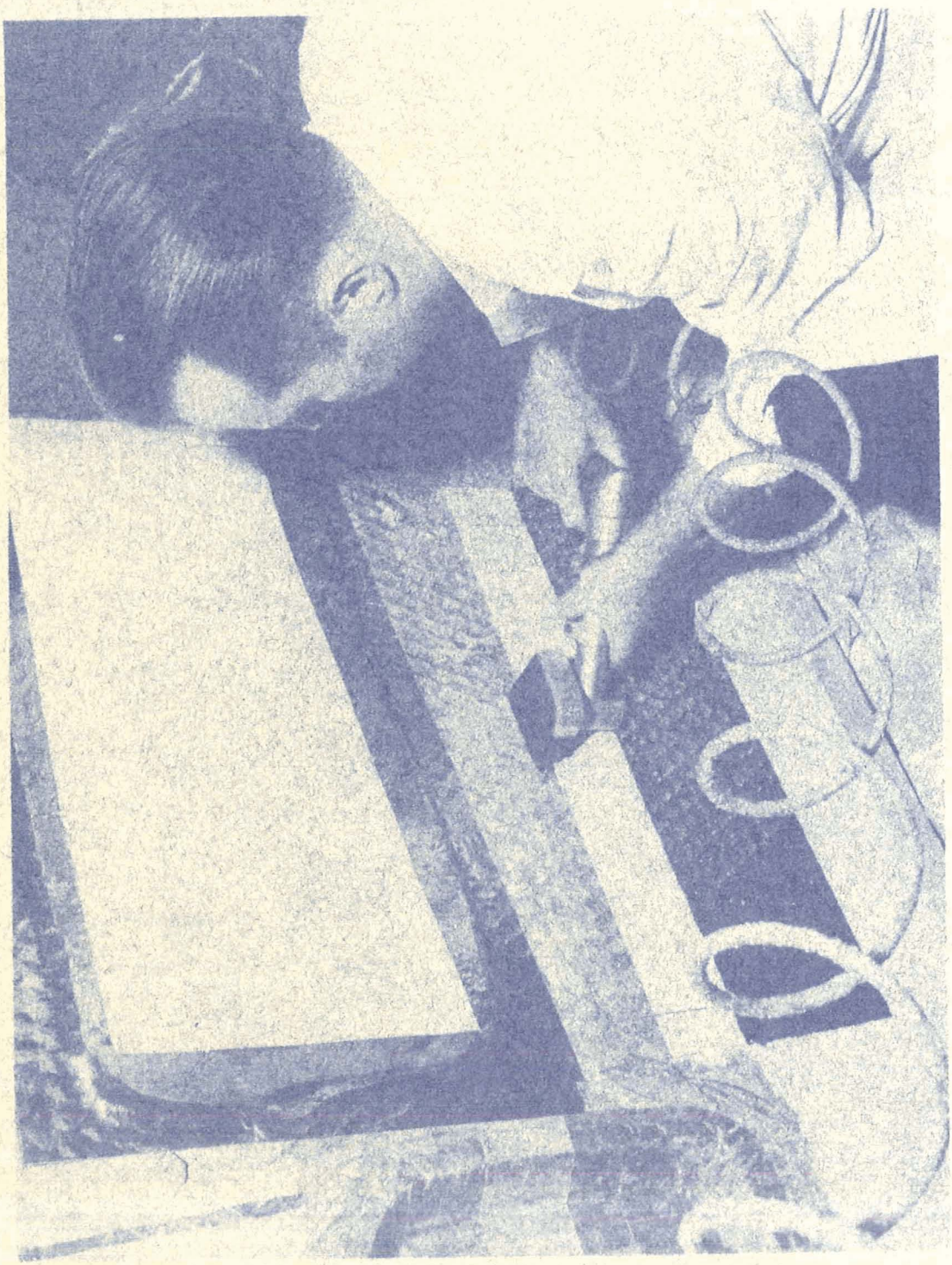

7006-81-2121G

Figure 126. Air-Motor-Driven Cutting Tool Removing Section of Defective Skin

7006-81-21458

Figure 127. Application of CPR 369-3 Foam Using Glascraft Gun Forming U-Shape Pattern Around Periphery of Repair

7006-81-2145F

Figure 128. Trimming the Spray Foam Insulation Repair, Using a Carpenter's Hand Saw

7006-81-2141A

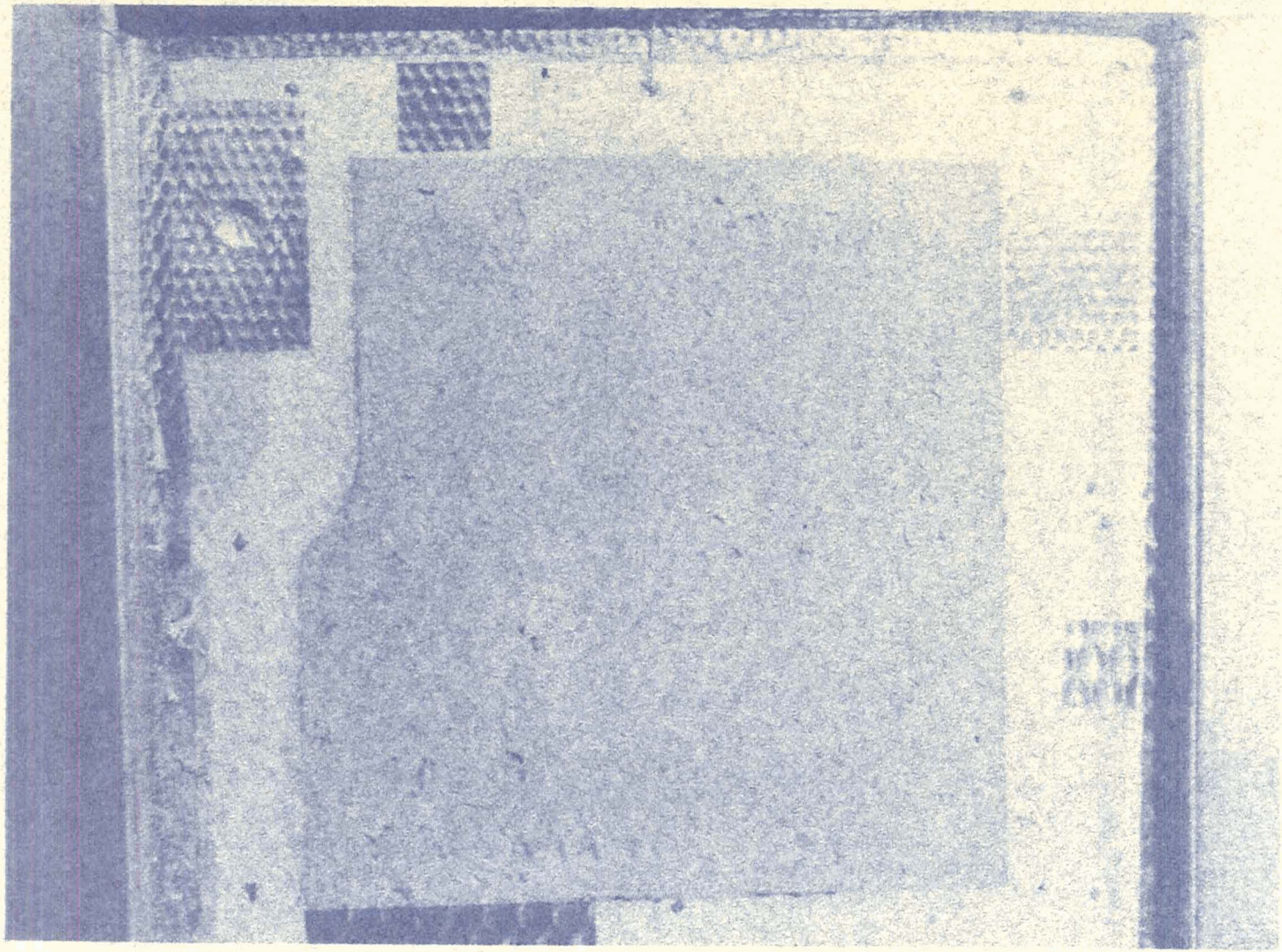

Figure 129. CPR 369-3 Spray Foam Repair Finished to Surface of Core and Flush With Adjacent Tedlar Skin Insulation Leak-Checked at Ambient Using Helium at 5 psi

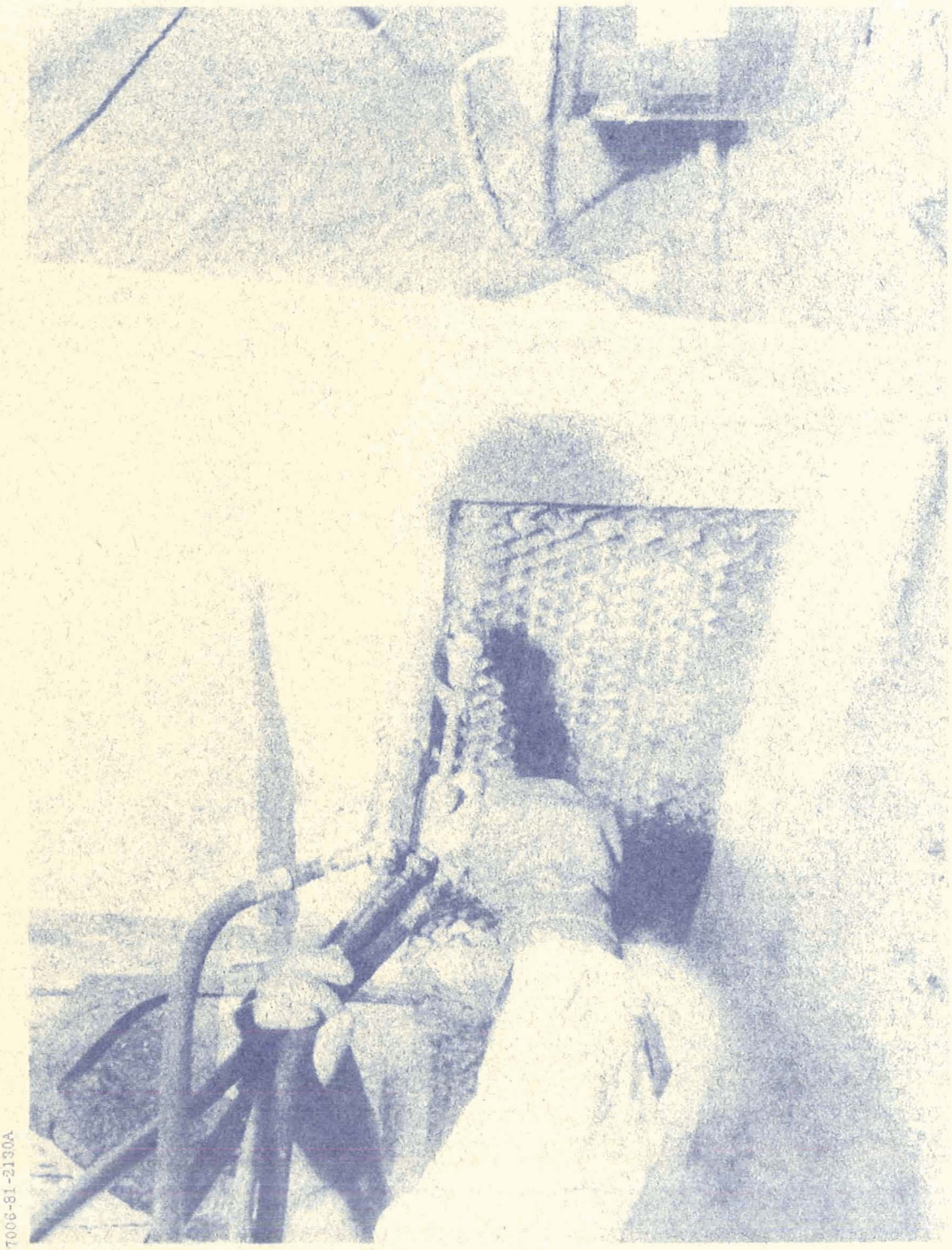

Figure 130. Application of CPR 369-3 Foam to Prechilled < -280 F) Insulation Repair Area Using Glascraft Gun

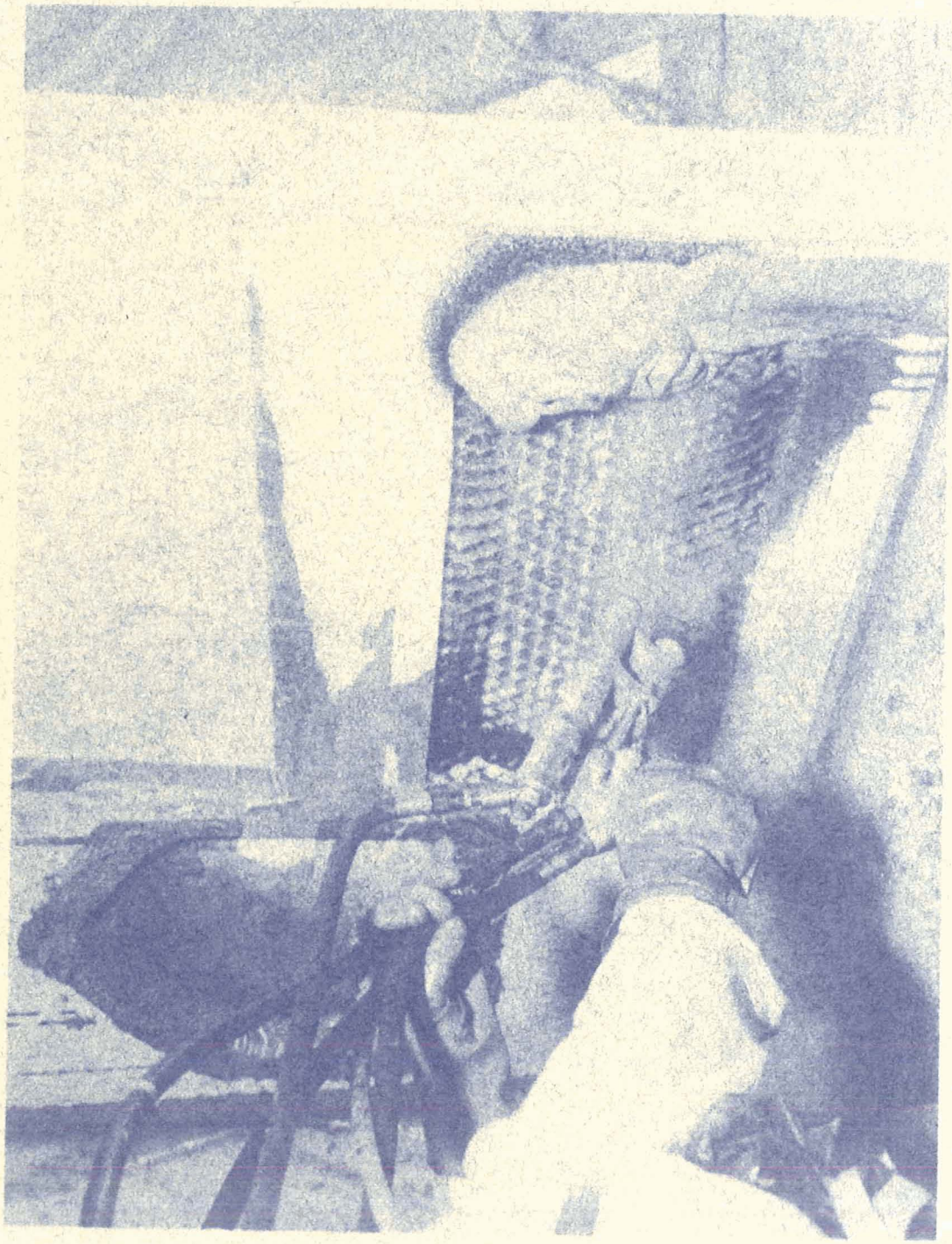

7006-81-2130B

Figure 131. Application of CPR 369-3 Foam Across Peripheral Area of Repair Insulation (Aluminum Plate is at < -280 F)

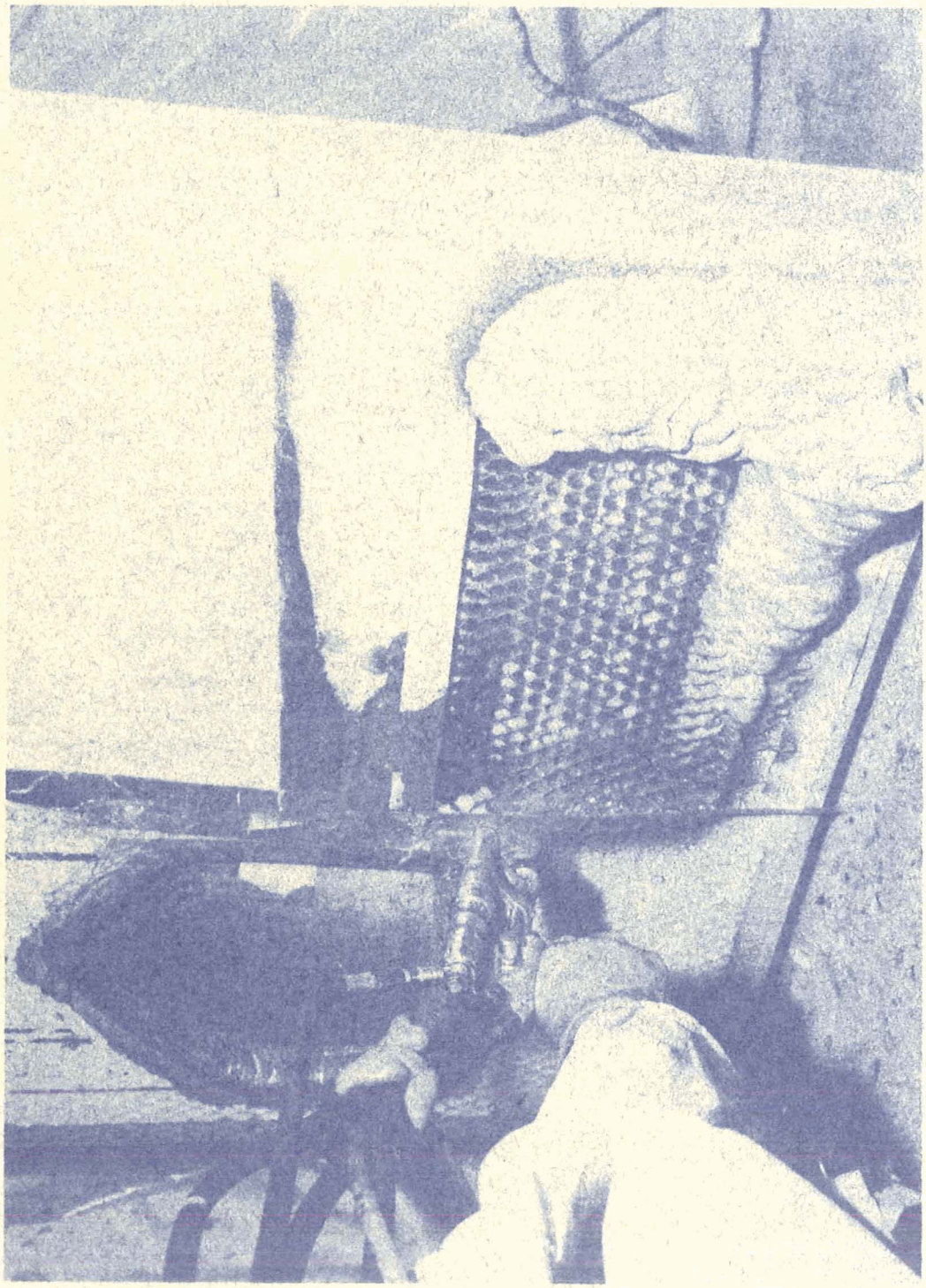

7006-81-2133A

Figure 132. Sealing Left-Hand Peripheral Area of Chilled (-280 F) Repair Using CPR 369-3 Foam and Glascraft Gun

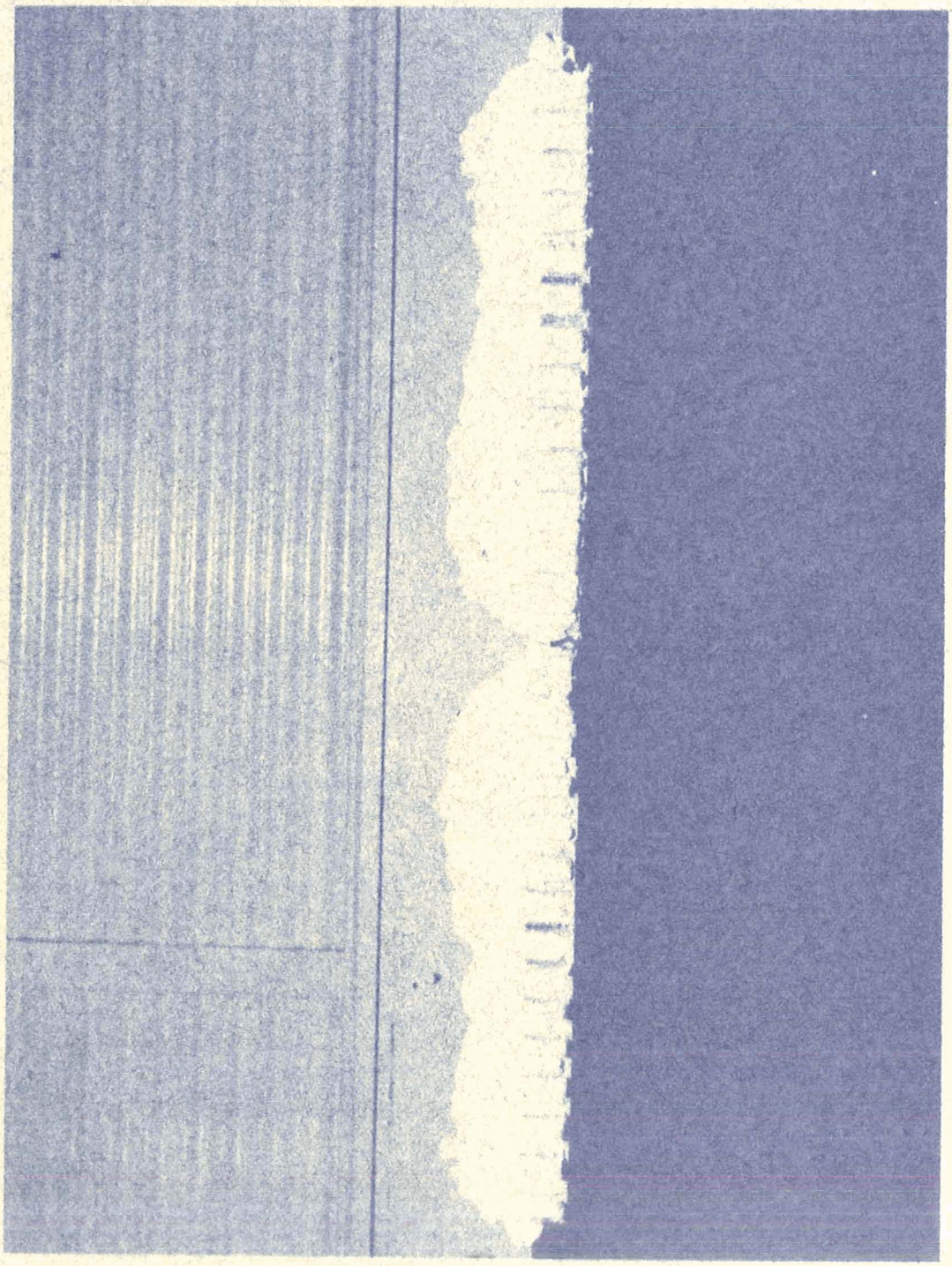

7006-81-2116

Figure 133. Cross-Section of CPR 396-3 Spray Foam Applied into 3/4-Inch Cell Honeycomb With Aluminum Backing Plate (Aluminum Plate Immersed in LH_2)

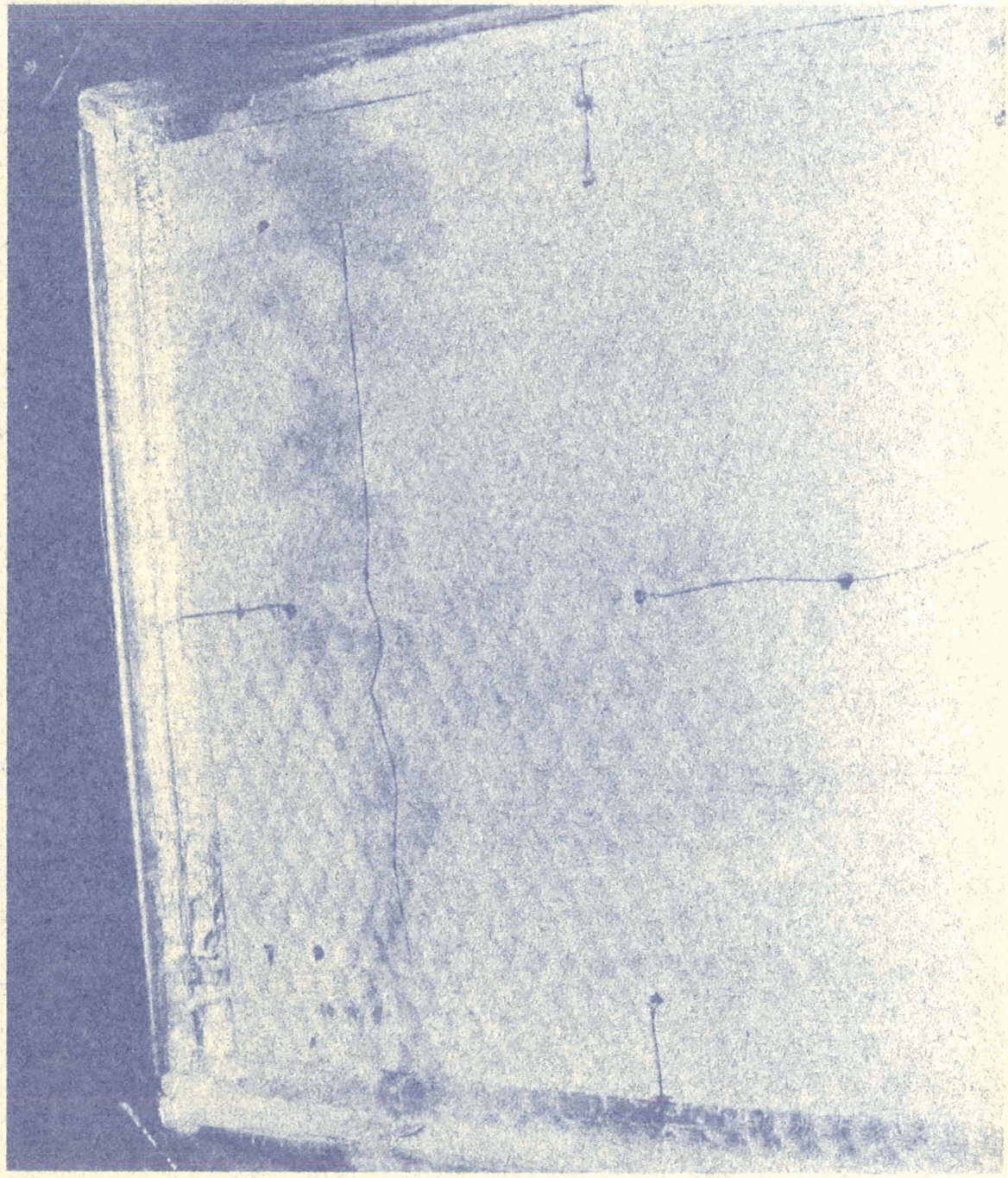

7006-81-2101 "O"

Figure 134. Tedlar Laminate Cut as Shown With Knife 1/16 x 16 Inch (Note Chilled Helium Purge Escaping Through Crack)

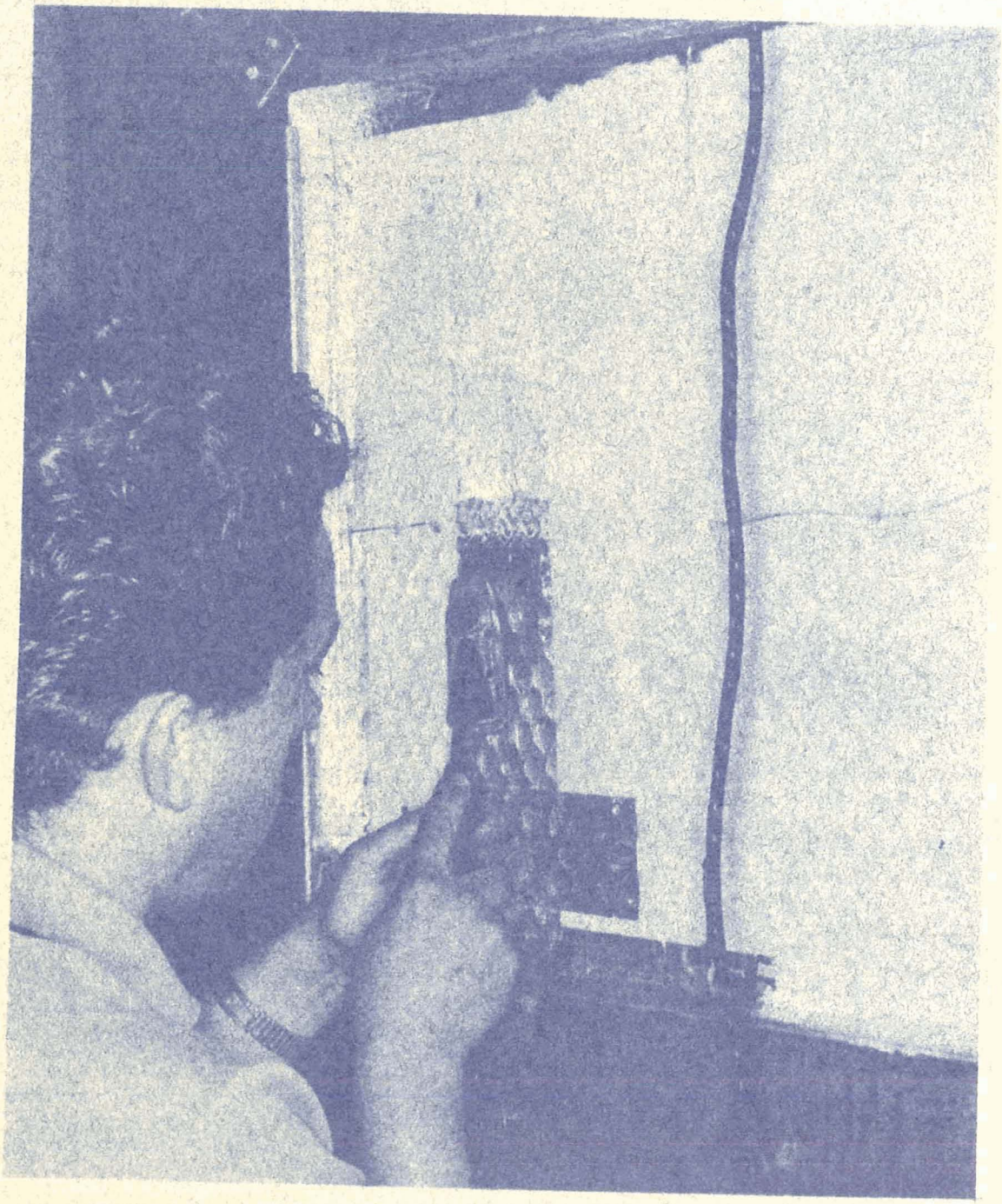

7006-81-2101F

Figure 135. Application of Johns Manville B-FF Tape to Prechilled (-80 F) Tedlar Surfaces Over Cracked Area, Iron is Approximately 475 F

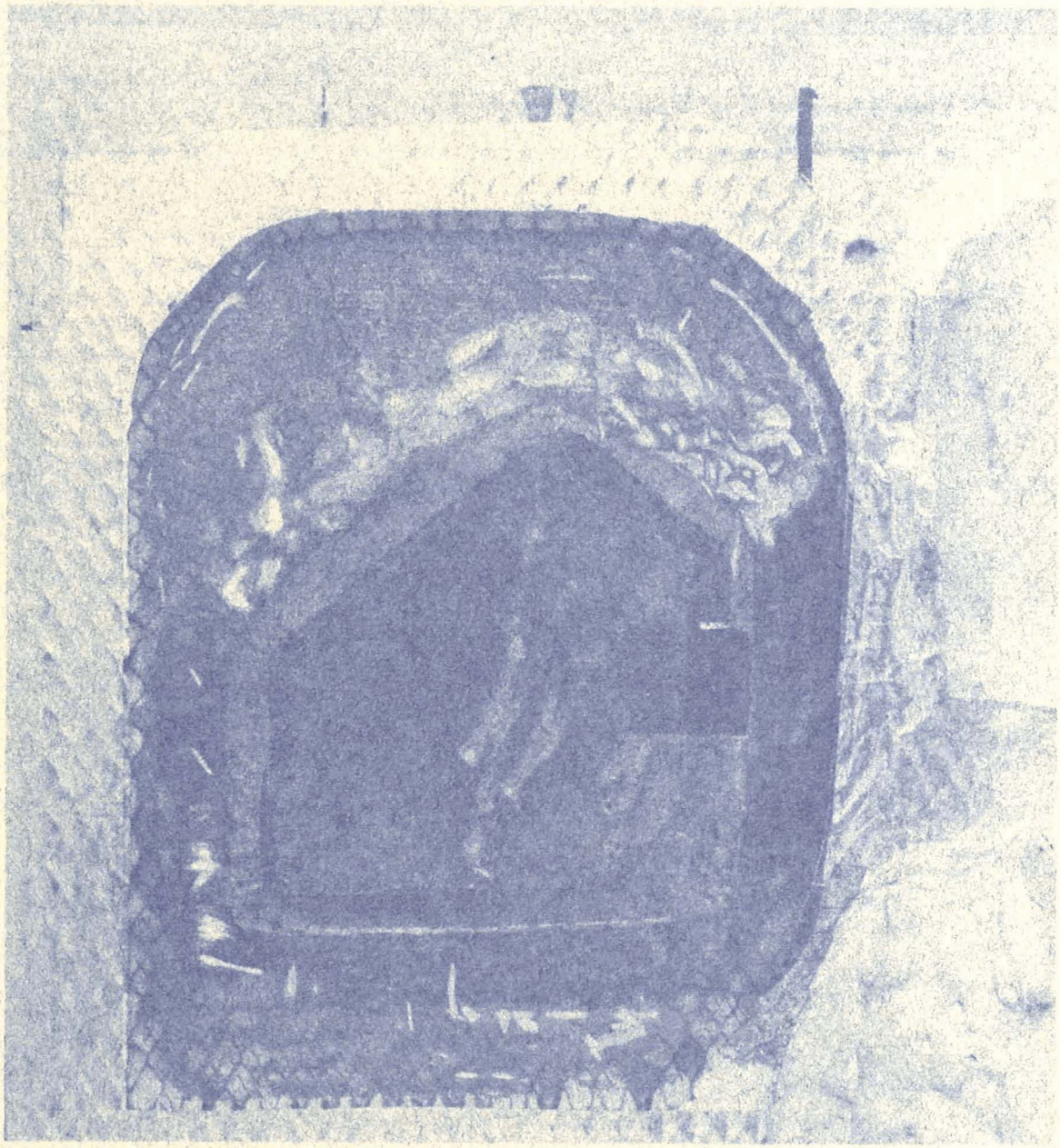

7006-81-2136A

Figure 136. Typical Repair Area—Core Removed to HT-424 Surface of Tank Wall—Primed with Primer M

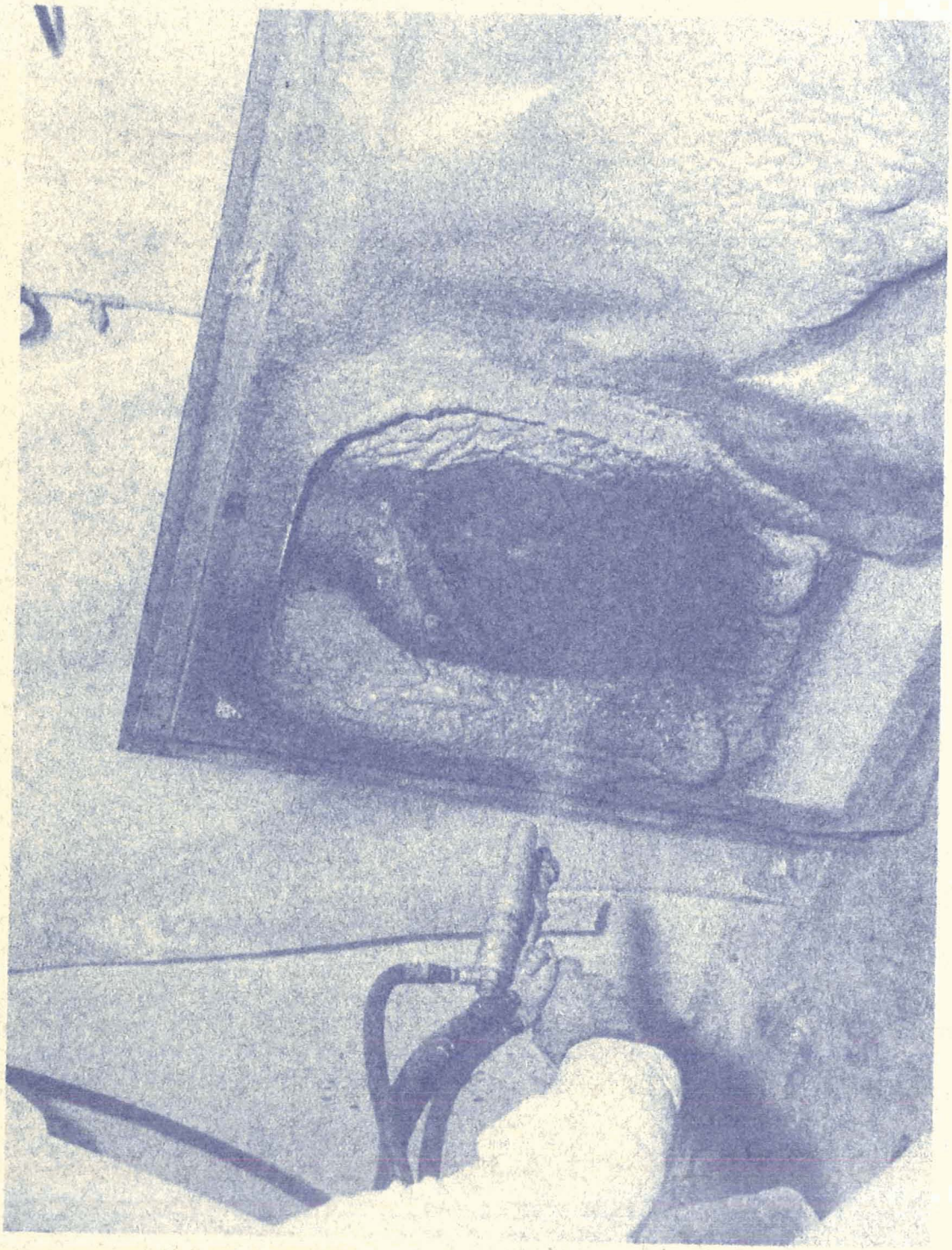

7006-81-2141D

Figure 137. Application of CPR 369 Foam in Center Section of Insulation Repair Area

MINIMUM SATURN S-II TANK WALL TEMPERATURE FOR ADHESIVE APPLICATION

INTRODUCTION

Damaged Saturn S-II sidewall tank insulation frequently must be repaired at off-site test facilities where the atmospheric temperature cannot always be controlled. The large size of the S-II stage usually requires its exposure to normal outside atmospheric environment that can go as low as freezing in the winter months at the test facility.

Laboratory test programs investigated the handling and mechanical properties of Lefkoweld 109 and the Narmco 7343/Primer M system at application temperatures from 30 to 80 F.

After application of Lefkoweld 109 adhesive, tensile shear specimens were cured as follows:

1. 48 hours at 60 to 70 F and 5- to 10-psi bonding pressure
2. 6 hours at 115 to 135 F and 5- to 10-psi bonding pressure

After application of the Narmco 7343/Primer M adhesive system, the following cure cycles were used to cure the adhesive:

1. 24 hours at 75 to 85 F and 2- to 10-psi bonding pressure
2. 12 hours at 115 to 135 F and 2- to 10-psi bonding pressure

CONCLUSIONS

Lefkoweld 109, when applied at various simulated tank wall temperatures, gave tensile shear results, after curing for 48 hours at 60 to 70 F that did not always meet the minimum room temperature requirement of 2000 psi. Six hours at the 115 to 135 F cure cycle gave tensile shear results that met the material specification room temperature requirement at all tank wall temperatures tested down to 35 F.

One disadvantage of applying the Lefkoweld 109 adhesive to low temperature surfaces is that the adhesive becomes very tacky and difficult to spread at temperatures below 55 F.

Narmco 7343/Primer M adhesive system, applied to specimens and cured for 24 hours at 75 to 85 F, gave tensile shear results that did not meet the room temperature material specification requirements of 1000 psi at any application temperature tested. The same type of specimens cured for 12 hours at 115 to 125 F met the minimum tensile shear requirements at all adhesive application temperatures tested, down to 40 F. Test data show that the tensile shear results were higher and had less variance at adhesive application temperatures of 55 F and above.

PROCEDURE AND RESULTS

The tensile shear coupons used in this test program were immersion-etched in accordance with MA0110-024, and the adhesive or primer was applied to the coupons within 8 hours after cleaning.

Two sets of tensile-shear coupons were put into the climatic control chamber at each of the indicated temperatures and humidity ranges listed in Table 35. The test coupons were allowed to stabilize at the temperature indicated before application of Lefkoweld 109 adhesive. The Lefkoweld 109 bonded specimens were put under 5-psi positive pressure. They were allowed to remain in the humidity chamber for 24 hours at the specified temperature conditions. Then one set was cured for 48 hours at 60 to 70 F, and the other for 6 hours at 115 to 135 F. Test specimens controlled at 60, 65, and 70 F were not conditioned 24 hours before starting the cure cycles. Cure cycles for specimens at these three application temperatures were started immediately following fabrication of the specimens.

Two sets of tensile-shear coupons were also put into the climatic control chamber at each of the temperature and humidity ranges indicated in Table 36. The test coupons were allowed to stabilize at the temperatures indicated before three brush coats of Primer M were applied. The Primer M was allowed to cure four hours in the climatic control chamber at the indicated controlled temperatures. Narmco 7343 adhesive was applied to the M-primed coupons and maintained under 5-psi positive pressure in the humidity chamber for 24 hours prior to starting the 24-hour cure cycle at 75 to 85 F on one set of tensile shear specimens and the 12-hour cure cycle at 115 to 135 F on the remaining set. The specimens having adhesive applied at 75 F were not given the 24-hour conditioning prior to starting the cure cycles, but the 24-hour cure cycle at 75 to 85 F was started immediately after application of the adhesive. The specimens to be cured for 12 hours at 115 to 135 F were allowed to stabilize for 12-hours at room temperature before starting the cure cycle.

Table 35. Average Lefkoweld 109 Room Temperature Tensile Shear Results

Adhesive Application Environment	Control Shear Strength (psi)	Specimens Cured for 48 Hours at 70 F Shear Strength (psi)	Specimens Cured for 6 Hours at 125 F Shear Strength (psi)
35±5 F and 65±5 percent relative humidity	4910	3090	4970
40±5 F and 65±5 percent relative humidity	4650	3142	4475
45±5 F and 65±5 percent relative humidity	4150	3020	4040
50±5 F and 65±5 percent relative humidity	4440	1720	2930
55±5 F and 65±5 percent relative humidity	4080	1650	3130
60±5 F and 65±5 percent relative humidity	4130	1820	2510
65±5 F and 65±5 percent relative humidity	4410	3240	3450
70±5 F and 65±5 percent relative humidity	4230	2965	2820

Table 36. Average Narmco 7343 Room Temperature Tensile Shear Results

Adhesive Application Environment	Control Shear Strength (psi)	Specimens Cured for 24 Hours at 80 F Shear Strength (psi)	Specimens Cured for 12 Hours at 125 F Shear Strength (psi)
40±5 F and 65±5 percent relative humidity	1416	388	1027
50±5 F and 65±5 percent relative humidity	405	77	271
55±5 F and 65±5 percent relative humidity	1545	70	1350
60±5 F and 65±5 percent relative humidity	1850	780	1818
65±5 F and 65±5 percent relative humidity	1940	203	2240
75±5 F and 65±5 percent relative humidity	2000	123	1520
Requirements MB0120-024	1000	1000	1000

TEST DATA FOR A POLYURETHANE-COATED NYLON FABRIC TO REPLACE MEMBRANE SEAL

INTRODUCTION

In accordance with a design requirement from Saturn S-II Engineering, an evaluation was conducted on a stretchable fabric impermeable to water and permeable to gases.

CONCLUSION

Urethane-coated nylon fabric, Style 3514, supplied by Reeves Vulcan, Division of Reeves Brothers Corporation, met the requirements noted.

PROCEDURE AND RESULTS

Hydrostatic Resistance

The hydrostatic permeability was zero when determined in accordance with ASTM D 751 and using a 2-inch head of water for an exposure period of 24 hours.

Nitrogen Permeability

With a pressure differential across the test area of 0.1±0.05 psia at ambient room temperature, the permeation of nitrogen was within the required minimum of 1500 scc/hr/sq in.

EVALUATION OF SILICONE RUBBER FLEXIBLE CLOSEOUT SEAL INSTALLATIONS AT EXTREME COLD TEMPERATURES

INTRODUCTION

The foam occasionally falls out of the edges of the 1.6-inch thick foam-filled honeycomb insulation panels and closeout assemblies during application to the S-II tank wall quarter panels. This condition creates relatively large open areas between core cells exposed in the insulation joints. The open-cell areas between the insulation joints allow convective flow and relatively large volumes of cold helium purge gas (as compared to joints filled with foam) to come in contact with the underside of the nylon/Tedlar insulation facing sheet and flexible closeout seal. The cold helium gas causes the flexible closeout seal installation to drop below minimum operating temperature. Open closeout joint configurations were investigated to determine if the flexible closeouts were affected by impingement of extremely cold helium gas.

The investigation consisted first of determining the low-temperature working characteristics of flexible closeout seals installed on insulation panel nylon/Tedlar facing sheets over open honeycomb core cell joints, and then developing a method for isolating a portion of the open joint from the cold helium purge gas.

CONCLUSIONS

Flexible closeout seals installed over insulation joints where the foam has been removed from the core cells may crack when exposed to the cold helium purge gas during tanking operations.

Tests demonstrated that a cork filler strip installed in open joints between insulation panels and under the flexible closeout seals would prevent the flexible closeout seals from cracking during the LH_2 tanking and GHe purging operations.

Where known foam voids exist in honeycomb core insulation joints, it is recommended that the flexible closeout seal be removed, and a 0.12-inch-thick MB0130-020 Type I cork filler strip be installed (Figure 138).

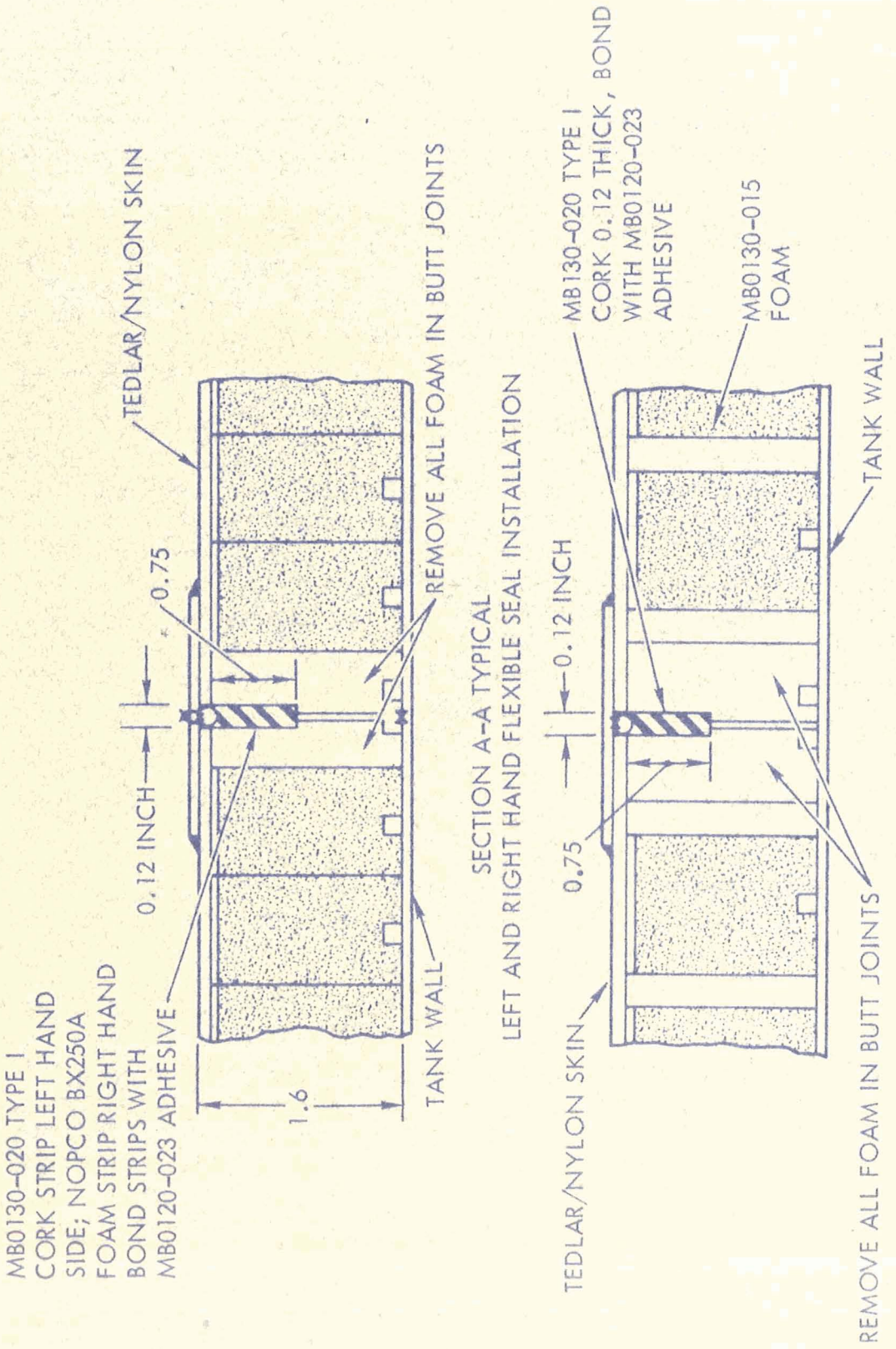

Figure 138. Modified Joint Configuration for Flexible Closeout Seal

PROCEDURE AND RESULTS

Preparation of Test Panel 252A

An insulation panel was bonded to a flat, double-faced LH_2 test tank, in compliance with MA0606-027, using MB0120-048 Type II adhesive.

Insulation Test Panel 252A was made by modifying the panel; a 20-inch square section of the nylon/Tedlar facing was removed and replaced with a new nylon/Tedlar facing sheet. The new facing sheet was bonded to the core with MB0120-023 adhesive, in compliance with MA0606-027, using a MB0135-008 fiberglass scrim cloth carrier to facilitate an even application of adhesive.

Slots were cut in the nylon/Tedlar skin and through the core to the tank wall approximately 1/16-inch wide using a Cleco saw. Two of the slots were cut along the center line of the cells where the foam had been removed. The other two slots were made in core cells filled with foam.

Flexible closeout seals were installed over the slots in the skin of the insulation panel, in compliance with MA0606-042. A 0.12-inch-diameter Teflon shaft was sealed in place in the bond joint of one flexible closeout seal used to release the helium purge during test. Upon removing the shaft from the flexible closeout seal, the helium purge leakage rate and any cold cracking in the closeout seal at the leakage point could be determined.

Testing Panel 252A, Run 1 and Results

The insulation test panel was filled with liquid hydrogen, and the 3-psi helium purge was started. After approximately 30 minutes, a leak developed through a crack in the lower horizontal flexible closeout seal, and purge pressure dropped to 0.3 psig. This seal had been installed over an open-core cell section of the test panel. The approximate top surface temperatures of the seal at the time of failure was -175 to -189 F.

Examination of the cracked flexible closeout seal revealed that the crack extended through the MB0130-072 silicone rubber strip, MB0120-041 Type I adhesive and nylon/Tedlar phenolic laminate. (See Figures 139 and 140.)

Rework of Insulation Panel 252A

The insulation panel was repaired by removing and replacing the defective flexible closeout seals as follows:

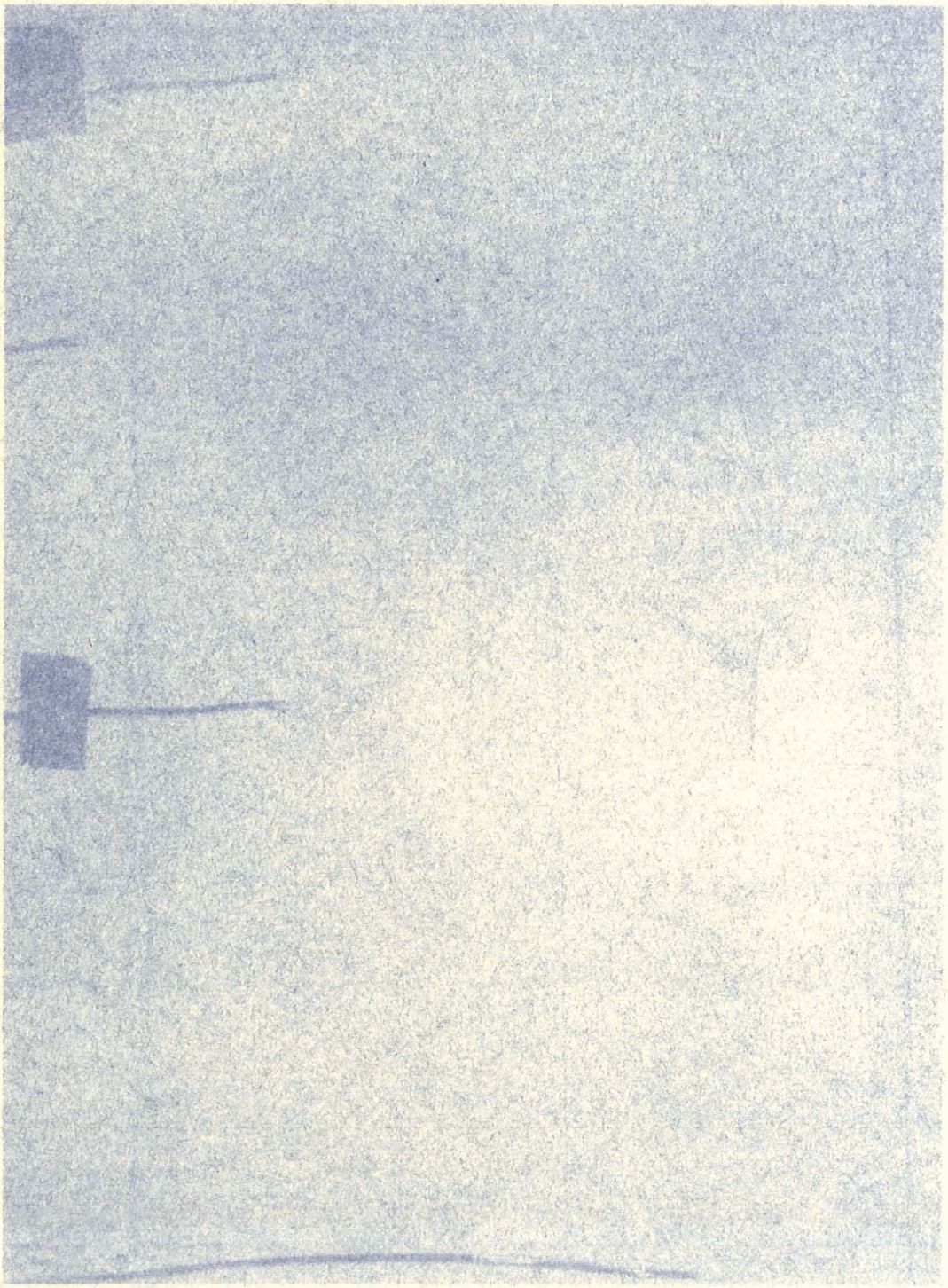

Figure 139. Closeup of Cracked Rubber Doubler and Tedlar Skin, Panel 252A

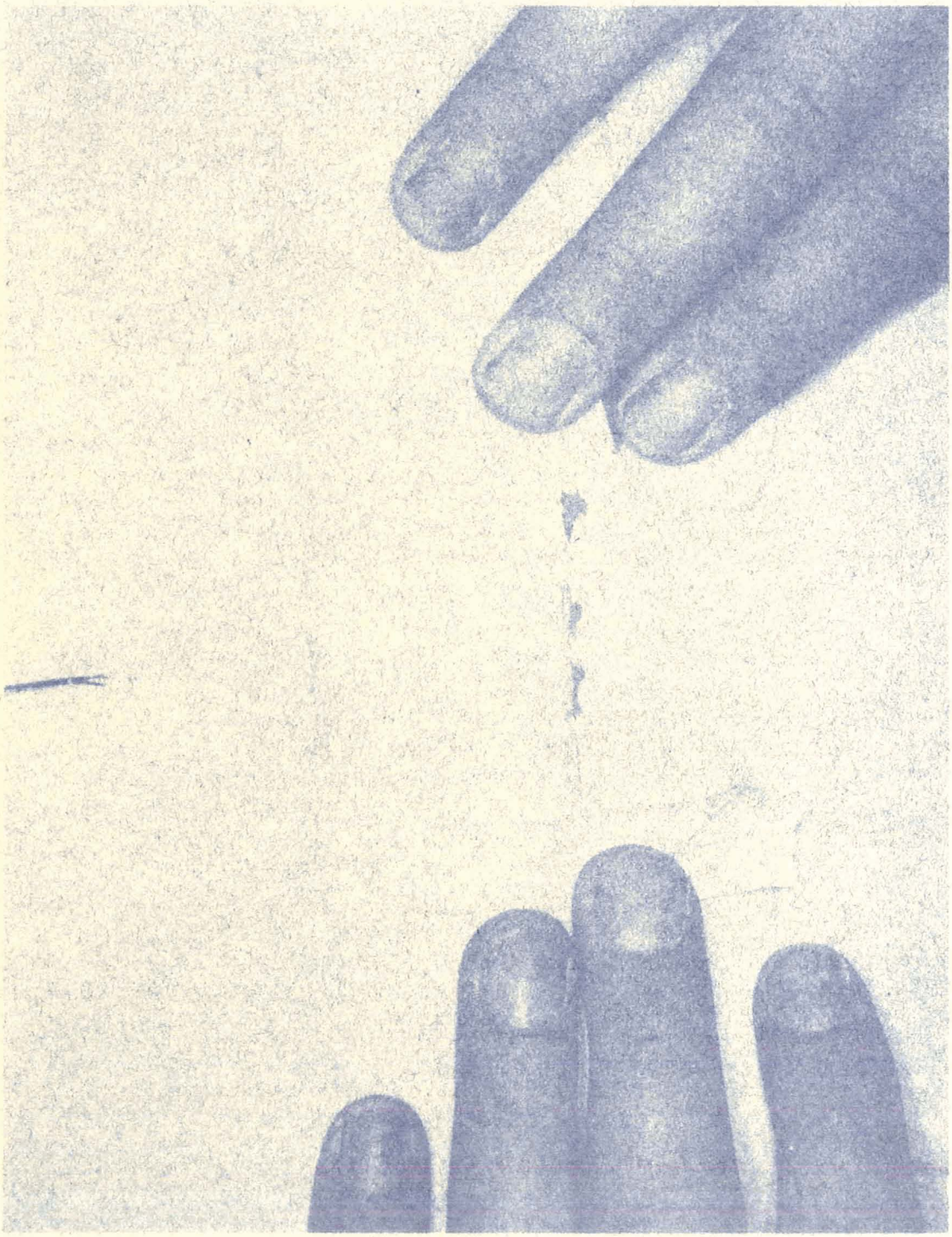

7006-81-2386C

Figure 140. Flexible Closeout Seal Pulled Back Exposing Cracked Nylon/Tedlar Skin, Panel 252A

The defective closeout silicone rubber seal and adhesive materials were removed from the surfaces of the Tedlar and adjacent flexible seals. The repair area was masked-off, solvent-cleaned with methyl ethyl ketone, and then primed with MB0125-038 primer in accordance with MA0606-042. The cracks were repaired by applying a 3000/14-nylon fabric/MB0120-041 Type II adhesive laminate, specified in MA0606-049A and shown in Figure 140. A section of flexible closeout seal was installed over the patch, Tedlar surfaces, and adjacent flexible closeout seals, as specified in MA0606-042 and shown in Figures 141 and 142.

Testing Panel 252A, Run 2 and Results

After about 40 minutes, while filling the reworked test tank with LH_2, a leak developed in the lower horizontal flexible closeout seal. The leak was detected initially by a thin stream of cold gaseous helium emitting from the area. The outside and inside surface temperatures of the flexible closeout seals at the time the leak occurred were approximately -81 F and -166 F, respectively.

The temperature rapidly decreased to -270 F on the inside surface and -116 F on the outside surface of the flexible seal within 10 minutes. During this 10-minute period, the flexible closeout seal and nylon/Tedlar skin cracked in the area of leakage. A photograph of the test panel cracked area is shown in Figure 143.

The probable cause of the crack failures in the nylon/Tedlar skin was attributed to the MB0135-008 fiberglass adhesive carrier and an excess of MB0120-023 adhesive used in making the skin-to-core bond during the modification of the insulation panel to Panel 252A configuration.

The relative difference in maximum elongation between fiberglass fabric and nylon/phenolic laminates is approximately three percent for fiberglass and 16 to 24 percent for three-ply nylon phenolic laminate. The low elongation characteristics of the fiberglass fabric, in combination with the thick MB0120-023 bond-line, restrained the nylon/phenolic laminate from deflecting with the remainder of the insulation panel and test tank during the LH_2 tank process. Crack failure in the facing sheet occurred when the fiberglass and adhesive cracked, locally overloading the facing sheet.

Preparation of Panel 272

Insulation Panel 272 was bonded to a 30-inch by 30-inch square, 198-inch radius of curvature LH_2 test tank, in compliance with MA0606-027,

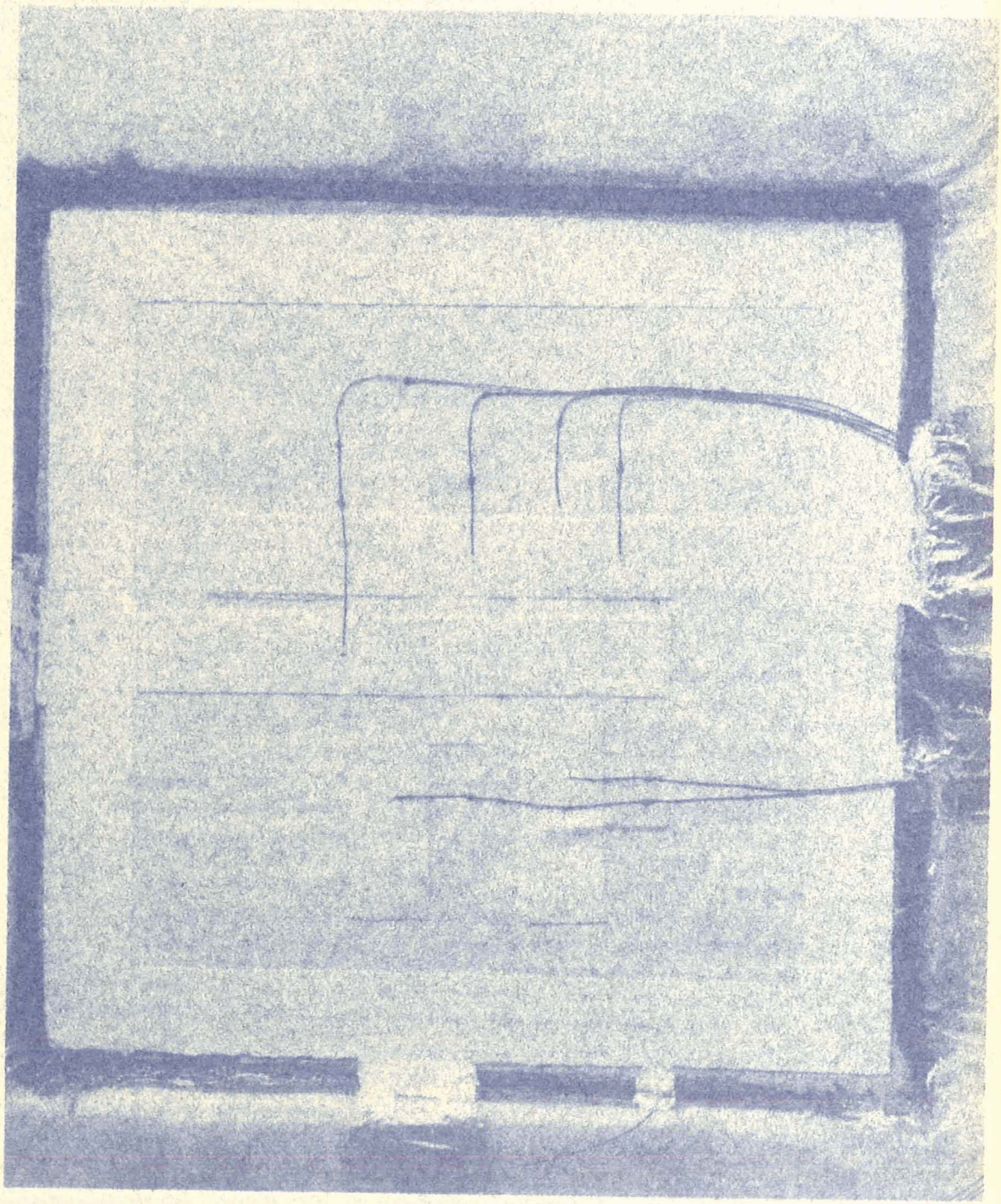

7006-81-2509A

Figure 141. Panel 252A After Second Test Cycle

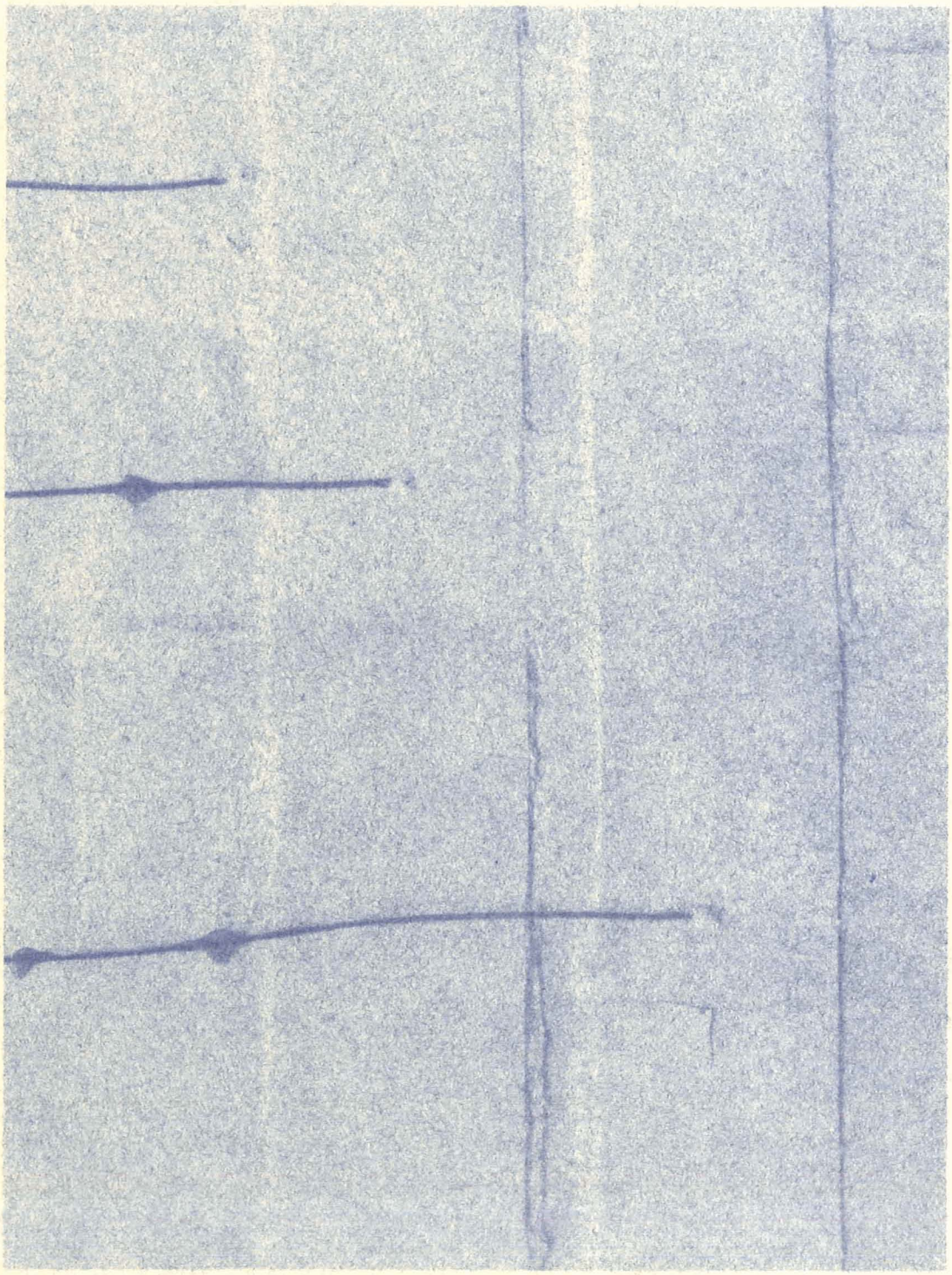

7006-81-2509B

Figure 142. Closeup of Cracked Flexible Closeout Seal, Panel 252A

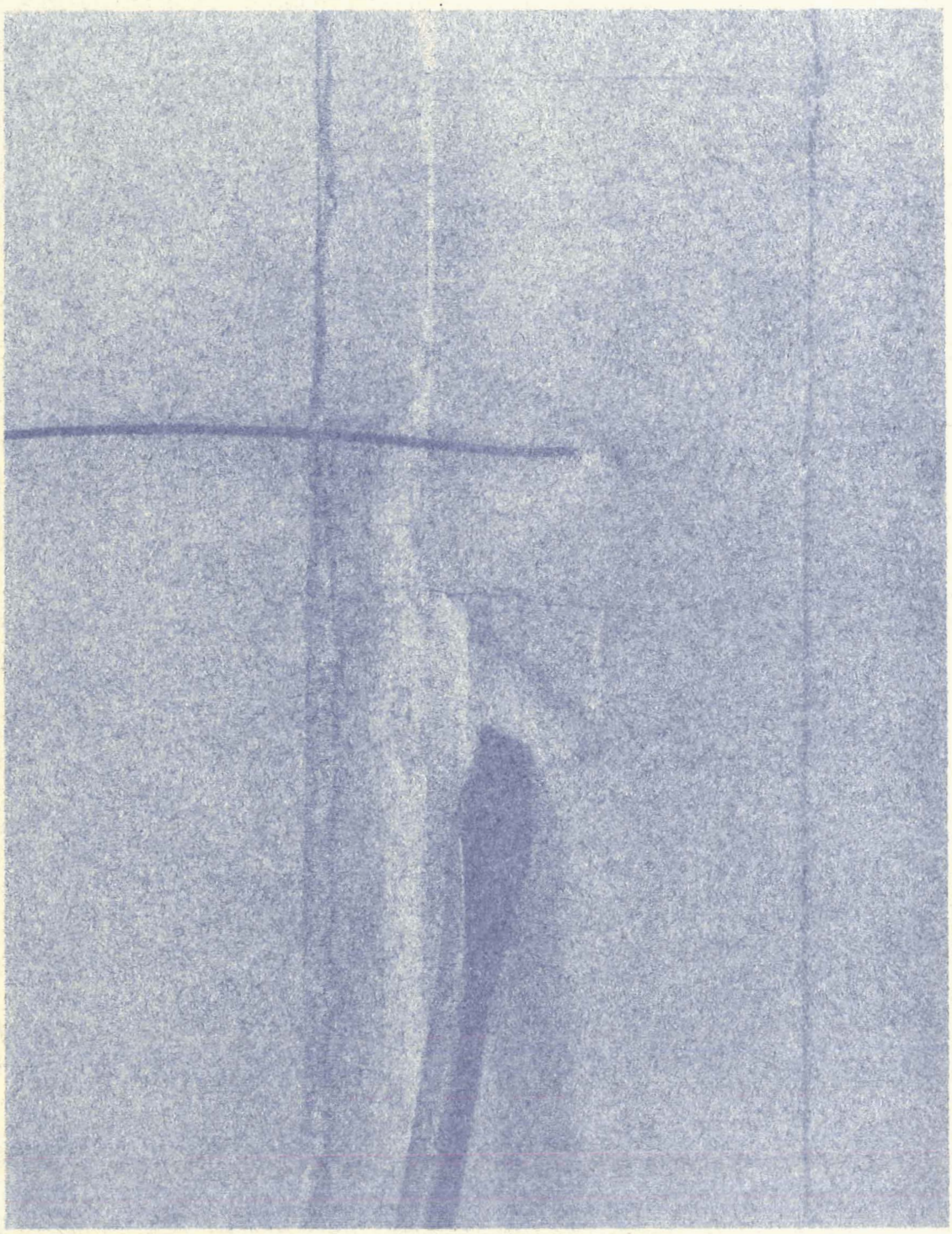

7006-81-2509C

Figure 143. Flexible Closeout Seal Pulled Back Exposing Cracked Tedlar/Nylon Skin

using MB0120-048 Type II adhesive. The tank wall thickness was 0.187 inch. Insulation edge seals were applied to the LH_2 tank and test panel in accordance with MA0105-049.

An 8- by 20-inch area of the insulation was removed from the center of the insulation panel to the tank wall. The MB0120-048 Type II adhesive was completely removed, and the exposed tank surface was paste-etched in conformance with MA0610-023.

A section of insulation representing a closeout was bonded in the prepared 8- by 20-inch area to the tank wall, complying with MA0606-027, using MB0120-023 adhesive which was cured at room temperature. The MB0130-015 foam was completely removed from the edges of both the insulation panel and closeout assembly before bonding in the closeout.

Slots 0.12-inch wide were cut in the insulation skin and core to a depth of 0.75-inch (Figure 138). A strip of 0.12-inch thick, 0.75-inch-wide MB0130-020 Type-I cork was cut to fit the left-hand vertical slot in the insulation. A strip of 0.12-inch thick, 0.75-inch-wide MB0130-077 spray foam was cut to fit the right-hand vertical slot in the insulation. A photograph of the filler strips before installation in the insulation panel is shown in Figure 144.

Both the cork and foam strips were bonded with MB0120-023 adhesive in the left- and right-hand insulation slots flush with the Tedlar surface. The adhesive was cured at room temperature. The top and bottom slots were left open.

Flexible closeout seals were bonded to the insulation test panel according to MA0606-042 as shown in Figures 138 and 145. Before installing the left-hand closeout seal, a 0.12-inch diameter Teflon rod was positioned in the bond joint. A 0.12-inch diameter hole was drilled through the cork filler strip to allow leakage of helium upon removal of the Teflon shaft during Test 2.

Testing Panel 272, Run Number 1 and Results

The test panel tank was filled with liquid hydrogen and insulation-purged with 5-psig helium. After approximately two and one-half hours during the first pressure cycle, a leak was noted in the lower flexible closeout seal.

Post-test examination of the lower flexible closeout seal revealed that three cracks occurred transverse to the length of the seal. The cracks did not propagate into the nylon/Tedlar skin. Details of the cracked flexible closeout seal are shown in Figure 146.

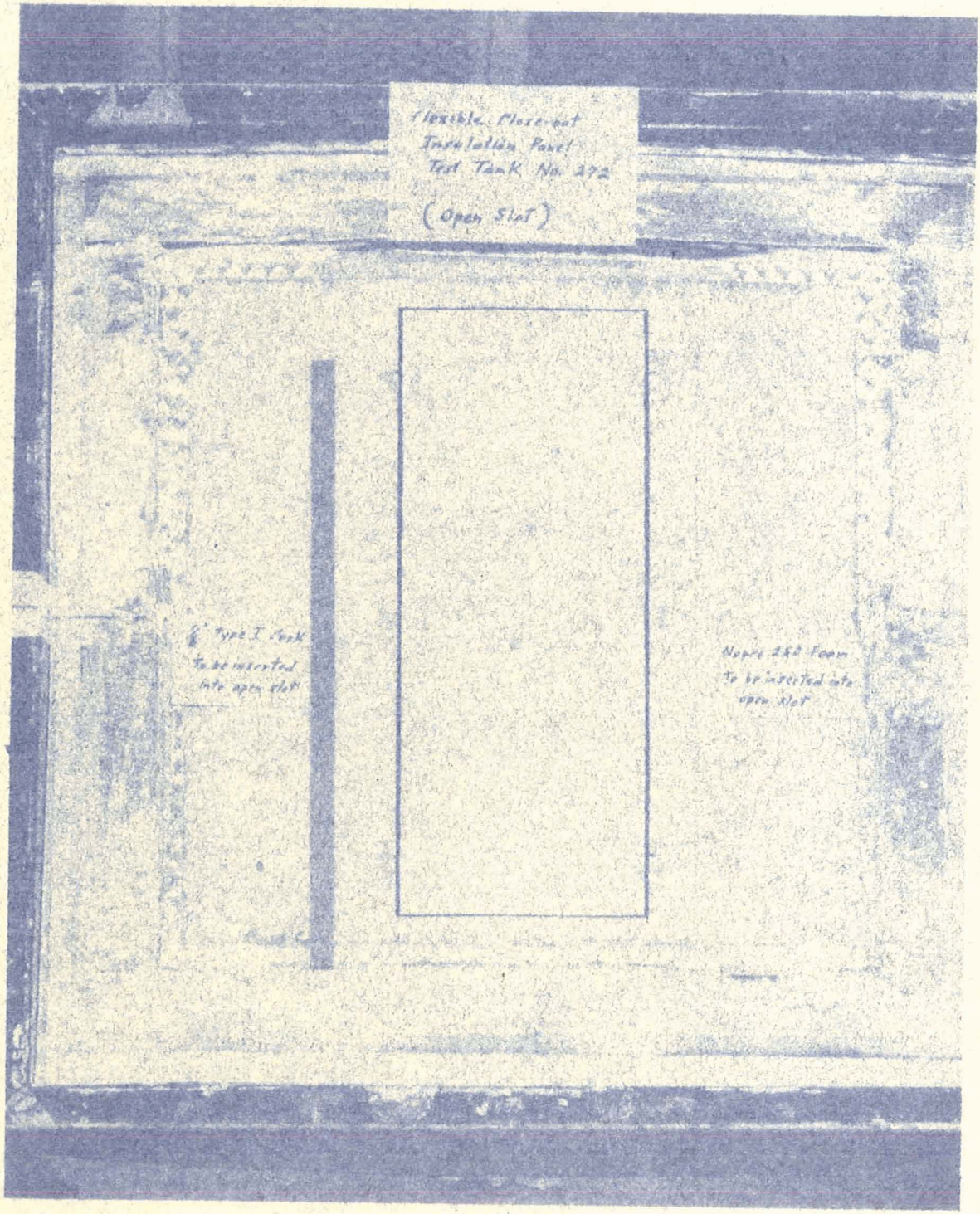

7006-81-2417A

Figure 144. Panel 272 Prior to Bonding in Cork and Foam Filler Strips

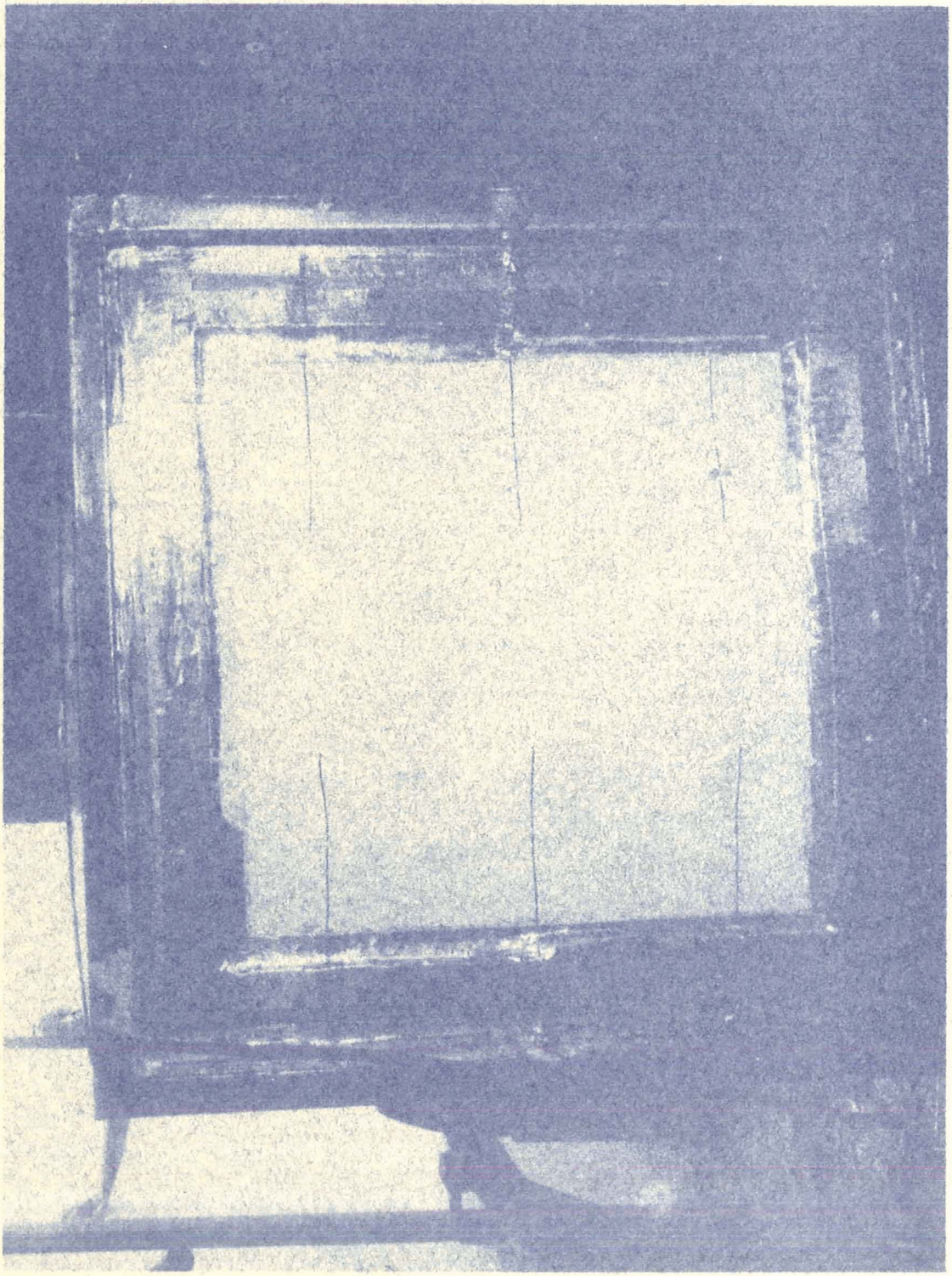

7000-81-2434A

Figure 145. Panel 272 After First Test, 17 Purge Cycles

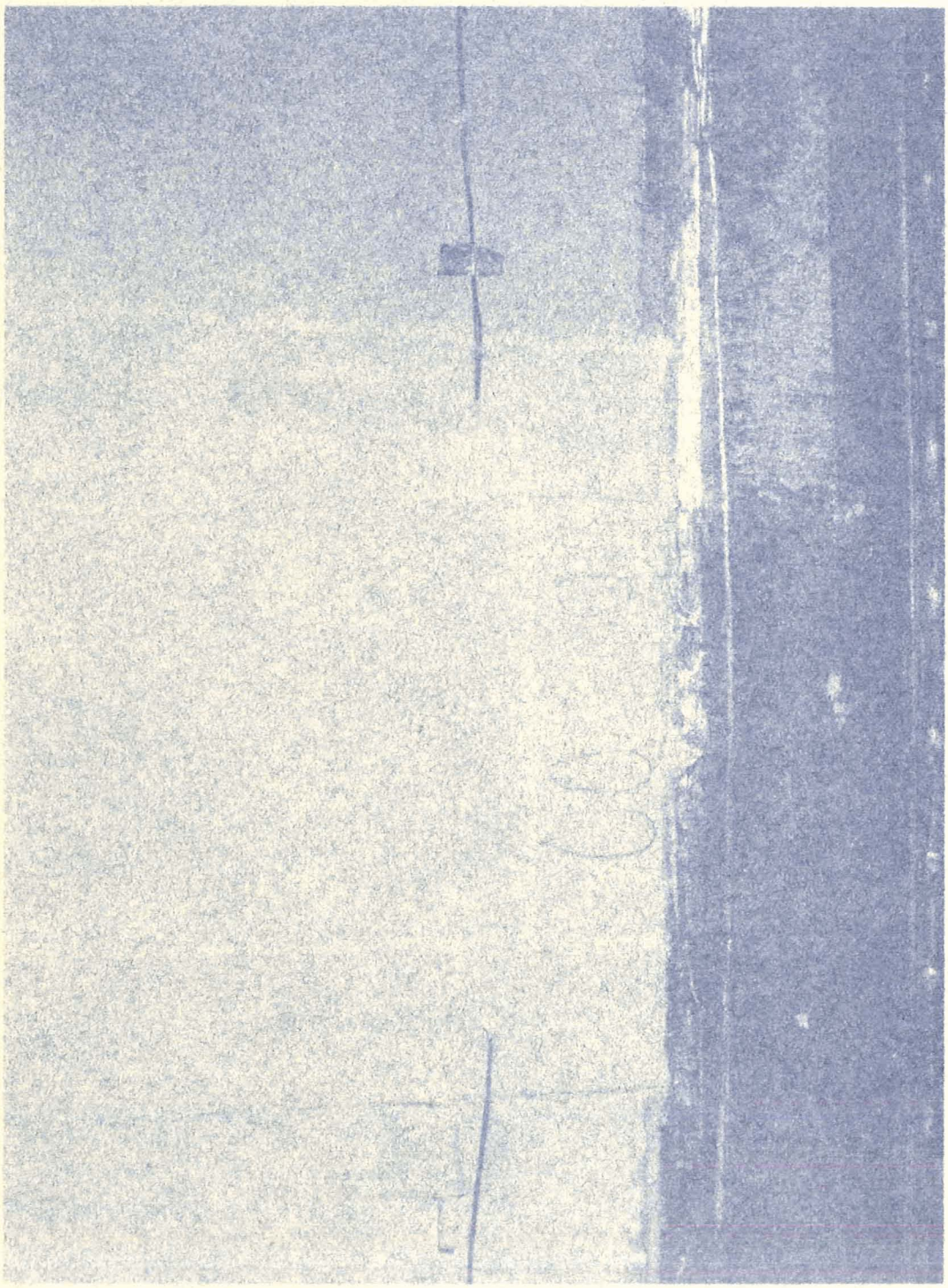

7000-81-2434B

Figure 146. Panel 272 Closeup of Cracked Lower Flexible Closeout Seal

The defective flexible closeout seal was removed and two strips of MB0130-020 Type I cork were prepared and installed in the top and bottom slots in the insulation, Figure 138. The top and bottom flexible closeout seals were then replaced in accordance with MA0606-042, as shown in Figure 138, Section B-B.

Testing Panel 272, Run 2 and Results

The test panel tank was filled with liquid hydrogen, and the insulation was purged with helium. The test was terminated after a leak in the Teflon shaft installation was noted. The flexible closeout seal cracked after dynamic flow of helium started through the leak in the Teflon shaft installation.

The defective flexible closeout seal was removed and then replaced, as specified in MA0606-042. The Teflon shaft was not replaced, and the 0.12-inch diameter helium bleed hole through the cork filler strip was plugged with MB0120-023 adhesive.

Testing Panel 272, Run 3 and Results

The test panel tank was filled with liquid hydrogen. The insulation panel was considered thermally stable in approximately one hour.

A 5.0-psig leak check was made by plugging the outlet and reading the inlet pressure gauge. A leak developed almost immediately in the lower flexible closeout seal installation, and the helium outlet pressure dropped to 0.0. Temperatures on the underside of the nylon/Tedlar skin in the region of the defect were as low as -210 F at the time of failure. The temperature decreased to -321 F at the point of leakage within 10 minutes.

It was determined that a helium leak occurred through the thermocouple installation, and that the flexible closeout seal cracked at approximately -210 F in the center of the lower seal installation. A 3-inch strip of the defective center portion of the lower flexible closeout seal was removed; 2-inch-wide strip of 3000/14 nylon fabric impregnated with MB0120-041 Type II adhesive was bonded in place in accordance with MB0606-049. A butt joint, rather than a lap joint, was made between the nylon/silicone adhesive lay-up and existing flexible closeout seals.

Testing Panel 272, Run 4 and Results

The test panel tank filled with liquid hydrogen and 3.0-psig helium purge was started.

A leak was detected in the left side of the lower flexible closeout seal installation during the second pressure cycle. The leak rate of the insulation panel at 5 psig was 2100 scim. It was determined that the leak occurred in the MB0120-041 Type I adhesive bond joint around a thermocouple installation. The lower flexible closeout seal was removed and then replaced according to MA0606-042.

Testing Panel 272, Run 5 and Results

The insulation panel was pressurized with helium to 3 psig, and the flexible closeout seal installations were leak-checked with liquid soap. No leakage was detected.

The test panel tank was filled with liquid hydrogen and the 2.8-psig helium purge was started. The lower flexible closeout seal failed during the first pressure cycle, 3 minutes into the 5-minute hold period. It was determined that the nylon fabric/MB0120-041 Type-II silicone adhesive laminate installation failed in a butt joint with the flexible closeout seal.

Testing Panel 272, Run 6 and Results

After filling the tank with liquid hydrogen, and after helium purging was started, a leak occurred in the lower flexible closeout seal installation.

Since it was decided to complete the test, the insulation panel was gradually pressurized to 5 psig within 5 minutes, and held at 5 psig for five minutes. After the 5-minute hold, the pressure was rapidly decreased to 0.25 psig. This cycle was repeated 25 times. During the 25 pressure cycles, the helium leak rate remained constant at 4500 scim. Then the helium outlet was shut off, and the helium was allowed to flow through the defective closeout seal.

At the time and at the point of leakage, the temperature of the flexible closeout seal bond joint was approximately -216 F. The temperature decreased to -258 F in 10 minutes, and to -308 F in 16 minutes. The flexible closeout seals did not fail in any other area during the remainder of the test, although the temperatures at the termination of the test were as low as -262 and -231 F at the flexible closeout seal/Tedlar film interface.

The helium leakage occurred through a thermocouple lead in the right-hand side of the lower flexible closeout seal bond joint. The flexible closeout seal cracked when contacted by the cold (approximately -258 F) helium. Further testing of the insulation panel was terminated.

DISCUSSION

Testing of Insulation Panel 252 was terminated after the second LH_2 tanking process. At this point, it was concluded that the insulation panel would not produce satisfactory test data because the adhesive bond was causing the nylon/Tedlar skin to crack during the tanking process.

Panel 272 was tested primarily to evaluate methods for thermal protection and for stabilizing flexible closeout seal installations over foam-voided core cells in insulation panel joints. A flexible closeout seal installation configuration (Figure 163), involving highly insulative bonding filler strips in grooves between insulation panels, was fabricated and tested. The filler strips insulated locally and stabilized the bottom surface of the flexible closeout seal that is normally exposed to cold helium gas in the gap between insulation panels.

It is felt that the flexible closeout seals would not have failed if the thermocouple wire installations were not present in the bond line.

The test series indicated that flexible closeout seals will perform satisfactorily over open-core cell-insulation panel joints filled with insulative cork or foam strips. The tests did not prove what the flexible closeout seal/insulation composite would do when exposed to expansion and contraction stresses experienced by the S-II LH_2 tank during tanking operations.

EVALUATION OF NYLON CLOSEOUT DOUBLER FOR USE UNDER FAIRINGS ON SATURN S-II

INTRODUCTION

Wet lay-up doublers on 1.6-inch-thick basic insulation, using nylon fabric MB0135-021 Type II and MB0120-024 resin under the fairing areas, were evaluated as replacements for the flexible silicone rubber doublers. The cryogenic temperature under the fairing areas can exceed the cryogenic temperature capabilities of the flexible silicone rubber doublers; consequently, a failure could occur in these areas.

CONCLUSION

The wet lay-up (nylon fabric and 7343 resin) doublers on 1.6-inch-thick basis insulation withstood pressurization and cryogenic tests, indicating that this is a suitable replacement for the flexible silicone rubber doublers used under the S-II stage fairing areas.

PROCEDURE

Fabrication

A 30- x 30-inch cryogenic test tank was prepared, and 1.6-inch-thick insulation was bonded to the tank in accordance with MA0606-027. Wet lay-up (nylon fabric - 7343 resin) closeout doublers were fabricated in accordance with MA0605-014. The wet lay-up doublers and exterior surface of the 1.6-inch-thick insulation were instrumented with thermocouple wires (Figure 147).

Testing

The exterior surface of the insulation panel was bagged and sealed. The bag was purged with GN_2, and LH_2 was introduced into the tank. The temperature of the tank wall and exterior surface of the insulation was stabilized, and 40 insulation purge-pressure cycles were performed. The purge pressure was increased from approximately 0.15±0.05 psig at a rate of 1 psi per minute until a pressure of 4.0 psig was reached. The pressure was maintained for one minute and then released. The temperature of insulation was stabilized in the range of -200 and -225 F. After the

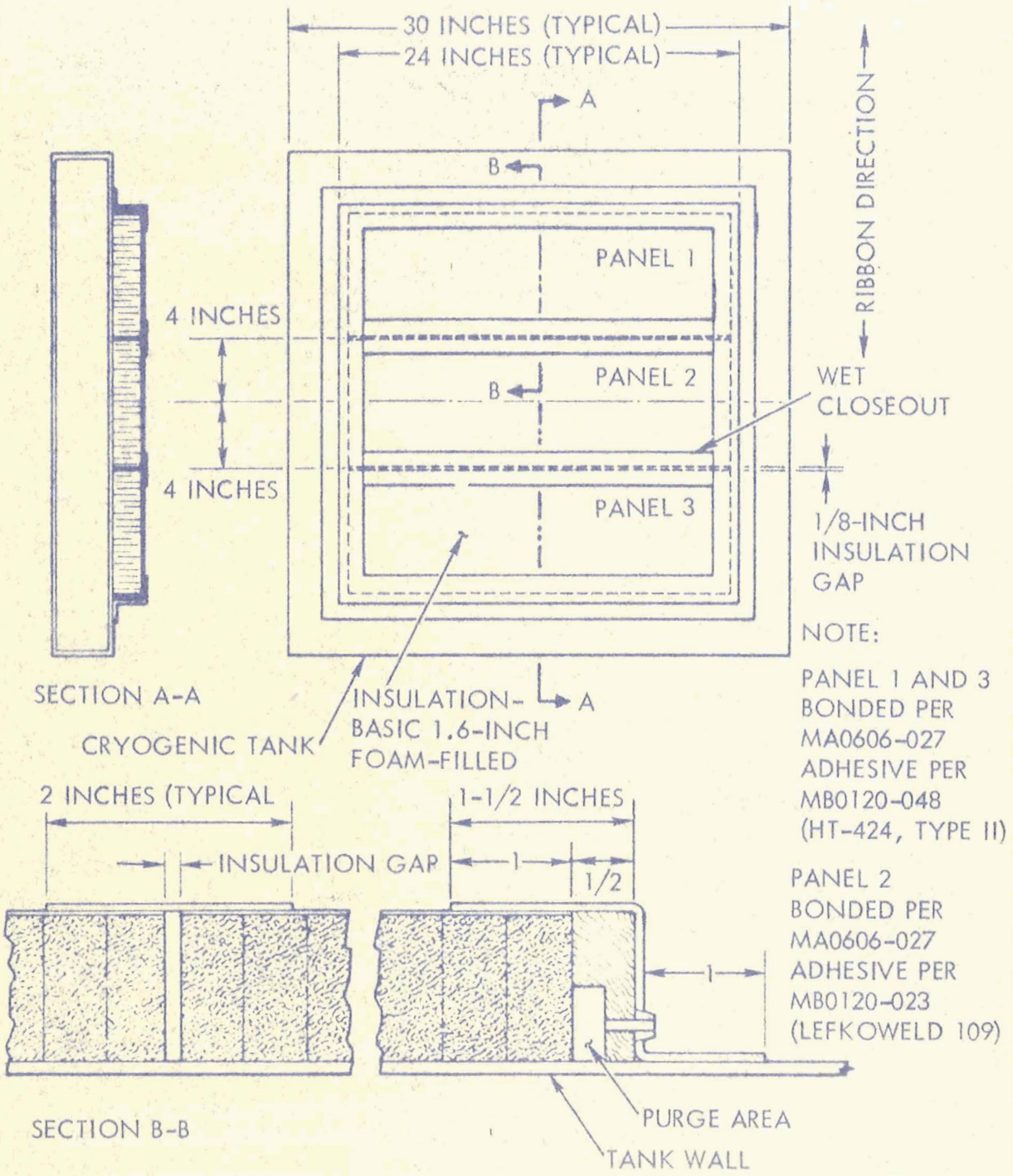

Figure 147. Nylon Closeout Doubler Panel Configuration

40th cycle, the pressure was increased at a rate of 1 psi per minute until a pressure of 10 psig was reached and was held for 1 minute. The pressure was released to 0.15 psig, and the cycle was repeated five times.

The insulation was helium-purged with a flowrate of 400 scim at an outlet pressure of 3 psig, and the insulation surface was stabilized at -230 to -250 F. The helium purge flow was stopped at the outlet, and the inlet pressure was increased to 3 psig per minute. Failure of the insulation occurred at 37 psig (Figure 148).

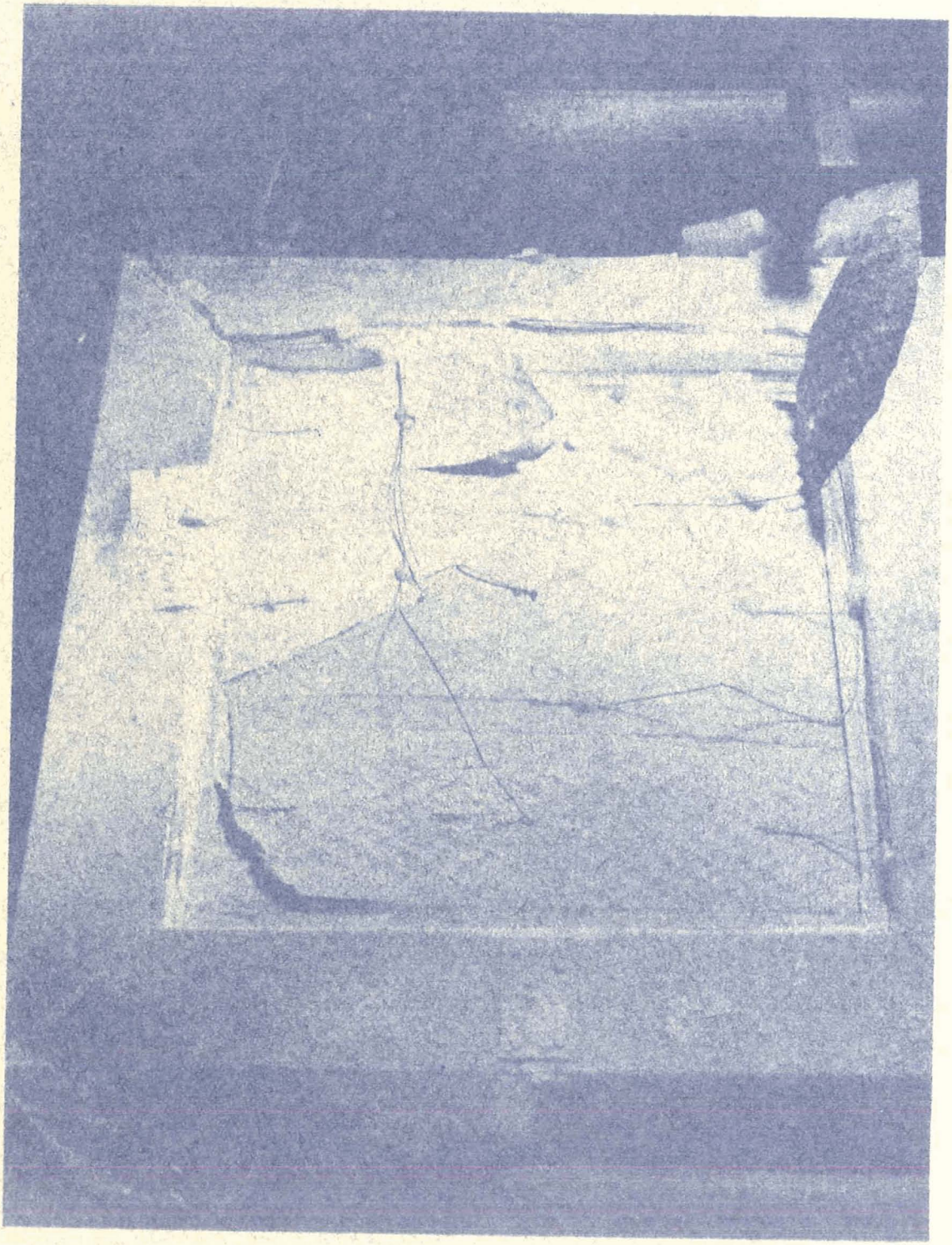

7066-81-24528

Figure 148. Cryogenic Test Tank After Pressurization Failure

FOAM INSULATION

PROGRESS SUMMARY

A pigmented spray foam was studied to improve the consistency of the spray mix ratio and the ultimate physical properties of the foam insulation. The spray foam system studied had a longer reaction time than that currently specified.

Various methods were evaluated for improving the interface bond strength of successively applied layers of foam. Foam insulation with specifically prepared debond areas was subjected to LH_2 cycling. The debond areas did not propagate during LH_2 cycling.

The flammability and/or explosibility associated with the application and machining of the spray foam were investigated. The airborne spray proved relatively nonflammable; however, the airborne-cured foam dust was explosive.

Environmental and verification tests were conducted on the CPR 369-3 spray foam insulation. The tests did not prove conclusively that the S-II insulation would withstand the stresses imposed by the environmental conditions during ground hold and boost.

The Hypalon-coated spray foam insulation was tested under estimated heat fluxes of 0.36 Btu/ft^2/sec at 625 F to 0.88 Btu/ft^2/sec at 925 F. The ballooning of the Hypalon during the simulated boost aerodynamic heating posed the question as to whether large pieces of the coating would become detached and endanger antenna functions. Cork (0.040-inch thick), bonded to the foam in the hot zone areas, did not provide satisfactory protection to the foam insulation.

PIGMENTED SPRAY FOAM - PRELIMINARY DATA ON SELECTROFOAM SYSTEMS

INTRODUCTION

A laboratory study is provided screening data on candidate pigmented materials in the selection of an alternate two pound per cubic foot spray foam system. The object was to meet S-II Engineering requirements for cryogenic insulation as well as to provide a color indication of the spray foam mix characteristics.

The prime purpose of this effort was to compare preliminary technical data of each of two candidate foam materials to data concerning the MB0130-077 specification.

CONCLUSIONS

The Selectrofoam 6516-6411 foam system best meets the general requirements of the MB0130-077 specification.

An alternate foam system with a color additive appears feasible in affording visual inspection of foam mixing characteristics while still providing the physical and strength properties necessary to meet specific S-II foam insulation requirements.

A pigmented foam system similar to Selectrofoam 6516SP-6411, but with a shorter reaction time, should be considered for additional study. This would provide technical support data for establishing conformance with MB0130-077 requirements.

PROCEDURES

Foam Material Systems (Furnished by Pittsburgh Plate Glass Co.)

Foam material systems used are as follows:

Selectrofoam 6516SP-6411 (blue-grey pigmented)

Selectrofoam 6574-6411 (blue-grey pigmented)

Specimen Fabrication and Testing

Foam specimens (each 24- x 24- x 1-inches) for determination of flatwise tensile, flatwise compression, coefficient of thermal expansion and flammability properties, were machined (parallel to rise) from foam blocks and tested in accordance with specification MB0130-077. Testing was conducted at room temperature (RT), +150 F and -300 F.

RESULTS

Technical data furnished by Pittsburgh Plate Glass Co. plus data obtained in this study are as follows:

Supplier-submitted physical and chemical data on each foam system and on isocyanate and polyol components are shown in Table 37. The flatwise tensile results from the Selectrofoam test specimens are shown in Table 38. The flatwise compression test results are shown in Table 39. The thermal expansion data are shown in Table 40.

DISCUSSION

Each Pittsburgh Plate Glass Co. foam system series is a typical polyether polyol-polyisocyanate foam system with a trichlorofluoromethane blowing agent. In many respects, these foam materials are similar to the MB0130-077 material in current usage. However, the isocyanate component, Selectrofoam 6411, has been modified by the addition of a purple-black dye. This provides a visual color indication of the ratio control and the mixing characteristics of the foam component materials. White or yellow spots in the foam material indicate problems within the isocyanate feedlines of the spray equipment. Conversely, a dark, or purple-black color in the foam indicates trouble within the polyol component feedline. A uniform blue-grey color represents a properly proportioned spray foam material.

The color additive is considered a fugitive dye, it does not impart a permanent pigmentation to the spray foam.

Table 37. Physical and Chemical Data of Selectrofoam Systems*

Liquid Foam Components	Isocyanate Component 6411	Polyol Component 6516SP	Polyol Component 6574
Viscosity cps	250 at 77 F	250 at 65 F	270 at 65 F
Specific gravity	1.239 at 77 F	1.24 at 65 F	1.23 at 65 F
NCO equivalent	132		
Hydroxyl Number - Base		515	480
- Component		349	325
NCO index (base)		1.21	1.27
Refractive index	1.62	1.46	1.55
H_2O content (percent)		0.062	0.064
Fluorocarbon content (percent)		33.1	30.0
Color	Purple-black	Amber	Amber
Flash point (ASTM D-1310)	>300 F	>300 F	>300 F

Mixed and Foam Components	Foam Systems	
	6411 - 6516SP	6411 - 6574
Cream time (seconds)	7 to 10	7 to 10
Tack free (seconds)	25 to 29	16 to 20
Rise time (seconds)	38 to 42	23 to 27
Core density (pcf)	2.40±0.1	2.50±0.1
Color	Blue-grey	Blue-grey
Closed cell-percent	90 to 95	90 to 95
F/W Tensile: psi at room temperature		
Parallel to rise	42.5	49.0
Perpendicular to rise	34.5	35.0
F/W Compression: psi at room temperature		
Parallel to rise	31.0	33.0
Shear Test at room temperature**		
Perpendicular to rise	79.0	89.0
Burning characteristic D-1692	Self-extinguishing <1 inch at 45 seconds	Self-extinguishing <1 inch at 45 seconds
Thermal Cond. "K" ASTM-D-1162	0.12 at 72 F	0.12 at 72 F
Mix by weight or volume	50/50	50/50

*Data supplied by PPG Company
**Shear test per ASTM D-732

Table 38. Average Flatwise Tensile Strength, Parallel to Rise

Material System	Test Temperature (F)	Ultimate Stress (psi)	Modulus of Elasticity (psi)
Selectrofoam	Room	73.6*	2850
6516SP-6411	+150	56.8	2142
	-300	50.5	4462
Selectrofoam	Room	64.1*	2012
6574-6411	+150	40.1	1008
	-300	49.6	4605
*MB0130-077 requirement is 60 psi average and 45 psi low			

Table 39. Average Flatwise Compressive Strength, Parallel to Rise

Material System	Test Temperature (F)	Ultimate Stress (psi)	Modulus of Elasticity (psi)
Selectrofoam	Room	33.9*	1402
6516SP-6411	+150	27.1	987
	-300	67.6	1699
Selectrofoam	Room	31.8*	664
6574-6411	+150	27.1	675
	-300	57.0	1024
*MB0130-077 requirement is 25 psi average and 20 psi low			

Table 40. Thermal Expansion Data

Material System	Temperature Range (F)	Density (lb/cu ft)	Coefficient of Linear Thermal Expansion (in./in.-F)
Selectrofoam	75 to 200	2.10	8.3×10^{-5}*
6516SP-6411	50 to -300	2.09	4.4×10^{-5}*
Selectrofoam	75 to 200	2.30	6.8×10^{-5}*
6574-6411	50 to -300	2.38	3.9×10^{-5}*

*MB0130-077 requirement is an average of 7.2×10^{-5} in./in. degree F at 75 to 200 F and 4.2×10^{-5} in./in. degree F at 50 to -300 F

ENVIRONMENTAL VERIFICATION TESTING OF CPR 369-3 SPRAY FOAM INSULATION

INTRODUCTION

This report presents concluding verification test efforts performed on CPR 369-3 spray foam, MB0130-075, intended for S-II stage insulation. One test was previously conducted on a bolting ring and Cylinder Tank 1, as reported during the previous reporting period.

This investigation sought to verify the capability of CPR 369-3 foam to function as a suitable insulation on the bolting ring, Cylinder 1, and forward bulkhead of the S-II stage.

CONCLUSION

Cryogenic and environmental tests conducted on spray-foam insulated 30- x 30-inch cryogenic test tanks have not proved conclusively that CPR 369-3 spray foam insulation will withstand the environmental stresses during ground hold and boost without incurring failures that might possibly endanger the S-II mission.

RECOMMENDATIONS

Subsequent tests should be conducted to verify the CPR 369-3 foam as a suitable insulation for the S-II vehicle. These should consist of larger scale-up cryogenic tank tests, plus developing tests that would create deflection loads plus other stresses simulating those to be expected under actual LH_2 tanking, detanking, and boost conditions.

PROCEDURES

Fabrication of Cryogenic Test Tanks

Two types of test tanks were used as the test vehicle for the spray foam insulation: one was fabricated from a section of an S-II bolting ring; the other was a smooth-walled contoured tank for simulation testing of the forward bulkhead configuration. Both were designed to withstand cryogenic and vibration stresses induced during environmental testing.

Specimen Fabrication

Test specimen 538: a 30- x 30-inch bolting ring and Cylinder 1 test tank were prepared for priming in accordance with MA0610-023. M-602 primer was applied, air-dried for one-half hour, and cured at 290 F for four hours.

Hard-spot details (foam-filled honeycomb core used for potted-in insert locations for hardware attachment points) were fabricated in compliance with MA0606-033. Three sides of each detail were machined to a 75-degree angle, as related to the plane surface of the tank. The sides of the details were then coated with Narmco 7343 polyurethane resin, MB0120-024, and cured for 16 hours before bonding to test tank surface with Lefkoweld 109 adhesive, MB0120-023. The details were bonded with a minimum of 2-psi positive pressure for 16 hours before releasing pressure. Primer M, MB0120-042 primer, was then applied over the cured M-602 primer and cured at room temperature for a minimum of 16 hours. Figure 149 shows the positioning of hard spots on the test tank.

The foam was sprayed on with Glascraft equipment in two separate applications, simulating one of the proposed techniques in insulating the bolting ring with prebonded hard spot details.

Cavities 1, 2, and 4 (Figure 150) were covered with kraft paper and Teflon-coated aluminum strips, in producing a smooth foam edge following removal of the coated strips after applying foam to the third cavity. The foam was sprayed over the hard spot details using a bottom-to-top spray pattern. The foam was then allowed to cure a minimum of 16 hours and machined to within 1/2 inch of the stringer surfaces. The edges of the foam were then coated with Narmco 7343 resin. (See Figure 151.)

Following a 16-hour cure, the remainder of the bolting ring was then spray foamed. After curing a minimum of 16 hours, the foam was machined to within 1/2 inch of the stringer surfaces (Figure 152).

Voids exceeding 1/8 inch but less than 1/2 inch in diameter were filled with a mixture of foam dust (retained from machining process) and Narmco 7343 resin. Two larger voids (over 1/2 inch in diameter) were repaired by cutting out a section about 1/4 inch deep and bonding precut foam to fit the void with Lefkoweld 109 adhesive.

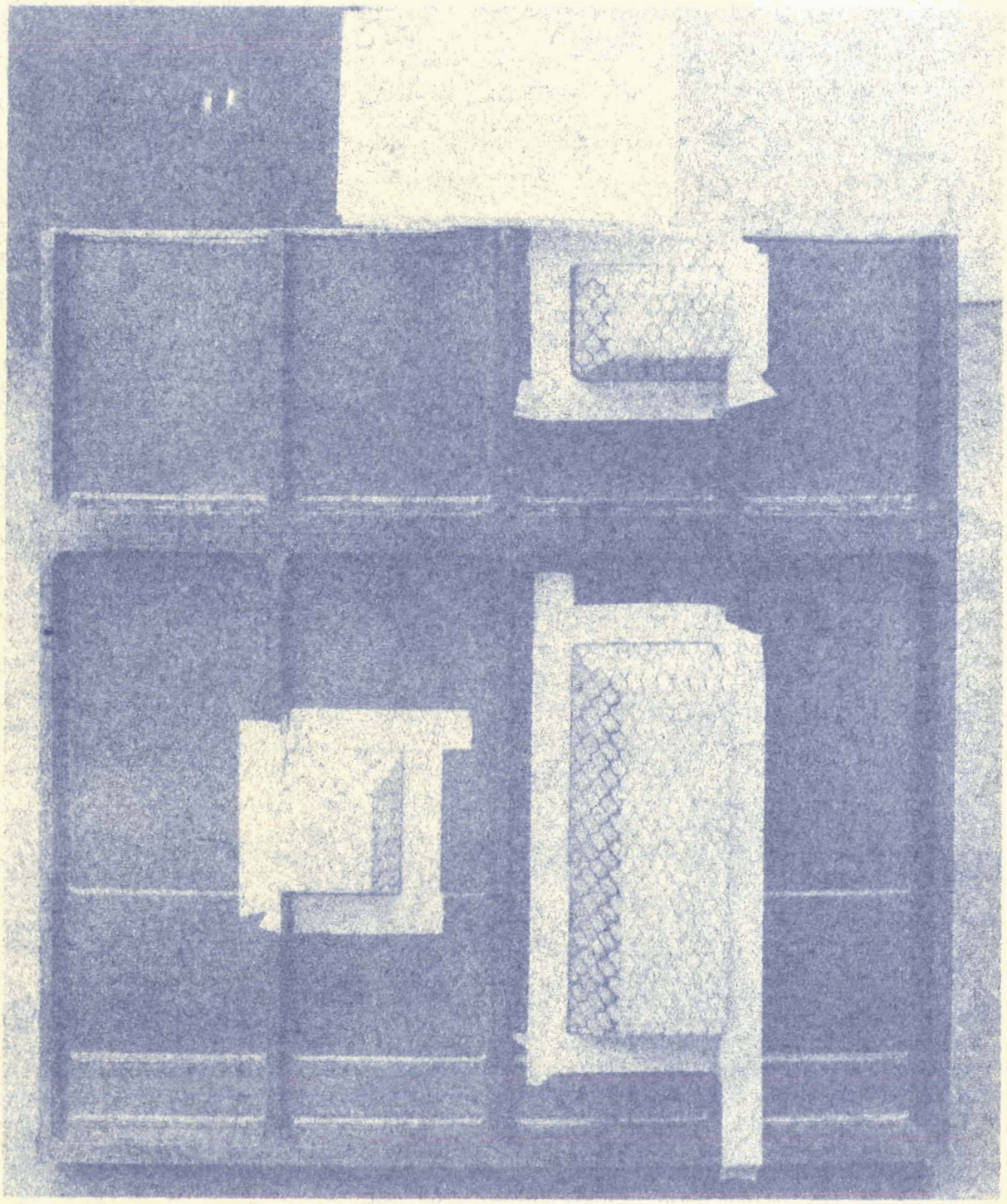

7009-81-2063

Figure 149. Hard Spot Details Bonded to Bolting Ring Test Tank 538

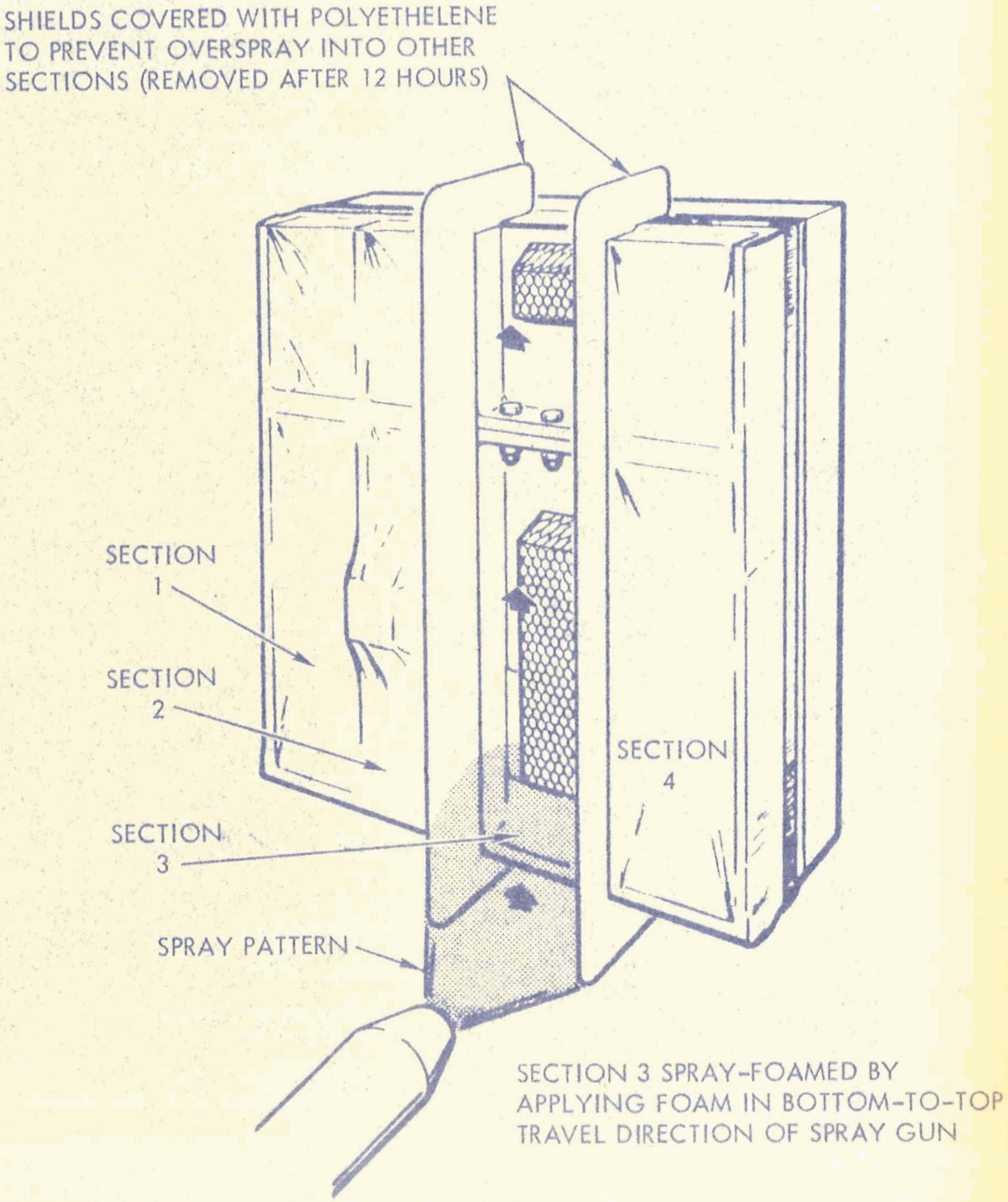

Figure 150. Schematic - Application Technique of Spray Foaming Section 3 of Bolting Ring Test Tank 538

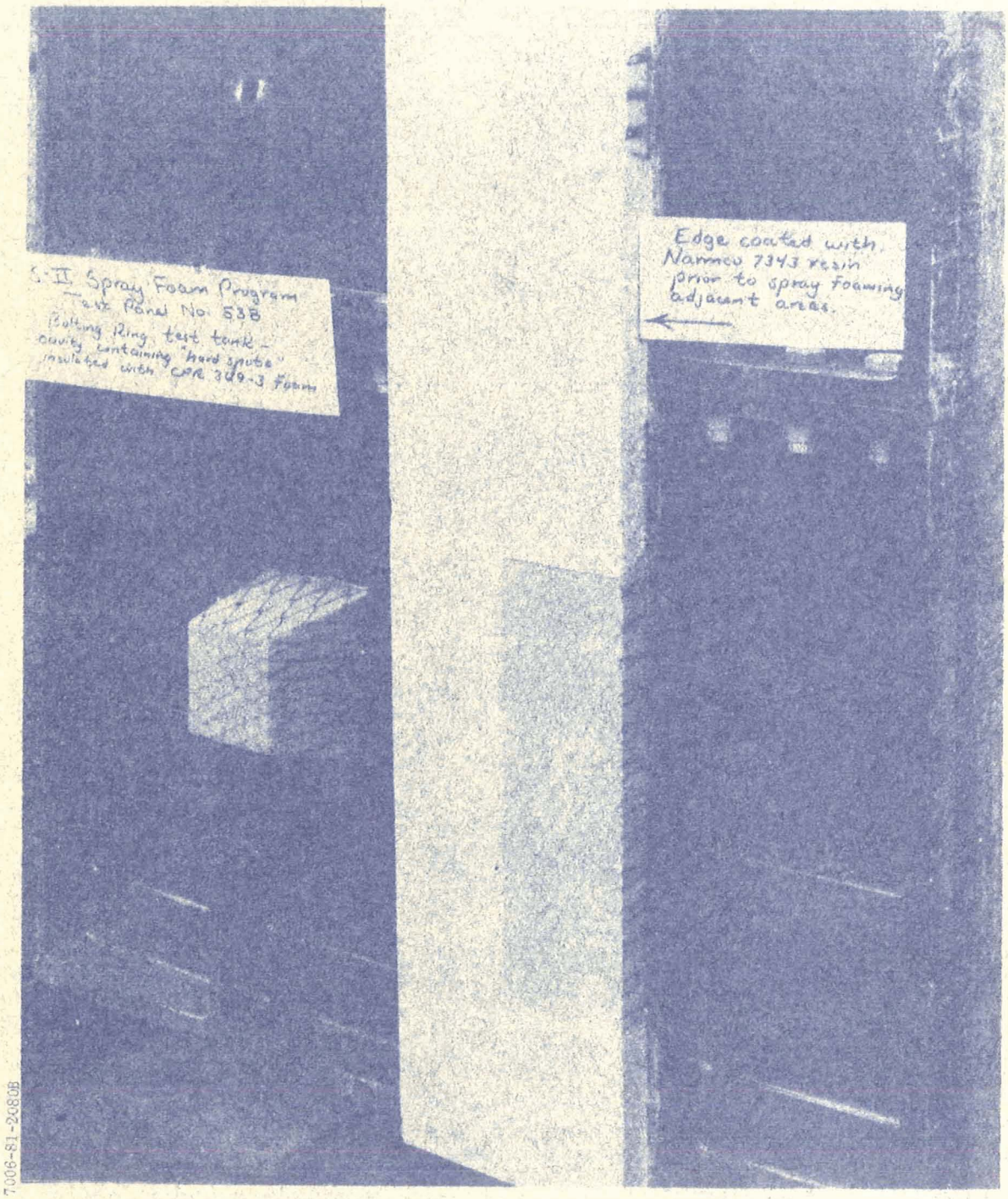

Figure 151. Machined Foam and Hard Spot Details in Cavity 3 of Bolting Ring Test Tank 538

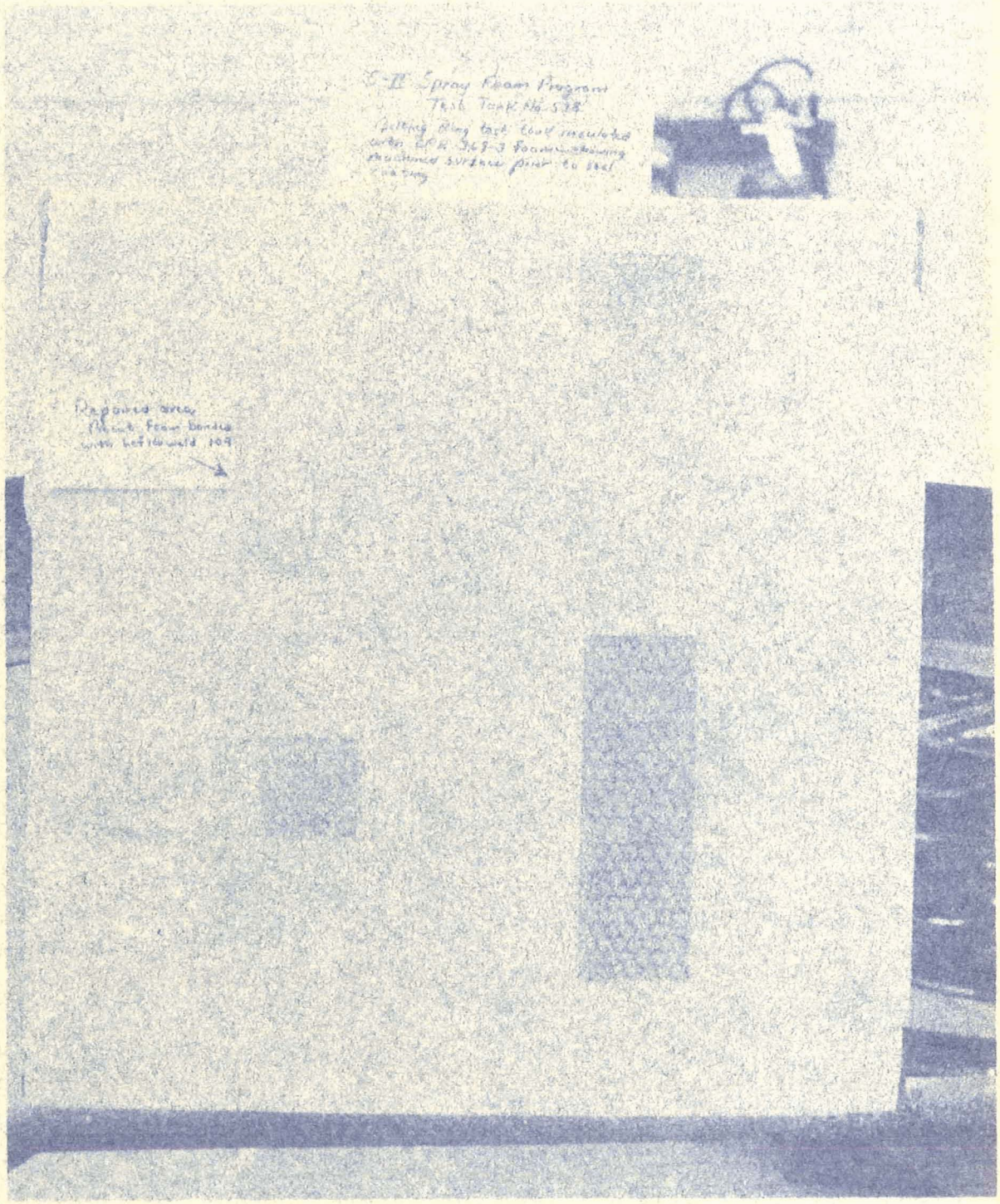

Figure 152. Bolting Ring Test Tank 538 Showing Machined Foam and Hard Spot Details

The hard-spot details were coated with Narmco 7343 resin. Following a minimum 48-hour, room-temperature cure of 7343, the insulation surface was sealed with a coating of Hypalon, MB0125-044 to comply with MA0608-014.

The coated insulated tank was then prepared for environmental test by foaming the uninsulated surfaces with a two-pound density pour foam covered with an aluminum heat shield (Figure 153).

Test specimen 539: a 30- x 30-inch test tank simulating the sidewall configuration was prepared for priming in conformance with MA0610-023, then primed with M602. Foam was applied with two Glascraft guns simultaneously in an overlapping spray pattern that covered the vertically-positioned tank surface in one pass. The foam was cured for 16 hours minimum, then machined to within 0.50-inch of the tank surface. Voids were filled and a moisture barrier was similarly applied to the previous tank.

Test specimen 547: a 30- x 30-inch configuration simulating the bolting ring was prepared prior to priming in accordance with MA0610-023. M-602 primer, MB0120-032, was applied, air-dried for one-half hour, and cured at 290 F for 4 hours. Primer M (MB0120-043 primer) was then applied over the cured M-602 primer and cured at room temperature for a minimum of 16 hours.

Hard-spot detail locations were prepared as shown in Figure 154. Foam was applied to the tank in an overlapping pattern, using two Glascraft guns simultaneously. Holes were then machined in the foam at the hard-spot locating positions. Pre-machined hard-spot details were then bonded in place with Narmco 7343 resin, using about two-psi positive pressure for 16 hours. (See Figure 155.)

The application of moisture barrier coating was accomplished as described for Test Tank Specimen 538. The specimen was prepared for testing as shown in Figure 156.

Test Setup

The test specimens were installed for testing in the cryogenic facility test cells. (Figures 157 and 158.) The test installation consisted of the following elements:

1. A cryogenic system that provides a liquid hydrogen flow from a 1000-liter liquid hydrogen dewar to the test specimen and a vent system for the boil-off gas

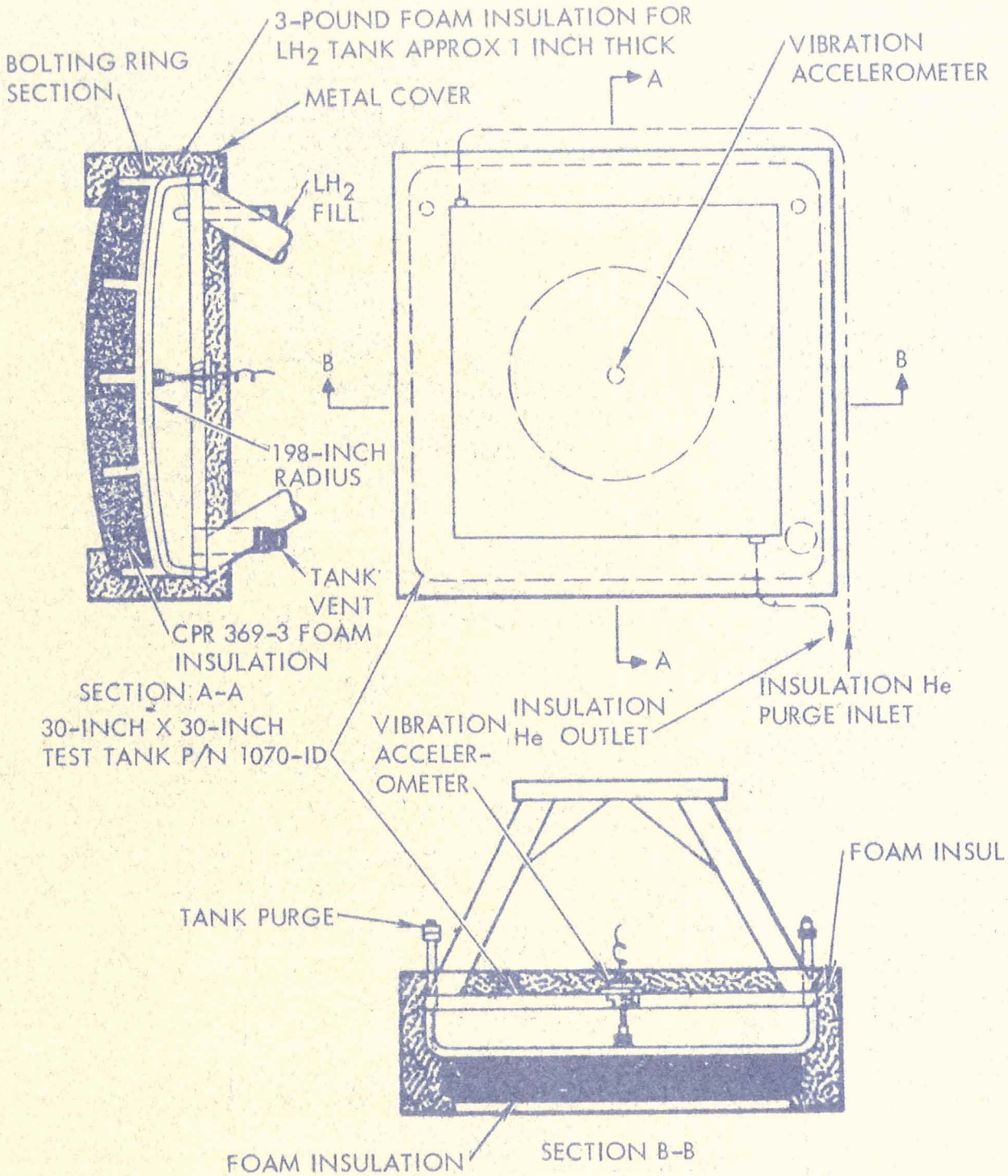

Figure 153. Test Assembly for Bolting Ring Test Tanks

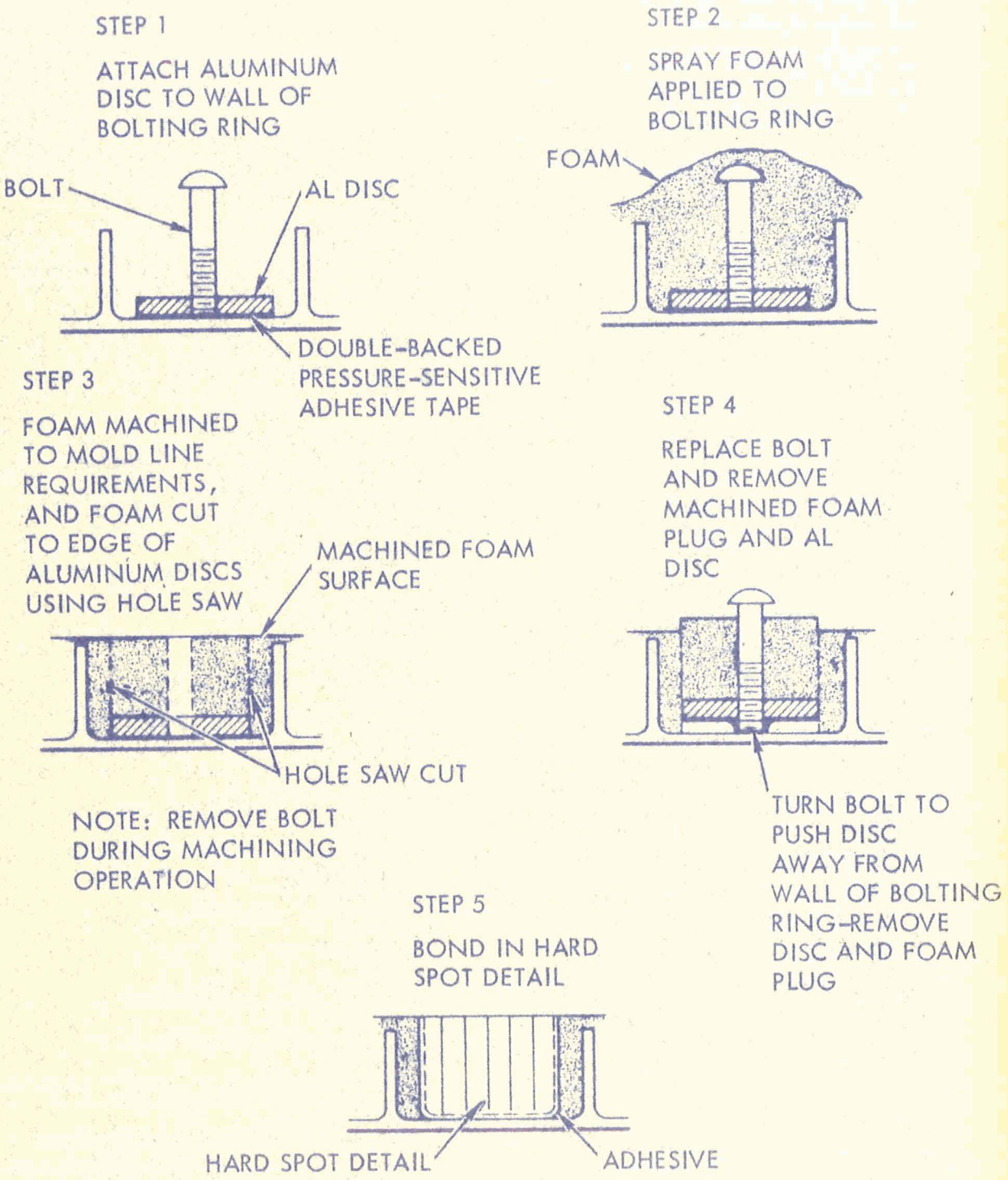

Figure 154. Processing Sequence for Locating and Bonding of Hard Spot Details in Predetermined Locations in Spray Foam Insulated S-II Bolting Ring Section

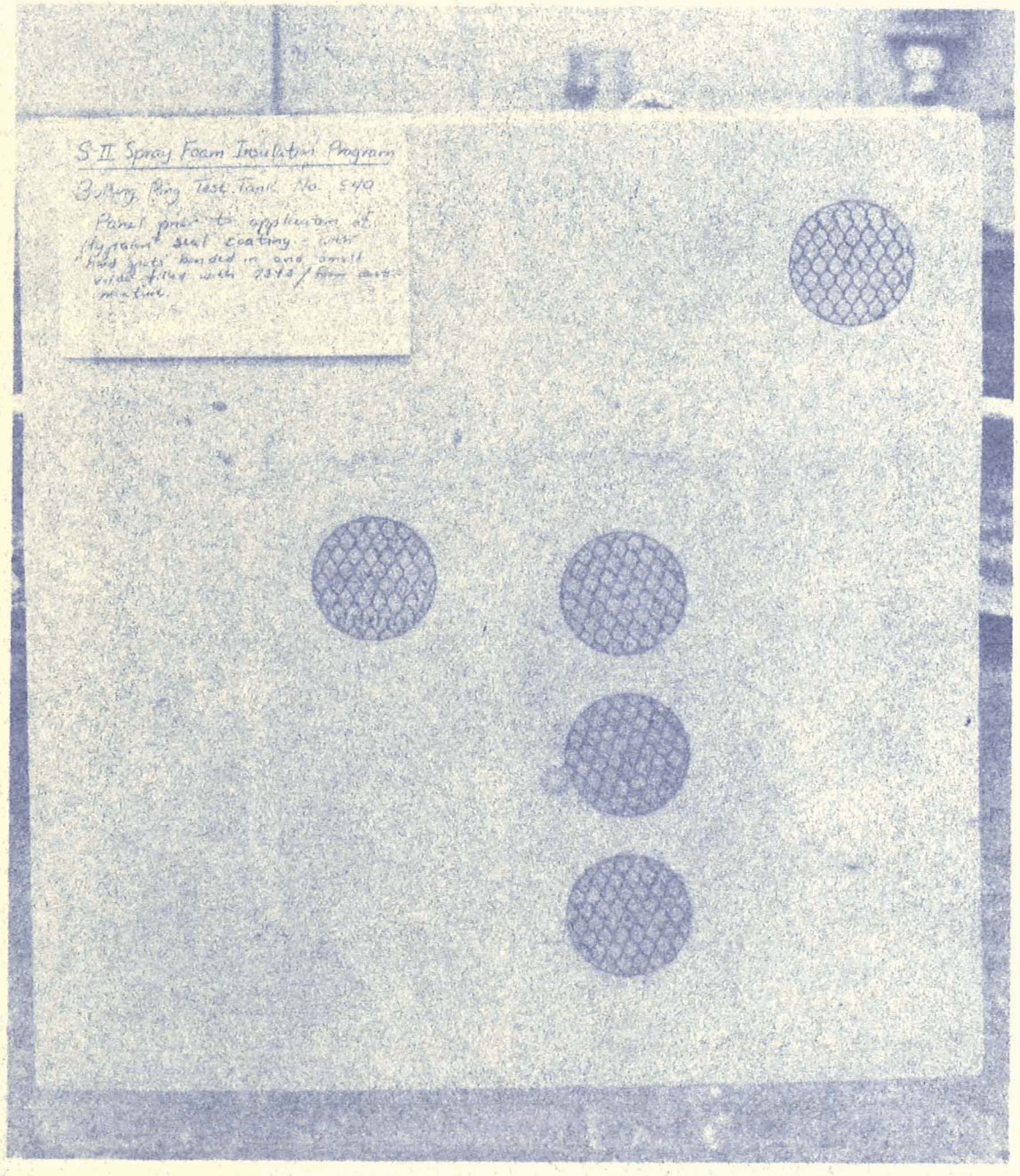

Figure 155. Bonded Hard Spot Details in Test Tank 547

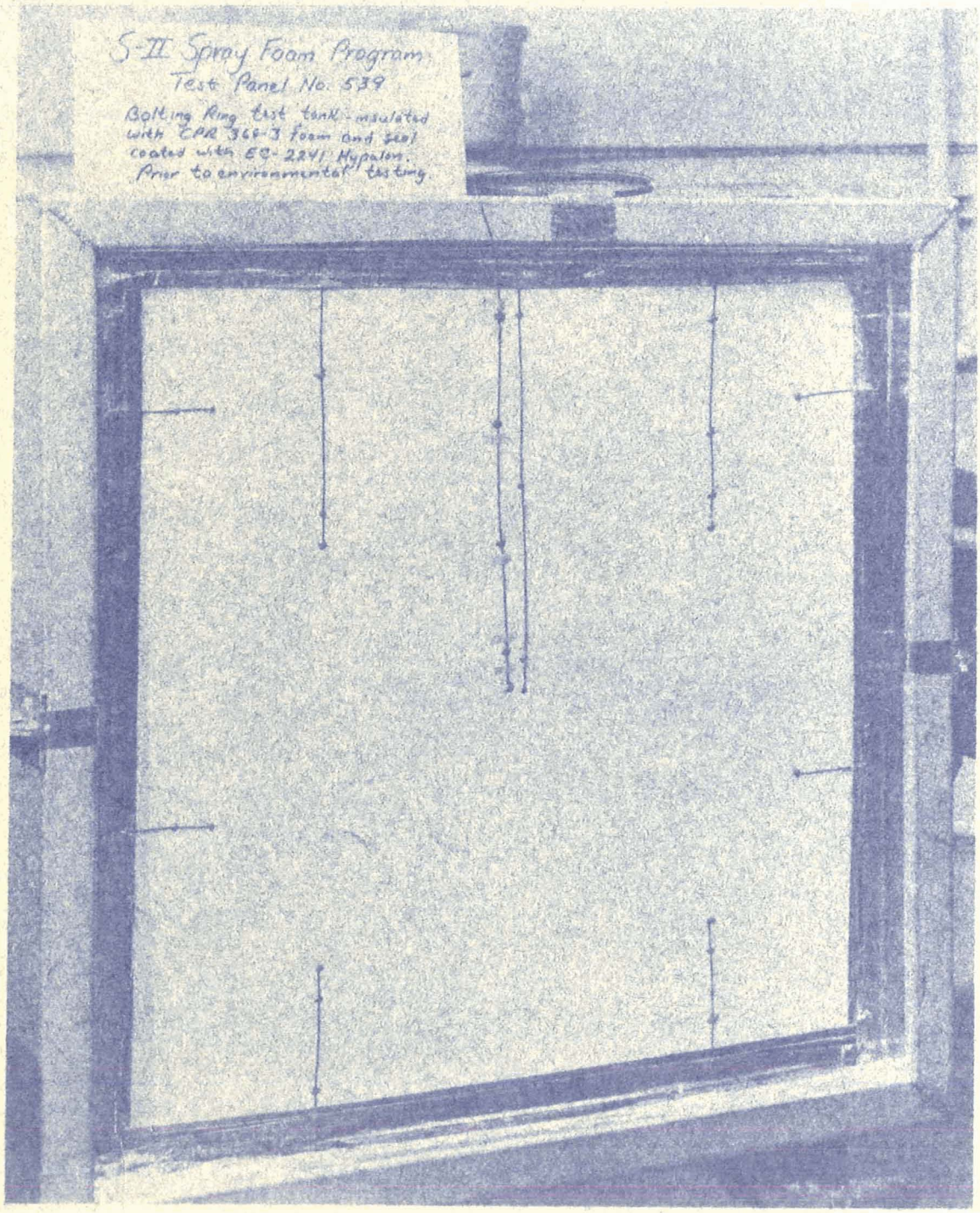

Figure 156. Test Tank 538 Prior to Environmental Testing

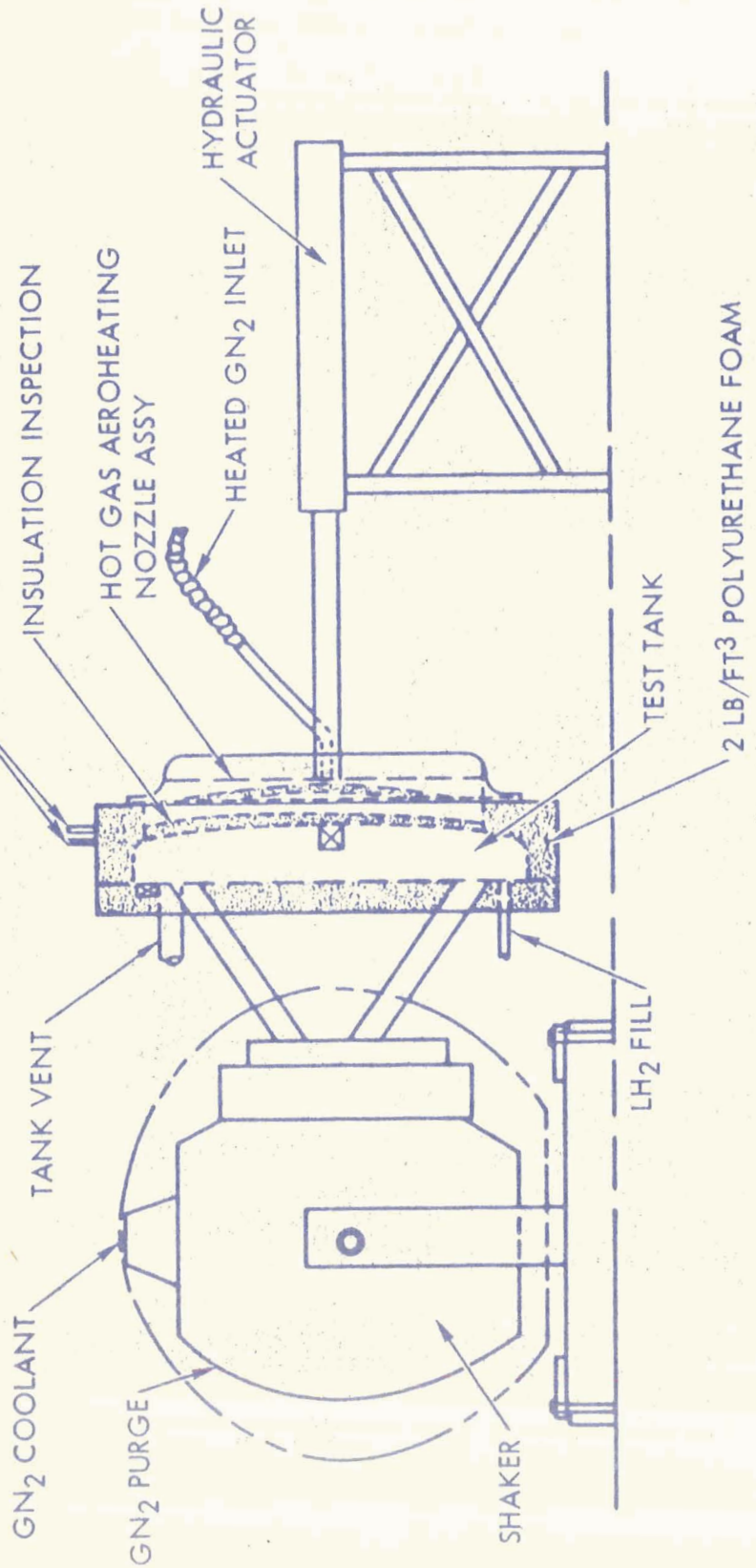

Figure 157. Test System Schematic for Combined Environmental Testing of S-II Insulation

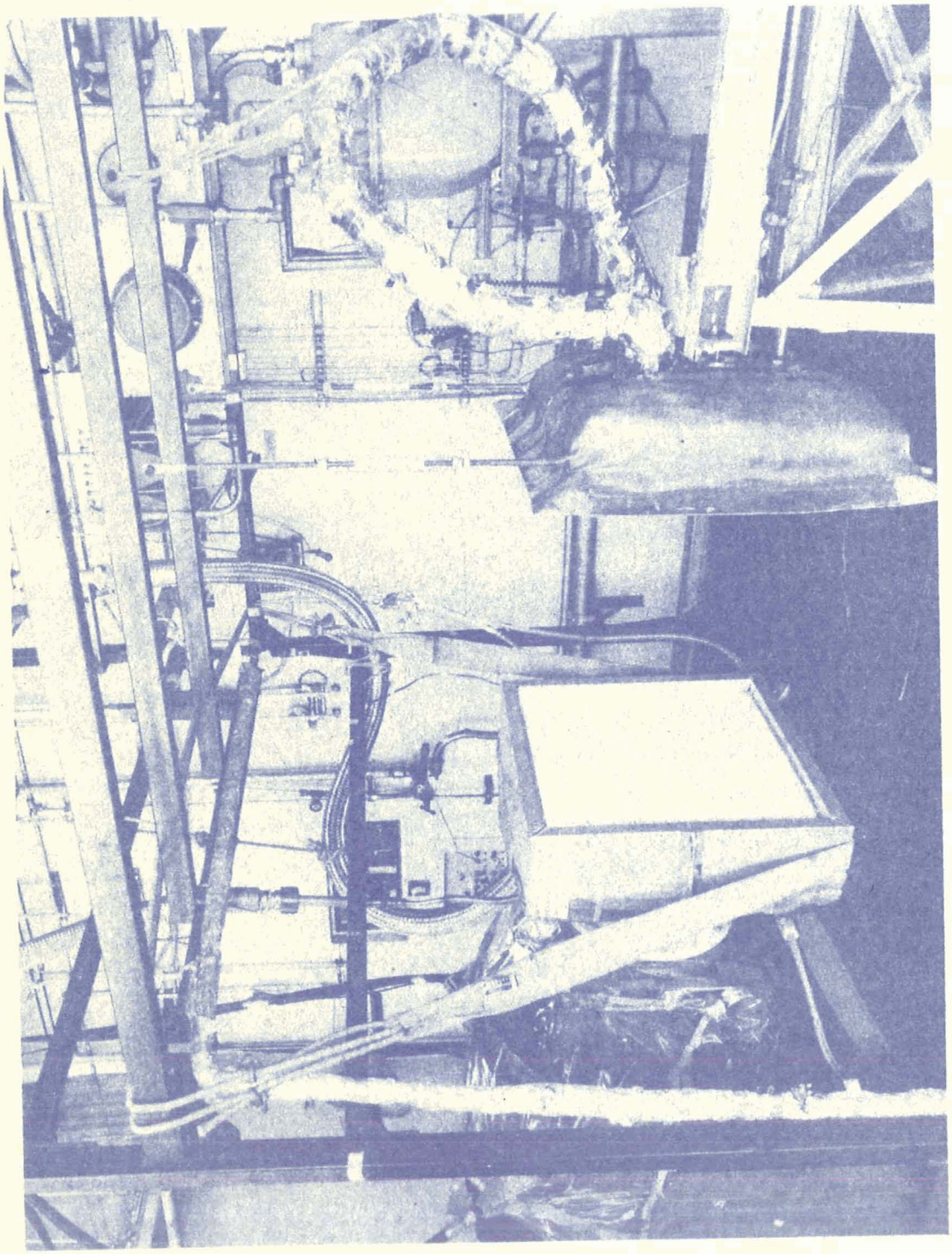

7006-81-1963

Figure 158. Typical Test Setup for Combined Environment Tank Test of S-II Insulation

2. A data acquisition system which utilizes a 100-channel digital data system to record the output of 30-gauge, copper-constantan thermocouples

3. A Ling vibration system using a C-25 vibration exciter

Test Procedure

Each test tank was cycled six times to cryogenic temperatures. During the last cryogenic cycle, the tanks were subjected to vibration and aerodynamic heating simulating S-II pad and launch conditions. Each of the first five cryogenic cycles consisted of filling the test tank with liquid hydrogen and holding for 1 hour before draining. During the sixth cycle, the cryogenic temperature was held 2 hours after which the exterior of the test tank specimen was subjected to the aerodynamic heating profile shown in Figure 159.

RESULTS

Test Tank 538

During the third one-hour LH_2 cycle, failure occurred in the specimen. A diagonal line of frost was noted with a bubble forming in the upper right-hand corner of the test specimen. The fourth one-hour LH_2 cycle caused multiple cracking in the foam structure and Hypalon coating.

Foam failures incurred during test are shown in the following figures:

1. Figure 160 shows the cracks in the Hypalon coating that occurred after five one-hour LH_2 cycles of environmental testing.

2. Figure 161 shows foam cracks noted after removal of the Hypalon coating.

3. Figure 162 shows specimens following dissection of foam in failure areas.

Test Tank 539

This specimen withstood five one-hour LH_2 cycles without incurring a failure. During these cycles, ambient temperatures were 60 to 70 F.

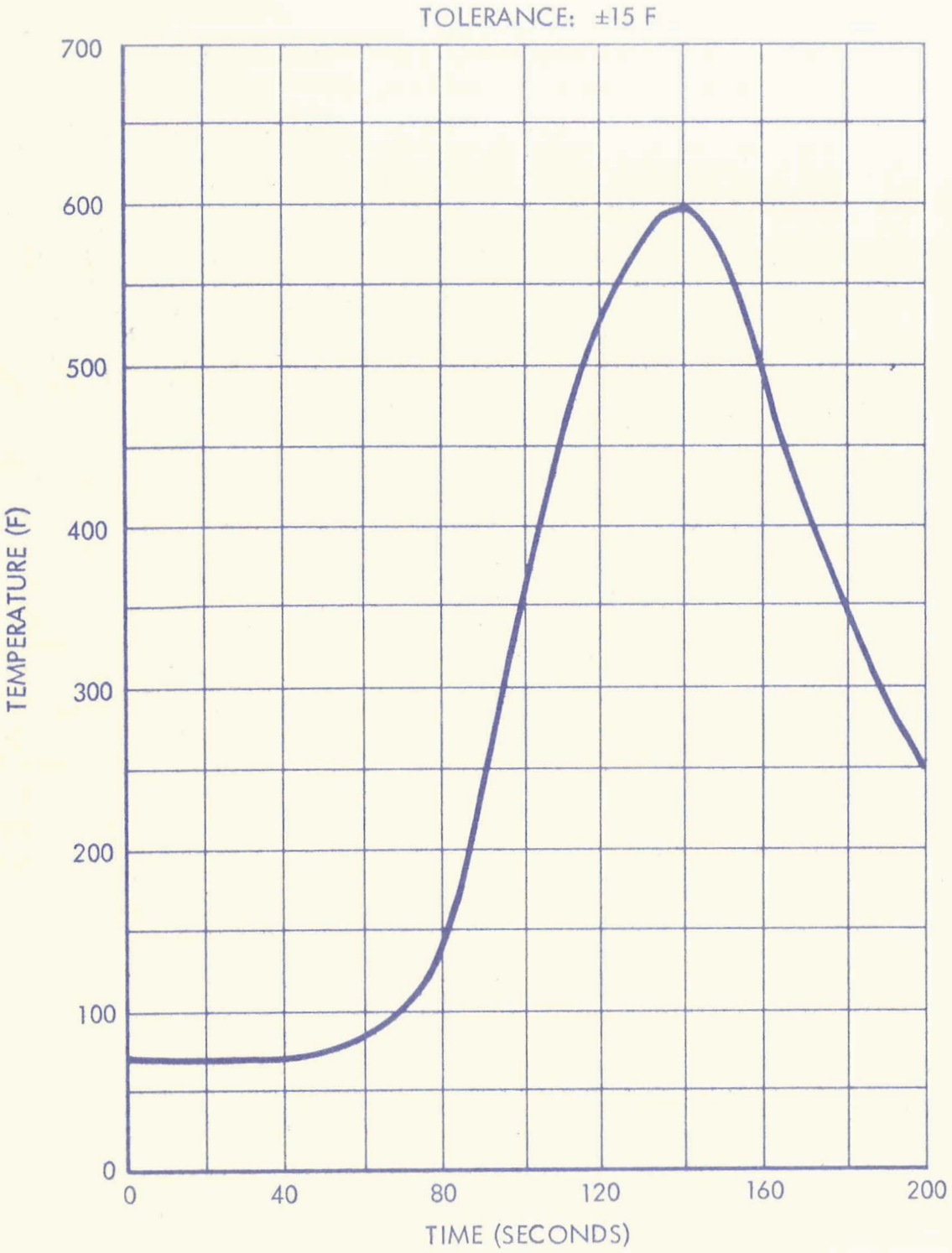

Figure 159. Test Tank Aerodynamic Heating Profile

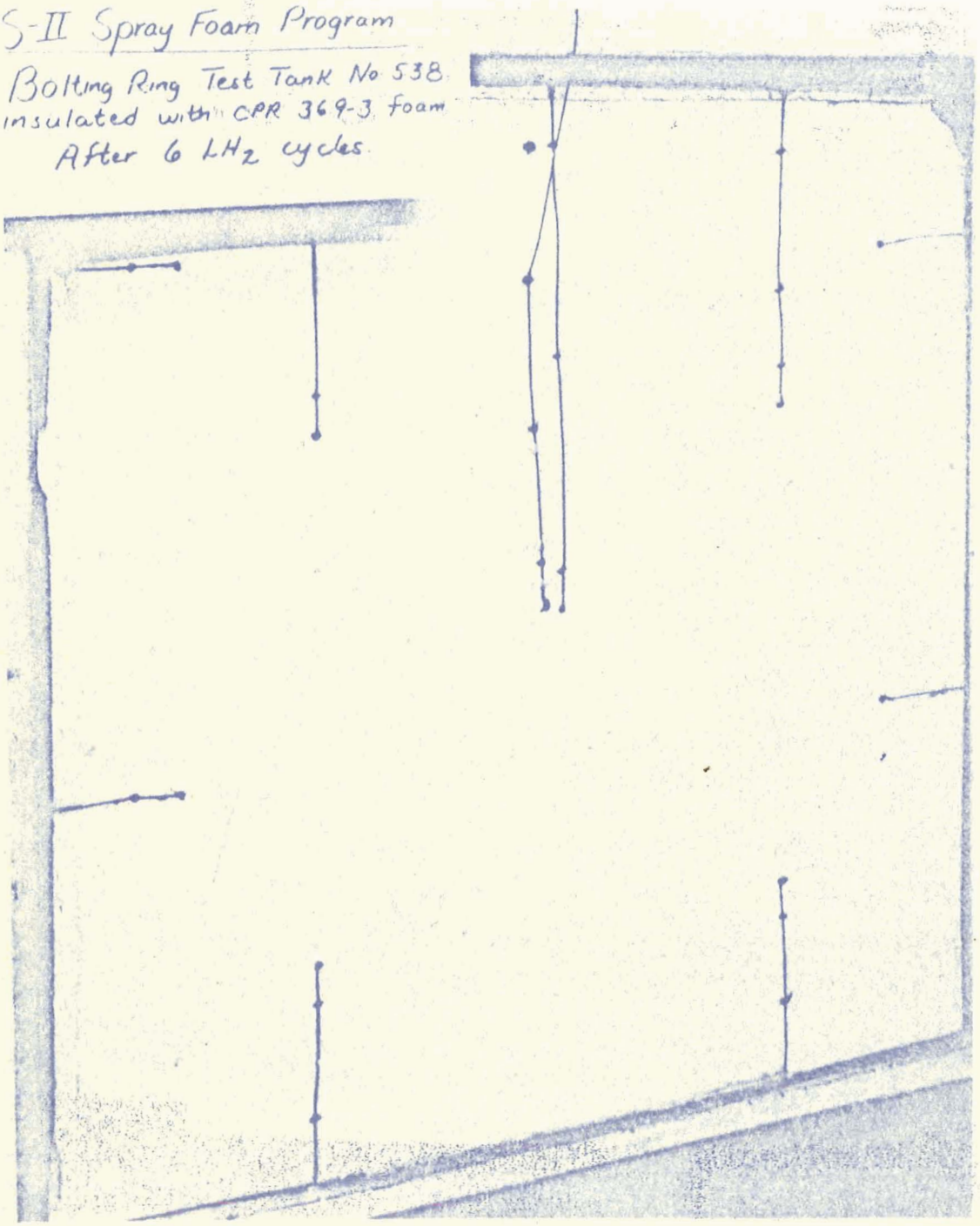

Figure 160. Bolting Ring Test Tank 538 After Environmental Tests

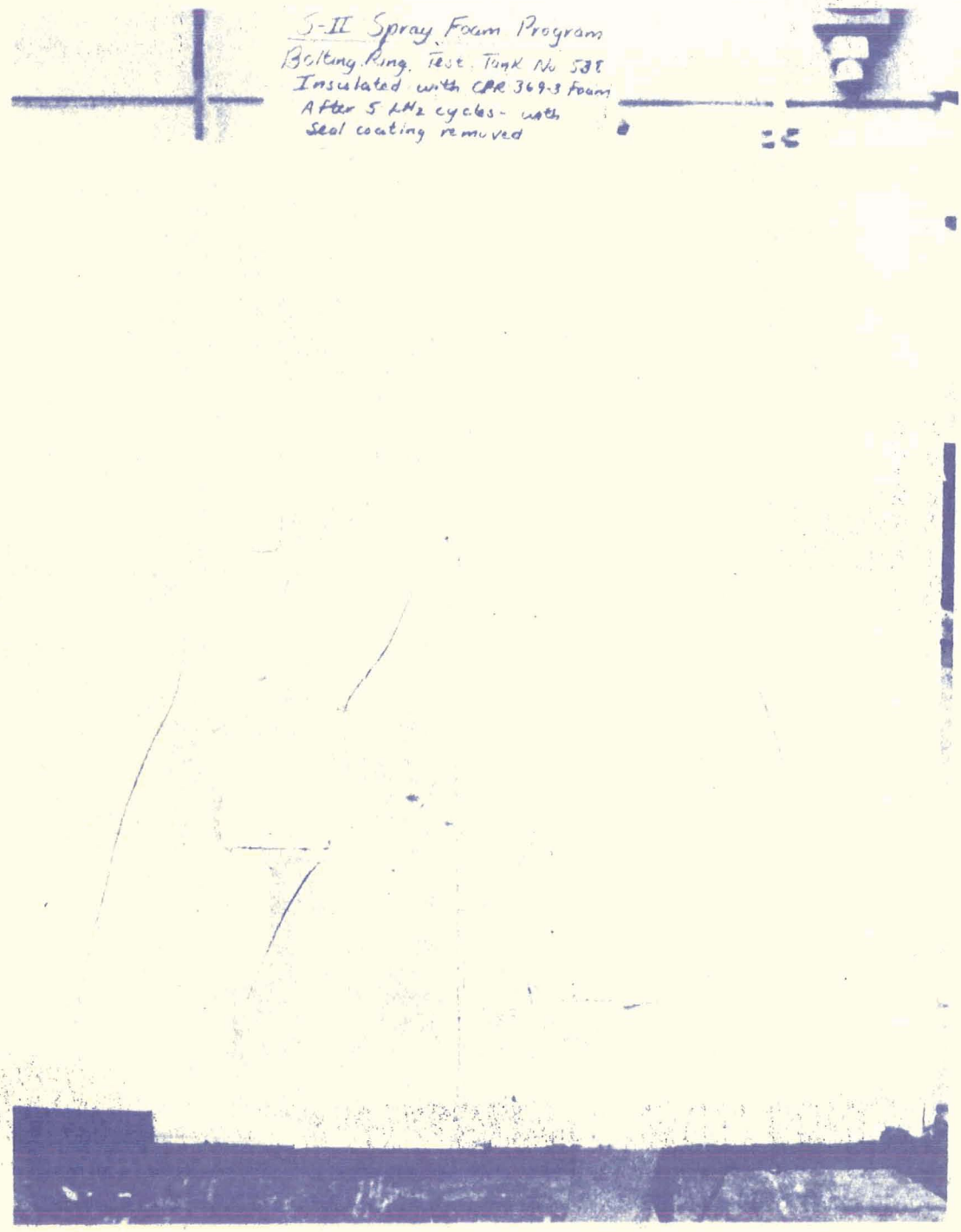

Figure 161. Bolting Ring Test Tank 538 After Environmental Testing with Hypalon Coating Removed

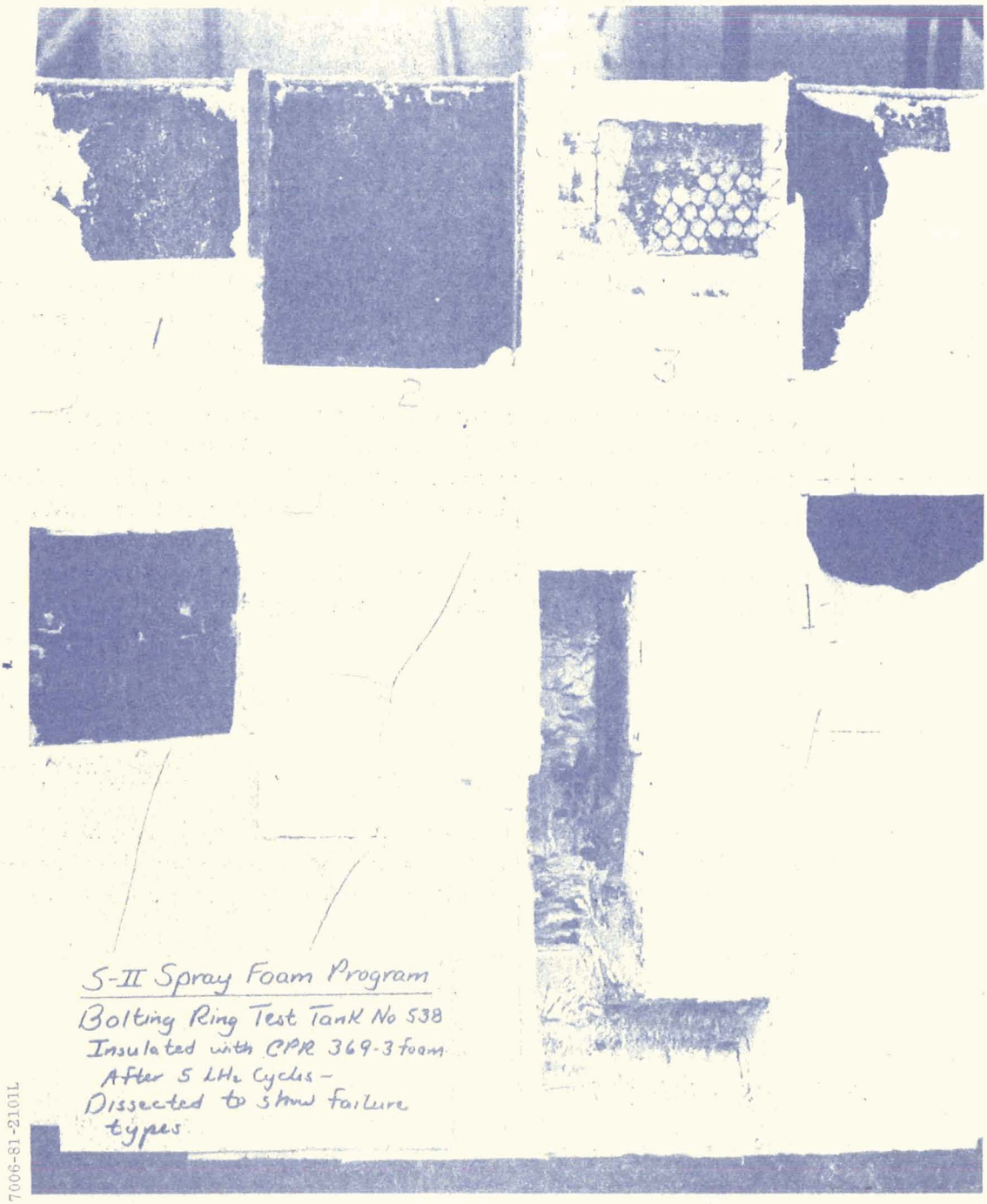

Figure 162. Bolting Ring Test Tank 538 After Dissection of Form in Failure Areas

During the final, or sixth, LH_2 cycle, the Hypalon coating cracked, when the facing was exposed to a -250 F temperature. This also caused cracks in the foam structure. Figure 163 shows hairline cracks in the Hypalon that occurred following the sixth LH_2 cycle when the coating was exposed to -250 F. (Figures 164 and 165 show similar cracks.)

Bolting Ring Test Tank 547

There was no visual evidence of structural changes or failures in the foam structure during or after test or following dissection of the specimen. Wrinkling and ballooning of the Hypalon coating developed under exposure to aerodynamic heating during the last LH_2 cycle, as had occurred in all previous tests with similar environmental exposure. Figure 166 shows the test tank before test.

Figure 167 shows the ballooning of the Hypalon coating during the final environmental cycle under exposure to the S-II aerodynamic heating profile. Figure 168 shows the foam surface and hard-spot details with the Hypalon coating removed. Note the absence of any visible cracks.

Removing the foam from the tank surface revealed excellent adherence to the primer; a sharp pointed chisel-like tool was required to remove the foam from the tank wall.

FAILURE ANALYSIS

Test Tank 538

Examination of the processing techniques and materials used in the test tank revealed the following discrepancies that might have induced the cracks and separation of the foam from the primer surface:

1. Foam was applied to the tank at relatively high humidity conditions, at 75±5 F and 60- to 65-percent relative humidity. Earlier investigations showed some decrease in the flatwise strength of foam applied during temperatures exceeding 75 F and 60-percent relative humidity. This may have contributed to the cracking of the foam structure.

2. During Section 3 cavity machining (Figure 151), the remaining tank surface was left unprotected. As a consequence, foam dust may have adhered to the primed surface (Primer M), although this was cleaned off with a clean stiff bristle brush after machining. Remaining foam dust film could have caused the poor foam adherence in the areas shown in Figure 162. (Note that Section 3 foam was difficult to remove, being well adhered to the primed tank surface.)

Test Tank 539

Cracks in the Hypalon coating and foam structure coincided in all cases. Figure 165 shows the typical crack that, in no case, extends to the tank surface. Indications are that the cracks were all propagated by the shrinkage of the Hypalon when exposed to the -250 F temperature. However, exposure to -250 F is not required for the Hypalon material when applied to the sidewall and bolting ring configuration.

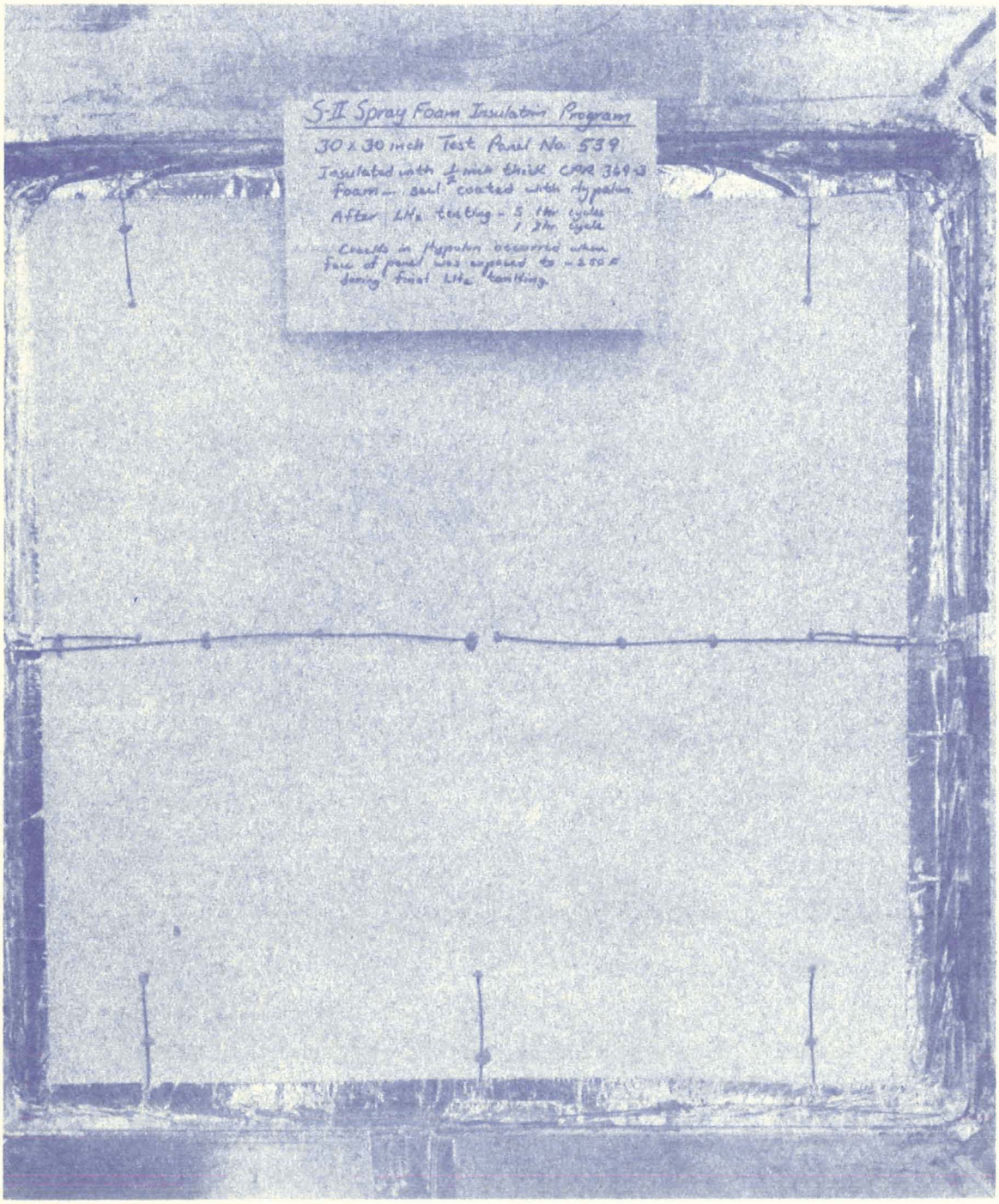

7006-81-2153A

Figure 163. 30-x 30-Inch Test Tank 539 After Test

7006-81-2196A

Figure 164. 30-x 30-Inch Test Tank 539 After Test— With Hypalon Coating Partially Removed

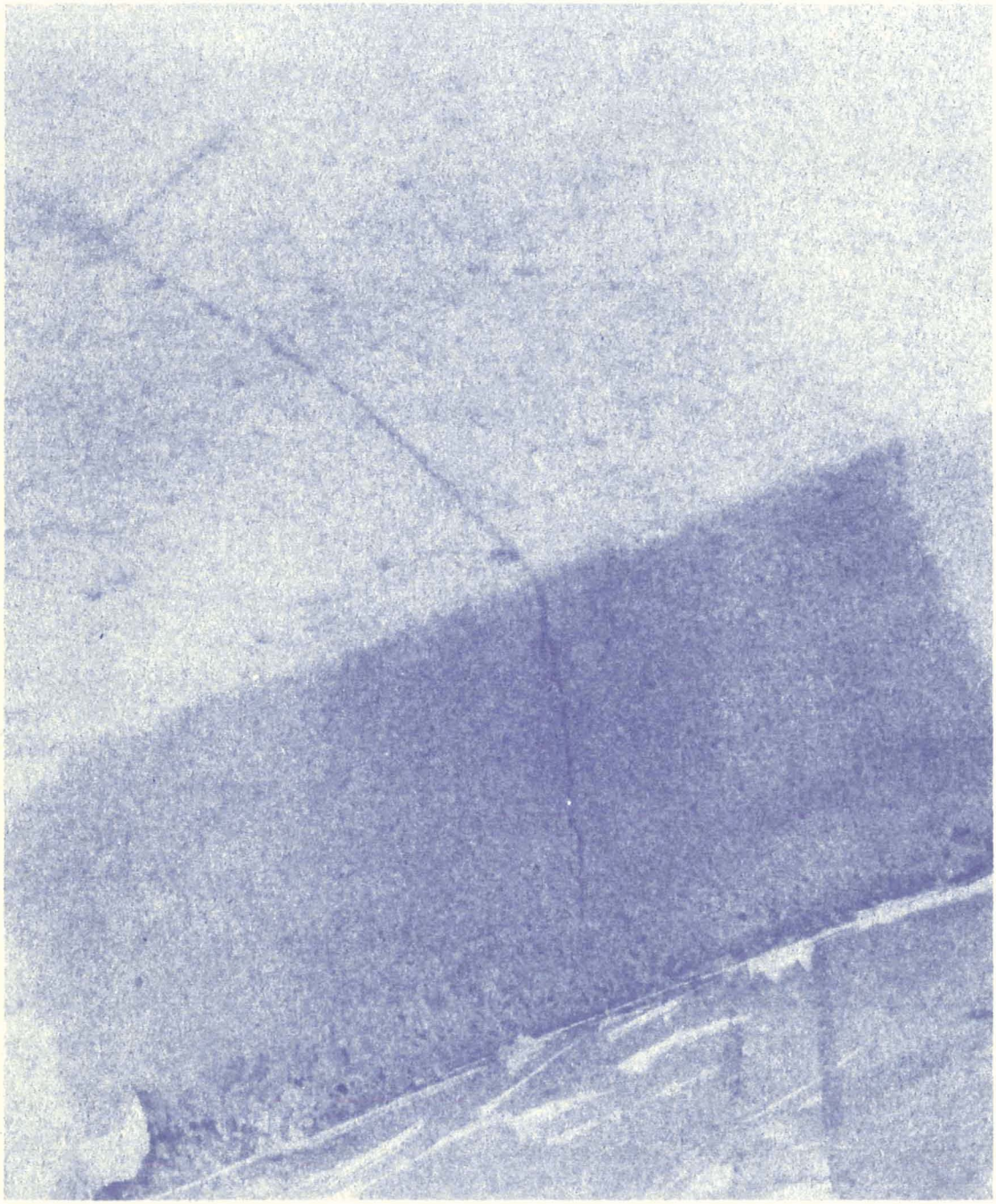

7006-81-2196C

Figure 165. 30-x 30-Inch Test Tank 539 After Test—Showing Depth of Cracks in Foam Structural

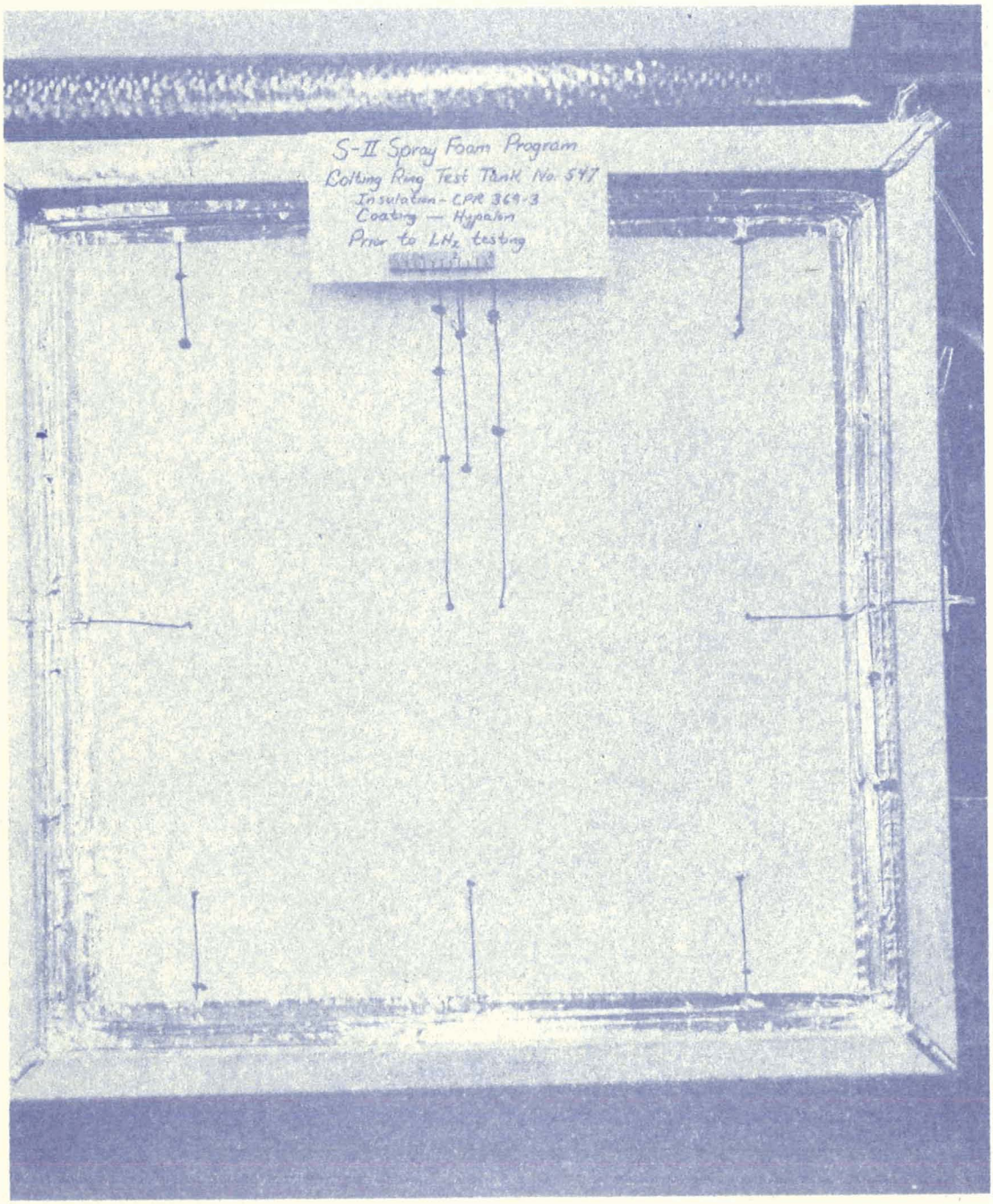

7006-81-2216A

Figure 166. Bolting Ring Test Tank 547 Before Test

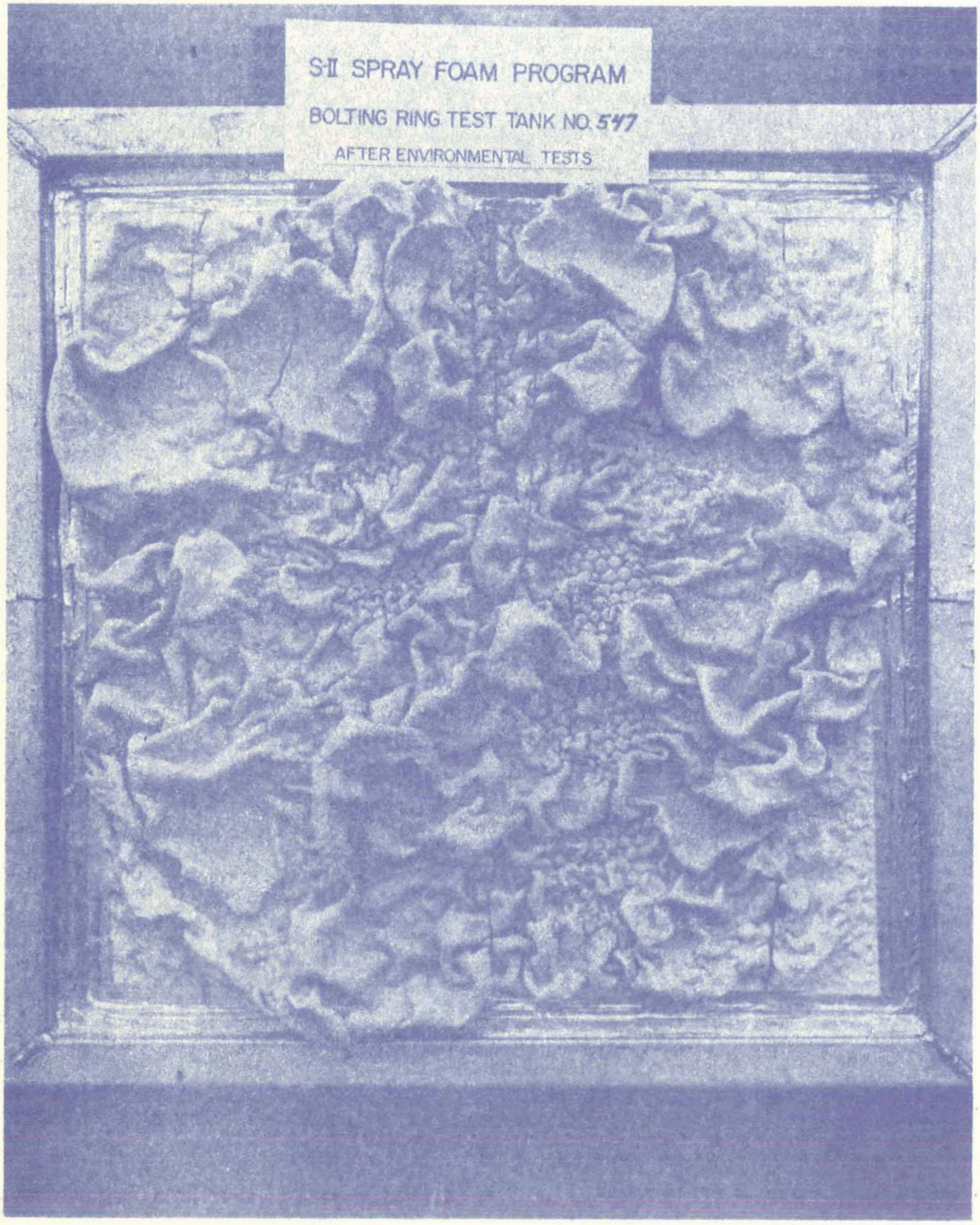

Figure 167. Bolting Ring Test Tank 547 After Test—Showing Ballooning of Hypalon Coating

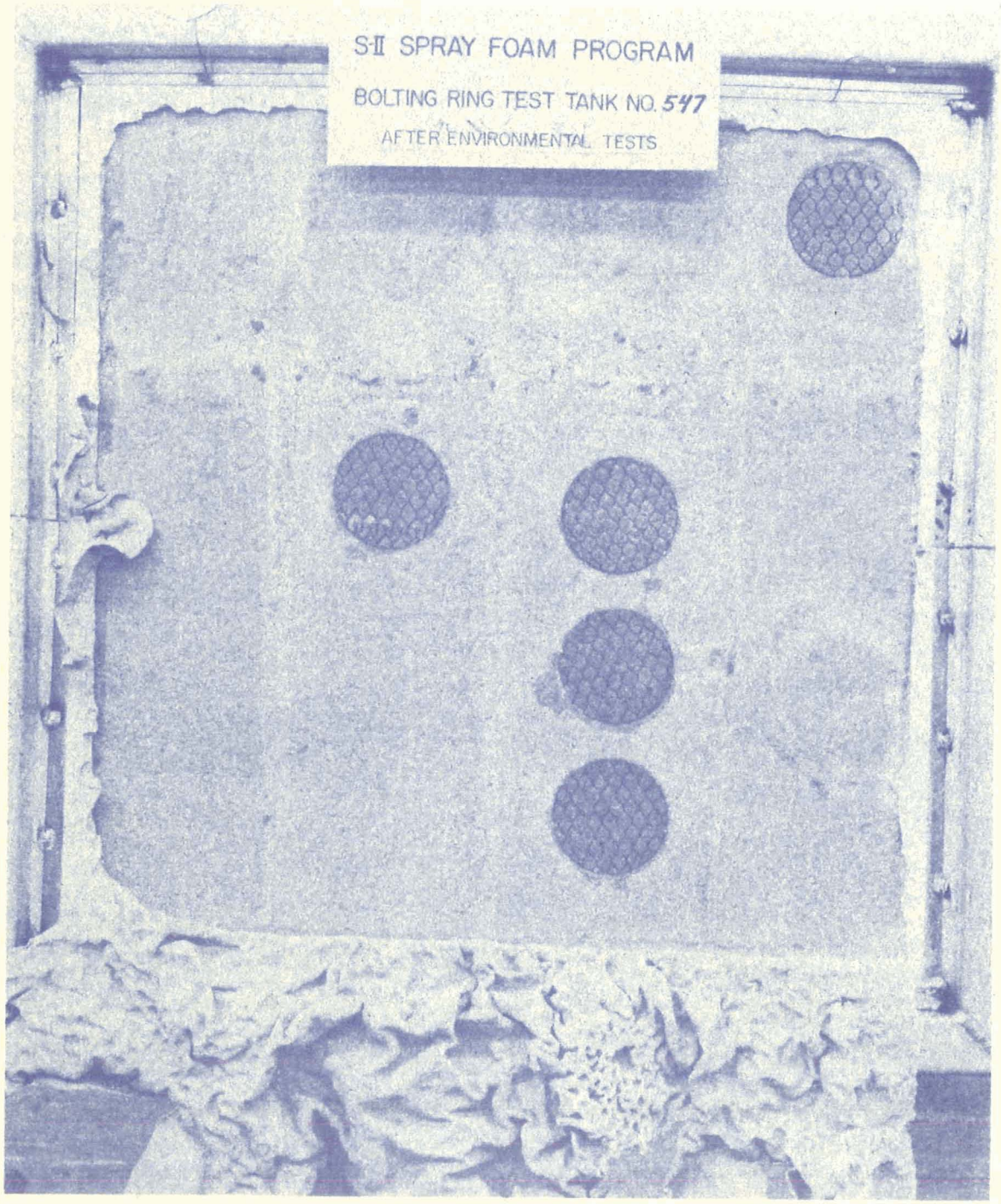

Figure 168. Bolting Ring Test Tank 547 After Test—Showing Foam Surface with Hypalon Coating Removed

DESIGN VERIFICATION, CPR 369-3 SPRAY-ON FOAM INSULATION, THREE-POUND DENSITY

INTRODUCTION

As a result of an agreement between NASA and S-II Engineering, a test program was initiated to verify Upjohn's CPR-369-3 spray-on foam insulation for Saturn S-II vehicles.

The program was to verify the structural cryogenic strain capabilities of spray foam, weighing 3 pounds per cubic foot. Foam specimens made from a minimum of three batches of material using three different pieces of spraying equipment were evaluated. Structural and thermal capabilities were verified after vibration, cryogenic temperature cycling, aeroheat testing and reduced atmospheric pressures.

CONCLUSIONS

Structural cryogenic strain compatibility was not verified since failures occurred in all batches of foam material with all three types of foam application equipment. However, CPR 369-3 foam demonstrated a capability of withstanding cryogenic cycling, aerodynamic heating, and vibration during testing simulating the vehicle launch condition profile.

PROCEDURES

Specimen Fabrication

Cryogenic Strain Compatibility Specimens

Metal tensile specimens were machined from 0.125-inch thick 2014-T6 aluminum sheet. The aluminum specimens were cleaned, primed with M-602 primer, and cured at 290±10 F for 3 hours. The thickness of the M-602 primer was then measured with a Permascope.

Five tensile specimens were mounted on a backing board with filler plates between the specimens. A 9 x 24 x 0.125-inch-thick 2014-T6 aluminum plate, processed identically to the aluminum tensile specimens, was placed at each end of the board. The five tensile specimens and end plates were then solvent-cleaned with methyl ethyl ketone or equivalent. After solvent cleaning, the group of specimens was primed with Primer M and allowed to cure for 16 hours minimum at ambient temperature (60 to 90 F). The specimen setup before foam application is shown in Figure 169.

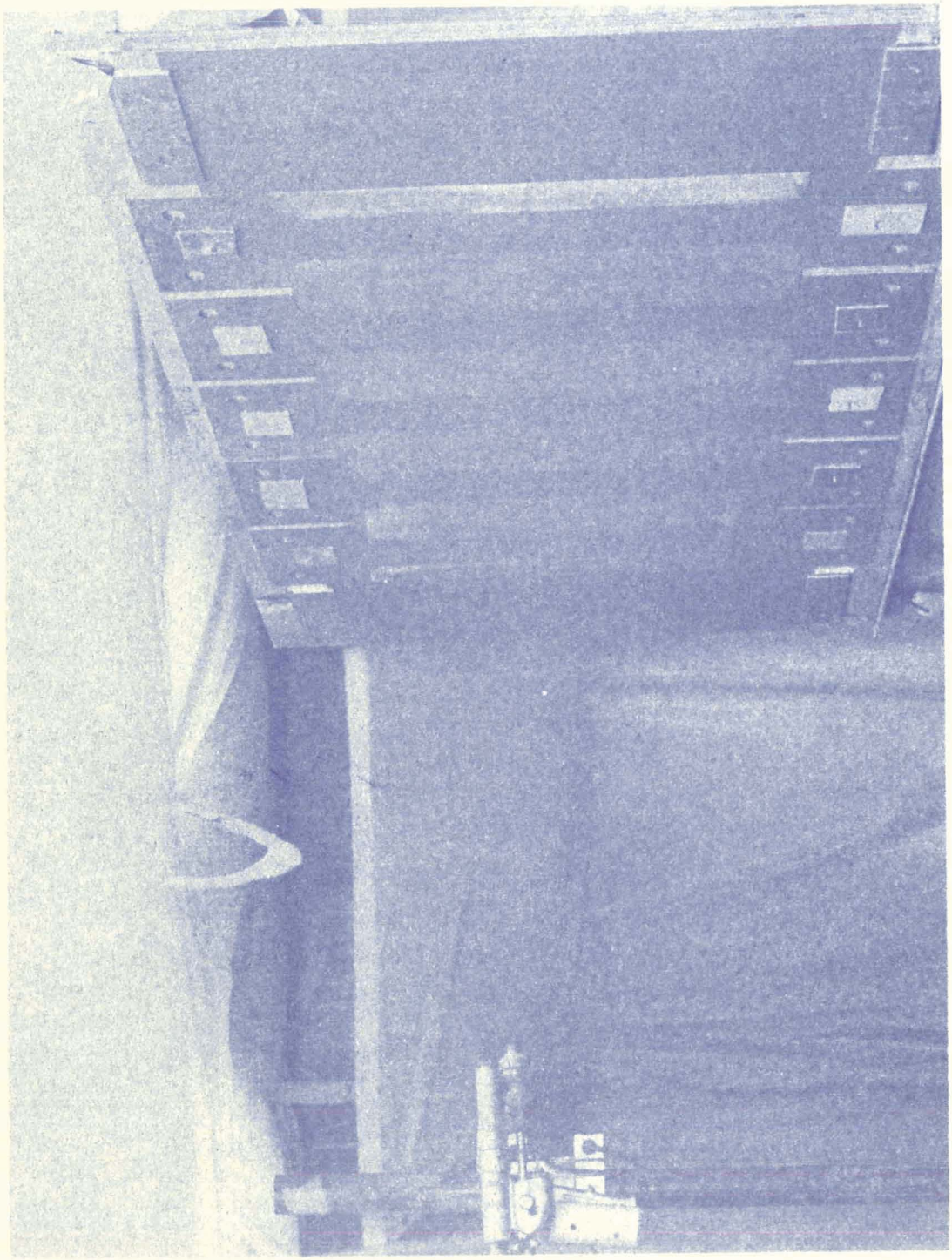

7006-81-9276A

Figure 169. Specimen Plate Setup Before Foaming

Polyurethane foam (CPR 369-3) was applied with a Glascraft Model 290 (or Binks or Lemco) spray gun with a flat fan nozzle (fan vertical). The spray setup was not distributed for a minimum of one hour after foam application. Specimens in the as-foamed condition are shown in Figure 170.

The foam was allowed to cure for a minimum of 24 hours before machining. The specimens were then machined to the overall configuration shown in Figure 171. Specimen code is described in Table 41 and specimen configuration is shown in Figure 172.

Figure 171 shows the nylon-phenolic end-block configuration. The nylon block was bonded to the end of the foam and to the aluminum tensile specimen with polyurethane adhesive to comply with MB0120-024.

Flatwise Foam Composite Tensile Specimens

When the cryogenic strain compatibility specimens were foamed, a metal plate at the beginning and end of each group was also simultaneously foamed (see Figure 169). Flatwise tensile specimens parallel to rise were cut from the plates and bonded to circular-etched aluminum blocks using adhesive described in specification MB0120-023 (Lefkoweld 109/LM52R). The adhesive was cured a minimum of 48 hours at room temperature prior to test.

Specimen Preparation - Density, Thermal Expansion

Density and thermal expansion specimens were cut from polyurethane foam removed from filler plates between the cryogenic strain compatibility specimens. Density specimens were 2 x 2 x 3/4 inches and weighed to the nearest 0.01 gram.

Thermal expansion specimens, 1/2 x 1/2 x 3 inches, were cut from the same area.

Six-Inch Debond 30- x 30-Inch Tank Specimen Preparation

A 30- x 30-inch test tank was cleaned with the paste-etched process described in specification MA0610-023 and primed with M-602 primer according to MB0120-032. The M-602 primer was masked except for a 6-inch-diameter area in the center of the tank. A spray coating of S-122 Teflon mold-release agent was applied to the exposed M-602 primed surface. After a drying period, the release coating was polished, the protective maskant was removed, and the M-602 primer was solvent wiped with methyl ethyl ketone. The tank was then primed with MB0120-042 Type-II primer and cured for a minimum of 16 hours at room temperature. CPR 369-3 polyurethane foam was sprayed on the tank surface, the mold release providing

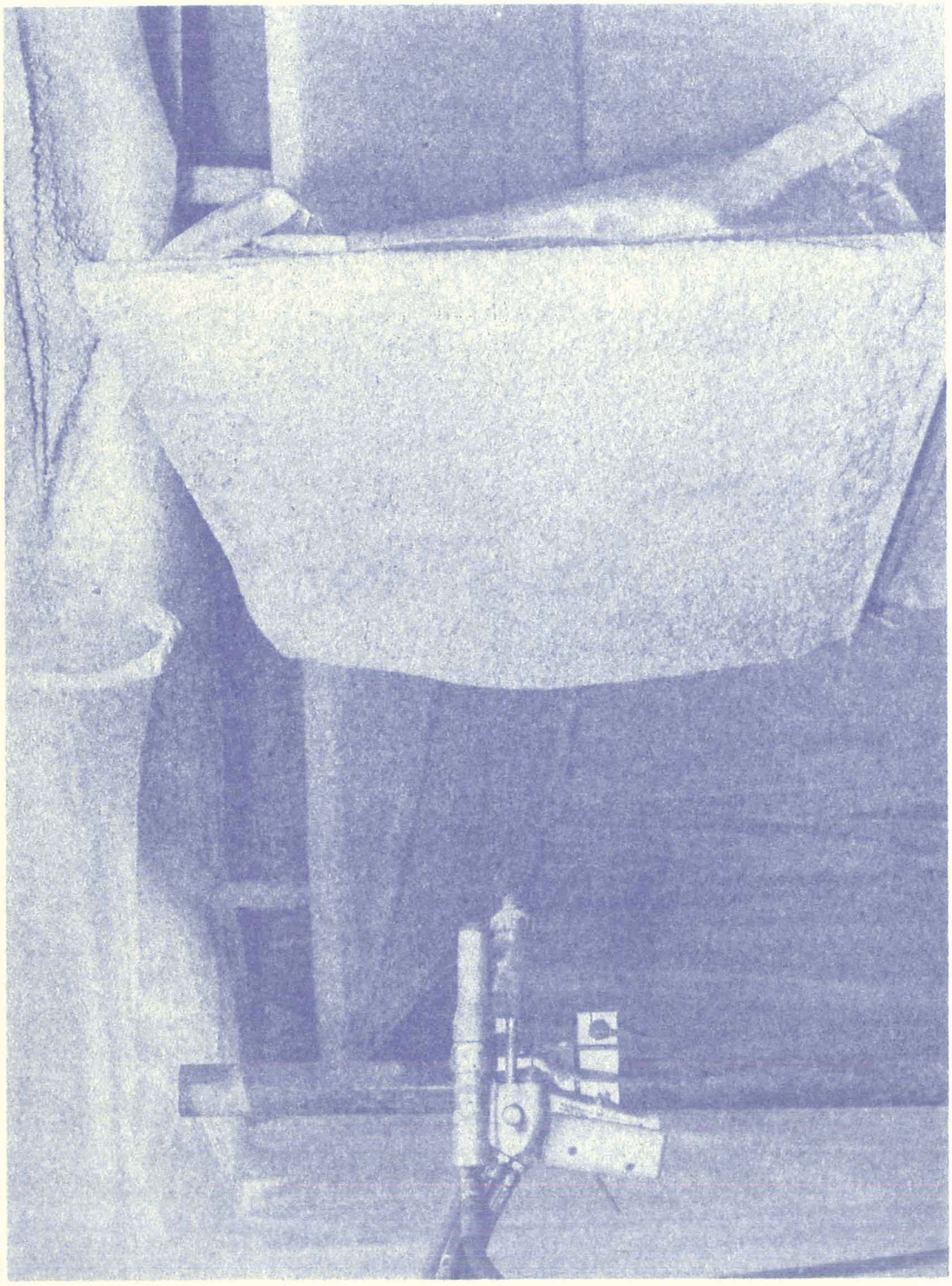

7006-81-2276B

Figure 170. Specimen After Application of Spray Foam

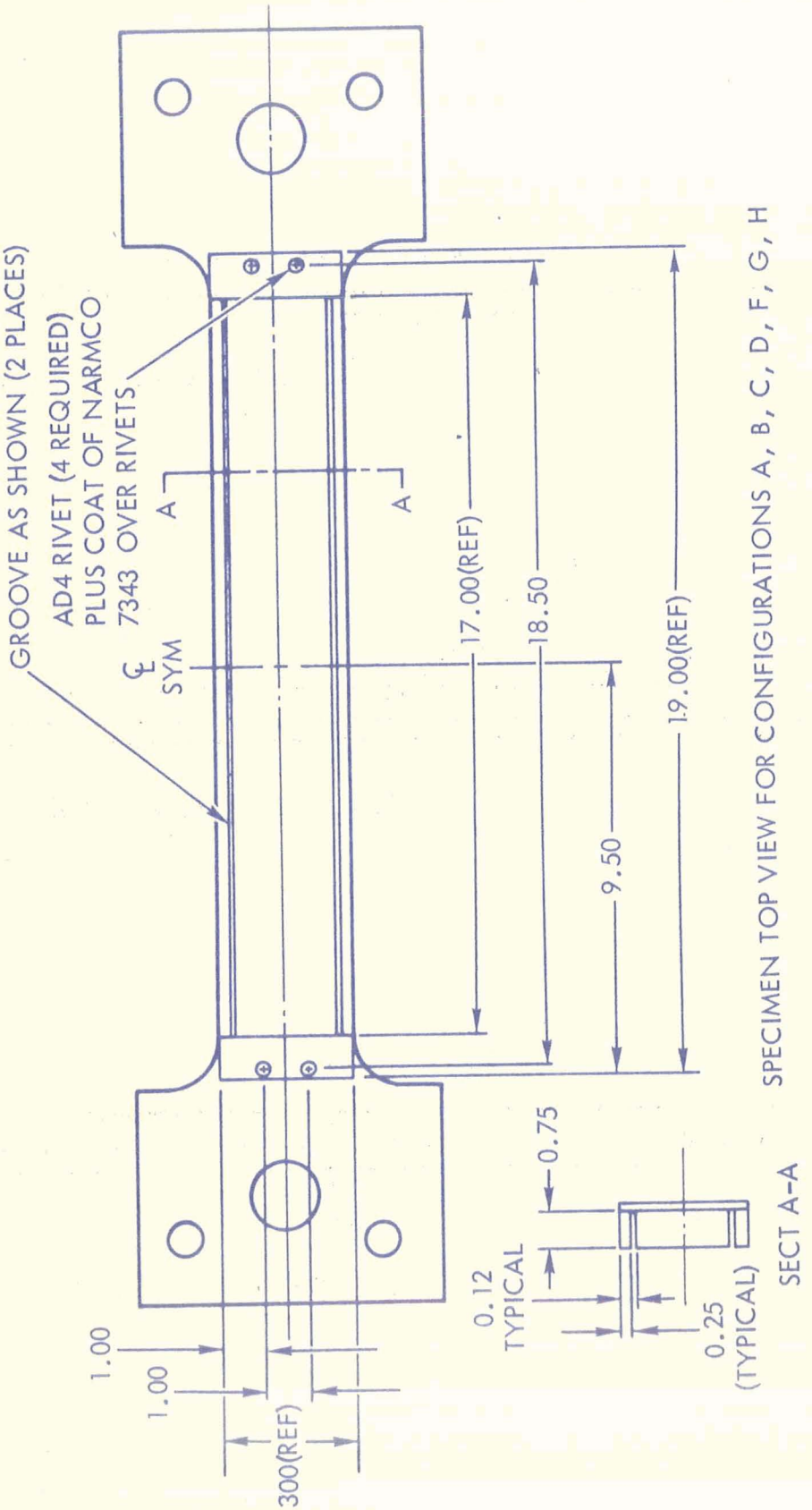

Figure 171. Sketch of Foam Composite Tension Specimen

CONFIGURATION A (REGULAR)

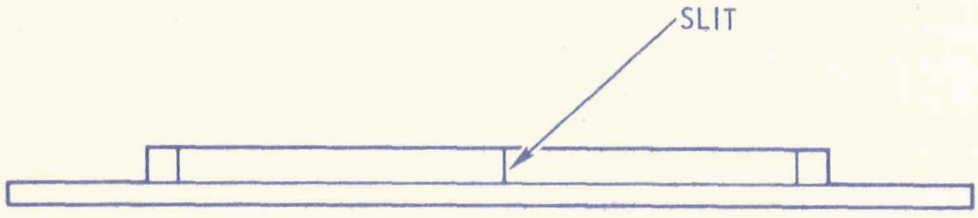

CONFIGURATION B (FULL DEPTH SLIT)

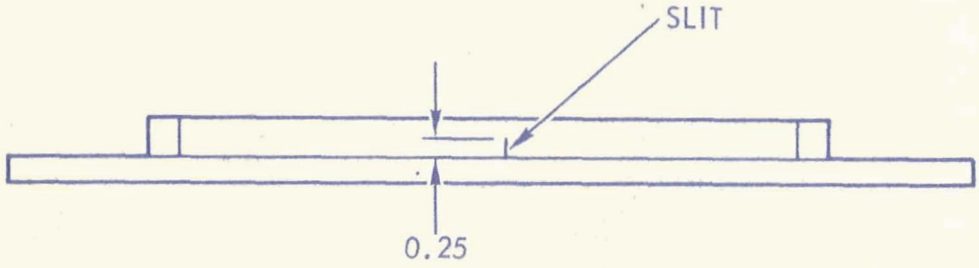

CONFIGURATION C (MODIFIED SLIT)

Figure 172. Sketch of Foam Composite Tension Specimen Configuration

Table 41. Legend of Specimen Code

Type of test	A - Regular
	B - Crack
	C - Modified crack
	D - Debond
	E - Cyclic
	F - Closeout
	G - Overlap
	H - Aeroheat test
Spray gun	G - Glascraft
	B - Binks
	L - Lemco
Foam material batch	1, 2, 3, etc.
Department spraying foam	L - Laboratory
	M - Seal Beach Manufacturing

X X X X
- X: Type of test
- X: Department spraying foam
- X: Foam material batch
- X: Spray gun

Example: ALIG - Regulator configuration, sprayed by Laboratories and Test, using Batch 1 with the Glascraft spray gun

Foam Batch	Cut Number
1	C710/C793
2	C710/D1045
3	D1084/D1191
4	D1084/D1258

a 6-inch diameter debond between the foam insulation and the tank wall. After a 24-hour cure, the foam was machined to a 1-inch thickness. An organic edge-seal of nylon fabric MB0135-021 Type II impregnated with polyurethane resin (Narmco 7343/7139) was applied to the edges of the 2-foot-square foam specimen. Nine thermocouples were installed on the foam specimen and four thermocouples on the tank wall (Figure 173). The 30- x 30-inch tank was completely installed with poured polyurethane foam, Nopco BX-249N-2. A vacuum bell of approximately 9-1/2-inch diameter was installed over the 6-inch debond with RTV according to MB0130-019 (Figure 173).

Twelve-Inch Debond 30- x 30-Inch Tank Specimen Preparation

A 30- x 30-inch test tank prepared by S-II Manufacturing was processed similarly to the 6-inch debond tank, except that a moisture-barrier coating was applied to the specimen surface, and no vacuum bell was installed Figure 174 shows the tank before test.

Forward Bulkhead Configuration Cryogenic Strain Compatibility Specimen Fabrication Procedure (118, 119, 194, 195)

Four specimens previously tested were machined to the contour shown in Figure 175. Applied over the foam specimen surface was a one-ply nylon fabric (MB0135-021) Type II impregnated with Narmco 7343/7139 polyurethane resin according to MB0120-024.

Instrumented Cryogenic Strain Specimen

A Configuration A cryogenic strain compatibility specimen (Figure 172) was instrumented with thermocouples to measure temperature gradients in the polyurethane foam.

Test Procedure

Foam Composite Tension Test

Foam composite tension tests were conducted with only the 2014-T6 aluminum parts of the specimen composite in liquid hydrogen. The surface of the foam was maintained at a temperature between 40 to 125 F.

The test setup was a load frame and load train consisting of a 50,000-pound hydraulic strut, a load cell, and miscellaneous rods and clevises. The test cryostat was a welded aluminum box insulated with styrofoam. The foam composite specimens were set in the cryostat. Thermocouples were attached to the bottom side of the aluminum coupon (in contact with liquid hydrogen) and to the top surface of the foam. A preload of 2600±500 psi was applied to the specimen and maintained during chilldown.

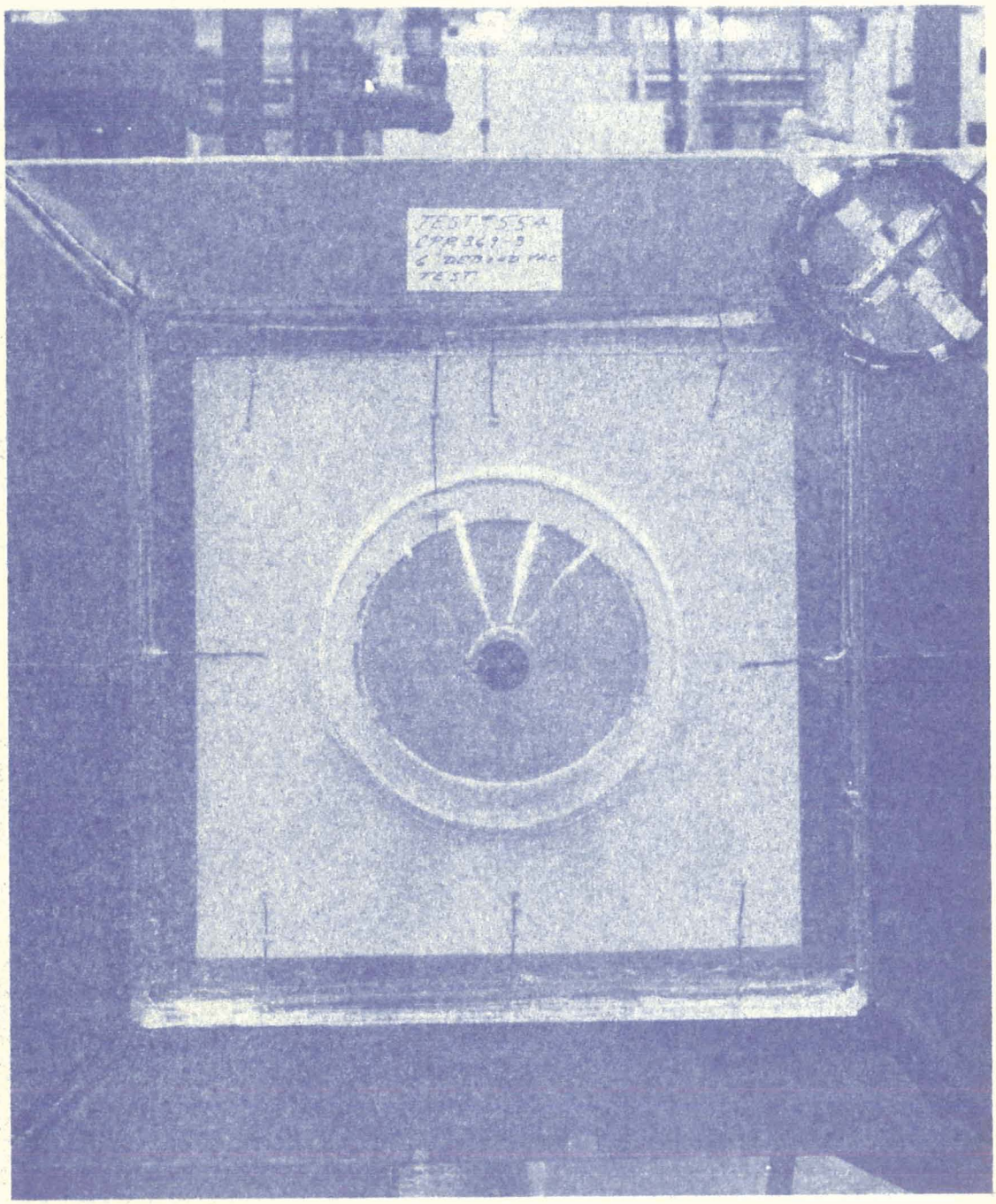

7006-81-2344A

Figure 173. Six-Inch Debond 30-x 30-Inch Tank Specimen

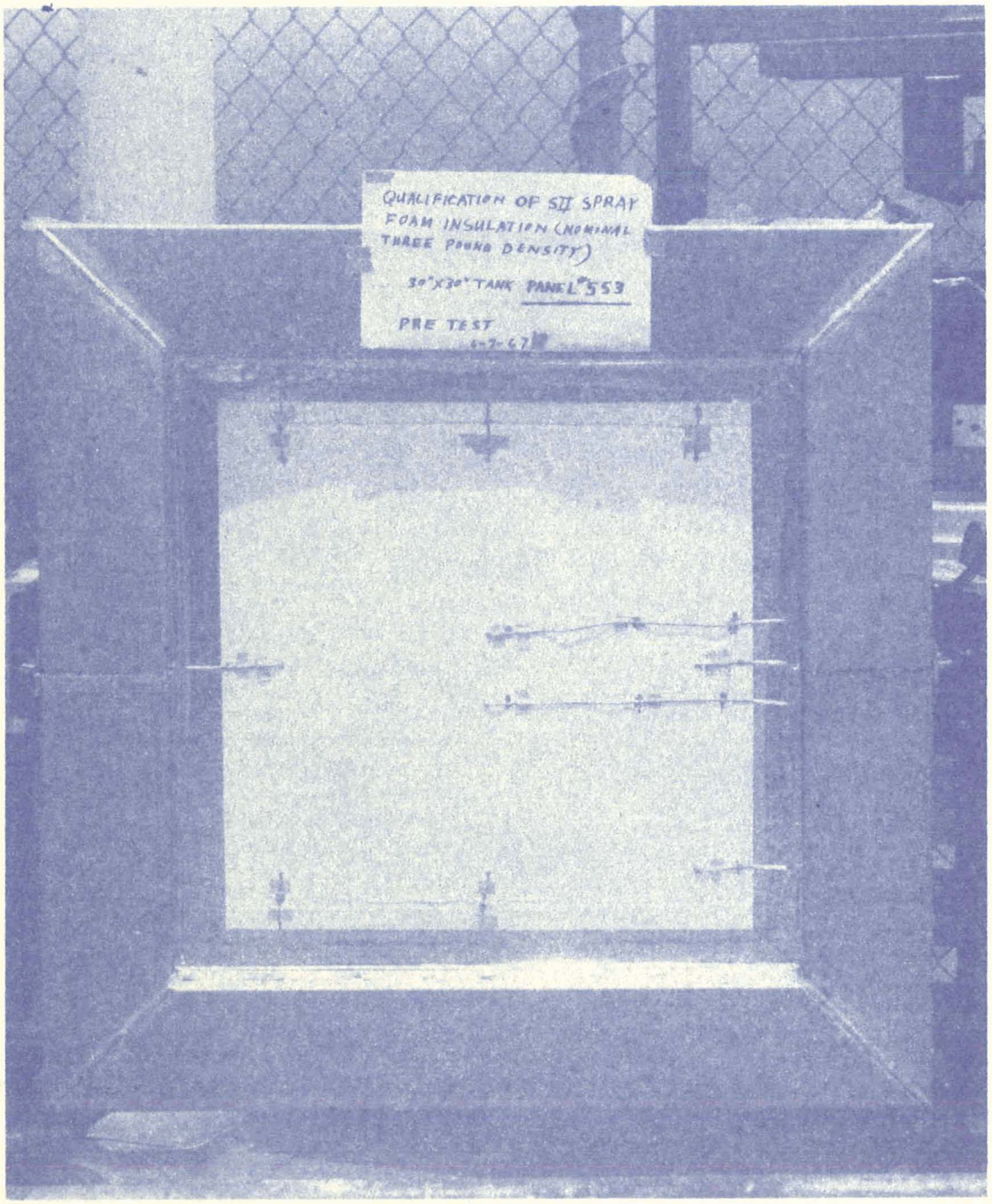

7006-81-2340

Figure 174. Twelve-Inch Debond 30-x 30-Inch Tank Specimen

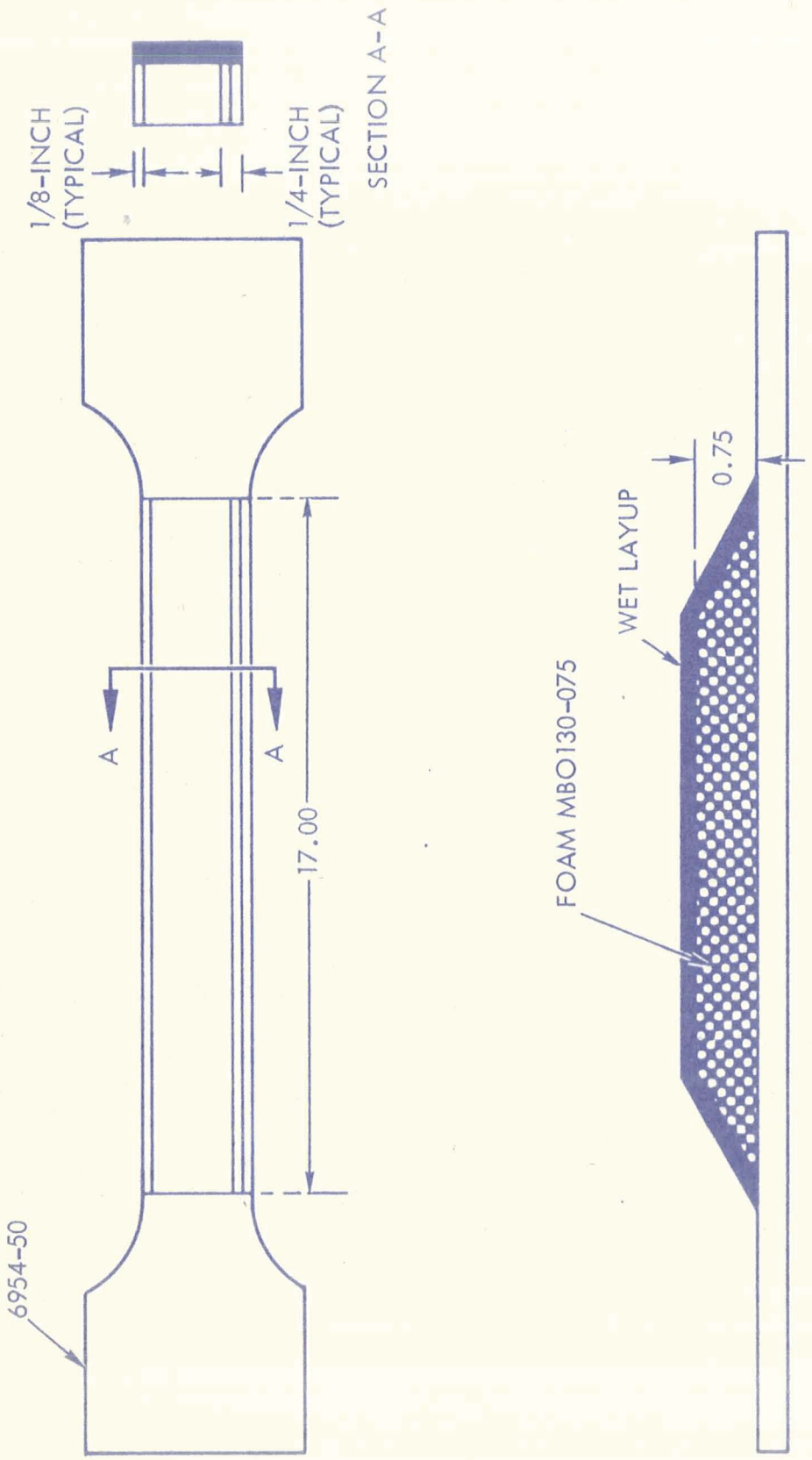

Figure 175. Bulkhead Configuration Composite Test Specimen

To maintain proper foam surface temperature, a copper plate with copper tubes was placed on the foam, and gaseous nitrogen was circulated through the tubes. In addition, a styrofoam box was placed over the foam portion of the specimen, and the entire test chamber was sealed with a lid. The test chamber and the inner styrofoam box were then purged with helium gas. As the liquid hydrogen flowed into the test cryostat, the hot gaseous nitrogen and helium purge were regulated so that the foam top surface remained between 40 and 125 F. When the aluminum reached -423 F (liquid hydrogen in contact with the metal), a tension stress was applied to the specimen in 45 to 90 seconds and gradually removed. A nominal stress level of 71,000 psi was then applied to each specimen. A minimum of 30 minutes was allowed after start of chilldown, before applying the load. After the test, the specimen was warmed to a temperature above -200 F, removed from the setup, and visually examined to determine if cracks had developed in the foam to primed metal bond or in the foam.

Foam Flatwise Tension Tests

The foam flatwise tension specimens were tested in a Riehle Universal test machine. The load was applied to a crosshead travel rate of 0.05-inch-per-minute, and the strain-load measurements were autographically recorded with a Baldwin LVDT microformer and a Riehle RD5XY null-balance strain-load recorder.

For the liquid hydrogen cryogenic tests, the specimens were immersed in liquid hydrogen before testing.

Thermal Expansion Test

Thermal expansion tests conducted from +50 to -300 F on CPR 369-3 polyurethane foam specimens employed a Vycor dilatometer tube (ASTM D-696-44).

Thermal Profile Test of Cryogenic Strain Specimen

The instrumented cryogenic strain specimen was tested in the same manner as were the foam composite tension specimens, except that no load was applied.

Vibration, Aerodynamic Heating and Cryogenic Cycling of 12-Inch Debond, 30- x 30-Inch Tank

The test tank was subjected to liquid nitrogen checkout followed by five 1-hour liquid hydrogen cycles. Following these cryogenic cycles, the test tank was installed on a Ling 249 shaker at Wyle Laboratory. The tank

was filled with LH_2 and allowed to stabilize for a 2-hour hold. After this, vibration tests were conducted, starting with the sinusoidal levels and finishing with random levels (Table 42).

Testing of 6-Inch Debond, 30- x 30-Inch Tank

The test tank was subjected to a 1-hour hold with LH_2 in the tank. Following the 1-hour stabilization, a vacuum was introduced in the bell jar over the 6-inch diameter debond and held for 15 minutes.

TEST RESULTS

Cryogenic strain compatibility test results are listed in Table 43. The flatwise tensile strength, density, and thermal expansion results are listed in Table 44.

The 12-inch debond test tank withstood the cryogenic cycling, aerodynamic heating, and vibration without any propagation of the debond. Figures 176 and 177 show the specimen after test and dissection, respectively.

The 6-inch debond test tank withstood the cryogenic cycling and vacuum pressure on the debond without any foam insulation failure. Figure 178 shows the test specimen after dissection.

Table 42. Vibration Levels

Sinusoidal Levels	
Z - axis (radial)	5 to 27 cps 0.3-inch double amplitude 27 to 100 cps 11.5 g peak 100 to 180 cps 0.0224-inch double amplitude 180 to 2000 cps 38.0 g peak
Random Levels	
Z - axis	20 to 2000 cps 0.6 g^2/cps

Table 43. Results of CPR 369 Spray Foam Composite Tension Tests

Specimen Number	Specimen Configuration Code	Foam Cure Prior to Test	Specimen Temperature (F)		Nominal Tensile Load (psi)	Remarks
			Metal	Top of Foam		
140A(2) (4)	FL1G	21	-423	55	73,000	Passed
141A	FL1G	21	-423	57	71,000	Failed
142A	FL1G	21	-423	73	72,400	Passed
143A	FL1G	21	-423	73	71,900	Passed
144A	FL1G	21	-423	64	71,700	Passed
145	AL1G	11	-423	71	71,700	Passed
145-1	H	11	-423	65	72,300	Passed
146	AL1G	11	-423	80	72,100	Passed
147	AL1G	11	-423	66	71,700	Passed
147-1	H	11	-423	82	71,700	Passed
148	AL1G	11	-423	73	71,700	Passed
149	AL1G	11	-423	53	71,700	Passed
156	GL1G	9	-423	73	70,500	Passed
157	GL1G	9	-423	91	71,400	Passed
158	GL1G	9	-423	71	71,100	Passed
159	GL1G	9	-423	64	71,200	Passed
160	GL1G	9	-423	73	71,200	Passed
161	BL1G	11	-423	31	70,600	Passed
162	BL1G	11	-423	84	71,100	Passed
163	BL1G	11	-423	95	70,800	Passed
164	BL1G	11	-423	78	70,800	Passed
165	BL1G	11	-423	87	71,500	Passed

Table 43. Results of CPR 369 Spray Foam Composite Tension Tests (Cont)

Specimen Number	Specimen Configuration Code	Foam Cure Prior to Test	Specimen Temperature (F)		Nominal Tensile Load (psi)	Remarks
			Metal	Top of Foam		
166	BL1G	11	-423	77	71,400	Passed
167	BL1G	11	-423	71	70,300	Passed
168	BL1G	11	-423	62	72,200	Passed
169	BL1G	11	-423	61	71,200	Passed
170	BL1G	11	-423	80	71,100	Passed
171	CL1G	9	-423	100	71,100	Passed
172	CL1G	9	-423	77	71,100	Passed
173	CL1G	9	-423	91	71,000	Passed
174	CL1G	9	-423	87	70,600	Passed
175	CL1G	9	-423	69	71,200	Passed
176	DL1G	11	-423	68	71,400	Passed
177	DL1G	11	-423	91	72,000	Passed
178	DL1G	11	-423	68	71,400	Passed
179	DL1G	11	-423	60	71,600	Passed
179-1	B		-423	69	71,700	Passed
180	DL1G	11	-423	57	72,300	Passed
180-1	B		-423	61	71,800	Passed
181	HL1G	17	-418	478	71,000	Passed
182	HL1G	17	-423	337	71,000	Passed
183	HL1G	17	-423	467	73,000	Passed

Table 43. Results of CPR 369 Spray Foam Composite Tension Tests (Cont)

Specimen Number	Specimen Configuration Code	Foam Cure Prior to Test	Specimen Temperature (F)		Nominal Tensile Load (psi)	Remarks
			Metal	Top of Foam		
226	AM1B	12	-423	62	71,000	Passed
227	AM1B	12	-423	49	71,300	Passed
228	AM1B	12	-423	41	70,000	Passed
229	AM1B	12	-423	73	70,900	Passed
230	AM1B	12	-423	78	71,700	Failed (4)
231	AM2B	10	-423	83	71,700	Passed
232	AM2B	10	-423	82	72,700	Failed (4)
233	AM2B	10	-423	84	72,500	Passed
234	AM2B	10	-423	62	72,400	Failed (4)
235	AM2B	10	-423	81	72,000	Passed
236	AM1L	15	-423	80	71,000	Passed
237	AM1L	15	-423	111	71,000	Passed
238	AM1L	15	-423	75	71,000	Passed
239	AM1L	15	-423	97	71,000	Passed
240	AM1L	15	-423	113	71,000	Passed
246	GM1B	24	-423	65	44,000	Passed
246-1		24	-423	101	71,000	Failed (4)
250	GM1B	24	-423	75	44,000	Passed
250-1		24	-423	66	71,000	Passed
261	AM3L	17	-423	79	44,000	Passed
261-1		17	-423	83	71,000	Passed
261-2		24	(5)	(5)	(5)	Passed

Table 43. Results of CPR 369 Spray Foam Composite Tension Tests (Cont)

Specimen Number	Specimen Configuration Code	Foam Cure Prior to Test	Specimen Temperature (F)		Nominal Tensile Load (psi)	Remarks
			Metal	Top of Foam		
262	AM3L	17	-423	77	44,000	Passed
262-1		17	-423	73	71,000	Passed
262-2		24	(5)	(5)	(5)	Passed
263	AM3L	17	-423	89	44,000	Passed
263-1		17	-423	90	71,000	Passed
263-2		24	(5)	(5)	(5)	Passed
264	AM3L	16	-423	100	44,000	Passed
264-1		16	-423	92	71,000	Passed
264-2		23	(5)	(5)	(5)	Passed
265	AM3L	16	-423	98	44,000	Passed
265-1		17	-423	97	71,000	Passed
265-2		23	(5)	(5)	(5)	Passed
275	AM4B	14	-423	90	71,000	Passed
276	AM4L	10	-423	98	44,000	Passed
276-1		10	-423	95	71,000	Failed
277	AM4L	10	-423	103	44,000	Passed
277-1		10	-423	50	71,000	Passed
278	AM4L	10	-423	80	44,000	Passed
278-1		10	-423	91	71,000	Passed
279	AM4L	10	-423	91	44,000	Passed
279-1		10	-423	80	71,000	Passed
280	AM4L	10	-423	106	44,000	Passed
280-1		10	-423	104	71,000	Passed

Table 43. Results of CPR 369 Spray Foam Composite Tension Tests (Cont)

Specimen Number	Specimen Configuration Code	Foam Cure Prior to Test	Specimen Temperature (F)		Nominal Tensile Load (psi)	Remarks
			Metal	Top of Foam		
336	AM2L	41	-423	96	71,000	Passed
337	AM2L	41	-423	97	71,000	Passed
338	AM2L	41	-423	110	71,000	Passed
339	AM2L	41	-423	105	71,000	Passed
118-1	(6)		-423	-184	34,000	Passed
118-2			-423	-221	71,000	Passed
119-1	(6)		-423	-192	34,000	Passed
119-2			-423	-205	71,000	Passed
194-1	(6)		-423	-196	34,000	Passed
194-2			-423	-200	71,000	Passed
195-1	(6)		-423	-204	34,000	Passed
195-2			-423	-206	71,000	Passed

Notes:

(1) Foam and metal temperature at peak stress of nominal 71,000 psi. The maximum foam temperature, prior to application of tension stress, was 495 F, 450 F, 503 F for specimens 181, 182, and 183, respectively.
(2) Failure occurred at one end of the specimen, not in the closeout area.
(3) Specimens visually examined in test fixture for radial cracks. Since these specimens were not removed from the test fixture, only 10 to 15 minutes were required to recool the metal to -423 F.
(4) Failure is defined as a debond between the metal and the foam associated with a full depth radial crack.
(5) These tests were cycling: 5 cycles at room temperature at 56,000 psi; 40 cycles at -423 F at 34,000 psi; and one cycle at -423 F at 71,000 psi.
(6) Specimens were tested during development and modified as shown in Figure 213.

Table 44. Foam Physical Properties Data

Specimen Group	Test Temperature (F)	Flatwise Tensile Strength (psi)		Apparent Modulus Range (psi)	Density (lb/ft^3)	Thermal Expansion (in./in./F x 10^{-5})
		Range	Average			
FL1G	75	70 to 91	80	2,690 to 4,050	2.9	3.7
FL1G	-423	53 to 65	58	5,090 to 8,570		
AL1G	75	73 to 90	84	2,940 to 4,230	3.3	
AL1G	-423	53 to 77	62	6,200 to 9,540		
GL1G	-423	45 to 59	49	7,150 to 9,510	2.83	3.6
BL1G	75	87 to 96	93	2,750 to 4,750	2.92	4.0
BL1G	-423	52 to 67	61	6,000 to 9,620		
BL1G	75	76 to 87	80	3,570 to 3,900	2.86	
BL1G	-423	54 to 66	56	6,740 to 8,307		
CL1G	75	56 to 95	76	2,900 to 5,300	2.84	
CL1G	-423	47 to 63	54	5,580 to 11,660		
DL1G	75	73 to 86	82	3,520 to 4,620	2.87	
DL1G	-423	45 to 59	49	7,150 to 9,520		
AL2G	75	81 to 83	82	4,180 to 4,470	2.80	
AL2G	-423	54 to 74	61	3,900 to 9,320		
AL3G	75	67 to 75	72	3,201 to 3,650	2.79	
AL3G	-423	48 to 58	53	5,020 to 7,850		
AM1B	75	96 to 103	100	4,350 to 4,690	3.08	
AM1B	-423	56 to 68	62	10,400 to 11,070		
AM2B	75	94 to 108	102	4,000 to 4,920	3.19	3.6
AM1L	75	96 to 117	102	4,590 to 5,330	3.25	
AM1L	-423	48 to 76	66	10,870 to 11,320		
GM1B					3.0	3.15

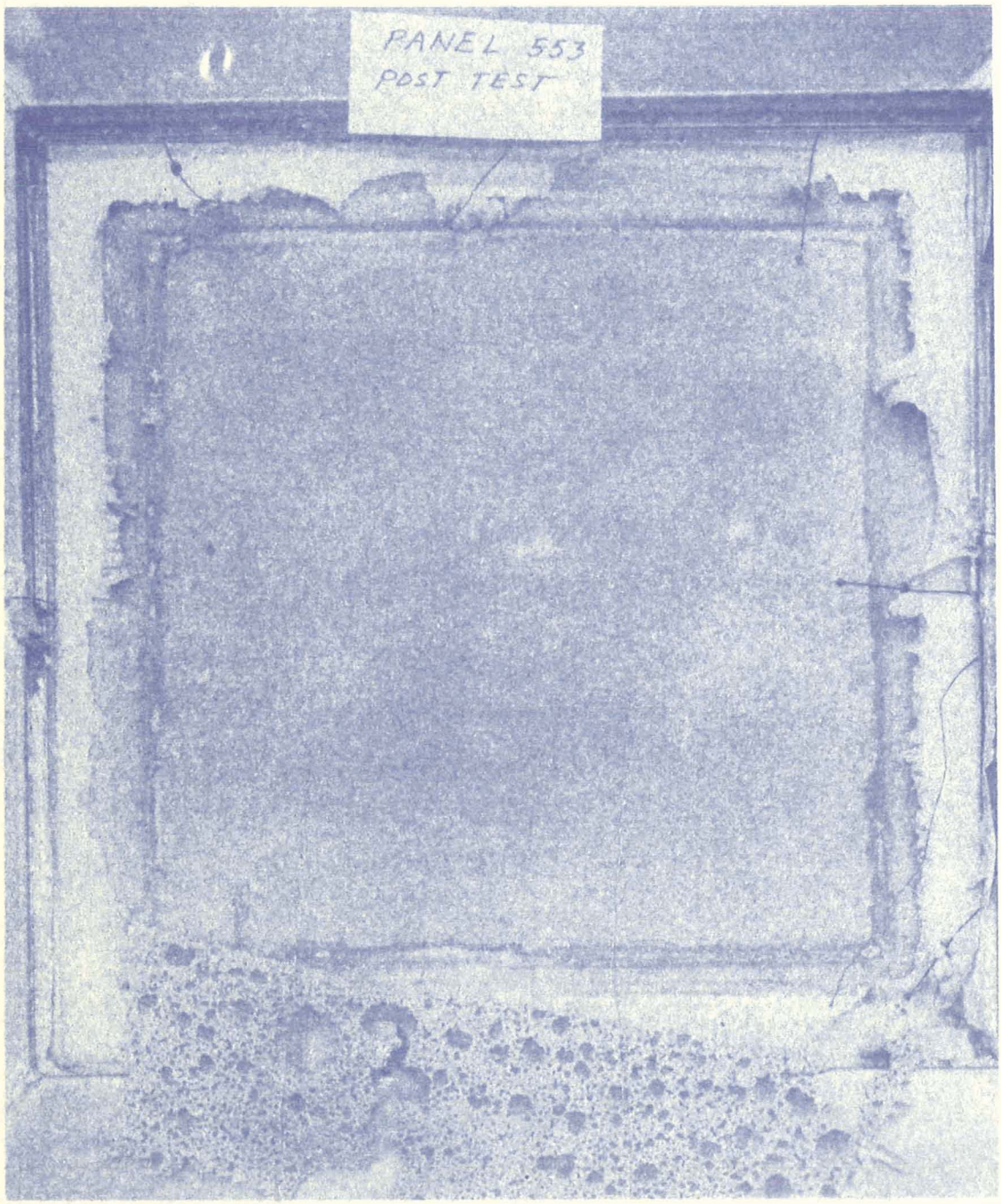

7006-81-2345I

Figure 176. Twelve-Inch Debond 30-x 30-Inch Tank After Test

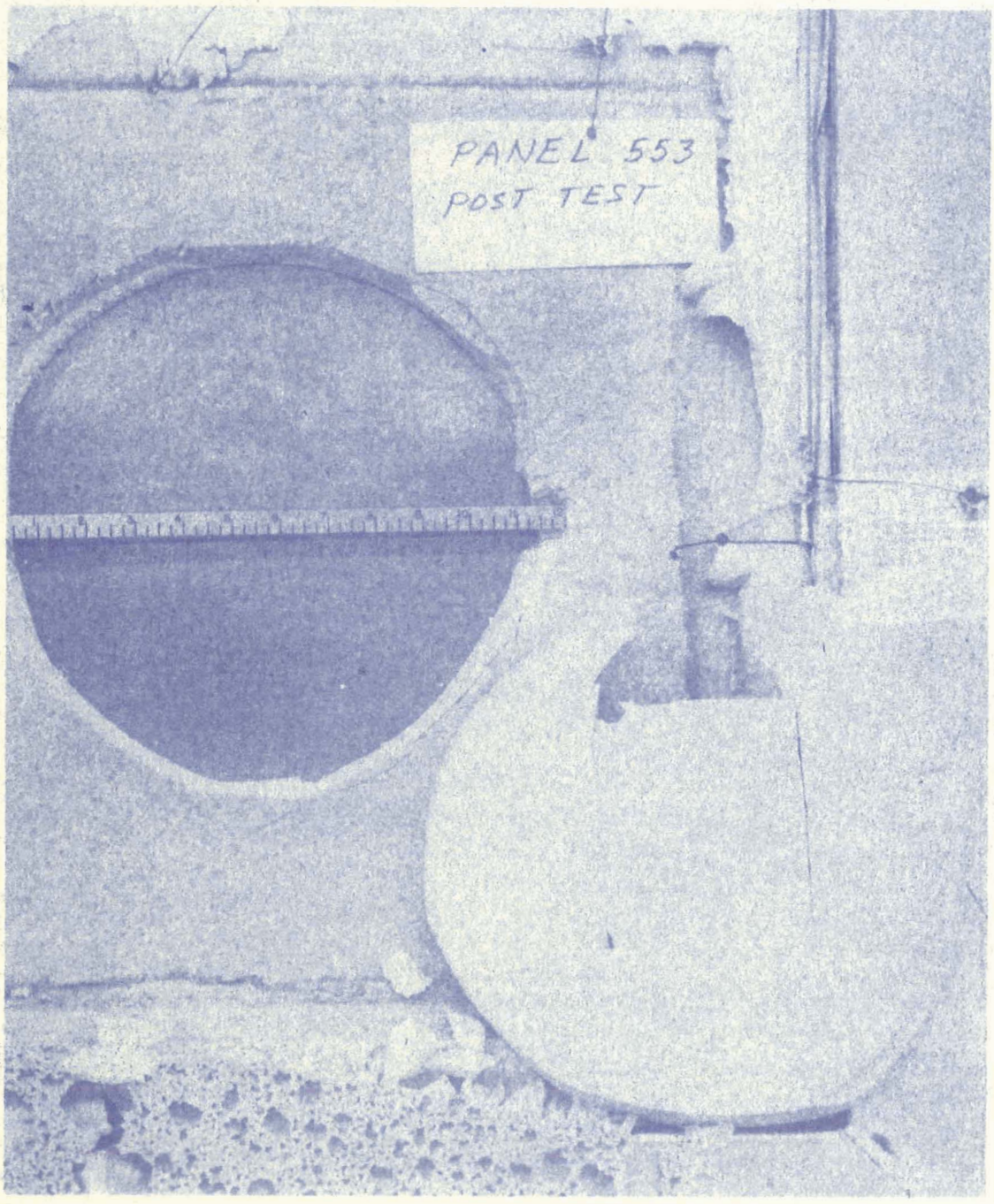

7006-81-2345D

Figure 177. Twelve-Inch Debond 30-x 30-Inch Tank After Dissection

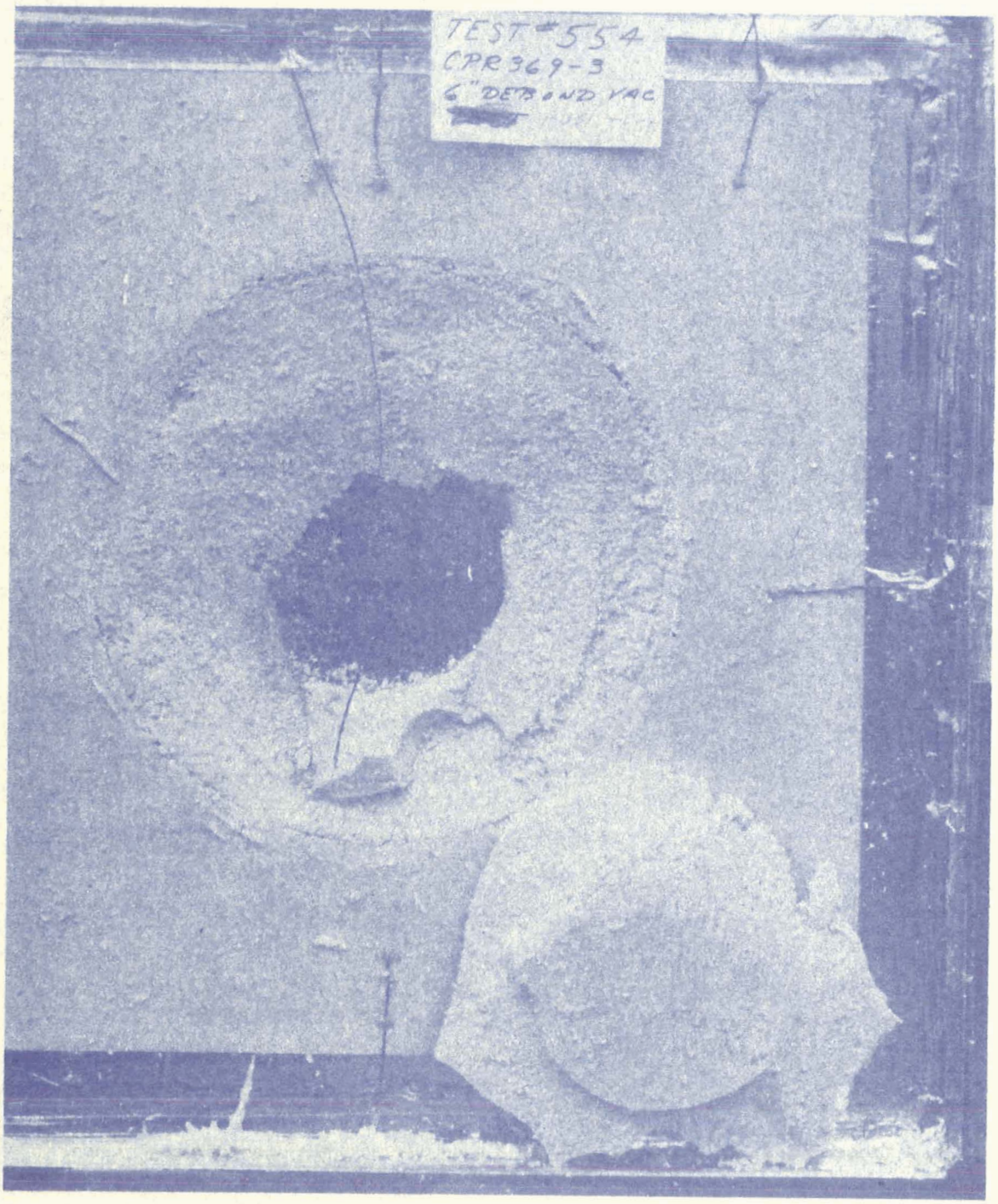

7006-81-2345F

Figure 178. Six Inch Debond 30-x 30-Inch Tank After Dissection

DETERMINATION OF MAXIMUM TEMPERATURE LIMITATIONS OF SPRAY-FOAM INSULATION

INTRODUCTION

During boost, the S-II hydrogen tank insulated surface will be exposed to elevated temperatures ranging from 525 to 925 F (with heat inputs to all areas varying from 0.18 to 0.22 Btu/ft^2/sec). The smooth-wall insulation surface that comprises the greater part of the structure will be exposed to maximum temperatures of approximately 525 F. Predicted peak temperatures for protuberance areas are from 650 to 925 F.

Combined environmental tests, consisting of LH_2 cycling and exposure to 525 F, have been conducted on the insulation composite, polyurethane foam sealed with a moisture barrier coating. Analysis of the test results by S-II Engineering indicated questionable performance at the 525 F temperature. Because of the predicted hot spots on protuberance areas, the Hypalon-coated foam insulation was tested at 625 to 925 F to determine its maximum temperature limitations.

Testing was conducted on Hypalon-coated polyurethane spray foam and similar specimens for comparison analysis purposes.

CONCLUSIONS

The Hypalon-coated spray foam insulation, tested under estimated heat fluxes of 0.36 Btu/ft^2/sec at 625 F to 0.88 Btu/ft^2/sec at 925 F, did not meet the requirements specified by Saturn S-II Engineering.

The ballooning of the Hypalon during exposure to simulated S-II environmental boost conditions posed a question as to whether large pieces of this material would become detached and endanger antenna functions during the flight of the S-II stage.

Cork, 0.040-inch thick, bonded to the foam did not provide adequate foam insulation protection through the predicted temperature profile for the S-II stages in the hot zone areas.

Fabrication of Test Specimens

Aluminum plates, 2014-T6 1/4-inch thick, were etched to comply with MA0110-024 and primed with M-602, MB0120-032 primer. They were then

cured for three hours at 290 F and primed with Primer M, MB0120-042. The plates were then sprayed with CPR 369-3, MB0130-075 foam to a thickness of 2 to 3 inches. Following a 24-hour cure, the foam was machined to a thickness of 0.75 inch. The surface of the foam was then vacuumed to remove the loose foam particles, and the foamed plates were cut to 6- x 10-inch individual specimen sizes.

Specimen configurations were prepared as shown in Figure 179 and as described below:

Unprotected foam—These specimens were not coated and were used as control specimens.

Cork insulation foam—MB0130-020, Type I, 0.040-inch thick cork was bonded to the foam surface with Epon 934, MB0120-008.

Hypalon-coated foam—Hypalon EC-2241 was applied to the foam surface to a nominal thickness of 0.020 inch according to MA0608-014. The coating was air-dried beyond the 7-day minimum requirement before testing.

Ablative-coated foam—Desoto Corporation Korotherm 13732, a low-temperature ablative compound, was applied to the foam surface using a De Vilbis Type JGA-5024 pressure cap spray gun to a nominal thickness of 0.040-inch.

Test Procedures

The specimens were tested in an altitude chamber with the evacuation simulating an altitude of approximately 200,000 feet or about 0.2 Torr. The heat source used was a radiant strip heater. The test setup schematic is shown in Figure 180.

Surface temperatures were monitored by control thermocouples affixed to the specimen edge in the same plane as the surface of the specimens. This was done so that the ballooning of the coating anticipated during the temperature profile would not mask off the thermocouple from the radiant heat source.

TEST RESULTS

Cork-Insulated Foam Specimen

Premature failure of the cork-to-foam bond, indicated by buckling of the cork, occurred at from 350 to 400 F. Following exposure to a peak temperature of 890 F, the cork was completely charred and friable. Figure 181 shows one specimen after test.

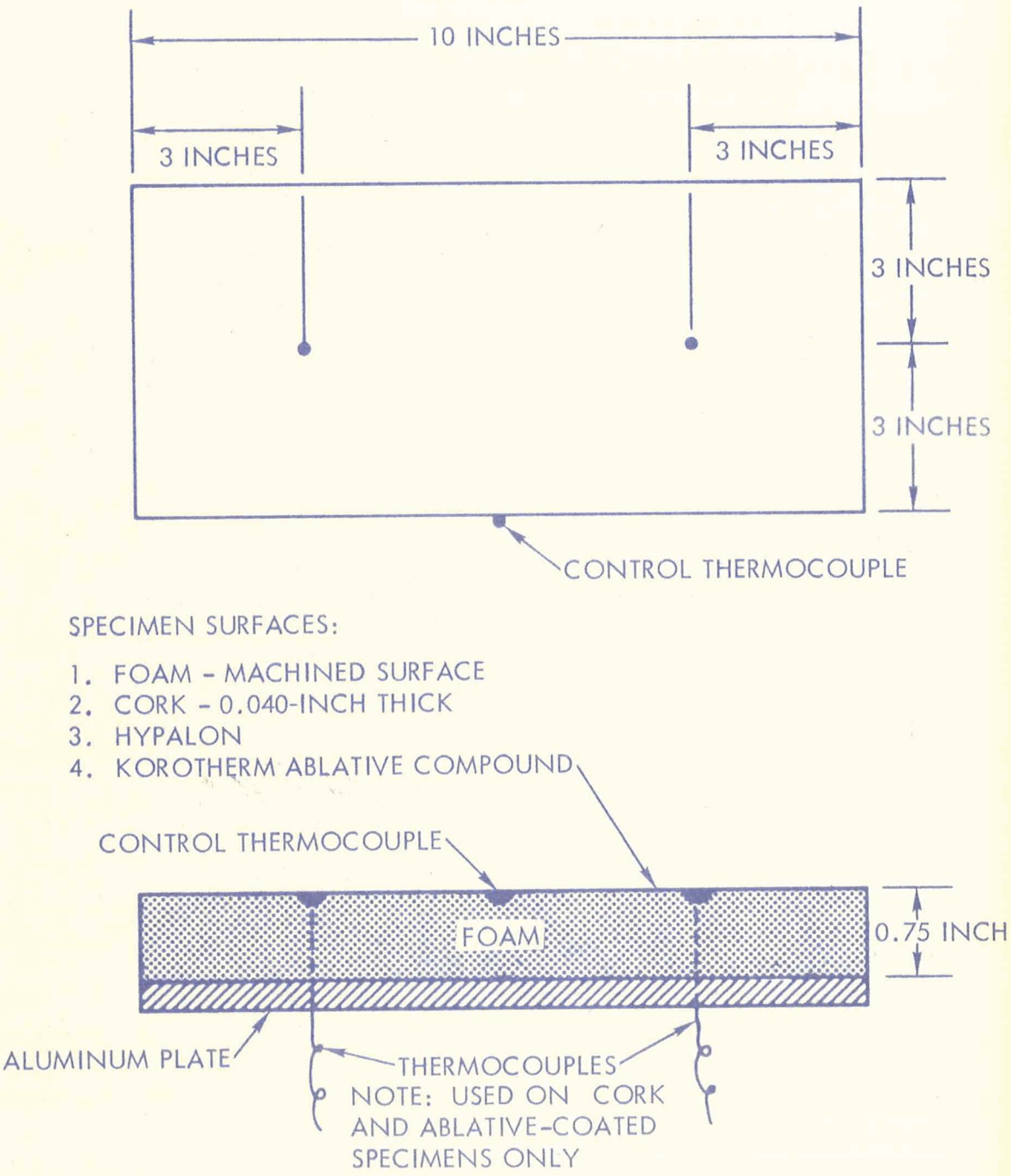

Figure 179. Typical Specimen Configuration for Determining Effect of Elevated Temperatures on Spray Foam Insulation

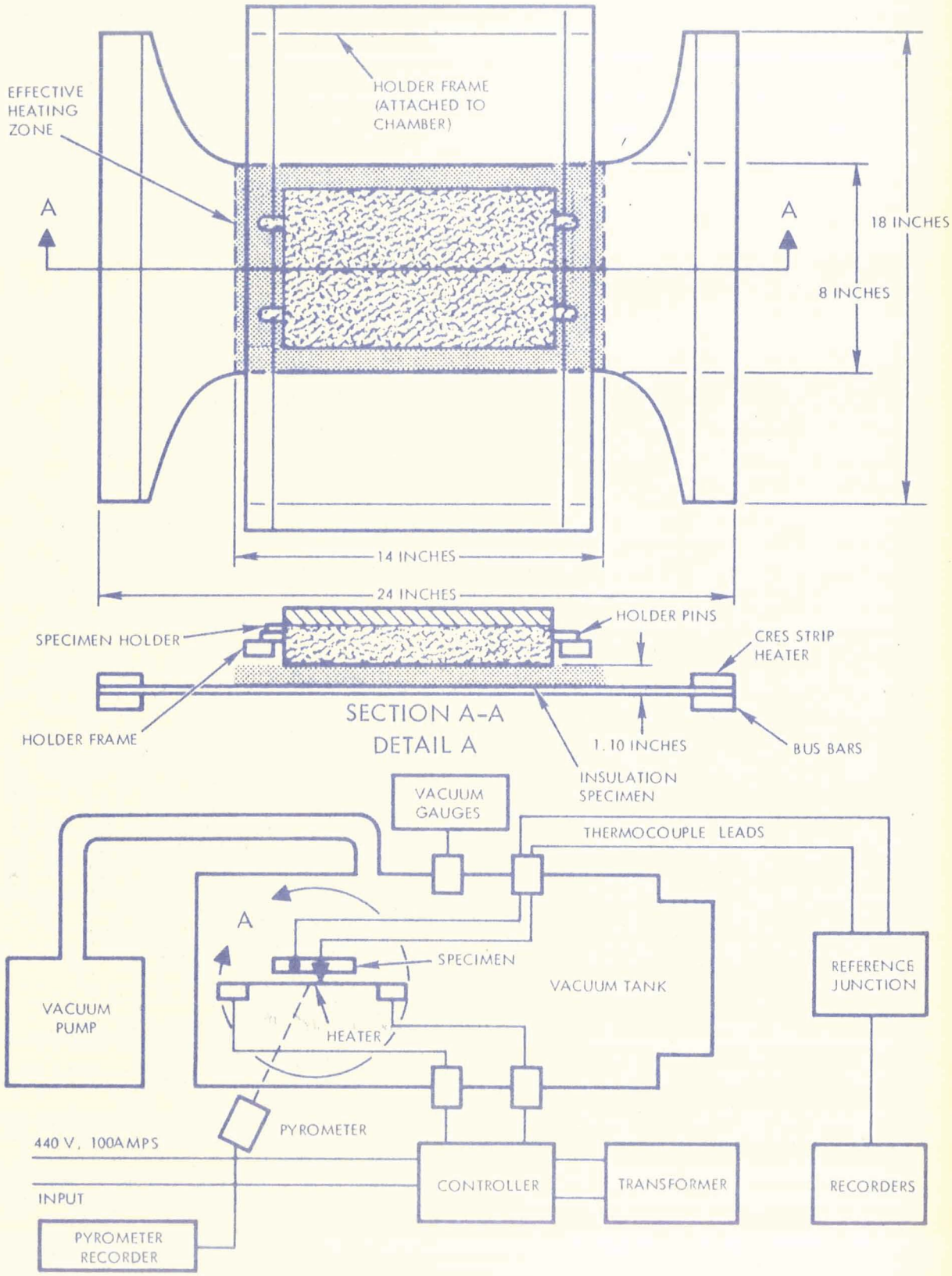

Figure 180. Radiant Heat/Altitude Chamber Test Apparatus

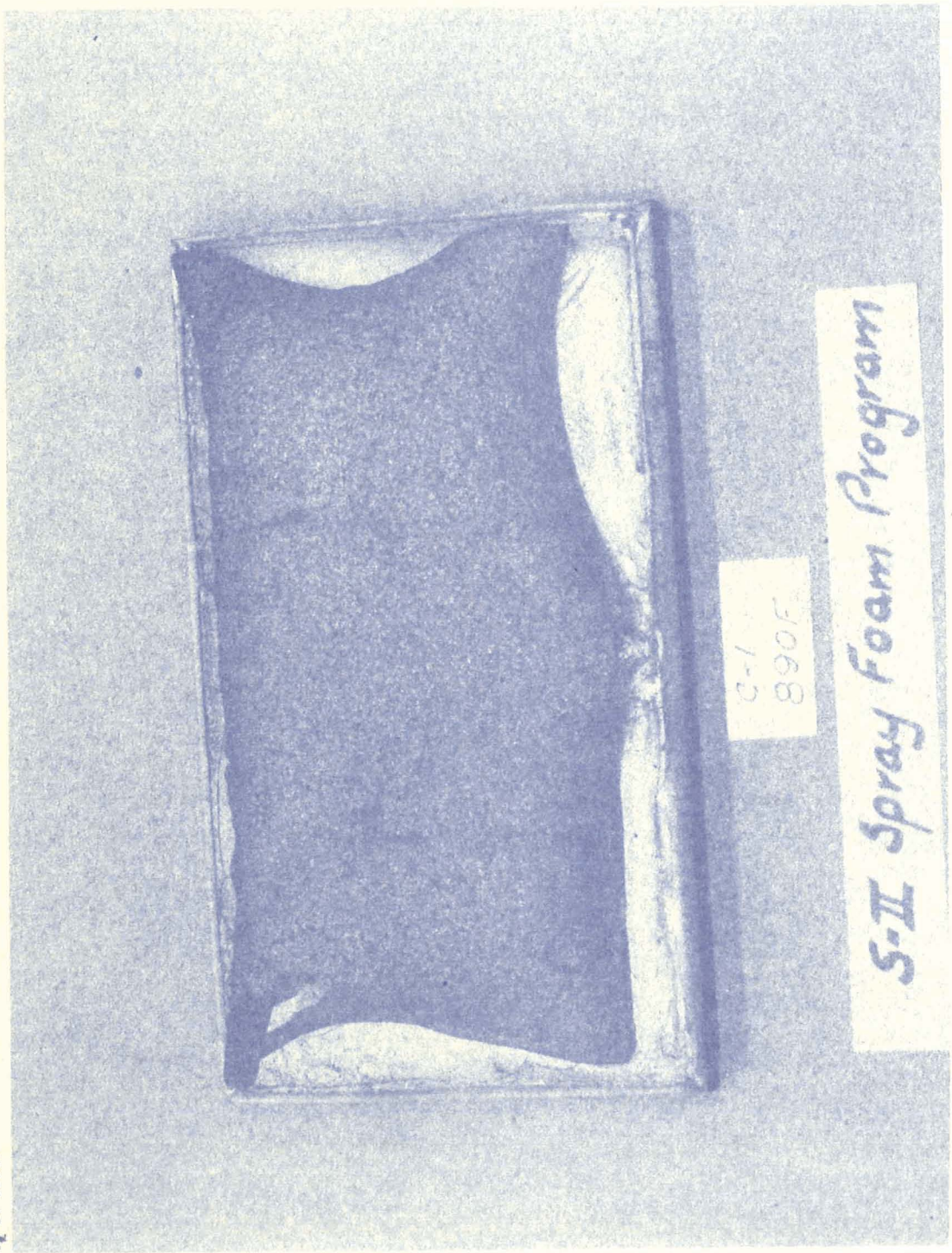

7006-81-2283B

Figure 181. Cork-Insulated Spray Foam Specimen After Exposure to Peak Temperature of 890 F

Unprotected Foam Specimens

These specimens frothed and bubbled as the temperature was increased. There was an accompanying loss of foam in various degrees, depending on the peak temperature to which the specimens were exposed. In all cases, a minimum of 0.5-inch thickness of the original 0.75-inch-thick foam layer was melted or ablated during the elevated temperature profile. Figures 182 through 186 show the specimens after test.

Hypalon-Coated Specimens

The Hypalon coating began to balloon at approximately 300 F. As the temperature increased, the bubbles burst, exposing the foam to the elevated temperatures. Subsequently, the foam melted and ablated. Figure 187 shows the blistering and subsequent rupturing of the blisters that transpired as the temperature rose to a peak temperature of 625 F. Figures 188 through 191 show the specimens after test.

Ablative-Coated Specimens

The ablative coating reacted similarly to the Hypalon, the ballooning being initiated at approximately 325 F. The coating appeared to ablate at low temperatures, becoming charred and very friable following the heat profile peak temperature of 625 F. Figure 192 shows the initiating of blistering and subsequent ballooning of the ablative coating. Figure 193 is a photograph of the specimens after the environmental testing.

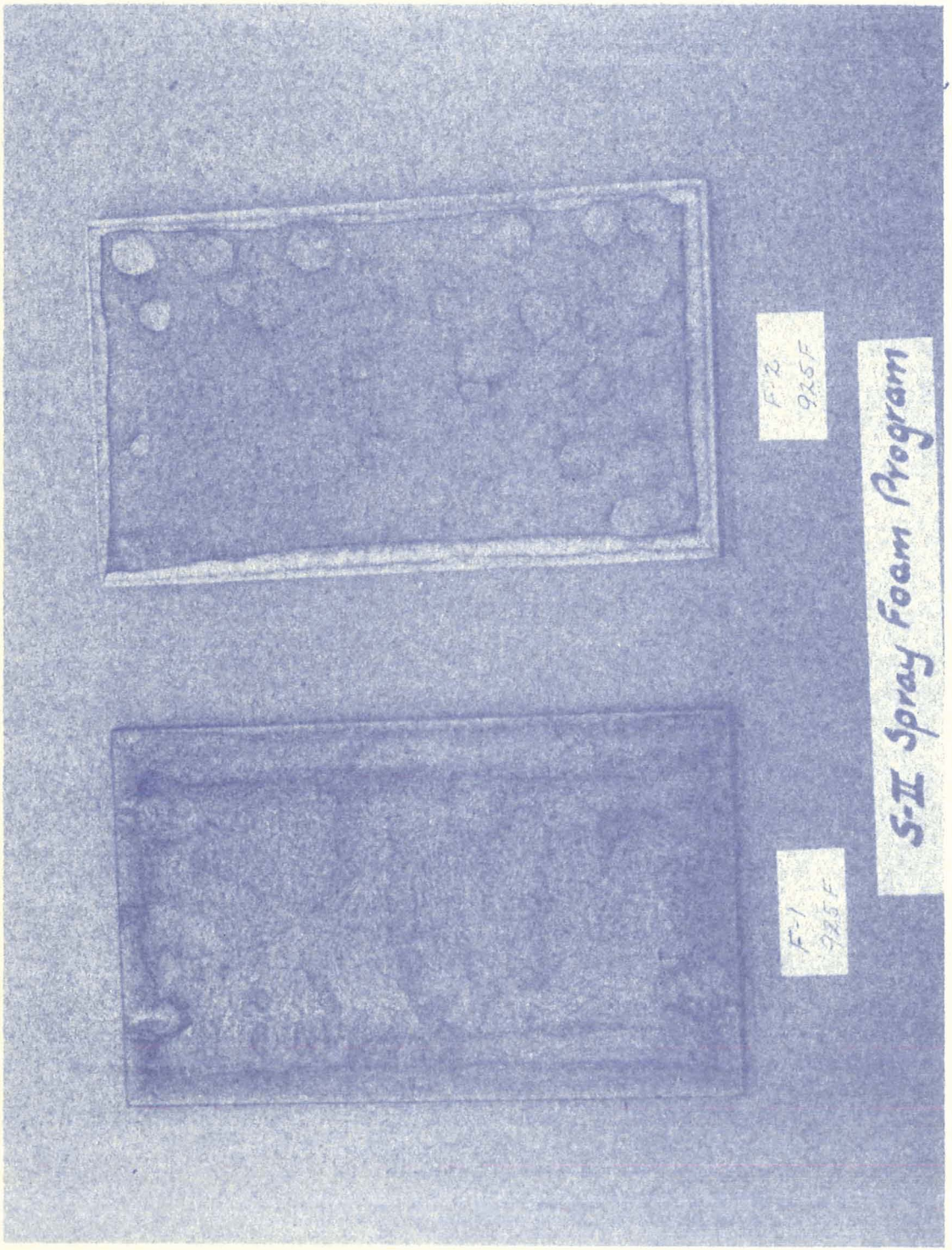

7006-81-2288H

Figure 182. CPR 369-3 Spray Foam Specimens After Environmental Testing at 925 F and 0.2-Torr Pressure

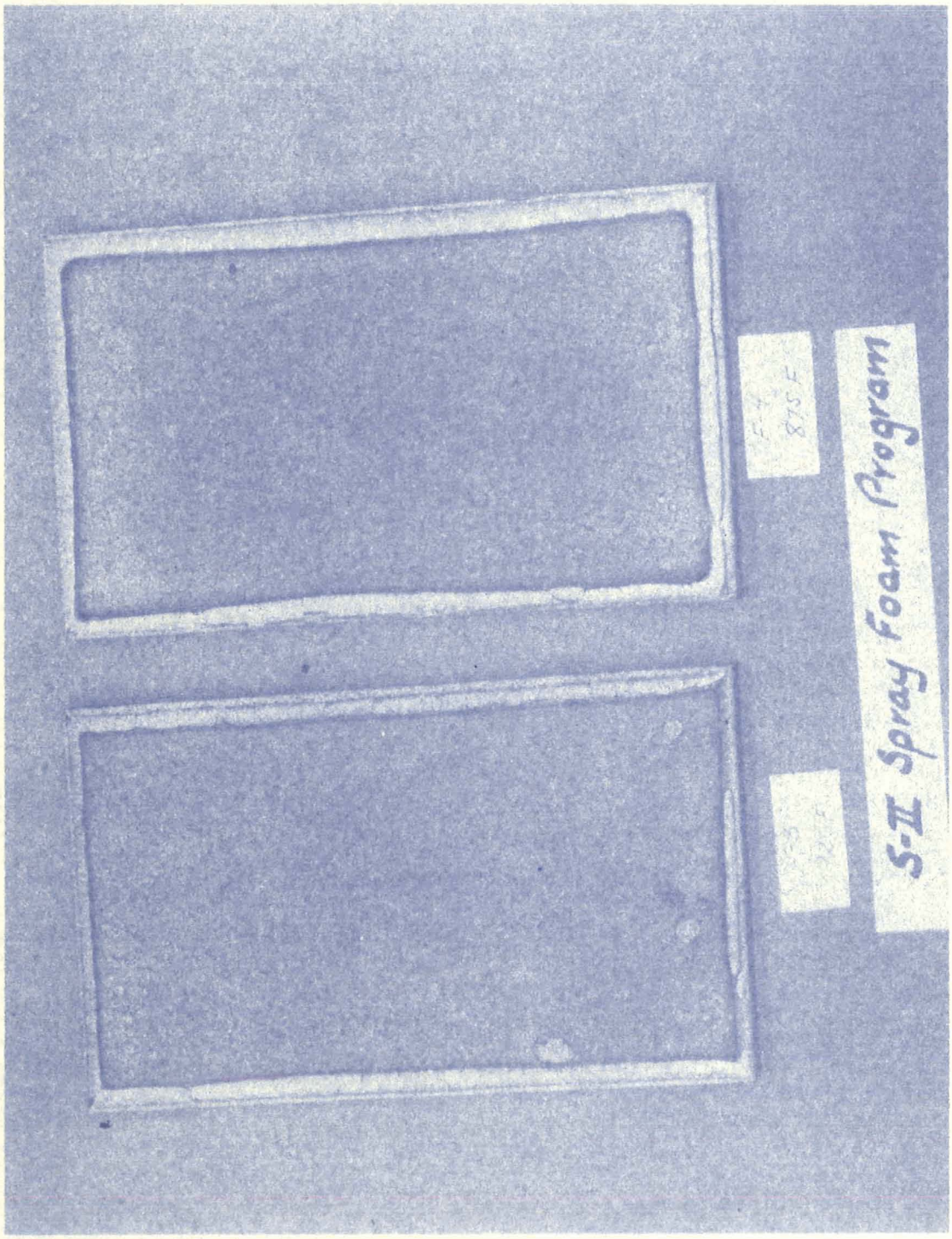

7006-81-2288F

Figure 183. CPR 369-3 Spray Foam Specimens After Environmental Testing at 875 F and 920 F at 0.2-Torr Pressure

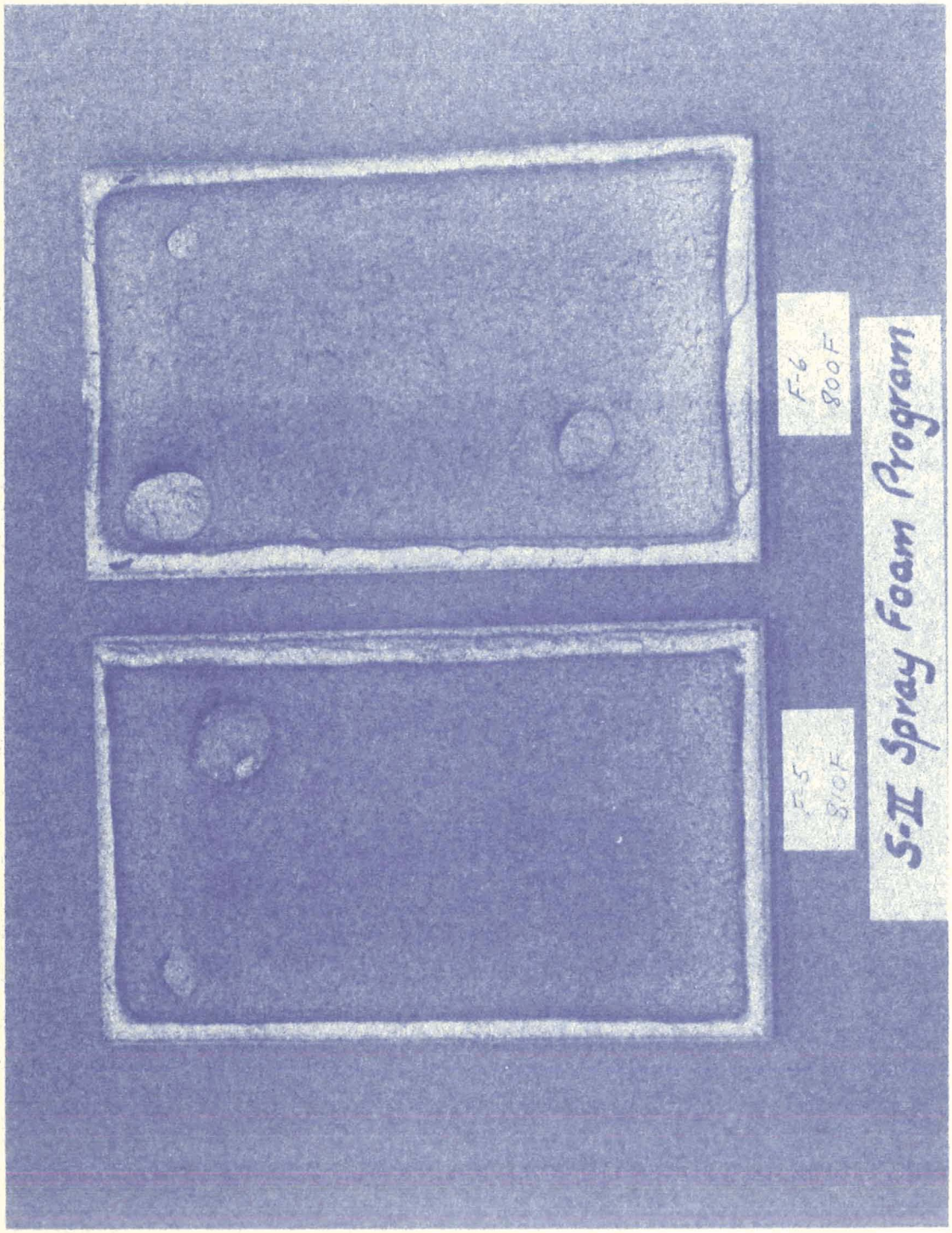

7006-81-2288E

Figure 184. CPR 369-3 Spray Foam Specimens After Environmental Testing at 800 F and 810 F at 0.2-Torr Pressure

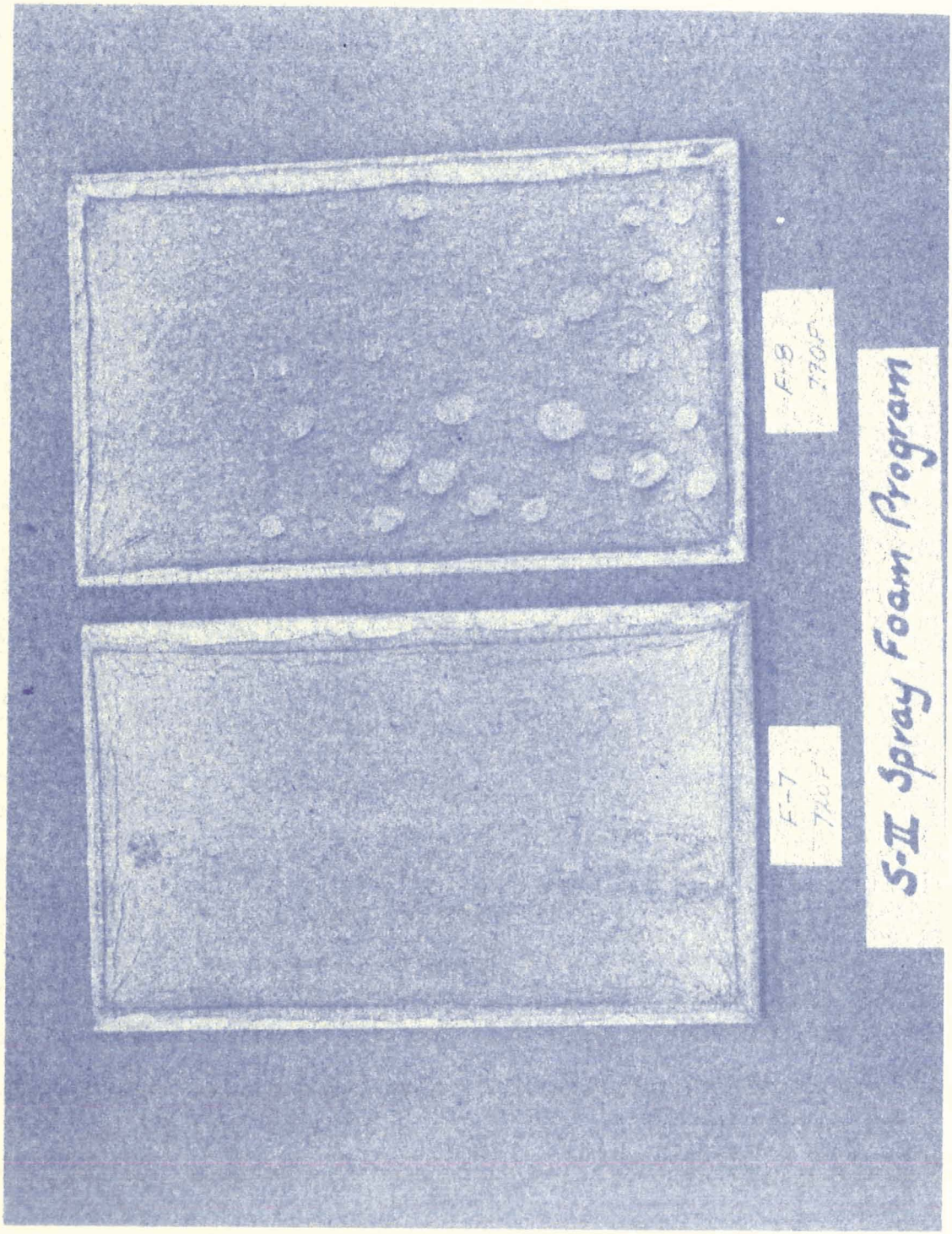

7006-81-2288D

Figure 185. CPR 369-3 Spray Foam Specimens After Environmental Testing at 720 F and 770 F at 0.2-Torr Pressure

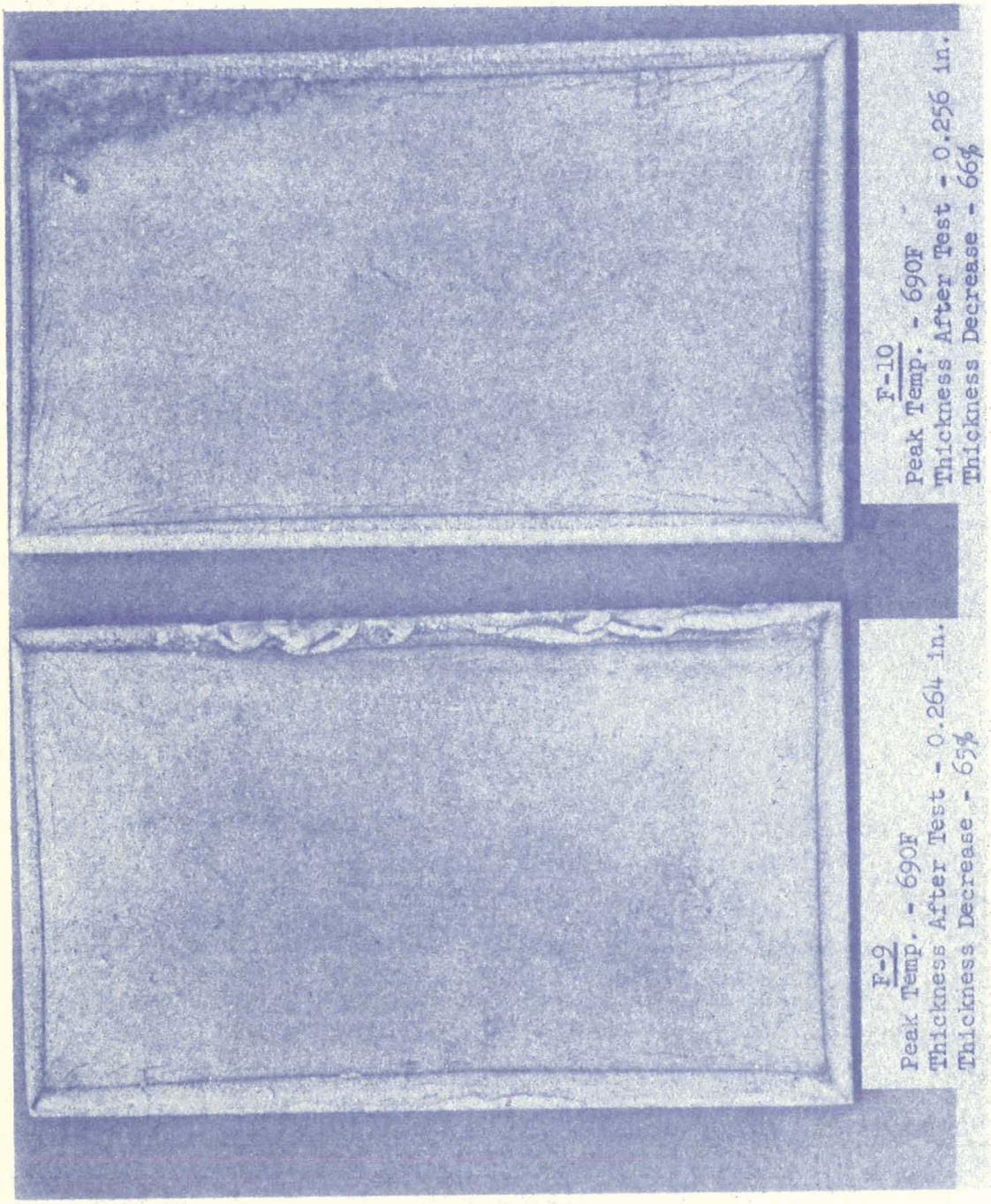

7006-81-2288C

Figure 186. CPR 369-3 Spray Foam Specimens After Environmental Testing at 690 F at 0.2-Torr Pressure

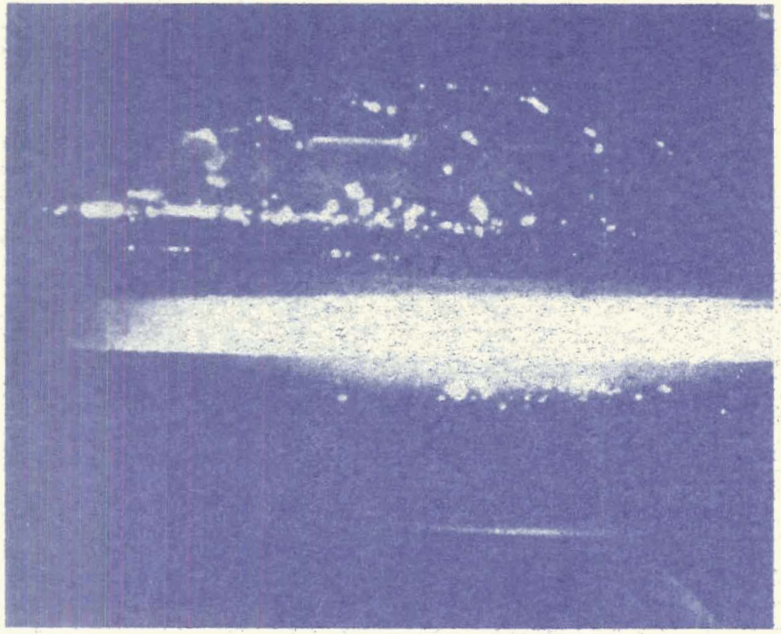

BLISTERING AND SUBSEQUENT BALLOONING OF HYPALON COATING INITIATED 45 SECONDS AFTER START OF PROFILE.
ESTIMATED TEMPERATURE CONTROL THERMOCOUPLE 275 F TO 300 F.

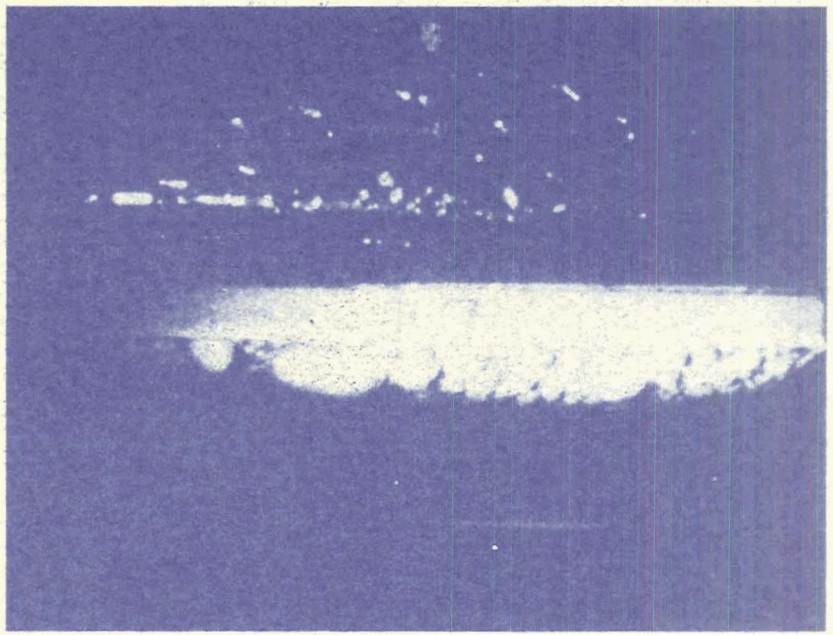

THE BLISTERS PROPAGATED AND INCREASED TO THE NUMBER AND SIZE SHOWN ABOVE ABOUT 2 SECONDS FOLLOWING RECORDER FAILURE

Figure 187. Effect of Aerodynamic Heat Profile on Hypalon-Coated Foam Specimens After Exposure to 590 F and 650 F at 0.2-Torr Pressure

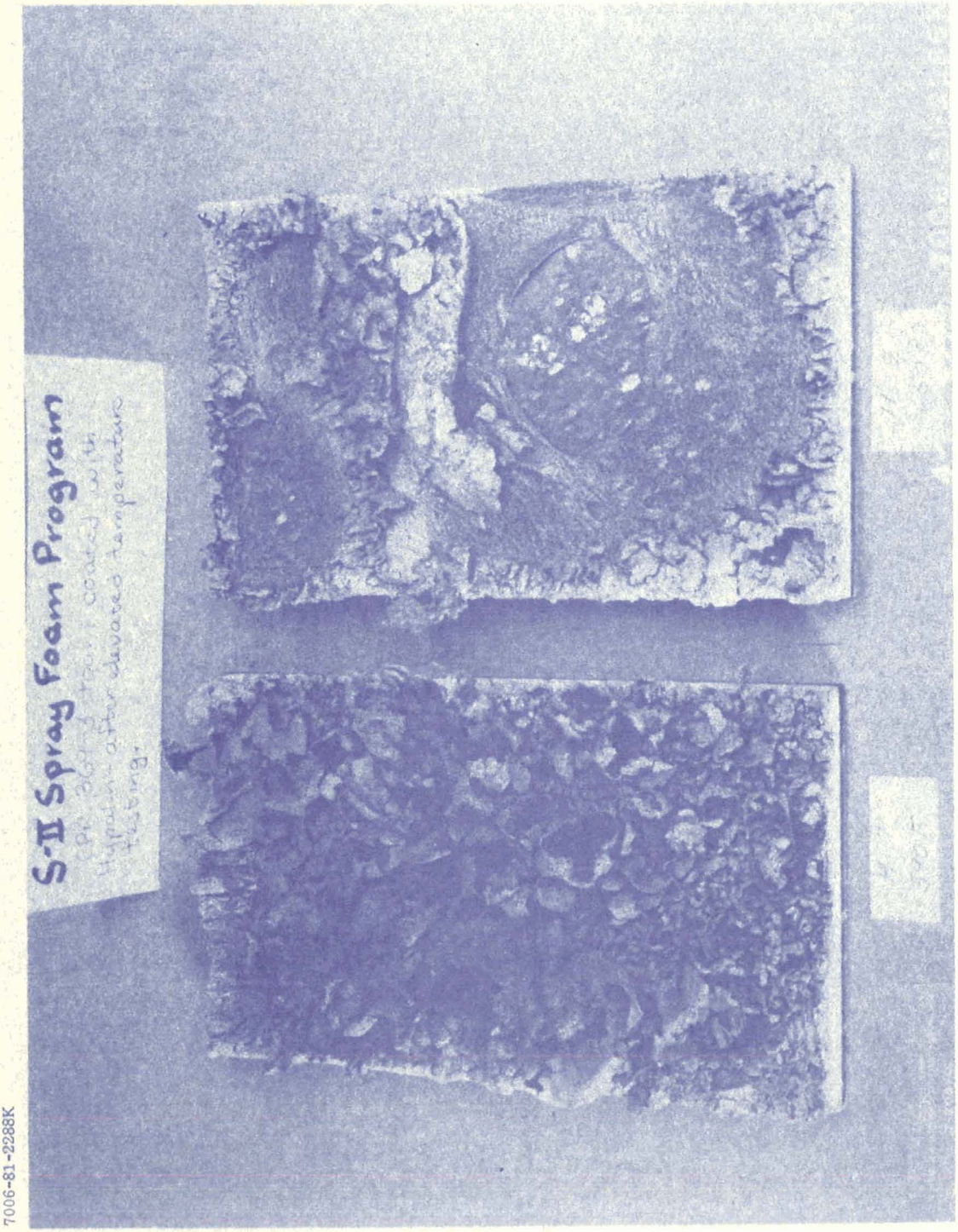

Figure 188. Hypalon-Coated Foram Specimens After Exposure to 590 F and 650 F at 0.2-Torr Pressure

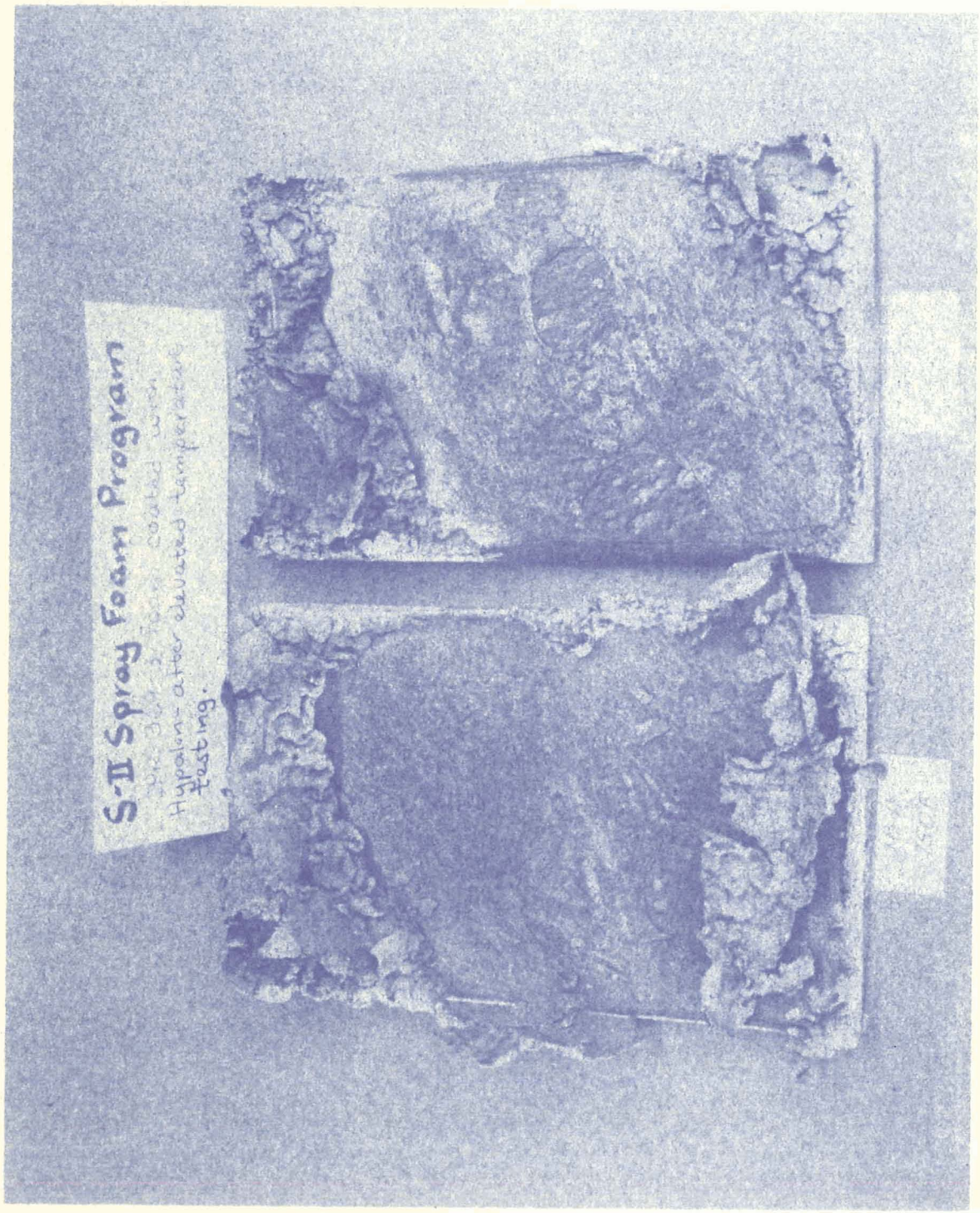

Figure 189. Hypalon-Coated Foam Specimens After Exposure to 710 F and 750 F at 0.2-Torr Pressure

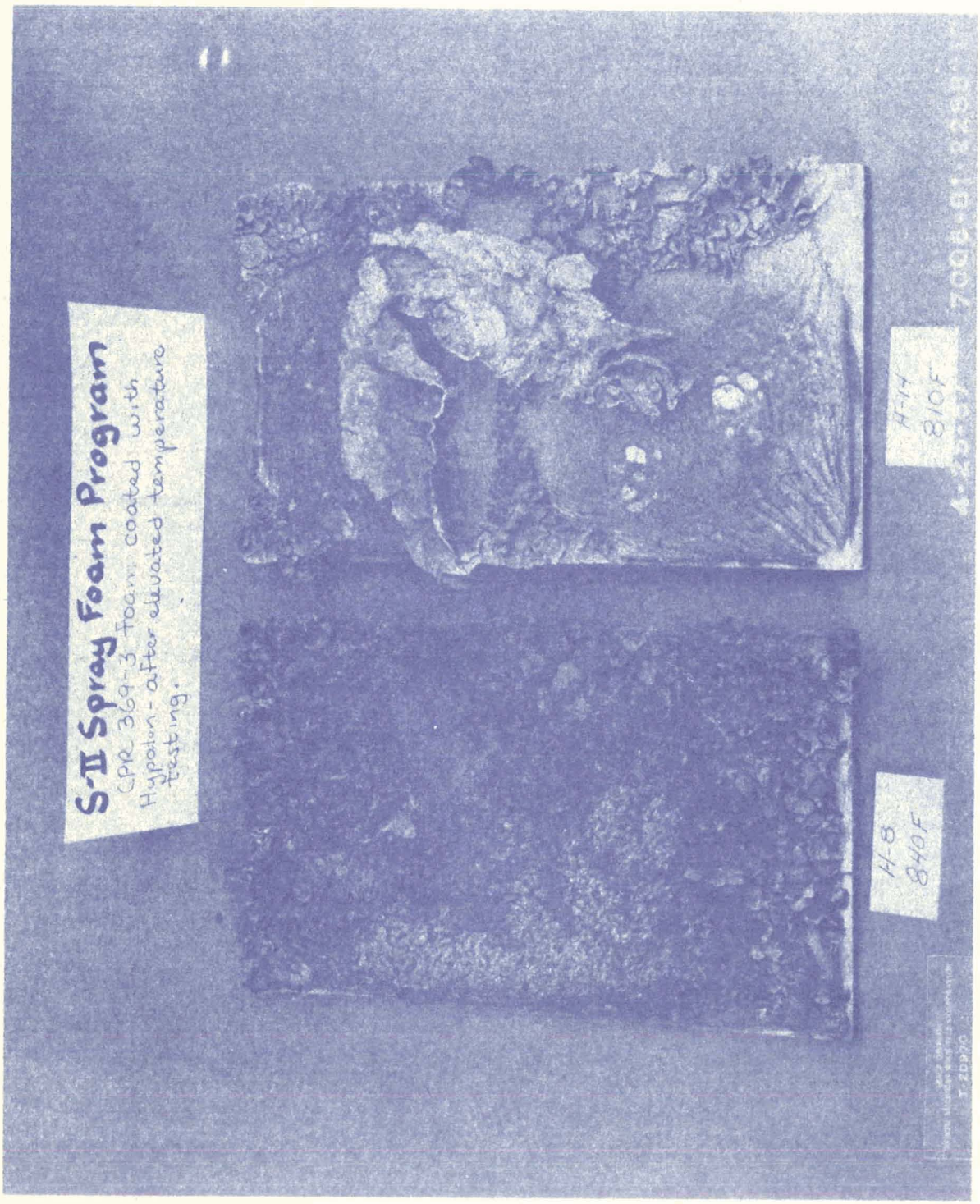

Figure 190. Hypalon-Coated Foam Specimens After Exposure to 810 F and 820 F at 0.2-Torr Pressure

7000-81-2286I

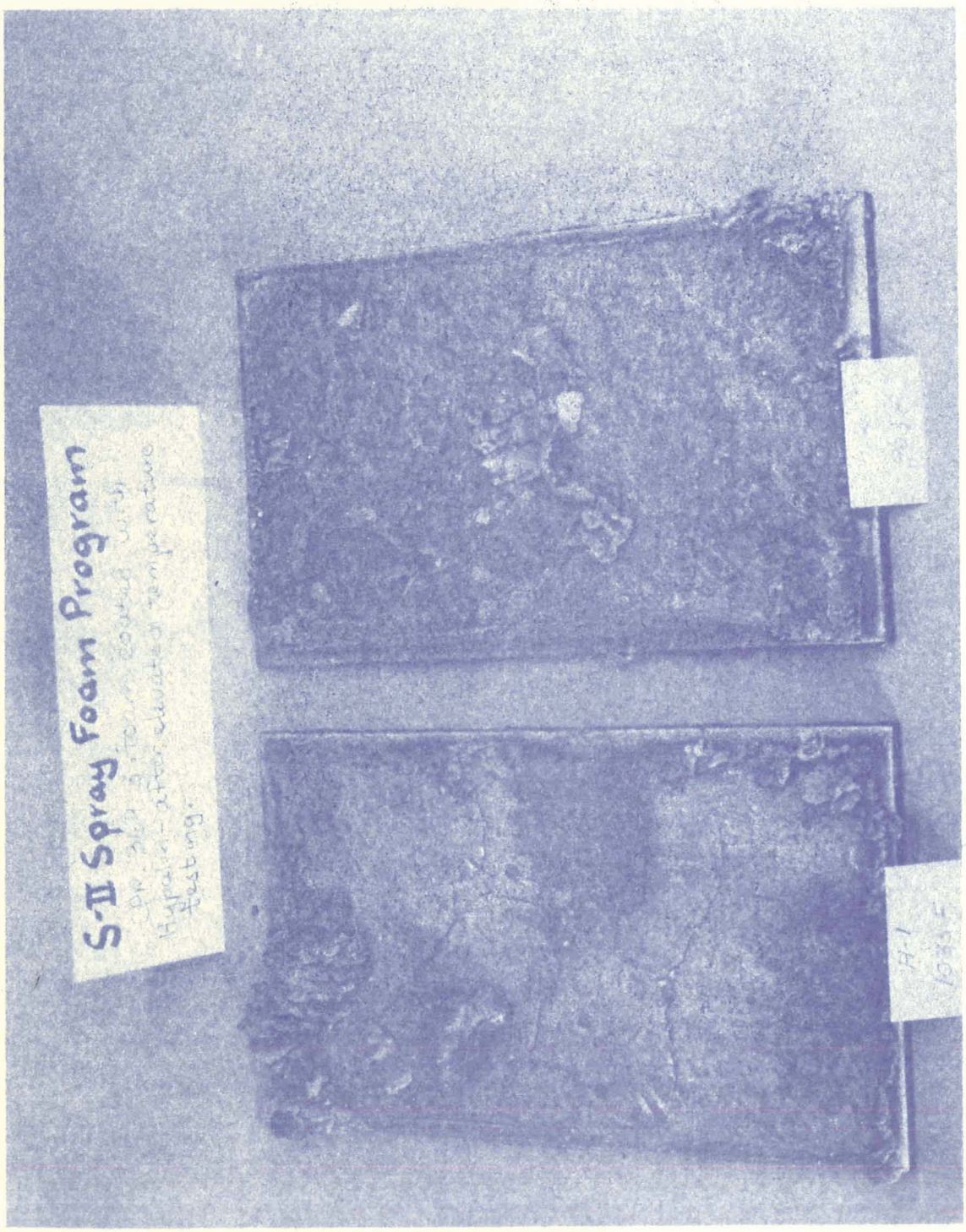

7006-81-2288G

Figure 191. Hypalon-Coated Foam Specimens After Exposure to 930 F and 1035 F at 0.2-Torr Pressure

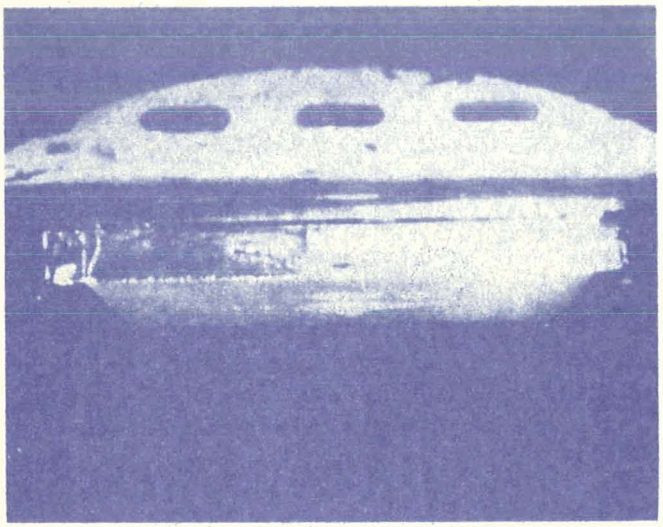

BLISTERING AND SUBSEQUENT BALLOONING OF ABLATIVE COATING INITIATED 48 SECONDS AFTER START OF PROFILE:
CONTROL THERMOCOUPLE - 340 F
THERMOCOUPLES AT SURFACE OF FOAM 1 - 280 F
(INTERFACE OF FOAM AND COATING) - 2 - 290 F

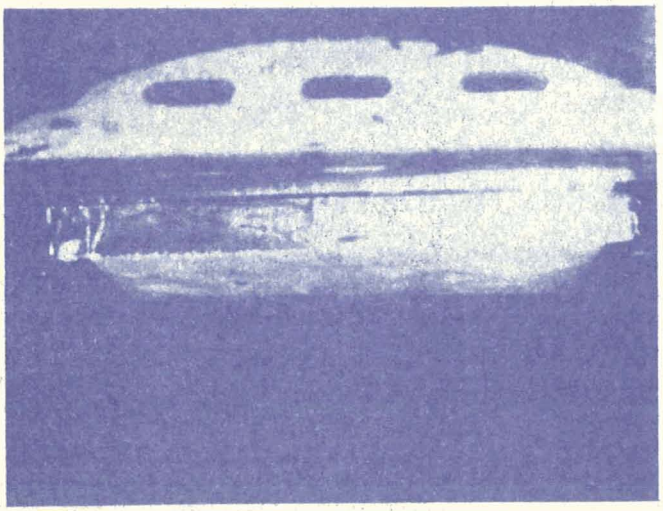

RUPTURING OF THE LARGE BLISTER ON THE ABLATIVE COATING OCCURRED AT:
TIME FROM START OF PROFILE - 58 SECONDS
CONTROL THERMOCOUPLE - 520 F
THERMOCOUPLES AT FOAM SURFACES: 1 - 380 F
(INTERFACE OF FOAM AND COATING) 2 - 355 F

Figure 192. Effect of Aerodynamic Heat Profile on Ablative-Coated CPR 369-3 Spray Foam in 0.2-Torr Pressure

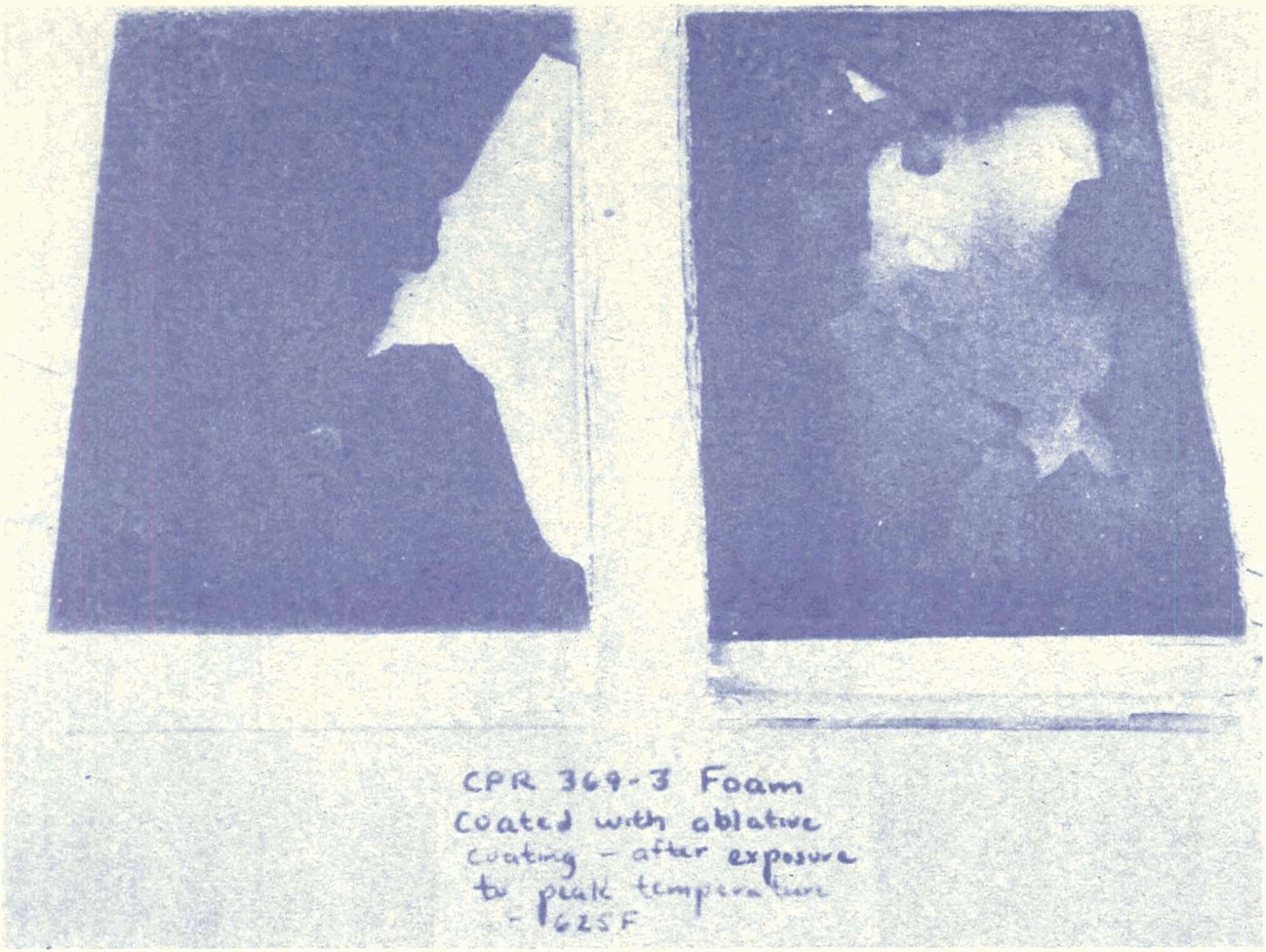

Figure 193. Ablative-Coated CPR 369-3 Spray Foam Specimens After Environmental Testing at 625 F and 0.2-Torr Pressure

SPACE DIVISION OF NORTH AMERICAN ROCKWELL CORPORATION

QUALIFICATION TESTS OF SPRAYABLE POLYURETHANE FOAM INSULATION (CPR 369-3) FOR S-II TANK SIDEWALL

INTRODUCTION

Qualification tests (i.e., cryogenic cycling and combined environments of aerodynamic heat and vibration) were conducted on specimens fabricated by S-II Manufacturing to demonstrate the capability to apply spray-on foam insulation for sidewall configuration and closeout configuration to a process specification.

CONCLUSION

The spray-on foam insulation test panels exhibited satisfactory insulative properties during combined environment testing of cryogenic cycling, vibration, and aerodynamic heating and demonstrated manufacturing capability to apply spray-on foam insulation for sidewall application.

RESULTS

Except for the aerodynamic heat wrinkling of the coatings of each 30- x 30-inch test tank spray foam specimen, there was no visual evidence of structural changes resulting from cryogenic cycles or vibration as indicated by Figures 194 through 197 showing conditions of the specimens before and after test.

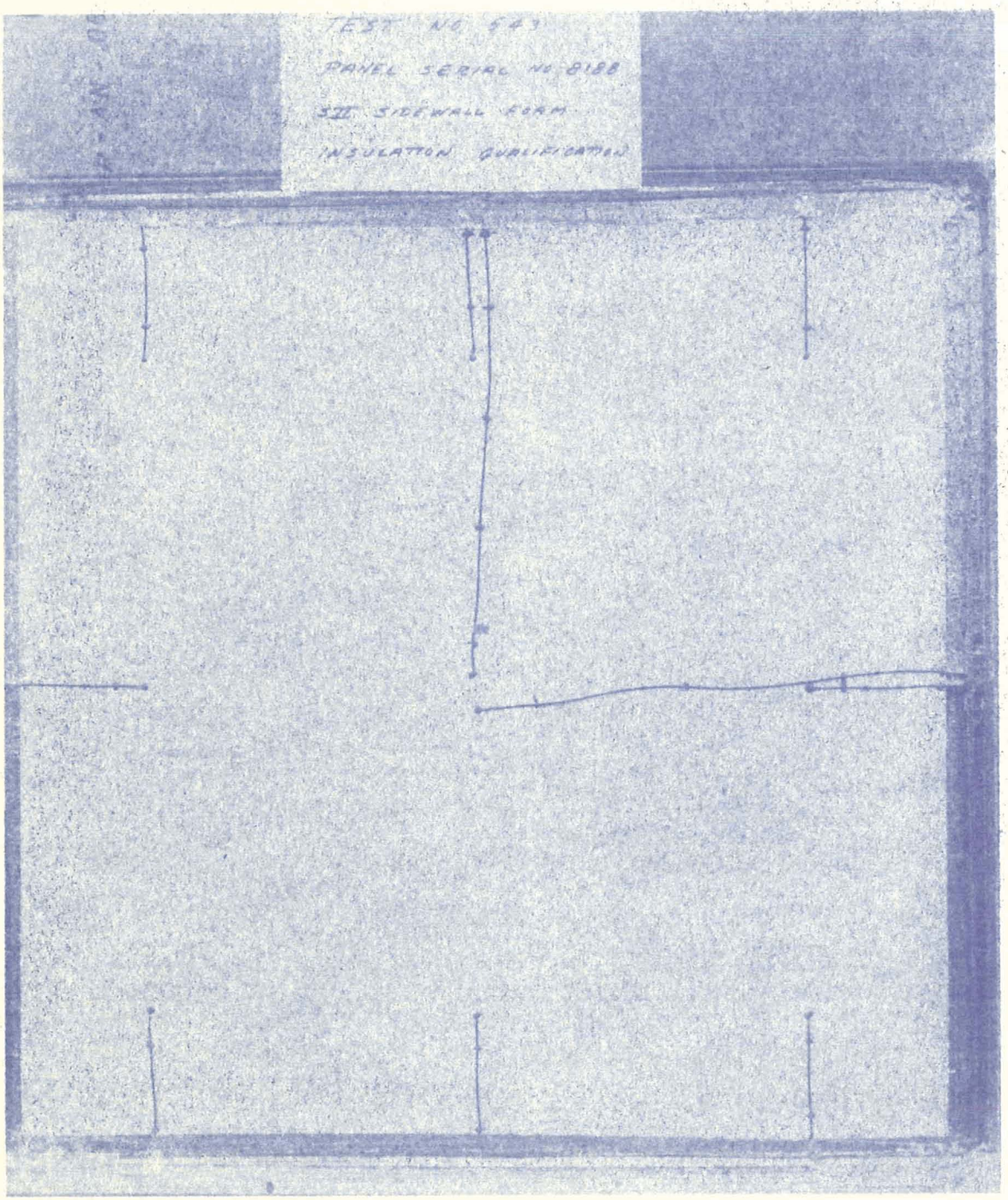

7006-81-2159B

Figure 194. S-II Sidewall Foam Insulation Test Panel 542 Before Test

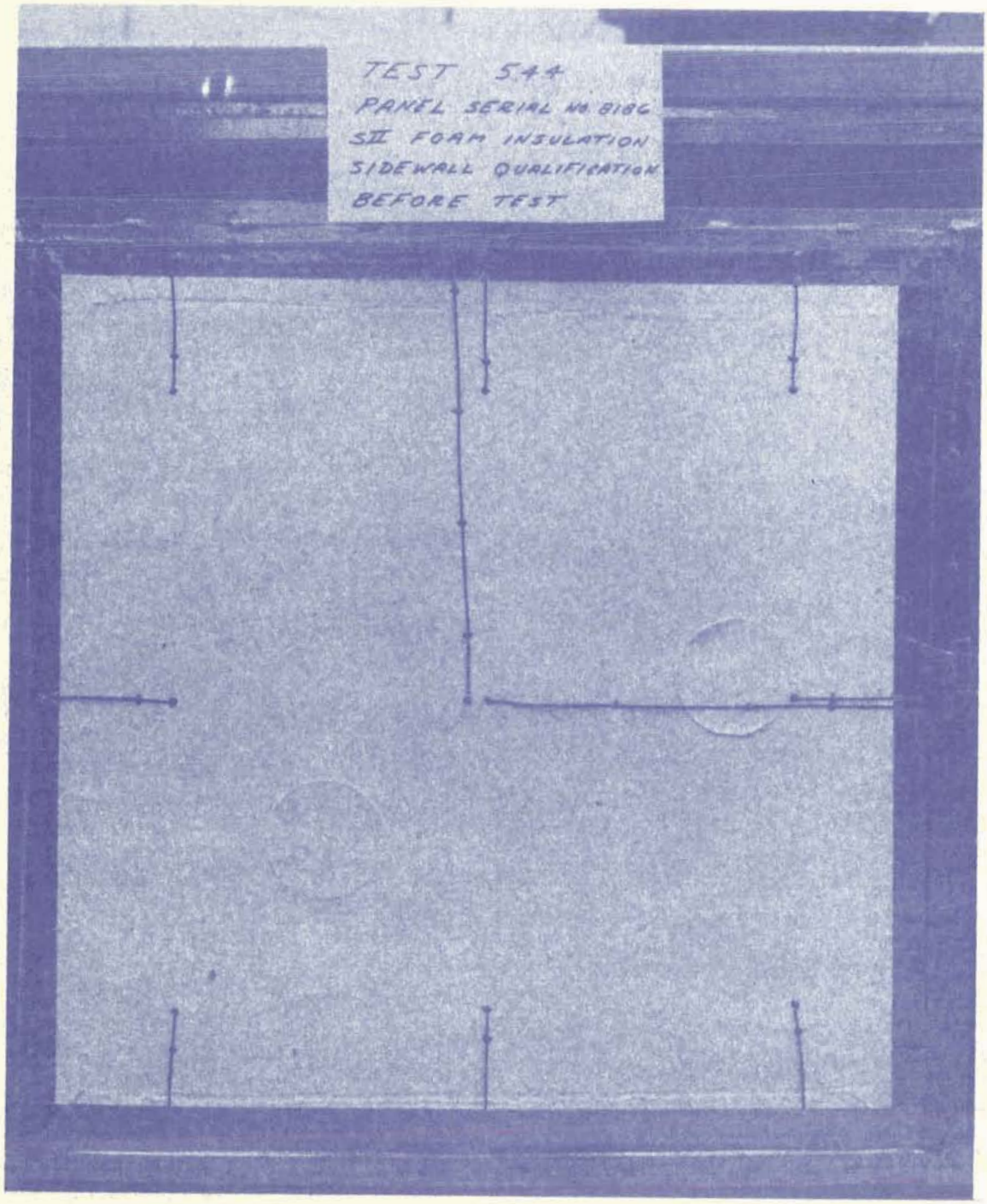

7006-81-2186A

Figure 195. S-II Sidewall Foam Insulation Test Panel 544 Before Test

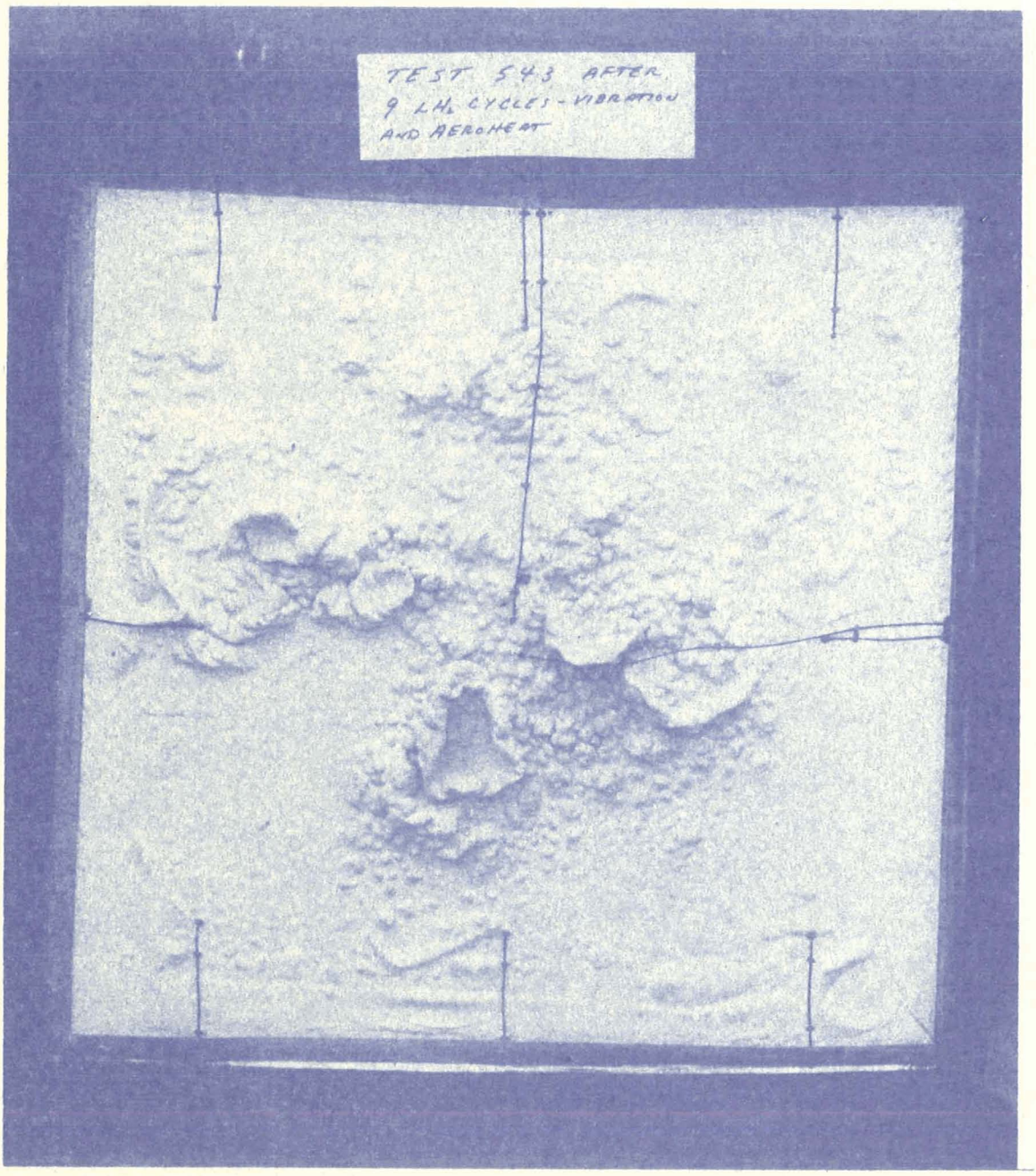

7006-81-2231B

Figure 196. S-II Sidewall Foam Insulation Test Panel 542 After Test

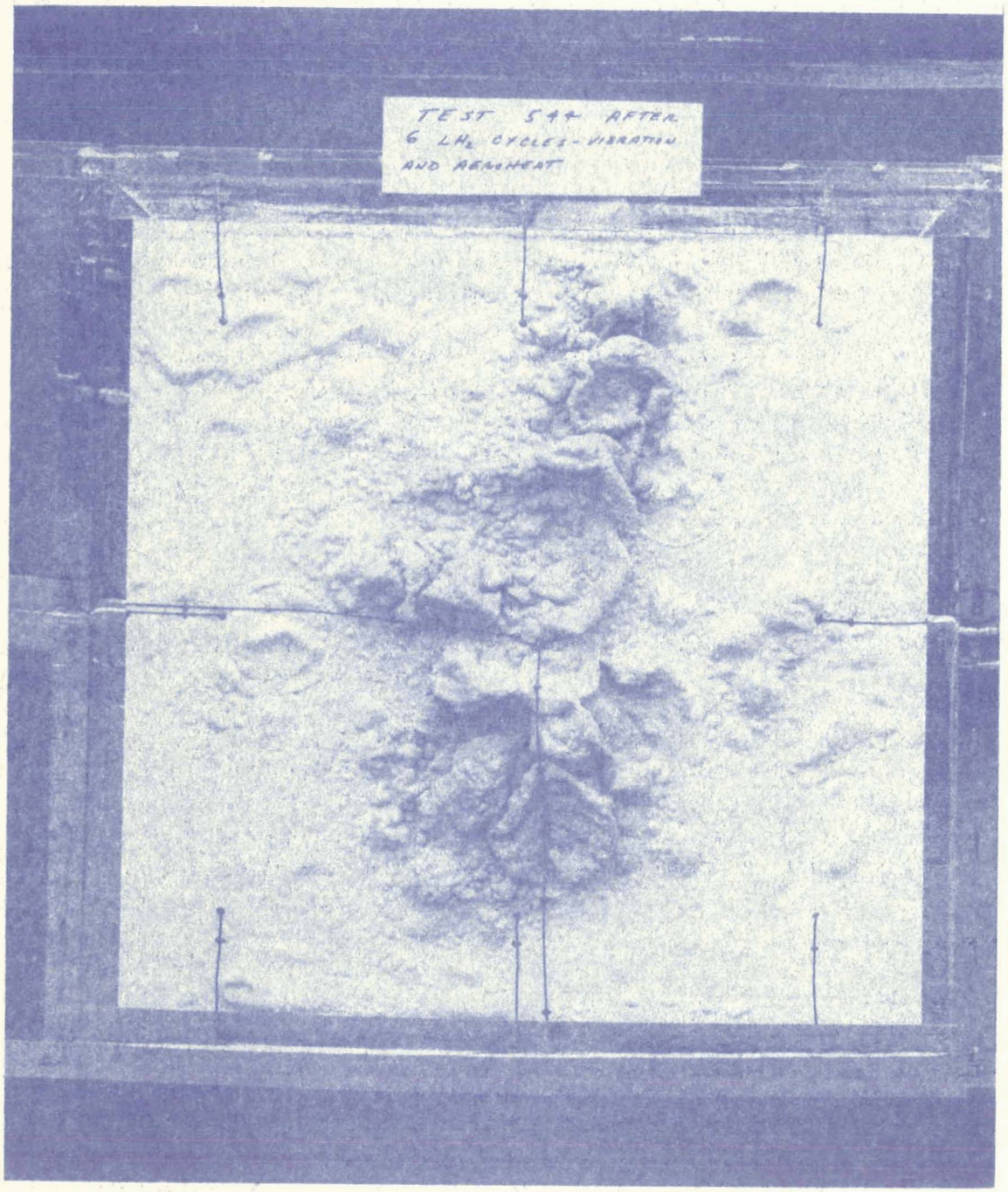

7006-81-2231A

Figure 197. S-II Sidewall Foam Insulation Test Panel 544 After Test

OVERLAP PRIMER STUDY ON CPR 369-3 FOAM AND EVALUATION OF CRYOGENIC STRAIN COMPATIBILITY OF NOPCO BX-250 SPRAY FOAM INSULATION

INTRODUCTION

A test program was conducted to improve the overlap joint bond between successively applied layers of CPR 369-3 foam (MB 0130-075). Various primer coatings applied between the successive layers of foam were evaluated.

A concurrent program was conducted to evaluate Nopco BX-250 for conformance to the cryogenic strain compatibility requirements (dog-bone tests) of MA0605-050. Also determined was whether a simulated debond of Nopco BX-250 foam to a cryogenic tank surface would propagate when cycled cryogenically.

CONCLUSIONS

The application of various resins or primers between successively applied layers of CPR 369-3 foam generally decreases the interface bond strength between the two layers.

Nopco BX-250 foam will meet the cryogenic strain compatibility requirements of MA0605-050.

A 6-inch debond of Nopco BX-250 foam introduced into a sprayed-on foam structure applied to a 30- x 30-inch test tank did not propagate when subjected to LH_2 cycling.

PROCEDURES

Overlap Joint Study

Aluminum 2014-T6 plates, 24 inches square by 1/8 inch thick, were prepared. Each was etched according to MA0610-023 primed with M-602 (MB0120-032). Primer M (MB0120-042) was then applied. Then CPR 369-3 foam was applied to the plates to obtain a final cured thickness of 1 to 2 inches. The panel was attached to a traversing fixture so a uniform layer of foam could be applied. A primer coating was then applied to the foam surface 30 seconds after the start of application of the first foam layer. Table 45 describes the various specimens, materials, and procedures.

Table 45. Specimen Data for Overlap Joint Processing Evaluation

Specimen	Primer	Company or Specification	Heat Applied
1 (control)	None		No
2	Primer M	MB0120-042	Yes
3	Primer M	MB0130-042	No
4	Polyol Component A	MB0130-075	No
5	PRC 1534	Products Research Co.	Yes
6	PRC 420	Products Research Co.	Yes
7	PRC 1531	Products Research Co.	Yes
8	8018	Furane Plastics	Yes
9	Epocast 25-3-946	Furane Plastics	Yes
10	Pro-Seal 775	Coast Pro-Seal	Yes
11	Korotherm 390-003	DeSoto Chemical	Yes

Hot air was then applied to the primed surface with a heat gun. The air-blast temperature at the surface was 250 to 300 F. The hot air blast was moved back and forth across the panel surface for 4 to 5 minutes.

Ten minutes after the start of the first spray application, a second foam layer was applied. A control panel was also produced for comparison purposes. No primer was used between successive applications of the foam of the control panel. Figure 198 shows the specimen configuration and area from where flatwise tensile specimens were cut.

Cryogenic Strain Compatibility (Dogbone Tensile) Specimens

2014-T6 aluminum, etched in accordance with MA0610-023, was used for all specimens. The aluminum dog-bone specimens were primed with M-602 followed by Primer M, mounted on plywood, and rigidly affixed to eliminate or minimize warping during and after the foam spray application.

The foam was then applied by S-II Manufacturing and the specimens were allowed to cure for a minimum of 48 hours before machining.

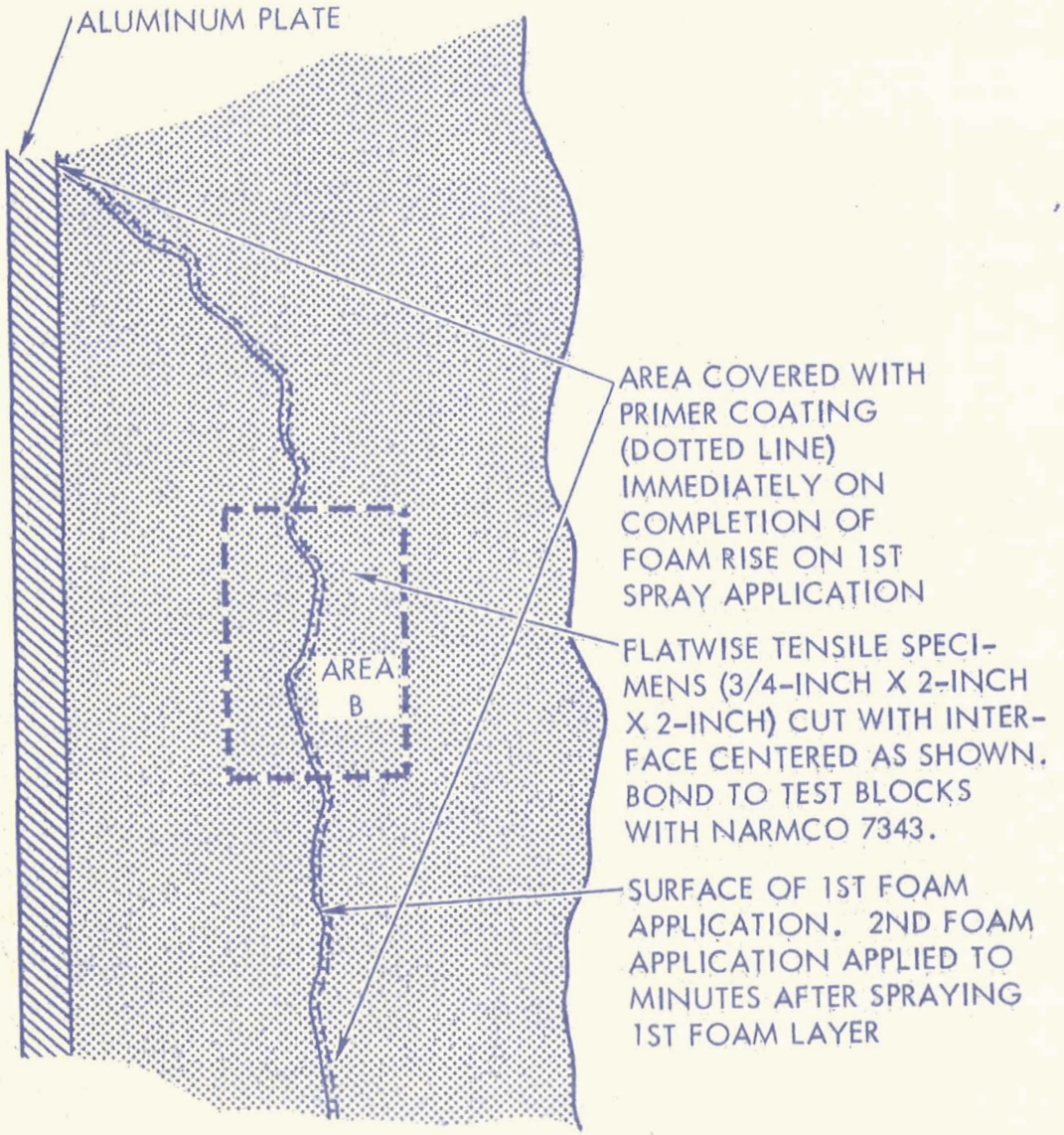

Figure 198. Test Panel Configuration For Overspray and Interface Strength Evaluation

Prepared specimen types or configurations are described as follows:

Standard - uninterrupted foam structure in machined specimen

Overlap - the foam applied in two successive overlapping applications with overlap joint in middle of specimen

Closeout - the foam applied with an area through the center of the specimen masked off as a closeout area; the edges of the foam then coated with Narmco 7343; MB0120-024 resin, cured for 16 hours; and then foam-sprayed into the closeout area

Debond - a debond actually introduced in the center of the specimen at the foam-primed metal surface interface

Slit - slits made normal to the machined foam surface near the ends of the specimens

30- x 30-Inch Panel - Debond Test Panel 555

A 30- x 30-inch cryogenic test tank was prepared for spray foaming by etching to comply with MA0610-023. The test tank was primed with M-602 and cured for 3 hours at 290 F.

The surface of the tank was masked off, except for a 6-inch-diameter circle in the center of the tank. This 6-inch-diameter area was sprayed with a Teflon release agent. The maskant was removed, and the masked area was cleaned with methyl ethyl ketone. Primer M was then applied to the entire faying surface of the tank. Following a 16-hour room temperature cure, Nopco BX-250 foam was applied to the tank surface in accordance with MA0606-050.

The uninsulated portions of the test tank were foamed with a 2-pound density foam and thermocouples affixed. A vacuum bell was bonded over the debond area (Figure 199) with a silicone adhesive sealant.

TEST PROCEDURES

Overlap Primer Specimens

Flatwise tensile specimens were cut from Area B, as shown in Figure 198. The foam was bonded to flatwise tensile blocks with Narmco 7343 After a 7-day cure of the 7343 adhesive, the specimens were tested in accordance with standard flatwise tensile test procedures.

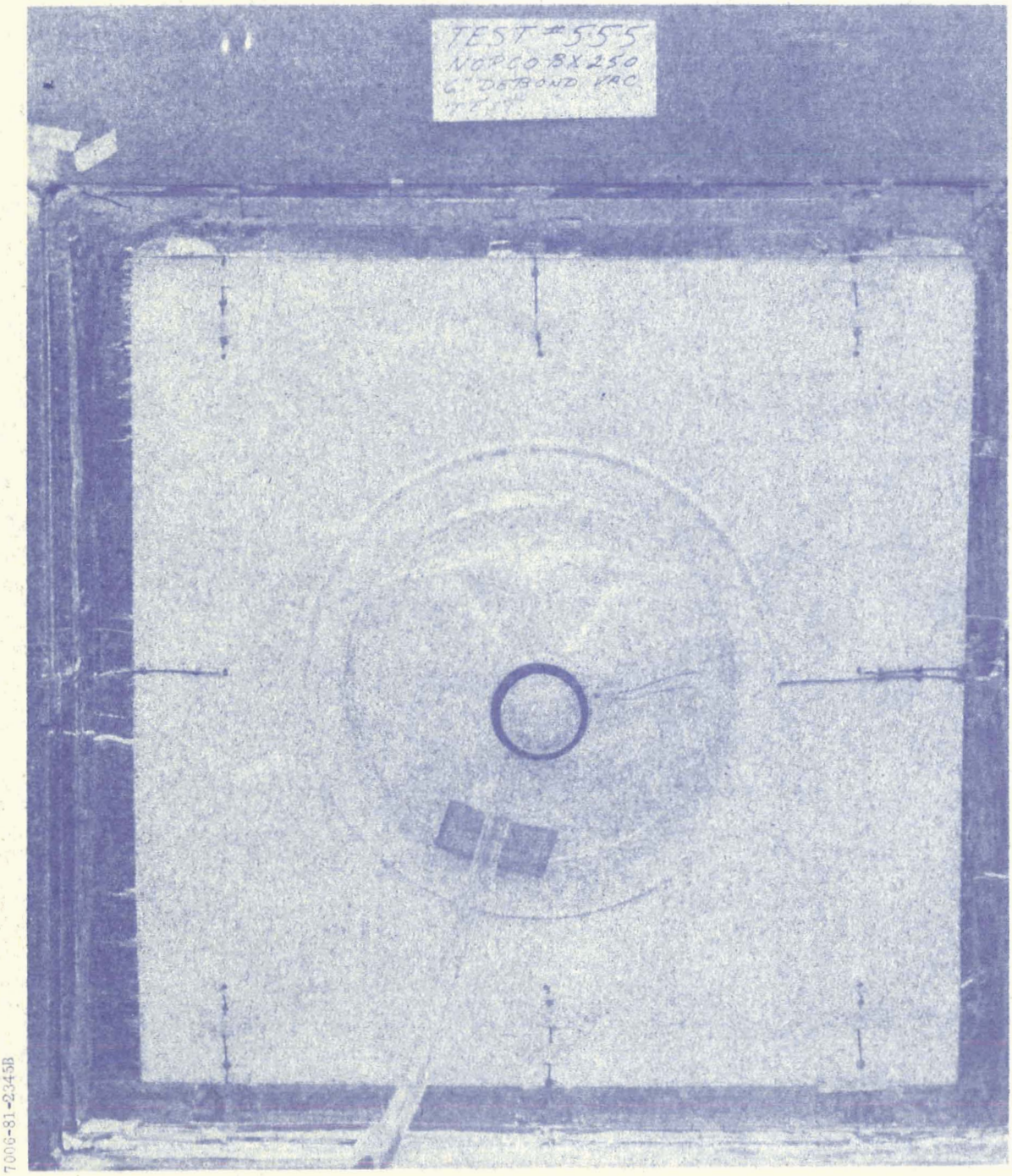

Figure 199. Test Panel 555 Showing Vacuum Bell Bonded Over Debond Area in Foam-Tank Interface

Cryogenic Compatibility Foam Tensile Tests

The foam composite tension tests were conducted with only the 2014-T6 aluminum parts of the specimen composite in liquid hydrogen. The surface of the foam was maintained at a temperature between 40 to 100 F.

A preload of 2600±500 psi was applied to the specimen and maintained during chilldown. To maintain the proper surface temperature on the foam, a copper plate with copper tubes was placed on the top surface of the foam. Hot water (150 to 250 F) was circulated through the tubes on the copper plate to control the foam surface temperature.

A nominal stress level of 71,000 psi was applied to each specimen. After the test, the specimens were visually examined to determine if cracks had developed either in the foam-to-primed metal bond or in the foam.

Cyclic tensile tests were conducted by stressing the specimen from 0 to 56,000 psi in five cycles at ambient temperature. The temperature of the aluminum was then lowered to -423 F with the surface of the foam stabilized at 40 F. A nominal stress of 34,000 psi was applied to the specimen in 20 consecutive cycles, and the specimen was examined for failures. After examination, the specimen was then again chilled to the -423 F level (metal temperature) and stressed to 71,000 psi.

Tensile Testing of Specimens With Narmco 7343/Nylon Wet Layup Applied to Foam

This testing was conducted on previously tested specimens. The specimens were remachined, and a wet layup of 7343 resin/nylon fabric was applied to the foam to simulate the S-II bulkhead insulation composite.

The testing was conducted in the same manner as was the tensile testing except that the surface of the 7343/nylon skin was exposed to temperatures from -295 to -310 F during the tension testing.

Testing of Debond Panel 555

Vacuum debond pressure was determined by using a mass spectrometer leak detector attached to a glass bell jar bonded on a 1-foot-square area of foam specimen surface. The lowest stable vacuum debond pressure was obtained from the leak detector prior to test, during liquid hydrogen fill and foam surface temperature stabilization, and after test when tank wall temperatures were ambient.

RESULTS

Overlap Joint Study

Superior void-free interface bonds were obtained with the control specimens on which no primer nor adhesive was applied between the successive layers of foam (Figure 200). Low-strength interface bonds were obtained when Primer M was applied between the successive layers of foam.

All other specimens, except for the PRC 1534 and Furane 8018-coated overlap specimens, resulted in extremely low strength interface bonds and generally massive void areas in the joints (Figures 201, 202, and 203). Average results of the flatwise tensile testing, which were 40.8 psi for the PRC 1531 and 21.4 psi for the PRC 1534 specimens, were considerably lower than the 50- to 70-psi nominal values for overlap joint strengths for uncoated interface bond strengths.

Cryogenic Compatibility Specimens (Dog-Bone Tests)

Close examination of all Nopco BX-250 foam dog-bone specimens after testing revealed that no cracks or debond failure had occurred during the test. Three specimens had debonds in the overlap areas noted after machining and before tension testing. However, these did not appear to propagate during testing.

Debond Panel 555

Though the debond was stressed by evacuating the surface of the foam above the debond area, no propagation of the debond was evidenced on close examination (Figure 204).

Some cracking of the foam was noted along the inner periphery of the vacuum jar. However, this was the result of the extremely high stress concentration induced by the pressure differential when the bell was evacuated.

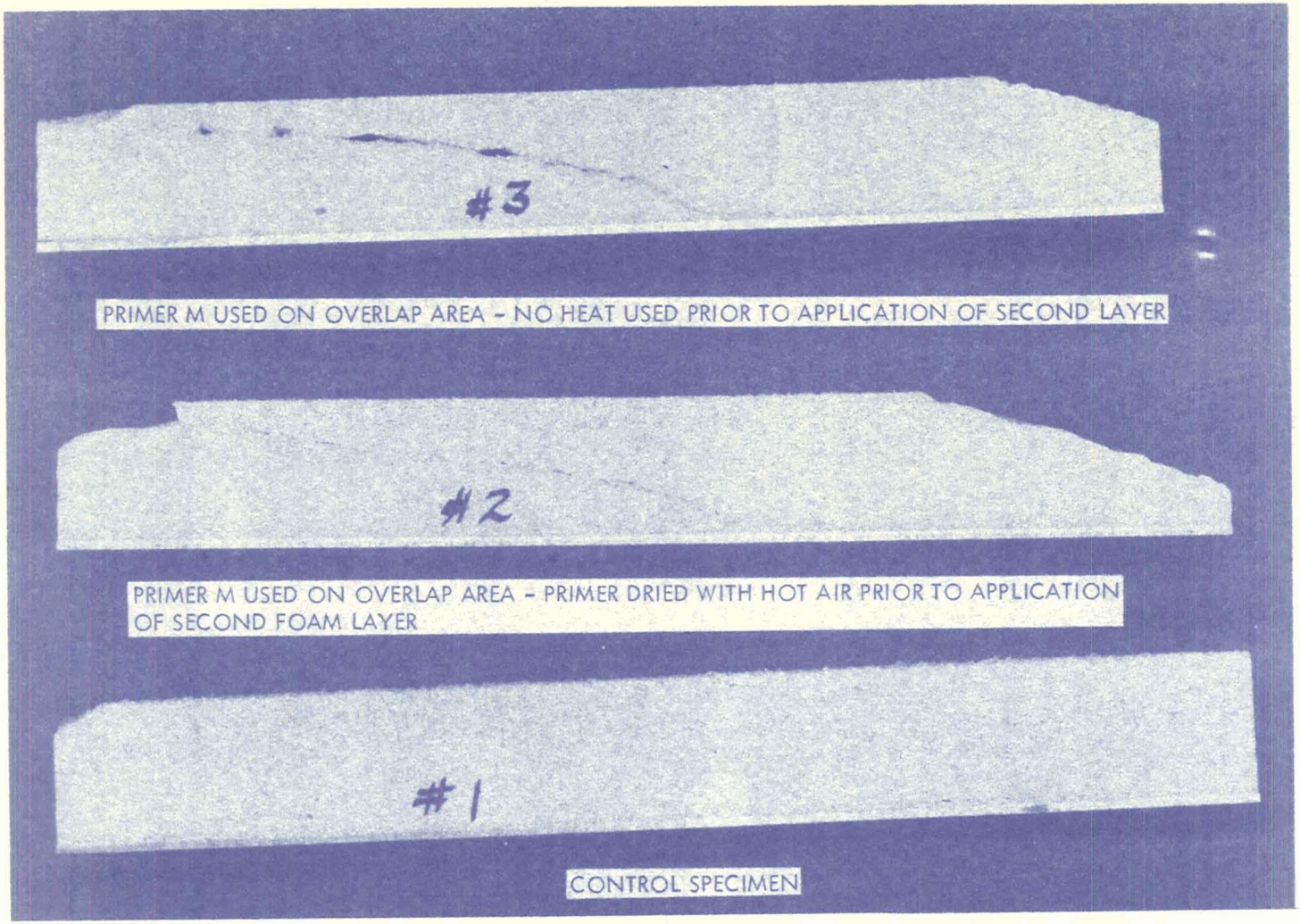

Figure 200. Cross-Section of Overlap Interfaces on Control Foam Specimens and Foam Specimens With Primer M-Coated Overlaps

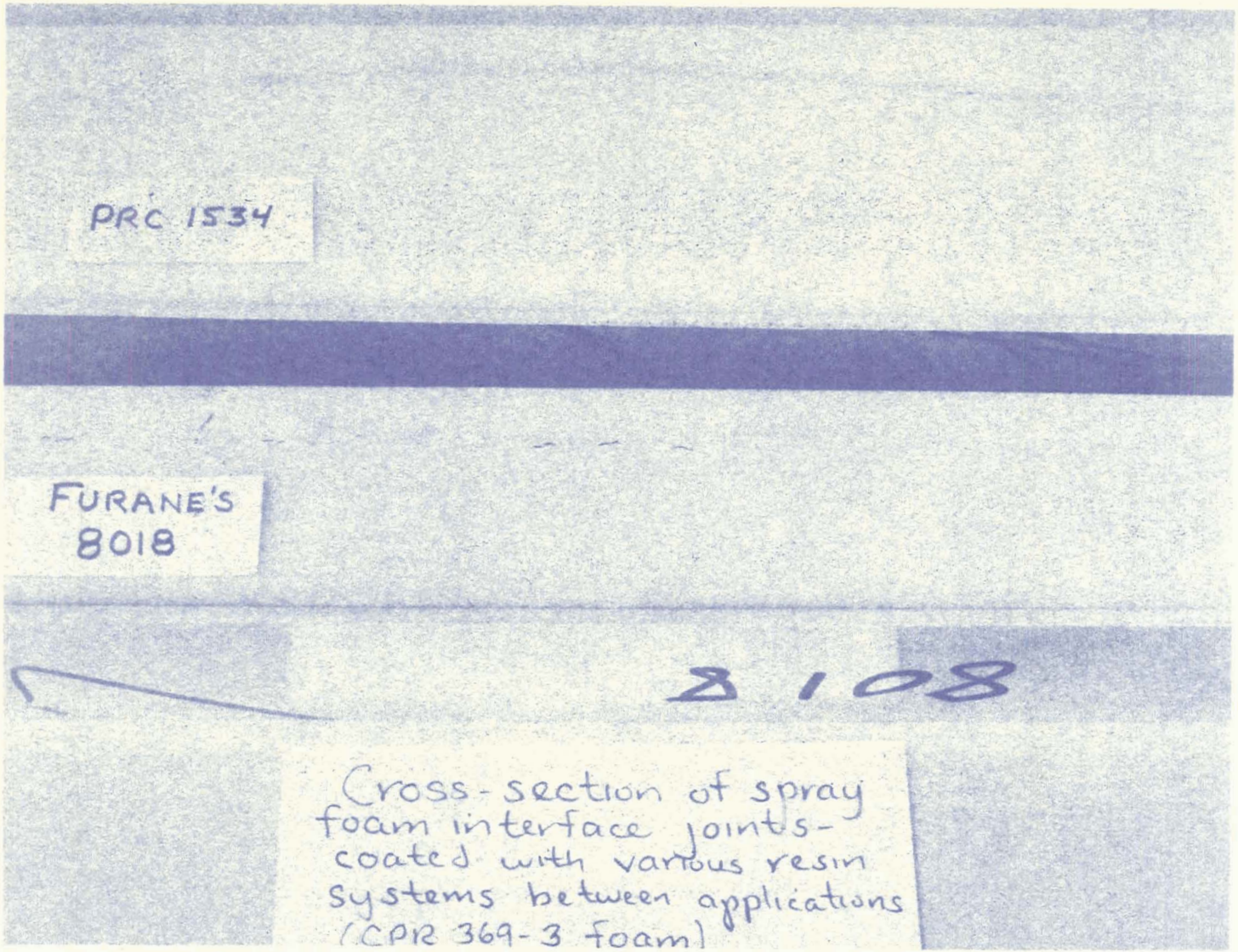

Figure 201. Cross-Section of Overlap Interfaces on Foam Specimens Coated With PRC 1535 Primer and Furane 8018 Resin System

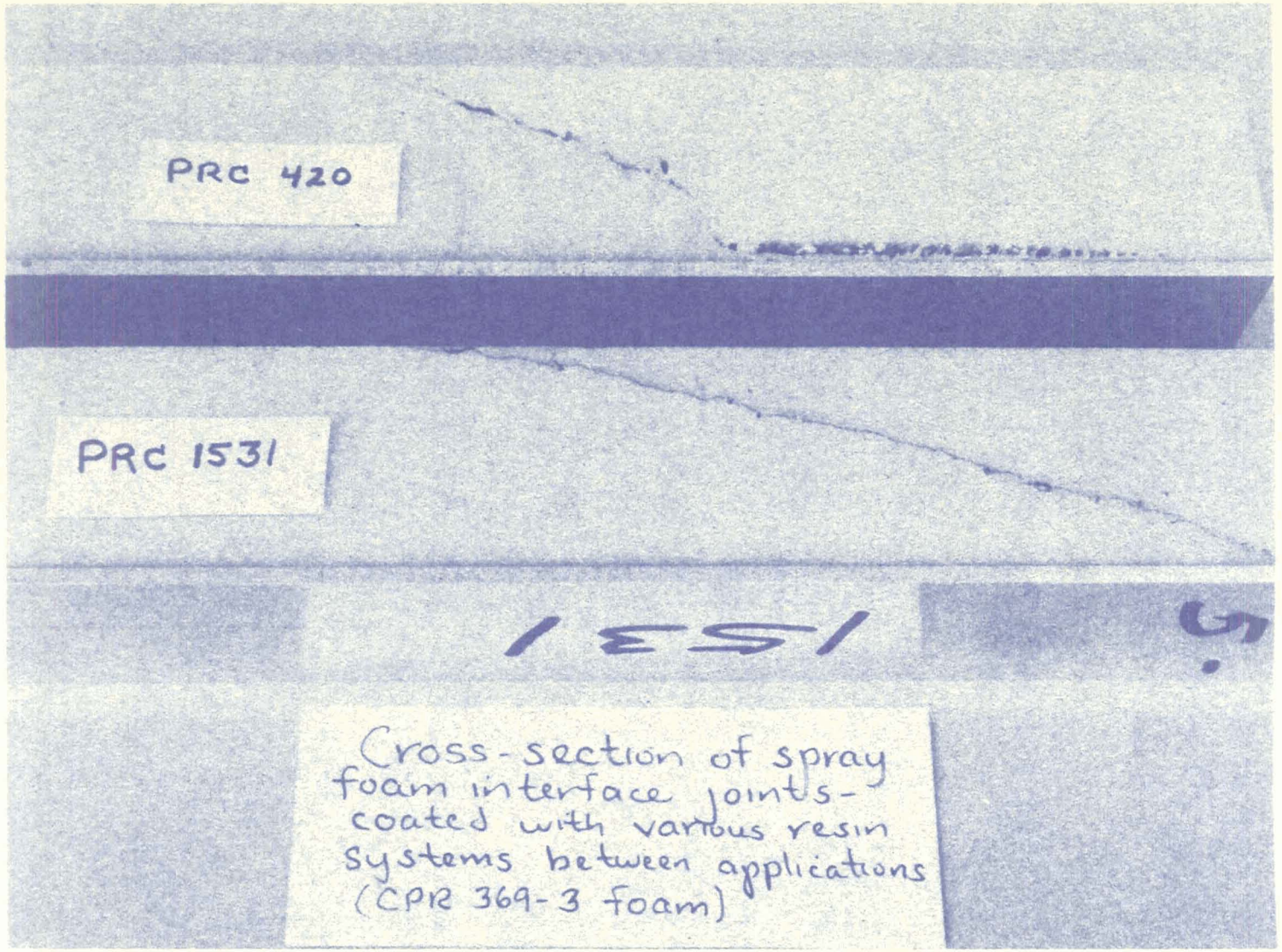

Figure 202. Cross-Section of Overlap Interfaces on Foam Specimens Coated With PRC 410 and PRC 1531 Primer Systems

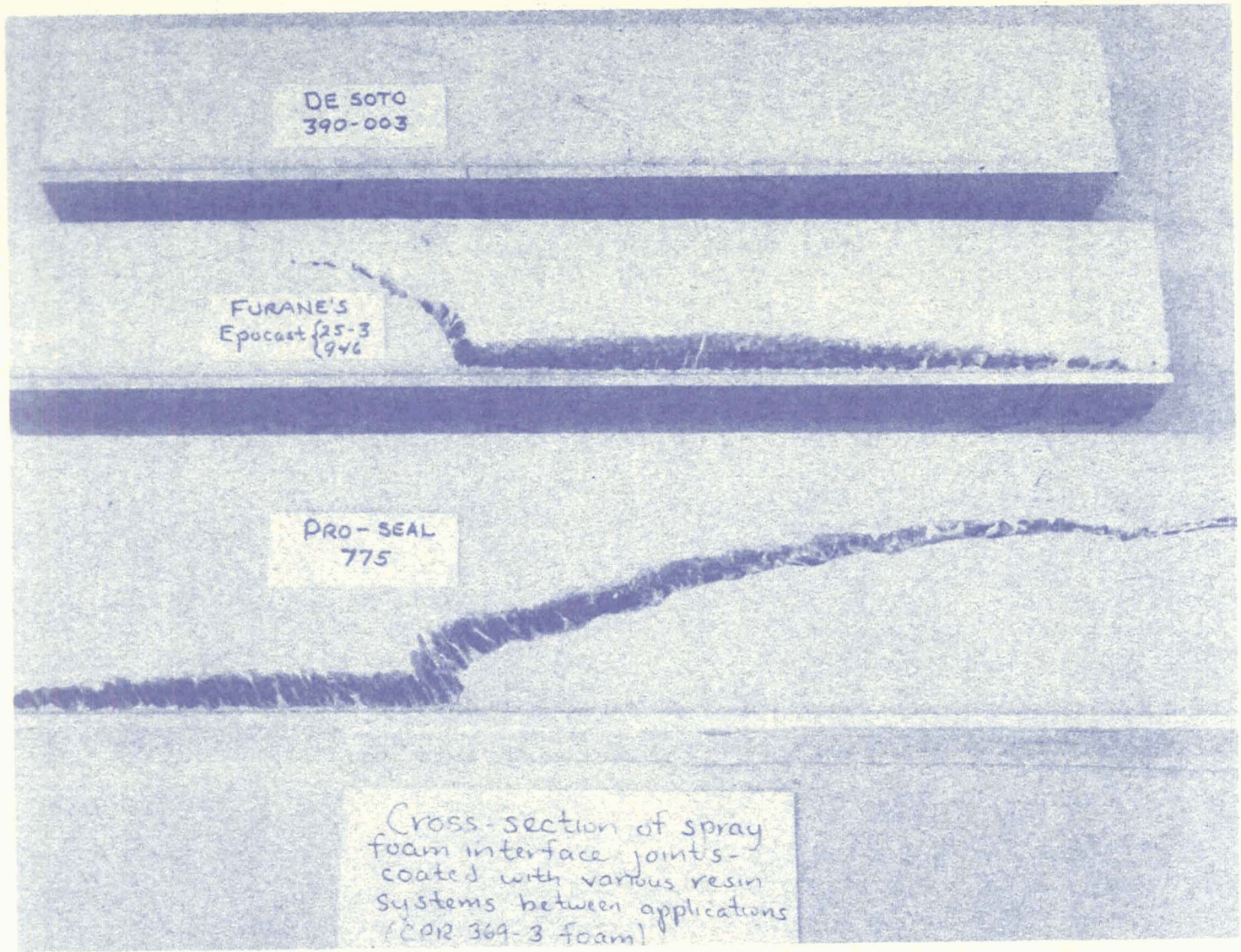

Figure 203. Cross-Section of Overlap Interfaces on Foam Specimens Coated With De Sota 390-003 Resin, Furan's Epo Coat 25-3-946 Resin and Proseal 775 Primer Systems

SPACE DIVISION OF NORTH AMERICAN ROCKWELL CORPORATION

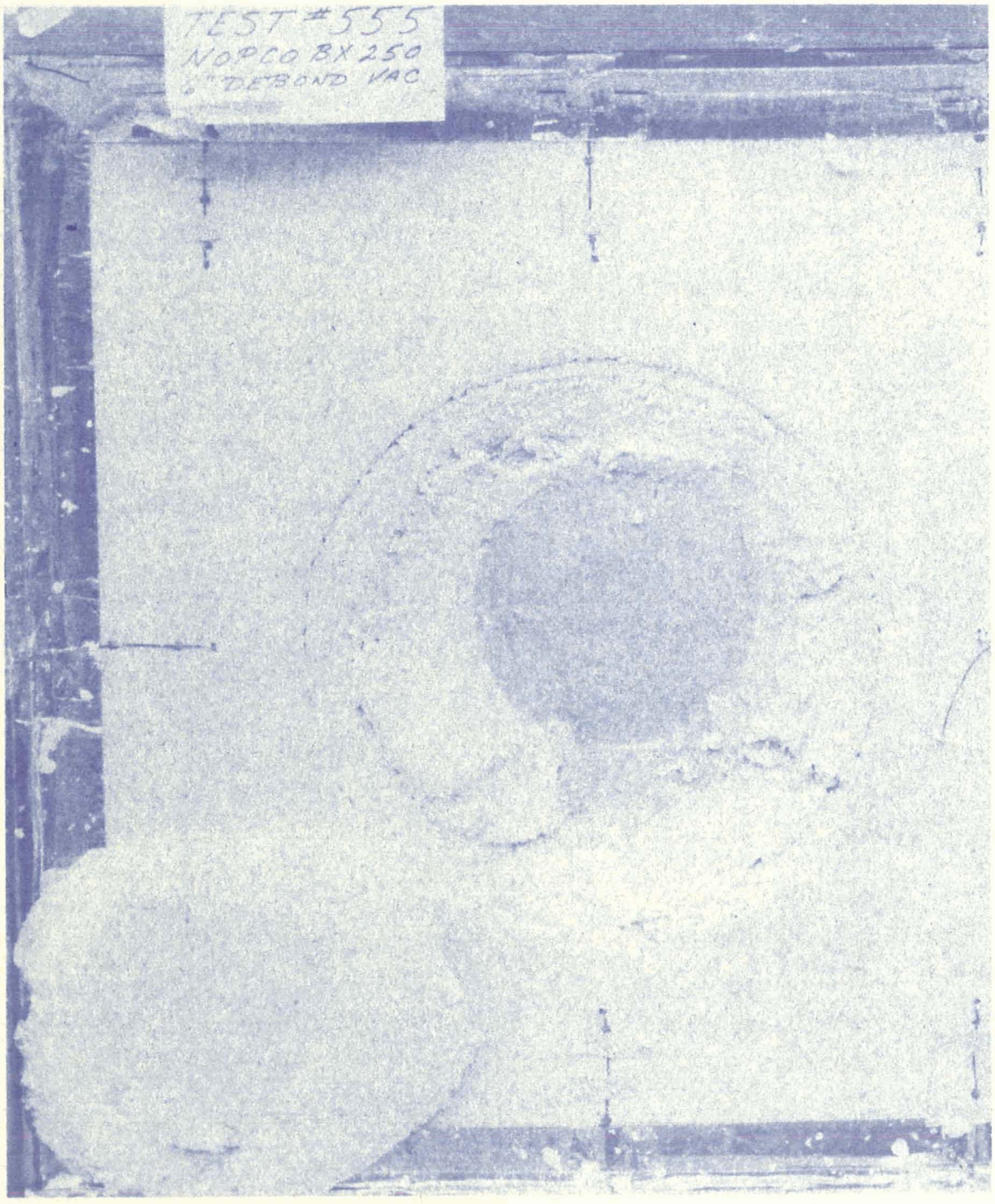

7006-81-2345E

Figure 204. Debond Test Panel 555 After Test and Dissected

MATERIAL PROPERTIES OF NOPCO BX-250A SPRAY FOAM

Laboratory effort was undertaken to provide additional technical data on Nopco BX-250A material, a 2-pound density sprayable polyurethane foam system. The purpose of this laboratory investigation was to determine the following physical and mechanical properties:

Flatwise tensile, flatwise compression, and block shear properties of foamed specimens at a temperature range from -423 to +200 F

Physical properties of foamed specimens, including density, closed cell, water absorption, thermal expansion, thermal conductivity, and specific heat

Helium permeability characteristics of foamed specimens at both ambient and cryogenic conditions

Thermal conductivity data under cryogenic conditions of a Hypalon-coated, 1-inch foam-insulated, round-guarded calorimeter tank before and after exposure to a climatic environment and salt spray exposure

RESULTS

The mechanical properties of BX-250A foam at 200 through -423 F are tabulated as follows:

Flatwise tensile data, parallel to rise, are shown in Table 46.

Flatwise tensile data, perpendicular to rise, are shown in Table 47.

Flatwise compression results, parallel to rise, are shown in Table 48.

Flatwise compression results, perpendicular to rise are shown in Table 49.

Block shear test data, parallel to rise, are shown in Table 50.

Block shear test data, perpendicular to rise, are shown in Table 51.

Table 46. Average Flatwise Tensile Test Data at Room Temperature, +200 F, -100 F, -300 F, and -423 F Parallel to Rise

Test Temperature (F)	Ultimate Stress (psi)	Strain (in./in.) (ϵ)	Apparent Modulus of Elasticity (psi)	Remarks
Room	42.9	0.0242	1850	Failure foam
+200	22.8	0.0247	1835	Secondary bond failure
-100	51.8	0.0183	2836	Foam
-300	46.8	0.0133	3333	Secondary bond
-423	52.5	0.0089	6270	Foam
-423	50.1	0.0076	6653	Foam and secondary adhesive bond

Table 47. Average Flatwise Tensile Test Data at Room Temperature, +200 F, -200 F, -300 F, and -423 F Perpendicular to Rise

Test Temperature (F)	Ultimate Stress (psi)	Strain (in./in.) (ϵ)	Apparent Modulus of Elasticity (psi)	Remarks
Room	54.4	0.0425	1923	Foam
+200	28.2	0.0491	1648	Secondary adhesive bond failure
-100	46.6	0.0195	2525	Foam
-300	39.4	0.0124	3260	Secondary adhesive bond
-423	39.7	0.0100	4123	Foam

Table 48. Average Flatwise Compression Test Data at Room Temperature, +200 F, -100 F, -320 F and -423 F Parallel to Rise

Test Temperature (F)	Ultimate Stress (psi)	Strain (in./in.) (ϵ)	Apparent Modulus of Elasticity (psi)
Room	36.7	0.0637	1090
+200	25.9	0.0732	808
-100	48.9	0.1166	1448
-320	82.5	0.0613	2267
-423	92.1	0.1200	4475

Table 49. Average Flatwise Compression Test Data at Room Temperature, +200 F, -100 F, -300 F, and -423 F Perpendicular to Rise

Test Temperature (F)	Ultimate Stress (psi)	Strain (in./in.) (ϵ)	Apparent Modulus of Elasticity (psi)
Room	23.8	0.1000	540
+200	19.0	0.1142	497
-100	32.6	0.1000	742
-300	47.3	0.0500	979
-423	51.2	0.0500	1529

Table 50. Average Block Shear Test Data at Room Temperature, +200 F, -100 F, -300 F, and -423 F Parallel to Rise

Test Temperature (F)	Ultimate Stress (psi)	Strain (in./in.) (ϵ)	Apparent Modulus of Elasticity (psi)	Remarks
Room	36.2	0.2644	591	Foam and secondary bond
+200	10.9	0.0656	395	Foam and secondary bond
-100	40.9	0.0814	764	Foam and secondary bond
-300	33.7	0.0323	1384	Foam or bondline
-423	27.6	0.0248	1326	Foam to adhesive

Table 51. Average Block Shear Test Data at Room Temperature, +200 F, -100 F, -300 F, and -423 F Perpendicular to Rise

Test Temperature (F)	Ultimate Stress (psi)	Strain (in./in.) (ϵ)	Apparent Modulus of Elasticity (psi)	Remarks
Room	31.9	0.3000	442	Secondary adhesive bond
+200	20.4	0.0901	1030	Secondary adhesive bond
-100	41.6	0.1022	634	Secondary adhesive bond
-300	29.5	0.0593	1051	Foam to adhesive bond
-423	24.7	0.0255	1100	Foam to adhesive bond

The Poisson's ratio for the BX-250A foam, at various temperatures, is shown in Table 52. As calculated, at room temperature, μ is 0.563 parallel to rise, and 1.179 perpendicular to rise. In comparison, Poisson's ratio for aluminum is 0.33 at room temperature.

The physical properties of the BX-250A foam are tabulated as follows:

Cream time is shown in Table 53, as well as the density, viscosity, and specific gravity of the BX-250A foam components used in the study.

Thermal conductivity results are shown in Table 54.

Water absorption characteristics of the BX-250A foam are shown in Table 55.

Coefficient of thermal expansion data for BX-250A foam, both parallel and perpendicular to rise, are shown in Table 56.

Closed-cell test results for the BX-250A foam specimens are shown in Table 57.

The specific heat of the BX-250A foam is 0.33 cal/gram-C at a mean temperature of 129 F.

Flammability testing was conducted on two different lots of BX-250A foam; both were classified nonburning according to ASTM D-1692.

The helium permeation test data for BX-250A foam are as follows:

1. At -423 F, the helium permeation rate was 1.37×10^{-6} scc/sec

2. At room temperature, the helium permeation rate was from 1.13×10^{-5} to 3.8×10^{-5} scc/sec

Thermal conductivity determinations were made with a round guarded calorimeter tank. Conductivity measurements were made before and after an exposure of 60 days at 100-percent relative humidity and 120 F climatic condition, and a salt-spray test of 50 hours at 95-percent relative humidity and 95 F. Table 58 summarizes thermal conductivity test results and respective cryogenic cyclic exposure before and after climatic salt-spray conditioning.

Table 52. Poisson's Ratio of BX-250A at Room Temperature, +200 F, -100 F, -300 F, and -423 F, Average Values

Specimen	Test Temperature (F)	Average Modulus of Elasticity in Shear - g (psi)	Average Modulus of Elasticity in Tension - E (psi)	Poisson's Ratio (in./in.)	Shear Strain (in./in.)	Tension Strain (in./in.)
Parallel to rise	Room	591	1850	0.563	0.2644	0.0242
	+200	395	1835	1.323	0.0656	0.0247
	-100	764	2836	0.841	0.0814	0.0183
	-300	1384	4254	0.523	0.0323	0.0128
	-423	1326	6270	1.361	0.0248	0.0089
Perpendicular to rise	Room	442	1923	1.179	0.3000	0.0425
	+200	1030*	1648	*	0.0901	0.0491
	-100	634	2535	0.999	0.1022	0.0195
	-300	1651	3260	0.550	0.0593	0.0124
	-423	1100	4143	0.882	0.0255	0.0100

*Modulus of elasticity data not realistic for a 200 F environment

Table 53. Properties of BX-250A Foam Components and Mix

Component Nopcofoam BX-250A	Temperature (F)	Spindle Number	Viscosity (cps)
Component A (T)	70	2	450
	76	2	338
	80	2	275
Component B (R)	70	2	383
	76	2	345
	80	2	282

Viscosity: Brookfield RVF

Specific Gravity: BX-250A Foam
Component A (T): 1.26 (25/25C)
Component B (R): 1.20 (25/25C)

Cream Time: 7.0 to 7.5 seconds
Tack free time: 22 seconds
Rise time: 22 seconds
Density: 2.2 pounds/cubic foot

Table 54. Thermal Conductivity Test Data of Nopco BX-250A Foam

Specimen Pair Number	Average Density (lb/cu ft)	Mean Temperature (F)	Hot Side Temperature (F)	Cold Side Temperature (F)	T (F)	Apparent Thermal Conductivity, k (Btu-in./sq ft-hr-F)
1B	2.36	101.9	126.5	77.3	49.2	0.148
		185.0	279.4	89.5	189.9	0.183
2B	2.42	100.1	125.1	75.0	50.1	0.144
		184.8	277.2	92.3	184.9	0.187
		6.13	89.5	33.1	56.4	0.127
3B	2.29	-88.1	-68.2	-108.0	39.8	0.169
		-302.1	-284.0	-320.2	36.2	0.083
		61.5	90.1	32.8	57.3	0.127
4B	2.29	-87.1	-65.9	-108.1	42.2	0.153
		-301.5	-282.8	-320.1	37.3	0.084

Table 55. Average Water Absorption Test Data

Foam Density (lb/cu ft)	Water Absorption			Volume Penetration (percent)
	Surface Area per Unit		Volume per Unit (gms/1000 cu cm)	
	(gms/1000 sq cm)	(lb/sq ft)		
2.52	5.9	0.012	7.0	0.7
2.21	6.6	0.014	7.8	0.8
2.27	5.8	0.012	6.9	0.7
Material: BX-250A Foam Batch Number: R/T 02-2594-2/02-47475-1 Test Method: ASTM D-2127-62T				

Table 56. Average Thermal Expansion Test Data

Temperature Range (F)	Density (lb/cu ft)	Coefficient of Linear Thermal Expansion, (in./in.)
Direction Perpendicular to Foam Rise		
75 to 200 +50 to -300	2.27 2.25	5.1×10^{-5} 3.3×10^{-5}
Direction Parallel to Foam Rise		
75 to 200 +50 to -300	2.28 2.30	7.2×10^{-5} 4.0×10^{-5}
For all tests: Specimen dimensions - 3- x 1/2- x 1/2-inches Test environment - 1 atmosphere air above room temperature 1 atmosphere helium below room temperature		
Material: Nopco BX-250A Batch Number: R/T 02-2594-2/02-47475-1 Test Method: Below room temperature - ASTM D-696-44 Above room temperature - Optical extensometer		

Table 57. Average Closed Cell-Porosity Test Results

Density (lb/cu ft)	Percent Open Cells	Percent Cell Wall	Percent Closed Cells
2.24	9	3	88
2.35	8	3	89
2.30	9	3	88

Calculation of percent closed cells:

Percent closed cells = 100 percent - percent open cells - percent cell wall

Where percent cell wall = 100 percent x $\frac{\text{Foam density}}{\text{Density of solid polymer}}$

Density of solid polymer is taken to be 80 pound per cubic foot.

Material: Nopco BX-250A
Batch Number: R/T 02-2594-2/02-47475-1
Test Method: ASTM D-1940-62T

Table 58. Round Guarded Calorimeter Test Data

Cycle	Stabilization Period (minutes)	Surface Temperature Average (F)	Cold Wall Temperature (F)	ΔT (F)	Gas Flow Rate (cu ft/hr)	Gas Density (lb/cu ft)	F/μt (F)	Cell		$\left(\frac{k \text{ Btu-in}}{\text{Hr-F-Ft}_2}\right)$
								Temperature (F)	Relative Humidity (%)	
Condition: Preclimatic Exposure										
LN_2	90	+44.9	-320	364.9	5.41	0.0752	60.2	58.5	84.6	0.1214
1st LH_2	90	+45.6	-420	465.6	38.18	0.0054	60.0	58.0	86.0	0.1088
2nd LH_2	90	+49.8	-420	469.3	38.14	0.0054	64.0	62.0	77.5	0.1062
3rd LH_2	90	+45.1	-420	465.1	36.98	0.0053	63.0	60.2	79.4	0.0986
4th LH_2	90	+44.0	-420	464.0	35.43	0.0053	63.3	63.2	63.0	0.0986
5th LH_2	300									
3rd hour		+48.8	-420	468.8	35.11	0.0053	69.2	69.0	51.0	0.0980
5th hour		+49.9	-423	472.9	35.88	0.0053	66.0	64.0	63.0	0.0982
Condition: Post-Climatic Exposure										
LN_2	90	+48.4	-311	359.4	13.52	0.0728	66.5	65.0	70.0	0.2909
1st LH_2	90	+46.0	-420	466.0	45.86	0.0053	65.2	65.2	65.0	0.1262
2nd LH_2	90	+47.0	-420	467.0	46.68	0.0052	67.5	64.0	73.0	0.1272
3rd LH_2	90	+45.0	-420	465.0	45.78	0.0053	65.0	65.1	67.5	0.1267
4th LH_2	90	+45.0	-420	465.0	45.54	0.0053	65.8	62.0	66.0	0.1259
5th LH_2	300									
3rd hour		+42.8	-423	465.8	44.32	0.0052	66.0	66.5	75.0	0.1222
5th hour		+45.0	-423	468.0	46.80	0.0053	62.8	65.0	64.0	0.1292

NOTE: F/μt is the flowmeter temperature
k is thermal conductivity

COMPARATIVE BLOCK SHEAR PROPERTIES OF BX-250A FOAM SPECIMENS PERPENDICULAR TO RISE

INTRODUCTION

A laboratory study was conducted to establish comparative test data on two types of foam block shear test specimens at -300 F, room temperature and +200 F. The block shear specimens were developed from BX-250A spray foam blocks machined perpendicular to foam rise and assembled into Type I and Type II configurations shown in Figure 205.

CONCLUSIONS

The strength data of the Type I specimens of BX-250A foam are slightly higher than those attained with Type II test specimens. The average modulus of elasticity value obtained for each specimen type tested is comparable at corresponding temperature conditions. (See Tables 59 and 60.)

The Type I test specimens are easier to machine, assemble, and adhesively bond to form block shear fixture plates. In addition, they can be fabricated in less than half the time required for Type II specimens. Consequently, the Type I configuration is considered best for determining block shear strength of foam material cut perpendicular to rise.

PROCEDURE

The foam sections were cut and machined into 2- x 7- x 5/8-inch coupons for Type I test specimens (Figure 205). Foam specimens were cut and machined into 2- x 2.33- x 5/8-inch coupons for Type II test specimens.

Densities of the foam sections were determined before their assembling and adhesive bonding with Narmco 734317139 adhesive (MB0120-024) into respective block shear specimens.

DISCUSSION

The slightly lower ultimate stress values obtained with Type II specimens are attributed to difficulties in maintaining uniformity in the alignment of the individual foam test sections. However, the modulus of elasticity data for both Type I and Type II configurations were remarkably similar at corresponding test temperatures.

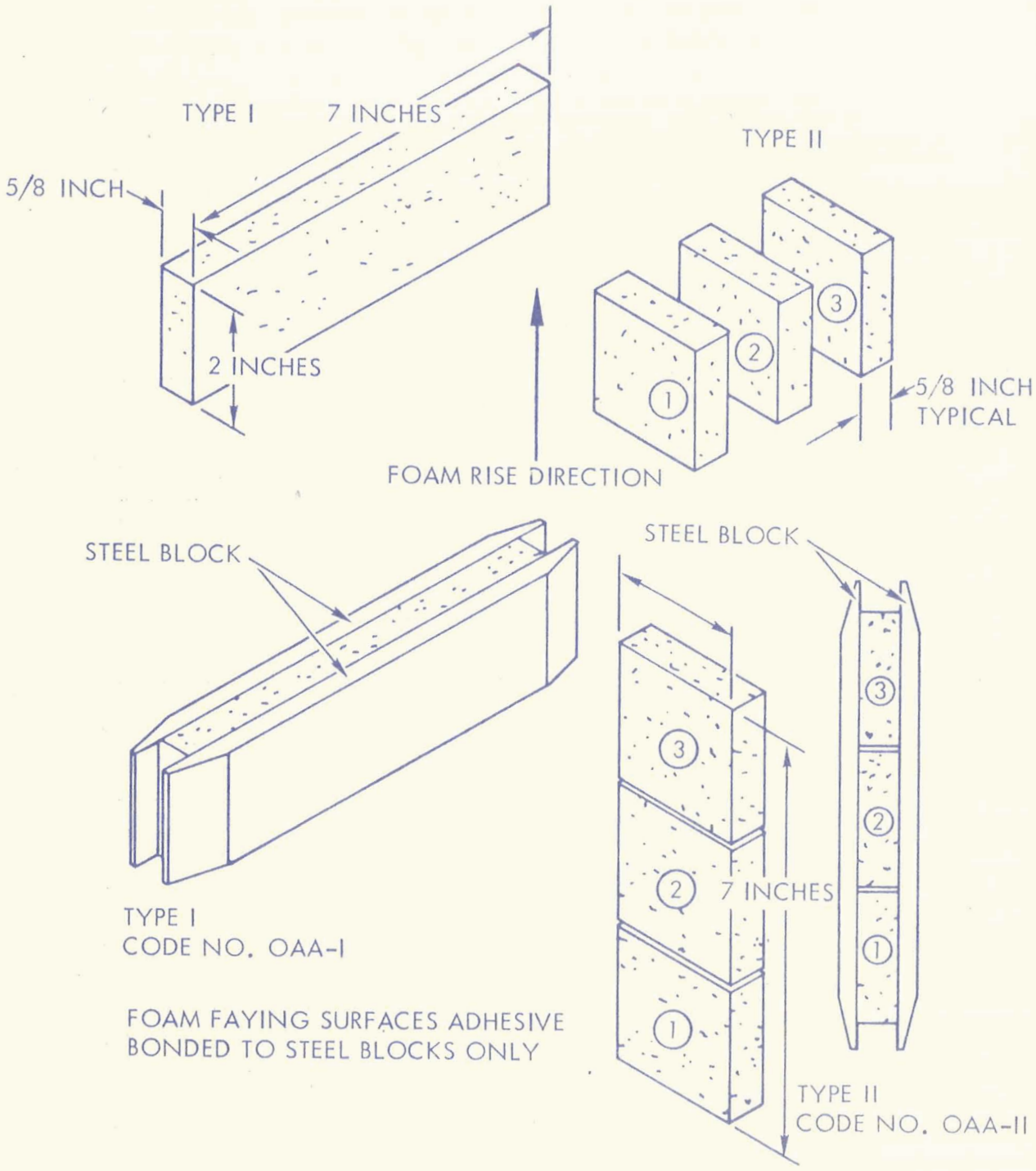

Figure 205. Block Shear Specimens, Type I and Type II Configuration

Table 59. Average Block Shear Test Data - Type I Configuration Specimens

Test Temperature (F)	Ultimate Stress (psi)	Apparent Modulus of Elasticity (psi)	Type of Failure
-300	25.6	657	Secondary adhesive bond
+200	20.2	235	Foam and secondary adhesive bond
Room	26.1	252	Secondary adhesive bond
Crosshead load rate of 0.05 inch per minute Soak time minimum of 30 minutes at temperature			

Table 60. Average Block Shear Test Data - Type II Configuration Specimens

Test Temperature (F)	Ultimate Stress (psi)	Apparent Modulus of Elasticity (psi)	Type of Failure
-300	18.1	660	Secondary adhesive bond
+200	16.3	256	Foam and adhesive bond
Room	20.7	267	Secondary adhesive bond
Crosshead load rate of 0.05 inch per minute Soak time minimum of 30 minutes at temperature			

DEVELOPMENT OF NEW PROCEDURE FOR FLATWISE TENSILE TESTING OF SPRAY FOAM INSULATION MATERIAL

INTRODUCTION

The concept of using spray foam for S-II vehicle insulation created a need for refined methods of testing the new material. Standard procedures for fabricating and testing of flatwise tensile specimens resulted in erratic data which made accurate evaluations of flatwise tensile properties impossible. The methods of test and the configuration of the test specimen were studied, and the cause for erratic test results appeared to be a load misalignment in the test specimen that caused unequal distribution of strain.

Four-square-inch aluminum blocks were being used for preparation of test specimens. After test the blocks were prepared for rinse by etch cleaning. However, repeated etch cleaning caused the blocks to become irregular in shape and size. The result was some mismatch of specimens prepared later.

A test specimen was designed using down pins to ensure alignment during the bonding process. The test specimen configuration is shown in Figure 206. Removal of the dowel pin after bond cure permits attachment of loading fixtures and strain measuring instrumentation. The assembly of the fixtures and instrumentation is shown in Figure 207. The microformer extensometer, used in conjunction with a strain recorder of a universal test machine, provides an autographically recorded plot of load versus strain. The assembled test specimen with loading and strain measuring instrumentation is shown in Figure 208.

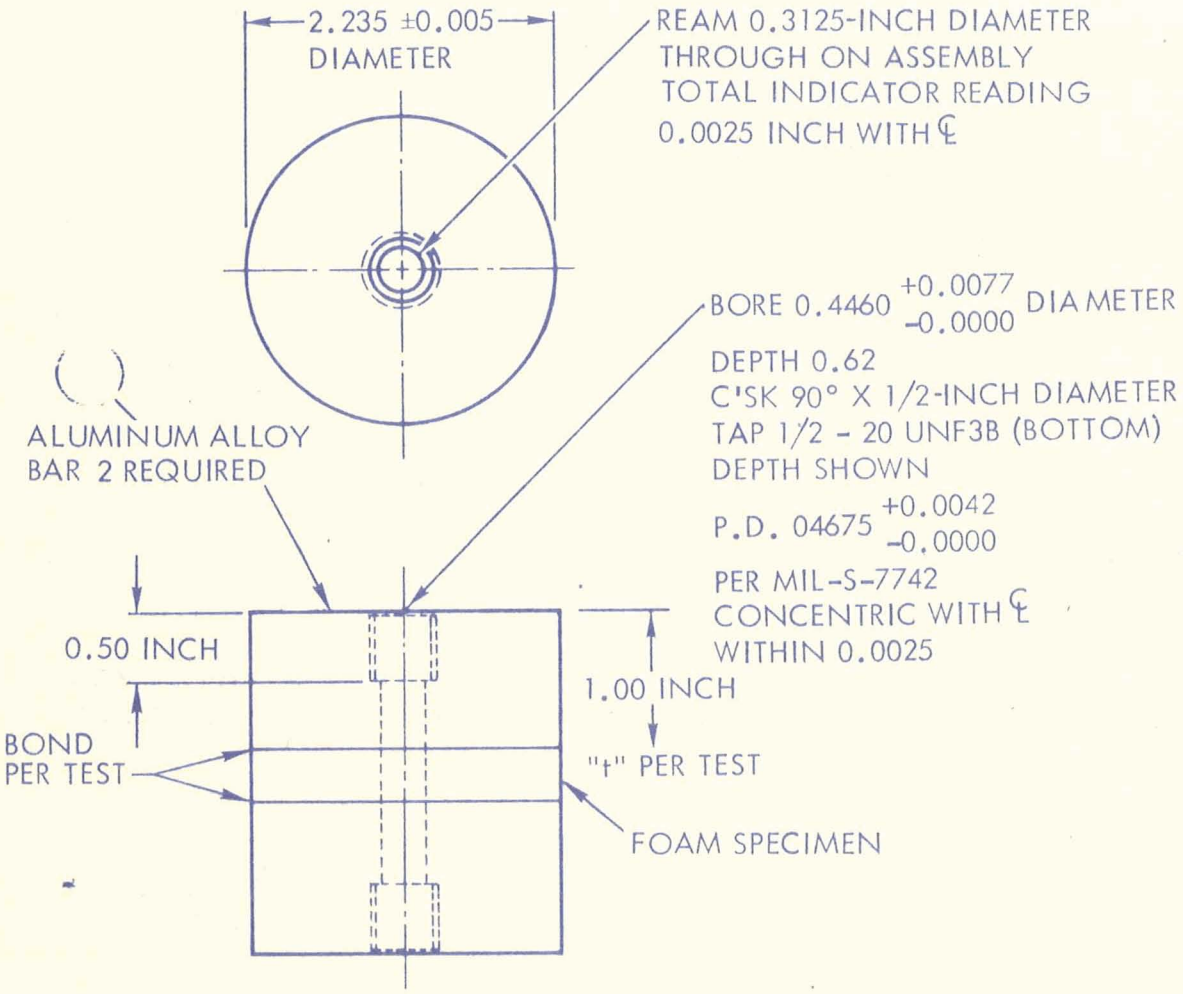

Figure 206. Configuration of Flatwise Tensile Test Specimens

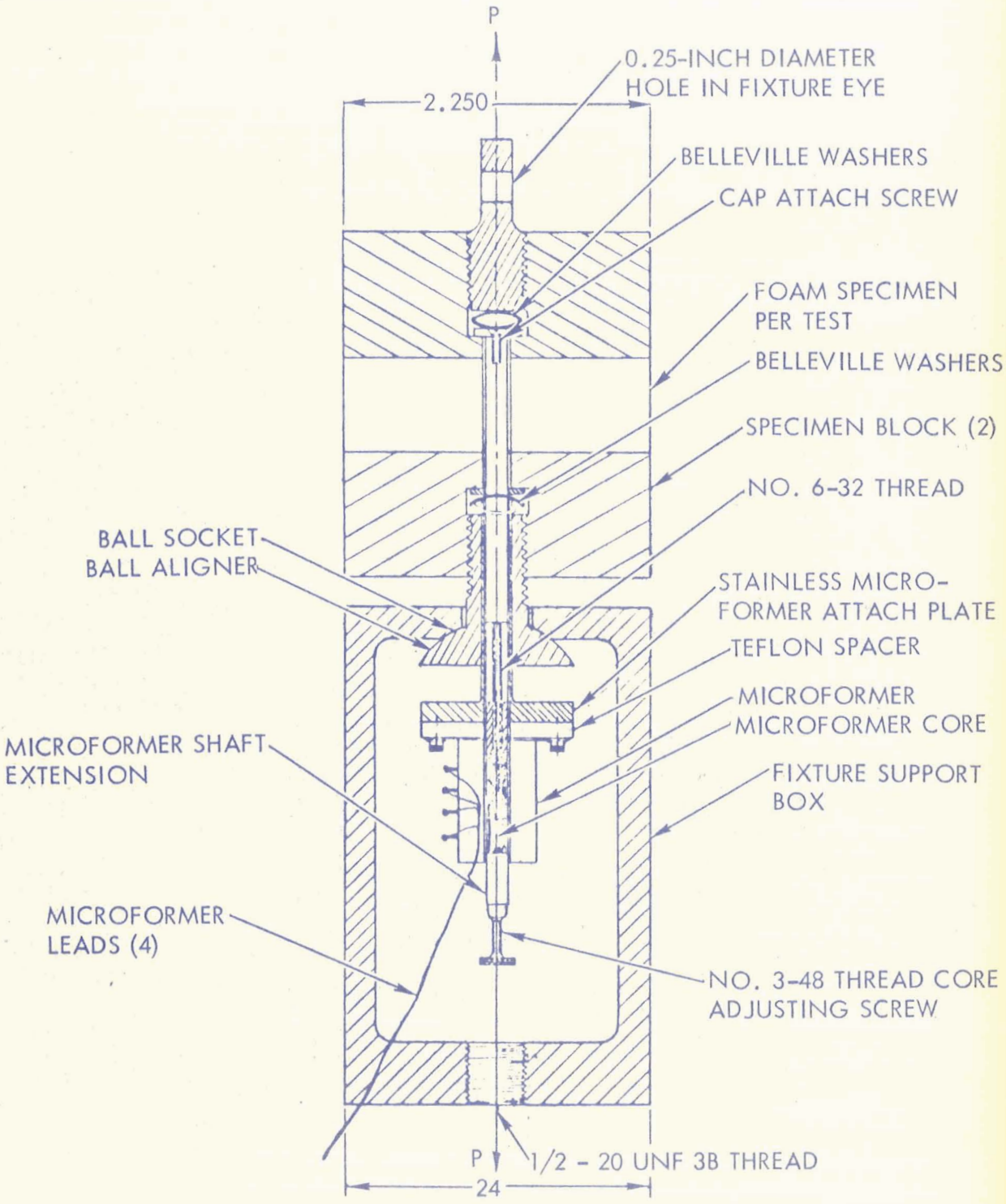

Figure 207. Sketch of Load-and-Strain Measuring Fixture for Foam Flatwise Tensile Testing

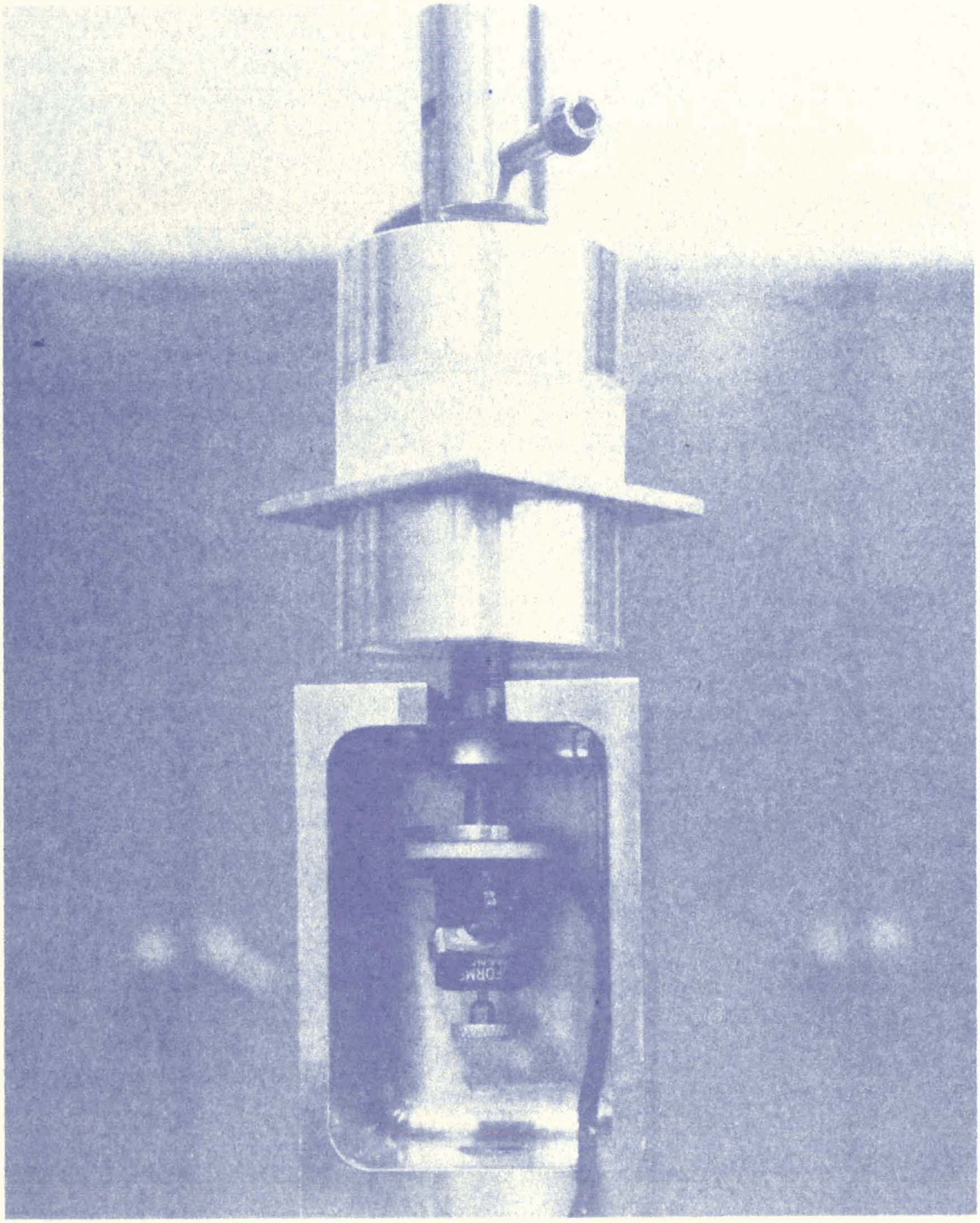

7006-81-2505B

Figure 208. Flatwise Tensile Specimen Installed in Loading Fixture

THERMOPHYSICAL PROPERTIES OF NOPCO SPRAY FOAM BX-250A

INTRODUCTION

Thermophysical properties tests conducted on two different batches of Nopco spray foam BX-250A determined the following:

Apparent density and water absorption of the foam at room temperature

Thermal conductivity of the foam in the direction parallel to foam rise at mean temperatures of -300, -90, +60, +100, and +185 F

Thermal expansion of the foam in two directions, perpendicular and parallel to foam rise, from room temperature to -300 F and from room temperature to +200 F

Closed cell content of the foam

Specific heat of the foam at 130 F

Flame-retardant properties of the foam

RESULTS AND DISCUSSION

Average test results are contained in Tables 61 through 67.

Gas Absorption

When the external gas pressure was changed from 0 to +2 psig in an air atmosphere, the foam absorbed only a small initial amount of air (about 5 percent by volume). However, when the gas pressure in a pure helium environment was suddenly increased from 0 to 1.8 psig, the foam showed a continuous increase in helium absorption with time (Figure 209). The rate of absorption decreased as the pressure inside the foam approached the pressure of the helium environment.

While the extent of testing was limited, the foregoing results suggest that for a small pressure increase (2 psi) in its gas environment, the foam will not (for practical purposes) absorb air. It will, however, continue to absorb helium until the gas pressure inside the foam approaches that outside the foam.

Table 61. Apparent Density Test Results (Average)

Material: Nopco BX-250A Test Method: ASTM D-1622-63	
Batch Number	Apparent Density (lb/cu ft)
02-2594-2/02-55546-1	2.05
02-2594-2/02-47475-1	2.39

Table 62. Water Absorption Test Results (Average)

Material: Nopco BX-250A Test Method: ASTM D-2127-62T					
		Water Absorption			
		Per Unit Surface Area		Per Unit Volume	
Batch Number	Density (lb/cu ft)	(g/1000 sq cm)	(lb/sq ft)	(g/1000 cu cm)	Volume Penetration (Percent)
02-2594-2/02-55546-1	2.04	8.2	0.017	9.7	1.0
02-259 - 2/02-47475-1	2.33	6.1	0.013	7.2	0.7

Table 63. Thermal Conductivity Test Results

Material: Nopco BX-250A (in direction parallel to foam rise) Test Method: ASTM C-177-63						
Batch Number	Average Density (lb/cu ft)	Mean Temperature (F)	Hot Side Temperature (F)	Cold Side Temperature (F)	T (F)	Apparent Thermal Conductivity, k (Btu-in/sq ft-hr-F)
02-2594-2/02-55546-1	1.89	73.4	113.4	33.4	80.0	0.132
		- 89.7	- 71.4	-107.9	36.5	0.164
		-302.2	-284.7	-319.7	35.0	0.080
02-2594-2/02-55546-1	2.18	70.9	110.6	31.2	79.4	0.135
		- 87.7	- 67.5	-107.8	40.3	0.170
		-302.2	-285.4	-319.0	33.6	0.080
02-2594-2/02-55546-1	2.36	101.9	126.5	77.3	49.2	0.148
		185.0	279.4	89.5	189.9	0.183
02-2594-2/02-55546-1	2.42	100.1	125.1	75.0	50.1	0.144
		184.8	277.2	92.3	184.9	0.187
02-2594-2/02-4745-1	2.29	61.3	89.5	33.1	56.4	0.127
		- 88.1	- 68.2	-108.0	39.8	0.169
		-302.1	-284.0	-320.2	36.2	0.083

Table 63. Thermal Conductivity Test Results (Cont)

Material: Nopco BX-250A (in direction Parallel to foam rise)
Test Method: ASTM C-177-63

Batch Number	Average Density (lb/cu ft)	Mean Temperature (F)	Hot Side Temperature (F)	Cold Side Temperature (F)	T (F)	Apparent Thermal Conductivity, k (Btu-in/sq ft-hr-F)
02-2594-2/02-47475-1	2.29	61.5	90.1	32.8	57.3	0.127
		- 87.1	- 65.9	-108.1	42.2	0.153
		-301.5	-282.8	-320.1	37.3	0.084

Test Environment for all tests was 1 atmosphere dry nitrogen

Test Specimen dimension: 13 x 13 x 1 inch for pairs 1A, 2A, 1B, and 2B
6-1/4 x 6 x 1 inch for pairs 3B and 4B

Table 64. Thermal Expansion Test Result Average

Temperature Range (F)	Density (lb/cu ft)	Coefficient of Linear Thermal Expansion, α (in./in. - F)
MATERIAL: NOPCO BX-250A BATCH NUMBER: 02-2594-2/02-55546-1		
Direction Perpendicular to Foam Rise		
80 to 200	1.97	2.7×10^{-5}
+50 to -300	1.96	3.1×10^{-5}
Direction Parallel to Foam Rise		
80 to 200	2.05	3.4×10^{-5}
+50 to -300	2.01	3.1×10^{-5}
MATERIAL: NOPCO BX-250A BATCH NUMBER: 02-2594-2/02-47475-1		
Direction Perpendicular to Foam Rise		
75 to 200	2.27	5.1×10^{-5}
+50 to -300	2.25	3.3×10^{-5}
Direction Parallel to Foam Rise		
75 to 200	2.28	7.2×10^{-5}
+50 to -300	2.30	4.0×10^{-5}
For all tests: Specimen Dimensions - 3 x 1/2 x 1/2 inch Test Environment - 1 atmosphere air above room temperature - 1 atmosphere helium below room temperature Test Method: ASTM D-696-44		

Table 65. Closed-Cell Test Results

Material: Nopco BX-250A
Batch Number: R/T 02-2594-2/02-47475-1
Test Method: ASTM D-1940-62T

Dimensions (in.)	Density (lb/cu ft)	Percent Open Cells	Percent Cell Wall	Percent Closed Cell
3 x 0.8 x 0.8	2.33	9	3	88
	2.35	8	3	89
	2.28	9	3	88
	2.30	9	3	88

Calculation of percent closed cells:

Closed cells = 100 percent - percent open cells - percent cell wall

Where percent cell wall = 100 percent $\times \frac{\text{foam density}}{\text{density of solid polymer}}$

Density of solid polymer is taken to be 80 lb/cu ft

Table 66. Specific Heat Test Results

Material: Nopco BX-250A
Batch Number: R/T 02-2594-2/02-47475-1
Test Method: ASTM C-351-61 (DROP calorimeter)

Mass (g)	Initial Temperature (F)	Final Temperature (F)	Mean Temperature (F)	Specific Heat (cal/g-C)
10.8424	178.0	79.7	128.8	0.32
11.4194	178.0	81.3	129.7	0.33
10.3385	175.6	81.1	128.4	0.33

Test specimen prepared by compressing as much foam as possible into 2- x 15/16-inch diameter brass drop capsule

Table 67. Flammability Test Results

Material: Nopco BX-250A
Batch Numbers R/T: 02-2594-2/02-47475-1 and
02-2594-2/02-55546-1

According to ASTM D-1692-59T

Specimen

Number tested: 10 of each batch

Dimensions: 6 x 2 x 1/2 inch

Preconditioning: 24 hours in laboratory environment*

Results**

Foam classification: nonburning

Observations

Portion of specimen exposed to flame gave off black smoke and was charred after test

According to Federal Specification LP 406B, Method 2021.1

Specimen

Number tested: 10 of each batch

Dimensions: 6 x 1/2 x 1/4 inch

Preconditioning: 24 hours in laboratory environment*

Results**

Foam classification: self-extinguishing

Observations: Same as above

*Approximately 70 F, with 60 percent relative humidity
**Identical results for both batches

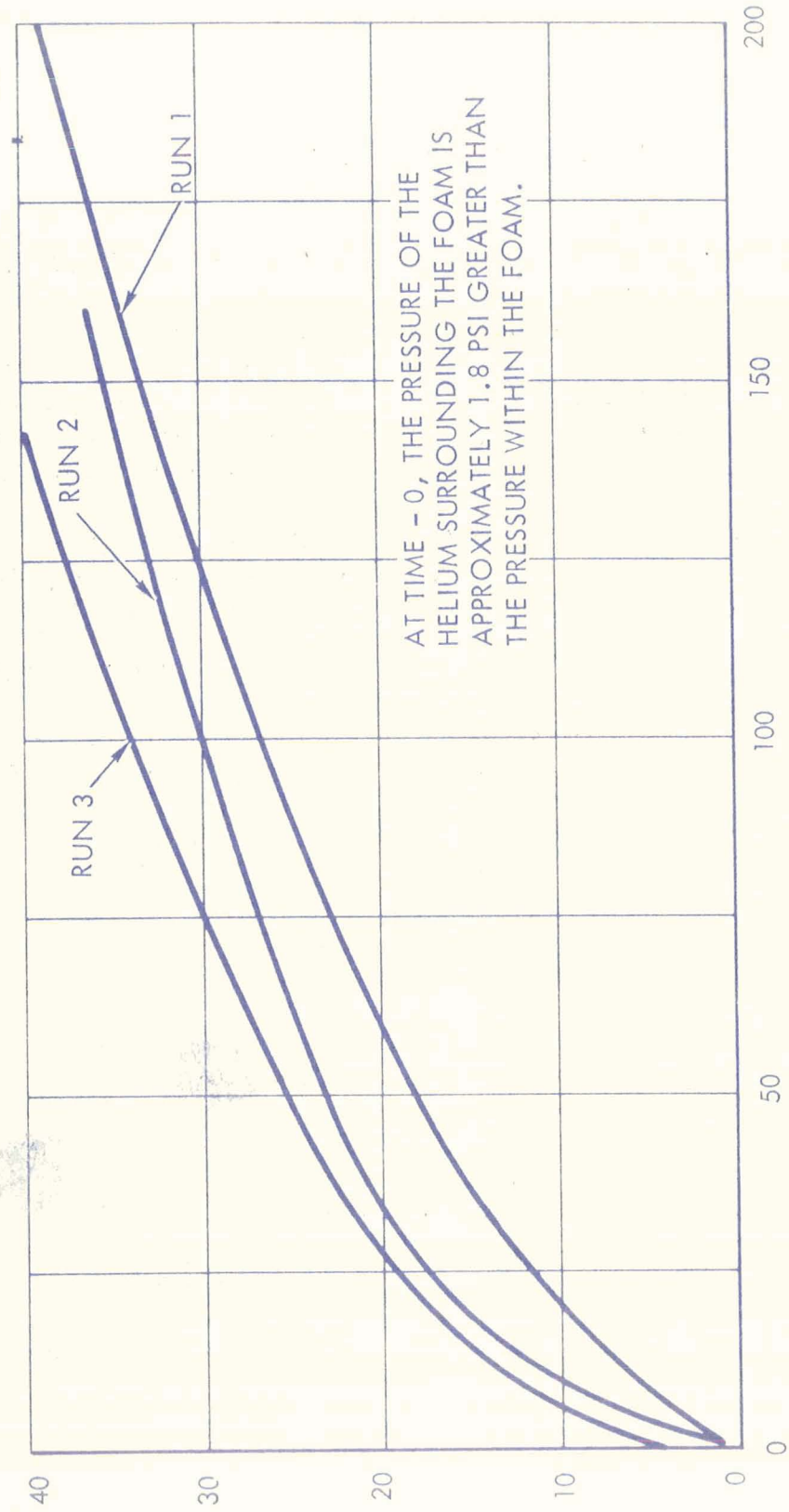

Figure 209. Helium Absorption Versus Time

OVERLAP JOINT PROCESSING TECHNIQUES

INTRODUCTION

An 8- x 22-foot diameter tank was insulated with Nopco BX-250 (MB0130-077) foam and tested cryogenically to verify spray foam insulation for S-II stages. Initial attempts at Seal Beach to apply the Nopcofoam with Binks equipment to the McDonnell Douglas tank resulted in large voids in the overlap areas.

A laboratory program was conducted to determine spray foam processing conditions that might cause voids in overlapping areas during the Nopcofoam BX-250 application.

CONCLUSIONS

Laboratory investigation revealed that the following processing conditions could contribute to the occurrence of voids:

High-velocity impingement of the spray foam components when applying a second pass overlapping previously sprayed foam

Application of relatively thick layers of foam (thicker than 3 inches) when overlapping previously sprayed foam

Using insufficient overlap spray pattern to wet previously applied foam surfaces (i. e. , using an overlap pattern of 1 inch or less)

PROCEDURES

Four different panels were sprayed with Nopcofoam BX-250 using the following processing conditions on overlapping successive foam applications:

Method Number	Nozzle Distances (inches from panel)	Overlap Spray Pattern (inches)	Cured Foam Thickness (inches)
1	10	1	4 to 5
2	10	4 to 5	2 to 3
3	20	1	2 to 3
4	20	4 to 5	3 to 4

The following conditions were equivalent for all panels:

1. The time interval between successive applications was five minutes.

2. The flowrate was approximately 4 pounds/minute

3. Glascraft equipment with a flat fan spray nozzle was used to apply foam.

RESULTS

Figure 210 is a photograph of the overlap cross-section using processing Method 1. It shows the large overlap void that occurred when impingment velocity was relatively high. The overlap spray pattern was at a minimum, and foam layers of from 4 to 5 inches were applied.

Figures 211, 212, and 213 show relatively good overlap joints resulting from the processing parameters described in Methods 2, 3, and 4.

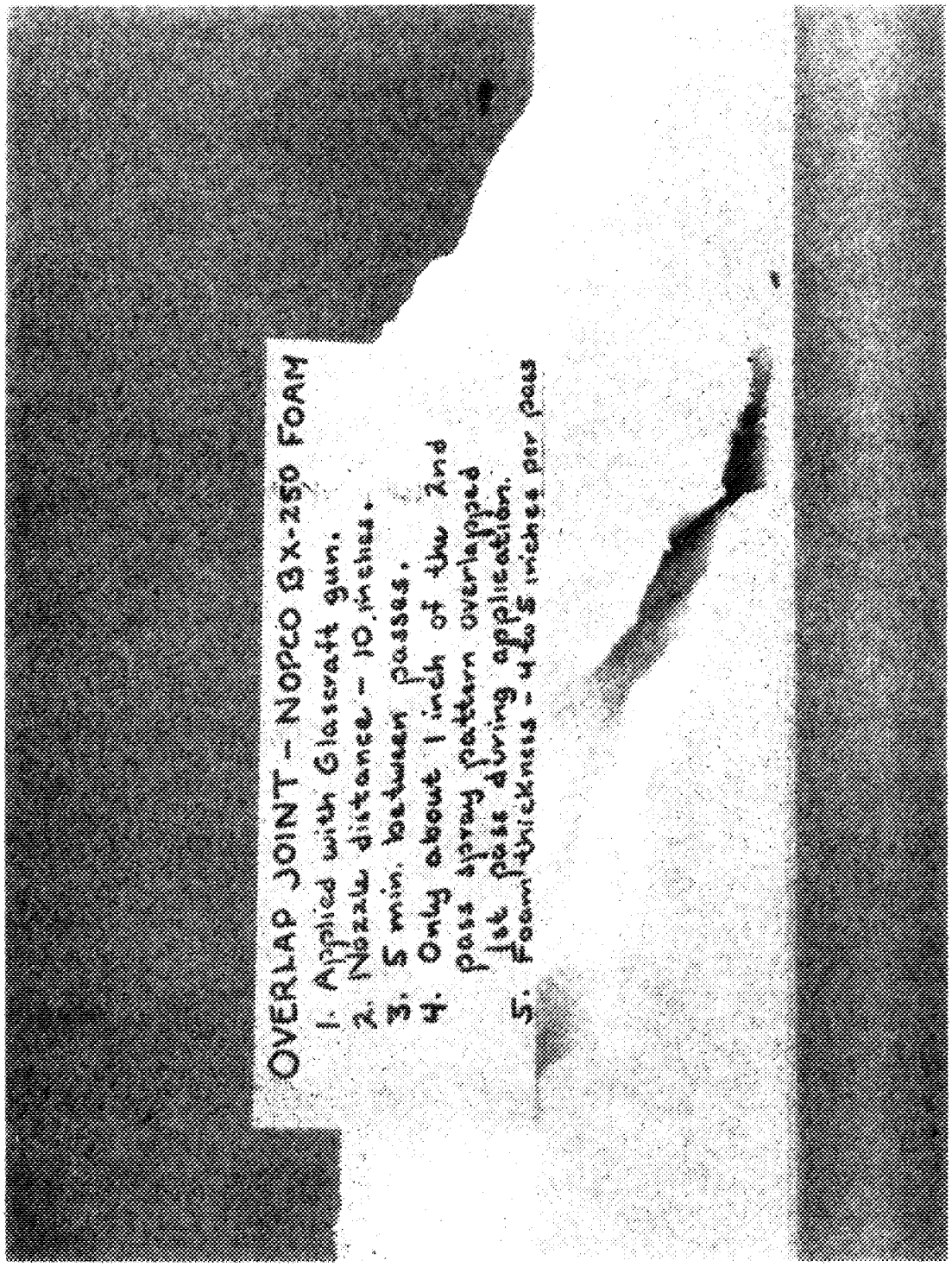

7006-81-2376A

Figure 210. Cross-Section of Overlap Joint Using Processing Method 1

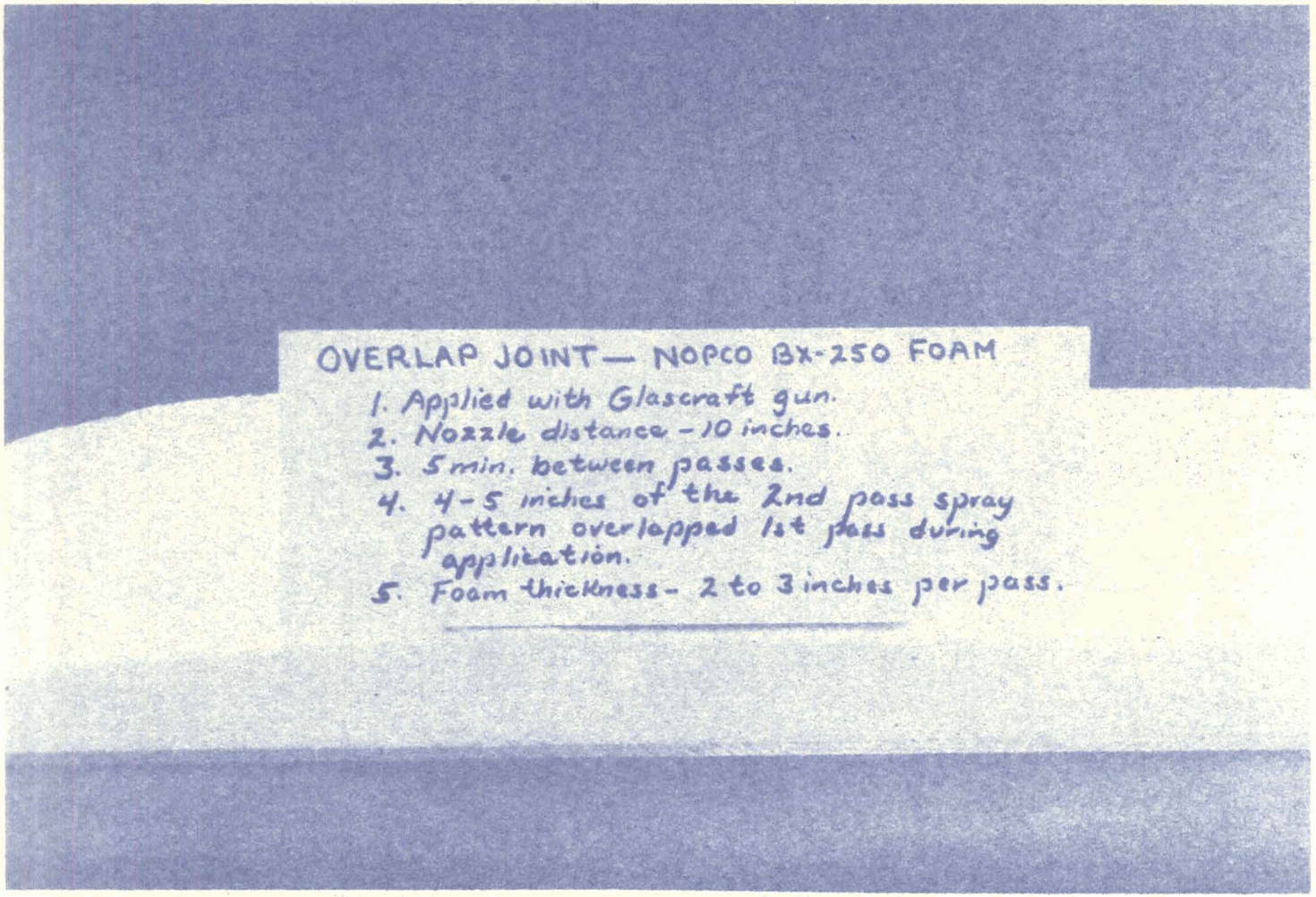

Figure 211. Cross-Section of Overlap Joint Using Processing Method 2

SPACE DIVISION OF NORTH AMERICAN ROCKWELL CORPORATION

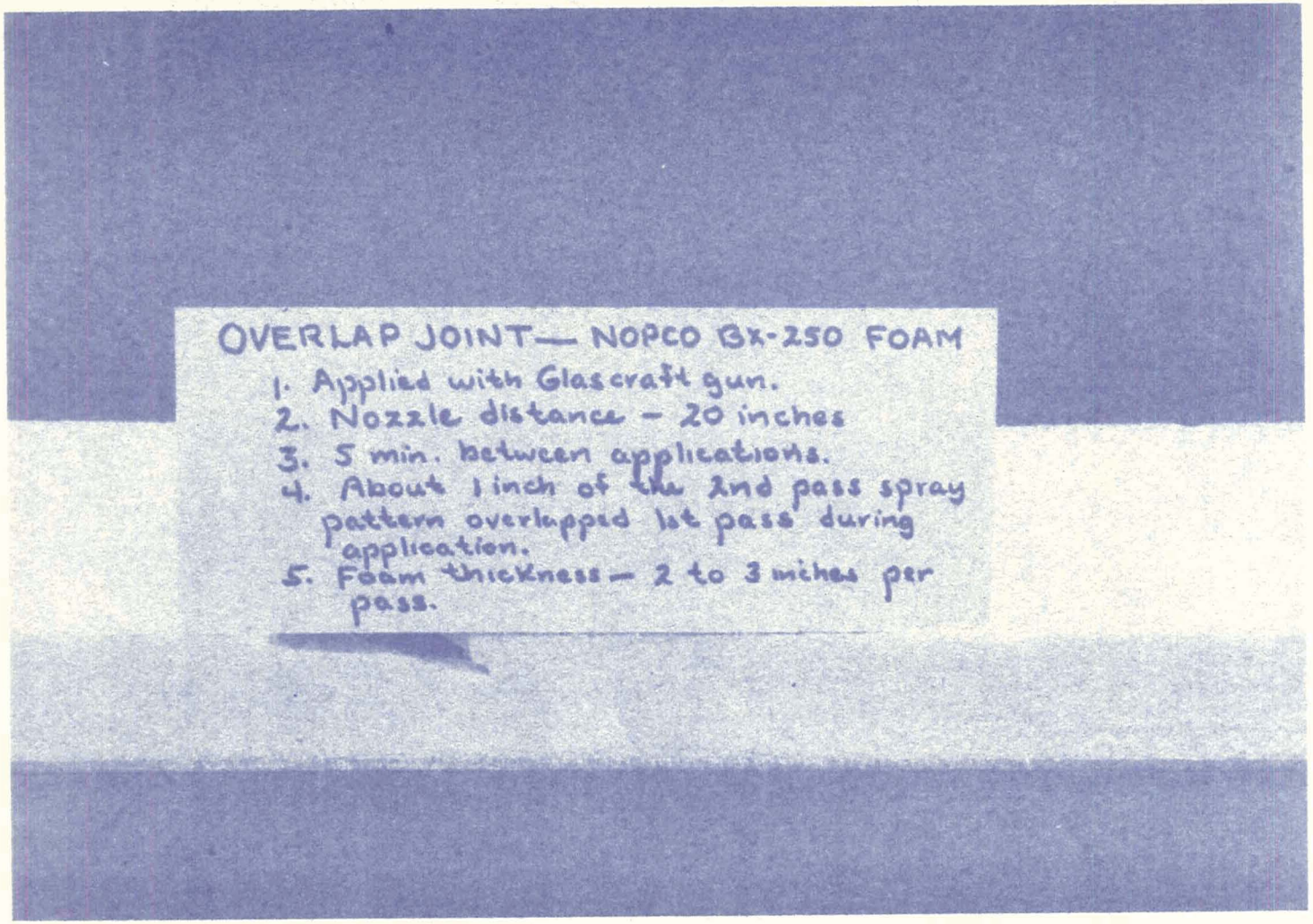

Figure 212. Cross-Section of Overlap Joint Using Processing Method 3

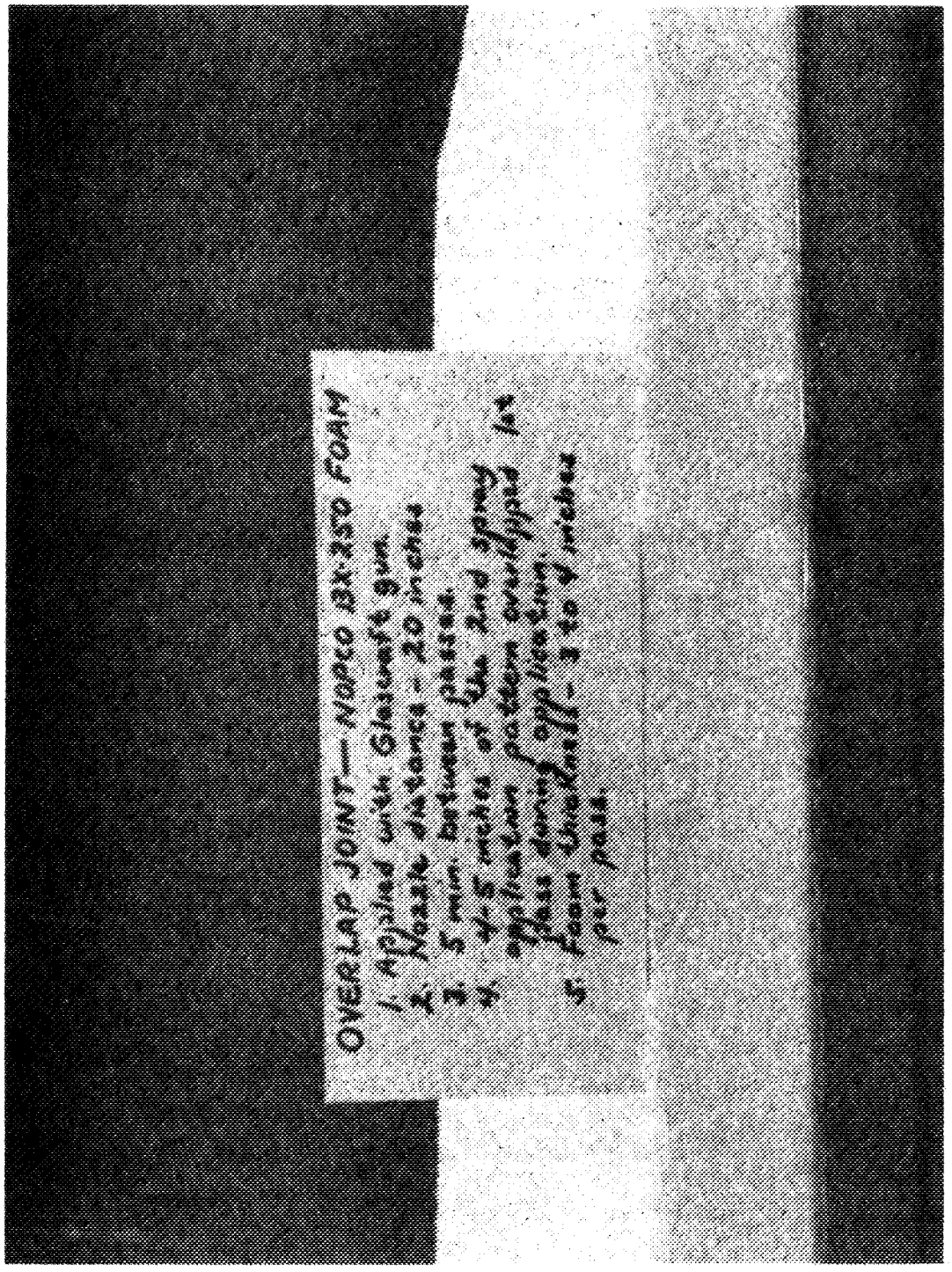

7006-81-237GD

Figure 213. Cross-Section of Overlap Joint Using Processing Method 4

FLAMMABILITY/EXPLOSIBILITY HAZARD ASSOCIATED WITH APPLICATION OF SPRAY FOAM (NOPCO BX-250)

INTRODUCTION

An investigation was conducted to evaluate the potential flammability and explosibility hazard associated with the application of polyurethane foam. Two potential hazards recognized were: flammability of the spray foam in the air after leaving the gun and flammability of the volatiles evolved from the surface during the subsequent foaming process, and explosibility of the polyurethane dust suspension in air created during the final machining operation.

PROCEDURE

Flammability of Airborne Spray

A high-voltage electric arc transformer and electrodes were located in the approximate center of a concrete walled room. The hand-held gun was operated for several seconds through a small hole in the room wall. A suspension of fine spray droplets, requiring considerable dispersal time, was produced in the air inside the room. The electric arc turned on as the interior was viewed through the cell window, but no reaction was observed.

After the preliminary test, with its negative result, all tests were made with the manually-operated spray gun while the ignition source was on. As before, the nozzle was passed through a small hole in wall of the room. The spray was directed on to the electric arc for several seconds and observed through the window. The arc was produced across a gap of about 1/2 inch by a transformer rated to deliver 12 kilovolts and 30 milliamperes.

An oxy-acetylene torch flame was substituted for the electric arc and the spray directed on to it. The flame had an inner cone about one inch long and an outer cone about 6 inches long.

Four tests were run, with the igniter flame 7, 4, 2, and 1 foot from the spray gun nozzle.

Dust Explosibility

A weighed amount of foam dust, passing through a Number 200 sieve, was placed inside the 1-cubic-foot test chamber. The igniter arc was switched on, the dust was suspended by an air blast, and the test was observed through the viewing window.

RESULTS

Flammability of Airborne Spray

Preliminary flammability tests of airborne spray were carried out by using an electric arc igniter and a Glascraft spray gun. Reaction was limited to the material passing through the arc itself, and no propagation was observed. In subsequent testing, the ignition source was an oxyacetylene flame. Limited testing indicates that the spray is not flammable (Table 78). The only indication of flame propagation was observed one instant during the initial test with the oxyacetylene flame: a few spray droplets ignited by the flame appeared to continue burning several inches beyond the flame.

The negative results are not unexpected. Freon is a major constituent of the spray, and large amounts of this noncombustible component may be expected in the vapor and liquid phases during spraying. A flame-inhibiting additive is also incorporated in the spray foam.

The results of dust explosibility are given in Table 69. Nominal dust concentrations greater than 0.01 ounce per cubic foot of air are explosive.

Table 68. Results of Flammability Tests on Airborne Droplets During Spraying Operation

Type of Spray Gun	Distance from Torch Flame to Nozzle of Gun (feet)	Results
Foametic	1	Spray droplets ignited only in torch flame; no propagation
Glascraft	2	
Foametic	4	
Foametic	7	
Ignition source - Oxyacetylene torch flame (inner cone 1 inch and outer cone 6 inches long, approximately)		

Table 69. Results of Dust Explosion Tests

Test Material: Nopco BX-250 Polyurethane Foam Dust, Passing through Number 200 Sieve (74 Microns)		
Weight Dust (ounces)	Number of Tests Conducted	Results
0.01	3	Negative
0.02	3	Positive
0.03	3	Positive
A test was judged positive if a flash (explosion), and an audible report with rupture of the plastic chamber wall resulted. A negative test gave only a flash (rapid ignition, no significant pressure rise). Test chamber volume was 1 cubic foot.		

SIMULATED DEBOND AREAS IN SPRAY FOAM INSULATION

INTRODUCTION

A laboratory study was undertaken to investigate the cryogenic behavior of insulation with simulated debond areas as noted on the Douglas tank. The purpose of the study was to determine: if gaseous hydrogen can cause the type of failure experienced in the insulation of the Douglas tank and if induced cryopumping of air will cause debonding-type failure as noted in the tank.

CONCLUSIONS

No failures were noted in the test panel foam insulation that could be attributed to passage of gaseous hydrogen. No foam insulation failures were observed after test caused by induced cryopumping of air. There was no comparison of the test results and simulated debond areas of this effort with those noted on the Douglas tank.

PROCEDURES

Test Panels

Several 12- x 12- x 3/4-inch foam-insulated panels with 1/8-inch thick aluminum plate backing were prepared with Hypalon external coating. Holes of 0.063-, 0.250-, and 0.875-inch diameter were made through the aluminum plate without impairing the foam interface. Two-inch-square aluminum plates fitted with gas inlet fittings were bonded over the holes with Lefkoweld 109 adhesive.

Gaseous nitrogen, at ambient temperature, was used to pressurize the foam insulation of the panels in an attempt to create debond areas in the test specimens.

The foam-insulated test panels were subjected to gaseous nitrogen at pressures from 40 to 90 psi. Panels with 0.875-inch holes in the metal plate were fitted with a sheet of acrylic with a two-inch diameter opening over the pressurized area to restrict balooning of the Hypalon coating during pressurization. Six coated panels with 0.875-inch holes were pressurized at about 40 psi with nitrogen to create debond foam areas.

TEST TANK

A 30- x 30-inch tank was prepared with BX-250A foam according to MA0606-050, subsequently modified and refoamed as follows:

A section of foam, 8 inches wide and 30 inches long, was removed from the center of the foam insulation attached to the tank surface. Three 2-1/2-inch lengths of 1/8-inch diameter nylon cord (MIL-C-5040, Type II) were bonded with MB0120-024 resin at specific intervals along the upper horizontal foam closeout area at the tank surface.

A coating MB0120-050 resin was applied to the lower horizontal foam closeout area as well as to the upper closeout area. Spray foam according to MA0606-050 was applied to the treated 8- x 30-inch horizontal closeout area.

The foam-insulated test tank, after trimming, was edged with balsa wood, nylon cloth, and MB0120-024 resin. A Hypalon surface coating in accordance with MA0608-014 was applied to the exterior foam surface. A series of 0.063-inch holes was drilled vertically through the coated foam insulation to contact the nylon cord debond areas at the tank surface after Cycle 1, LH_2 run.

TESTING

Six panels with debonded areas were checked at ambient temperature with gaseous hydrogen at a pressure of 0.025 psig; however, one panel was further tested with hydrogen while cooling the panel metal side with LN_2 spray ring (-320 F). Leak detection testing was conducted on the coated areas of the debond section using a mass spectrometer. After testing, the coatings were removed from the foam insulation panels to check the foam condition.

Testing of Test Tank Panel

Cryogenic cycling tests with LH_2 were conducted with and without holes in panel insulation. After the foregoing cycling LH_2 tests, the panel was modified by plugging the 0.063-diameter holes with zinc chromate vacuum-bag putty; in addition, 1/8-inch diameter wire was used to provide horizontal channels through the insulation at the foam/tank surface interface extending from panel edges. A cryogenic cycling test with a 2-hour LH_2 stabilization period was then conducted on the modified Panel 611.

RESULTS

Test Panels

Gaseous hydrogen was readily detected during test at both ambient and cryogenic temperature (-300 F) emitted through the foam and Hypalon coating over the created debond or void areas. Hydrogen pressures did not produce the same type of failure as evidenced in the Douglas tank insulation.

Test Tank Panel

Cryopumping of air through the openings induced in the foam insulation was evident during cryogenic cycling with LH_2. There was no apparent degradation, void areas, or separation in the foam insulation of the panel after completion of the cryogenic cyclic runs.

DEVELOPMENT AND VERIFICATION OF CPR 349-3 POUR FOAM MATERIAL FOR NONSPRAYABLE APPLICATIONS AND SMALL REPAIRS ON THE S-II INSULATION

INTRODUCTION

CPR 349-3, a pour-foam material, was evaluated for such thermal insulation applications as the LH_2 recirculation systems hardware, between stringers, structural ties and hard spots in the bolting ring and Cylinder 1, and for small repairs on the S-II sidewall insulation.

The objectives of the evaluation were to:

1. Develop surface preparation processes for the application of the material to metallic surfaces and hardware or repair areas that may or may not have spray-on foam interfaces
2. Develop foam-in-place techniques
3. Conduct mechanical and physical properties tests
4. Verify the adequacy of the materials and processes
5. Develop sufficient data for establishment of material and process specifications

CONCLUSIONS

Standard existing surface preparation materials and processes currently used for spray foam and foam-in-place applications on the S-II program provided adequate bonding surfaces for the CPR 349-3 foam. Foam-in-place techniques that are standard practice in the state-of-the-art are adequate for applications mentioned. Physical properties of CPR 349-3 pour foam-in-place were similar to spray-on foam CPR 369-3, compared with batches of materials of equivalent density.

PROCEDURE AND RESULTS

Material Properties

Mechanical and physical properties of CPR 349-3 pour foam are reported in Tables 70 through 78.

Temperature and Humidity Evaluation

The Foam materials and mixing equipment were placed in an environmental chamber and allowed to stabilize at the specific test conditions noted in Table 89 before mixing and foaming the test panels. The test panels were cured for a minimum of two hours at each of the specific test conditions before machining the test specimens for determination of density. Density values are given in Table 79.

Heat Sink Effect and Heat of Reaction Evaluation

Aluminum plates (2014-T6) of each respective thickness referenced in Table 80 were machined into 3.5-inch-diameter circles. Each aluminum plate was instrumented with thermocouple wires and placed at the bottom of a paper mixing cup. A 100-gram mix of pour-foam resin was prepared for each aluminum plate. The resin was mixed with a 2800 rpm air motor and a 2-inch diameter propeller for 20 to 23 seconds. The mixed resin was immediately poured over the prepared aluminum plates and allowed to free-foam. The time required for temperature of the foam to stabilize is presented in Table 80.

Foam-In-Place and Coating of LH_2 Elbow Feedline

A test LH_2 feedline elbow was prepared for foam-in-place in accordance with the surface preparation requirements of MA0606-023. Because of the configuration of the elbow, aluminum tape was used as a mold to contain the foam-in-place resin during the foaming operation. The foam operation was performed in several pour operations with a minimum time lapse between pours in order to obtain maximum adhesion at the unmachined foam interfaces. After the foaming operation was completed, the foam was cured for 24 hours at room temperature. The elbow was subjected to combined cryogenic and vibration environment in accordance with NASA 63-2-15. Post-test examination revealed no cracks, blistering, or other insulation failures.

Cryogenic Test Tank

A 30- x 30-inch cryogenic test tank was prepared in accordance with MA0606-045. After the spray foam was machined to the required 1-inch thickness, a 1- x 20- x 20-inch dissection was prepared to simulate a repair. The spray foam in the 20- x 20-inch repair area was removed to the primed metal surface, and the interface surfaces of the existing spray foam were cut at 90 degrees to the surface of the test tank. The spray foam interfaces were sealed in accordance with MA0606-045 using MF0120-024 adhesive. Prior to foam-in-place with the CPR 349-3 foam, the surfaces

Table 70. Average Flatwise Tensile Data Perpendicular to Rise, CPR 349-3 Pour Foam

Test Temperature (F)	Average Flatwise Tensile (psi)
+200	39.4
Room	48.1
-100	41.0
-300	32.8
-423	31.4

Table 71. Average Flatwise Tensile Data Parallel to Rise, CPR 349-3 Pour Foam

Test Temperature (F)	Average Flatwise Tensile (psi)
+200	54.4
Room	75.6
-100	66.7
-300	53.9
-423	45.8

Table 72. Average Flatwise Compressive Data Perpendicular to Rise, CPR 349-3 Pour Foam

Test Temperature (F)	Average Flatwise Compressive (psi)
+200	15.0
Room	24.3
-100	34.9
-300	49.1
-423	34.3

Table 73. Average Flatwise Compressive Data Parallel to Rise, CPR 349-3 Pour Foam

Test Temperature (F)	Average Flatwise Compressive (psi)
+200	22.1
Room	47.6
-100	52.4
-300	53.8
-423	31.3

Table 74. Average Block Shear Data Perpendicular to Rise, CPR 349-3 Pour Foam

Test Temperature (F)	Average Shear Strength (psi)
+200	28.6
Room	35.0
-100	29.4
-300	25.7

Table 75. Average Block Shear Data Parallel to Rise, CPR 349-3 Pour Foam

Test Temperature (F)	Average Shear Strength (psi)
+200	37.4
Room	49.5
-100	44.2
-300	34.7

Table 76. Average Water Absorption of CPR 349-3 Pour Foam (ASTM D-2127-62T)

Density (lb/cu ft)	Water Absorption			Volume Penetration (percent)
	Per Unit Area		Per Unit Volume (g/1000 cu cm)	
	(g/1000 sq cm)	(lb/sq ft)		
2.43	5.5	0.011	6.4	0.7

Note: Specimen - Dimensions = 4 x 4 x 1 inch
Preconditioning of 24 hours in laboratory environment

Table 77. Thermal Conductivity of CPR 349-3 in Direction Parallel to Foam Rise (ASTM C-177-63)

Specimen Pair Number*	Average Density (lb/cu ft)	Hot Side Temperature (F)	Cold Side Temperature (F)	Temperature Difference (F)	Mean Temperature (F)	Apparent Thermal Conductivity, K $\frac{(Btu)(in.)}{(sq\ ft)(hr)(F)}$
1	2.46	121.2	74.5	46.7	97.9	0.185
2	2.39	119.1	66.9	52.2	98.0	0.173
3	2.59	121.8	72.2	49.6	97.0	0.170
1	2.46	257.6	81.4	176.2	169.3	0.246
2	2.49	255.0	80.8	174.2	167.9	0.246
3	2.59	257.2	78.8	178.4	168.0	0.245

Test Apparatus: Air cooled guarded hot plate

Test Environment: 1 atmosphere dry nitrogen

Specimen Dimensions: 13 x 13 x 1 inch

*Each of the three pairs of specimens was tested at two temperatures

Table 78. Average Thermal Expansion of CPR 349-3
(ASTM D-696-44)

Temperature Range (F)	Average Density (lb/cu ft)	Average Coefficient of Linear Thermal Expansion (inches/in/F)
Perpendicular to Foam Rise		
+80 to +200	2.56	4.5×10^{-5}
+50 to -300	2.59	4.3×10^{-5}
Parallel to Foam Rise		
+80 to +200	2.51	2.4×10^{-5}
+50 to -300	2.52	1.9×10^{-5}
Test Environment:	1 atmosphere air for 80 to 200 F range 1 atmosphere helium for 50 to -300 range	
Specimen Dimensions:	3 x 1/2 x 1/2 inch	

Table 79. Effect of Temperature and Relative Humidity on Density of CPR 349-3

Relative Humidity (percent)	Temperature (F)	Density (lb/ft^3)	
		Mixed by Hand	Mixed by Air Motor
30	60	2.63	3.99
50	60	2.26	3.58
70	60	2.36	3.28
30	75	2.46	3.82
50	75	2.92	3.51
75	75	2.52	3.28
30	90	2.50	4.21
50	90	2.41	3.19
75	90	2.35	3.02

Table 80. Heat Sink Effect

Aluminum Thickness (inches)	Initial Aluminum Temperature (F)	Maximum Temperature Rise of Aluminum* (F)	Time Required for Temperature to Stabilize (minutes)
0.020	75	115	2.50
0.020	75	115	3.00
0.020	80	118	3.50
0.040	75	107	3.25
0.040	77	110	3.50
0.040	75	110	2.75
0.075	75	105	3.75
0.075	75	105	2.50
0.075	75	105	2.50
0.100	80	120	3.75
0.125	80	102	2.75
0.125	120	115	0.75
0.125	50	95	5.25

*The maximum temperature rise of the aluminum was measured on the back side of the aluminum test plate or the surface not in contact with the foam.

were lightly solvent-wiped with methyl ethyl ketone. The foam-in-place resin was mixed and poured into the prepared area and allowed to free foam. After a 24-hour room temperature cure, the foam in the repair area was machined to a uniform 1-inch thickness consistent with the existing spray-on foam surface. The machined foam surface of the tank was coated with the moisture barrier coating in accordance with MA0608-014. After the moisture barrier coating was cured, the tank was instrumented and insulated for environmental testing (Figures 214, 215, and 216).

After vibration and simulation aerodynamic heating under cryogenic conditions, the moisture barrier coating was removed from the foam surface. Product qualification verification (PQV) tests (MQ0501-034) were conducted on the foam to determine the effects of the environmental conditioning. Figure 217 provides the results of the PQV tensile testing. The values noted illustrate the integrity of the foam.

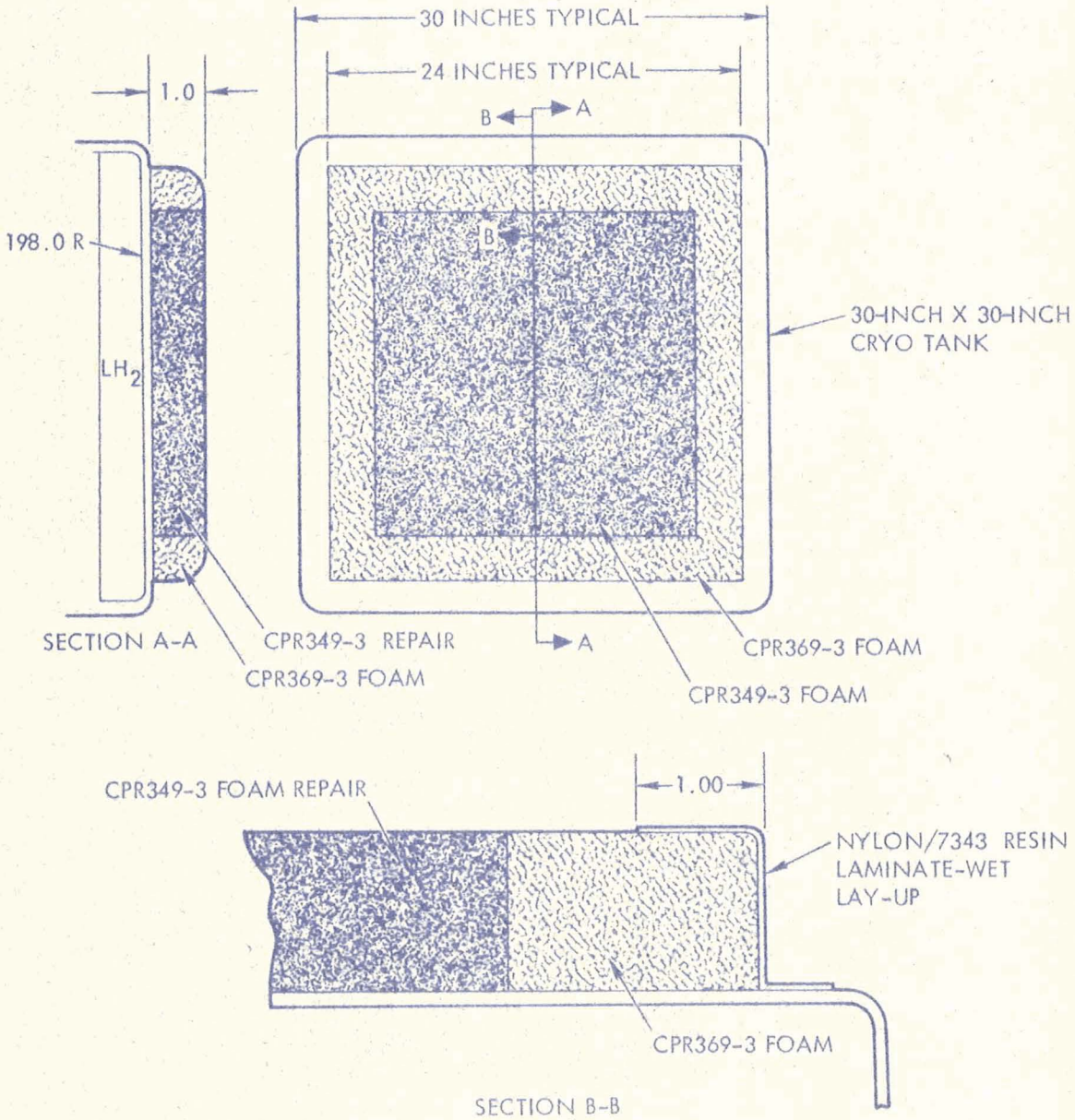

Figure 214. Spray Foam and 20-x 20-Inch Foam-In-Place Repair on 30-x 30-Inch Cryogenic Test Tank

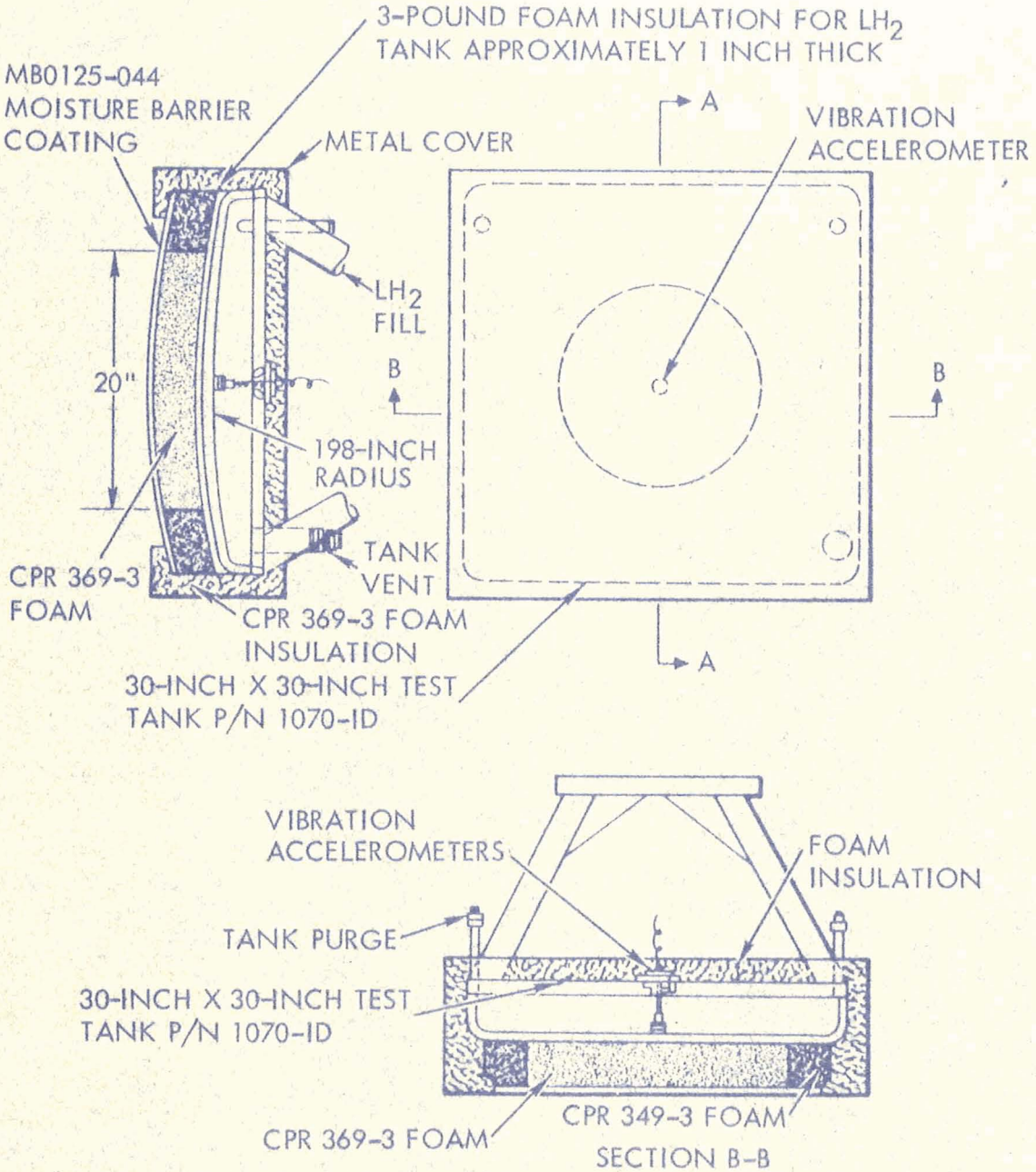

Figure 215. Final Configuration of 30- x 30-Inch Cryogenic Tank Test With Foam-In-Place Repair

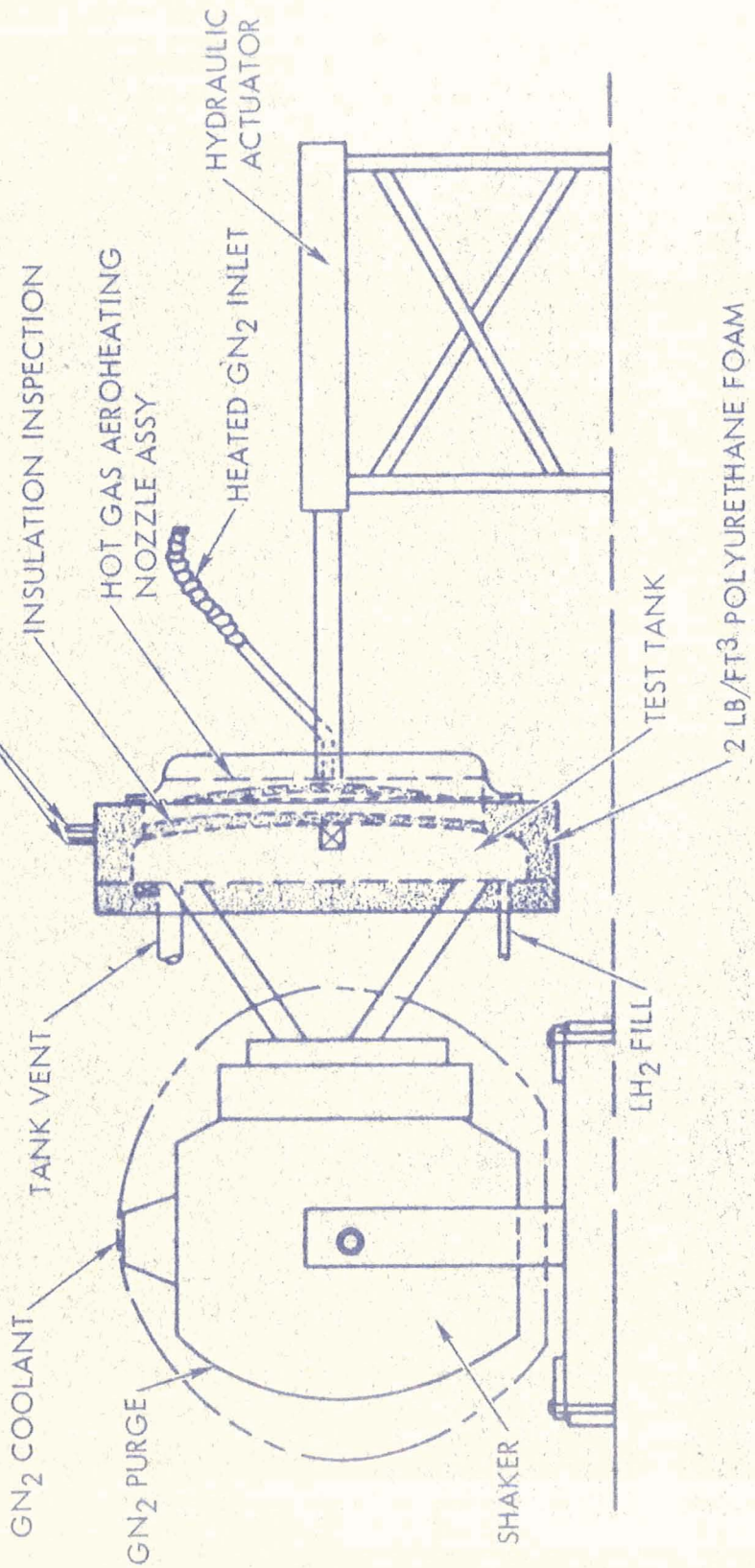

Figure 216. Final Setup of Shaker, Cryogenic Test Tank, and Hydraulic Actuator

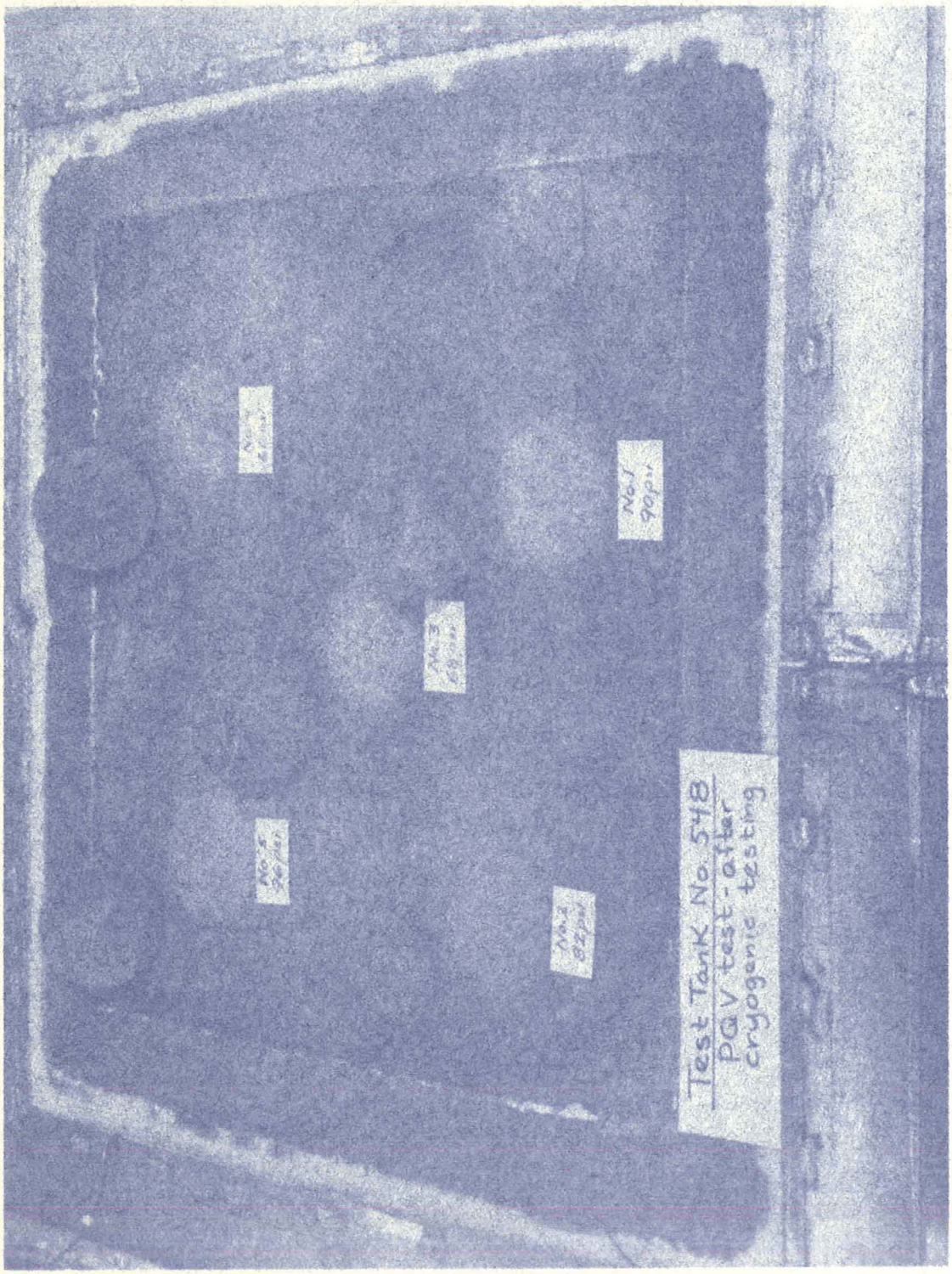

Figure 217. PQV Test Values Obtained After Cryogenic Testing

7006-81-2320A

CRYOGENIC STRAIN COMPATIBILITY OF CPR 349-3 POUR FOAM

INTRODUCTION

CPR 349-3 pour foam was evaluated for possible use as a repair material for sprayed sidewall foam insulation. To be qualified, the pour foam must meet the cryogenic strain compatibility requirements of the sprayed foam insulation described in MB0130-077.

CONCLUSION

Based on the results of the cryogenic compatibility testing, CRP 349-3 pour foam should not be used in the insulation of aluminum substrates that will be exposed to -423 F temperature and stressed to a level of 71,000 psi.

SPECIMEN PREPARATION

A 1/8-inch thick 2014-T6 aluminum coupon was etched in conformance with MA0110-024, primed with M-602 (MB0120-032), in accordance with MA0106-045, and primed with Primer M (MB0120-042 Type II). The Primer M was cured for more than 16 hours at 70 to 80 F before foam application.

The plates were attached to plywood as shown in Figure 218, and the wooden forms were clamped together. Five hundred grams of CPR 349-3 foam components were mixed in the required proportions and poured into the trough. The aluminum cryogenic strain compatibility specimens were positioned on edge during the pour foam operation so that the flat surface was parallel to the rise direction of the foam. (See Figure 219.)

After a 48-hour room temperature cure, the specimens were machined, and foam-filled honeycomb core blocks were bonded to the ends of the foam specimen. (See Figure 220 for details of the specimen configuration.)

Cryogenic Compatibility Tests

Testing was conducted 6 days after the pour foaming operation. Figure 221 shows test specimens before testing.

The test specimens were instrumented, installed in a test fixture, and tested as follows:

1. The metal specimens were brought to a temperature of -423 F in 30 minutes.

2. The surface temperatures were held at:

   Specimen 445 - 64 F

   Specimen 446 - 63 F

   Specimen 447 - 82 F

3. Tension stresses were applied as follows:

   Specimen 445 - 71,000 psi

   Specimen 446 - 35,000 psi

   Specimen 447 - 71,000 psi

RESULTS

The results were as follows:

Specimen 445 - 40 percent debond

Specimen 446 - no debond

Specimen 447 - 90 percent debond

Figure 222 shows the extent of debonds in Specimen 445 and 447.

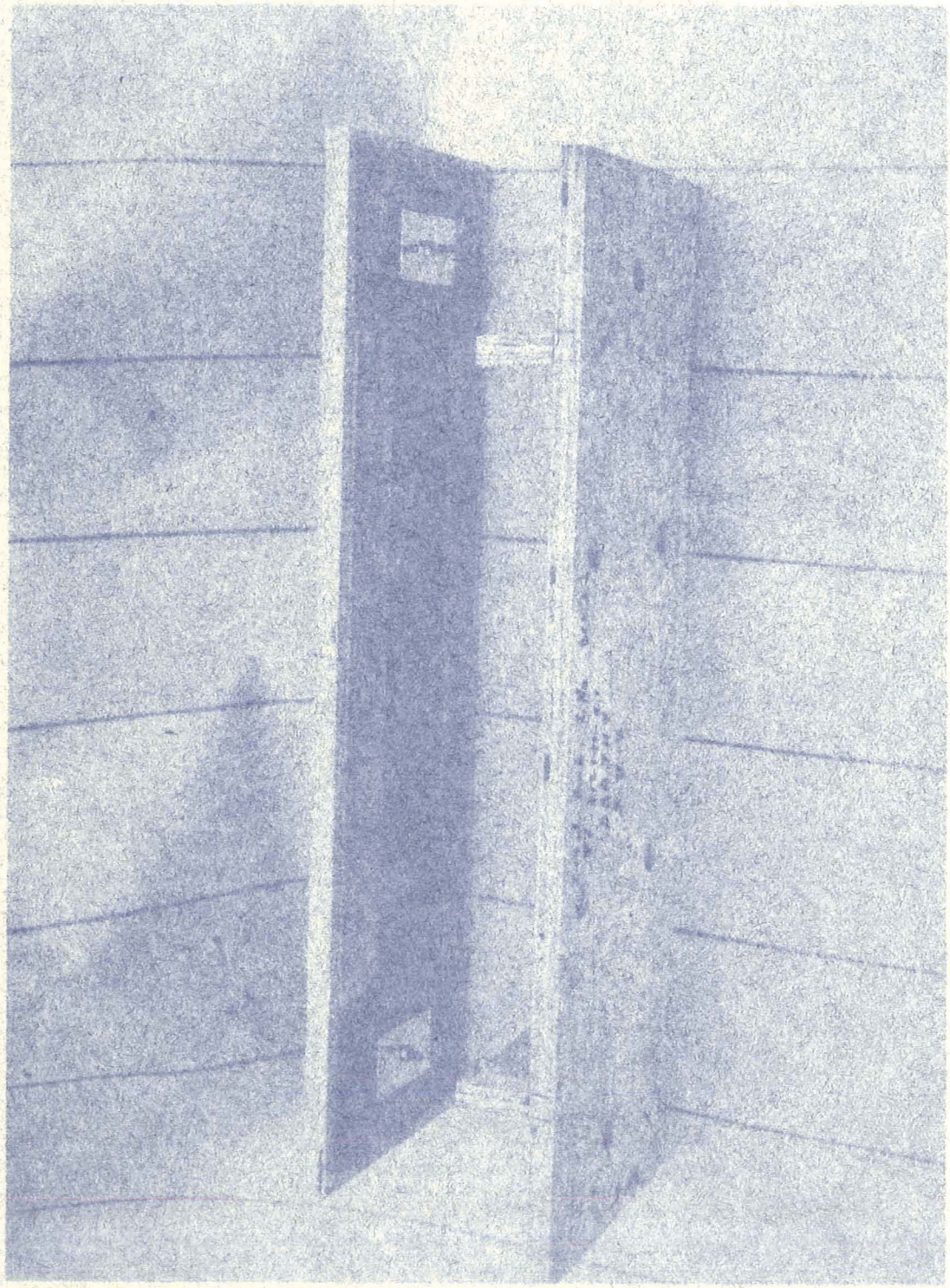

700-81-1109C

Figure 218. Fixturing for Pouring of Cryogenic Strain Compatibility Specimen

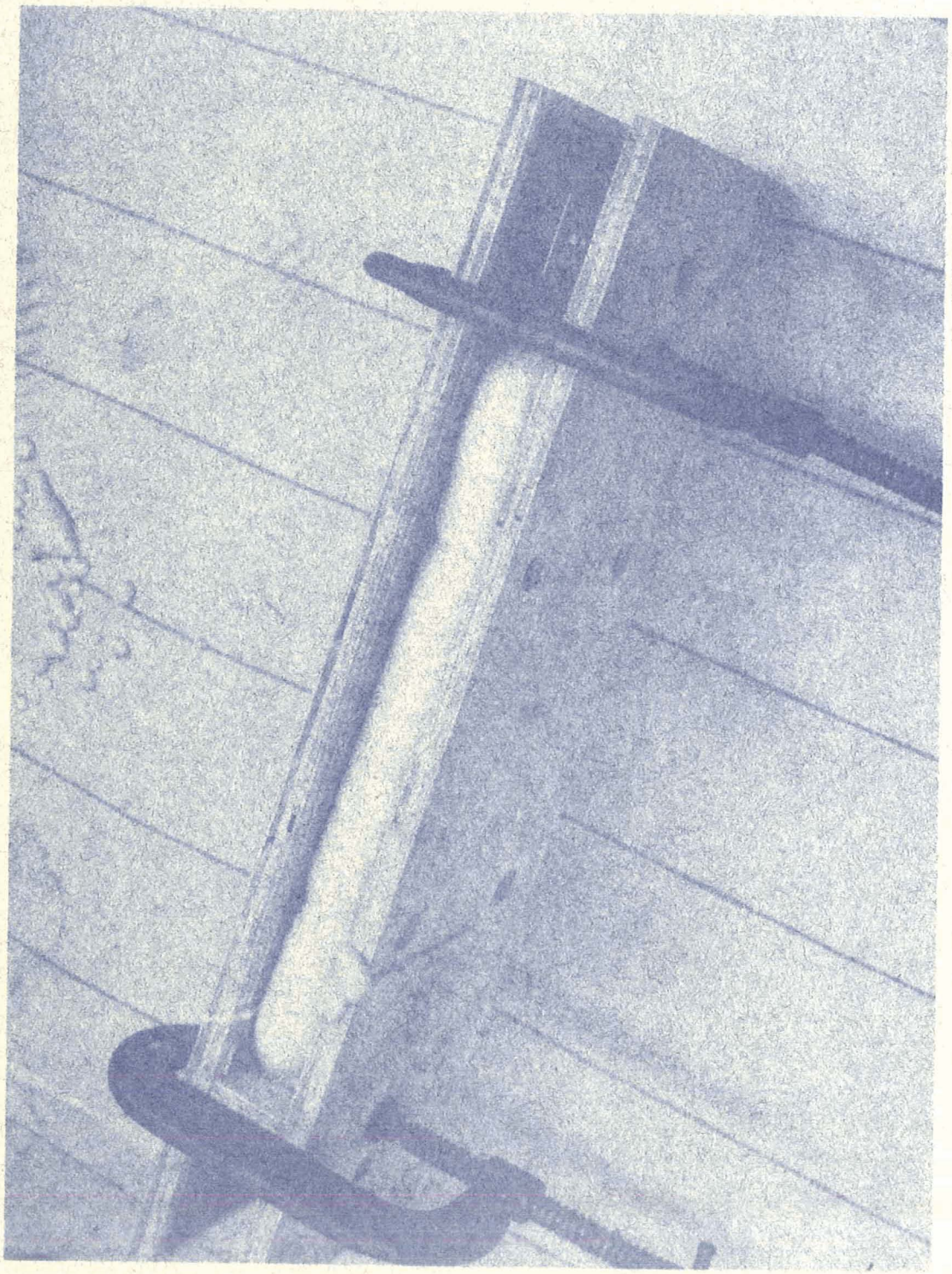

700-63-1109B

Figure 219. Fixture Clamped in Position and Foam Poured

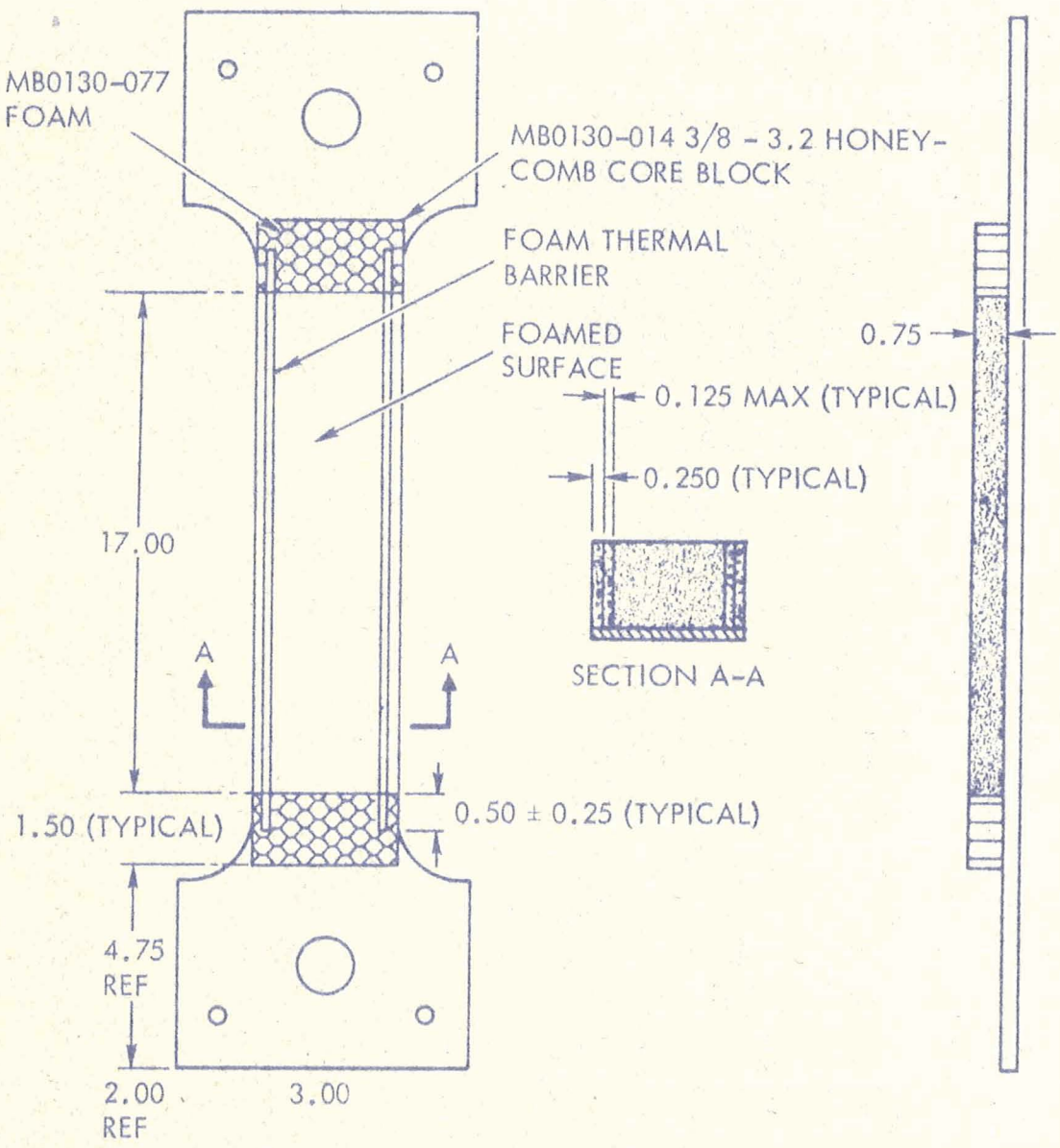

Figure 220. Configuration of Cryogenic Strain Compatibility Specimens

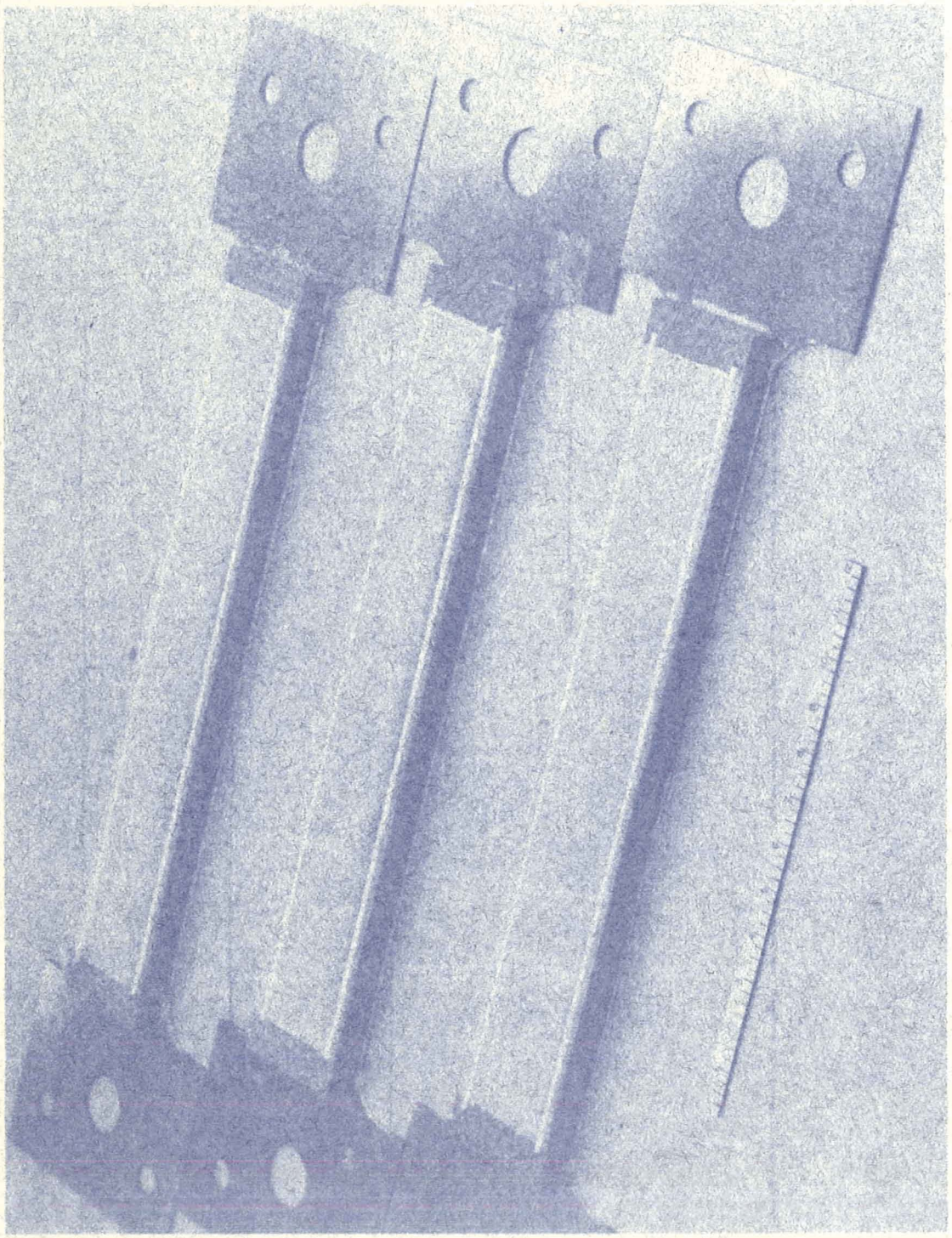

7006-81-2499E

Figure 221. Specimens 445, 446, and 447 Prior to Test

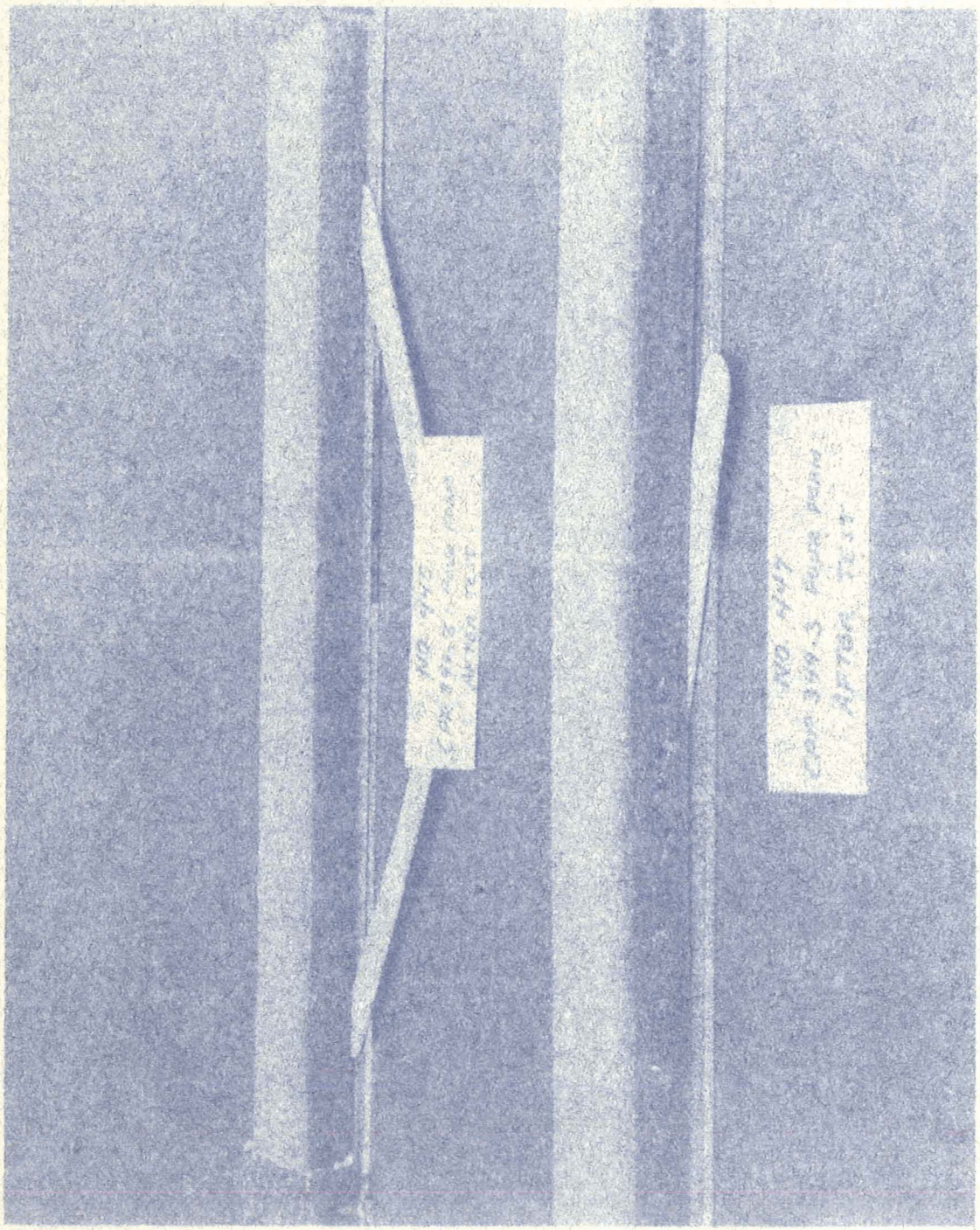

Figure 222. Specimens 445 and 447 After Test

7006-81-2511L

ADHESIVES AND PRIMERS

PROGRESS SUMMARY

The engineering decision to replace the basic honeycomb insulation on the S-II stage skirt with foam insulation resulted in the proposal to apply the foam directly to a Chem-filmed epoxy-painted surface. An investigation revealed that the Chem-filmed, epoxy-painted surfaces with applied spray foam would withstand the thermal shock of liquid nitrogen immersion. However, the lap-shear strength of the bond was considerably below current requirements.

An engineering decision to replace the 2020 aluminum in the S-II stage skirts with 7075 aluminum necessitated a curing temperature change in the processing of the M-602 primer. However, the physical properties of 7075 aluminum are sensitive to temperatures above 260 F. It was determined that M-602 primer cured at 240 F for a minimum of 12 hours could be used as a corrosion-preventive coating and as a substratum for spray foam insulation.

Adhesion inconsistencies in the bonding of foam and hard spots to M-602 primed surfaces with Narmco 7343 was experienced. An investigation revealed that cured Narmco 7343 adhesive peels from Primer M-coated M-602 primer more readily than from M-602 primer that has not been coated with Primer M.

EVALUATION OF THE MECHANICAL PROPERTIES OF CHEMICAL FILM, EPOXY PAINT SURFACE FOR ADHESIVE BONDING

INTRODUCTION

It had been proposed to apply Nopco BX-250 spray foam (MB0130-077) directly to the paint surface at the forward skirt, which would eliminate the need for changing current process specifications and procedures. It would also remove the need to strip, clean, and prepare forward skirt sections that have already been processed both at Seal Beach and at Tulsa.

The investigation consisted of determining the feasibility of adhesive bonding to a chemically filmed surface-coated with epoxy paint, primed and not primed with Primer M.

CONCLUSIONS

The lap shear strengths of the epoxy paint surface with and without the use of Primer M primer were below the present requirements for surface preparations before foam application (MA0606-050).

The bonding surfaces with and without Primer M and spray foam applied according to MA0606-050 are capable of withstanding the thermal shock of liquid nitrogen immersion. No paint-to-primer or primer-to-foam failures were noted.

Metal-to-Metal Lap Shear

The 7075-T6 aluminum sheet specimens were immersion-cleaned to comply with MA0610-023, chemically filmed according to MA0610-002, and then processed with two box coats of epoxy paint in accordance with MA0108-009.

One-half of the specimens was coated with Primer M to agree with MA0106-032. Other specimens for control samples were primed with M-602 primer over the bare cleaned aluminum surface. Narmco 7343 adhesive was applied to lap shear specimens in accordance with MA0106-032 and cured for 16 hours at room temperature followed by 4 hours at 160 F. All specimens were cured at the same time, on the same platen and with the same vacuum pressure.

Thermal Shock Specimens

A 24- x 24- x 0.125-inch panel of 7075-T6 aluminum sheet was chemically filmed and coated with epoxy paint. Half of the painted panels were primed with Primer M. Aluminum panels were also immersion cleaned and primed with M-602. All the panels were spray-foamed with Nopco BX-250A according to MA0606-050 and machined to 0.75-inch thickness of foam after curing. Test panels, 6 x 6 inches, were cut from the center of each of the 24- x 24-inch panels.

Test Method

The metal-to-metal lap shear specimens were tested in accordance with Federal Specification MMM-A-132.

Thermal shock specimens were subjected to LN_2 thermal shock, and examined for foam-to-metal separation. The specimen was allowed to return to room temperature and again subjected to LN_2. The test was repeated for ten cycles for each specimen.

RESULTS

The results of the metal lap shear strength tests are listed in Table 81. The thermal shock specimens indicated that there were no failures on any of the three sets of specimens.

The specimens with the chem-film, epoxy paint, and Primer M achieved only 36 percent at room temperature and 30 percent at -300 F of the lap shear strengths attained by the control specimens. The specimens with the chem-film, epoxy paint, and without Primer M were only 36 percent at room temperature and 26 percent at -300 F of the lap shear strength attained by the control specimens.

Table 81. Average Primer Lap Shear Test Data

Condition	Test Temperature (F)	Ultimate Stress (psi)	Type Failure
Epoxy paint with Primer M and Narmco 7343 adhesive	Room -300	925 867	Adhesive Adhesive to primer
Epoxy paint, no primer, and Narmco 7343 adhesive	Room -300	933 970	Cohesive - adhesive Adhesive to primer
Control specimens - M-602 primer with Narmco 7343 adhesive	Room -300	2597 3293	Adhesive - cohesive Metal to primer

EVALUATION OF M-602 PRIMER CURED AT 240 F

INTRODUCTION

A laboratory study was conducted to determine the feasibility of curing M-602 primer (MB0120-032) at a lower temperature. This study was initiated by an S-II Engineering decision to change the forward skirt components to 7075 aluminum, the physical properties of which are sensitive to temperatures above 260 F. It is therefore imperative that the primer system used in the foam insulation process be cured at a temperature below 260 F. A cure temperature of 240 F was selected, and the cure time was determined for M-602 primer to meet the following physical properties:

1. The cured primer shall be sufficiently tack-free, firm, and adherent to be used alone as a corrosion preventive coating.

2. The cured primer shall be capable of withstanding solvent-wipe with methyl ethyl alcohol in accordance with MA0110-010.

3. Bonds made over the cured coating shall exhibit a minimum lap-shear strength on 7075 aluminum of 1500 psi at room temperature, -300 F, and -423 F.

4. The cured primer, with Nopco BX-250 foam applied over it, shall be capable of withstanding ten thermal shock cycles consisting of exposure of the metal surfaces to liquid nitrogen.

CONCLUSIONS

M-602 primer, cured for 12 hours at 240 (+5, -0) F, will meet the target requirements given in the Introduction.

PROCEDURE

The metal-to-metal lap-shear specimens were tested in accordance with Federal Specification MMM-A-132, using a loading rate of 0.05 inch per minute on the 6000-pound range. The thermal shock specimens were subjected to LN_2 and then examined for foam-to-metal separation. The test was repeated for ten cycles. The corrosion test panels were subjected to a 5-percent salt fog exposure at 95 degrees for 10 days, in agreement with MIL-STD 810, Method 509.

RESULTS

Results of the metal lap-shear strength tests for the various cure cycles of the M-602 primer are listed in Tables 82 and 83.

Thermal shock specimens indicated that there were no primer-to-metal or primer-to-foam failures for either the 12-hour cure at 240 F or for control specimens cured at 290 F for 3 hours.

The results of the effects of 5-percent salt spray corrosion tests for the 12-hour cure at 240 F and the control specimens (3 hours at 290 F) were comparable. There were no corrosion pits after 240 hours salt-spray exposure on the three panels cured at 240 F. There were four corrosion pits after 240 hours salt-spray exposure on the three panels cured at 290 F.

Results of the methyl ethyl ketone wipe-on M-602 indicated that extra care must be taken when cleaning M-602 cured only 3 hours at 240 F. All other cure cycles—6, 12, 18, and the control—evidenced no signs of deterioration when rubbed vigorously with methyl ethyl ketone-soaked cheese cloth.

Table 82. Average Cure Lap Shear Test Data

Cure Time at 240 F (hours)	Test Temperature (F)	Ultimate Stress (psi)
3	Room	1520
3	-300	1617
6	Room	1960
6	-300	1687
12	Room	2183
12	-300	1776
18	Room	2190
18	-300	1761
12	-423	1671

Table 83. Average Lap Shear Test Controls

Cure Time at 290 F (hours)	Test Temperature (F)	Ultimate Stress (psi)
3	Room	1760
3	-300	2157
3	-423	1624

ADHESIVE AND PRIMER COMPATIBILITY WITH M-602

INTRODUCTION

A laboratory study was conducted to determine the compatibility of various adhesives and primers currently in use on the spray foam program for Saturn S-II.

The purpose of this investigation was to determine the compatibility of Narmco 7343 adhesive (MB0120-024) and Primer M with M-602 coatings that have been cured for 3 hours at 290 F, 6 hours at 290 F, and 30 minutes at room temperature, 30 minutes at 240 F, then 1 hour at 340 F.

Also investigated was the adhesion of cured Narmco 7343 adhesive with M-602 coatings that have been cured for 3 hours at 290 F, 6 hours at 290 F, and 30 minutes at room temperature, 30 minutes at 240 F, then 1 hour at 340 F.

CONCLUSIONS

Applications of MB0120-024 resin, curing agent and Primer M, allowed to remain in contact at room temperature for time periods up to 30 days with M-602 primer, and cured by the three test conditions did not visibly degrade the M-602 primer. Cured MB0120-024 resin peels from the Primer M-coated M-602 primer more readily than from M-602 primer uncoated with Primer M. This was true for the three M-602 primer cures evaluated. Peel failures were confined to the Primer M to M-602 bond where the two primers coexisted.

PROCEDURES

Six 2024-T6 aluminum sheet panels were immersion-cleaned according to MA0610-023 to remove chemical film or anodized surface. M-602 primer was applied in accordance with MA0106-045, except for the cure cycle. Two panels (A-1 and A-2) were cured for 3 hours at 290 F. Two panels (B-1 and B-2) were cured for 6 hours at 290 F. Two panels (C-1 and C-2) were cured for 30 minutes at 240 F and 1 hour at 340 F.

Each of the six panels was divided into 2- by 2-inch squares. Along the top of the panel were the numbers 5, 10, 15, 20, and 30, indicating the number of days per exposure prior to test. Along the sides of the panels were the following letters indicating the coatings applied to the panels:

a. MB0120-024 uncatalyzed 7343 resin

b. MB0120-024 curing agent for 7343

c. MB0120-042, Primer M in accordance with MA0606-045

d. MB0120-024 catalyzed resin

e. MB0120-024 catalyzed resin over Primer M

Test panels were allowed to cure for 5, 10, 15, 20, and 30 days. At the end of the various cures, an X-acto knife with a No. 10 blade was used to begin peeling or lifting the overlying adhesive or primer films. If the film could be removed, the panel was examined under 20X magnification for visible degradation of the M-602.

RESULTS

The results of compatibility and adhesion of Narmco 7343 and Primer M with M-602 are listed in Table 84. Figure 223 shows a typical test panel.

Although there was no visible degradation of the M-602 in any of the three different cure cycles, the testing resulted in enough inconsistencies to indicate an interaction in various conditions.

Table 84. Adhesion of Cured Adhesive Films to M-602

		Overlying Adhesive or Primer (See Text)				
Panel Number	Number of Days Cure	a	b	c	d	e
A-1	5	DP	CO	DP	DP	DP
	10	DP	CO	DP	DP	PO
	15	DP	CO	DP	DP	PO
	20	PO	CO	DP	DP	PO
	30	DP	CO	DP	DP	PO
B-1	5	DP	CO	DP	DP	PO
	10	PO	CO	DP	PO	PO
	15	PO	CO	DP	DP	PO
	20	PO	CO	DP	DP	PO
	30	DP	CO	DP	PO	PO
C-1	5	DP	CO	DP	DP	PO
	10	DP	CO	DP	DP	PO
	15	DP	CO	DP	PO	PO
	20	DP	CO	DP	DP	PO
	30	DP	CO	DP	DP	PO
A-2	5	DP	CO	DP	DP	PO
	10	DP	CO	DP	PO	PO
	15	DP	CO	DP	PO	PO
	20	PO	CO	DP	DP	PO
	30	DP	CO	DP	DP	PO
B-2	5	DP	CO	DP	PO	PO
	10	PO	CO	DP	PO	PO
	15	PO	CO	DP	PO	PO
	20	PO	CO	DP	PO	PO
	30	PO	CO	DP	PO	PO
C-2	5	DP	CO	DP	PO	PO
	10	DP	CO	CP	PO	PO
	15	DP	CO	DP	PO	PO
	20	DP	CO	DP	DP	PO
	30	DP	CO	DP	PO	PO

DP: Does not peel
PO: Peels off
CO: Chips off

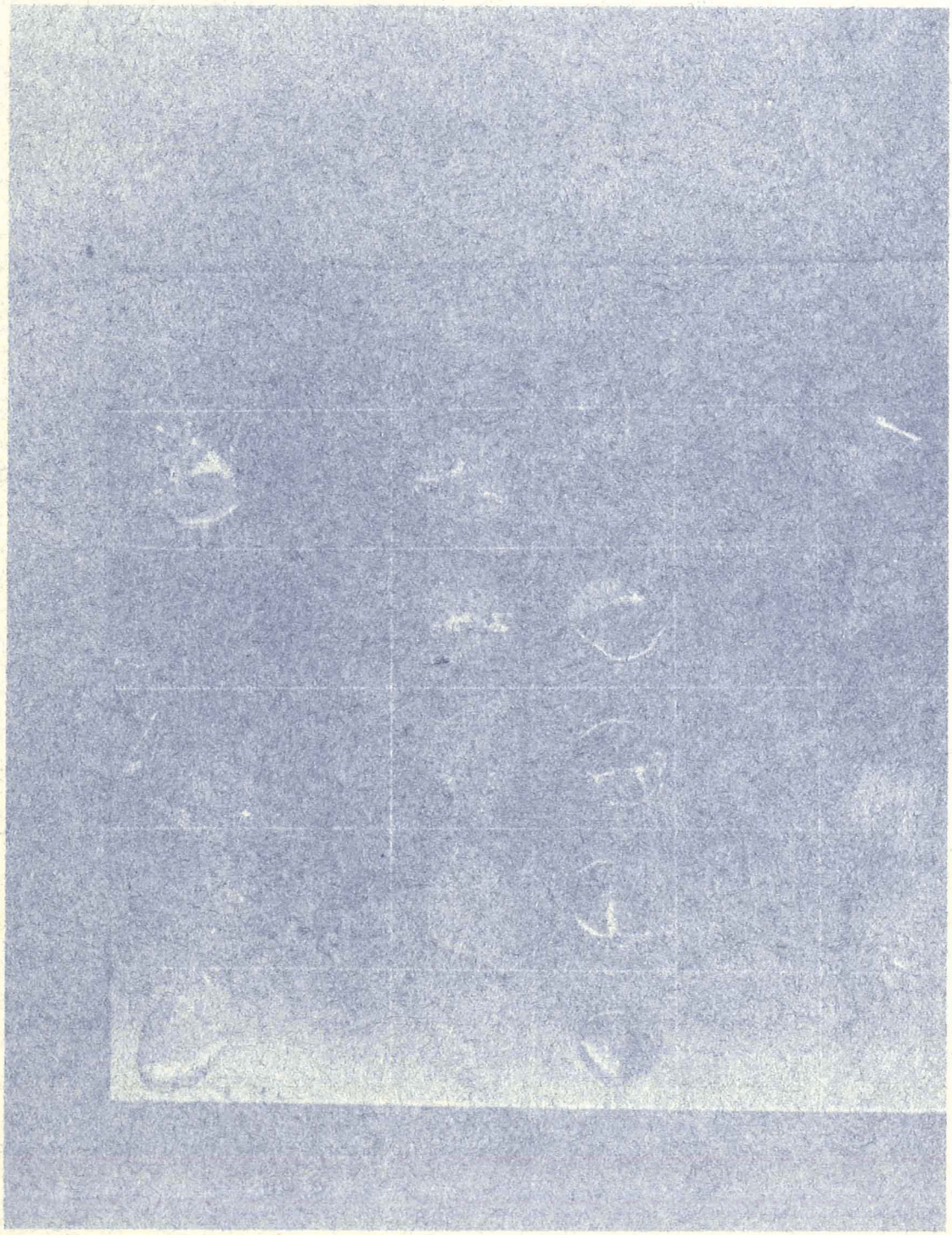

7006-81-2511D

Figure 223. Panel B-1—M-602 Cured 6 Hours at 290 F and Adhesive Applied, Cured, and Tested

PLASTICS

TEFLON CORRUGATED TUBING PRESSURE TEST

INTRODUCTION

Teflon corrugated tubing attached to the S-II LOX pumps allows excess LOX leakage to be dumped overboard during flight. Pressure buildup as high as 30 psig was anticipated, although engineering data were lacking at pressure this high. Typical deformation characteristics versus pressure were obtained on the corrugated tubing designated as Penntube No. 400.

PROCEDURES

The entire test setup, including pressure source, nitrogen and gauges, is shown in Figure 224. To determine burst pressure, the tube was secured at three points in a straight line position. Water was used as the pressure medium.

RESULTS

Deformation of the 26-inch tubing under pressure is shown in Figures 225 and 226. The tube did not burst at pressures up to 150 psig, so further burst pressure testing was discontinued.

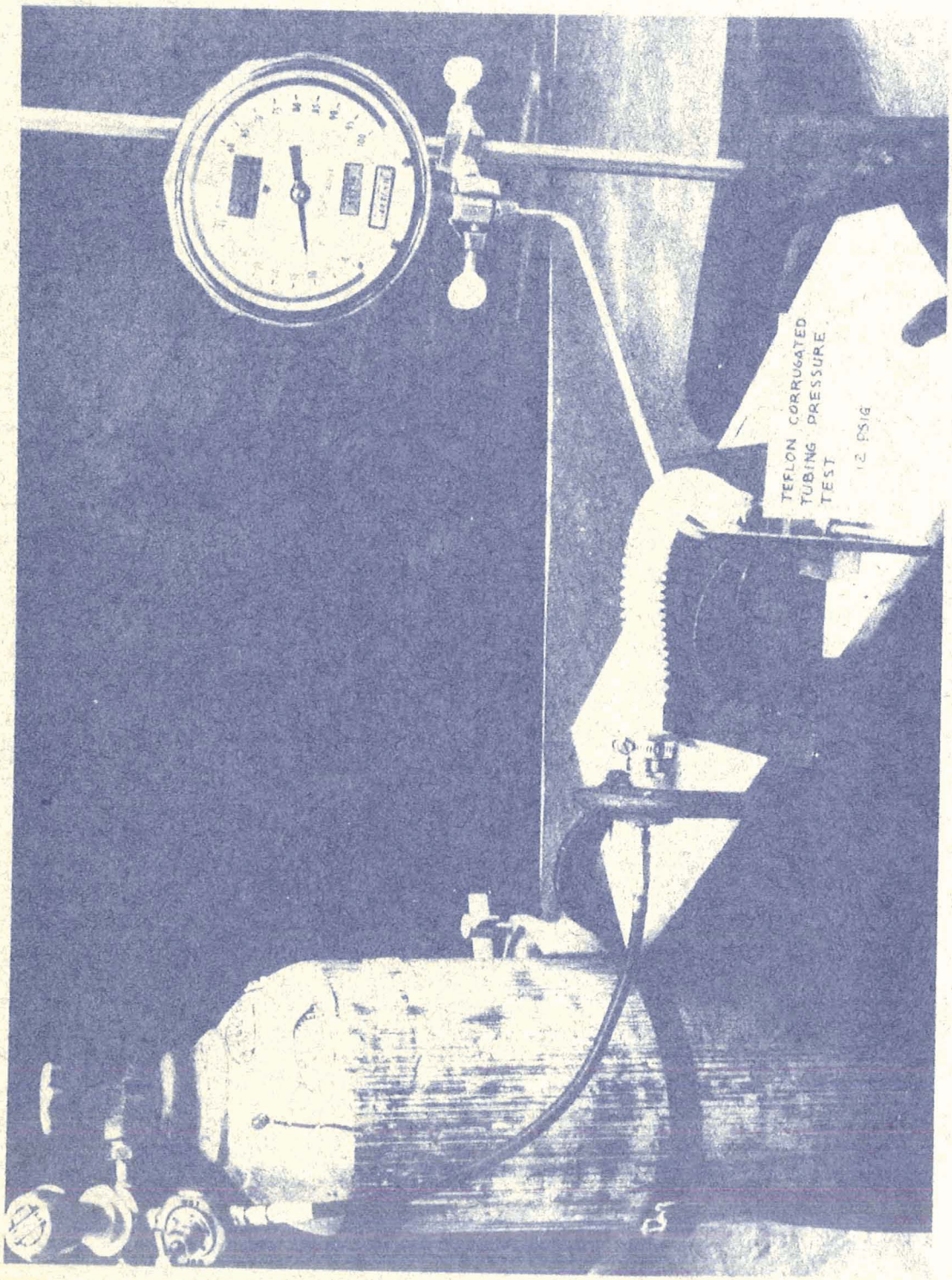

Figure 224. Test Setup With 14-Inch Tube

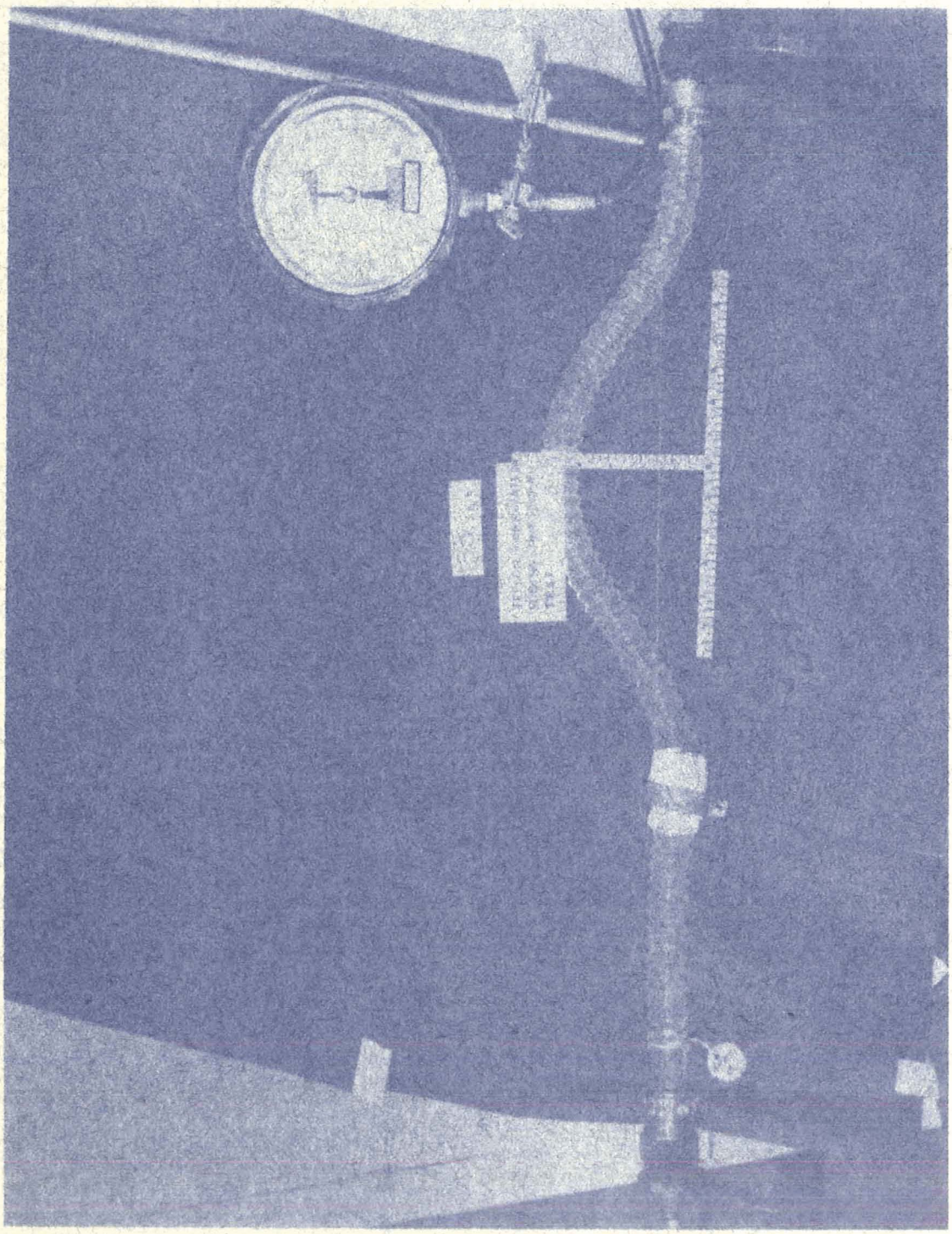

7006-81-2467P

Figure 225. Straight Line Position of 26-Inch Tube at 50 psig

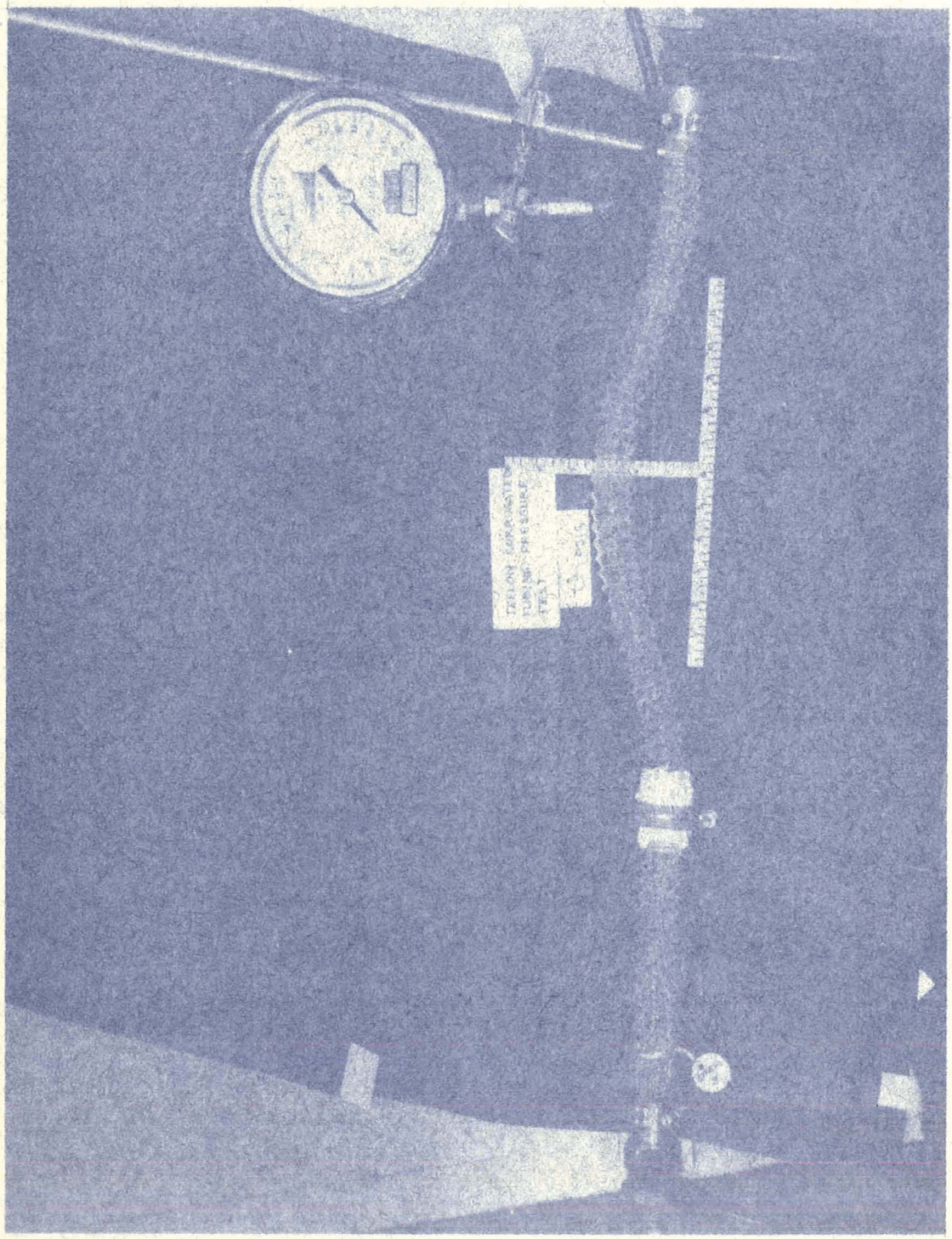

Figure 226. Straight Line Position of 26-Inch Tube After Relief of Pressure

7006-81-2467M

NEW SPECIFICATIONS

MATERIAL SPECIFICATIONS

The following S-II Material Specifications were released during this reporting period:

Specification Number	Title
MB0130-077	Polyurethane Foam, Two-Pound Density for Spray Application
MB0130-078	Fabric, Nylon, Polyurethane Coated
ST0210GB0002	Trichloroethane 1, 1, 1 Stabilized, Vapor Degreasing and Solvent Flushing Grade
MB0125-045	Polyurethane Coating for Foam Insulation
MB0150-044	Weldable Lead and Interconnect Material for Electric Components
MB0125-046	Coating, Vinyl Top Coat for Foam Insulation

PROCESS SPECIFICATIONS

The following S-II process specifications were released during this reporting period:

Specification Number	Title
MA0606-050	Spray Application of Two-Pound Density Polyurethane Foam Material for Saturn S-II Test Articles
MA0605-018	Fabrication and Installation of Saturn S-II Debris Barrier
MA0621-001	Finish Specification - Saturn S-II Stage
MA0606-052	Application of Primer, 250-F Curing For Saturn S-II
MA0608-015	Application of Polyurethane Coating to the Saturn S-II Foam Insulation
MA0606-053	Application of Cork Insulation on Exterior Surfaces of Saturn S-II Aft Skirt and Interstage
MA0606-054	Application of Sealing, Locking, and Retaining Compounds to Threaded Fasteners - Saturn S-II

INDEX TO PREVIOUS REPORTS

The topics listed below have appeared in previous issues of this report. The SID 63-600 dash number and page number are shown in the right-hand column. The original document, SID 63-600, is indicated by -0.

Topic	Volume and Page
Adhesives and primers	
Epoxy curing rates	SID 63-600-7, 71
FM-1000	-3, 55
HT-424	-0, 65
HT-424 and Aerobond 430	-0, 71
HT-424B primer variables	-7, 69
HT-424F roller coating	-5, 83
Lefkoweld 109	-5, 79
Lefkoweld 109 and 211	-6, 69
M-10 Primer	-8, 415
Metlbond 329 - high peel	-7, 65
Narmco 7343	-3, 88
Narmco 7343 primers	-4, 79 -5, 69 -6, 77
Aging of 2014-T6 during adhesive cure	-1, 3
Aging rates in aluminum weldments	-5, 25
Alternate bulkhead design	-0, 65 -2, 61 -3, 47

Topic	Volume and Page
Aluminum alloy, 2014-T6 (see cracking)	SID 63-600-1, 3 -3, 3
Aluminum fusion welding (see welding)	
Antiseize compounds	-2, 41
Arc-percussive welding	-4, 63
Automatic repair welding	-4, 16
Barrier films	-0, 79
Base heat shield	-1, 103 -2, 73 -4, 57
Flexible shield tests	-7, 59
Mechanical attachments load carrying	-8, 239
Rigid panel test	-7, 55
Bolts, titanium	-5, 3
Bonded doublers	-0, 66 -4, 83
Brazing, tube	-0, 41
Bulkhead failure analysis	-3, 3
Castings	-4, 3 -5, 15 -6, 3
Chemical milling	-0, 61 -1, 43
Chemical investigation of cracked ribs	-7, 19

Topic	Volume and Page
Chemical processing	
Etching of 2014 plate	SID 63-600-8, 169
Seal Beach facility	-1, 35
Circuit boards	-1, 117
	-2, 89
Cleaning	-0, 49
Coating, foam insulation	-8, 415
Columbium plume shield	-2, 74
Common bulkhead studies	-1, 61
Conformal coatings	-1, 119
Contamination control	-0, 45
Core, vented honeycomb	-1, 64
Corrosion	
Aluminum components of S-II stage	-8, 163
Protective coating	
Chem-Mill-type maskant	-8, 177
Evaluations for 2014-T6 aluminum	-8, 181
Evaluation of M-602 primer	-8, 185
Protection	
During hydrostat	-1, 49
In transit	-1, 50
Refurbishment of susceptible parts	-8, 175
Covers, LSC	-5, 85

Topic	Volume and Page
Conversion coatings	SID 63-600-1, 43
Cracking	
Chemical investigation of cracked ribs	-7, 19
Mechanical properties of as-received and formed tank panels	-8, 11
Mechanically fastened reinforcement	-8, 33
Metallurgical analysis of	-7, 3-17
Misalignment test program	-8, 21
Notch sensitivity of rib ends	-8, 5
Tensile evaluation	-8, 31
Cryogenic testing	-0, 97
Cylinder burst tests	-3, 41
Deoxidizers for aluminum	-2, 47 -3, 61
Diffusion bonding	-0, 29
Discoloration of terminal boards	-5, 55
Dollar welding	-5, 29
Double-seal insulation	-3, 82 -4, 91 -5, 57
Drying large tanks	-2, 47
Dye penetrants	-1, 38 -2, 52 -4, 42
Edge preparation	-4, 13

Topic	Volume and Page
Edge seals	SID 63-600-2, 57
Elastomeric mats	-4, 105
Electrical cable harnesses	-6, 83
Electrical cables	-6, 79
Electrical connections	-0, 25 -4, 63
Encapsulation	-0, 31
Epoxy-phenolic adhesives	-0, 71
Equipment containers	-1, 111 -2, 74
Explosion hazard	-2, 67
External insulation (see insulation cryogenic)	
Extrusions	-5, 9' -6, 11
Facings, properties of honeycomb insulation	-7, 73
Failure analysis	
Angle, Saturn thrust structures splice	-8, 105
Bellows, S-II-2 LOX fill and drain	-8, 111
Bolts, deformation of thrust block	-8, 149
CBTT hydrogen tank	-8, 115
Interstage, test support of S-II	-8, 99
Line, LOX vent	-8, 141
Line, S-II forward LOX vent	-8, 139

Topic	Volume and Page
Value, GSE self-sealing disconnect	-8, 103
Value, mounting flange calmec vent	-8, 93
Web, S-II interstage frame	-8, 155
Fasteners, self-sealing	
Alternate	-7, 51
Huck bolts, self-broaching	-7, 51
Test methods	-7, 47
Foam block insulation	-6, 37
Foam-in insulation	-6, 19
Foam helium barriers	-6, 47
Finishing	-0, 63 -1, 57 -4, 37 -5, 91
Fire hazards	-2, 67
Fit-up tests, bulkhead	-0, 21
Flammability of LH_2 tank insulation	-1, 83
Flexible curtain	-1, 106 -2, 73
Fluorescent penetrant	-2, 52
Fluoroelastomers	-3, 97
FM-1000 adhesive	-3, 55
Forgings, weldable hand	-1, 9

Topic	Volume and Page
Fusion welding aluminum (see welding)	
Groove-out repairs	SID 63-600-5, 39
Hand forgings, 2014, weldable	-1, 9
Harnesses, electrical	-6, 83
Heat shield	-0, 105 -4, 57
Heat shrinkable Teflon sleeving	-3, 67
Honeycomb core	-0, 69 -1, 64
Identification	-1, 57
Impact tests on LH_2 tank insulation	-1, 83
Induction soldering	-5, 43
Inserts for sandwich parts	-2, 29
Threaded	-7, 81
Insulation	
Ablative	
Aft skirt and interstage	-8, 215
Interstage spray-on	-8, 235
Resin-bonded cork	-8, 231
Base heat shield	-1, 103 -2, 73 -4, 57
Flexible shield tests	-7, 59

Topic	Volume and Page
Mechanical attachments load carrying	SID 63-600-8, 239
Rigid panel tests	-7, 55
Basic honeycomb	
Adhesive bond for	-0, 71
Adhesives for repair of	-5, 75
Edge seals for	-2, 57
Evacuated	-3, 73
Facing composites for	-6, 59
Flammability of	-1, 83
Hazards of	-2, 63
Helium-purged	-3, 73
Impact tests of	-1, 83
Laminates, lightweight	-2, 57
Laminate seals for	-2, 61
Materials for helium-purged	-3, 73
Repair, emergency	-8, 423
Retrofit of 0. 8-inch	-1, 80
Specifications for helium-purged	-5, 75
Vacuum decay test of	-8, 237
Double-seal	-5, 57 -3, 82 -4, 91

Topic	Volume and Page
Foam	
Block	
Flame-retardant	SID 63-600-8, 259
Qualification of	-8, 247
Hazards	
Explosive	-8, 409
Mechanical properties	
CPR 368-3	-8, 323 -8, 333
NOPCO BX-250A	-8, 333
Physical properties	
CPR 348-3	-8, 265
CPR 368-3	-8, 307 -8, 323
CPR 369-3	-8, 265
Spray	
Application of CPR 369-3	-8, 389
Cryopumping of CPR 369-3	-8, 277
Evaluation of CPR 369-3	-8, 269
Interface bond strength of	-8, 403
Process development of CPR 369-3	-8, 371
Structural test of CPR 369-3	-8, 281
Verification of CPR 368-3	-8, 355

Topic	Volume and Page
Technology of	SID 63-600-7, 85 -8, 245
J-section welding	-0, 10 -2, 3
J-section finishing	-5, 91
Lacing and typing materials	-3, 67
Laminates	-0, 75 -2, 57
Leak detection	
Study	-0, 95
Bolt, aft LOX bulkhead	-8, 193
Foil seal	-8, 191
Lightweight outer laminates	-2, 57
Linear-shaped-charge covers	-5, 85
LOX compatibility	-2, 50
Markings	-1, 57
Mechanical fasteners	-0, 23 -1, 23
Mechanical seals	-1, 95 -2, 93 -4, 55
Model 12 calorimeter	-1, 100
Module welding	-2, 89
Nickel-plated wire	-4, 63

Topic	Volume and Page
Notch strength of 2014-T6 weldments	SID 63-600-0, 3 -1, 3
Sensitivity of rib ends	-8, 5
Overaging 2014-T6 during adhesive cure	-1, 3
Paint systems for S-II	-1, 57
Planishing of welds	-1, 18 -2, 7
Polyurethane adhesives	-4, 79 -5, 69
Polyurethane adhesives, primers for	-6, 77
Potting	-0, 31 -2, 82 -3, 67
Percussion stud welding	-1, 27
Percussion welding wire to connector pin	-8, 87
Pressure-sensitive tapes	-0, 83
Primers for polyrethane	-5, 69
Printed-circuit boards	-0, 34
Purging studies	-0, 93
Quarter-scale tank	-0, 85
Repair welding	-0, 15 -4, 16 -4, 20
Repair adhesives	-5, 79
Resistance-welded electrical connectors	-0, 25
RF shielding	-0, 31

Topic	Volume and Page
Roller coating adhesives	SID 63-600-5, 83
Sandwich inserts	-2, 29
Sealants, cryogenic	-6, 53
Sealing, bolted splice plate	-3, 97 -5, 47
Seals	
Flanged joints	-0, 111 -2, 93 -4, 55 -6, 13
Foil	
Allowable back pressure	-8, 213
Leakage tests	-8, 191
LH_2 feedlines	-8, 187
LOX compatible	-8, 199
Plug	
Soldered for small holes	-8, 213
Seal welds, LOX tank	-0, 15
Sleeving	-1, 120 -3, 67
Soldering	-0, 25
Thermofit solder sleeve	-8, 85
Specifications for foam-filled insulations	-5, 75
Spray cleaning	-2, 47

Topic	Volume and Page
Spraying conversion coatings	SID 63-600-1, 43
Spray processing	-0, 49
	-1, 52
	-2, 47
Stress corrosion	-1, 10
	-4, 42
Surface preparation for bonding	-1, 52
	-2, 47
	-3, 61
Terminal boards	-1, 119
	-5, 55
Thermal conductance apparatus	-0, 101
	-1, 97
Thermal conductivity	-1, 97
	-2, 64
Thermal stability of 340L	-1, 33
Threaded inserts	-2, 29
	-4, 69
Titanium bolts	-5, 3
Tube joint welding	-1, 29
	-2, 19
Tungsten inclusions in 2014-T6 weldments	-1, 18
Vented honeycomb core	-1, 64
Welding, aluminum fusion,	
Coupon, geometry	-3, 25
Cryogenic shock test of	-3, 28

Topic	Volume and Page
Cylinder burst test of	SID 63-600-3, 41
Edge, preparation of	-4, 13
Thinning of	-8, 67
Elbow, CBTT	-8, 71
J-section	-0, 10 -2, 13
Land thickness	-3, 36
Leak testing	-8, 81
Mechanical properties	
Effect of porosity on	-8, 75
Misalignment	
Uniaxial strength	-7, 31
Notch strength	-1, 3
Offset	-1, 18
LOX tank girth, S-II-5	-8, 57
Peaking	-1, 18
Biaxial strength	-7, 25
Planishing	-1, 18
Post-weld treatment	-3, 34
Seal welds	-0, 10
Welding, Inconel	
Filler material Inconel 82	-8, 69

Topic	Volume and Page
Mechanical properties	
Alloys 625 and 718	SID 63-600-8, 73
Welding, percussion, wire to connector pin	-8, 87
Welding, repair	-7, 37
Analysis, coupon	-7, 38
Automatic	-4, 16
Inspection of	-7, 37
Manual	-4, 20
Specimens, preparation of	-7, 35
Specimens, preparation of physical	-7, 37
Testing procedures, physical	-7, 37
White lines in aluminum weldments	-5, 33